RCEM 2019

THE 11TH SYMPOSIUM ON RIVER, COASTAL AND ESTUARINE MORPHODYNAMICS

BOOK OF ABSTRACTS

AUCKLAND, NEW ZEALAND
16TH–21ST NOVEMBER 2019

manatiaki kōawa
rivers
GROUP
A joint technical interest group of Engineering New Zealand & Water NZ

IAHR AIRH
International Association for Hydro-Environment Engineering and Research

Hosted by
Spain Water and IWHR, China

RCEM 2019

THE 11TH SYMPOSIUM ON RIVER, COASTAL AND ESTUARINE MORPHODYNAMICS

AUCKLAND, NEW ZEALAND
16TH–21ST NOVEMBER 2019

BOOK OF ABSTRACTS

EDITED BY:
HEIDE FRIEDRICH AND KARIN BRYAN

2019

COMMITTEE MEMBERS

RCEM Local Organising Committee

Heide Friedrich (Chair)
University of Auckland, Auckland

Giovanni Coco
University of Auckland, Auckland

Karin Bryan
University of Waikato, Hamilton

Jon Tunnicliffe
University of Auckland, Auckland

Julia Mullarney
University of Waikato, Hamilton

Jo Hoyle
NIWA, Christchurch

Kyle Christensen
Christensen Consulting, Wellington

Tumanako Fa'aui
University of Auckland, Auckland

James Brasington
University of Waikato, Hamilton

Ian Fuller
Massey University, Palmerston North

Edwin Baynes
University of Auckland, Auckland

Renske Terwisscha van Scheltinga
University of Auckland, Auckland

I.S.B.N.: 978-0-473-50422-9

KEYNOTE SPEAKERS

MONDAY—18 NOV, 9:30AM

MURRAY HICKS

Principal Scientist for River and Coastal Geomorphology at NIWA, Christchurch, NZ

Murray Hicks is Principal Scientist for River and Coastal Geomorphology at the National Institute of Water and Atmospheric Research Ltd (NIWA) in Christchurch. With undergraduate honours degrees in geology and civil engineering from Otago and Canterbury Universities, his PhD at the University of California focussed on sediment transport by coastal and river processes. His career since has stayed in the same domain, working mostly at NIWA as a researcher and consultant. With NIWA colleagues and international collaborators, much of this has been devoted to measuring and modelling the morphodynamics of braided rivers and applying results to assessing the effects of water-use schemes, dams, and gravel extraction on river morphology and physical habitat. He has also used coastal sediment budgets, remote-sensing, and morphological models to investigate the effects of changing river sand/gravel yields on the stability of adjacent coasts in the context of rising sea level and changing wave climate. He has also led projects, and trained many others, to measure and analyse the suspended load of New Zealand rivers, producing guidance manuals and national scale GIS models to predict sediment yield.

MCRE–NZ: Morphodynamic Challenges in Braided River Environments of New Zealand

This talk introduces morphodynamics research challenges to assist environmental/engineering issues in New Zealand's braided rivers, which are becoming increasingly threatened by demands for irrigation water, braidplain conversion to farmland, and extreme events associated with earthquakes and climate change.

With baseflows and groundwater fully allocated, the water demand is now directed at flood-harvesting. Effects include fine-sediment deposition on recessions and long-term morphological change, compounded by interactions with vegetation and wind-blown sediment, with impacts on ecosystems and human values. Key morphodynamic challenges are to detect and predict event-scale and long-term consequences.

Braidplains on range-front alluvial fans are prone to flooding associated with aggradation accelerated by gravel-supply events from earthquakes and floods and by engineered channel confinement. Sustainable management often stalls from a vicious circle of low confidence in predicted river response to high-cost intervention with limited funding. Novel research exploring the interaction of transient morphological events (e.g. avulsions) and confinement on bedload transport efficiency offers a chance to break this impasse.

Most braided rivers enter the sea via "hapua" – elongated lagoons fronted by wave-built barriers with unstable outlets prone to closing. This produces a risky environment, particularly for flooding and fish-migration, sensitive to changes in river regime and wave climate. The morphodynamic challenge is to numerically predict the consequences of changing controls on these 3-d, hybrid river/coastal features.

TUESDAY—19 NOV, 8:30AM

LAURA J. MOORE

The University of North Carolina, USA

Laura J. Moore is an Associate Professor in the Department of Geological Sciences and the Environment, Ecology and Energy Program at The University of North Carolina at Chapel Hill. Laura's interdisciplinary research program in coastal geomorphology focuses on the response of low-lying coastal environments to climate change. Her recent and ongoing work relies on the merging of numerical and observational approaches to investigate coastal foredune ecomorphodynamics, barrier island response to climate change; couplings among barrier islands, back-barrier marshes and back-barrier bays; large-scale coastline response to changing wave climate; and coupled natural-human coastline dynamics. Laura has been an Investigator at the Virginia Coast Reserve Long-term Ecological Research site in the U.S. since 2008. Recently, she was the lead editor of *Barrier Dynamics and Response to Changing* Climate published in 2018 by Springer and served as a member of the National Academy of Sciences Committee, *Long-term Coastal Zone Dynamics: Interactions and Feedbacks between Natural and Human Processes along the U.S. Gulf Coast*.

The Role of Ecomorphodynamic Feedbacks, Landscape Couplings and Natural-Human Dynamics in Determining the Fate of Coastal Barrier Systems

Because coastal barriers are low-lying and dynamic landforms, they are especially sensitive to changing environmental conditions. The effectiveness of storms in building elevation and moving a barrier landward as conditions change is largely determined by foredune morphology, which is a product of feedbacks between vegetation and sediment transport processes. For example, the cross-shore and alongshore shape of coastal foredunes is influenced by the distance from the shoreline that vegetation can grow, the lateral and vertical growth rate (and form) of dune-building grasses, and the rate of lateral vegetation growth relative to the rate of shoreline change. Coastal foredune morphology largely determines barrier state (including the possibility for bistable dynamics) and, thus, the degree to which connectivity with back-barrier environments will influence overall barrier system response to changing conditions. Coupled natural-human dynamics also alter ecomorphodynamic processes, barrier morphology, and sediment flux, further influencing the future evolution of developed coastal barrier systems worldwide.

TUESDAY—19 NOV, 5:00PM

DANIEL PARSONS

University of Hull, UK

Professor Dan Parsons leads the Energy and Environment Institute (EEI) at the University of Hull, UK. The EEI gathers together multidisciplinary researchers from across the University to conduct impactful research on the global challenges presented by environmental change and securing a low-carbon energy transition. Dan is an active researcher in areas related to fluvial, estuarine, coastal and deep marine sedimentary environments, exploring responses of these systems to climate and environmental change. He has research interests in anthropogenic disturbances to these systems and determining necessary societal adaptations to mitigate the impact of change – for example understanding how evolving flood risk on large mega-deltas can impact populations and their related livelihoods through to understanding and quantifying and predicting the magnitude of risk and hazard from natural system function.

The Impact of Unsteadiness and Non-stationarity in Riverine and Estuarine Systems: Morphodynamic Response and (In)stability

Riverine and tidal flows are inherently non-stationary, varying on a range of timescales. These variations in flows field strength alter a suite of morphodynamic processes. For example, during flow field unsteadiness bedforms change in size and shape over time and in space, altering bed roughness and imparting system hysteresis between flows and form. However, our knowledge of how these bedforms adapt to changing flows remains inadequately understood. Moreover, how these variations, and hysteresis between flow and form, manifest at broader scales and control the morphodynamic evolution of the wider system is also poorly understood.

Herein I will present a mix of laboratory flume experiments, field case studies and numerical experiments to explore some of these relationships and their controls. The result indicate how changes in primary sediment transport mechanisms can dominate how dunes change with unsteady flows and how sediment redistribution over greater spatial scales can also play a significant role. Where substrate sediments are comprised of mixed sand and mud, the results indicate how this can play a first-order control on bedform size and aspect ratios, also altering adaption styles and rates as well as impacting the levels of hysteresis between flow and form.

How this work extends our knowledge on the impact of variable flows on riverine and esturine processes will be discussed and the broader impact and significance of the findings for a wide variety of purposes, such as improving morphodynamic modelling over large spatio-temporal scales, environmental and engineering management, and more reliable flood predictions will also be highlighted.

WEDNESDAY—20 NOV, 8:30AM

DOUGLAS J. JEROLMACK

University of Pennsylvania, USA

Professor Doug Jerolmack's research focuses on the spatial and temporal evolution of patterns that emerge at the interface of fluid and sediment on Earth and planetary surfaces. His group uses laboratory experiments, combined with field work and theory, to elucidate the minimum number of ingredients that are required to explain physical phenomena. Particular foci include: granular physics of fluid-driven (water and wind) sediment transport; landform dynamics including dunes, river channels, deltas and fans; stochastic and nonlinear transport processes; and landscape response to dynamic boundary conditions such as climate. Doug is currently Professor and Graduate Chair in Earth and Environmental Science, with a secondary appointment in Mechanical Engineering and Applied Mechanics, at University of Pennsylvania, USA. Doug received a B.S. in Environmental Engineering at Drexel University in 2001, PhD in Geophysics from MIT in 2006, and was a postdoctoral researcher at Saint Anthony Falls Lab at University of Minnesota 2006-2007. Doug has been at Penn since 2007.

All Rivers Are Threshold If You Average the Hell out of Them

A laundry list of factors have been proposed to control alluvial river size. Near-universal scaling relations between channel geometry and discharge, however, suggest a common organizing principle. Numerous metaphysical explanations have been advanced. We propose an extension of Parker's original theory for gravel-bed rivers: River geometry adjusts to the threshold fluid entrainment stress of the most resistant material lining the channel. For gravel-bed rivers this is gravel, but for sand-bed rivers this is muddy bank material. This "threshold limiting material" model describes the hydraulic state of natural rivers - so long as we appropriately average over all of the time and space scales of variation in the flow. It is also compatible with dynamics: erosion and deposition associated with meandering represent higher-order variations in fluid stress around the mean state. Thus, we consider the generalized Parker model as a mean field theory for alluvial river geometry, that highlights the importance of the entrainment threshold. Increasing the relative threshold of bank to bed material leads to a proportionate reduction in channel width and increase in channel depth; in this manner, muddy banks encourage sand-bed rivers to adopt a meandering (rather than braided) morphology. All kinds of important implications may be imagined for managing rivers, dealing with climate change, and of course Mars."

WEDNESDAY—20 NOV, 4:30PM

CATHERINE KNIGHT

Writer and Environmental Historian, Manawatu, NZ

Dr Catherine Knight is a writer and environmental historian. She is a Senior Associate at the Institute for Governance and Policy Studies, Victoria University of Wellington and Honorary Research Associate at the School of People, Environment and Planning, Massey University. She has published four books relating to New Zealand's environmental history, including New Zealand's Rivers: An environmental history (Canterbury University Press, 2016), which was long-listed for the Ockham New Zealand Book Awards, short-listed for the New Zealand Heritage Book Awards and selected as one of The Listener's Best Books for 2016. Her other books are: Beyond Manapouri: 50 years of environmental politics in New Zealand (Canterbury University Press), which was a finalist in the New Zealand Heritage Book Awards; Ravaged Beauty: An environmental history of the Manawatu (Dunmore Press), which was the winner of the J.M. Sherrard Award for Regional and Local History; and Wildbore: A photographic legacy (Totara Press). Catherine works as a policy and communications consultant at KHM Consulting, based in the Manawatu.

The Changing Meaning of Rivers in Aotearoa New Zealand

In this talk Dr Catherine Knight will explore how perceptions of rivers in Aotearoa New Zealand has evolved since the country's settlement by Europeans, two centuries ago. For most of our post-colonial history, rivers have been viewed as something to be controlled and managed – even 'improved'. But today, rivers are increasingly being recognised as embodying a broad range of values from the ecological to the spiritual – not simply as a 'channel of water' that can be exploited for human ends. While much of this evolving understanding stems from the advance in scientific knowledge, much too has its roots in our collective past.

ABSTRACT INDEX

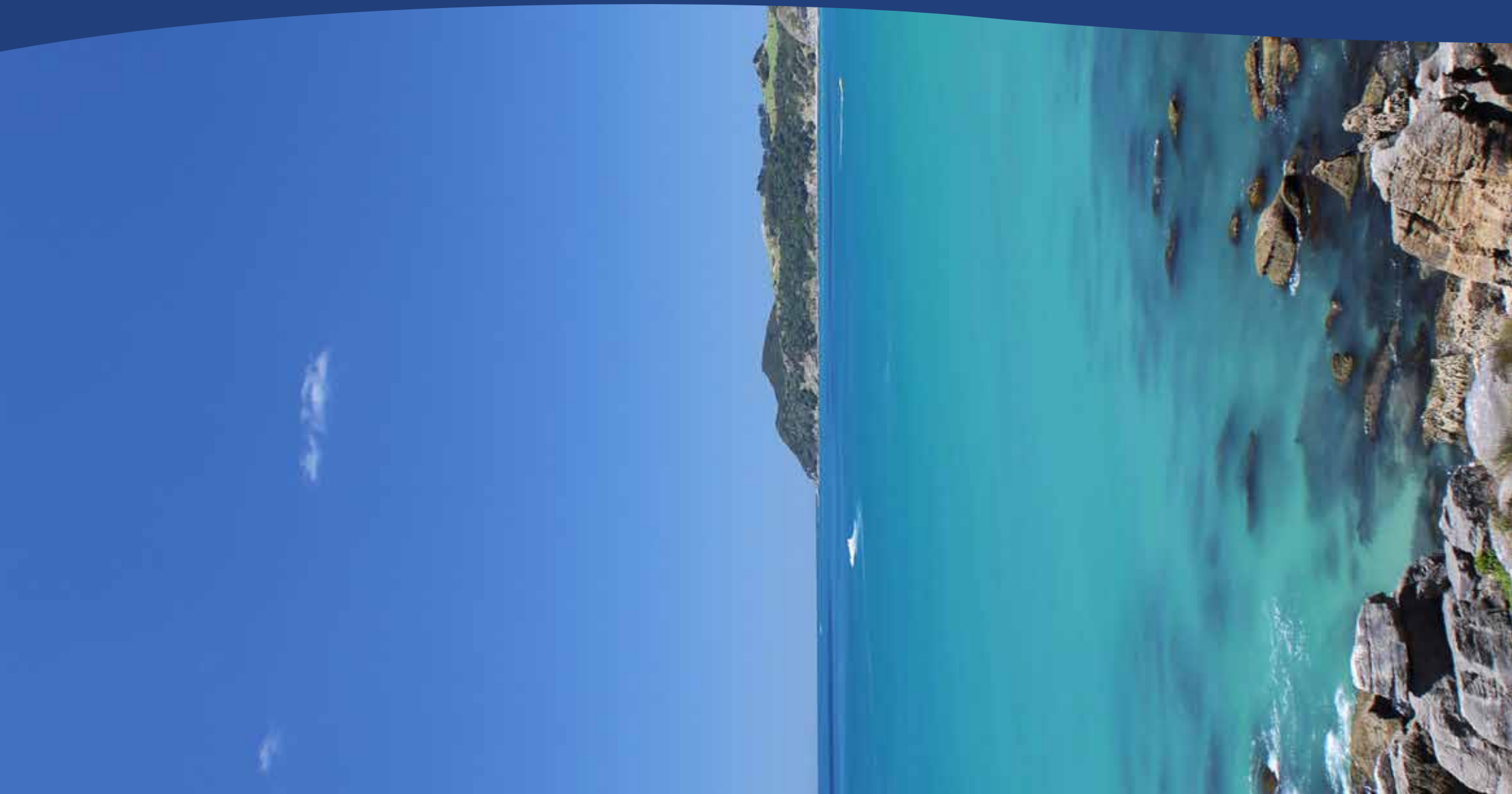

INDEX—MONDAY, 18 NOV

Oral Presentations

Estuaries

Coastal Sediment Transport

Marshes and Intertidal Flats

INDEX—MONDAY, 18 NOV

Oral Presentations

Anthropogenic Effects on Morphodynamics

River Morphodynamics

River Modelling

INDEX—MONDAY, 18 NOV
Oral Presentations

Bank Erosion

Instrumentation and Methodology Advances

INDEX—MONDAY, 18 NOV

Poster Presentations

INDEX—MONDAY, 18 NOV

Poster Presentations

INDEX—TUESDAY, 19 NOV

Oral Presentations

Tidal Morphodynamics

Morphodynamics Around the World

Marshes

INDEX—TUESDAY, 19 NOV
Oral Presentations

River Sediment Transport

River Sediment Transport

River Sediment Transport

INDEX—TUESDAY, 19 NOV

Poster Presentations

INDEX—TUESDAY, 19 NOV

Poster Presentations

INDEX—WEDNESDAY, 20 NOV
Oral Presentations

Beach and Barrier Morphodynamics

Dunes and Bedforms

Tidal Shoals

INDEX—WEDNESDAY, 20 NOV
Oral Presentations

Vegetation in Rivers

Small-Scale Effects

Climate Change Effects on Morphodynamics

INDEX—WEDNESDAY, 20 NOV
Oral Presentations

NZ Applied Case Studies

NZ River Research

Sediment-Wood Interaction

INDEX—WEDNESDAY, 20 NOV

Poster Presentations

INDEX—WEDNESDAY, 20 NOV

Poster Presentations

Determining morphological stability of tidally-influenced bifurcations

A.P. Iwantoro[1], M. van der Vegt[1] and M.G. Kleinhans[1]

[1] Department of Physical Geography, Utrecht University, Utrecht, the Netherlands. a.p.iwantoro@uu.nl

1. Introduction

The morphology of river bifurcations often evolves asymmetrically, resulting in an avulsion (i.e. unstable bifurcations). Bolla Pittaluga et al. (2015) proposed a stability theory of bifurcations for gravel and sand bed rivers using an idealized model. They found that for high and low values of the Shields number the bifurcation is unstable, while for a limited range of Shields numbers the bifurcation can be stable. Observations suggest that bifurcations in tidally influenced systems are stable; however, the stability theory has not been applied to tidal systems. This is because of the presence of bi-directional flows induced by tides, suspended load dominated condition, and typical low channel slopes in tidal deltas and estuaries. Here we study the morphological evolution of bifurcations in the range from river- to tide-dominated systems.

2. Method

We developed a 1D numerical model that solves the 1D shallow water equations, sediment transport and the sediment mass conservation equation for a system consisting of one upstream channel and two downstream branches. To solve the sediment division at the bifurcation we used an improved version of the nodal point relationship of Bolla Pittaluga et al. (2015). It includes both bed-load and suspended load transport and can cover the changing flow directions in tidal systems. The division of bed-load at the junction was affected by both cross-channel flow and transverse bed slopes, while for suspended load, in contrast to Bolla Pittaluga et al. (2015), it is only affected by cross-channel flow. The results of the 1D model has been well-verified against fully-numerical 2D model (Delft3D). Furthermore, this 1D model is also applied to analyse the morphodynamic of channel networks in urbanized delta (Dordtsche Kil channel network, Rhine-Meuse delta, the Netherlands).

To analyse the stability of the bifurcations, identical branches were initially defined. Then a small depth difference between branches was prescribed. When this depth asymmetry grows in time the system is unstable, when it decays it is stable. The channel configuration and other model settings were based on observed bifurcations. In shown results, the Shields number was varied by varying the D_{50} in the range of sandy material (0.1-1 mm).

3. Results and conclusions

For river-dominated systems, we found that systems with lower channel slope have a narrower range of Shields number for which stable solutions are present, as shown in Figure 1. Thus, besides a larger width-to-depth ratio (W/h), a lower channel slope also causes a more limited range of Shields numbers for stable bifurcations.

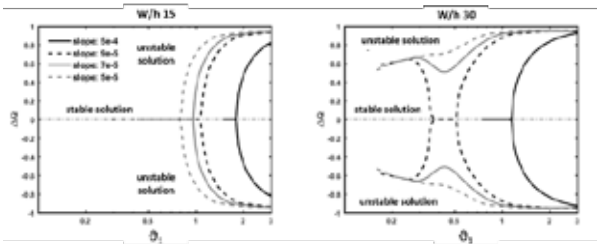

Figure 1: stability of bifurcations for different slopes with w/h of 15 (left) and 30 (right). ΔQ is discharge difference between branches.

Based on a first set of simulations for tide-dominated systems, we conclude that tides oppose this asymmetric development and results in a stable bifurcation for all tidally averaged Shields numbers (Figure *2*). Meanwhile, with the same configuration, the opposite behaviour is shown in river only conditions.

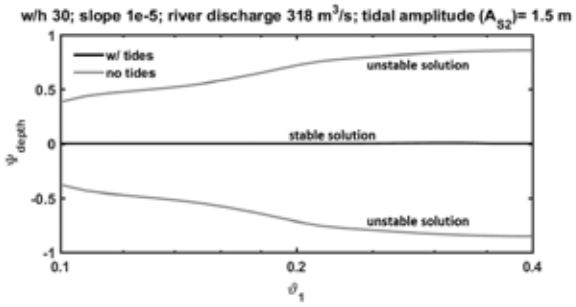

Figure 2: stability of bifurcations for tidally influenced and river-only condition for w/h = 30 and slope = 1e-5. Ψ_{depth} is tidally averaged depth ratio (H_2-H_3/H_2+H_3). H_i is tidally averaged depth for different branches.

From these results, we proof that tides can counteract the avulsion process that would occur in river-dominated deltas. Using this new model, we can start analysing how different combinations of tide and river forcing determine the morphological stability of bifurcations, and how this depends on the geometry of the bifurcation.

Acknowledgments

This research is funded by Indonesia Endowment Fund for Education (LPDP).

References

Bolla Pittaluga, M., Coco, G., & Kleinhans, M. G. (2015). A unified framework for stability of channel bifurcations in gravel and sand fluvial systems. *Geophysical Research Letters*, *42*(18), 7521–7536. http://doi.org/10.1002/2015GL065175

A Theoretical Study on the Width-To-Depth Ratio of a Tidal Channel

Fan Xu[1], Qing He[1], Giovanni Coco[2], Zeng Zhou[3] and Jianfeng Tao[3]

[1] State Key Laboratory of Estuarine and Coastal Research, East China Normal University, Shanghai, China.
[2] Faculty of Science, University of Auckland, Auckland, New Zealand.
[3] College of Harbor, Coastal and Offshore Engineering, Hohai University, Nanjing, China.

1. Introduction

The width-to-depth ratio is a key feature characterizing the equilibrium profile of tidal channels. Field observations have been carried out in different coastal regions (e.g., Marani et al., 2002). However, a unified framework that addresses the width-to-depth ratio is still lacking, despite several theoretical relationships being proposed for riverine cross-sections (e.g., Ikeda and Izumi, 1990).

In this study, a unified and general framework is proposed to describe the width-to-depth ratio that characterizes the morphodynamic equilibrium of a tidal channel. A generic form of momentum balance is employed including the water pressure gradient, the bed resistance and the lateral turbulent diffusion (Lanzoni and D'Alpaos, 2015). The equilibrium profile is simulated using a lateral one-dimensional numerical model, which allows the cross-section to evolve following simple erosion and deposition rules. This equilibrium profile leads to an analytical form of the width-to-depth ratio, which agrees well with available field measurements.

2. Methods

The numerical model consists of a flow model and a sediment balance model. The flow model simulates the lateral distribution of the bed shear stress, which is calculated by the generic momentum equation:

$$\tau = -\rho g h S + \frac{\partial}{\partial y}\int_0^h \tau_{yx} dz \qquad (1)$$

where x and y are the longitudinal and the lateral coordinates (m), τ is the bed shear stress ($\mathrm{kg/ms^2}$), ρ is the water density ($\mathrm{kg/m^3}$), g is the gravity ($\mathrm{m/s^2}$), $h = \eta - z_b$ is the total water depth (m), in which η is the water surface elevation and z_b is the bed elevation, and τ_{yx} is the turbulent shear stress ($\mathrm{kg/ms^2}$). The sediment balance model is governed by a simple mass continuity law:

$$\frac{\partial h}{\partial t} = E - D \qquad (2)$$

where D and E are local deposition and erosion terms ($\mathrm{m/s}$). The deposition term D is constant ($D = D_0$). A linear function $E = Q_{e0}(\tau/\tau_e - 1)\mathbb{H}(\tau - \tau_e)$ is used to evaluate the local erosion, where Q_{e0} is a characteristic erosion rate ($\mathrm{m/s}$), τ_e is the critical bed shear stress for erosion and $\mathbb{H}$ is a Heaviside step function.

3. Results and Discussions

Since the mass balance condition $E = D$ must be satisfied at equilibrium, the bed shear stresses over the profile are evenly distributed. This simple configuration follows the concept of the dynamic equilibrium, where some sort of null spatial gradient conditions is satisfied, such as sediment flux (e.g., Friedrichs and Aubrey, 1996). Taking the bed shear stress at its equilibrium value and employing the Manning friction and eddy viscosity closures, the governing equation for the equilibrium profile can be derived, which further leads to the analytical solution of the width-to-depth ratio:

$$\frac{B}{h} \approx 1.62\sqrt{\frac{\Lambda}{\sqrt{g}n}}h^{1/12} \qquad (3)$$

where B is the bankfull width of the tidal channel (m), Λ is the non-dimensional eddy viscosity and n is the Manning friction coefficient ($\mathrm{s/m^{1/3}}$). The analytical width-to-depth ratio is compared with field data (Figure 1) and is consistent with relatively small tidal channels. Small cross-sections are mainly observed in sheltered salt marshes, where longitudinal tidal flow is dominant and bank stability issues are less important due to the relatively small channel depth. Therefore, the assumption that the tide-induced bed shear stresses are uniformly distributed can be valid and equation (3) gives an estimate of the minimum value of the bankfull width that the cross section of a tidal channel can reach.

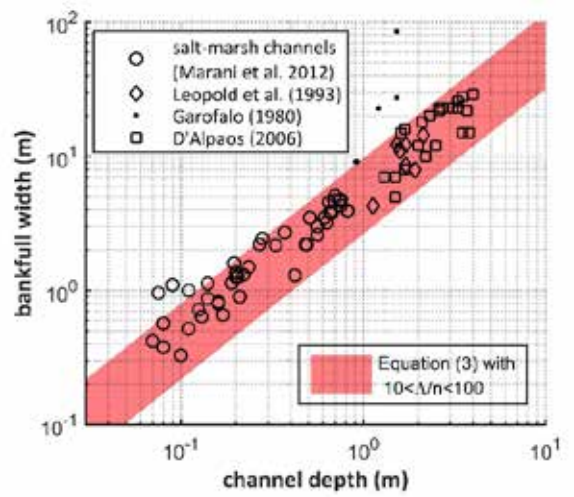

Figure 1. Comparison between the analytical width-to-depth ratio (Equation 3) and field data.

References

Friedrichs, C.T., Aubrey, D.G., (1996). Uniform bottom shear stress and equilibrium hyposometry of intertidal flats. *Mix. estuaries Coast. seas* 405–429.

Ikeda, S., Izumi, N., (1990). Width and depth of self-formed straight gravel rivers with bank vegetation. *Water Resour. Res.* 26, 2353–2364.

Lanzoni, S., D'Alpaos, A., (2015). On funneling of tidal channels. *J. Geophys. Res. Earth Surf.* 120, 433–452.

Marani, M., Lanzoni, S., Zandolin, D., Seminara, G., Rinaldo, A., (2002). Tidal meanders. *Water Resour. Res.* 38, 7–14.

Morphodynamic Equilibria and Linear Stability in Tidal Estuaries: Influence of Coriolis and Planform Geometry

H.M. Schuttelaars[1], T. Boelens [2], T. De Mulder [2], X. Deng [1] and G.P Schramkowski[1,3]

[1] Delft Institute of Applied Mathematics, Delft University of Technology, The Netherlands.
H.M.Schuttelaars@tudelft.nl, X.Deng@tudelft.nl
[2] Hydraulics Laboratory, Civil Engineering Department, Faculty of Engineering and Architecture, Ghent University, Belgium. Thomas.Boelens@ugent.be, TomFO.DeMulder@ugent.be
[3] Flanders Hydraulics Research, Belgium. George.Schramkowski@mow.vlaanderen.be

1. Introduction

Complex bottom patterns are often observed in tidal basins, found in for example the Wadden Sea along the Dutch, German and Danish coast. These patterns consist of branching channel-shoal patterns, that often exhibit cyclic behavior. Using an idealised morphodynamic model, we aim at finding morphodynamic equilibria and assess their stability, with a specific focus on their sensitivity to Coriolis forcing and planform geometry.

2. Model Description

The geometry we consider consists of either a single or double inlet system, with arbitrary planform geometry, see Fig. 1.

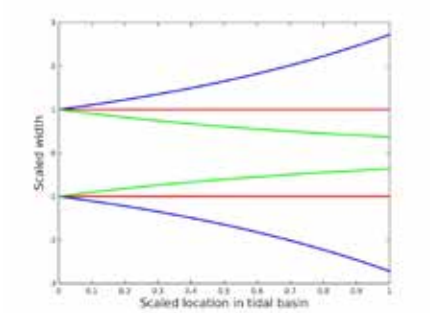

Figure 1. Various examples of geometries considered.

The physics are modeled using the depth–averagerd shallow water equations, suspended sediment transport equation the bed evolution equation. As a first step, the equations are scaled, using typical order of magnitudes for the various physical parameters. After scaling, a small parameter is identified, namely the ratio of the amplitude of the sea surface elevation and the water depth at the seaward side. This allows for an asymptotic analysis of the system of equations, resulting in a systematic solution method to obtain the various physical variables. Since the water motions and sediment transport take place on a much shorter timescale than the bed evolution, the bed is considered fixed on the fast hydrodynamic timescale. Only the tidally averaged divergences and convergences of the sediment transport result in a change of the bed profile on the long timescale. The model equations are discretized using the finite elements method, and morphodynamic equilibria are obtained using a continuation method: instead of integrating the equations in time, a solution of the equations is sought for such that there are no convergences and divergences of tidally averaged sediment transport. By including the Coriolis force and a general planform, previous results are extended.

3. Model results

In Fig. 2, left panel, an example of a bed profile in morphodynamic equilibrium in a converging single tidal inlet is shown. The water depth at the seaward side (lefthand side) is maximum, while the undisturbed water depth vanishes at the landward side. To more clearly illustrate the symmetry–breaking by including the effects of Coriolis forcing, the difference in bed profile between the morphodynamic equilibrium with and without Coriolis effects is depicted in the panel on the right.

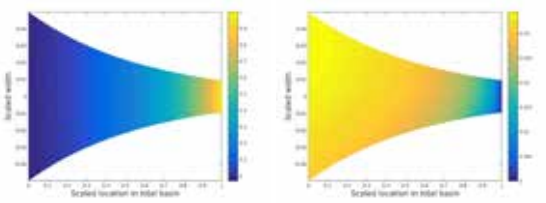

Figure 2. Left panel: Equilibrium bed profile in a converging channel, including Coriolis forcing. Right panel: difference between the equilibrium bed profile with and without Coriolis effects.

Apart from influencing the morphodynamic equilibria, Coriolis effects also influence the linear stability. For a rectangular basin, inclusion of Coriolis effects results in more negative eigenvalues, implying that with Coriolis the underlying morphodynamic equilibrium is linearly more stable.

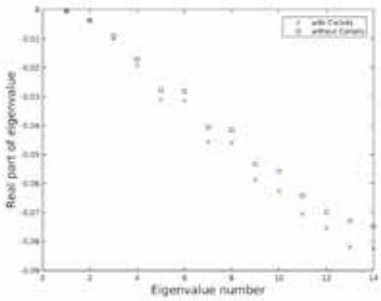

Figure 3. Real part of the eigenvalues of the 14 most unstable eigenpatterns.

4. Conclusions

In this presentation, the influence of the planform geometry and Coriolis forces on the morphodynamic equilibria and their linear stability will be systematically analysed and the underlying physical mechanisms will be explained.

Influence of the inlet geometry on the deflection of bed material into lateral river branches

Karl Kastner[1,2], A. J. F (Ton) Hoitink[1,3]

[1]Hydrology and Water Management, Wageningen University, The Netherlands
[2]kastner.karl@gmail.com [3]ton.hoitink@wur.nl

1. Introduction

The division of sediment at river bifurcations is crucial for the morphodynamics of delta channel networks. Many natural bifurcations are strongly asymmetric so that a small channel branches off from the side of a large channel. The secondary currents at such an asymmetric bifurcation preferentially direct water that flows near the bottom towards the side branch. As the sediment concentration near the bottom is high, side branches receive a larger fraction of the approaching sediment load than of the water discharge. This causes side branches in scale experiments to fill in rapidly. However, there are many asymmetric bifurcations in river deltas that appear to be morphologically stable. This suggests that under certain conditions, less sediment is diverted than expected from small scale experiments. Recent surveys of bifurcations of the Kapuas River show that side branches can have entries that are much wider than their cross-sections further downstream. This may counteract sedimentation and increase their morphological stability. To test this hypothesis, we analyze the flow and sediment division at an idealized lateral diversion with a potential flow model. Our analysis confirms that a large inlet area moderates the fraction of the diverted sediment. We compare our findings to existing empirical relations derived from scale experiments and find that these do not necessarily scale up to the size of rivers.

2. Method

We employ a potential flow model to determine the depth averaged flow in a wide channel with flat bed from which water is diverted into a lateral branch. We find analytic solutions for the flow velocity and the streamline curvature, from which we determine the near bed flow as well as the water to sediment division ratio.

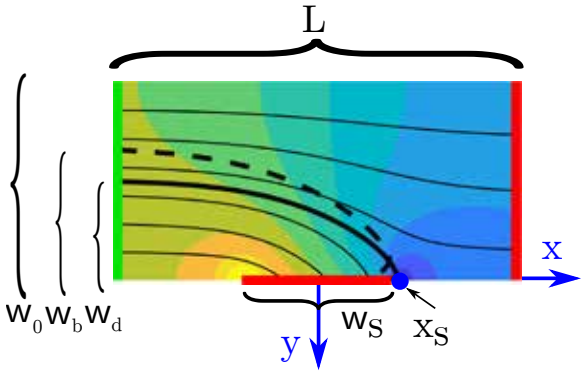

Figure 1. Magnitude (shades) and streamlines of the flow at an open channel diversion, bold and dashed line indicate streamline at mid-depth and near the bed

3. Results

We show that the flow field is uniquely determined just by a single parameter, independently of the scale of the diversion. The sediment to water division ratio is uniquely determined in combination with a second parameter. These parameters are related to the area and aspect ratio of the inlet to the side branch.

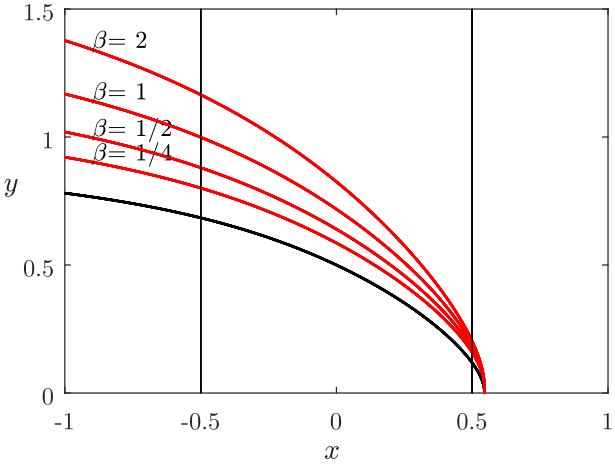

Figure 2. Dividing streamline on the near bed flow, depending on the width-to-depth ratio (β) of the inlet to the side branch (normalized unit length)

We confirm that the size and geometry of the inlet to the side branch strongly influences the water to sediment division ratio. We put our results in context with various empirical relations for the division of sediment.

4. Conclusion

Our results show, that the local channel width at river bifurcations strongly influences the division of sediment. Models that predict the long term stability of alluvial river bifurcations have therefore to account for the migration of the river banks as this can either narrow or widen the inlet to the side branch over time. Our parametrisation can aid the design further numerical and laboratory experiments as well as empirical relations based thereon to cover the full parameter space.

References

Kästner, K. and Hoitink, A. J. F. (2019a). Flow and sediment division at two asymmetric bifurcations of a tidally influenced river delta: implications for channel stability. *Submitted to Journal of Geophysical Research: Earth Surface*.

Kästner, K. and Hoitink, A. J. F. (2019b). The effect of the inlet width of lateral bifurcation branches on the division of sediment. *Submitted to Journal of Fluid Mechanics*.

Morphodynamic evolution of a funnel shaped tidal estuary: an idealized modeling study

M. Olabarrieta[1], W. R. Geyer[2], G. Coco[3], C. Friedrichs[4] and Z. Cao[5]

[1] Civil and Coastal Engineering Department, ESSIE, University of Florida, USA, molabarrieta@ufl.edu
[2] Applied Ocean Physics and Engineering, WHOI, Woods Hole, USA, rgeyer@whoi.edu
[3] School of the Environment, University of Auckland, Auckland, New Zealand. g.coco@auckland.ac.nz
[4]Virginia Institute of Marine Science, William & Mary, Gloucester Pt., USA, carl.friedrichs@vims.edu
[5] Los Alamos National Laboratory, Los Alamos, USA, caozd999@gmail.com

1. Introduction

The morphology of an estuary is primarily controlled by river flow, tides, waves, and sediment supply. Computational advances in the last decade have facilitated remarkable progress in the understanding of the long-term (decades to centuries) evolution of estuaries. However, despite the relevance of the density driven flows and Earth's rotation in nutrient, pollutant, larvae and sediment dispersal in estuaries, these processes are usually disregarded when modelling estuarine morphodynamics. Here, we provide a summary of the study by Olabarrieta et al. (2018), in which the morphodynamic evolution of an idealized funnel-shape estuary, considering 3-dimensional effects and water density variations, is analysed.

2. Model setup

The 3-dimensional Regional Ocean Modelling System (ROMS) is applied to numerically analyse the long-term morphodynamic evolution of idealized funnel-shaped estuaries. The geometry of the generic 3-dimensional estuary, its sediment characteristics, and the considered boundary conditions are representative of the types of estuaries along the northeast coast of the United States. This generic idealized estuary is funnel-shaped with a maximum width of 1.2 km at the mouth (Figure 1, top). The initial bathymetry has a symmetric Gaussian shape in the cross-channel direction. At the offshore boundary a symmetric M2 tidal wave with a range of 1.5 m and a constant salinity of 35 psu are imposed. At the landward boundary a fresh water discharge of 150 m^3/s is specified. Our base case is located at 41˚ North. A single sediment class, equivalent to medium silt (or flocculated estuarine mud), with the fall velocity equal to 0.6 mm/s and the critical shear stress for erosion of 0.05 Pa is considered. The morphodynamic model is run for 200 years.

3. Results

The bathymetric evolution is shown in Figure 1. During the initial evolution (0-15 years) bathymetric changes are maximal because the initial morphology is far from the equilibrium. The central part of the estuary erodes while close to the head, in the bed-load convergence zone, the formation of a bar is observed. Intertidal flats start to develop in the upper-middle estuary, and the growth of some instabilities or bars can be identified. Between years 15 to 50, the bar formed close to the head evolves into meanders and point bars. After 100 years 3 different regions can be identified along the estuary: 1) the upper estuary, which is characterized by a meandering system with a shallow and narrow main channel flanked by tidal flats with elevations close to the high-tide level; 2) the middle estuary, which is characterized by a straight and asymmetric cross-section, with the main channel in the right and intertidal areas in the left; and 3) the lower estuary, which is characterized by an asymmetric cross-section that also shows along-channel bars.

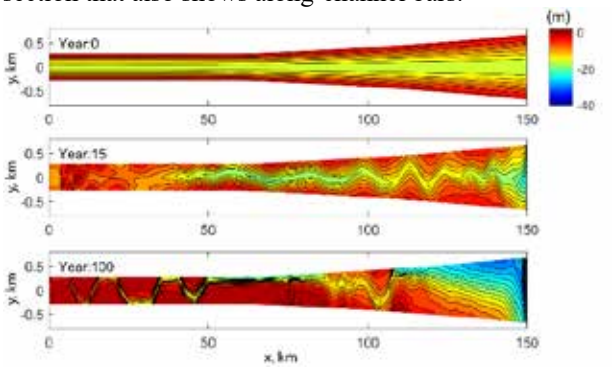

Figure 1: Temporal bathymetric evolution over 100 years. Modified after Olabarrieta et al. (2018).

As the morphology evolves, the formation of a tidal maximum zone is observed in the salt intrusion limit. The tide tends towards a hyper-synchronous behaviour and tidal asymmetry reduces. Subtidal flows are characterized by an inflow in the main channel and outflow in the shallower flanks.

4. Conclusions

The morphodynamic evolution in all the analysed cases reproduced structures identified in many tidal estuaries: a meandering region in the fluvial-tidal transition zone, a tidal maximum area close to the head, and a turbidity maxima region in the brackish zone. As the morphology of the estuaries evolved, the tidal propagation, the salinity gradient, and the strength of subtidal flows changed, which reflects the strong bathymetric control of these systems.

Acknowledgments

MO, WRG and CTF acknowledge support from NSF projects OCE-1554892, OCE-1634480 and OCE-1459708 respectively.

References

Olabarrieta, M., Geyer, W. R., Coco, G.,Friedrichs, C. T., & Cao, Z. (2018). Effects of density-driven flows on the long-term morphodynamic evolution of funnel-shaped estuaries. *Journal of Geophysical Research: Earth Surface*, 123, 2901–2924.

The impact of basin geometry on the long-term morphological evolution of barrier coasts: an exploratory modelling study.

K.R.G. Reef[1], P.C. Roos[1], H.M. Schuttelaars[2], S.J.M.H. Hulscher[1]

[1] Water Engineering and Management, University of Twente, Enschede, the Netherlands. K.r.g.reef@utwente.nl
[2] Applied mathematics, Delft University of Technology, Delft, the Netherlands.

1. Introduction

Barrier coasts cover 10% of the worlds coastline (Stutz and Pilkey 2011) and are important coastal systems that are often found near densely populated areas. Because of their importance, human interventions in barrier coast systems are common. A frequently applied intervention is the reclamation of land, resulting in a reduction of the tidal basin. Even though land reclamations in barrier coast systems are common, only little is known about their effect on the long-term (decades to centuries) morphological evolution of barrier coasts.

In this work we aim to investigate the effect of a basin reduction in one part of a tidal basin on the equilibrium configuration (i.e. size and spacing) of tidal inlets in the entire basin (i.e. both the affected and unaffected parts of the basin). Because a basin reduction is essentially a sudden change from one geometry to another, we study the equilibrium configuration of inlets for various basin geometries (reflecting different basin reductions). This reveals how the equilibrium configuration of the inlets would change if a new geometry is imposed through a basin reduction.

2. Methods

We use an idealized barrier coast model that is an extension to the model of Roos et al. (2013), but now allowing for arbitrary basin geometries instead of only a rectangular basins. The model simulates the morphological evolution of multiple tidal inlets (n=50) towards an equilibrium configuration. The morphological evolution is based on the stability concept of Escoffier (1940), while the hydrodynamic part of the model is based on the linearized shallow water equations that are solved analytically. An example model run is shown in Figure 1.

3. Results

By performing a sensitivity analysis of basin geometry (with a wide and narrow part in the basin as in Figure 1), we studied the effect that basin geometry has on the equilibrium configuration of tidal inlets.

Our results show that three processes affect the equilibrium configuration of tidal inlets. First, there are wider inlets in the wider part of the tidal basin for a larger basin width. Second, there is an equilibrium value for both the inlet width per km and number of inlets per km, due to bottom friction. Third, resonance affects the width and number of inlets in both the wide and narrow part of the basin.

4. Conclusions

We studied the effect of basin geometry on the long-term morphological evolution of barrier coasts using an idealized model, that allows arbitrary tidal basin geometries; and identified the most relevant processes.

Acknowledgement

This research was carried out within the WADSnext! project, funded by the `Simon Stevin Meester' prize (awarded by NWO to S.J.M.H. Hulscher), Deltares, and the 4TU centre for fluids and solid mechanics.

Bibliography

Escoffier EF (1940) The stability of tidal inlets. Shore and Beach 8:114–115

Roos PC, Schuttelaars HM, Brouwer RL (2013) Observations of barrier island length explained using an exploratory morphodynamic model. Geophys Res Lett 40:4338–4343.

Stutz ML, Pilkey OH (2011) Open-ocean barrier islands: Global influence of climatic, oceanographic, and depositional settings. J Coast Res 27:207–222.

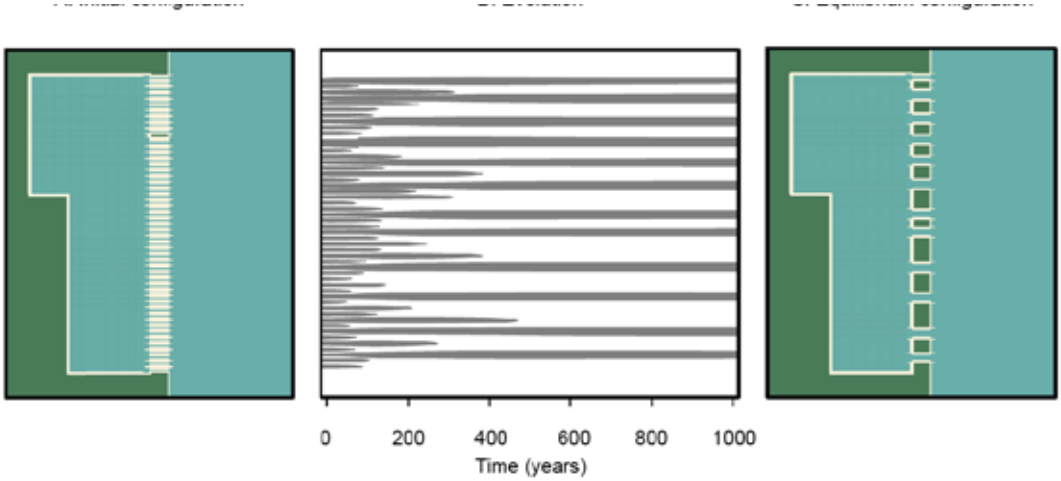

Figure 1: Example run of our barrier coast model with non-rectangular geometry; showing: A: the initial over-saturated barrier coast (top view), B: the evolution of the tidal inlets (line stack), C: the equilibrium configuration (top view).

Entraiment of Very Fine Sediment in Treating the Estuary Bed Evolution

S. Egashira[1], D. Harada[2] and T. S. Ahmed [3]

[1, 2, 3]International Centre for Water Hazard and Risk Management, Public Works Research Institute, Japan.
[3] PhD Student, Graduate Institute for Policy Studies, Japan.
[1]s-egashira77@pwri.go.jp, [2]d-harada77@pwri.go.jp, [3]tanjirsaifahmed@gmail.com

1. Introduction

A depth averaged 2-d convection-diffusion equation is employed to describe the mass conservation of sediment within the flow body, and a temporal change of bed surface elevation is formulated by means of the mass conservation equation of bed sediment. An erosion rate term plays an important role in these equations, and associated formulas have been proposed (Itakura et.al. 1980, Garcia et.al. 1991). However, it is difficult to evaluate the erosion rate of estuary bed composed of sediment particles finer than silt grains, because existing formulas are out of their applicable range. This study discusses formulas for erosion rate and bed load to treat sediment transport processes in estuaries composed of such very fine sediment. In addition, we provide numerical results on the formation processes of deltas and sand bars in the estuaries.

2. Formulas for Erosion Rate and Bed-load

Figure 1 is a schematic diagram to formulate the erosion rate and bed-load, in which h_s is the thickness of bed-load layer, c_s is the sediment concentration of bed-load layer. It is assumed the bed is composed of very fine sediment and its surface layer is formed by loosely deposited sediment. Using the idea of entrainment coefficient for density stratified flows, the erosion rate of bed sediment can be described as follows.

$$E(=w_e c_s) = (k / R_{i*})\overline{v} c_s \quad (1)$$

in which E is the erosion rate, w_e is the entrainment velocity, R_{i*} is the overall Richardson number, k is the empirical constant as $k = 0.0015$ specified by Ashida et.al. (1977) and $\overline{v}$ is the average velocity of the upper layer. In addition, it is assumed that stress-strain rate relation can be evaluated by means of a quasi-Bingham model, resulting in bed-load formula such as

$$q_b = (1/6)(u_* h_s / \nu_s) c_s u_* h_s \quad (2)$$

in which h_s is given by

$$h_s = u_*^2 / \{(\sigma/\rho - 1) c_s g \tan\phi_a\} \quad (3)$$

q_b is the bed load rate in unit width, u_* is the shear velocity, ν_s is the kinematic viscosity of bed-load layer (water and very fine sediment mixture), σ is the mass density of sediment particles, ρ is the mass density of water and ϕ_a is the apparent friction angle of sediment.

3. Result and Discussion

Flume experiments were conducted to test the validity of Eq. (1), which will be explained precisely in full manuscript. According to the experimental data, Equation (1) is verified for the bed composed of water-sediment mixture with sediment concentration from 8% to 12 % by volume.

Introducing Eqs. (1) and (2) into governing equations for sediment transportation and associated channel changes, formation processes of delta and sand bars in an estuary are simulated. Figure 2 shows delta formation process which is computed in a simple basin; the width=8km, the length=6km, bed slope=0.0001, the downstream flow depth=4m. A stream channel of 100m in width attaches this basin. (A) is a flow pattern and corresponding bed elevation in an initial stage when the flow stretches straightforward, (B) shows that the flow separates toward the both sides, and (C) illustrates that the left side stream decayed already.

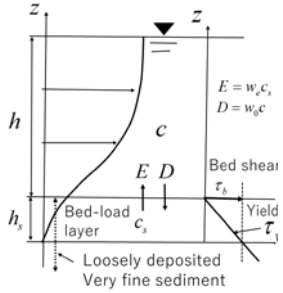

Figure 1 Schematic diagram for erosion and bed-load

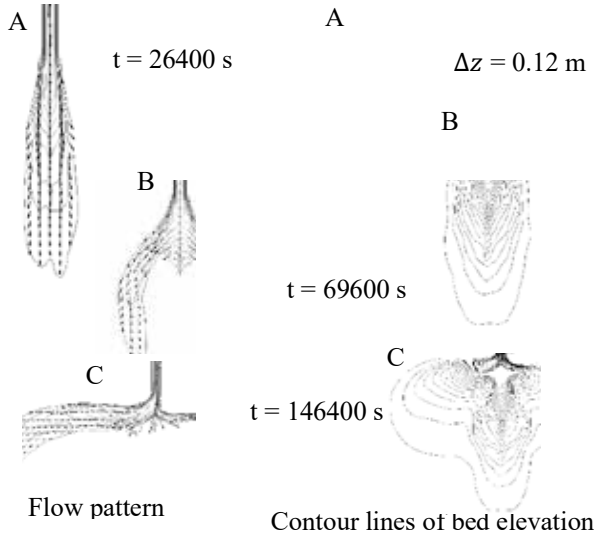

Figure 2 Delta formation process

4. Conclusions

New formulas for erosion rate and bed-load transport rate are proposed to evaluate sediment transport processes and corresponding geomorphologic changes in estuary bed composed of very fine sediment. Numerical simulation on delta formation process suggests some possibilities of the proposed formulas.

References

K. Ashida and S. Egashira (1977). Proc. 17th Cong. IAHR, Vol.2, 33-40.

M. H. Garcia and G. Parker (1991). Jour. Hydraulic Eng., ASCE, Vol. 4, 414-435.

T. Itakura and T. Kishi (1980). Jour. Hydraulic Div., Vol. 106, HY.8, 1325-1343.

Analysis of Mud Deposit Characteristics using the Vertical Profile in an Estuary

G. Azhikodan[1] and K. Yokoyama[2]

[1,2]Tokyo Metropolitan University, Tokyo, Japan. gubash@gmail.com; k-yoko@tmu.ac.jp

1. Introduction

Mud deposits in estuaries are of critical importance since it can cause a reduction in navigation depth and flood carrying capacity, contaminant accumulation, etc. The presence of mud deposits has been reported in many estuaries worldwide (Becker et al., 2013). It has a profound influence on the erosion and sedimentation cycles in estuaries and thereby its morphology. Hence, it is necessary to study the characteristics of mud deposits in detail to understand its dynamics in estuarine systems. Based on the above discussions, this study aims to analyse the impact of cohesiveness and remoulding effect of mud on its erodibility in a macro-tidal estuary.

2. Methodology

The Chikugo River estuary, Japan (Azhikodan and Yokoyama, 2018) is a highly turbid macro-tidal estuary. A sediment core with a diameter of 105 mm was sampled by a diver on the riverbed from the middle of the estuarine channel at 14 km upstream from the river mouth using a 2 m acrylic cylinder on May 27, 2006. The original stratification of the sampled material was maintained. The viscosity of undisturbed mud at every 10 cm thickness was measured 3-5 times at the fishing port immediately after sampling using a rotational viscometer (Toki Sangyo Co. Ltd. TVC–5). The rotational speed of the stainless-steel rod no. 5 was 5 rpm. Then each sample was stirred to become uniform and its viscosity was measured 3 times. Further, the particle-size distribution (using SALD–3100, Shimadzu), water content (WC), and loss on ignition (LOI) of the sediment core were determined in the laboratory.

3. Results and Discussion

The river discharge observed from September 2005 to June 2006 was below 55 $m^3 s^{-1}$ with few peaks but <500 $m^3 s^{-1}$. The SSC near the bed at the 14.6 km upstream during the considered period was high with values ranging between 4,000–6,000 mg L^{-1} at the spring tides and was <100 mg L^{-1} at neap tides. As a result, the depth of the channel cross-section decreased during the period due to the tidally induced upward sediment transport and deposition process as shown in Figure 1 which was obtained from the topographic survey of the channel.

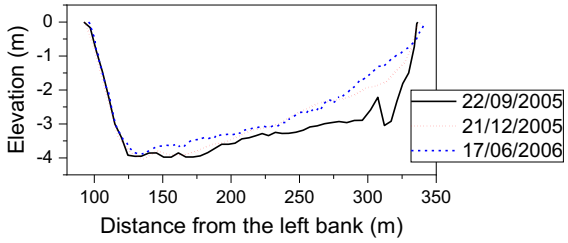

Figure 1: Channel cross-section of the 14 km station.

The length of the core sample, 1.5 m, corresponds to the thickness of the mud layer in the study area (Figure 2). The sediment on the riverbed at 14 km mainly consisted of 70% silt and 25% clay with 5% fine sand. The D50 of the sample was ranged between 11–16 µm. The WC of the sediment was >200% for the top layer, 150–200% for the middle layer and <150% for the bottom layer with an LOI ranged between 6–9%. There was a rapid increase in viscosity of the undisturbed mud from the top to bottom layer and it ranged between 80–470 Pa s. The viscosity of the mud sample decreases when it was disturbed (stirring) and was still high at the bottom layer. It represents the initial condition of the mud before consolidation.

The viscosity ratio, VR (ratio of the viscosity of undisturbed mud to the disturbed mud) represents the adhesive strength acquired during the consolidation, which is known as the thixotropic behaviour. The sediment gained 5 and 2.5 times strength at the top and bottom layers respectively. This further revealed that the consolidation of mud begins at the early stages of deposition due to the strong internal bonding resulted from thixotropy, and the presence of organic matter and this process in the natural environment will be several times higher than that of the disturbed mud. Therefore, the erosion resistance of the sediment surface will enhance, and will eventually lead to deposition without further erosion and resuspension even at high velocities.

References

Azhikodan, G. and Yokoyama, K. (2018). Sediment transport and fluid mud layer formation in the macro-tidal Chikugo river estuary during a fortnightly tidal cycle. *Estuar. Coast. Shelf Sci.*, 202:232–245.

Becker, Marius, et al. (2013). Formation and entrainment of fluid mud layers in troughs of subtidal dunes in an estuarine turbidity zone. *J. Geophys. Res. Ocean*, 118(4):2175–2187.

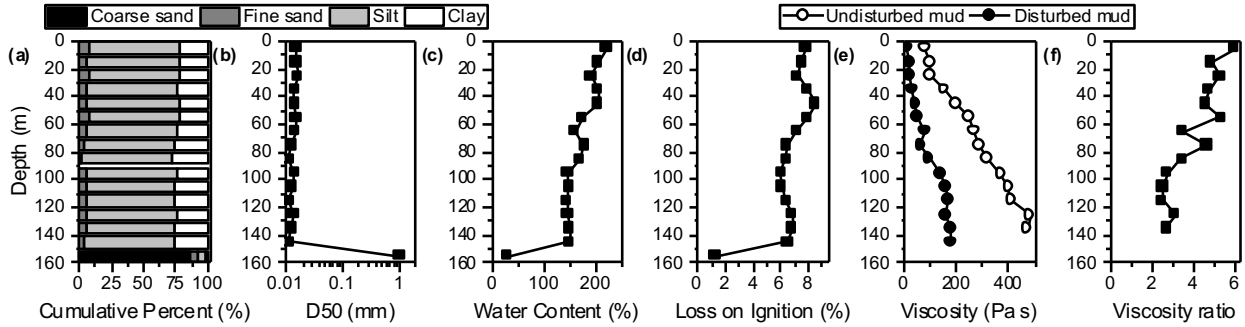

Figure 2: Vertical profile of (a) texture, (b) D50, (c) water content (WC), (d) loss on ignition (LOI), (e) viscosity, and (f) viscosity ratio (VR) of the bottom mud layer.

Bottom stress and hydrodynamics: field study on Perkpolder (NL)

E. Santirosi[1], L. Schippa[2]

[1] Department of Engineering, University of Ferrara, Ferrara, Italy. elena.santirosi@student.unife.it
[2] Department of Engineering, University of Ferrara, Ferrara, Italy. Leonardo.schippa@unife.it

1. Introduction

A big part of The Netherlands territory is below sea level; for this reason, a lot of lands have been reclaimed through the years by means of the creation of polders. However, this process caused the loss of intertidal areas, that are essential for the safeguard of natural habitats. From the last century the European governments provided the depoldering of some areas. The study area (Perkpolder, NL, located in the Western Scheldt) it is one of these pilot locations. The morphology and the evolution of the entire area and of the channels network have been influenced, over the last four years (since the tidal basin was created), by the local tidal conditions inside the basin. These conditions, in turn, determine the flux of sediment, nutrients and biota. With the aim to evaluate the hydrodynamic condition and its effects on sediment transport in the Perkpolder area, water velocity and depth have been continuously measured in six different locations in the Perkpolder area, four in the channels and two in the mudflat

2. Bed Shear Stress (BSS) and critical bed shear stress calculation

Starting from the velocity measurements, the BSS and the critical values of the BSS, on both mudflat and channels, have been evaluated according to two different approaches suggested by van Rijn: the formula used for the BSS is (van Rijn, 1984):

$$\tau(t) = \frac{\rho}{c^2}\bar{u}(t)^2 \qquad (1)$$

Where ρ is the density, $\bar{u}$ is the horizontal velocity averaged on the vertical and c is the adimensional Chézy coefficient, while the critical values of the BSS have been calculated by taking into account the cohesion and the packing effect, as explained in the formulas (van Rijn, 2007):

$\mathrm{d}_{50} < 62\mu\mathrm{m}$ $$\tau_{cr,bed,fine} = \left(\frac{d_{sand}}{d_{50}}\right)^{0,5}\tau_{cr,0} \qquad (2)$$

$$\tau_{cr,bed,sand} = (1 + p_{cs})^3\tau_{cr,0} \qquad (3)$$

$\mathrm{d}_{50} > 62\mu\mathrm{m}$ $$\tau_{cr,bed} = (1 + p_{cs})^3\tau_{cr,0} \qquad (4)$$

Where $\mathrm{d}_{sand} = 62\mu\mathrm{m}$, p_{cs} is the percentage of clay and silt and $\tau_{cr,0}$ is the critical BSS calculated without considering the cohesion and the packing effects.
The values as obtained have been compared to evaluate the sediments transport capacity of the water flow.

3. Tidal Phase Prevalence Index (TPPI)

To have a better qualitative factor, that allows to compare the impact of the water flow, both in ebb and flood phase, and the behaviour of the different cross sections, a new parameter has been introduced.
This parameter is called "Tidal Phase Prevalence Index" (TPPI) and it is expressed through the following equations:

for $\theta > \theta_{cr}$ $$TPPI = \frac{1}{T/2}\int_0^{T/2}(\theta - \theta_{cr})\,dt \qquad (5)$$

for $\theta < \theta_{cr}$ $$TPPI = 0 \qquad (6)$$

Where T is the tidal period, θ is the Shields parameter and θ_{cr} is the critical Shields parameter.
Since θ_{cr} and, consequently, the TPPI value depends on the equivalent *Nikuradse roughness* K_s, a sensitivity analysis has been carried out changing the value of K_s.
In the table below the TPPI values calculated with the K_s value suggested by van Rijn are reported:

Ks	Measurement Point	$d_{50} < d_{sand}$				$d_{50} > d_{sand}$	
		TPPI fine flood	TPPI fine ebb	TPPI sand flood	TPPI sand ebb	TPPI flood	TPPI ebb
D90*3	BC3_1	0.323	0.301	0	0	NA	NA
	AC3_1	0.23	0.214	0	0	NA	NA
	BC4_1	NA	NA	NA	NA	0.002	0.002
	AC2_1	NA	NA	NA	NA	0	0
	MC2_1	NA	NA	NA	NA	0	0
	MC2_2	0.009	0.007	0	0	NA	NA

Table 1: TPPI values

4. Conclusions

The bed shear stress results much higher in the channels than on the mudflat. The sediment dynamic on the mudflat are dominated by deposition, whereas in the channels are governed by erosion, and it is in agreement with the observed morphological evolution. Mudflat and channels, are still getting modified by the action of the water, making difficult the vegetation engraftment. TPPI gives a qualitative indication about erosion-deposition rate TPPI values confirm that the intertidal basin is characterized by a flood dominance.

References

van Rijn L. C. (1984). *'Sediment Transport, Part I: Bed Load Transport'. Journal of Hydraulic Engineering* 110(10):1431–56.

van Rijn L. C. (2007). *'A Unified View of Sediment Transport by Currents and Waves, Part 1: Initiation of Motion, Bed Roughness and Bed Load Transport'. Journal of Hydraulic Engineering,* 133(6):649-667

Variability in estuarine vertical mixing as an influencing factor in suspended sediment flux in weakly stratified estuaries

X. Wei[1], M.E. Williams[1,2], H.M. Schuttelaars[3], J.M. Brown[1], P.D. Thorne[1], L.O. Amoudry[1]
[1] National Oceanography Centre, Joseph Proudman Building, 6 Brownlow Street, Liverpool L3 5DA, United Kingdom.
xwei@noc.ac.uk; jebro@noc.ac.uk; pdt@noc.ac.uk; laou@noc.ac.uk
[2] Departamento de Obras Civiles, Universidad Técnica Federico Santa María, Avenida España 1680, Valparaíso, Chile.
megan.williams@usm.cl
[3] Delft Institute of Applied Mathematics, Delft University of Technology, Delft, Netherlands.
h.m.schuttelaars@tudelft.nl

1. Introduction

Vertical mixing of momentum and density, which is strongly related to flow-generated turbulence and density-induced stratification (Simpson et al., 1990), can significantly influence the tidal flow, estuarine circulation, salt intrusion, sediment transport and trapping. Hence, advancing understanding of the interactions between the vertical mixing, turbulence and stratification is essential for predicting the response of estuarine sediment transport to natural changes (e.g., storms, spring-neap tidal variations, fluctuating river discharge, sea level rise) and human activities (e.g., land reclamation, damming). Some attempts have been made to systematically investigate mixing with given estuarine parameters. MacCready et al. (2018) and Burchard et al. (2019) proposed an estimate for the long-term averaged estuarine mixing in relation to exchange flow and vertical salinity variance. However, their approach was based on a box-type estuary model, which is not sufficient for predicting the along-channel variations of mixing, velocity, salinity and sediment concentration. Therefore, our work attempts to resolve the spatially and temporally varying interacting system of vertical mixing, tidal/residual flow and salinity, and evaluate its influence on the suspended sediment flux in estuaries.

2. Methods

This work will be realised by resolving the coupled water motion, salinity and vertical mixing, and using the flow information to calculate the suspended sediment concentration, extending the work by Wei et al. (2018). Assuming the estuary to be weakly stratified, the model solves the three-dimensional shallow water equations, salinity and sediment equations using a perturbation method and finite element method. The perturbation method allows for an analytic decomposition of processes contributing to estuarine circulations and sediment transport. In this model, the residual circulation and salinity-induced stratification resulting from eddy viscosity-shear covariance (Dijkstra et al., 2017) will be taken into account. Impacts of flow and stratification on the vertical mixing will be also considered in the model by assuming the vertical eddy viscosity A_v and vertical eddy diffusivity K_v to be functions of the Richardson number (Nunes Vaz and Simpson 1994). These functions will be obtained by fitting A_v and K_v, which are calculated based on the measurements of the vertical shear and Reynolds stress $A_v = K_v = \frac{\overline{u'w'}}{\partial u/\partial z}$ (Scully and Friedrichs 2003), to the measured vertical gradients of velocity and salinity. Here, K_v is assumed to be equal to A_v, u' and w' are respectively the turbulently fluctuating components of the along-channel and vertical velocities (with overbar indicating a tidal average), u is the along-channel velocity and z the vertical coordinate positive upward.

3. Results

The model will be applied to the Blackwater estuary, Essex, UK, where measurements of turbulence, velocity, salinity and suspended sediment concentration were made for 1 month in the winter of 2017/18. The contributions of the dynamic mixing to the residual circulation, salt and sediment transport in estuaries will be systematically investigated. A sensitivity study of these contributions to varying tide and river discharge will be conducted.

Acknowledgments

This work is funded by the NERC BLUEcoast project (NE/N015894/1).

References

Dijkstra, Y.M., Schuttelaars, H.M. and Burchard, H., Generation of exchange flows in estuaries by tidal and gravitational eddy viscosity-shear covariance (ESCO). *Journal of Geophysical Research: Oceans*, 2017, 122(5): 4217-4237.

Burchard, H., Lange, X., Klingbeil, K. and MacCready, P., Mixing estimates for estuaries, *Journal of Physical Oceanography*, 2019, 49:631-648.

MacCready, P., Geyer, W. R. and Burchard, H., Estuarine exchange flow is related to mixing through the salinity variance budget. Journal of Physical Oceanography, 2018, 48(6): 1375-1384.

Nunes Vaz, R.A. and Simpson, J.H., Turbulence closure modeling of estuarine stratification. *Journal of Geophysical Research: Oceans*, 1994, 99(C8): 16143-16160.

Scully, M.E. and Friedrichs, C.T., The influence of asymmetries in overlying stratification on near-bed turbulence and sediment suspension in a partially mixed estuary. *Ocean Dynamics*, 2003, 53(3): 208-219.

Simpson, J.H., Brown, J., Matthews, J. and Allen, G., Tidal straining, density currents, and stirring in the control of estuarine stratification. *Estuaries*, 1990, 13(2): 125-132.

Wei, X., Kumar, M. and Schuttelaars, H.M., Three-dimensional sediment dynamics in well-mixed estuaries: importance of the internally generated overtide, spatial settling lag, and gravitational circulation. *Journal of Geophysical Research: Oceans, 2018, 123 (2), 1062-1090.*

Unravelling creek formation on intertidal flats

J.L.J. Hanssen[1], B.C. van Prooijen[1], P.L.M. de Vet[1,2], P.M.J. Herman[1,2], Z.B. Wang[1,2]
Department of Hydraulic Engineering, Delft University of Technology, Delft, Netherlands. j.l.j.hanssen@tudelft.nl
[2] Department of Marine and Coastal Systems, Deltares, Delft, Netherlands.

1. Introduction

For a good observer, tidal flats are not flat at all (*Figure 1*) Morphological features like creeks and gullies run through in various shapes and sizes (Whitehouse et al., 2000). The small-scale features are shaped by interconnected biological, morphological and hydrodynamic processes. The morphodynamics of tidal flats develop during very shallow water when the small scale topography is important. Such small scale topography is however often not accounted for in predicting the large scale morphology of the tidal flats (Coco, 2013). We aim to understand the evolution of creeks and their relation with the flat morphodynamics.

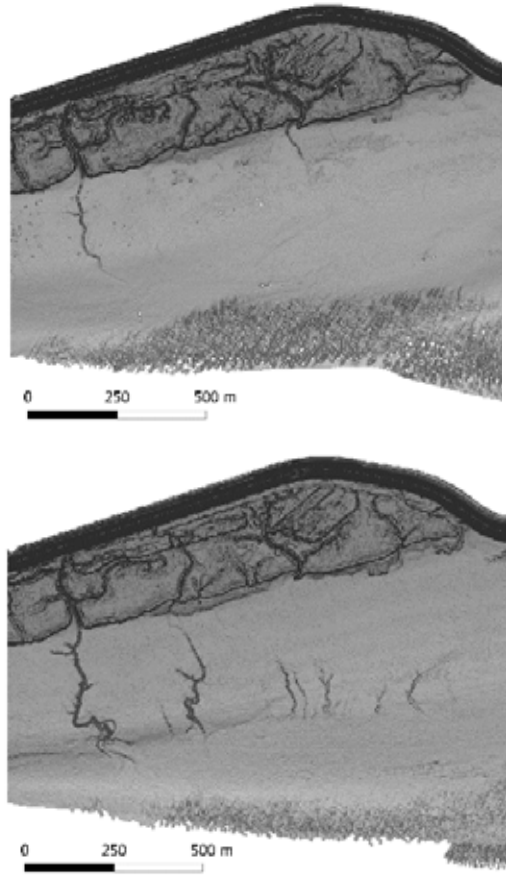

Figure 1: Tidal flat in the Western Scheldt, the Netherlands. Upper: 2009, lower: 2014. On the left side of the picture a creek originating from the salt marsh can be seen. On the right side we see creeks developed at the flat inclination.

2. Methods

We selected tidal flats in the Western Scheldt, the Netherlands. Bathymetry data from 2009 – 2014 and areal pictures in the period 2005 – 2018 have been used. They have a high spatial resolution of 2.0 x 2.0 [m^2] and 0.1 x 0.1 [m^2] respectively. The Lidar data were used to identify the creeks digitally. Despite the high resolution, some creeks were defined manually, based on the areal pictures. Tidal flat bulk parameters, like steepness and bed level, were derived from the Lidar data. Where available, the grain size was used. A 1D model was used to estimate the velocity distribution over the flat.

3. Results

From the historical data two types of mud flat creeks have been defined. Creeks of the first type originate in the salt marsh and may or may not continue on the mudflat. The planform of the creek in the salt marsh is static, on the mudflat it can be dynamic. The discharge through the creek and its dimensions depend mainly on the volume of water drained from the salt marsh. Whether the salt marsh creek ends blindly on the flat, or continues in a tidal flat creek, depends on the height difference between the marsh and the flat.

The second type of creeks establishes on the bare mudflat depending on the height gradient. The cross shore bare flat profile has an upper part with a slope of 0.1 – 0.5 %, an inclination point and a lower part with a slope between 1.0% – 25.0%. During the analysed period sedimentation occurred on the upper flat, leading to a steepening of the slope in the lower part As a result new creeks developed close to the inclination point. Creeks will not form if the cross shore slope is too flat and mean flow velocities are too low to cause erosion.

Results of the 1D model with flow over a bare mud flat are in agreement with the historical data. The maximum mean flow velocities occur close to the inclination point. Flow velocity scales linearly with the cross shore width of the flat, and non-linear with the tidal amplitude.

Creeks on the flat can grow towards the salt marsh where they find a connection with existing creeks in the marsh. This enhances the dewatering of the salt marsh.

4. Conclusions

Two different types of creeks have been identified on mud flats; one develops in the salt marsh, the other is initiated at the mud flat. The first is fixed by vegetation and its continuation on the flat depends on the flat topography and discharge from the marsh. The second is initiated on the mud flat close to the inclination point. We conclude that these are found if the bed slope exceeds a threshold. The 1D numerical model proves this concept and gives confidence to make the step to a 2D model. Connection of the two types of creeks leads to persistent channels that are effectively dewatering the salt marsh-mudflat system.

References

Coco, G. et al., (2013). Morphodynamics of tidal networks: Advances and challenges. *Elsevier, Marine Geology 346*, 1-16.

Whitehouse, R.J.S. et al., (2000). The influence of bedforms on flow and sediment transport over intertidal mudflats. *Continental Shelf Research 20*, 1099-1124.

Long-term morphological evolution of intertidal flats: how do storms affect this?

P.L.M. de Vet[1,2], B.C. van Prooijen[1], I. Colosimo[1], N. Steiner[3], T. Ysebaert[3], P.M.J. Herman[1,2] and Z.B. Wang[1,2]

[1] Department of Hydraulic Engineering, Delft University of Technology, Delft, Netherlands. p.l.m.devet@tudelft.nl
[2] Department of Marine and Coastal Systems, Deltares, Delft, Netherlands.
[3] NIOZ and Wageningen Marine Research, Yerseke, Netherlands.

1. Introduction

The morphology of intertidal flats is driven by anthropogenic and natural forces. These may lead to (quasi-)equilibrium states, but there is especially also interest in the (slow) evolution over years and decades. A key question is how this evolution is influenced by storm events. It is known that such events can suddenly change the morphology of intertidal flats. The question is whether such events just impose fluctuations around a stable and predictable long-term evolution, or if their impacts persist because they change the subsequent system trajectory.

2. Methodology: field measurements

This question is addressed using decades of data on morphology measured in the Eastern Scheldt and Western Scheldt, The Netherlands. Transects were measured yearly, and fixed points were measured ~7-14 times a year (average of 15 samples each time). These data were combined with measurements from our one-month field campaign that included, apart from 14 ADCPs, two frames placed on one of the intertidal flat transects in the Western Scheldt. Bed level changes were measured every 10 minutes, simultaneously with measurements on the flow, waves, and suspended sediment concentrations. A storm event was captured with wind speeds up to 22 m/s.

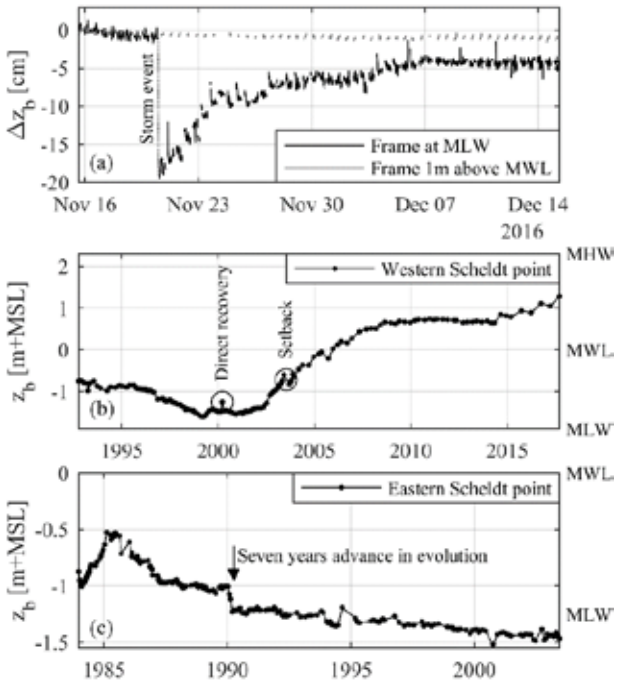

Figure 1: (a) Bed elevation time series of the frame measurements at the Western Scheldt transect. (b) Long-term bed elevation time series as measured at a point on the same intertidal flat. (c) Long-term bed elevation time series as measured at an intertidal flat in the Eastern Scheldt.

3. The impact and recovery of an individual event

Two insights from the frame campaign are highlighted:

First, we observed a substantial inhomogeneous impact by the storm event (Figure 1a). The impact at the highest frame was negligible, while the erosion at the lowest location was 20 cm by this event only. This inhomogeneity is explained by a combination of breaking waves, wind-driven flow and a long duration of a shallow water depth, which was only present at the lowest location (see also De Vet et al., 2017).

Second, 15 cm of the impact recovered within two weeks. This means that still 5 cm of the impact persisted, i.e., 25% of the impact had a long-term consequence.

4. Effects of events on the long-term evolution

All studied transects had a relatively gradual evolution over decades. This also appears in the long-term time series in Figure 1b. Changes in trends relate to structural changes in forcings (mainly human interventions). Events, such as the one captured in our frame campaign, affect these time series suddenly. Some impacts only induced short-term deviations (*direct recovery*), while others had persisting consequences (*setbacks* or *advances*). For example, the setback marked in Figure 1b delayed the evolution by half a year. At a less tide-dominated site in the Eastern Scheldt (Figure 1c), the impact by major storms early 1990 advanced the background evolution by seven years. However, we found no examples where sudden events fundamentally reversed the evolution of the system.

5. Conclusions

The local impact of events results from a favorable superposition of the individual forcings, each fluctuating on different time scales. This introduces spatial inhomogeneous impacts across intertidal flats.

Even if the largest part of the impact recovers already within days, a significant net impact may persist (25% in our case). We identified various impacts in the long-term time series database that significantly affected the speed of the evolution (years delay/advance), but none where the trend was reversed. The level to which events persist relate to the spatial extent of the impact and the local characteristics of the sites, such as bed composition and hydrodynamics.

We conclude that idealized models that exclude temporal fluctuations in forcing may correctly estimate the direction of the evolution, but incorrectly estimate the speed and the spatial inhomogeneity of the evolution.

References

De Vet, P.L.M., Van Prooijen, B.C., Walles, B., Ysebaert, T., Schrijver, M. and Wang, Z.B. (2017). The Inhomogeneous Impact of Low-water Storms on Intertidal Flats. *RCEM 2017*

Wind wave-induced erosion in the Venice Lagoon in the last four centuries: a statistical characterization

L. Carniello[1], A. D'Alpaos[2], D. Tognin[1], L. Tommasini[2], L. D'Alpaos[1], and A. Rinaldo[1,3]

[1] Department of Civil, Environmental and Architectural Engineering, University of Padova, Italy.
luca.carniello@unipd.it, davide.tognin@phd.unipd.it
[2] Department of Geosciences, University of Padova, Italy. andrea.dalpaos@unipd.it
[3] Laboratory of Ecohydrology ECHO/IEE/ENAC, Ècole Polytechnique Fèdèrale de Lausanne, Lausanne, Switzerland.

1. Introduction

The morphodynamic equilibrium of shallow tidal basins is strongly influenced by wind-wave induced erosion events (Fagherazzi et al., 2006; Green and Coco, 2014). The Venice Lagoon provides a clear example in this framework, as it has experienced strong erosion processes in the last centuries, which progressively deepened tidal flats, promoted the loss of fine cohesive sediments after storms, and led to extensive salt-marsh loss. We employed a fully-coupled finite element model to six historical configuration of the Venice Lagoon, namely 1611, 1810, 1901, 1932, 1970, and 2012, in order to analyse spatial and temporal characteristics of wind-wave induced erosion events, with the aim to develop a synthetic theoretical framework to study the long-term biomorphodynamic evolution of tidal environments.

2. Methods

We applied the fully-coupled wind-wave tidal model, developed by Carniello et al. (2011), to the six different configurations of the Venice Lagoon to analyse the temporal evolution and spatial distribution of the local bottom shear stress (BSS) on the basis of a "Peak Over Threshold" method, once a critical shear stress for the erosion of cohesive sediments, τ_c, was assumed. This allowed us to identify single erosion events, their interarrival time (the time between two consecutive cross-up occurrences), intensity, and duration for each historical configuration of the Lagoon. We performed a Kolmogorov-Smirnov goodness-of-fit test, to test the hypothesis that the interarrival time of events is a random variable described by an exponential distribution, and, consequently, the wind-wave induced over-threshold exceedances can be modeled as a Poisson process (D'Alpaos et al., 2013; Carniello et al., 2016). Where this hypothesis is verified, the erosion work (i.e., the annual erosion *sensu* Mariotti and Fagherazzi (2013)) is computed as a function of the mean interarrival, mean duration and mean intensity of the over-threshold event.

3. Results and Conclusions

For all the analysed historical configurations of the Venice Lagoon, our results suggest that the interarrival time between two events, their durations and intensities are exponentially distributed random variables over most of the tidal and subtidal flats within the lagoon and, thus, resuspension events can be modeled as a marked Poisson process. In general, we show that, along the last four centuries, the interarrival times of erosion events have increased, as well as their durations and intensities, thus leading to less frequent but stronger events. Interestingly, the erosion work, which is a combination of frequency, duration and intensity of resuspension events, remained almost constant until the beginning of the 20th century, when it rapidly increased showing a maximum in 1970 and finally decreaseg in the present configuration. We therefore highlight that because of the generalized deepening of the basin, the wind-wave induced erosive trend is slightly decreasing over time after having reached a peak in the recent past.

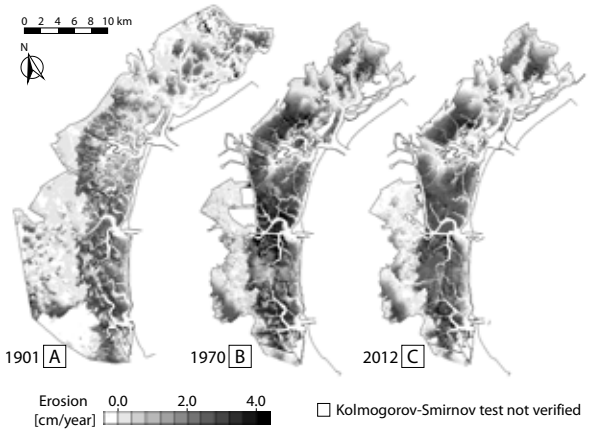

Figure 1. Spatial distribution of the erosion work, at sites where bed shear stress can be modelled as a marked Poisson process, for three different configurations of the Venice Lagoon: 1901 (a), 1970 (b), and 2012 (b).

References

Carniello, L., D'Alpaos, A., Botter, G., and Rinaldo, A. (2016). Statistical characterization of spatiotemporal sediment dynamics in the Venice lagoon. *Journal of Geophysical Research: Earth Surface*.

Carniello, L., D'Alpaos, A., and Defina, A. (2011). Modeling wind waves and tidal flows in shallow micro-tidal basins. *Estuarine, Coastal and Shelf Science*.

D'Alpaos, A., Carniello, L., and Rinaldo, A. (2013). Statistical mechanics of wind wave-induced erosion in shallow tidal basins: Inferences from the Venice Lagoon. *Geophysical Research Letters*.

Fagherazzi, S., Carniello, L., D'Alpaos, L., and Defina, A. (2006). Critical bifurcation of shallow microtidal landforms in tidal flats and salt marshes. *Proceedings of the National Academy of Sciences*.

Green, M. O. and Coco, G. (2014). Review of wave-driven sediment resuspension and transport in estuaries. *Reviews of Geophysics*.

Mariotti, G. and Fagherazzi, S. (2013). Wind waves on a mudflat: The influence of fetch and depth on bed shear stresses. *Continental Shelf Research*.

Disentangling interactions of salt marsh species and mud accretion in dynamic estuaries

M.Z.M. Brückner[1], C. Schwarz[1], L. Braat[1] and M.G. Kleinhans[1]

[1] Utrecht University, Utrecht, The Netherlands. m.z.m.bruckner@uu.nl

1. Introduction

The interactions of salt marsh vegetation and cohesive sediments modify the large-scale morphology of estuaries by strengthening of channel banks and higher bed accretion rates on bars and in sheltered areas. Previous research suggests that mud is preferably deposited in intertidal areas, with enhanced mud sedimentation rates in areas covered by vegetation (Braat et al., 2018; Lokhorst et al., 2018; Kleinhans et al., 2018). However, whether vegetation establishment or mud settling comes first or under what conditions they take place simultaneously remains unclear. We hypothesize that vegetation zonation and succession along the estuarine gradient play a substantial role in accretion rates of muddy sediments, which in turn govern the survival of the marsh.

2. Methods

We developed a novel eco-morphodynamic model that couples species-specific, literature-based vegetation establishment, seasonal growth, mortality and life-stage development at a biweekly interval to the 2D-hydromorphodynamic model Delft3D with sand and mud. The model reproduces growth and cover of a generic salt marsh species as well as species assemblages using the Western Scheldt (the Netherlands) as a test case. This setup allows the investigation of interactions between mud accretion, vegetation cover and hydrodynamics on estuary and bar-scale.

3. Results and conclusions

Our results show that mud settling is correlated with inundation time while the latter is enhanced around and within sparse vegetation patches. Velocities are strongly reduced by the vegetation, however, their effect on mud accretion rates is limited. Species preferring muddy sediments show a more gradual growth pattern than species favouring sand, which delays vegetation establishment and mud accretion rates (Figure 1). We show that species types and assemblages have an effect on accretion location and rate, which is particularly important with regard to changes in vegetation diversity and sea level due to climatic changes. Our results give new insights into the role of species-specific mud accretion patterns on morphology of estuarine systems.

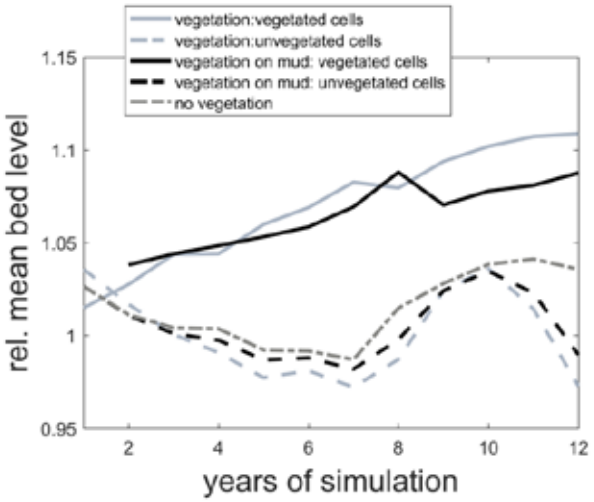

Figure 1: Relative mud accretion linked to two types of vegetation, indicating that different vegetation strategies affect accretion rates. Light grey is a general vegetation scenario; black is vegetation that can only grow on mud and the dark-grey dotted line the reference scenario without vegetation. Dashed versus solid line indicates the difference between vegetated and unvegetated cells. Accretion mainly takes place on the marsh while away from the marsh erosion is dominating and the bed is more dynamic.

References

Braat, L., Kessel, T. V., Leuven, J. R., & Kleinhans, M. G. (2017). Effects of mud supply on large-scale estuary morphology and development over centuries to millennia. *Earth Surface Dynamics*, 5(4), 617-652.

Kleinhans, M. G., de Vries, B., Braat, L., & van Oorschot, M. (2018). Living landscapes: Muddy and vegetated floodplain effects on fluvial pattern in an incised river. *Earth surface processes and landforms*, 43(14), 2948-2963.

Lokhorst, I. R., Braat, L., Leuven, J. R., Baar, A. W., Van Oorschot, M., Selaković, S., & Kleinhans, M. G. (2018). Morphological effects of vegetation on the tidal-fluvial transition in Holocene estuaries. *Earth Surface Dynamics*, 6(4), 883-901.

Salt marsh loss affects tides and sediment fluxes in shallow bays

S. Fagherazzi[1], C. Donatelli[2], X. Zhang[1], N.K. Ganju[3], and N. Leonardi[2]

[1]Department of Earth and Environment, Boston University, 685 Commonwealth Avenue, Boston, MA 02215, USA
[2]Department of Geography and Planning, School of Environmental Sciences, Faculty of Science and Engineering, University of Liverpool, Roxby Building, Chatham St., Liverpool L69 7ZT, UK
[3]U.S. Geological Survey, Woods Hole Coastal and Marine Science Center, MA 02543, USA

Introduction

There have been extensive studies on both vertical and horizontal salt marsh dynamics, and on the response of these ecosystems to changes in hydrodynamics and sediment inputs. However, there is not a specific knowledge about the reverse problem, that is, the impact of marsh loss on tides and sediment budget in coastal embayments. In this paper we investigate how geomorphic modifications caused by marsh lateral erosion can alter tides and transport dynamics across the whole bay system, and this can in turn affect the survival of marsh ecosystems.

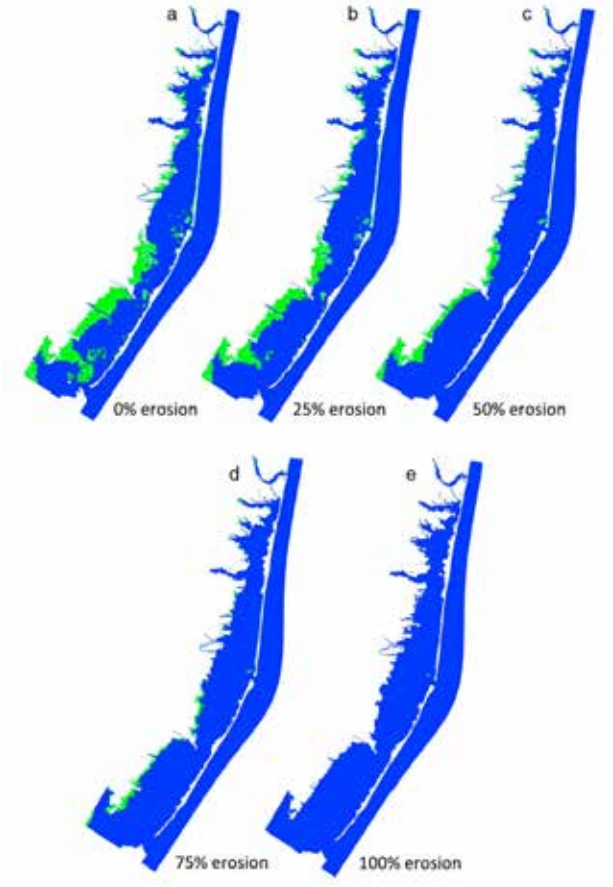

Figure 1. Barnegat Bay-Little Egg Harbor Estuary, USA, under different salt marsh erosion scenarios (From Donatelli et al. 2018),

Methods

The Coupled Ocean-Atmosphere-Wave-Sediment Transport (COAWST) modeling framework (Warner et al., 2010) was used to simulate the hydrodynamics and sediment transport processes in the Barnegat Bay-Little Egg Harbor system, USA. Different salt marsh loss scenarios are tested, which represent a uniform erosion of the marsh areas (Figure 1).
Loss percentage ranges from 25% to 100% (when all vegetated areas are removed). The erosion of salt marshes was simulated by removing vegetation from the eroded marsh cells and by matching the corresponding bathymetry values with the elevation of the surrounding tidal flats.

Results and conclusions

Salt marsh erosion influences the sediment budget of bay systems, and for our case study salt marsh loss has been found to largely decrease the capability of the bay to retain sediments.
This decline is connected to two mechanisms:
(i) a direct impact associated to the decrease in the spatial extent of vegetated areas where deposition is possible and (ii) an indirect impact connected to the decrease in tidal amplitude and associated reduced delivery to marsh platforms; the latter has been found to be less important in marsh sediment trapping. The amount
of sediments deposited on tidal flats shows a linear decrease with salt marsh lateral erosion. Generally, as the marshes erode, the capability of the system to retain sediments decreases; therefore, positive feedbacks between marsh erosion and a decrease in the available sediment could be triggered, which is detrimental for salt marsh survival and especially for the maintenance of vertical accretion rates.

References

Donatelli, C., Ganju, N. K., Zhang, X., Fagherazzi, S., & Leonardi, N. 2018. Salt marsh loss affects tides and the sediment budget in shallow bays. Journal of Geophysical Research: Earth Surface, 123. https://doi.org/10.1029/2018JF004617

Warner, J. C., Armstrong, B., He, R., & Zambon, J. B. 2010. Development of a coupled ocean-atmosphere-wave-sediment transport (COAWST)
modeling system. Ocean Modelling, 35(3), 230–244. https://doi.org/10.1016/j.ocemod.2010.07.010

Building and raising land: the effect of mud and vegetation on the development of infilling estuaries

S.A.H. Weisscher[1], K. Van den Hoven[1] and M.G. Kleinhans[1]

[1] Department of Physical Geography, Utrecht University, The Netherlands. s.a.h.weisscher@uu.nl

1. Introduction

Stratigraphic records show that many Holocene estuaries were infilled and closed off from the sea (e.g. De Haas et al., 2019), but how is unclear. Yet, understanding on how to build and raise land to keep up with future sea level rise is urgently needed. Current understanding and analogies with rivers suggest that mud and vegetation play a key role in this process by elevating bars and confining flow. We aim to unravel experimentally how these local processes affect the filling up of entire estuaries, and what the resulting stratigraphy becomes.

2. Methods

We used a 20 m long by 3 m wide tilting flume (the www.uu.nl/Metronome) to simulate complete tidal systems at an approximate scale of 1:1000 that develop from an initially long rectangular basin with barrier islands. Tidal flow was driven by periodical tilting of the flume, which caused sediment transport in both the flood and ebb direction at similar Shields numbers as in nature. Tilting was done asymmetrically such that sediment was net imported (flood asymmetry; M2+M4), which is in contrast to former exporting systems simulated in the Metronome (Braat et al., 2018; Leuven et al., 2018). We ran three experiments, one with only sand, a second with sand and mud, and a third with sand, mud and vegetation. Mud was simulated as crushed walnut shell, which was added to the river discharge and at the tidal inlet. Sprouts of three species with different colonising strategies simulated natural vegetation. The experiments were run for 10,000 tidal cycles, and the following data were acquired: time lapse imagery, bathymetry maps for every 100 to 1,000 tidal cycles, and stratigraphic cross-sections. Based on these data, flow was simulated by the numerical model Nays2D to acquire high resolution flow charts, and preliminary analysis of the channel network development was done using a novel network extraction tool (Kleinhans et al., 2017).

3. Preliminary results

Mud in the infilling estuaries with perpetual channel-shoal migration was deposited on top of bars and in abandoned channels, reduced overall dynamics due to its cohesivity, and its preservation potential increased in the landward direction. Vegetation effectively trapped most fluvial mud, resulting in considerable topographic variation on the fluvial bayhead delta, and strongly reduced bar mobility. Vegetation colonised both muddy and sandy bars, suggesting that mud is not a prerequisite for vegetation settlement in estuarine environments. Vegetation, and to a lesser extent mud, raised bars above the high water level (=land) by catching in new fines (Figure 1). The succession from tidal bar to land is also reflected in the vegetation settling patterns, such as successive bands at the rims of bars. Peat layers formed in the stratigraphic record by vegetation burial.

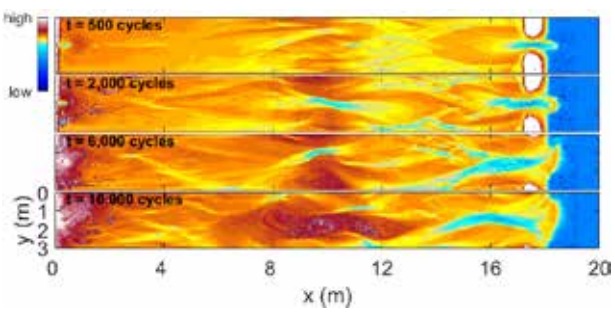

Figure 1. Morphological development of the experiment with vegetation. Elevation is not yet calibrated.

4. Conclusion

The large-scale effect of mud and vegetation is lower dynamics, especially in the upstream part of the estuary, and faster accumulation, effectively narrowing the estuary. Building and raising land was most pronounced in the experiment that included vegetation.

Acknowledgments

This research was funded by the European Research Council (ERC Consolidator grant 647570 to MGK). We would also like to thank the technical staff of Physical Geography for their support.

References

Braat L., Leuven J.R.F.W., Lokhorst I.R., and Kleinhans M.G. 2018. Effects of estuarine mudflat formation on tidal prism and large-scale morphology in experiments. *Earth Surface Processes and Landforms*. doi: 10.1002/esp.4504

De Haas T., Van der Valk L., Cohen K.M., Pierik H.J., Weisscher S.A.H., Hijma M., Spek A.J.F., and Kleinhans M.G. 2019. Long-term evolution of the Old Rhine estuary: Unravelling effects of changing boundary conditions and inherited landscape. *The Depositional Record*, 5(1):84–108. doi: 10.1002/dep2.56

Kleinhans M.G., Van Kreveld M.J., Ophelders T.A.E., Sonke W.M., Speckmann B., and Verbeek K.A.B. 2017. Computing Representative Networks for Braided Rivers. *33rd International Symposium on Computational Geometry* (SoCG 2017):48:1–48:15. doi: 10.4230/LIPIcs.SoCG.2017.48

Leuven J.R.F.W., Braat L., Van Dijk W.M., De Haas T., Van Onselen E.P., Ruessink B.G., and Kleinhans M.G. 2018. Growing forced bars determine non-ideal estuary planform. *Journal of Geophysical Research: Earth Surface*, 123(11):2971–2992. doi: 10.1029/2018JF004718

Sediment erosion mechanisms driving local scour around a patch of emerged vegetation in a river

W.Y. Chang[1] and G. Constantinescu[2]

[1] National Center for High Performance Computing, National Applied Research Laboratories, Hsinchu, Taiwan
0303106@narlabs.org.tw
[2] Department of Civil and Environmental Engineering, The University of Iowa, USA, sconstan@engineering.uiowa.edu

1. Introduction

Morphodynamics and sediment entrainment and deposition mechanisms around patches of vegetation present in rivers are controlled to a large extent by the large-scale coherent structures generated by the interaction between the incoming flow and the plant stems (Chen et al., 2012). 3-D detached eddy simulations (DES) are used to discuss how sediment entrainment mechanisms and local scour processes around an isolated, circular patch of emerged plant stems change between conditions present at the start of the erosion-deposition process and its end (equilibrium scour bathymetry). The paper also discusses how these mechanism change with the solid volume fraction (SVF) of the patch.

2. Numerical model

A series of DES is conducted with flat bed and equilibrium scour bathymetry for SVF=0.034 (37 plant stems) and 0.092 (100 plant stems). The equilibrium bathymetry (see Fig. 1 for SVF=0.092) is the one measured experimentally by Follett and Nepf (2012). Results are also compared to the limiting case of a non-porous (solid) cylinder with SVF=1. The circular porous patch of diameter D contains solid cylinders of diameter d=0.03D placed in an open channel of depth h≈0.5D. The channel Reynolds number is 35,000 and the mesh contains close to 10 million cells. The simulations resolve the wakes past the individual solid cylinders in the array, which is essential to investigate erosion and deposition mechanisms inside the patch. The numerical model and validation are discussed in Keylock et al. (2012).

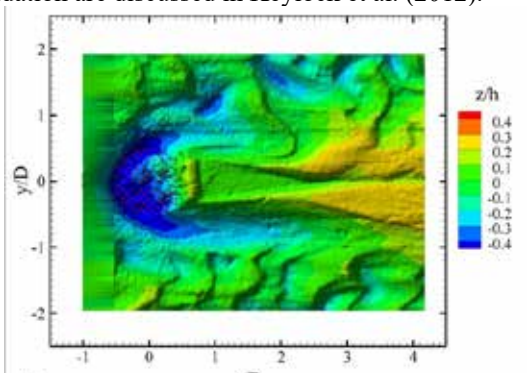

Figure 1: Equilibrium scour bathymetry measured by Follett and Nepf (2012) for SVF=0.092

3. Results

Figure 2 visualizes the coherent structures for the SVF=0.092 case with a flat bed. It visualizes the necklace vortices around the upstream face of the patch and the vortex tubes in the separated shear layers that play an important role in scour around the patch. Results also suggest that scour inside the patch increases with increasing SVF, in agreement with the observations of Follett and Nepf (2012). Results also show that for SVF>0.2 the bleeding flow is quite week and the small distance between the solid cylinders suppresses the generation of large-scale energetic eddies in the wakes of the stems. Thus, scour inside the patch is expected to start decreasing past a certain threshold value of the SVF. Given, the large capacity of the large-scale eddies shed in the wake of the stems to amplify the instantaneous bed shear stress, both variables should be used to assess the erosive capacity of the flow inside the porous region. In the flat bed cases, regions of high bed friction velocity inside the porous region and around its upstream base matched fairly well the regions where scour developed in the corresponding movable bed experiments.

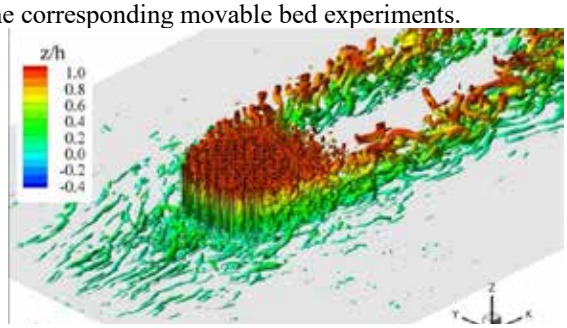

Figure 2: Coherent structures in the instantaneous flow for SVF=0.092 with flat bed (initiation of scour)

3. Conclusions

While for relatively high SVFs the scour in front of the patch is driven by necklace vortices, that are qualitatively similar but less coherent than those observed past solid cylinders, in the case of low SVFs severe scour is observed inside the upstream part of the patch and on its sides. The scour inside the patch is driven by the bleeding flow that creates corridors of strong flow acceleration as it passes around the plant stems, while the scour on the sides of the patch is driven by the flow acceleration around the patch. As only a small fraction of the bleeding flow exits the patch at its back, the downstream part of the patch is a region where deposition occurs.

References

Chen, Z., Ortiz, A., Zong, L. and Nepf, H. (2012). The wake structure behind a porous obstruction and its implications for deposition near a finite patch of emergent vegetation, *Water Res. Res.*, 48, W09517.

Follett, E. and Nepf, H. (2012). Sediment patterns near a model patch of reedy emergent vegetation. *Geomorphology*, **179**:141-151.

Keylock, C., Constantinescu, G. and Hardy, R.J. (2012). The application of computational fluid dynamics to natural river channels: Eddy resolving versus mean flow approaches, *Geomorphology,* 179:1-20.

Human versus Autogenic Controls on River Morphodynamics: The Rhine River from source to mouth

R.M. Frings[1], G. Hillebrand[2], T. Hoffmann[2]

[1] RWTH Aachen University, Aachen, Germany. frings@iww.rwth-aachen.de
[2] Federal Institute of Hydrology, Koblenz, Germany. hillebrand@bafg.de, thomas.hoffmann@bafg.de

1. Introduction

Integrated river management requires a profound understanding of river morphodynamics on the basin-scale. However, contemporary management of large rivers is often fragmented between different regions (states) within the river basin. In this contribution we present a unique, highly-detailed, basin-wide, morphological analysis of one of the world's larger rivers, the Rhine in Western Europe. The objectives of this study were to characterize the basin-scale morphodynamics of the Rhine River in the period 1991-2010, distinguishing between human and autogenic controls. We analysed the full 1,232.7 km long river from source to mouth.

2. Methods

First we quantified the downstream variation of the fluxes of clay, silt, sand, gravel and cobbles from measurement data. Next, we identified the sources and sinks of these sediments from a sediment budget analysis.

3. Results and Conclusions

From source to mouth, the Rhine traverses four sections with fundamentally different morphodynamic behaviour: the Alpine, impounded, free-flowing and delta section. Sediment fluxes are discontinuous, primarily because of a glacial lake trapping all sediments from upstream. The lake caused sediment fluxes to be discontinuous already before the Anthropocene. Today's sediment fluxes are strongly influenced by dredging and nourishment operations. From a global perspective, sediment fluxes in the river's headwaters are large, whereas sediment output from the Rhine towards the sea is small. A special feature of the Rhine is the fact that more sediment is transported in upstream direction from the sea into the delta than vice versa. On a basin-scale, nourishment represents the biggest source of gravel and cobbles, and tributaries the biggest source of clay, silt and sand. In the lower Rhine delta, also large amounts of clay, silt and sand are supplied by the sea. Dredging represents the main sediment sink for all size fractions. For silt and clay, also floodplain deposition and deposition in ports represent major sinks. The Rhine is an example of a river in disequilibrium: large parts of the river are subject to erosion or sedimentation. A-typically it has net deposition upstream and net erosion downstream. Although human interventions contributed to the disequilibrium, the pristine Rhine already was in a state of disequilibrium. Even today, natural factors determine the location of the main sedimentation areas. The budget analysis shows that the behaviour of the clay/silt, sand and gravel/cobble fractions strongly differ from each other. A particularity is that in many reaches gravel is deposited, whereas simultaneously sand is being eroded. The budget analysis also shows that sediment dynamics in rivers are much higher than is suggested by echosoundings or transport measurements. This study provides valuable insights into the basin-scale morphodynamics of the Rhine, helps to see smaller-scale studies of parts of the Rhine Basin in a correct perspective, provides a good data basis to improve numerical prediction models, and helps to optimize nourishment, dredging and monitoring strategies in the Rhine. Furthermore, the Rhine represents an excellent reference case for other large river systems for which less data are available. Knowledge gaps of supra-regional importance identified in this study relate to (A) the fundamental disequilibrium of large river systems, (B) the effect of natural and human factors on the future morphodynamic development of the large river systems, (C) the morphodynamic role of sand in gravel-bed rivers and (D) the long-term effects of sediment nourishment.

Reference

Frings, R.M., Hillebrand G., Gehres, N., Banhold, K., Schriever, S. and Hoffmann T. (2019). From source to mouth: Basin-scale morphodynamics of the Rhine River. Earth-Sci Rev. 10.1016/j.earscirev.2019.04.002

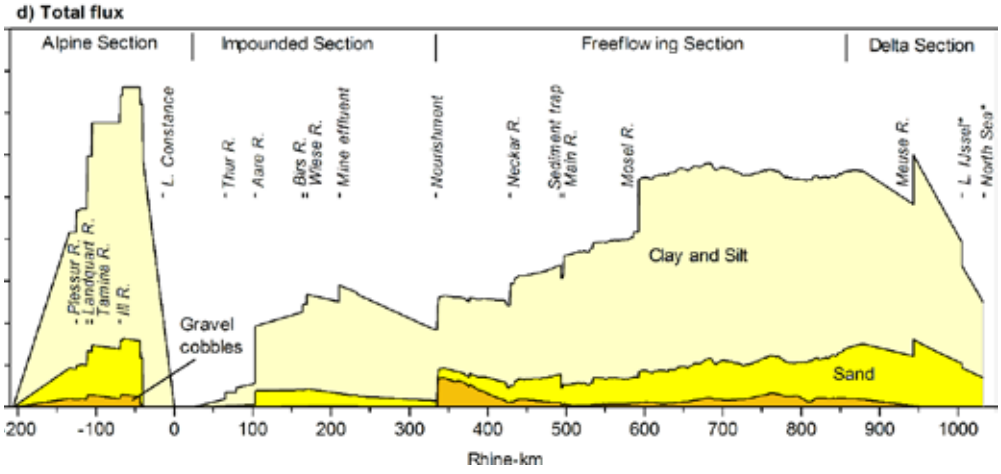

Figure 1: Sediment fluxes in the Rhine River from source to mouth (Frings et al., 2019)

Needles in a Haystack: Twitter for Coastal Morphodynamics

E.B. Goldstein[1], T. Beuzen[2], S. Sayedahmed[3], S. D. Mohanty[3], and E.D. Lazarus[4]

[1] Department of Geography, Environment, and Sustainability, University of North Carolina at Greensboro, Greensboro, NC, USA, ebgoldst@uncg.edu, @ebgoldstein (Twitter)
[2]Water Research Laboratory, School of Civil and Environmental Engineering, UNSW Sydney, NSW, Australia
[3] Department of Computer Science, University of North Carolina at Greensboro, Greensboro, NC, USA
[4] School of Geography and Environmental Science, University of Southampton, Southampton, UK

1. Introduction

Streaming social media is a source for real time impacts of extreme events. How can morphodynamicists use these data? What are the possibilities and the pitfalls of social media data as a record of morphodynamic phenomena? Here we explore several examples of connections between social media and coastal morphodynamics, consider some inherent problems when using social media data, and discuss ongoing work integrating social media with coastal morphodynamic models.

2. Making Twitter Data Useful

We use a dataset of geolocated tweets from Sept. 10th to 12th 2017 to investigate the digital trace of Hurricane Irma, FL, USA (2017). The dataset includes 54k tweets with 3000 images. We use machine learning to exclude tweets that are jokes/memes, and use subset via spatial attributes to find tweets relevant to coastal morphodynamics. A final manual processing is required to find tweets directly relevant to morphodynamics. Initial work suggest that there are just hundreds of relevant images (Figure 1). Text analysis is ongoing.

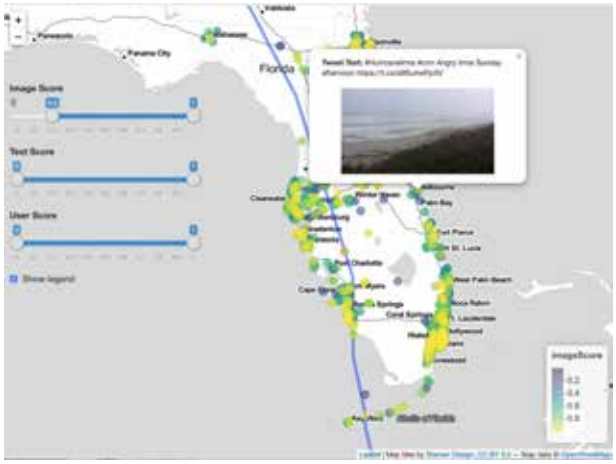

Figure 1. Screenshot of interactive map of geo-tagged twitter photos from Hurricane Irma (2017).

These observations are spatially and temporally sparse compared to high temporal resolution data (e.g., buoys, tide gauges) or high spatial resolution data (e.g., lidar). Many areas of interest for coastal modelling have no geolocated tweet.

3. Results from Preliminary Analysis

3.1 Novel anthropogenic behaviour

Scouring this dataset provides some indication that there is potentially interesting and novel information for a morphodynamicist, such as observations of during-storm mitigation measures (Lazarus and Goldstein, 2019) and how humans interact with the landscape (e.g. Hooke, 1994; Haff, 2002, 2010).

3.2 Capturing storm impacts before clean-up

A key benefit of social media data is the ability to capture storm impacts in built settings before cleanup occurs, which can inform future models of coupled human-landscape systems (e.g. Werner and McNamara, 2007; McNamara and Werner, 2008).

4. Future Directions

We identify several future directions for merging social media data with morphodynamics research. Two examples are 1) Understanding how to store and reuse the data in a way that does not violate the terms-of-service of a specific platform. A key hurdle is the fact that users can delete tweets at any moment, erasing potentially useful information; 2) It remains unclear how to effectively use social media data in morphodynamic models, or how a model can be built to explicitly use social media data (e.g. Referee 2, 2017). We give an example using a coastal dune erosion model presented in Beuzen et al. (2019).

Acknowledgments

The authors acknowledge financial support from DOD DARPA (EBG; HR001118200064), The Leverhulme Trust (EBG, EDL; RPG-2018-282), and a UNCG strategic seed grant (SM). We thank Dr. Arthur Cosby (Miss. State Univ.) for the Irma twitter data.

References

Beuzen, T., Goldstein, E., and Splinter, K. (2019). Ensemble models from machine learning: an example of wave runup and coastal dune erosion. *NHESSD*.

Haff, P. (2002). Neogeomorphology. *Eos*, 83(29):310–317.

Haff, P. (2010). Hillslopes, rivers, plows, and trucks: mass transport on earth's surface by natural and technological processes. *ESPL*, 35(10):1157–1166.

Hooke, R. L. (1994). On the efficacy of humans as geomorphic agents. *GSA Today*, 4(9):217.

Lazarus, E. D. and Goldstein, E. B. (2019). Is there a bulldozer in your model? *JGR-ES*.

McNamara, D. and Werner, B. (2008). Coupled barrier island–resort model: 1. emergent instabilities induced by strong human-landscape interactions. *Journal of Geophysical Research: Earth Surface*, 113(F1).

Referee 2 (2017). Interactive comment on "Citizen observations contributing to flood modelling: opportunities and challenges" by Assumpção et al. *HESS*.

Werner, B. and McNamara, D. E. (2007). Dynamics of coupled human-landscape systems. *Geomorphology*, 91(3-4):393–407.

Biogeomorphic evolution of a modern mangrove forest in a sediment-rich estuary, New Zealand.

A. Swales[1], S.J. Bentley[2], G. Reeve[1] and C.E. Lovelock[3]

[1] Coastal and Estuarine Physical Processes Group, NIWA, Hamilton, New Zealand, Andrew.Swales@niwa.co.nz
[2]Department of Geology and Geophysics, Louisiana State University, Baton Rouge, USA, sjb@lsu.edu
[1] Coastal and Estuarine Physical Processes Group, NIWA, Hamilton, New Zealand, Glen.Reeve@niwa.co.nz
[3] School of Biological Sciences, The University of Queensland, Brisbane, Australia, c.lovelock@uq.edu.au

1. Introduction

Mangrove forests in New Zealand's northern estuaries have rapidly colonised intertidal flats since the 1930s (averaging 4% yr^{-1}, Morrisey et al., 2010). This forest expansion has followed order-of-magnitude increases in fluvial-sediment fluxes to estuaries after catchment deforestation in the mid-1800s. Mangrove forests are vulnerable to sea level rise (SLR) as they occupy a narrow elevation zone (i.e., mid-to-upper-intertidal) and must accrete sediments to maintain their elevation relative to sea level.

Development of models to simulate long-term biogeomorphic evolution of mangrove forests is at an early stage. Formulation and validation of these models require quantitative data that integrate processes over the annual-to-decadal time timescales relevant to mangrove-forest development. Biogeomorphic reconstructions from sedimentary records have typically lacked sufficient temporal resolution to observe process-response feedbacks (Swales et al., 2015). Insights on biophysical processes controlling mangrove-forest surface-elevation dynamics have come from studies employing Surface Elevation Tables (SET, e.g., Krauss et al., 2014). With few exceptions these studies have focused on fluvial sediment-poor systems whereas the largest mangrove forests occur in fluvial sediment-rich settings. In this study we identify key formative processes and feedbacks controlling the long-term biogeomorphic evolution of a sediment-rich *Avicennia marina* forest in the Firth of Thames (37.25°S, 175.4°E), New Zealand.

2. Methods

The biogeomorphic evolution of the Firth mangrove forest was reconstructed using dated sediment cores collected along an 800-m shore-normal intertidal transect; and (2) detailed aerial photographic record of forest development since the 1950s. Excess lead-210 ($^{210}Pb_{xs}$) sediment accumulation rates (SAR) were used as a proxy for surface-elevation gain. Sediment accretion and surface-elevation trends were measured at triplicate SET stations (2007–2018) located along the transect in fringe, scrub and a relict-fringe forest zones of varying elevations and distance from the unvegetated mudflat. Hydroperiod was measured using pressure sensors and cameras (2011–2014) deployed at a SET station located in each forest zone. These data, along with other environmental variables, were analysed using Boosted-Regression-Tree (BRT) methods.

3. Results

Two- to ten-fold increases in $^{210}Pb_{xs}$ SAR occurred years to decades before seedling recruitment events on the intertidal flats. This demonstrates that mangroves did not measurably enhance sedimentation over annual to decadal timescales. Sediment accretion and resulting surface-elevation trends (0 to 28 mm yr^{-1}) in the mangrove forest over seasonal to interannual time scales are controlled by the coupling of frequent onshore winds and resulting resuspension of intertidal muds by small estuarine waves, with the fortnightly cycle of spring tide inundation. Sediment desiccation and resulting compaction during the summer (4 to 16 mm yr^{-1}) and deep subsidence of the entire forest (~8 mm yr^{-1}) are key processes controlling surface-elevation dynamics (Figure 1).

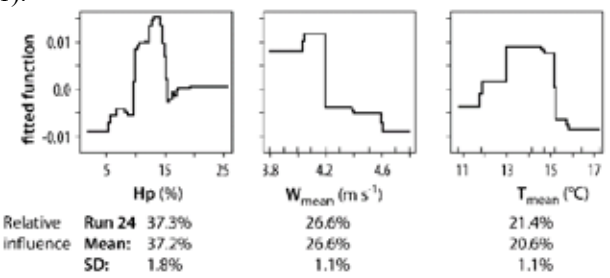

Figure 1: BRT partial-dependency plot of retained predictors for sediment accretion in the mangrove forest: hydroperiod (Hp), mean onshore wind speed (W_{mean}) and mean air temperature (T_{mean}).

3. Conclusions

The negative feedback between surface elevation and hydroperiod is a key process controlling mangrove-forest evolution. Regular ''day-to-day'' processes, rather than extreme events ultimately drives the long-term biogeomorphic evolution of the Firth mangrove forest.

Acknowledgments

This study was supported by the NZ Ministry of Business, Innovation & Employment (NIWA Managing Mud Programme – contract FWCE1911).

References

Swales, A., Bentley, S.J., and Lovelock, C.E. (2015). Mangrove-forest evolution in a sediment-rich estuarine system: opportunists or agents of geomorphic change? *Earth Surface Processes and Landforms* 40: 1672–1687.

Morrisey D.J., Swales, A., Dittmann, S., Morrison, M.A., Lovelock, C.E., Beard, C.M. (2010). The ecology and management of temperate Mangroves. *Oceanography and Marine Ecology: An Annual Review* 48: 43–160.

Krauss, K.W., McKee, K.L., Lovelock, C.E., Cahoon, D.R., Saintilan, N., Reef, R., Chen, L. (2014). How mangroves adjust to rising sea level. *New Phytologist* 202: 19–34.

Antidunes on steep slopes: variability of wave geometry and migration celerity

I. Pascal[1], C. Ancey[1] and P. Bohorquez[2]

[1] École Polytechnique Fédérale de Lausanne, Lausanne, Switzerland. ivan.pascal@epfl.ch, christophe.ancey@epfl.ch
[2] Centro de Estudios Avanzados en Ciencias de la Tierra, University of Jaén, Jaén, Spain. patricio.bohorquez@ujaen.es

1. Introduction

As a result of interactions between streamflow and sediment, riverbeds are seldom smooth, but depending on hydraulic and sediment transport conditions, they exhibit bedforms, which grow and migrate over time (upstream or downstream). Morphology migration may explain bedload transport pulses observed in field surveys and laboratory experiments, even under steady supply conditions (Gomez et al., 1989; Dhont and Ancey, 2018). Experimental investigations into the coupling between stream and bedform commonly focus on downstream migrating forms (dunes or bars). Guala et al. (2014) documented the importance of considering the scale-dependent relationship between wave geometry and migration celerity for estimating the sediment fluxes due to downstream migrating dunes.

Taking inspiration from their work, we investigated the case of upstream migrating bedforms, called *antidunes,* on steep slopes. Antidunes of variable wavelengths have been observed in gravel-bed streams (see Video Clip S2 in Froude et al., 2017). Well-controlled flume experiments are useful for assessing how bedform geometry and celerity are interrelated.

2. Methods

To investigate antidune formation and migration, we ran experiments in a 2.5-m long 4-cm wide flume with well-sorted gravel (d_{50} = 2.9 mm). The experiments were performed under steady conditions for water discharge and sediment supply. We studied four cases with different transport intensities and the same value of mean slope angle, ϑ = 3°. For each run we selected the unit flow discharge value q_w which ensures balance between erosion and deposition for a given sediment feeding rate $q_{s,in}$ (values from $2.0 \cdot 10^{-5}$ to $6.1 \cdot 10^{-5}$ m^2/s). The flow conditions were supercritical and fully turbulent.

The bed-topography data were collected using a side camera that covered a 75-cm long window in streamwise direction. The acquisition window was located near the middle of the flume. The resulting topographic profiles were characterized by a temporal resolution of 1 s and by a spatial resolution around 1 mm. Data acquisition started only after the system reached quasi-equilibrium between the sediment supply at the inlet and the sediment discharge sampled at the outlet (sampling time in the 60–120-s range). Moreover, the sediment feeding rate and the bedload transport rate at the outlet were monitored using high-speed cameras and image processing techniques. The duration of the experiments ranged between 35 and 77 minutes.

3. Results

During these experiments, antidune patterns developed and migrated upstream over almost the entire length of the flume. The bed topography was characterized by high stability of the mean bed slope in time. Considering the bed elevation matrix $Z(x,t)$, we extracted the typical modes applying a 2D Fast Fourier Transform in terms of wavenumber and frequency. This analysis allowed us to determine the statistical distribution of spatial scales and timescales. The spectra revealed a multiscale behaviour of the bedform geometry and its migration celerity. In particular, this study revealed the existence of a positive relationship between wavelength λ and celerity c. The normalization of the variables enabled us to better understand this dependence.

4. Conclusions

The experimental investigation demonstrated that, even under well-controlled conditions, antidunes exhibit varying shapes and migration celerity. In our experiments, we observed that longer antidunes (high λ) travelled upstream faster than shorter ones (low λ). Thus, we developed a scaling functional relationship that described the trends (celerity vs. wavelength) observed for different sediment transport intensities. The multiscale nature of this relationship is key to estimating friction parameters and sediment fluxes in the presence of antidunes and when interpreting field and laboratory data. The outcomes could improve the estimation of bedload transport fluxes in mountain streams and help paleohydraulic reconstructions.

Acknowledgments

P.B. was supported by the Spanish Ministry of Science, Innovation and Universities (MICINN/FEDER, UE) under Grant SEDRETO CGL2015-70736-R.

References

Dhont, B., & Ancey, C. (2018). Are Bedload Transport Pulses in Gravel Bed Rivers Created by Bar Migration or Sediment Waves? *Geophysical Research Letters*, 45(11), 5501-5508.

Froude, M. J., Alexander, J., Barclay, J., & Cole, P. (2017). Interpreting flash flood palaeoflow parameters from antidunes and gravel lenses: An example from Montserrat, West Indies. *Sedimentology*, 64(7), 1817-1845.

Gomez, B., Naff, R. L., and Hubbell, D. W. (1989). Temporal variations in bedload transport rates associated with the migration of bedforms. *Earth Surface Processes and Landforms*, 14(2), 135-156.

Guala, M., Singh, A., BadHeartBull, N., & Foufoula–Georgiou, E. (2014). Spectral description of migrating bed forms and sediment transport. *Journal of Geophysical Research: Earth Surface*, 119(2), 123-137.

Stratomorphodynamics of the Selenga River Delta, Lake Baikal: the Premier Modern System for Investigating Autogenic and Allogenic Influences on Stratigraphy

Jeffrey A. Nittrouer[1], Tian Dong[2] and Brandon McElroy[3]

[1] Rice University, Houston, U.S.A. nittrouer@rice.edu
[2] Rice University, Houston, U.S.A.. tian.dong@rice.edu
[3] University of Wyoming, Laramie, U.S.A. bmcelroy@uwyo.edu

On January 12, 1862, an earthquake of magnitude 7.5 struck the Selenga River delta at Lake Baikal, Siberia (Fig. 1). This event instantly lowered an area of 230 km^2 of the delta's northeastern region by 3-4 meters below lake elevation, creating "Proval Bay", which in Russian appropriately translates to "Failure Bay". Not long after the 1862 earthquake, a major distributary channel of the Selenga River avulsed into this newly created accommodation space. Presently, this eastern distributary channel delivers approximately 45% of the total water and sediment discharge of the Selenga River into Proval Bay; consequently, the eastern delta lobe has prograded ~ 62 m yr^{-1}, building approximately 90 km^2 of subaerial deltaic deposit (Il'icheva, 2008). This seismic event and subsequent rapid fluvial response reflects an important convergence of sedimentary dynamics and tectonics: a significant portion of the Selenga delta landform was downthrown via tectonic activity; the locally enhanced topset slope facilitated a channel avulsion, and fresh sediment deposits are now entombing and the underlying former topset stratigraphy into the geologic record.

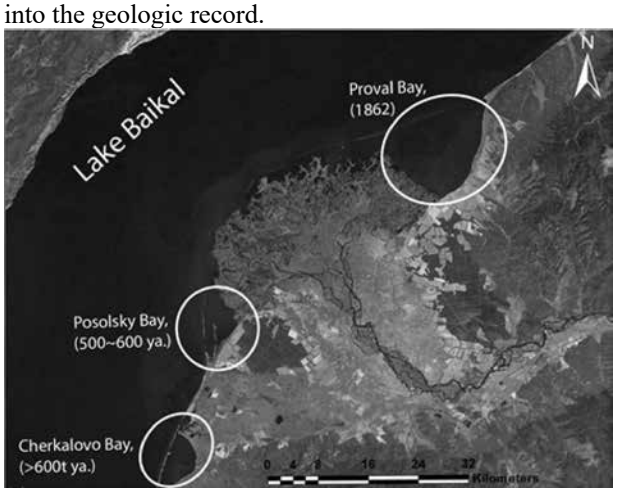

Figure 1 ***The Selenga River delta and Lake Baikal. Seismic activity subsides parts of subaerial delta below lake level, converting these regions into embayments. The most recent event generated Proval Bay (1862), and others are also indicated.***

Prior studies of modern river delta systems have sought to link surface processes to stratigraphy. However, signals measured in modern deltas are dominated by autogenic processes (internal dynamics of the system) with little means to evaluate how allogenic (external) perturbations manifest and impact the depositional record. Hence, existing theories linking delta morphodynamics and stratigraphy have developed primarily from physical experiments and numerical models, where boundary conditions can be controlled and constrained. For example, experimental studies demonstrate that the competition between autogenic lobe switching and allogenic influences (e.g., tectonic perturbations) plays an important role affecting sediment accumulation and the production of stratigraphy. However, validating these predictions using studies from modern field observations has not yet occurred

Located on the Baikal Rift margin, the Selenga River delta consists of three distinct lobes that receive varying amounts of water and sediment as a function of their respective slope and developmental history (Dong et al., 2016). This location therefore provides an excellent natural laboratory to test the following hypothesis: *the competition between autogenic and allogenic forcing on delta lobe development can be assessed by comparing morphological development over two discreet timescales – natural channel extension and commensurate reduction in slope and sediment transport capacity, and episodic tectonic subsidence that disrupts lobe development.* To constrain the autogenic lobe switching timescale, field measurements of water and sediment discharge are collected for the three lobes of the Selenga River delta, covering the 2018 summer flood hydrograph, whereby measurements occurred continuously from low to bankfull discharge. These data are combined with robust historical records (1908-2018), which include significant earthquake subsidence events affecting shoreline position. Water and sedimentation patterns of the delta lobes, and natural extension of these lobes, are compared to the production of accommodation via tectonic activity. This allows for a first-order comparison of autogenic and allogenic impacts on development for the Selenga delta lobes.

We determine that the lobe-scale strata of the Selenga River delta are reflective of autogenic depositional processes; however, on decadal timescales, deposition is disrupted by allogenic (tectonic) forcing. Moreover, the compensational stacking time scale can be established based on morphodynamic activity combined with subsidence patterns that derive from punctuated tectonic events. This information can be used to predict the internal stratigraphy of the Selenga delta system arsing over the past several centuries.

References

Il'icheva, E.A. (2008). Dynamics of the Selenga River network and delta structure. *Geography and Natural Resources*, v. 29, p. 343-347

Dong, T. Y., Nittrouer, J. A., Il'icheva, E., Pavlov, M., McElroy, B., Czapiga, M. J., Ma, H., and Parker, G. (2016). Controls on gravel termination in seven distributary channels of the Selenga River Delta, Baikal Rift basin, Russia. Geological Society of America Bulletin, 128(1-7): 1297-1312.

Initiation, growth and interactions of bars in a sandy-gravel bed river

J. Le Guern[1], S. Rodrigues[1, 2], P. Tassi[3], P. Jugé[4], T. Handfus[4] and A. Duperray[4]

[1] UMR CNRS CITERES, University of Tours, Tours, France. leguern@univ-tours.fr
[2] Graduate School of Engineering Polytech Tours, University of Tours, Tours, France. srodrigues@univ-tours.fr
[3] EDF R&D – National Laboratory for Hydraulics and Environment (LNHE) & Saint-Venant Laboratory for Hydraulics, Chatou, France. pablo.tassi@edf.fr
[4] CETU Elmis ingénieries, University of Tours, Chinon, France –juge@univ-tours.fr

1. Introduction

Dunes and bars are bedforms commonly observed in alluvial channels. Their interactions is seldom analysed in rivers, specifically the formation and growth of bars from a relatively flat bed composed of dunes. This field-based study sheds light on this formation process and on the interactions between the new formed bar appeared on the site ("autochthonous") and migrating bars coming from upstream ("allochthonous").

2. Study site & method

The study site is located near Saint-Mathurin-sur-Loire, in the downstream reach of the Loire River (France, [Figure 1D]), about 150 km upstream of the estuary. The study reach is 2.5 km long and nearly straight with a bed slope of 0.0002 m m^{-1}. The bed is composed of sands and gravels with a median diameter = 0.8 mm. The width-to-depth aspect ratio ranges between 120 and 550 according to discharge variations. The significant variation of the aspect ratio with hydrology leads to different bar modes (Cordier, 2018). To understand the initiation and the morphological evolution of bars, we carried out bathymetric surveys along longitudinal profiles for various discharge conditions. Flow velocities were also measured using aDcp surveys.

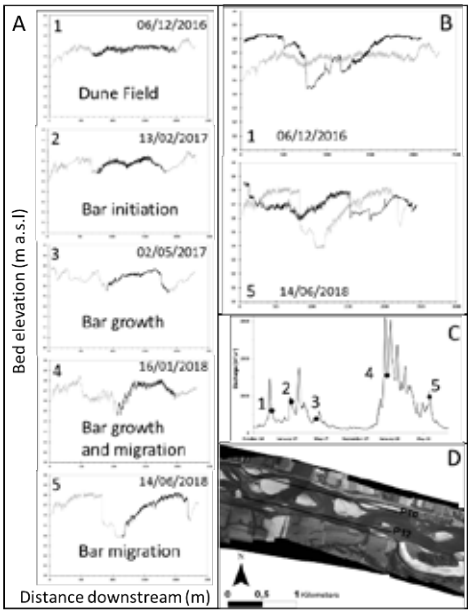

Figure 1: A: Initiation and evolution of a bar (highlighted in black); B: Initial (1) and final (5) river bed (left and right banks indicate in grey and black resp.); C: Hydrogram with bathymetric surveys; D Study reach in 2017.

3. Results & Discussion

During the first survey (06/12/2016, after an annual flood), bars were not present on the left side of the channel. A large dune field, almost flat, was present (Figure 1A). In this area, dune tracking measurements show that averaged dune height, length and celerity are about 0.3 m, 6 m and 30 $m.d^{-1}$, respectively. The second survey (13/02/2017, during an annual flood, [Figure 1C]) shows the initiation of a bar from a bed initially covered by dunes. The dune field oscillates into two small bars characterized by a wavelength of 500 m and an amplitude of about 1 meter. During the falling stage of the flood, these two bars merged into one unit of 2 m high and 1000 m long. During the subsequent biennial flood, the bar aggradation continued (3 m in height and 1000 m long) and the macroform started to migrate downstream. During its migration, the bar deflected the flow towards the right bank. This process led to the erosion and migration of a bar in this area ([Figure 1B], Claude et al., 2014; Cordier, 2018). According to the hydrology, bar initiation and aggradation processes lasted 5 months. The biennial flood allowed the migration of the bar with an average celerity of 2.5 $m.d^{-1}$.

3. Conclusions

This study suggests that bars can arise from a spontaneous initiation in a channel, apparently controlled by the dynamics of dunes (Ashworth et al., 2000; Claude et al. 2014). These newly-created bedforms interact with pre-existing bars migrating from upstream, leading to a highly dynamic environment, according to the hydrological forcing.

Acknowledgments

This work is part of the PhD thesis of the first author and the RTEMUS I & II research programs co-funded by the Agence de l'Eau Loire-Bretagne (convention n°150569501) and European Union (FEDER convention n° 2016-110475).

References

Ashworth, P. J., Best, J. L., Roden, J. E., Bristow, C. S., and Klaassen, G. J. (2000). Morphological evolution and dynamics of a large, sand braid-bar, Jamuna River, Bangladesh. *Sedimentology.* 47, 533-555.

Claude, N., Rodrigues, S., Bustillo, V., Bréhéret, J.-G., Tassi, P., and Jugé, P. (2014). Interactions between flow structure and morphodynamics of bars in a channel expansion/contraction, Loire River, France. *Water Resour. Res.*, 50, 2850-2873.

Cordier, F., (2018). Bars morphodynamics in trained rivers with heterogeneous sediment. PhD Thesis. University of Paris-Est.

Discharge variations and bar patterns in a channel contraction/expansion of a sandy-gravel river (Middle Loire, France)

F. Cordier[1], P. Tassi[1], N. Claude[1], A. Crosato[2], S. Rodrigues[3] and D. Pham Van Bang[4]

[1] EDF R&D LNHE, Chatou, France; [2] IHE Delft and Delft University of Technology, Delft, The Netherlands;
[3] Université de Tours, Tours, France; [4] INRS-ETE, Quebec, Canada

1. Introduction

Periodic bars are a common feature of rivers and correspond to large sediment deposits alternating with deeper areas that arise from an instability phenomenon of the alluvial bed. Linear stability theories show that periodic bars are primarily governed by the width-to-depth ratio of the flow, which is a crucial parameter to define the threshold between stability and instability regimes as well as the bar "mode" a parameter that indicate the number of bars that form in the river cross-section. Classical approaches to study bar formation and migration have considered separately the forcing effects of hydrology and channel geometry. Because the width-to-depth ratio is a function of water depth and thus of discharge, the latter is thus a crucial parameter for bar stability and dominant bar modes. Furthermore, geometrical channel changes not only modify directly the width-to-depth ratio, but also induce local areas of erosion or deposition. The present study is meant to better understand the impact of combined complex hydrology and channel geometry on bar morphodynamics in alluvial riverbeds. To this goal, a two-dimensional morphodynamic model (Cordier et al., 2019b) is used to simulate the bed evolution of a 1 km long reach of the Loire River, corresponding to an area of contraction/expansion wherein complex bar dynamics have been observed.

2. Numerical Scenarios and Results

Four scenarios are proposed to investigate bar morphodynamics processes and patterns, with a special focus on the hydrological conditions. The first proposed scenario (run A, also referred to as reference scenario) consists on reproducing numerically the bar evolution observed *in situ* by Claude et al. (2014) starting from March 15^{th} 2010 and lasting one year, using the hydrogram of 2010-2011. The influence of the hydrology on resulting bar dynamics is investigated by comparing results from the reference scenario and three derived scenarios considering uniform water inflow (runs B, C and D). The three last runs are defined by water discharges representative of the low flow period (run B, Q_w =200 m^3/s), mean annual flow (run C, Q_w =500 m^3/s) and two-year flood peak (run D, Q_w =2000 m^3/s).

Computation of the most probable bar mode m using the predictor of Crosato and Mosselman (2009) at different stages of run A and bar modes obtained from the numerical model (Fig. 1) suggest a strong variation of the bar pattern in the study area, varying between alternate bars ($m = 1$), central bars ($m = 2$) and a multi-channel -or braided- pattern ($m \geq 2.5$).

In every single scenario considering a constant flow rate, a dominant bar pattern is observed in the expansion area in the late stage of the simulations (Fig. 2). In run B, the bed topography consists in a multiple channel pattern with relatively short bars. Conversely, in run D, the riverbed is characterized by the presence of alternate bars. In run C, an intermediate state is obtained, where transverse bars and central bars patterns are alternating over time (Cordier et al., 2019a).

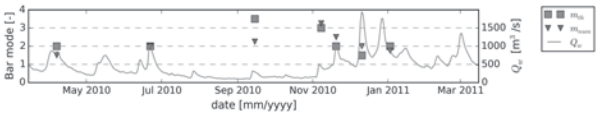

Figure 1. Time-series of the theoretical and numerical bar modes obtained with run A.

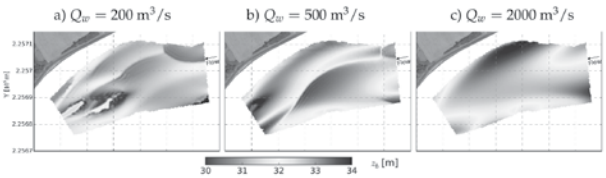

Figure 2. Planform bed topography computed with the morphodynamic model after a period of 300 days with a uniform inflow with a) run B, b) run C and c) run D.

3. Conclusions

The model predicts satisfactorily the bar evolution with respect to field observations, such as the transition from an alternate bar to a transverse bar system. In agreement with theory, varying discharge creates a competition between low and high bar modes. High flow rates induce bar mode reduction, whereas low-flow rates induce higher bar modes. The forcing effect of channel contraction/expansion on bar dynamics appears strongly mediated by discharge variations.

References

Claude, N., Rodrigues, S., Bustillo, V., Bréhéret, J.-G., Tassi, P., and Jugé, P. (2014). Interactions between flow structure and morphodynamic of bars in a channel expansion/contraction, Loire River, France. *Water Resources Research*, 50(4):2850–2873.

Cordier, F., Tassi, P., Claude, N., Crosato, A., Rodrigues, S., and Pham Van Bang, D. (2019a). Bar pattern and sediment sorting in a channel contraction/expansion: application to a sandy-gravel river reach (Middle Loire, France). Submitted to ESPL.

Cordier, F., Tassi, P., Claude, N., Crosato, A., Rodrigues, S., and Pham Van Bang, D. (2019b). Numerical study of alternate bars in alluvial channels with non-uniform sediment. *Water Resources Research*, Accepted.

Crosato, A. and Mosselman, E. (2009). Simple physics-based predictor for the number of river bars and the transition between meandering and braiding. *Water Resources Research*, 45(3):1–12.

A framework to better understand river side channel development

R. Pepijn van Denderen[1], Ralph M.J. Schielen[1,2] and Suzanne J.M.H. Hulscher[1]

[1] Water Engineering & Management, University of Twente, The Netherlands. r.p.vandenderen@utwente.nl
[2] Ministry of Infrastructure and Water Management-Rijkswaterstaat, The Netherlands

1. Introduction

Side channels are small secondary channels that are generally connected to the main channel at both ends. Side channels are (re)constructed to reduce the flood risk and to increase the ecological value of a river. Many such artificial side channels quickly aggrade (Riquier et al., 2015; Van Denderen et al., 2019) and therefore costly maintenance is needed. There are several parameters and processes such as the channel length and secondary flow at the bifurcation that affect the sediment supply and the transport capacity in side channels. The imbalance between supply and capacity results in bed level changes within the side channel system. Here, we first present the development of a side channel system in the river Waal. We then propose a framework to estimate the development of side channels.

2. Side channel system at Gameren

The side channel system at Gameren was constructed between 1996 and 1999 (Figure 1). Their objective is to compensate a water level increase that was a result of a levee relocation. At the upstream side of the East channel and the West channel, weirs were constructed to control the discharge in the channels such that the East channel flows 100 d/yr and the West channel flows 265 d/yr. The Large channel is much longer compared to the other two channels and is permanently connected to the main channel.

All the three channels show large aggradation, but the type of sediment that is deposited in the side channel differs. In the East and West channel are mainly filled with fine sand that in the main channel is transported as suspended bed-material load. The East channel has reached a bed level at which vegetation is able to grow and wash load is trapped. In the Large channel, the bed shear stress is lower due to its large width variation and the channel length. This also results in the deposition of wash load material. In each of the channels different mechanisms are important that result in the aggradation of a side channel and these mechanisms seem to be linked to the sediment that is deposited in the side channels.

3. Side channel characterization

The side channel system at Gameren is an example that depending on the channel and its development different processes are important that cause the side channel aggradation. A similar distinction in the sedimentation processes can be found in other rivers such as the river Rhône in France (Riquier et al., 2015). We define three categories: (1) bed load supplied side channel, (2) suspended bed-material load supplied side channels and (3) wash load supplied side channels. These categories are based on how the sediment that is deposited in the side channel is transported in the main channel. Each category is related to mechanisms. Knowing these mechanisms, we can give a first estimation of the development of a side channel and its corresponding time scale.

4. Conclusions

Side channel development can be characterized based on the sediment that is deposited in the side channel. The sediment that is deposited in the side channel gives an indication of which mechanisms are important for the development of the side channel system.

Acknowledgments

This research is supported by the Netherlands Organisation for Scientific Research (NWO), which is partly funded by the Ministry of Economic affairs, under grant number P12-P14 (RiverCare Perspective Programme) project number 13516. This research has benefited from cooperation within the network of the Netherlands Centre for River studies (https://ncr-web.org).

References

Riquier, J., H. Piégay, and M. S. Michalková, 2015: Hydromorphological conditions in eighteen restored floodplain channels of a large river: linking patterns to processes. *Freshwater Biology*, 60, 1085-1103, doi:10.1111/fwb.12411.

Van Denderen, R. P., R. M. J. Schielen, S. G. Westerhof, S. Quartel, and S. J. M. H. Hulscher, 2019: Explaining artificial side channel dynamics using data analysis and model calculations. *Geomorphology*, 327, 93-110, doi:10.1016/j.geomorph.2018.10.016.

Figure 1 An aerial image of the side channel system at Gameren in the river Waal.

Estimation of riverbed evolution at hydrometric stations using the stage record

M. Darienzo[1], J. Le Coz[1], B. Renard[1] and M. Lang[1]

[1] Irstea Lyon-Villeurbanne, UR Riverly, 5 rue de la Doua, 69100 Villeurbanne, France. matteo.darienzo@irstea.fr

1. Introduction

We propose an original method for estimating riverbed evolution at hydrometric stations through the analysis of stage recessions. The main goal is the detection and automatic estimation of variations in the mean bed elevation using stage record only, in the absence of discharge measurements (aka gaugings), rating curves and bathymetry measurements. The method assumes the stage recession physically tends towards the riverbed elevation as streamflow tends towards zero (Lapuszek, 2003). Thus, a change in the shape of the recession may indicate a potential riverbed evolution. This work focuses on rivers subjected to sudden morphological changes.

2. Methodology

The first step of the proposed method is the identification of recessions from the stage record. A threshold parameter is used to separate two successive recession curves, based on a minimum difference between the start of period i and the end of period $i-1$.

The second step is based on a Bayesian regression of each recession using a two-exponential model and the asymptotic stage h_∞ (Equation 1),

$$h(t) = \theta_1 \, e^{-\theta_2 \, t} + \theta_3 \, e^{-\theta_4 \, t} + h_\infty \qquad (1)$$

where h is the stage, t is the recession time and $\theta_1, \theta_2, \theta_3, \theta_4, h_\infty$ are the inferred parameters.

The last step consists in the segmentation of the asymptotic stage time series. To account for uncertainties a Bayesian segmentation method has been implemented. The inferred parameters are the mean of each homogeneous segment and the change point times. The choice of the optimal number of segments is relative to the minimum value of the Bayesian Information Criterion (Schwarz, 1978).

3. Results

The proposed method has been applied to the Ardèche River at Meyras (Barutel) in France, a river with a gravel bed degrading during each flood. We considered the period 07/11/2001 - 01/01/2015. Figure 1 shows the results of the segmentation method applied to the asymptotic stage time series. The dashed vertical lines and the horizontal gray lines are the change point times and the mean for each homogeneous period, respectively, obtained by the proposed segmentation method with quantitative uncertainties. The results evidence three detected change points. If we compare them with the official shift times (provided by the hydrometric service and represented by crosses in Figure 1) we observe in general a good agreement, except for the first shift time (at 1835 days). However the results of the riverbed estimation using gaugings and rating curves for each official stable period (obtained by Mansanarez et al. (2019) and represented by horizontal black lines in Figure 1) show that the bed variation is quite negligible for that time. It seems that the recession analysis is able to detect net riverbed change only. Furthermore, a seasonal variability of the estimated asymptotic stage is observed, approaching to the estimated riverbed elevation during the dry season only. This variability causes the overestimation of the segments mean. Nevertheless, since the riverbed variations mainly occur during the rainy season, we need to analyse all available recessions (including uncertain ones) to avoid missing change times.

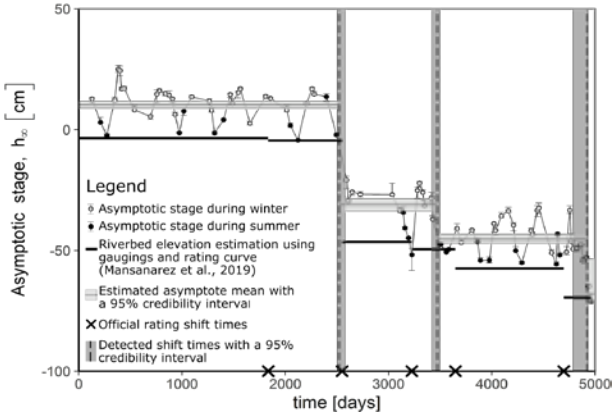

Figure 1. Results of the stage recessions segmentation for the Ardèche River at Meyras, France, for the period 07/11/2001-01/01/2015.

4. Conclusions and perspectives

The proposed method for detecting riverbed change through stage recession analysis yielded encouraging results with the detection of net riverbed change. However, the seasonal variability of the estimated asymptotic stage requires further investigation. Perspectives include the validation of the method by considering more challenging case studies, e.g. the Wairau River at Barnett's Bank in New Zealand. Furthermore, the prediction of the asymptotic stage after the flood may be possible, providing real-time information about potential riverbed change.

Acknowledgments

We would like to thank EDF, CNR and SCHAPI for the financial support to this project.

References

Lapuszek, M. (2003). The investigation of riverbed erosion in a mountainous river. *Archives of Hydro-Engineering and Environmental Mechanics : AHEM*.

Mansanarez, V., Le Coz, J., Renard, B., Lang, M., and Darienzo, M. (2019). Shift happens! adjusting stage-discharge rating curves to riverbed morphological changes at known times. in press. *Water Resources Research*.

Schwarz, G. (1978). Estimating the dimension of a model. *Ann. Statist.*, 6(2):461–464.

Influence of the position and angle in the trapped efficiency of flow in a bifurcation along a bend

C. Caballero[1], L. Domínguez Ruben[2] A. Mendoza[3], R. Szupiany[4] and M. Berezowsky[5],

[1] Instituto de Ingeniería, Universidad Nacional Autónoma de México, México. ccaballeroc@ii.unam.mx
[2]Universidad Nacional del Litoral, Santa Fe, Argentina. ldominguez@fich.unl.edu.ar
[3] Instituto de Ingeniería, Universidad Nacional Autónoma de México, México. amendozar@ii.unam.mx
[4]Universidad Nacional del Litoral, Santa Fe, Argentina. ldominguez@fich.unl.edu.ar
[5] Instituto de Ingeniería, Universidad Nacional Autónoma de México, México. mberezowskyv@ii.unam.mx

1. Introduction

Although some past studies described the flow partition in a bifurcation (Klienhans et al., 2012), there is still little understanding for some specific cases such as bifurcations on a bend. In general, the previous studies of 2D numerical modeling have been solved for bifurcation in straight channels only (Dutta et al., 2018). This research intends to carry out an approximation of the effects produced by the location and bifurcation angle in a bend evaluating the trapped efficiency of the secondary channel. The question to answer is what effect of both parameters (location or angle) is more important for a secondary channel to remain or to be abandoned. For that purpose, it is utilized 2D numerical modeling based on the Telemac System coupled with Sisyphe sediment transport module.

2. Methods

Nine study cases were defined, varying the position ($\pm$10º from apex and apex) and bifurcation angle ($\pm$10º and 0º) along with a bend in the main channel (Figure 1). For the 2D simulations, it is considered bed and suspended load. Table 1 shows the general parameters utilized for the geometries. Geometrical conditions were set to guaranty the secondary flow effects (Dietrich, 1987) and previous geometry studies (Edmons et al., 2016).

Parameter	Main	Secondary
Channel width to Depth ratio	33.3	33.3
Wavelength to channel width ratio	120	120
Main channel to secondary channel width ratio		0.7

Table 1: Geometrical parameters of both channels

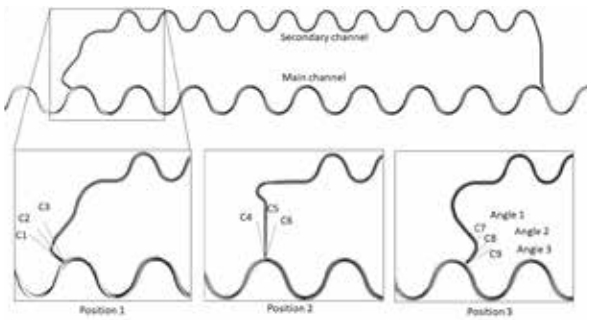

Figure 1: Position and angle of the start of the secondary channel

It was considered in the domain, 1) all the secondary channels have the same length, 2) the secondary channels reconnect to the main channel in the same location and angle, 3) the main channel was modeled until it reached bed equilibrium, before connecting the secondary channel, 4) all the secondary channels have the same width to depth ratio and the initial condition was flat bed.

3. Conclusions

Preliminarily results show that both, location and angle bifurcation have a significant impact on the temporal evolution of the flow partition in the secondary channel "life". Figure 2 shows the flow distribution for some cases C1, C5, C7, and C8. The secondary channel that starts upstream the apex bend (C1) captures a 7% and 25 % more flow than the located in the apex and downstream the apex (C7 and C8), respectively.

Comparing the bifurcation angle for C7 and C8 the changes in the capture of flow varies no more than 1%.

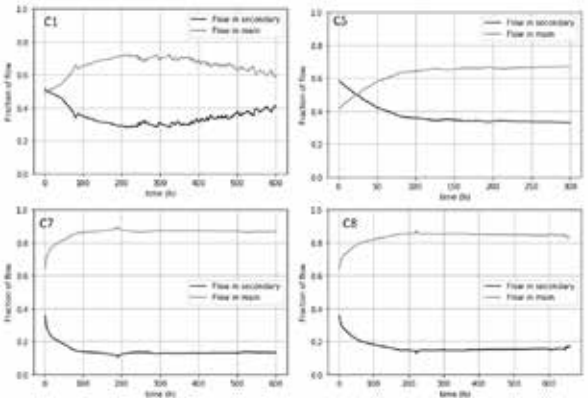

Figure 2: Flow partition for some study cases (C1, C5, C7, and C8). See Figure 1.

When the initiation of the secondary channel is in the apex, it captures more flow at the beginning of the simulation; however, gradually and consistently the main channel recovers the largest fraction of the flow. It would be interesting to increase the elapse of time simulated for cases C1 and C5 to determine if in C1 the secondary channel keeps increasing its capacity to capture the flow, and for C5 if the secondary channel losses its capacity; note that C5 show results up to 300 hours.

References

Dietrich, W. E. (1987), Mechanics of flow and sediment transport in river bends, in: River Channels: Environment and Process, K. S. Richards (ed.), Institute of British Geographers Special Publication No. 18, Basil Blackwell, Inc., 179-227.

Dutta, S., Wang, D., Tassi, P. y Garcia, M. H. (2017), Three-dimensional numerical modeling of the Bulle effect: the nonlinear distribution of near-bed sediment at fluvial diversions, Earth Surface Processes and Landforms, DOI: 10.1002/esp.4186.

Edmons, D., Hajek, E., Downton, N., and Bryk, A (2016), Avulsion flow-path selection on rivers in foreland basins, The Geological Society of America. DOI: 10.1130/G38082.1.

Klienhans, M.G., Ferguson, R.I., Lane, S.N, y Hardy, R. J. (2012), Spliting rivers at their seams: bifurcations and avulsion. Earth Surfaces Processes and Landforms. DOI:10.1002/esp.3268.

Testing long-term channel network incision models using a natural experiment in postglacial landscape evolution

G.E. Tucker[1,2], K.R. Barnhart[1,2], S.G. Doty[3], R.C. Glade[2,4], M.C. Hill[5], M.W. Rossi[1,2], and C.M. Shobe[1,2]

[1] Cooperative Institute for Research in Environmental Sciences (CIRES), Univ. of Colorado, Boulder, Colorado, USA
[2] Department of Geological Sciences, University of Colorado, Boulder, Colorado, USA
[3] Consultant, Denver, Colorado, USA
[4] Institute for Arctic and Alpine Research (INSTAAR), University of Colorado, Boulder, Colorado, USA
[5] Department of Geology, University of Kansas, Lawrence, Kansas, USA

1. Introduction

A key challenge in fluvial geomorphology lies in understanding the mechanics that govern channel incision over millennial time scales. Channel incision into rock or cohesive sediment plays a key role in the evolution of landscapes. In the case of engineered landforms or storage sites for hazardous material, long-term stewardship relies on an ability to forecast potential future rates and patterns of erosion. Many different mathematical formulations have been proposed as approximate descriptors of the channel incision process. It remains unclear, however, which of these gives the best and most parsimonious representation of the process for any given environmental setting, geological material, or scale. Here we test and compare a set of alternative erosion laws. To do so, we exploit a natural experiment in rapid post-glacial channel network incision. A series of 37 different numerical models, representing various combinations of alternative channel and hillslope erosion laws, are tested for their ability to reproduce the modern topography of a $\sim$5 km^2 watershed, given a reconstruction of the immediate postglacial topography and an estimate of the downcutting history at the watershed outlet.

2. Approach

The case study is a small watershed east of Lake Erie, in the state of New York, USA. Following the retreat of the Laurentide ice sheet, channel incision carved a network of ravines and gullies up to 50 m deep into an initially low-relief surface. Remnants of the original surface allow reconstruction of its pre-incision form, and dating of fluvial terraces and related features provides an estimate of the post-glacial history of incision in the main stem valley to which the catchment drains. The availability of "before and after" topography provides an opportunity to test a group of alternative erosion models based on their ability to reproduce the modern topography. We consider 37 different process models, which differ from one another on the basis of one or more of the following aspects: channel incision law, hillslope erosion law(s), representation of hydrology, and treatment of material properties. Here we focus on channel incision laws. The general formulation casts incision rate as the difference between rates of bed-material entrainment, E, and deposition, D:

$$\left.\frac{\partial \eta}{\partial t}\right|_{\text{channel}} = D - E \qquad (1)$$

where η is land surface elevation. We consider variations on this general form. In most cases, $D = 0$, but in some models D is treated as a function of sediment flux and discharge. E is represented as a power function of discharge and slope, with or without a threshold. Discharge is treated either as proportional to drainage area, as a modified function of drainage area that accounts for partitioning between surface and shallow subsurface flow, or as a linear function of a stochastic-in-time precipitation rate. Material erodibility is treated either as uniform, or with different erodibility coefficients assigned to shale and glacial till. To carry out this inter-model comparison and evaluation, we used the CSDMS **Landlab Toolkit** (Hobley et al., 2017) to construct the individual numerical models. The resulting open-source package is known as **terrainbento** (Barnhart et al., 2019).

3. Results

Formal calibration of the alternative models reveals that the greatest improvement in model performance comes when shale and cohesive glacial sediments are treated as distinct lithologies, with the shale more resistant to detachment than the glacial material. Inclusion of a threshold in the detachment term also substantially improves model performance. Stochastic representation of stream flow did not significantly improve model performance, nor did inclusion of a deposition term.

4. Discussion and Conclusions

Calibration and inter-comparison of 37 alternative long-term erosion models demonstrates that channel incision into relatively fine-grained materials at the test site can be approximated using a detachment-limited formulation based on unit stream power in excess of an erosion threshold. Despite the apparent similarity between the two primary lithologic units, reproducing the observed incision patterns requires treating the shale as more resistant than glacial till. More generally, the approach to hypothesis testing that we outline in this study can be applied to other natural experiments, and has the potential to improve our mechanistic understanding of long-term channel incision.

References

Barnhart, K. R., Glade, R. C., Shobe, C. M., and Tucker, G. E. (2019). terrainbento 1.0: a python package for multi-model analysis in long-term drainage basin evolution. *Geoscientific Model Development Discussions*.

Hobley, D. E., Adams, J. M., Nudurupati, S. S., Hutton, E. W., Gasparini, N. M., Istanbulluoglu, E., and Tucker, G. E. (2017). Creative computing with landlab: an open-source toolkit for building, coupling, and exploring two-dimensional numerical models of earth-surface dynamics. *Earth Surface Dynamics*, 5(1):21.

Comparing Non-Newtonian Approaches to Experimental Results: Validating Mud and Debris Flow in HEC-RAS

S. Gibson[1], I. Floyd[2], A. Sánchez[1], and R. Heath[3]

[1] Hydrologic Engineering Center, Davis, CA, USA. Stanford.Gibson@usace.army.mil
[2] Coastal and Hydraulics Laboratory, Vicksburg, MS, USA, Ian.Floyd@usace.army.mil

1. Introduction

Destructive mine-tailing, dam failures and post-fire, mud and debris flows destroy lives and property. These geologic hazards - and other similar processes - fall on a continuum between classic, Newtonian, flood analyses and geotechnical, stability analyses. The US Army Corps of Engineers (USACE) is developing a Non-Newtonian library (DebLib) that includes a suite of rheological and clastic approaches to hyper-concentrated, mud, and debris flow dynamics. The Hydrologic Engineering Center (HEC) has implemented these Non-Newtonian methods into the widely-used, public-domain, open-channel hydraulics and morphodymaic software, HEC-RAS (the River Analysis System). This work presents the Verification and Validation of several of these non-Newtonian approaches, applying several rheological and clastic approaches to non-Newtonian transport in HEC-RAS to experimental studies that include a range of concentrations and gradations.

2. Non-Newtonian Models and Validation Data Sets

The study team implemented a selection of rheological, clastic, and combined non-Newtonian closures in HEC-RAS. This study tested the linear Bingham model (with O'Brien parameter equations) and, Julian's turbulent, Bagnold's dispersive, quadratic terms. HEC-RAS also includes the non-linear Herschel–Bulkley (HB) approach that quantifies dilatant or thinning processes and clastic approaches including a Coulomb yeild stress and the Cross approach, which can be applied alone or as a yeild component in the rheological models.

In this study, these non-Newtonian approaches were applied to unsteady flow simulations of a wide range of experimental data with the different non-Newtonian closures. The experimental data include lower concentration (C_v between 1.5 and 9.2%) thinning (HB power between 0.55 and 1) experiments (Burger et al., 2010), high concentration (C_v>63%) experiments with a range of grain sizes and mixtures, including dilatant and thinning (HB power between 0.43 and 1.25) materials (Parsons et al., 2001), and clastic experiments (Mainali and Rajarathnam, 1994) with coarser materials (d_{50} between 0.22 and 0.43 mm) and a range of concentrations (C_v between 1 and 22%). Most of these studies measured or estimated yeild stress and viscosity and compute HB parameters, providing the opportunity to test the different non-Newtonian models in different settings. Empirical equations (e.g. Obrian and Einstein and Chen) that compute these parameters in the absence of measurements, which is the case for most prototype applications, are also evaluated.

Example results are included in Figure 1. Figure 1 compares measured velocities from the "fine" experiments in Parsons et al., (2001) (τ_{yield}=98Pa, μ=1.92Pa-s) with the HEC-RAS results with the standard, Newtonian, shallow water flow equations and the Bingham closure.

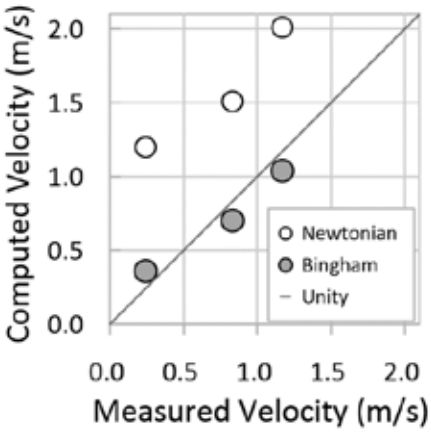

Figure 1: Depth averaged velocities measured by Parson et al. (2001) in three different experiments plotted with computed Newtonian and Bingham velocities.

3. Conclusions

The study team developed a non-Newtonian library leveraged by multiple, free, production level hydraulic and morphodyamic software packages, including HEC-RAS. These non-Newtonian closures improve results for hyper-concentrated flows, mudflows and debris flows. However, the appropriate algorithm must be selected for each case. The library includes dimensionless thresholds to automatically select algorithms based on condition.

Acknowledgments

This work was funded by the US Army Corps of Engineers Flood and Coastal Storm Damage Reduction Research and Development Program.

References

Burger, J., Haldenwang, R., and Alderman, N. (2010). Ëxperimental database for non-Newtonian Flow in four channel shapes, *J. of Hyd. Res.*, 48(3):363-370.

Mainali, A., and Rajarathnam, N. (1994). Experimental study of debris flows, *ASCE J. of Hydr. Eng.,* 120(1):104-123.

Parson, J.D., Whipple, K.X., and Simon, A. (2001).Experimental study of the grain-flow, fluid-mud transition in debris flows. *J. of Geology*, 109:427–447.

A well-posed model for 2D mixed-size sediment morphodynamics

Víctor Chavarrías[1], Willem Ottevanger[2], Ralph Schielen[3,4], and Astrid Blom[1]

[1] Delft University of Technology, Delft, The Netherlands. v.chavarriasborras@tudelft.nl
[2] Deltares, Delft, The Netherlands.
[3] University of Twente, Enschede, The Netherlands.
[4] Ministry of Infrastructure and Water Management, Lelystad, The Netherlands.

1. Introduction

The active layer model (Hirano, 1971) is the most widely applied model to account for mixed-size sediment in morphodynamic simulations. In this model, the bed is discretized into two parts: the active layer and the substrate. The sediment in the active layer is assumed to be perfectly mixed, whereas the substrate may be stratified. Sediment entrainment and deposition occurs within the active layer only. A flux of sediment from and to the substrate occurs in case of lowering or increase in the elevation of the interface between the active layer and the substrate.

Using this simplified view of the mixing processes, one is able to reproduce, up to a certain extent, a large amount of physical processes such as armoring, tracer propagation, downstream fining, and the formation of a gravel-sand transition. However, the model suffers from an important limitation: under certain conditions (specially under degradational conditions when the active layer is coarse with respect to the substrate) it may be ill-posed. An ill-posed model is incapable of representing any physical process, as the solution is unstable to short wave perturbations (e.g., noise in the initial condition and numerical truncation errors) and does not converge when the numerical grid is refined (Chavarrías et al., 2019). Ill-posedness indicates that a key physical process is missing in the model description.

Chavarrías et al. (2017) devised a regularization strategy that prevents the one-dimensional active layer model from being ill-posed. By increasing the time scale of the mixing processes, the regularized model is guaranteed to be well-posed. The strategy was tested against laboratory data. In the laboratory experiment, degradation into a fine substrate was imposed, which led to periodic entrainment cycles of fine sediment. The regularized model captures the mixing processes averaged over a time scale that includes several cycles of sudden entrainment of fine sediment. Although the strategy was shown to be successful, it has been applied under one-dimensional conditions only. Here we extend the strategy to two-dimensional conditions.

2. Regularization Strategy

Our first attempt is to modify the two-dimensional version of the active layer model in the same manner as Chavarrías et al. (2017) modified the one-dimensional version of the model. Interestingly, this straightforward extension of the one-dimensional solution to two dimensions does not regularize the model. We prove this fact conducting a perturbation analysis of the two-dimensional model accounting for the modification of the time scale.

We propose a new strategy for regularizing the two-dimensional model. As an increase of the time scale of the mixing processes appears to be the key element to regularize the one-dimensional model, we devise a different strategy that has similar physical implications. Diffusion accounts for the mixing processes on a short time scale not resolved by the model. The new strategy consists of adding a diffusive component to the active layer equation only (i.e., the Exner equation for bed elevation changes remains intact). By means of a perturbation analysis, we prove that a certain amount of diffusion guarantees that the active layer model is well-posed under two-dimensional conditions.

3. Application

The regularized two-dimensional model is guaranteed to be well-posed. Yet, well-posedness does not guarantee that mixing-processes are well represented. In testing whether diffusion accounts for the mixing processes occurring on a short time scale, we compare the results of the regularized model to laboratory and field data.

We implement the strategy in the software package Delft3D. We model the laboratory experiment conducted by Chavarrías et al. (2017) while considering the transverse direction and compare the results to the laboratory data. In this way, we not only compare results to laboratory data but also to the results of the regularization strategy of the one-dimensional model. A second test is to model the experiment conducted by Blom et al. (2003). In this second experiment fine sediment initially part of the substrate was entrained due to dune growth. This process is represented in the active layer model by an increase in the active layer thickness. Finally, we asses the consequences of ill-posedness and the regularization strategy in a field case. To this end, we use a two-dimensional schematization of the Rhine branches in the Netherlands that accounts for mixed-size sediment processes.

References

Blom, A., Ribberink, J. S., and de Vriend, H. J. (2003). Vertical sorting in bed forms: Flume experiments with a natural and a trimodal sediment mixture. *Water Resour. Res.*, 39(2):1025.

Chavarrías, V., Schielen, R., Ottevanger, W., and Blom, A. (2019). Ill posedness in modelling 2d morphodynamic problems: Effects of bed slope and secondary flow. *J. Fluid Mech.* (in press).

Chavarrías, V., Stecca, G., Labeur, R. J., and Blom, A. (2017). A strategy to avoid ill-posedness in mixed sediment morphodynamics. In Lanzoni, S., Redolfi, M., and Zolezzi, G., editors, *10th Symposium on River, Coastal and Estuarine Morphodynamics, Trento-Padova, Italy 15–22 September*, page 166.

Hirano, M. (1971). River bed degradation with armoring. *Proc. Jpn. Soc. Civ. Eng.*, 195:55–65.

Towards understanding the role of fatigue and rock damage accumulation on sea cliff erosion using seismic methods

C.C. Masteller[1*], N. Hovius[1], C. Thompson[2], H.B. Woo[3], P.N. Adams[2], M.E. Dickson[3], N.J. Rosser[4], A. Young[5], M.J. Brain[4], and E.C. Vann Jones[4]

[1] Helmholtz Centre, German Research Centre for Geosciences, Potsdam, Germany. *mastell@gfz-potsdam.de.
[2] University of Auckland, Auckland, New Zealand.
[3] University of Florida, Gainesville, Florida, USA.
[4] Durham University, Durham, UK
[5] Scripps Institution of Oceanography, University of California, San Diego, La Jolla, California, USA.

1. Introduction

Though they comprise ~80% of global coastlines, rocky shores are significantly understudied in comparison to their depositional counterparts. As winter wave heights and variability intensify across Western Europe, understanding the susceptibility of these coasts is becoming increasingly important. Though sea cliffs are subjected to persistent wave action, cliff erosion and collapse is episodic, making prediction difficult, as observations of cliff failures do not always coincide with the highest magnitude waves. In addition, there is a significant mismatch between the maximum pressures exerted by individual breaking waves (kPa) and the intact tensile strength of the bedrock that comprises these cliffs (MPa), suggesting that under almost all wave conditions, erosion should not occur as the tensile strength of the cliff rock is almost never exceeded by wave forcing.

These observations suggest that sea cliff stability is not purely dependent on the magnitude of a single wave, but is likely related to the additive effects of the full history of past wave action. Indeed, previous studies have suggested that the cyclic flexure of sea cliffs in response to wave action result in progressive weakening of cliff rock via fatigue processes. Here, we explore the influence of variable wave action on cliff flexure patterns using seismic methods. We present data from a coastal seismic observatory established on the Orkney Islands of Scotland, where 30m sea cliffs are subject to wave heights from 1-15 m, making it an ideal natural laboratory to characterize the contribution of varying wave heights towards cliff rock weakening and eventual erosion.

2. Quantifying cliff rock displacement in response to variable wave forcing

We pair high-resolution wave buoy data with a cliff-top seismic network to characterize the relationship between delivered wave energy and sea cliff response. Through comparison of wave and seismic spectra, we constrain the portion of ocean waves that most effectively translate into mechanical work. We characterize the relationship between wave height and cliff shaking. We find that cliff displacement as measured by a cliff face seismometer is strongly dependent on wave magnitude, such that the degree of cliff displacement scales nonlinearly with wave height. As such, larger waves appear to have a disproportionate effect on cliff flexure.

3. Characteristic cliff flexure in response to cyclic wave action

We also constrain the degree of cliff flexure in response to variable wave action by quantifying cliff displacement in a cross-shore seismic array. We find that cliff displacement decays nonlinearly with distance from the cliff face, driving cliff flexure. At Orkney, this cliff flexure, or decay in ground displacement, is insensitive to wave magnitude. Further, preliminary data shows that cliff flexure patterns derived from the Orkney seismic dataset are consistent with data from four previous studies where cross-shore seismic data has been collected. This suggests that coastal cliffs have a universal and characteristic response to wave action, such that cliff strain patterns can be predicted from measurements of displacement measured at the cliff face.

4. Cliff displacement as a proxy for rock fatigue

We hypothesize that both the magnitude of cliff displacement and patterns in cliff flexure will evolve with time as rock damage develops via low-magnitude, cyclic cliff flexure. Preliminary data confirm this hypothesis, indicating temporally coherent variations in the relationship between the intensity of cliff displacement and wave height, implying damage accumulation due to repetitive stressing of the cliff rock. Additionally, we find that, while insensitive to wave magnitude, the decay in cliff displacement landward also increases through time, suggesting more efficient loss of energy. We suggest that this energy may be consumed by an increased in the role of brittle fracture processes related to damage accumulation.

5. Conclusions and implications for sea cliff failure

Through the analysis of passive seismic data from sea cliffs on the Orkney Islands, we find:

- Larger waves increase intensity of cliff shaking
- Cliff flexure is insensitive to wave magnitude
- Spatial cliff displacement patterns may be universal across rocky coasts
- Temporal variations in cliff displacement patterns suggest damage accumulation via rock fatigue due to cyclic cliff flexure in response to wave action

These preliminary observations from Orkney, paired with previous work from four other sites, suggest that patterns of cyclic cliff flexure may be universal across many rocky coasts, and, as such, could act as a significant driver of cliff erosion and retreat.

Processes and Properties of Return-Flow Channels Cut Into San Jose Island During Hurricane Harvey, Texas, USA, August 2017

A. Ruangsirikulchai, D. Mohrig, K. Wilson and H.J. Hassenruck-Gudipati

Jackson School of Geosciences, The University of Texas at Austin, Austin, Texas, USA. mohrig@jsg.utexas.edu

1. Introduction

On August 25, 2017, Hurricane Harvey made landfall at the northeast end of San Jose Island, central Texas, USA. Offshore-directed winds on the left side of the eye caused bay water to pile up against aeolian dune ridges immediately adjacent to the beach (Fig. 1a). A wrack line of organic detritus on the landward sides of these dunes documented water-surface elevations ~ 3.8m above sea level. In addition, ADCIRC hindcast values for storm-driven water levels predicted water-surface elevations ~ 0.5m lower on the seaward than landward side of the island (Goff et al., 2019). This seaward-sloping water surface drove flow across the island and out into the Gulf of Mexico, and return-flow channels cut into the island (Fig. 1b).

2. Observations and hydrodynamic modelling

Seaward flow across the island scoured 31 channels to depths below mean lower low water. Fifteen of these channels can be seen in Figure 1b. With antecedent dune topography up to 6m in height and deepest scours as much as 2m below sea level, channels were associated with removal of columns of sand, meters in thickness. Oriented perpendicular to the coastline, trunk channels were up to 450m in length and 140m in width. Side channels oriented at right angles to trunk channels followed the swale between dune ridges. Median grain size for eroded island deposits was very fine or fine sand. The locations of channel heads spatially correlated with a change in vegetation and root density.

The ANUGA hydrodynamic modelling suite was run using the pre-storm topography (Fig.1a) and estimated water-surface elevations as boundary conditions. Model results point to the importance of (1) variability in dune-ridge topography on selection of channel locations, (2) topographically enhanced lateral flow in side-channel development, and (3) competing flow capture by adjacent channels in setting final channel size.

3. Conclusions

Within six months, a laterally continuous beach had rebuilt across the seaward-most necks of all channels. Since then, repeat measurements document no systematic filling of channels landward of this point, indicating persistence in the coastal landscape.

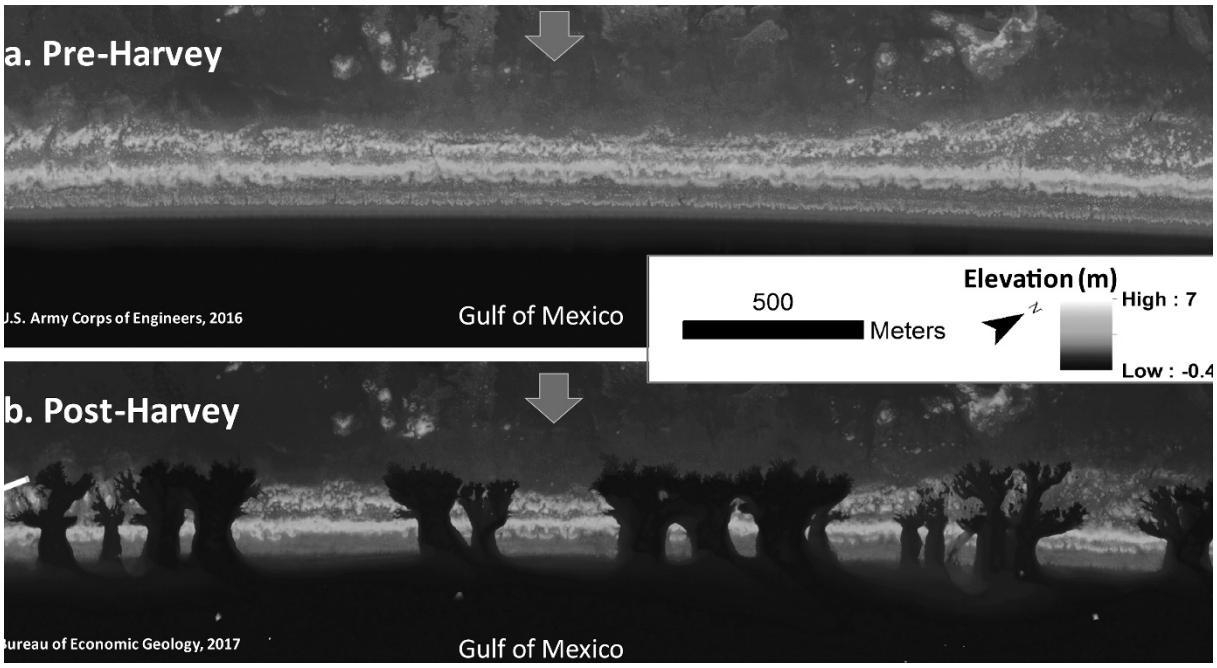

Figure 1. Images from two airborne lidar surveys collected shortly before (a) and after (b) Hurricane Harvey. Arrows point from bay-ward to seaward side on San Jose Island. (b) Return-flow channels cut into aeolian dune ridges and washover deposits by seaward-directed flow on the left side of hurricane. Notice the appearance (far left) of a large, rectangular barge that was ripped from its bay mooring and transported to the landward side of the dune ridge.

Acknowledgments

Funding provided by the Jackson School of Geosciences and a UT Undergraduate Research Fellowship. We thank J.M. Swartz for help with the airborne lidar surveys.

References

Goff, J.A., Swartz, J.M., Gulick, S.P.S., Dawson, C.N., and de Alegria-Arzaburu, A.R. (2019). An outflow event on the left side of Hurricane Harvey: Erosion of barrier sand and seaward transport through Aransas Pass, Texas. *Geomorphology*, 334(June): 44–57.

The role of bank height and near-bank water depth on bank failure patterns in tidal channels

Kaili Zhang[1], Zheng Gong[2], Kun Zhao[1], Keyu Wang[1]

[1] Jiangsu Key Laboratory of Coast Ocean Resources Development and Environment Security, Hohai University, Nanjing 210098, China.zhangkaili@hhu.edu.cn, zk1357@hhu.edu.cn, keyu_wang97@163.com
[2] State Key Laboratory of Hydrology-Water Resources and Hydraulic Engineering, Hohai University, Nanjing 210098, China. gongzheng@hhu.edu.cn

1. Introduction

Tidal channels on muddy flats with low vegetation cover are characterised by significant flow-induced bank erosion and consequently gravity-induced bank failure (Gong et al., 2018). The failure patterns (e.g., toppling, shear-type and tension failure) of tidal channel banks are subject to both bank height and near-bank water depth. Although some of the physical and numerical experiments have been conducted to investigate the effects of bank height and near-bank water depth on bank stability (Chu-Agor et al., 2008; Nardi et al., 2012), few of them attempt to combine these two factors and to define a threshold judging the type of bank failure. Here, on the basis of experiments evidences, we propose a numerical model to simulate the process of bank failure, taking into account the transition between saturated and unsaturated soil.

2. Methodology

In this research, ABAQUS software, version 6.14, was used to model the stress-strain behaviour of overhanging blocks resulting from flow-induced bank erosion. The dimensionless parameter *R*, defined as the bank height divided by near-bank water depth, is used to quantify the coupled effects of bank height and near-bank depth. To study the relation between bank failure type and *R*, eight series of numerical experiments (24 cases) on bank failure are performed with different bank height and near-bank water depth (Table 1).

Run ID	Bank height (cm)	R
Run A	100	4/2/1.3
Run B	80	4/2/1.3
Run C	70	4/2/1.3
Run D	60	4/2/1.3
Run E	50	4/2/1.3
Run F	40	4/2/1.3
Run G	30	4/2/1.3
Run H	20	4/2/1.3

Table 1: Parameters applied in each numerical experiment.

3. Results

We have conducted several physical experiments with different bank height (20cm, 40cm and 60cm) and near-bank water depth (15cm and 30cm). Laboratory experiment results show that for large bank height (e.g., bank height=60cm), bank failure is characterised by toppling (Fig. 1). Since near-bank water depth provides hydrostatic pressure, the volume of the collapsed bank soil decreases with increased near-bank water depth. In the context of small bank height (e.g., bank height=20cm), mass failure (e.g., toppling or shear-type failure) is absent and instead bank soil gently moves down into the water under gravity. This phenomenon is similar to soil creep reported in salt marsh channels (Mariotti et al., 2016). Numerical results indicate that soil cohesion in the middle of the bank decreases significantly with the decreased *R*. Since soil favors creep rather than torque in the case of small soil cohesion, mass failure is absent when *R* approaching 1.

Figure 1. Images of toppling failures as observed in the physical models with bank height of 0.6m and near-bank water depth of 0.15m.

Acknowledgments

National Natural Science Foundation of China (No. 51620105005, No. 51879095) and funding from the Graduate Student Innovation Project (No. 2018B638X14) is gratefully acknowledged.

References

Chu-Agor, M.L., Fox, G.A., Cancienne, R.M., and Wilson, G.V., 2008, Seepage caused tension failures and erosion undercutting of hillslopes: Journal of hydrology, v. 359, p. 247-259.

Gong, Z., Zhao, K., Zhang, C., Dai, W., Coco, G., and Zhou, Z., 2018, The role of bank collapse on tidal creek ontogeny: A novel process-based model for bank retreat: Geomorphology, v. 311, p. 13-26.

Mariotti, G., Kearney, W.S., and Fagherazzi, S., 2016, Soil creep in salt marshes: Geology, v. 44, p. 459-462.

Nardi, L., Rinaldi, M., and Solari, L., 2012, An experimental investigation on mass failures occurring in a riverbank composed of sandy gravel: Geomorphology, v. 163-164, p. 56-69.

Study on Estimation of bank erosion possibility in steep slope river channel －A Case study on Otofuke River in Japan －

Kazunori Okabe [1], Yasuyuki Shimizu [2], Tomoko Kyuka [3],
Kazuyoshi Hasegawa [4], Kho Shinjo [5] and Satomi Yamaguchi [6]

[1] Graduate school of the Engineering, Hokkaido University, Japan. k.okabe@ric.or.jp
[2] Graduate school of the Engineering, Hokkaido University, Japan. yasu@eng.hokudai.ac.jp
[3] Graduate school of the Engineering, Hokkaido University, Japan. t_kyuka@eng.hokudai.ac.jp
[4] Hokkaisuiko Consultant Corporation, Japan. k-hasegawa@suiko.jp
[5] Hokkaisuiko Consultant Corporation, Japan. k-shinjo@suiko.jp
[6] Civil Engineering Research Institute for Cold Region, Japan. kawamura-s@ceri.go.jp

1. Introduction

Disasters related to record breaking rainfall that may be caused by climate change have been increasing in recent years. Steep gradient rivers located in upstream basin are facing serious damages such as bank erosion, levee breaches and abutment damages. To prevent serious flooding damages caused by bank erosion and establish countermeasures for an erosion risk in such steep gradient rivers, it is important to predict and understand the patterns, locations, and scales of bank erosion due to the meander shift related to flooding events. However, the basic mechanisms to accelerate drastic and rapid channel migration (including bank erosion risk) in a steep gradient channel are unclear.

Channel meander in steep gradient rivers is affected by various hydraulic parameters such as original channel form, hydrograph, bed materials, patterns of growing vegetation, location of levee and revetments. In this study, we focused on a rapid, large channel meandering of the Otofuke River, Hokkaido, Japan that occurred in August 2018 as shown in Figure 1. In this area, the channel flow path expanded, and seven levee breaches were observed in one night due to the record-breaking rainfall. The timing was when the flow rate decreased, and it was the same as the previous report related to the levee breaches in the Otofuke River (Nagata et al., 2014; Iwasaki et al., 2016). The objectives of this study are to estimate the relationships between hydrograph shape and channel morphodynamics in steep gradient rivers by means of computational analysis.

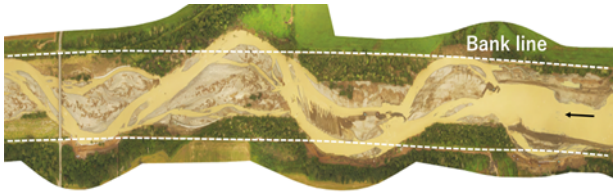

Figure 1. Disaster situation of the Otofuke River (Sep 15, 2016), White line: bank lines before flood

2. Investigation Methods

Numerical experiments are conducted using 2-dimensional shallow water flow model, Nays2D in iRIC, in which the reproducibility had been confirmed using DEM data of before and after the flood. The discharge hydrographs used were (a) observed one as a basis and modified as, (b) arriving peak discharge earlier, (c) arriving peak discharge later, and (d) increasing peak discharge larger, in which time integrated total volume of the discharge was kept constant, as shown in Figure 2.

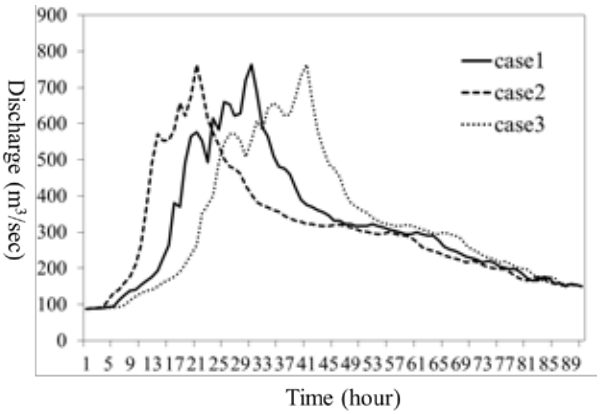

Figure 1. Hydrograph in the numerical simulation, Case 1, Case 2, and Case 3.

Based on the calculated results of these 4 cases, we compared the time dependent and special distributions of boundary shear stress, bed load transport rate, bank and bottom erosion width, and deposition rates.

3. Conclusion

The results showed that, both the shape of channel path and the locations of levee breach were almost same even if the timing of peak discharge was shifted under the same total flow and same peak discharge conditions.
Moreover, integrated flow rate and sediment transport rate until the breach was also substantially similar in each case.

Under this numerical condition, there is a possibility that the duration of high water is strongly influenced on channel formation than the peak flow rate itself.

References

Iwasaki, T., Shimizu, Y., Kimura, I. (2016). Numerical simulation of bar and bank erosion in a vegetated floodplain: A case study in the Otofuke River. Advances in Water Resources, 93, pp.118-134.

Nagata, T., Watanabe, Y., Yasuda, H., Ito, A., 2014. Development of a meandering channel caused by the planform shape of the river bank. Earth Surf. Dynam. 2, 255-270. https://doi.org/10.5194/esurf-2-255-2014.

How does marsh edge erosion vary across salinity gradients?

K. Valentine[1], G. Bruno[1], T. Quirk[1] and G. Mariotti[1]

[1] Department of Oceanography and Coastal Sciences, College of the Coast and Environment, Louisiana State University, Baton Rouge, Louisiana, USA. kvalen7@lsu.edu

1. Introduction

Considerable research has focused on wave impacts on the erosion of the marsh edge [*Schwimmer 2001, Marani et al. 2011, Leonardi et al. 2016, Bendoni et al. 2016*]. Wave power is the primary driver of how fast the marsh edge erodes, although much of the variability in the rate of erosion cannot be explained by waves [*Priestas et al. 2015*]. Field studies often attribute variability in erosion rates to vegetation [*Le Hir et al. 2007*] and soil characteristics [*Feagin et al. 2009*]. Models of coastline erosion typically incorporate all factors of marsh strength into one correction that is used as a calibration parameter. Not only is this value difficult to determine without extensive field experiments, but by using one value, the variability in individual marsh properties is largely ignored. This variability is further intensified in estuaries, where salinity gradients drive differences in soils and vegetation. The goal of this study is to determine how salinity gradients drive variability in erosion in estuarine marsh settings and how this can be incorporated in models of marsh erosion.

2. Methods

To explore how salinity gradients modify marsh edge erosion, we used Barataria Bay, Louisiana, USA as a case study. This estuary features fresh marsh in the north, and gradually transitions to salt marsh near the outlet (Figure 1). Forty-eight cores were collected in brackish and saline marshes within the estuary and were analysed for sediment and vegetation properties. We modified a wind-driven marsh edge erosion model [*Valentine and Mariotti 2019*] to allow for different erodibility coefficients depending on the salinity zone within an estuary, using the core data as validation for variations in erodibility.

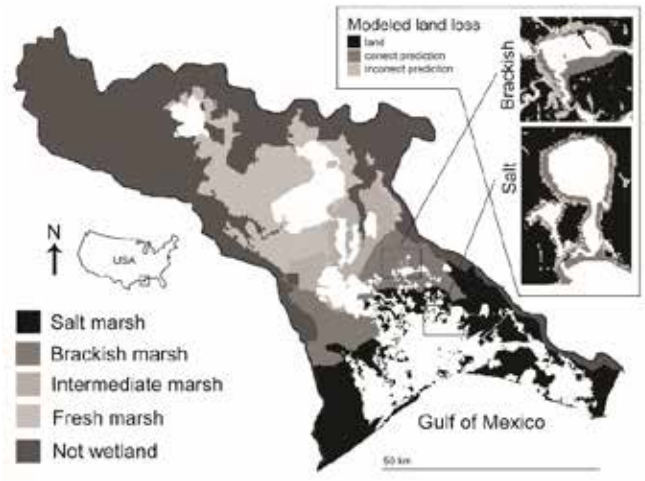

Figure 1: Marsh salinity in Barataria Basin. Inset shows modeled land loss results calibrated to a salt marsh. Erosion is predicted well in the salt marsh, but not in the brackish marsh (arrow indicates area of mismatch).

3. Results

A single erodibility parameter for the entire estuary yields poor estimates of edge erosion when comparing between salinity regimes. For example, if the model is calibrated to a salt marsh erodibility parameter, erosion at the marsh edge in intermediate and brackish marshes is underestimated (Figure 1). Allowing the erodibility of the marsh to depend on the salinity zone allows for a better prediction of wind-wave driven marsh edge erosion.

3. Conclusions

Accounting for variations in marsh type, in marsh edge erosion models through variations in erodibility improves model performance.

Acknowledgments

This research was made possible by a grant from the Gulf of Mexico Research Initiative.

References

Bendoni, M., Mel, R., Solari, L., Lanzoni, S., Francalanci, S., and H. Oumeraci, 2016, Insights into lateral marsh retreat mechanism through localized field measurements, *Water Resources Research* 52(2): 1446-1464.

Feagin, R.A., Lozada-Bernard, S.M., Ravens, T.M., Moller, I., Yeager, K.M., and A.H. Baird, 2009, Does vegetation prevent wave erosion of salt marsh edges?, *PNAS* 106(25): 10109-10113.

Le Hir, P., Monbet, Y., and F. Orvain, 2007, Sediment erodibility in sediment transport modelling: can we account for biota effects?, *Cont. Shelf Res.* 27(8): 1116-1142.

Leonardi, N., Ganju, N.K., and S. Fagherazzi, 2016, A linear relationship between wave power and erosion determines salt-marsh resilience to violent storms and hurricanes, *PNAS* 113(1): 64-68.

Marani, M., d'Alpaos, A., Lanzoni, S., and M. Santalucia, 2011, Understanding and predicting wave erosion of marsh edges, *GRL* 38(21).

Priestas, A.M., Mariotti, G., Leonardi, N., and S. Fagherazzi, 2015, Coupled wave energy and erosion dynamics along a salt marsh boundary, Hog Island Bay, Virginia, USA, *Journal of Marine Science and Engineering* 3: 1041-1065.

Schwimmer, R.A., 2001, Rates and processes of marsh shoreline erosion in Rehoboth Bay, Delaware, USA, *Journal of Coastal Research* 17(3): 672-683.

Valentine, K., and G. Mariotti, 2019, Wind-driven water level fluctuations drive marsh edge erosion variability in microtidal coastal bays, *Cont. Shelf Res.* 176: 76-89.

Chenier dynamics at an eroding mangrove-mud coastline in Demak, Indonesia

S.A.J. Tas[1*], D.S. van Maren[1,2] and A.J.H.M. Reniers[1]

[1] Civil Engineering and Geosciences, Delft University of Technology, the Netherlands. *s.a.j.tas@tudelft.nl
[2] Deltares, Delft, the Netherlands.

1. Introduction

The erosion of mangrove-mud coasts is a serious problem worldwide, affecting millions of people in their daily life. This research is part of the BioManCO project, which aims at unravelling key mechanisms responsible for the dynamics of (eroding) mangrove-mud coasts, and develop guidelines and tools to restore and protect such coastlines. The mangroves in Demak, Indonesia are fringed on their seaward side by cheniers (see Figure 1). A chenier is defined as a beach ridge, resting on silty or clayey deposits, which becomes isolated from the shore by a band of tidal mudflats (Augustinus, 1989). This work focuses on the role of cheniers in the dynamics of mangrove-mud coasts.

Figure 1. Drone photo of a chenier in front of the Demak coastline, Indonesia, December 2018 (Tas, 2018)

Satellite observations (van Bijsterveldt, 2015) reveal that cheniers reduce degradation rates of the mangroves. Cheniers create shelter, in which mangrove vegetation can recover and stabilise the coastline. However, cheniers can be extremely dynamic and little is known about the dynamics of cheniers in this area.
Therefore, the research questions this work aims to answer are: How do cheniers develop in general and along the eroding mangrove-mud coast of Demak, Indonesia? Which mechanisms are responsible for their generation, migration, and disappearance?

1.1 Hypotheses on the development of cheniers

Three mechanisms have been identified that may be responsible for the formation of the cheniers in Demak:

Hypothesis 1: Cross-shore, wave-driven Fines are washed out of the bed by wave action. The coarser particles are concentrated in a longshore bar, which migrates landward by wave asymmetry.

Hypothesis 2: Longshore Cheniers are formed as a river mouth spit and are transported alongshore by waves and/or tidal processes.

Hypothesis 3: Cross-shore, tide-driven Cheniers are formed in response to an increase in the tidal prism (resulting from flooding of the hinterland), which strengthens tidal currents.

2. Methods

2.1 Hydro- and morphodynamic field survey

An intensive field survey was conducted between October and December 2018 in Demak, Indonesia. The experiments were aimed at measuring the hydro- and morphodynamics of one single chenier.

2.2 Numerical modelling of the development and evolution of cheniers in one cross-section

The data of the fieldwork is used to set up and validate a numerical model in Delft3D. In a first phase, a 1D/2DV model is set-up (one cross-section, perpendicular to the coastline), which can be used to test hypotheses 1 and 3, as well as to perform a sensitivity analysis on the processes affecting such cheniers. In a second phase, this model will be extended to 2DH/3D.

3. Results

Despite the timing of the field survey around the start of the stormy NW monsoon season, no storms or extreme events were observed. In fact, wave heights rarely exceeded 0.5 m at a water depth of 12 m. Nevertheless, large changes have been observed in the chenier, with erosion and accretion up to 1 m at certain locations. Although the Demak coastline has a micro-tide (tidal range around 0.5 m), the most significant changes occurred around spring tide. While most coastal sandy ridges are wave-driven, it seems that cheniers can also be dominated by the tide.
During the field survey, no new cheniers have formed. Therefore, the generation of cheniers has been investigated through numerical modelling and remote sensing.

Acknowledgments

This work is part of the BioManCO project with project number 14753, which is (partly) financed by NWO Domain Applied and Engineering Sciences. The BioManCO project makes use of the framework set up by Building with Nature Indonesia, which is a programme by Ecoshape, Wetlands International, the Indonesian Ministry of Marine Affairs and Fisheries (MMAF), and the Indonesian Ministry of Public Work and Human Settlement (PU), in partnership with Witteveen+Bos, Deltares, Wageningen University & Research Centre, UNESCO-IHE, Blue Forests, and Von Lieberman, with support from the Diponegoro University, and local communities.

References

Augustinus, P. G. E. F. (1989). Cheniers and chenier plains: A general introduction. *Marine Geology*, 90(4):219–229.

van Bijsterveldt, C. E. J. (2015). *Natural mangrove restoration: how can it be induced?* Master thesis, Universiteit Utrecht.

Grain-Scale Roughness Classification in the Laboratory

C. Rachelly[1], V. Weitbrecht[1] and R.M. Boes[1]

[1] Laboratory of Hydraulics, Hydrology and Glaciology (VAW), ETH Zurich, Zurich, Switzerland.
rachelly@vaw.baug.ethz.ch

1. Introduction

The distribution of grain-scale roughness on river beds is of significant interest, among others, for restoration science. Several studies have shown that surface patchiness is closely linked to sediment supply (e.g. Nelson et al., 2009). Within a research project focusing on dynamic river widening processes under variable sediment supply conditions, an automated and robust measure of surface patchiness in laboratory flumes is developed. The resolution of the digital elevation model (DEM) generated by terrestrial laser scanning (TLS) is too low to directly evaluate grain-scale roughness, which is approximated by the standard deviation of point elevations σ_Z. However, the grain-scale roughness determined for selected areas of interest (AOI) with higher DEM resolution can be correlated to the values of the low-resolution DEM and therefore allows the classifiction of grain-scale roughness across the entire flume with limited measurement effort.

2. Methods

The workflow is presented using the example of a flume experiment with alternate bars in equilibrium condition. The mobile bed and feed material consisted of sediment grains of D_{50} = 1.94 mm, D_{90} = 6.27 mm, and σ_g = 3.8 and developed a distinct patchiness of coarse bar tops and fine pools. The topography was scanned with a Leica P15 TLS and transformed into a 10x10 mm DEM, a grid size close to the maximum grain diameter.

Over the course of several experiments, eight 100x100 mm AOIs were selected for the detailed evaluation of grain-scale roughness. Structure from Motion and MultiView-Stereo (SfM-MVS) were applied (Agisoft LLC., 2018) and the resulting 0.1x0.1 mm DEM was separated into grain and bedform vertical roughness with the methodology described in Bertin et al. (2017). The technique includes the application of a circular averaging filter with a diameter value dependent on the D_{90} of the analyzed surface. The grain size distribution of each AOI was determined by removing the uppermost sediment layer either with an adhesive surface or by manual extraction and subsequent square-hole sieving.

2.1 Results

The grain-scale roughness $\sigma_{Z,G}$ determined in detail for eight AOIs was linearly related to the total roughness σ_Z obtained from the low-resolution DEM of the same AOIs.

$$\sigma_{Z,G} = 1.49\sigma_Z - 0.74 \qquad (R^2 = 0.87) \qquad (1)$$

Figure 1 shows the topography of an alternate bar sequence in the experimental flume and the grain-scale surface roughness determined for the same reach based on eq. (1), discretized as 100x100 mm tiles. The coarse bar tops are clearly visible and finer patches follow the thalweg. The lateral expansion of the fine patches decreases in the pools and widens on the riffles.

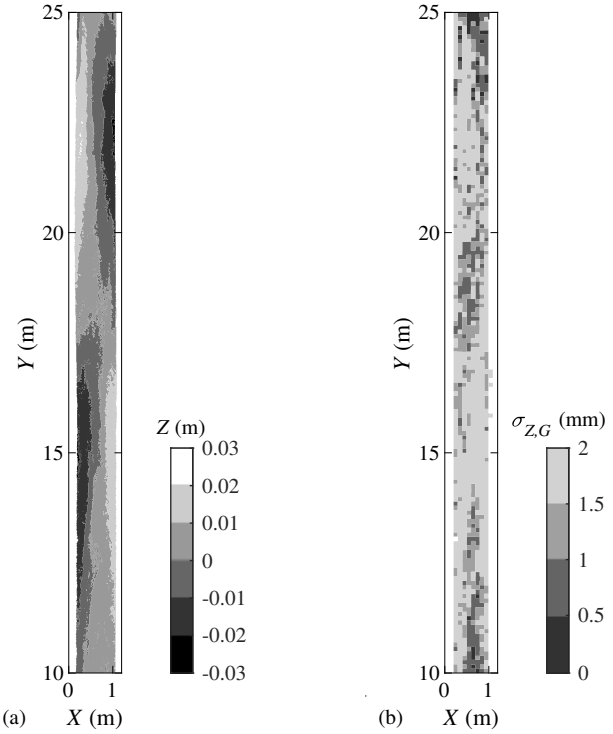

Figure 1. (a) Topography of an alternate bar sequence with (b) its surface grain-scale roughness.

3. Conclusions

The presented methodology shows how detailed information on grain-scale surface roughness may be obtained from a rather low-resolution DEM. The results generally represent the visually observed roughness distribution well, but a quantitative validation is pending. To further refine the workflow, future work will include a higher number of AOIs, a detailed exploration of the application range of the presented relation, and thorough validation by manually mapping the surface roughness distribution.

Acknowledgments

This research project is part of the interdisciplinary research program *Riverscapes - sediment dynamics and lateral connectivity* and the first author is financially supported by the Swiss Federal Office for the Environment (FOEN), Grant 16.0113.PJ/P501-1050.

References

Agisoft LLC. (2018). Agisoft Photoscan and Metashape (v 1.4.2 and v 1.5.1).

Bertin, S., Groom, J., and Friedrich, H. (2017). Isolating roughness scales of gravel-bed patches. *Water Resour. Res.*, 53:6841–6856. doi:10.1002/2016WR20205.

Nelson, P., Venditti, J., Dietrich, W., Kirchner, J., Ikeda, H., Iseya, F., and Sklar, L. (2009). Response of bed surface patchiness to reductions in sediment supply. *J. Geophys. Res. Earth Surf.*, 114. F02005, doi:20.1029/2008JF001144.

Estimating the attenuation of sound by sediment using a tilted ADCP transducer

J.Y. Poelman[1], A.J.F. Hoitink[1]
[1] Hydrology and Water Management Group, Wageningen University, Wageningen, the Netherlands.
judith.poelman@wur.nl

1. Introduction

Observations of sediment fluxes are essential for the understanding of observed morphological trends and the calibration and validation of numerical models that are used to predict (long-term) development of river systems. A well-accepted method to assess suspended load transport is to infer the suspended sediment concentration (SSC) from ADCP backscatter. This method requires relatively little effort, especially because ADCPs are regularly employed for discharge measurements, and offer a high spatial and temporal resolution.
However, the inversion of backscatter intensity to SSC requires extensive calibration, as the intensity of the acoustic signal does not depend on concentration, but also on the particle size distribution (PSD) and other parameters. In fine-grained rivers, mainly the coarse fraction (sand) contributes to backscattering, whereas the fine fraction (silt, clay) is not sensed, but it does affect the signal through attenuation. We aim to develop a method to estimate the attenuation of sound by sediment, by using a tilted transducer.

2. Approach

The estimation of attenuation is based on the assumption that the SSC and the particle size distribution (PSD) are horizontally homogeneous (over the distance between two beams). Attenuation is then estimated based on the sonar equation (Eq.1), which provides a relation of backscatter intensity, I, and instrument and sediment properties (Thorne and Hanes, 2002):

$$I = p_0^2 r_0^2 \frac{k_t^2 k_s^2 M_s}{r^2 \phi^2} e^4 (\alpha_w + \alpha_s) r$$

where α_w is the suspended sediment attenuation coefficient. With instrument and sediment properties know or equal between beams, the difference in received backscatter intensity between two beams I_1 and I_2 can now be attributed to attenuation over Δr (Figure 1).

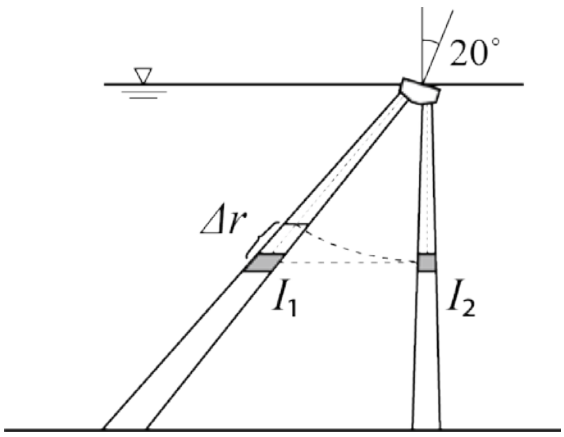

Figure 1: A conceptual drawing of an ADCP with two of four beams.

2. Data

The method will be developed and tested based on data obtained at two different location: at a tidal junction in the Rhine-Meuse estuary and in the Ems-Dollard estuary (the Netherlands). In the Rhine-Meuse estuary, velocity and backscatter were measured with a vessel-mounted ADCP over one tidal cycle (13 hours). In the Ems-Dollard estuary, velocity and backscatter data were measured with two ADCPs mounted on a frame, placed at the bottom. The ADCPs measured for approximately eight days. SSC values from samples in the Rhine-Meuse estuary go up to 83mg/L, whereas samples from the Ems-Dollard estuary reach values up to 2000mg/L.

Figure 2: Variation of SSC, backscatter intensity averaged over the cross-section and discharge over time, in the Rhine-Meuse estuary.

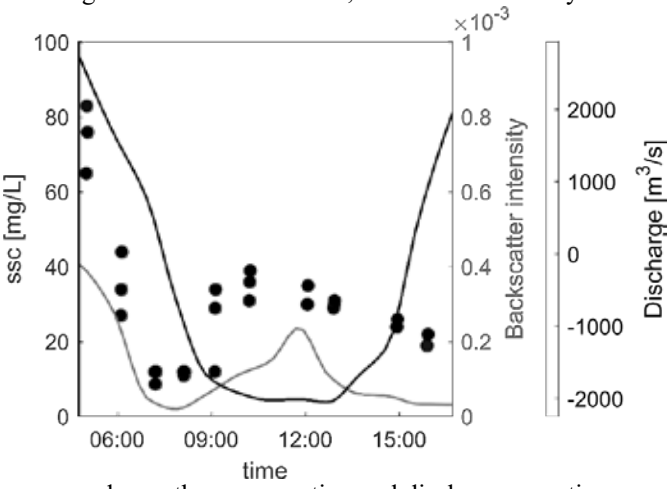

References

Thorne, P. D. and Hanes, D. M. (2002), A review of acoustic measurement of small-scale sediment processes, *Continental Shelf Research*, 22(4), 603–632. https://doi.org/10.1016/S0278 4343(01)00101-7.

Image-based 3D measurement of size, location, and orientation of gravel grains

M. Detert[1], C. Rachelly[1], L. Brezzi[2] and H. Biggs[3]

[1] ETH Zurich, VAW, Zurich, Switzerland. mdetert@ethz.ch | crachell@ethz.ch
[2] University of Padua, Dept. ICEA, Padua, Italy, lorenzo.brezzi@dicea.unipd.it
[3] NIWA, Christchurch, New Zealand, hamish.biggs@niwa.co.nz

1. Introduction

Earth's rivers transport over 10 billion tons of sediment each year. Quantifying the size distribution of sediment particles is essential to understand and predict many fluvial processes. Standard techniques such as laboratory sieving are labour intensive and provide limited spatial coverage. To overcome these limitations novel image-based methods have been developed. These methods are non-intrusive and low-cost, providing a more efficient way to obtain grain size distributions for coarse non-cohesive bed material (e.g., Buscombe et al., 2010; Detert and Weitbrecht, 2012). However, these approaches suffer from uncertainties when quantifying the geometry of 3D grains from 2D planform imagery. For water-worked gravel beds, issues arise due to foreshortening, overlapping, and imbrication of grains. A bulk grain size correction is only possible by empirical factors (Stähly et al., 2017). The use of Structure from Motion (SfM) techniques in combination with MultiView-Stereo (MVS) algorithms provide a promising tool to expand image-based grain size analysis to 3D (Detert et al., 2018). However, to the knowledge of the authors, no automated method has been developed and tested that is able to derive 3D size, location, and orientation of individual gravel grains out of images.

2. Methods

The steps for automatic 3D gravelometry are illustrated in Figure 1. Input data are comprised of a high-resolution 3D point cloud of a gravel patch obtained by SfM-MVS. An orthophoto is derived from the colour-values of the point cloud and then gets analysed by the free software BASEGRAIN (Detert and Weitbrecht, 2012). The separated top-view areas of individual grains are then transferred back to the 3D point cloud data. Next, ellipsoids are fitted to the 3D surface points of each separated grain. Finally, the ellipsoids are merged into the context of the initial gravel patch. The result gives an estimation of the grains' midpoint locations, orientations and axes lengths in 3D. The minimum grain size that can be resolved is not dependent on its absolute dimension (e.g., mm) but on the pixel resolution of the input images.

3. Outlook

In 2019 the following datasets will be analysed in more detail to test this methodology: (i) in-situ dry fine gravel from a laboratory scale model; (ii) dryly dumped coarse gravel; (iii) in-situ subaqueous gravel bed; and (iv) drone-based recorded coarse gravel bed. The main goal of this work is to demonstrate potential areas of application and to assess the limitations of this new technique.

Acknowledgments

Support by NIWA's 'Drone Flow Research Programme' (MBIE Grant: END19505) is gratefully acknowledged.

References

Buscombe, D., Rubin, D.M., and Warrick, J.A. (2010). A universal approximation of grain size from images of non-cohesive sediment. *J. Geophys. Res.*, 115(F02015).

Detert, M., and Weitbrecht, V. (2012). Automatic object detection to analyze the geometry of gravel grains – a free stand-alone tool. In R.M. Muños, editor, *River Flow 2012*, pages 595–600. London: Taylor & Francis.

Detert, M., Kadinski, L., and Weitbrecht, V. (2018). On the way to airborne gravelometry based on 3D spatial data derived from images *Int. J. Sed. Res.*, 33: 84–92.

Stähly, S., Friedrich, H., and Detert, M. (2017). Size ratio of fluvial grains intermediate axes assessed by image proc. and square hole sieving. *J. Hydr. Eng.*, 143(6).

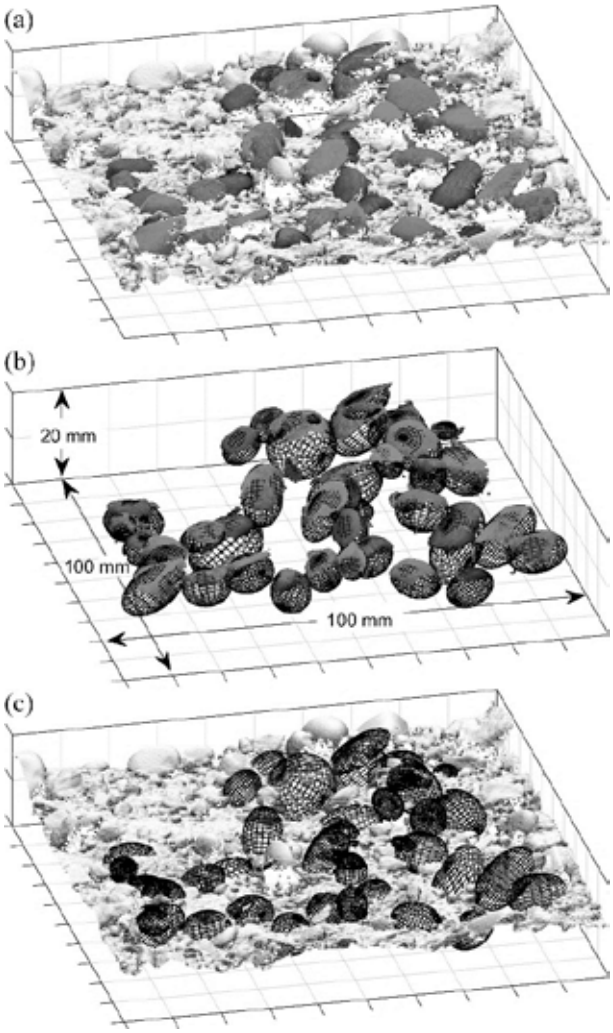

Figure 1: Steps of the method. (a) Separating single grains' 3D surface points based on their 2D coordinates found by BASEGRAIN, here exemplified for top view intermediate axes' lengths ≥ 5 mm, (b) Fitting ellipsoids, and (c) Merging the fits into the gravel bed context.

X-Ray CT Analysis of Vertical Porosity Variations in Sand-Gravel Mixtures

M. Tabesh[1,2], M. F Huguett Mejia[1], S. Vollmer[2], H. Schüttrumpf[1] and R.M Frings[1]

[1] Institute of Hydraulic Engineering and Water Resources Management, RWTH Aachen University, Aachen, Germany.
[2] Federal Institute of Hydrology, Koblenz, Germany.
tabesh@iww.rwth-aachen.de, maria.fiorella.huguett@rwth-aachen.de, vollmer@bafg.de, schuettrumpf@iww.rwth-aachen.de, frings@iww.rwth-aachen.de

1. Introduction

Sediment porosity (n) is one of the key structural properties of a river bed. It is defined as $n = V_p/V_t$, with V_p and V_t are the pore volume and total mixture volume, respectively. Porosity is vertically variable in sand-gravel mixtures, as the surface armor layer has a different sediment structure and grain size distribution than the fine subsurface layers. Although porosity measurement methods (Frings et al. 2011 and Tabesh et al. 2019, manuscript submitted to *Geomorphology*) provide values of bulk porosity, they do not provide information about porosity variations over depth. If such information is required, the sediment mixture must be stabilized prior to the sampling and the internal structure of the mixture must be mapped. In this contribution, we used X-Ray computed tomography (CT) to obtain non-destructive, vertical imaging of the sediment mixture structure to determine vertical porosity variations.

2. Description of the technique

To take undisturbed samples, sediment mixture must be first stabilized. Sample stabilization for sand-gravel mixtures is challenging, because of the absence of cohesion and the large sample volumes involved. It requires saturation of the pores of the sediment mixture with a quickly-solidifying liquid. We tested several stabilizer liquids (synthetic resin, sodium acetate and paraffin) in the laboratory, and found paraffin to be the most cost-effective and environmentally-friendly material which solidifies within few minutes. The stabilized sampling depth is related to the grain size distribution of sand-gravel deposits and the solidification duration. Therefore, our sample depths varied between 1 and 10 cm and can be increased by 25% by heating the sediment surface prior to paraffin application using a mobile heater. The paraffin volume shrinkage due to the changes from liquid to solid phase was measured in the laboratory to be 6 %, which was considered during the porosity calculation. Afterward, the stabilized samples (Figure1a) were transported to a specialized laboratory to scan the internal structure using 3D computed tomography. Using this process, gray-scale 3D images of the internal structure of samples with voxel resolution (three-dimensional analogue of a pixel) of 100 µm were obtained (Figure1b).

3. Vertical porosity variations

To evaluate the porosity of sediment sample from CT data, pores (includes paraffin) and grains must be distinguished from each other. For this purpose, the image segmentation method developed by Otsu (1979) was applied to create a threshold between pores and grains regions. During this process, the image was analyzed so that the grains were interpreted as white and pores as black areas (Figure 1b). By determining the number of voxels for each area, the porosity of the sediment sample was evaluated. Figure 1c shows a histogram of a CT image with two peaks indicating the two phases of grains and pores, and the defined threshold, which divides the sample into pores voxels and grains voxels.

To measure the vertical variation of porosity (Figure 1d), a subsampling region of 250 x 250 x 250 voxels (equivalent to 25 x 25 x 25 mm^3) was defined. Using a moving average, this subsample was moved every 50 voxels in the vertical direction. For each subsample the porosity value was calculated from the CT image following the image segmentation process shown in Figure 1d.

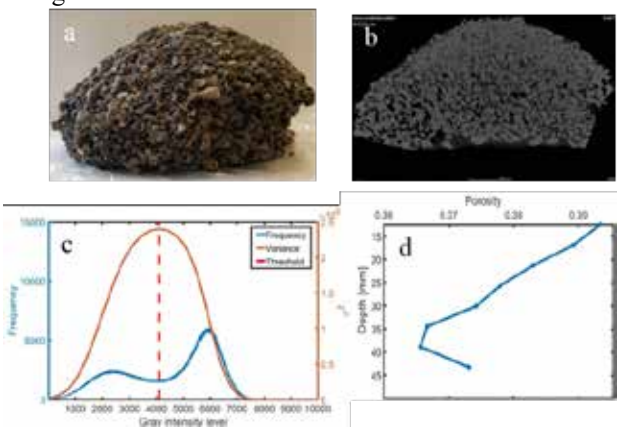

Figure 1: a) stabilized sediment sample, b) gray-scale image of internal structure of the sediment sample, c) histogram of gray-scale values of one subsample (n = 0.38) and defined threshold showed with red dash line, and d) vertical variation of the porosity.

4. Conclusions

Our method for porosity measurement combines sample stabilization using paraffin with X-Ray computed tomography (CT) to map the internal pore structure to determine vertical variation of the porosity. Our Tests in the laboratory showed this method to be a powerful tool for characterization of vertical variations of porosity.

References

Frings, R. M., Schüttrumpf, H., & Vollmer, S. (2011). Verification of porosity predictors for fluvial sand-gravel deposits. *Water Resources Research*, 47(7).

Tabesh, M., Hoffmann, T., Vollmer, S., Schüttrumpf, H. & Frings, R. M. (2019). In-situ measurement of river-bed sediment porosity using Structure-from-Motion image analysis. Submitted to *Geomorphology*.

Otsu, N. (1979). A threshold selection method from gray-level histograms. *IEEE transactions on systems, man, and cybernetics*, 9(1), 62-66.

Correlation of landslide area variation with occurrence of intensive rainfall events in an upstream region of the Midorikawa Reservoir, Japan.

K. Akiyama[1], S. Aoki[2], T. Ishikawa[3] and S. Takahashi[4]

[1] Token C. E. E. Consultants Co., Ltd, Tokyo Japan, akiyama-k@tokencon.co.jp
[2] Token C. E. E. Consultants Co., Ltd, Tokyo Japan, aoki-shi@tokencon.co.jp
[3] Tokyo Institute of Technology, workishikawa0612@yahoo.co.jp
[4] Token C. E. E. Consultants Co., Ltd, Tokyo Japan, takahashi-d@tokencon.co.jp

1. Introduction

Quantitative estimation of the stochastic feature of sediment influx becomes important for long-term reservoir management, with the frequency increase of intense rainfall due to the recent climate change. The total area of landslide spots is considered as an index to sediment yield in a reservoir catchment (Kawada and Uemoto, 1998). In this study, variation of the area of landslide spots upstream from the Midorikawa Reservoir which was built 45 years ago in Western Japan was estimated by image analysis of aerial photographs, and its dependency on the occurrence of intense rainfalls was discussed.

2. Study site

Figure 1 shows the study site. The reservoir is located near the Median Tectonic Line that runs the length of Western Japan. Landslide spots marked with dots in the figure are concentrated in the south half of the reservoir catchment where outcrop bands are formed by tectonic pressure. The image analysis was made for the watershed of Naidaijin River shown with a broken line in the figure where a lot of aerial photographs were available. The river catchment area is 44.2 km^2, and the altitude difference is 1,490m.

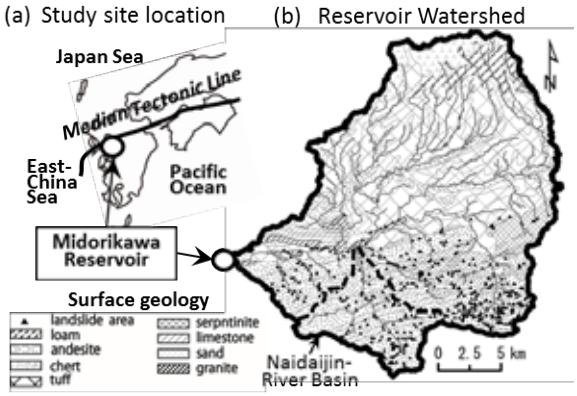

Figure 1: Study Site

3. Image analysis for landslide area

Ten Image data sets obtained from 1976 to 2016 were analysed after some fundamental data processing such as geometric correction, normalization of resolution and contrast, and removal of data influenced by diffused reflection. With the landslide spot data obtained from naked eye distinction for 2016 image data, the error ratio of image analysis was estimated for various threshold levels of relative luminance. From the results, $\sigma/\sigma_0 > 1.6$ was adopted to distinguish landslide spots from the surroundings, where σ is the luminance deviation from the mean value, σ_0 is the standard deviation.

4. Variation of landslide area

An equation to express the time variation of overall landslide area was assumed as follows:

$$Z(i) = Z(i-1) \cdot \exp(-\alpha \Delta t) + \beta \cdot R_j(i) \qquad (1)$$

where Δt is a time increment, $Z(i)$ is the landslide area at time step i. $R_j(i)$ is the cumulative rainfall amount when $R(t) > R_{pj}$, $R(t)$ is the time series of rainfall intensity and R_{pj} is a threshold to induce landslide. α is the reduction rate of Z when $R(t) < R_{pj}$, and β is a coefficient for response of Z to effective rainfall. R_{pj}, α and β are empirical parameters. Figure 2 shows the comparison of calculation results of two cases which have better results than others are shown with the results from image analysis. Figure 3 compares the annual sediment volume increase observed in the reservoir to the estimated overall landslide area shown in Figure 2. Although agreement is not enough in detail, timing and degree of large increments are well reproduced to some degree.

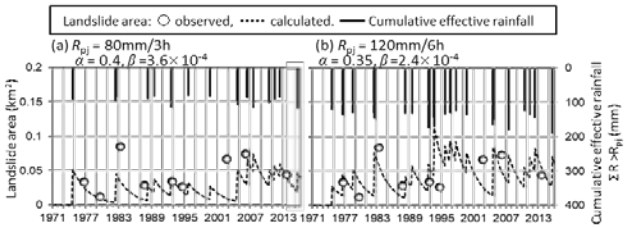

Figure 2: Test results of Equation 1

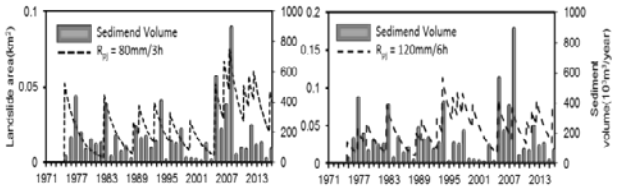

Figure. 3: Comparison with sedimentation in reservoir

5. Conclusion

This study showed the possibility that the variation of landslide area was related to the occurrence of intense rainfalls over some threshold as expressed by Equation 1. In addition, the variation of sediment influx to the reservoir had a rough correlation with the landslide area variation. Therefore, this kind of simple model would be useful for quantitative estimation of stochastic feature of sedimentation in a reservoir located in a small river basin.

References

Kawada, H. and Uemoto, M (1998). Control factors of reservoir sedimentation. Annual journal of Hydraulic Engineering, JSCE, Vol. 42, pp. 1027-1032.

Towards an understanding of sand-mud segregation in tidal basins

A. Colina Alonso[1], D.S. van Maren[1,2], Z.B. Wang[1,2] and P.M.J. Herman[1,2]

[1] Delft University of Technology, Delft, The Netherlands. A.ColinaAlonso@tudelft.nl
[2] Deltares, Delft, The Netherlands

1. Introduction

Anthropogenic interferences in tidal basins can irreversibly influence their morphological development and the large-scale sediment budgets. Examples of heavily impacted tidal basins are those in the Dutch Wadden Sea. The man-made partial closures of two tidal basins (the Zuiderzee in 1932 and the Lauwerszee in 1969) still influence the morphodynamics of the Wadden Sea basins (Wang et al., 2018), including the overall sediment budget. Key to understanding the impact of these interferences is how they influenced the sand balance and the mud balance. Establishing a realistic sediment balance for both sand and mud and determining how this balance was affected by the closures requires a better understanding of the mechanisms that determine the sand-mud patterns.

Analysis of recent field data shows that the Wadden Sea environments tend to be either mud-dominated or sand-dominated (see Figure 1). This suggests that we are dealing with a bistable system with two stable equilibrium states, and an unstable state in between (Herman et al., 2018). In this research we investigate physical mechanisms responsible for this bimodality.

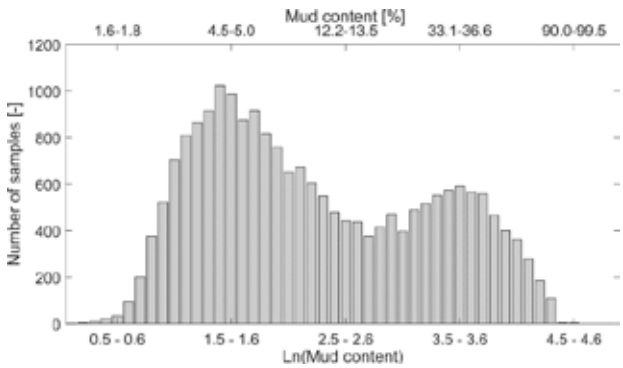

Figure 1: Distribution of the mud content in the Dutch Wadden Sea (data source: SIBES database 2008-2013)

2. Methods

We investigate the bimodality using a combination of data analysis and numerical modelling. Field data of spatial sand-mud patterns in the Dutch Wadden Sea dates back to the late 19th century. Since then, several datasets of the sediment types have been collected, allowing for a comparison of large-scale trends over the past 125 years. Additionally, simulations with a Delft3D model enable a study on the behaviour of sand-mud mixtures under various hydrodynamic forcing scenarios.

3. Results and conclusions

Fine-grained sediments tend to migrate from high-energy areas (channels) to low-energy areas (flats), and therefore many flats are muddy whereas channels are sandy. However, we do not yet know why transitions from muddy to sandy areas in basins as the Wadden Sea are fairly abrupt. Van Ledden (2003) established an equilibrium value for the mud content at the bed surface, based on the (critical) bed shear stresses, and the deposition and erosion capacity. From this, he concluded that sharp transitions exist when the mud deposition capacity is low (e.g. low suspended mud concentration).

Field data of the Wadden Sea reveal the existence of a threshold for the bed shear stress: Above this value, the bed consists of mainly sand with a very low mud content. Below this value, a large scatter in the mud content is observed. This shows that the mud content does not reach the theoretical equilibrium value.

Two physical mechanisms can explain the bimodality of the mud content in tidal basins. The erodibility of sand-mud mixtures influences the mud content such that a sediment sample with a high mud content will have a higher critical bed shear stress than a predominantly sandy sample. A sharp transition for the critical bed shear stress was found for a clay content around 7% (van Ledden, 2003). For the Wadden Sea, this corresponds to a mud content of 35%. Moreover, the hydraulic roughness decreases with decreasing sediment size in the surface layer of the bed, leading to lower bed shear stresses and hindering erosion in case of muddy beds. Besides the aforementioned physical mechanisms, ecological processes are also expected to contribute to the observed phenomenon.

The obtained insights on sand-mud mixtures are not only relevant to understand the natural sediment dynamics in the Wadden Sea; they are also applicable to many other systems, since large-scale sand-mud segregation is found in estuaries and tidal basins all over the world.

Acknowledgments

This project is funded by the Royal Netherlands Academy of Arts and Sciences (KNAW) within the framework of the Programme Strategic Scientific Alliances between China and The Netherlands, project PSA-SA-E-02.

References

Herman, P.M.J., van Kessel, T., Vroom, J., Dankers, P., Cleveringa, J., de Vries, B., Villars, N. (2018). Mud dynamics in the Wadden Sea. Report 11202177-000-ZKS-0011, Deltares, Delft.

Van Ledden, M. (2003). *Sand-mud segregation in estuaries and tidal basins* (PhD thesis). Delft University of Technology, Delft.

Wang, Z.B., Elias, E.P.L., Van der Spek, A.J.F.& Lodder, Q.L., 2018. Sediment budget and morphological development of the Dutch Wadden Sea-impact of accelerated sea-level rise and subsidence until 2100. Netherlands Journal of Geosciences, 97-3: 183-214.

A Model for Bedload Particle Motion Over Equilibrium Mobile Bedforms

T.C. Ashley[1], R.C. Mahon[2], S. Naqshband[3], K.C.P. Leary[4], and B.J. McElroy[1]

[1] University of Wyoming Department of Geology & Geophysics, Laramie, WY, USA. tashley3@uwyo.edu
[2] University of New Orleans Department of Earth & Environmental Sciences, New Orleans, LA, USA
[3] Wageningen University Department of Environmental Sciences, Wageningen, Netherlands
[4] UC Santa Barbara Department of Geography, Santa Barbara, CA, USA

1. Introduction

Probabilistic descriptions of particle motion represent a promising approach for developing large-scale morphodynamic models that are consistent with the physics of grain-scale sediment transport. However, experimental observations of particle motion on which these descriptions are based come almost exclusively from plane bed conditions. This is problematic because plane-bed topography is commonly unstable in alluvial rivers, leading to the development of bedforms.

Bedform topography is coupled with fluid flow, causing persistent zones of flow acceleration, expansion, and separation. This effect modulates the bed stress and sediment transport fields, which has a profound impact on particle behavior. Several recent studies show that instantaneous quantities like particle activity and velocity vary systematically in relation to topographic position, while retaining probability distributions that are similar to those observed under plane-bed conditions (Wilson and Hay, 2016). What remains unclear is how bedforms influence Lagrangian integral quantities like particle hop distance and travel time. These quantities are of primary importance in morphodynamic models because they are the centerpiece of the enrainment form of the Exner equation, a precise probabilistic statement of mass conservation that encapsulates the relationship between topographic evolution and sediment transport.

We report the results of experiments designed to clarify how bedforms influence the joint probability distribution of particle travel time, streamwise hop distance, and lateral hop distance. This is accomplished using videos of fluorescent tracer particles recorded under two conditions differentiated primarily by the presence or absence of equilibrium bedforms. Measured distributions are compared with probability distribution models proposed by Fathel et al. (2015).

2. Experiments

Particle tracking experiments were conducted in a laboratory flume capable of recirculating sediment and water. The bed was seeded with fluorescent tracer particles which were illuminated with ultraviolet light and recorded using a downward looking camera. Particle motions were measured over equilibrium bedforms and artificially-graded plane-bed topography without changing other boundary conditions like water discharge, outlet flow depth, or flume slope. The full data set comprises 360 hops for the plane-bed condition and 1170 hops for the bedform condition (Figure 1). Probability distributions were fit to these data using Bayesian estimation, and distribution fits were evaluated qualitatively using histograms and quantile-quantile plots.

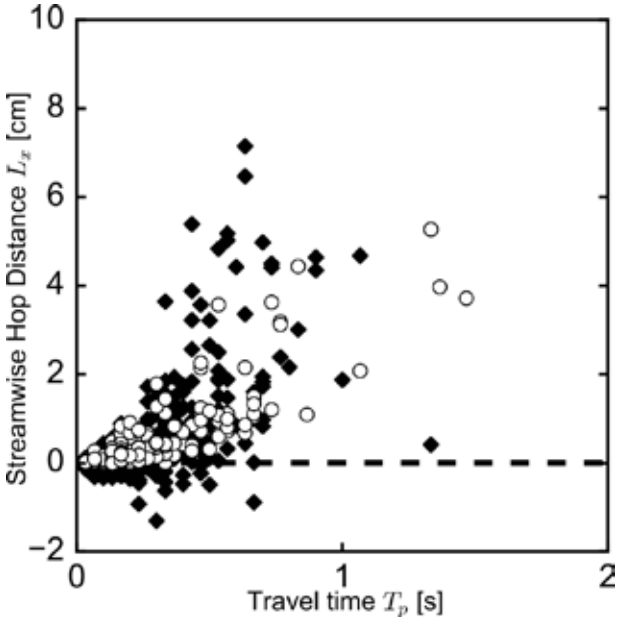

Figure 1. Measurements of particle travel time and streamwise hop distance over bedforms (diamonds) and plane-bed topography (circles). Dashed line corresponds to a streamwise hop distance of 0.

3. Conclusions

We find that measured probability distributions are similar in form and scale in both experiments with subtle but important differences. Qualitative observations reveal that a much larger fraction of hops occur in the upstream direction when bedforms are present, and there is more variability in transport direction. These observations correspond to an increased coefficient of variation (the ratio of the standard deviation to the mean) of particle hop distance, which is like a Peclet number in that it determines the relative importance of advective-like and diffusive-like transport. This means that bedforms increase the importance of both streamwise and lateral diffusion.

References

Fathel, S. L., Furbish, D. J., and Schmeeckle, M. W. (2015). Experimental evidence of statistical ensemble behavior in bed load sediment transport. *J. Geophys. Res. F Earth Surf.*, 120(11):2298–2317.

Wilson, G. W. and Hay, A. E. (2016). Acoustic observations of near-bed sediment concentration and flux statistics above migrating sand dunes. *Geophys. Res. Lett.*, 43(12):6304–6312.

Macrorugosities as promotors of the sediment movement

Bateman, A.[1]; Sosa, R.[1]; Onorati, B[2], Marín-Esteve, B.[1]

[1] GITS-UPC. Universitat Politècnica de Catalunya, Catalonia. allen.bateman@upc.edu.
[2] Scuola di Ingegneria. Università degli Studi della Basilicata, Italia.

1. Introduction

One of the most complex topics in hydraulics is the flow resistance. It is due to the interaction between the flow and the obstacles that finds in its way. Roughness produces a momentum exchange that results in what we know as Turbulence. Turbulence can also be produced by the addition of a local external force on the flow mass. When the flow impacts over the macrorugosity it tends to accelerate and change its direction. One of the consequences of this force exchange is the creation of vortexes; some of them would be able to produce bed shear stresses stronger than the natural ones. Nikuradse (1926), Sayre and Albertson (1961), Aguirre et al. (1986), Koloseus and Davidian (1966), Christodoulo (2014) are some of the authors that have already studied macrorugosities in firm bed.

The idea of this study is to test the efficiency of these macrorugosities for generating sediment transport in flows where the sediment is unable to move.

2. Experiments description

Different macrorugosities were tested, see Figure 1.

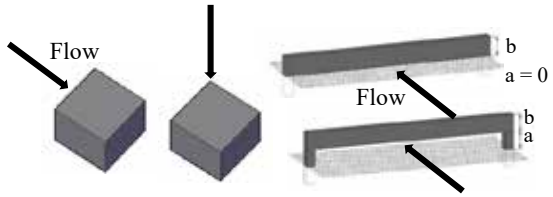

Figure 1: Examples of the analyzed shapes.

The experiments were carried out in the laboratory of Fluvial Morphodynamics I of GITS-UPC at the Civil and Environmental Engineering Department. A channel of concrete 9m long and 2.52 m wide was used, inside the channel there is a 2.5x2.5 m trench filled with 50 cm of sand. The sand had a D50=1.6 mm and it is flattened with a slope of $1 \cdot 10^{-3}$. The movement threshold of this sand in the experiments conditions it is reached for 100 l/s, a water depth of 10 cm and a bed shear stress of 1 N/m^2. Different arrangements of the macrorugosities were tested. The one that showed more efficiency was the plate elevated from the bed. Thus, around this macrorugosity different experiments were carried out in order to understand the velocity and stresses distributions in the vicinities of the plate. Three different discharges were tested (50, 75 y 100 l/s), always with a water depth of 20 cm. The velocity profiles were measured through a lateral ADV, measuring at a distance of 1 cm and 5 cm downstream the element. The experiments were carried out on the coarse sand bed (D50=1.6 mm) and it was expected that a fine sand of D50=0.2 mm moves over the bed. The dimensionless bed shear stress in these conditions is between 40 and 85% below the threshold movement condition of the fine grain, consequently the fine sand is not able to move without the aid of an external force to the flow.

3. Measurement results

For each parameter combination a detailed velocity distribution profile was measured.

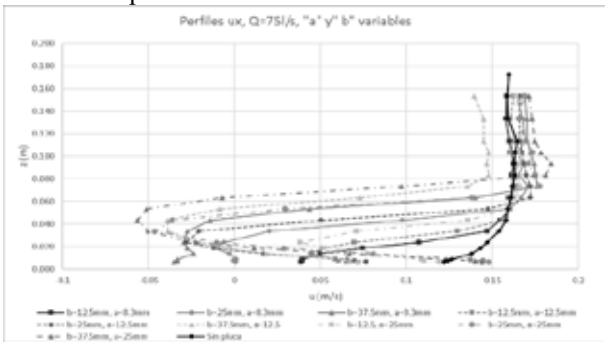

Figure 2: Velocity distribution Q = 75 l/s.

In Figure 2 it is shown how 5 cm downstream the plate the velocity it is decreased, reaching even negative values. The results show different values of elevation "a" and height "b" of the plate (Figure 1). The natural velocity profile when the flow has not reached the macrorugosity yet is added in Figure 2. It can be seen that there is still no influence of the plate on the superficial zones.

In addition, using the Reynolds theory about the averaged flow, the Reynolds shear stresses can be calculated and, thus, characterize its distribution. The results show a clear increase of the shear stresses, with peaks that reach to exceed 6 times the natural shear stress with no macrorugosity.

The plates increase the tensions over them and close to the bottom. More plate elevation means less bed shear stress, although, if the elevation is too small, the bed shear stress can drop to null. The mobilization of the sediment is guaranteed meanwhile the stresses under the plate are high enough and, once the sediment goes by and accumulates downstream, the upper stress mobilizes it until it reaches the next plate.

5. Conclusions

The macrorugosity increases the bed shear stresses. The elevated plates enable the sediment mobilization where naturally would not be able to move.

References

Nikuradse, (1926). Untersuchungen über die Geschwindigkeitsverteilungs in turbulenten Stromüngen. Thesis Göttingen, VDI Forschungsheft 281, Berlin, 1926.

Sayre and Albertson Roughness (1961). Spacing in rigid open channels. *Transactions,* ASCE, 128, 196 pp 343-427.

Aguirre, J; Olivero, M; Fuentes, R. (1986). Una formula para la fricción en escurrimientos rugosos a superficie libre. *Ciencia e ingeniería volumen XVIII*.

Koloseus and Davidian, (1966). Free surface instability correlation. *Geologicval survey*. Water Supply. Paper 1592C. U.S. Government Printing Office, 1966.

Sediment dynamics study under extreme tidal currents

O. Blanpain[1], G. Minster[2, 3], N. Le Dantec[2], J-F. Filipot[4], Y. Méar[5] and T. Garlan[1]

1. Service Hydrographique et Océanographique de la Marine, Brest, France. blanpain@shom.fr, garlan@shom.fr
2. IUEM, Domaines Océaniques UMR 6538, France. nicolas.ledantec@univ-brest.fr
3. ENSTA Bretagne, France. gaspard.minster@ensta-bretagne.org
4. France Energie Marine, France. jean.francois.filipot@france-energies-marines.org
5. Université de Caen, LUSAC, France. yann.mear@cnam.fr

1. Introduction

In extreme tidal environments, very high current and rough bottom generate large turbulence levels periodically. Theses turbulent bursts can potentially induced high sediment load of grains as coarse as pebbles. Some clues lead to think that unusual processes, like suspension of coarse particles or sheet flow of gravels may exist in such environment. Because sediment interactions with tidal stream turbines could affect engineering performance, maintenance operations and finally energy yield, an attempt to qualify and quantify this load in the Alderney race (English Channel) has been undertaken.

2. Methodology

To reach this goal we are simultaneously developing:

- A comprehensive measurement program based on several specific systems to be able to understand or model sediment dynamics in these kind of very energetic marine environments.
- A regional sediment dynamic model based both on semi analytical and experimental modelling results and on in-situ data acquired.

2.1 Data acquisition strategy

For each particle population, we want to highlight:

- Mobility threshold processes
- Mode of transportation (bed load, saltation or suspended load)
- Moving speed and height above seabed
- Sediment discharges

Five frames supporting have been moored this winter with a dozen of sensors: two ADCPs, three current meters, two stereovideo systems, one camera, five hydrophones, five accelerometers, one acoustic turbidity profiler, a sediment trap. Fifty pebbles with acoustic tags have been launched on the sea bottom. The data obtained should brought information on the load, the size and the height of the particles in movement.

2.2 Modelling strategy

Meanwhile, a modelling effort has been undertaken: a physical one in a current flume to study the transition from rolling to saltation; a semi analytical one to enlarge the flume results to the strong current conditions; and, in the future, a regional one to evaluate bedload and suspension load of different particle sizes.

An experimental study of saltated sphere over a rough bed was done. Different diameters (1.6cm, 3cm and 5cm), flow velocities (65cm/s, 85cm/s and 107cm/s) and roughness (1.2cm, 1.6cm, 2.6cm) are tested. The critical Shields number is estimated for each case and each individual jumps are analysed (height and length) with a fast camera.

A semi-analytical model is adapted from Berzi et al. (2016) to extend validity of experimental data. Hydro-sedimentary conditions that allow saltation are definied (Figure 1).

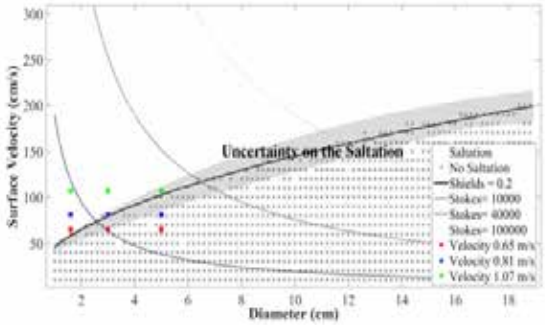

Figure 1: Results from the semi-analytical model. Dots are experimental data.

.

3. Conclusions

A comprehensive field campain has been done in rough hydro-sedimentary conditions. Analysis and interpretation of data is ongoing. They should brought information on the load, the size and the height of the particles in movement. Exceptionally intense forcing may induce other undocumented processes. These results will feed the different modelling approaches that are underway and will able to extend the validity of process predictors.

Acknowledgments

The work is supported by the project ANR FEM PHYSIC ANR-10-IEED-0006-10.

References

Berzi, D., Jenkins, J., and Valance, A. (2016). Periodic saltation over hydrodynamically rough beds: Aeolian to aquatic. *Journal of Fluid Mechanics,* 786, 190-209. doi:10.1017/jfm.2015.601

Physical modeling of sediment transport by bedload and suspensions

E. Bouvet[1], A. Jarno[1], O. Blanpain[2], T. Garlan[2] and F. Marin[1]

[1] Laboratoire Ondes et Milieux Complexes, Normandy University, Le Havre, France.
ellynn.bouvet@doct.univ-lehavre.fr

[2] SHOM, Brest, France. olivier.blanpain@shom.fr

1. Introduction

Measuring the total sediment transport is very challenging because of the complexity of the environmental conditions (e.g. Turowski et al., 2010). Though, it has a crucial role on morphologies, erosion and deposition and migration rate.

With the help of a physical model, we established a method to measure both bedload and suspension loads, allowing us to obtain the total sediment transport. This study investigates the impact of grain size on sediment transport using fine and medium well sorted sands. Grain shape is also considered using bioclastic and non-bioclastic sands. Tests are performed in a current flume and the method used is based on an ADCP.

2. Experimental setup and measurement techniques

The current flume of the LOMC[1] laboratory is $10m$ long, $0.49m$ deep and $0.49m$ wide. The current is generated with a pump that recirculates the water in a closed circuit (see Auzerais et al., 2016, for more in-depth descriptions of the flume).

For the present study, three sands are used: a fine sand ($D_{50} = 119\mu m$) and two medium sands ($D_{50} = 360\mu m$). One medium sand has 39% of shell debris so that the impact of particle shape can also be highlighted. Multiple current speed are applied.

The bedload is measured by weighting the sand that falls into traps situated at the end of the flume.

To measure the current velocity and the suspended load, we used an Acoustic Doppler Current Profiler (UB Lab from UBERTONE). The backscatter signal is proceeded to allow turbidity calculation. The acquisition signal depends on size and shape of particles and therefore results from the ADCP are calibrated with samples taken during the experiment.

These samples are withdrawn directly in the water column during the tests at different heights above the flume bed. The method is based upon the isokinetic method (Nelson and Benedict, 1950): a small tube is inserted at the desired depth facing the flow and withdraws water and sediments with the same speed that the medium flow speed in the flume. The samples are filtrated and sediments are dried and weighted.

The calibration curves show good correlations between the load of sediment contained in the sample and the ADCP data. It is then easy to estimate the suspended load for the sand types considered in this study.

3. Results

Bedload and suspension load are estimated for each sand and compared to commonly used formulas in the literature. Results from the experiments show a good trend of the suspension transport rate: comparison is made with Van Rijn (1984) formula and the relative error is relatively small (around 20%). Overall, concentrations from the ADCP are sightly lower than concentrations from Van Rijn (1984), especially near the bed.

The expected transport based on Van Rijn (1993) criterion for medium sands is a domination of the bedload transport with a small amount of suspension load. This is what is obtained with tests performed with the medium silicoclastic sand. However, we noticed that the suspension load increases with the bioclastic sand: the particle shape has an impact on the transport.

4. Conclusion

In this experimental study, bedload is measured by using traps at the end of the flume and suspension load is measured with an ADCP calibrated with water and sediment samples.

The method showed its reliability and results are in good accordance with existing formulas found in the literature and thus, provides a useful data base. The next step of this study is the investigation of sand heterogeneity and its impact on transport, both bedload and suspension by mixing up the sands described above.

References

Auzerais, A., Jarno, A., Ezersky, A., and Marin, F. (2016). Formation of localized sand patterns downstream from a vertical cylinder under steady flows: Experimental and theoretical study. *Physical Review E*, 94(5).

Nelson, M. and Benedict, P. (1950). Measurement and analysis of suspended sediment loads in streams. *Proc. ASCE*, 76:1–28.

Turowski, J. M., Rickenmann, D., and Dadson, S. J. (2010). The partitioning of the total sediment load of a river into suspended load and bedload: a review of empirical data: The partitioning of sediment load. *Sedimentology*, 57(4):1126–1146.

Van Rijn, L. C. (1984). Sediment Transport, Part II: Suspended Load Transport. *Journal of Hydraulic Engineering*, 110(11):1613–1641.

Van Rijn, L. C. (1993). *Principles of sediment transport in rivers, estuaries and coastal seas. 1: Principles of sediment transport in rivers, estuaries and coastal seas*. Aqua Publications, Amsterdam. OCLC: 832662677.

Effects of Sediment Strength on Sediment Transport Mechanisms and Morphology of a Dynamic Sandy Spit

N. Brilli[1] and N. Stark[1]

[1]Civil and Environmental Engineering, Virginia Tech, Blacksburg, Virginia. nickb96@vt.edu, ninas@vt.edu.

1. Introduction

In August 2018, a field survey was conducted off the coast of Point Carrew, a sandy spit near Yakutat, Alaska. The spit forms as strong longshore transport NW along the Gulf of Alaska reaches a peninsula at the mouth of Yakutat Bay (Yehle, 1971). Wave refraction around the peninsula deposits the sediment towards the Ankau estuary in the NE (Figure 1). After an unknown event in 1997 caused 400,000 meters^2 to erode, the spit has been steadily accreting at a rate of ~32,000 meters^2/yr. A portable free fall penetrometer (PFFP) was deployed along several transects in the nearshore zone of the spit to determine sediment strength. Using the method developed by Albatal et al. (2019), friction angles (ϕ) and relative densities (D_r) of the surficial seabed sediments were determined. The goal of this paper is to use the obtained strength and packing properties to draw conclusions about the dynamic morphology of the spit by studying their effect on and response to sediment transport processes.

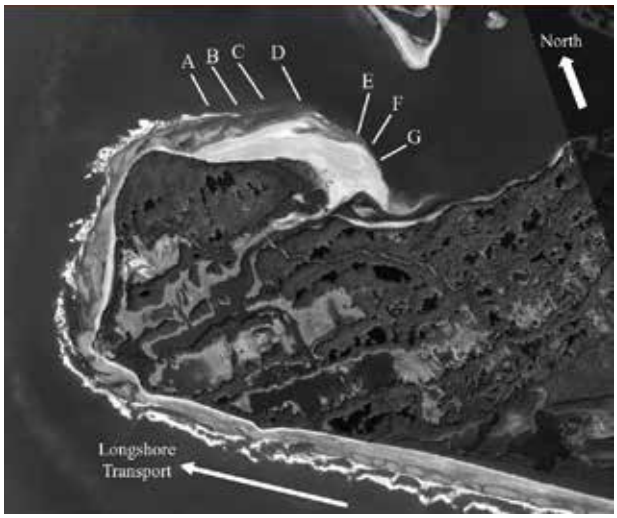

Figure 1: Site layout (Lettered line = transects) Source: Google Earth (59°32'23.42"N, 139°49'18.09"W)

2. Results

The deceleration profile produced by the PFFP yields a maximum deceleration and an estimate of bearing capacity (Stark et al. 2012). Relative density is obtained via direct correlation from the deceleration record, and the friction angle is back calculated using the bearing capacity (Albatal et al 2019). The results show higher friction angles and relative densities for transects (E-G) than transects (A-D). Average ϕ and D_r values in the middle of transects A-D were 45° and 23% respectively compared to 53° and 55% for transect E-G.

The area of A-D (N side of the spit) is the location with the highest deposition rate (20,000 meters^2/yr) because this side is exposed to the refracting waves and longshore transport. The combination of wave energy and large tidal range (~3m) leads to the formation of intertidal bars (Masselink et al. 2006). Despite the net deposition on the sub-aerial body of the spit, storms, tides, and waves constantly rework the sediment in the intertidal zone, producing these dynamic bars and contributing to high sediment mobility. In contrast, the high accretion rate to the North serves to protect the area of transect E-G thus it receives much lower wave energy and experiences lower deposition rates (2,500 meters^2/yr). This prevents the formation of an intertidal bar system, which leaves sediment in this area relatively undisturbed by hydrodynamic processes. Seismic activity would act to consolidate and densify the sediment everywhere on the spit, contributing to high ϕ and D_R values. This may be reflected in the results from transects E-G, which are mostly protected from hydrodynamic forcing.

3. Conclusions

Transects A-D are subject to constant reworking of surficial sediment and deposition processes by waves and sediment transport as seen by the presence of an intertidal bar system, which is the reason for the lower ϕ and D_R values. These processes likely work in a feedback loop by which the lower ϕ and D_R sediments are more mobile and enhance sediment transport, and the stronger, stiffer sediments are more resistant to transport mechanisms.

Acknowledgments

The authors would like to thank the City and Borough of Yakutat, specifically Rhonda Coston and Irving Grass. Funding was provided by NSF award CMMI-1751463.

References

A. Albatal, N. Stark, and B. Castellanos. (2019). Estimating in-situ relative density and friction angle of nearshore sand from portable free fall penetrometer tests. *Canadian Geotechnical Journal*.

G. Masselink, A. Kroon, and R. G. D. Davidson-Arnott, "Morphodynamics of intertidal bars in wave-dominated coastal settings — A review," *Geomorphology,* vol. 73, no. 1, pp. 33-49, 2006/01/01/ 2006.

Stark, N., Wilkens, R., Ernstsen, V. B., Lambers-Huesmann, M., Stegmann, S., & Kopf, A. (2012). Geotechnical properties of sandy seafloors and the consequences for dynamic penetrometer interpretations: quartz sand versus carbonate sand. *Geotechnical & Geological Engineering*, *30*(1), 1-14.

Yehle, L.A. (1971). *Reconnaissance Engineering Geology of the Yakutat Area, Alaska, With Emphasis on Evaluation of Earthquake and Other Geologic Hazards*, Geological Survey Professional Paper No. 1074, prepared for USGS

A model for tidal propagation in intertidal regions with mangroves

K.R. Bryan[1], Sergio Fagherazzi[2] and J.C. Mullarney [1]

[1]School of Science, University of Waikato, Hamilton, New Zealand. karin.bryan@waikato.ac.nz
[2] Dept. of Earth & Environment, Boston University, Boston, MA, USA

1. Introduction

Mangroves dissipate energy and change the propagation characteristics of long waves such as tides, surges and tsunami. As a result, they are often credited for protecting the coast against hazards, and play a role in accumulating sediment in the intertidal zone. Simple theoretical arguments have been used to show that high friction environments cause distortion of the wave shape (Friedrichs and Madsen, 1992), but distortion caused by vegetation-induced friction has only been studied through numerical modelling and field observations. In principle, the tide is flood-dominant within the forest, and ebb dominant seaward of the forest, an effect that is driven by the water level slope caused by delayed drainage from the intertidal.

In this work, we use a simple analytical model to study the coupled behaviour of the tidal wave in a vegetated intertidal area. The region of interest (Figure 1) is divided into three areas, the unvegetated flat (region 1), the fringe (region 2) and the heavily vegetated forest interior (region 3), with areas are connected by matching water level and discharge across boundaries.

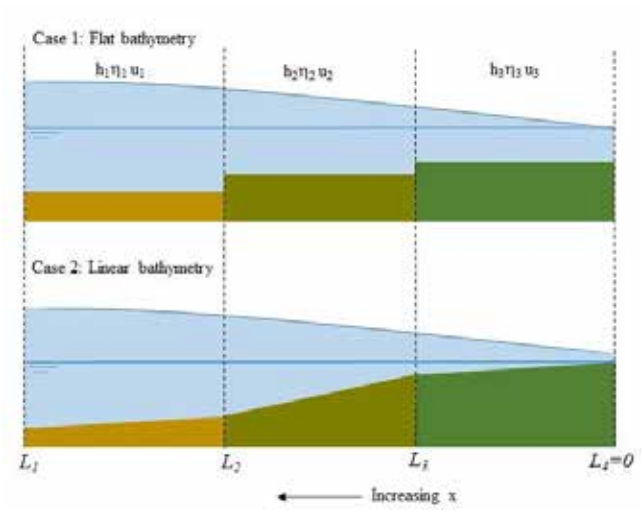

Figure 1: Schematic of the domain with the two cases, flat and sloping bathymetry.

2. Methods

Assuming that the momentum balance is dominated by friction and the water level gradient, and dividing the domain into regions where there is either no vegetation (*M*) or vegetation is much more important than bottom friction (*F*), yields a diffusion equation in each environment type

$$\frac{\partial \eta}{\partial t} - \frac{\partial}{\partial x}\left(D_{F,M}\frac{\partial \eta}{\partial x}\right) = 0 \qquad (1)$$

and

$$D_F = \left(\frac{gh^3}{C_d|\partial\eta/\partial x|}\right)^{1/2} \text{ and } \quad D_M = \left(\frac{2gh^2}{a_v C_D\left|\frac{\partial \eta}{\partial x}\right|}\right)^{\frac{1}{2}}, \qquad (2)$$

where η is sea-surface elevation, h is water depth, x is cross-shore distance (positive onshore), t is time, g is acceleration due to gravity, C_d is bottom drag, a_v is vegetation frontal area density and C_D is vegetation drag.

Following from Friedrichs and Madsen (1992), the time dependence of $D_{F,M}$ is incorporated by considering a frame of reference moving with the tide, including the possibility of a harmonic

$$\omega\tau = \omega t + \alpha\sin(\omega t) + \frac{\delta}{2}\sin(2(\omega t + \phi + \frac{\pi}{2})), \qquad (3)$$

where ω is the radian frequency, and ϕ is the phase of the seasurface gradient and δ is a constant. Equation 1 is solved separately in each region i assuming a wave solution,

$$\eta_m(x,\tau) \sim \xi_m e^{i(m\omega_i\tau+\varphi_{mi})} \qquad (4)$$

and by matching η and uh at each boundary, where u is cross-shore velocity, m is the harmonic, φ a phase shift, and

$$\xi_{mi} \sim \cosh(m^{1/2}k_i x)\prod_{q=1}^{i}\frac{\cosh(m^{1/2}k_{q-1}L_q)}{\cosh(m^{1/2}k_q L_q)} \qquad (5)$$

$$\xi_{mi} \sim x^{\sigma\nu^2} J_\nu(ik_{mi}\sigma^{-1}x^\sigma) \qquad (6)$$

for Case 1 and Case 2 respectively. The constants σ and ν differ in each region, and the radian wavenumber is $k_i = (im\omega_i/D_i)^{1/2}$, where $\omega_l = \omega$.

3. Conclusions

The model will provide a quick and easy tool which can be used to estimate surge waterlevels and asymmetries in mangrove coastlines. This tool is particularly useful in areas where only satellite/LiDAR data are available.

Acknowledgments

Work was done during a Fulbright Fellowship for KRB at the Boston University. Work was initiated as part of a Marsden Fund project (14-UOW-11).

References

Friedrichs, C. T., Madsen, O. S., 1992. Nonlinear diffusion of the tidal signal in frictionally dominated embayments. Journal of Geophysical Research, 97(C4), 5637– 5650. https://doi.org/10.1029/92JC00354.

The stochastic nature of vegetation removal driven by riverbed erosion

G. Calvani[1,2,3], P. Perona[1], H.M. Schöniger[2] and L. Solari[3]

[1] Institute for Infrastructure and Environment, School of Engineering, The University of Edinburgh, Edinburgh, UK
[2] Leichtweiß-Institute for Hydraulic Engineering and Water Resources, University of Braunschweig, Braunschweig, DE
[3]Department of Civil and Environmental Engineering, University of Florence, Florence, Italy. giulio.calvani@unifi.it

1. Introduction

Aquatic and riparian plants are recognized as fundamental components of fluvial systems. Vegetation influences both the biological factors and the morphodynamic evolution in river corridors, together with the hydrological alternation of low and high flow discharges and the sediment transport processes of erosion and deposition. In the same way, the establishment, growth and decay of riparian vegetation is governed by the plant ability to adapt to such morphodynamic evolution. Consequently, plant resilience to uprooting is governed by the mutual interactions between riparian vegetation and river processes, particularly by flow magnitude, hydrograph duration and erosion depth (Edmaier et al., 2011). As a result, plant removal driven by flow and bed erosion (Type II uprooting) is directly affected by stochasticity intrinsically involved in such processes, due to randomness in flow hydrograph and sediment transport (Perona and Crouzy, 2018).
In this work, we investigated the correlation between the return period of flood events and the associated resilience to uprooting of riparian vegetation from a stochastic point of view.

2. Materials and methods

To model the stochastic occurrence of flow discharges and calculate the correspondent return period, we adopted the Compound Poisson Process and the Peak-Over-Threshold (POT) analysis. Magnitude and duration $\tilde{T}_\xi$ of flow discharge above the critical threshold for sediment motion were defined according to the characteristics of the Compound Poisson Process (shot frequency λ_P, decay rate τ_P and average value μ_P). Plant resilience to uprooting R_τ was calculated using the stochastic model of Perona and Crouzy (2018), by considering different hydrological parameters of the Compound Poisson Process and characteristics of riparian vegetation (e.g., critical erosion depth at time of uprooting L_e), as well as factors governing the processes of sediment transport and bed erosion (e.g., the coefficient in bedload transport formula α_{BL}). Figure 1 shows an example of the performed calculation.

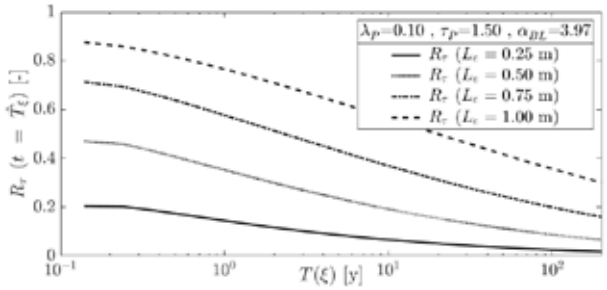

Figure 1. The computed riparian vegetation resilience R_τ against the return period $T(\xi)$ of flood events for different values of L_e (erosion depth at uprooting).

According to the performed analysis, we are able to highlight the key parameters determining the resilience of riparian vegetation to flood events. As a result, both the the characteristics of plants, the hydrological regime and the riverbed erosion process contribute to increase or decrease chances of riparian vegetation to survive and then establish in riverine environments.
To validate the proposed approach, the combined analysis of return period and stochastic resilience was then apply to the field measurements of mechanical uprooting of woody vegetation performed by Bywater-Reyes et al. (2015) on the Santa Maria River (Arizona, USA).

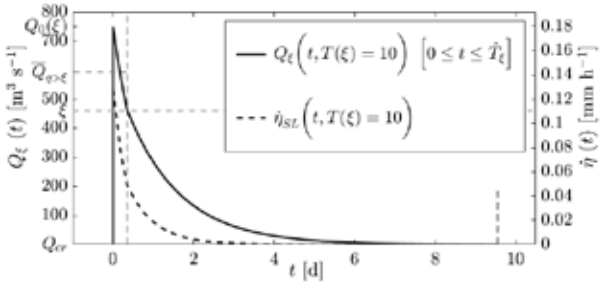

Figure 2. Flow hydrograph $Q_\xi(t)$ and the associated erosion rate $\dot{\eta}(t)$ for the 10-years return period flood event in the Santa Maria River (Arizona, USA).

3. Conclusions

Our analysis sheds lights on the correlations between hydro-morphological processes and riparian vegetation survival chances to flood events. The results show that species recruitment and resilience depends on both biomechanical properties of vegetation and flow magnitude and duration. The analysis suggests that changes in the hydrological regime due to climate change conditions may reflect in ecological shifts from native to invasive species.

References

Bywater-Reyes, S., Wilcox, A. C., Stella, J. C., and Lightbody, A. F. (2015). Flow and scour constraints on uprooting of pioneer woody seedlings. *Water Resources Research*, 51(11):9190–9206.

Edmaier, K., Burlando, P., and Perona, P. (2011). Mechanisms of vegetation uprooting by flow in alluvial noncohesive sediment. *Hydrology and Earth System Sciences*, 15(5):1615–1627.

Perona, P. and Crouzy, B. (2018). Resilience of riverbed vegetation to uprooting by flow. *Proc. R. Soc. A*, 474(2211).

A New Approach for Bathymetric Video-Inversion: Synthetic Case

D. Calvete[1], G. Simarro[2], P. Luque[3], A. Orfila[4] and F. Ribas[5]

[1] Universitat Politecnica de Catalunya, Barcelona, Spain. daniel.calvete@upc.edu
[2] Institute of Marine Sciences (ICM-CSIC), Barcelona, Spain. simarro@icm.csic.es
[3] Coastal Ocean Observing and Forecast System Balearic Islands (SOCIB-CSIC), Palma de Mallorca, Spain.
[4] Mediterranean Institute for Advanced Studies (IMEDEA-CSIC), Esporles, Spain. aorfila@imedea.uib-csic.es
[5] Universitat Politecnica de Catalunya, Barcelona, Spain. francesca.ribas@upc.edu

1. Introduction and Methods

Scientists and managers of the coastal zone need to know the coastal bathymetry to understand the behaviour of the beaches and be able to predict their evolution. Intensive monitoring programs through campaigns of direct measurements of the bathymetry are excessively expensive, so that in the last decades alternative methodologies have been developed. Many of them are based on video monitoring stations, and among the different existing algorithms, cBathy (Holman et al., 2013) is the algorithm that achieves the best results.

In a first step, cBathy gets the dominant frequencies and their corresponding wave numbers from the Cross Spectral Matrices (CSMs) of a given set of frequency bands. An estimation of the local water depth is then obtained from the dispersion equation. In the second step, the estimated bathymetries obtained for each video are smoothed through a Kalman filter to obtain the final hourly estimates. This algorithm, which has been used in a number of studies (e.g., Bergsma et al., 2016; Rutten et al., 2017) to obtain 2-D bathymetries, presents however some limitations and/or known problems that have been reported in the literature (Rutten et al., 2017).

The work being presented here is an alternative to the first step of cBathy. It consists of performing a Principal Component Analysis (PCA) to the matrix made of pixel intensities from a series of snaps. The result of the PCA is the decomposition of the video into a set of modes associated with the components of the wave field. The spatial part (the Empirical Orthogonal Function, EOF), is associated with the spatial phase of the wave from which a wave number can be derived. The amplitude of the mode (Principal Component, PC) is associated with the frequency of the wave component. To facilitate the decomposition of the videos in modes of travelling waves, a Hilbert transformation in time of the matrix of intensities has been carried out.

The objective of this work is to explore the feasibility of PCA of video images to obtain beach bathymetries. To this end, artificial videos have been generated by assigning pixel intensity to the elevation of the surface free of synthetic waves, both linear and nonlinear (Shi et al., 2012, for FUNWAVE), propagated over known bathymetries.

2. Results

It has been studied the influence on the results of: the discretization in time and space of the videos; the method to derive frequencies and wave numbers from PC and EOF, respectively; the characteristics of waves; and, finally, the complexity of the bathymetry. As a general result, the PCA is able to capture the individual wave components from which bathymetry can be derived, see Figure 1. For nonlinear waves the PCA also encounters the subharmomic components and reflections. For the most common coastal waves (from 5 to 15s), the method allows resolving the spatial structure of the waves with pixels that cover up to 4 m in real world coordinates and recording images with a frequency of 1Hz or greater.

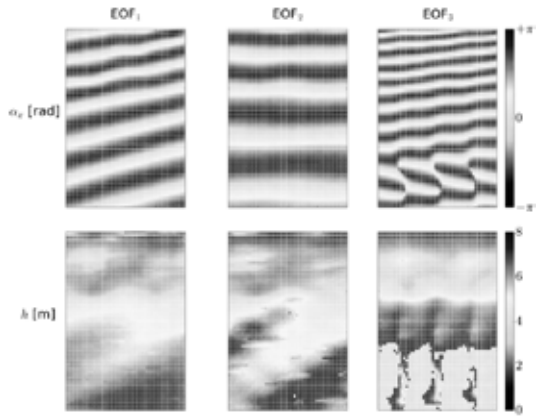

Figure 1. Example of results from PCA. On top the spatial phases, on bottom the recovered bathymetry.

3. Conclusions

PCA of video images allows to isolate the various wave components and determine their frequency and wave numbers, from which the bathymetry can be inferred.

Acknowledgments

This research was partly funded by the Spanish Government projects CTM2015-66225-C2-1-P, and CTM2015-66225-C2-2-P (MINECO/FEDER).

References

Bergsma, E., Conley, D., Davidson, M., and O'Hare, T. (2016). Video-based nearshore bathymetry estimation in macro-tidal environments. *Marine Geology*, 374:31–41.

Holman, R., Plant, N., and Holland, T. (2013). Cbathy: A robust algorithm for estimating nearshore bathymetry. *JGR: Oceans*, 118(5):2595–2609.

Rutten, J., De Jong, S., and Ruessink, G. (2017). Accuracy of nearshore bathymetry inverted from x-band radar and optical video data. *IEEE Transactions on Geoscience and Remote Sensing*, 55(2):1106–1116.

Shi, F., Kirby, J., Harris, J., Geiman, J., and Grilli, S. (2012). A high-order adaptive time-stepping tvd solver for boussinesq modeling of breaking waves and coastal inundation. *Ocean Modelling*, 43-44:36–51. cited By 201.

Simulation of the diverse fish habitat in alluvial rivers−A case study of Tsengwen river

C. N. Chen [1] C. H. Tsai[2]

[1] National Pingtung University of Science and Technology, Taiwan, ginrochen@mail.npust.edu.tw
[2] National Cheng-Kung University, Tainan, Taiwan, jht581212@gmail.com

1. Introduction

In the past, the river management was mostly human-oriented, focusing on development, utilization and safety, often ignoring the river habitat, leading to ecological destruction of rivers. The issues of river environment have recently been brought into focus and the importance of environmental protection and ecological balance has also been recognized. The ecological capability in the river in turn decreases due to artificial development or dredging. Henceforth, ecological protection and restoration were taken up in order to attain the purpose of river restoration. The purpose of this study was to develop a two-dimensional river habitat transition model to simulate the distribution of habitat. Six habitat types are established; type1: Shallow pool, type2: Medium pool, type3: Deep pool, type4: Slow riffle, type5: Fast riffle, type6: Run, which are defined by depth and velocity under ordinary flow (average discharge in dry season is 3.38cms, and 84.57cms in rainy season). The Shannon index and Simpson index are used as Habitat Diversity Index (HDI) and the habitat diversity of the river under the average discharge of ordinary flow is evaluated.

2. Results and Discussion

The simulation area is from the No.59 cross-section to the No.73cross-section. The computed cells are squared with $\Delta x = \Delta y = 25m$. The total cells are 11,953 and the time step (Δt) is 0.05 second. The Manning′s roughness coefficient is 0.035.

The simulation results indicate that the water flow is concentrated in the main channel under ordinary flow. According to the calculation results of water depth and flow velocity, combined with the classification of habitat types, the distribution of fish habitat types under the average discharge of ordinary flow was shown in Figures 1 and 2, respectively. The distribution of fish habitat types is obviously different, the area and proportion of each type of habitat under average discharge in dry and rain seasons are shown in Table 1. Figures 1 and 2 show that all habitat types are distributed in the main channel in the dry season (November-April), and the type 2 and 3 of habitats are the most, accounting for 38.3% and 52.4% of the water area, respectively. The fifth type of habitat does not exist at all. Under the average discharge in rainy periods (May to October), the type 0 of habitat is the water area without any habitat that accounts for 38.7% of the total water area. The type 3 of habitat is the most, accounting for 42% of the water area. The type 4 of habitat is quite rare and the type 5 of habitat does not exist in either the dry or rainy periods. The Shannon and Simpson habitat diversity indices are $H_{shan} = 0.97$ and $H_{simp} = 0.57$ in the dry season, $H_{shan} = 0.906$ and $H_{simp} = 0.48$ in the rainy season.

3. Conclusions

The habitat types are distributed in the main channel during dry and rainy periods. In the mid-stream of the Tsengwen River, the types 2 and 3 of habitats are the most and the types 4 and 5 of habitats are quite rare or do not exist. The habitat diversity under ordinary flow during dry season is higher than that of rainy seasons.

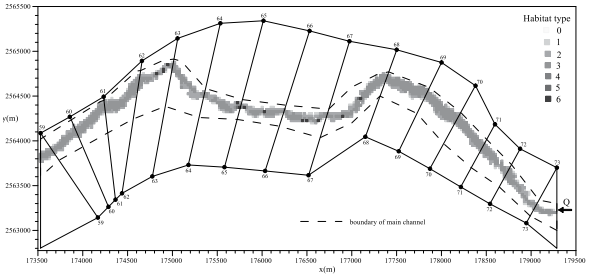

Figure 1: The habitat types under average discharge in dry periods (3.38 cms)

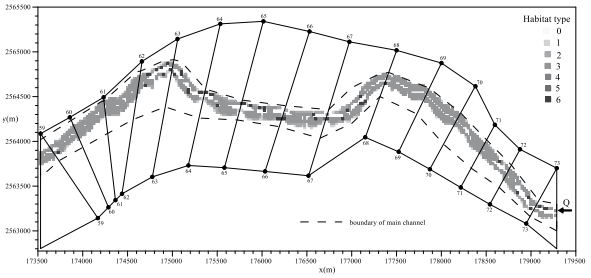

Figure2: The habitat types under average discharge in rainy periods (84.57 cms)

Table1 The area and proportion of each type of habitat during average discharge both in dry rainy periods.

Habitat types	Discharge in dry periods (3.38cms)		Discharge in rainy periods(84.57cms)	
	Area (m^2)	Proportion (%)	Area (m^2)	Proportion (%)
0	0	0.0	379375	38.8
1	55625	7.9	40000	4.1
2	269375	38.3	122500	12.5
3	368750	52.4	413125	42.2
4	1250	0.2	1250	0.1
5	0	0.0	0	0.0
6	8125	1.2	21875	2.2
Total	703,125	100	978125	100

References

Coarer, Y. L., “Hydraulic Signatures for Ecological Modelling at Different Scales,” Aquatic Ecology, Vol. 41, pp. 451-459 (2007).

Suen, J. P., Chen, C. N. and Tsai, C. H., “Creating Diverse Habitat Environment in Ecological Water Resources Management,” World Environmental & Water Resources Congress (EWRI), Hawaii, (2008).

Impact of dredging activities on salt marshes of Aveiro Lagoon

C.L. Lopes[1,2], R. Mendes[1,3], I. Caçador[2] and J.M Dias[1]

[1] CESAM, Departamento de Física, Universidade de Aveiro, Aveiro, Portugal, carinalopes@ua.pt; rpsm@ua.pt; joao.dias@ua.pt
[2] MARE, Faculdade de Ciências, Universidade de Lisboa, Lisboa, Portugal, micacador@fc.ul.pt
[3] CIIMAR, Faculdade de Ciências, Universidade do Porto, Porto, Portugal

1. Introduction

Salt marshes have a great ecological value for estuarine ecosystems, providing a broad range of services; however, their general decline is being observed worldwide, in large part due to undergoing threats posed by human actions. Accordingly, there is a growing concern about salt marsh preservation status towards their conservation and restoration. The main objective of this work is to evaluate the effects of bathymetric changes induced by local dredging operations on the estuarine vegetation of Aveiro Lagoon, a tidally dominated coastal system located on the NW Portuguese coast. The lagoon presents extensive salt marsh communities which high ecological importance was recognized by the National Classified Areas System (SNAP), integrating the Nature 2000 network as a Special Protection Area (SPA) and Site of Community Importance (SCI).

2. Methods

A historical review of the lagoon morphologic evolution was carried out, analysing the available dataset of topo-hydrographic surveys. The resulting bathymetric changes were related with the frequent dredging operations performed in Aveiro Lagoon. After was assessed their impact in alterations in estuarine vegetation through the interpretation of Landsat satellite imagery and determination of vegetation indices (Lopes et al., 2019).

3. Results

Over the last 30 years, the lagoon experienced mostly a deepening of its main channels. The inlet channel deepened over than 10 m in some regions and the main channels depth increased up to 8 m (S. Jacinto and Espinheiro) and 3 m (Mira and Ílhavo). These changes were motivated mostly by dredging activities performed: 1) regularly at the inlet; and 2) between 1996 and 1999 on the lagoon main channels (Lopes and Dias, 2015).

The interpretation of satellite images revealed that these morphologic alterations affected the intertidal regions vegetation cover, promoting mostly a decrease of vegetation indices (Figure 1). The Normalized Difference Vegetation Index (NDVI) decreased in the upper reaches of S. Jacinto channel and lagoon central area, and increased in restricted regions located at the heads of Mira, Ílhavo and Espinheiro channels. This pattern reveals that: 1) the vegetated area decreased; 2) the type of vegetation cover changed over this period. These results agree with Lopes et al. (2019), that found significant evidence that the vegetation indices patterns observed prior to and after 1999 are due to morphological changes in the lagoon, namely the deepening of the lagoon main channels.

4. Conclusions

This work revealed that the dredging activities occurring in Aveiro Lagoon are changing significantly the local morphology. These modifications were found to represent a major threat to salt marsh communities of this coastal system, endangering its ecological diversity.

Figure 1: NDVI variation between July 1987 and July 2017.

Acknowledgments

The first and second authors benefit from Post-Doctoral grants (SFRH/BPD/114906/2016, SFRH/BPD/115093/2016) given by the Portuguese Science Foundation (FCT). Thanks are due for the financial support to CESAM (UID/AMB/50017/2019), to FCT/MCTES through national funds.

References

Lopes, C.L. and Dias, J.M. (2015). Tidal dynamics in a changing lagoon: Flooding or not flooding the marginal regions. *Estuar. Coast. Shelf Sci.*, 167, Part A: 14-24.

Lopes, C.L., Mendes, R., Caçador, I., and Dias, J.M. (2019). Evaluation of long-term estuarine vegetation changes through Landsat imagery. *Sci. Total Environ.*, 653: 512-522.

The effect and evolution of a shoreface nourishment

W.L. Chen[1] and N. Dodd[1]

[1] Faculty of Engineering, University of Nottingham, Nottingham NG72RD, UK. wenlong.chen@nottingham.ac.uk

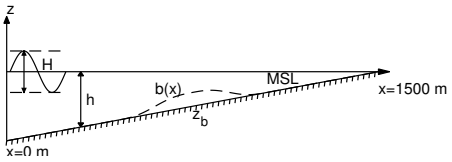

Figure 1. Geometry and coordinate system. Beach slope is 0.01, with shoreline located at $x = 1500$ m. Wave of 1 m high and 6 s period is applied along the offshore boundary ($x = 0$ m).

1. Introduction

Shoreface nourishments are effective methods in protecting the coast from erosion. It is important to study the physics underlying the evolution of a shoreface nourishment. In complex numerical models developed for a practical purpose, it can be difficult to isolate physics. We therefore have developed a one-dimensional idealized model to study the physics behind the effect and evolution of a shoreface nourishment.

2. Methodology

We assume that a nourishment ($b(x)$, with x denoting the cross-shore coordinate) is added onto an equilibrium seabed (referred to as $z_{b,0}(x)$) The evolution of nourishment is subject to

$$\frac{\partial b}{\partial t} + \frac{1}{1-p}\frac{\partial q'}{\partial x} - \gamma\frac{\partial^2 b}{\partial x^2} = 0, \qquad (1)$$

where $p = 0.4$ is the porosity of sediment. The perturbed sediment transport q' is given by,

$$q' = q(E_w(x), E_r(x), z_{b,0}(x)+b(x)) - q(E_{w,0}(x), E_{r,0}(x), z_{b,0}(x)), \qquad (2)$$

where q is the sediment transport consisting of sediment flux driven by wave skewness, wave asymmetry and return flow (Roelvink and Reniers, 2011). E_w and E_r are the wave and roller energy, solved from cross-shore wave energy transport equation (Battjes and Janssen, 1978). Subscript $_{,0}$ refers to the case without nourishment. The third term in (1) represents the diffusion of the nourishment due to gravity.

3. Results

Nourishments (see thick grey curve in Fig. 3 for its size and shape) are placed initially at x_n. The magnitude of q' increases (see Fig 2) as x_n approaches the coast. Placed offshore, a nourishment causes shoaling and a positive q'. As a result, the nourishment diffuses and gradually move to the coast (feeder effect, see dashed curve in Fig. 3). A nourishment placed close to the break point induces an earlier breaking, resulting in a negative (positive) q' around the newly formed (un-nourished) break point (see the dark and bright region in Fig 2). Wave energy is dissipated in this process (lee effect). The initial evolution of nourishment depends on the intensity of the wave break

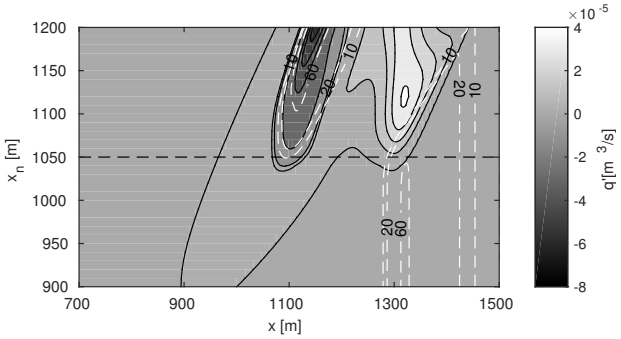

Figure 2. Sensitivity of q' to nourishment location x_n. Black and bright color refer to negative and positive q'. Dashed contour lines denotes the wave energy dissipation.

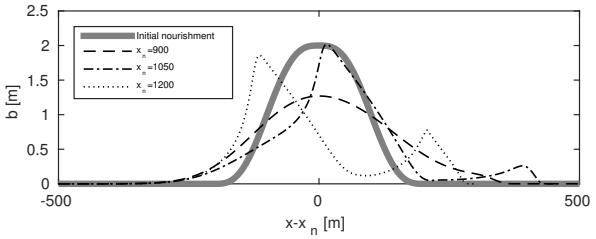

Figure 3. Evolution of nourishment after 160 days.

triggered by the nourishment. The nourishment either evolves into a skewed shape with its peak migrating onshore (weak break, for $x_n = 1050$ m in Fig. 3) or splits into onshore and offshore parts (strong break, for $x_n = 1200$ m in Fig. 3).

4. Conclusions

A shoreface nourishment changes the shoaling (placed well away from break point) or breaking (placed close to the break point) processes of a wave, and therefore, changes the sediment transport driven by wave skewness, wave asymmetry and return flow. The nourishment thus provide a feeder or lee effect. The approach we take illustrates and isolates these mechanisms and provides an alternative method by which nourishment can be studied.

Acknowledgments

The support of the UK Engineering and Physical Sciences Research Council (EPSRC) under the MORPHINE project (grant EP/N007379/1) and of the University of Nottingham is gratefully appreciated.

References

Battjes, J. A. and Janssen, J. (1978). Energy loss and set-up due to breaking of random waves. In *Proceedings of the 16th International conference Coastal Engineering*, page 569, USA,New York. American Society of Civil Engineering.

Roelvink, D. and Reniers, A. (2011). *A Guide to Modeling Coastal Morphology*. WORLD SCIENTIFIC.

Effect of Selective Withdrawal and Vertical Curtain on Reservoir Sedimentation: a 3-D Numerical Modelling Approach

M.A Duka[1], K. Yokoyama[2], T. Shintani[3] and K. Iguchi[4]

Tokyo Metropolitan University, Japan. [1]mauriceduka@gmail.com; [2]k-yoko@tmu.ac.jp; [3]shintani@tmu.ac.jp; [4]iguchi-kei@ed.tmu.ac.jp

1. Introduction

In reservoirs, selective withdrawal systems are installed to control the quality of the water downstream of dam. On the other hand, vertical curtains are placed near the river mouth to mitigate phytoplankton problems. Although these two structures were proven to work for their intended purpose, their direct effect to reservoir sedimentation has not been fully explored. This paper therefore presents a 3-D numerical simulation study of reservoir sedimentation considering the presence of these facilities after a flood event.

2. Study Site

The study area, located at Tokyo, Japan is the Ogouchi Reservoir, which serves largely for the city's water supply. It has an effective storage capacity of 185 Mm^3 and a water surface area of 4.25 km^2 at normal water level (NWL) of 101.5 m from dam bottom. A selective withdrawal facility, spanning up to a depth of 40 m from NWL is in operation. Meanwhile, two successive vertical curtains or fences with depths of 2 and 10 m, respectively are installed across Taba River, the main tributary.

3. Numerical Model

A 3-D hydrodynamic simulator, *Fantom Refined* (Shintani, 2017) was used, where equations of continuity and 3-D Navier-Stokes with incompressible and Boussinesq approximations are employed, together with temperature transport. The sediment transport model utilizes the advection-diffusion equation and takes into account sediment deposition under constant settling velocity. The equations were discretized based on a collocated finite volume method. Horizontal grids of 50 m were used alongside vertical grids of 0.25 m at surface gradually increasing up to 5 m at the bottom.

4. Calibration and Simulation

The effect to reservoir sedimentation of the July 15-17, 2015 flood was studied considering actual sediment inflow for 2- and 5-µm particles. Simulated temperature profiles and water level were found to be in good agreement with actual values. Six model cases were developed for three outflow locations (15, 40 and 70 m below NWL) without the fence (Cases 1a, 2a and 3a) and with the fence (1b, 2b and 3b). Water is discharged using selective withdrawal for the first two outflow settings, while the last one is purely directed towards the penstock.

5. Results and Discussion

The sediment budget in Figure 1 shows generally higher deposition for coarser particles (5 µm) while higher suspension for finer ones (2 µm). Shallower withdrawal without the fence (Case 1a) facilitates the largest release of sediment out of the reservoir at 40%, especially with finer sediments. This setting allows the transport of suspended sediments at the epilimnion, as facilitated by relatively same levels of inflow in the river and outflow in the selective withdrawal. Deeper withdrawals and presence of fence would result to higher sedimentation.

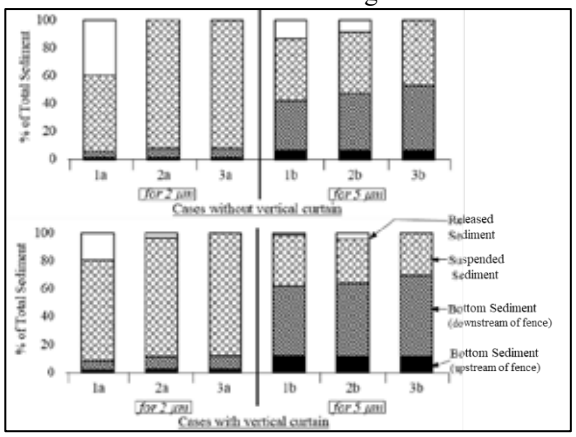

Figure 1: Sediment budget for all model cases.

Furthermore, vertical curtain enhances deposition in the reservoir particularly upstream of the fence, where around 20% of the bottom sediments are entrapped (Figure 2). It is likewise apparent that most of bottom sediments tend to accumulate at the shallower portions of the reservoir (near the shoreline) due to earlier settling.

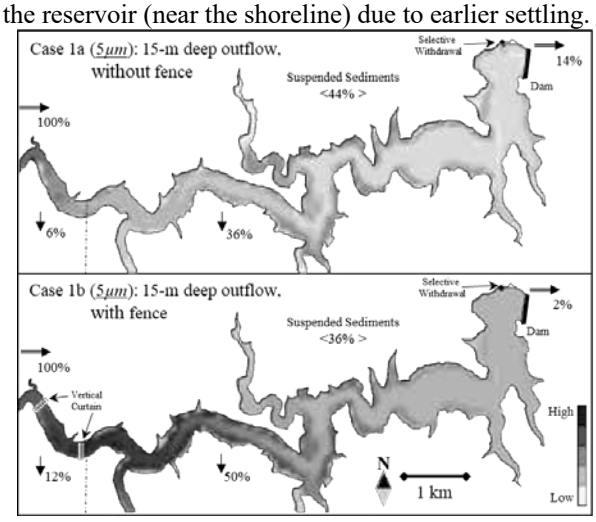

Figure 2: Bottom sediment distribution 24 days after flood peak for Cases 1a and 1b.

6. Conclusions

Shallower water withdrawal enhances release of fine sediments out of the reservoir while deeper withdrawal and presence of fence cause larger sediment deposition.

Reference

Shintani, T. (2017). An unstructured-Cartesian hydrodynamic simulator with local mesh refinement technique. *J. of JSCE, B1,* 73 (4), 967-972.

Impact of Bulle-Effect on Morphodynamics of Fluvial Diversions

S. Dutta[1], P. Tassi[2], D. Wang[3] and M.H Garcia[3]

[1] CSI, City University of New York (CUNY), New York, USA. somdutta.mail@gmail.com
[2] EDF R&D and Saint-Venant Hydraulics Laboratory, Paris, France.
[3] University of Illinois at Urbana-Champaign, Urbana, USA

1. Introduction

Bulle-Effect is the phenomenon in which disproportionately higher percentage of near-bed sediment enters the side-channel of a diversion, compared to the percentage of water. The phenomenon is named after Bulle (1926), who conducted the first extensive study about it. Recently, Dutta and Garcia (2018b) illustrated the applicability of the phenomenon to sediment distribution at diversions, and its importance for design of efficient sediment diversions (Dutta and Garcia, 2018a). The mechanics of the phenomena was recently studied using 3D numerical simulations at different spatio-temporal resolutions, using LES (Dutta et al., 2016) and Reynolds Averaged Navier-Stokes (RANS) based models (Dutta et al., 2017). The sensitivity of the sediment distribution process to the size of sediment showed that the phenomena is not only pertinent for the distribution of sediment traveling as bedload, but also for the sediment traveling in suspension (Dutta, 2017). The current study explores the implication of the phenomenon on the morphological evolution of diversions by analyzing the impact of Bulle-Effect on evolution of the channel-bed of an experimental diversion.The study also explores how the changing morphology impacts the hydrodynamics at the diversion. Based upon the available literature and knowledge of the processes, the study also discusses the impacts of the Bulle-Effect on morphological evolution of diversions beyond the set of conditions simulated for the current study.

2. Numerical Model

The 3D RANS based hydrodynamic model is used in conjunction with a morphodynamics model that accounts for the change in bed-elevation using the 2D Exner equation, and the bedload flux is calculated using the empirical bedload transport model by Meyer-Peter-Muller. Amount of bedload transported depends on the size of sediment and shear-stress on the bed, which is calculated using the classical quadratic relationship between the depth-averaged velocity and the friction-coefficient with the total bed shear stress. The bed friction was calculated using the Chezy formula. The hydrodynamic governing equations are discretized in space using the finite-element method, and integrated in time using a fractional step method. The computational-domain is composed of prismatic elements that are built from an unstructured triangulation of the two-dimensional domain, which are stacked in the vertical from the bed to the free-surface. The Exner equation is discretized in space using the finite-volume method.

3. Results and Discussion

The boundary conditions used for the simulations are similar to the ones used by Dutta et al. (2017), but with an erodible bottom that allows the bed to evolve in time. The simulations were run till the bed reaches equilibrium. Below we have reproduced equilibrium bed-elevation results for two of the cases. From the plots, one can observe the

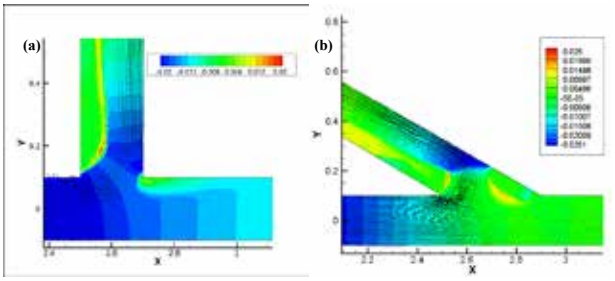

Figure 1. Equilibrium bed elevation contours for 90-degree and 150-degree diversions. The hydrodynamic and morphodynamic boundary conditions, and the size of sediment are exactly the same for all the cases.

appreciable scouring in the diversion-channel in the high-flow region, and formation of bar under flow-separation. This study lays the groundwork for future research on the topic of morphological evolution at diversions under the influence of Bulle-Effect, with implications for both engineered diversions and natural asymmetric bifurcations.

Acknowledgments

Major portions of the research by the first author was done while he was a PhD student at UIUC.

References

Bulle, H. (1926). *Untersuchungen über die Geschiebeableitung bei der Spaltung von Wasserläufen: Modellversuche aus dem Flussbaulaboratorium der Technischen Hochschule zu Karlsruhe*. VDI-Verlag.

Dutta, S. (2017). *Bulle-effect and its implications for morphodynamics of river diversions*. PhD thesis, University of Illinois at Urbana-Champaign.

Dutta, S., Fischer, P., and Garcia, M. H. (2016). Large eddy simulation (les) of flow and bedload transport at an idealized 90-degree diversion: Insight into bulle-effect. In Constantinescu, G. and Hanes, editors, *River Flow*, pages 101–109, Iowa City, USA. CRC Press.

Dutta, S. and Garcia, M. H. (2018a). Discussion of "evaluation of sediment diversion design attributes and their impact on the capture efficiency" by ahmed gaweesh and ehab meselhe. *J. Hydraulic Eng.*, 144(8):07018007.

Dutta, S. and Garcia, M. H. (2018b). Nonlinear distribution of sediment at river diversions: Brief history of the bulle effect and its implications. *J. Hydraulic Eng.*, 144(5):03118001.

Dutta, S., Wang, D., Tassi, P., and Garcia, M. H. (2017). Three-dimensional numerical modeling of the bulle effect: the nonlinear distribution of near-bed sediment at fluvial diversions. *Earth Surface Processes and Landforms*, 42(14):2322–2337.

Ten Reasons to Set up Channel Sediment Budgets for River Management

R.M. Frings[1] and W.B.M. ten Brinke[2]

[1] RWTH Aachen University, Aachen, Germany. frings@iww.rwth-aachen.de
[2] Blueland Consultancy, Utrecht, Netherlands. info@blueland.eu

1. Introduction

Rivers are dynamic systems with alternating patterns of sedimentation and erosion. Both sedimentation and erosion may have negative consequences from a perspective of river management. Sustainable river management calls for sufficient knowledge of a river's sediment dynamics. In order to identify areas and rates of sedimentation and erosion, river managers typically rely on acoustic echo soundings. Echo soundings, however, do not provide information on the provenance and fate of the sediment that is deposited or eroded. This essential information can be obtained by constructing a channel sediment budget (Figure 1). Channel sediment budgets represent the mass balance between the sediment entering the channel (I), the sediment leaving the channel (O) and the (change in) sediment stored in the channel (ΔS): I – O = ΔS. Whereas the value of catchment sediment budgets for management purposes is well recognized, the value of channel sediment budgets for management purposes is not. The main goal of this contribution is to provide scientists and river managers with arguments in favour of channel sediment budget studies.

2. Methods

Consultations of river managers and river scientists from within the Rhine River Basin.

3. Results and conclusions

Although drawing-up a sediment budget is time-consuming and complicated, it is very rewarding in that it strongly increases our understanding of the functional behaviour of a river system and the human impact thereon. Drawing-up a sediment budget helps river management in the following ways (Frings and Ten Brinke, 2018). It helps to: (1) create order in the apparent chaos of data, (2) identify morphological problems, (3) find smart solutions to problems, (4) set research agendas and monitoring strategies, (5) optimize dredging and nourishment strategies, (6) coordinate river management on basin-scale, (7) assess consequences of human interventions, (8) improve numerical models, (9) explain river management to society, and (10) train future generations of river managers.

References

Frings, R.M. and Ten Brinke, W.B.M. (2018). Ten reasons to set up sediment budgets for river management, International Journal of River Basin Management 16(1), 35-40, DOI: 10.1080/15715124.2017.1345916

Frings, R.M., Hillebrand G., Gehres, N., Banhold, K., Schriever, S. and Hoffmann T. (2019). From source to mouth: Basin-scale morphodynamics of the Rhine River. Earth-Sci Rev. 10.1016/j.earscirev.2019.04.002

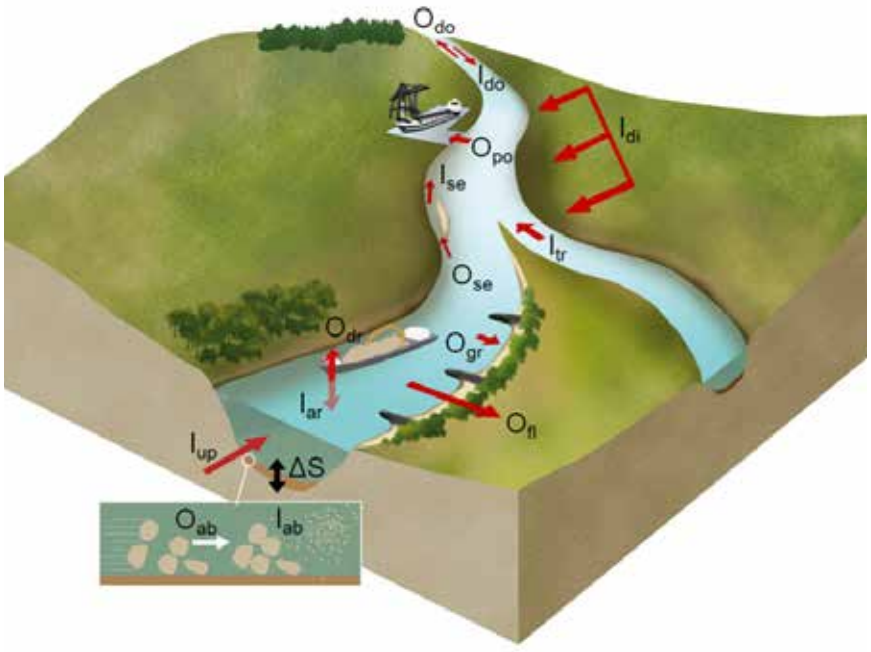

Figure 1: Cartoon of a channel sediment budget in a human-controlled river system, with different sediment inputs (*I*), outputs (*O*) and the storage term (Δ*S*) (after Frings et al, 2019). I_{up}, I_{tr}, I_{se}, I_{di}, I_{ar}, I_{ab}, I_{do} : sediment input from upstream, by tributaries, from secondary channels, from diffuse sources, by nourishment, through abrasion, or from the downstream area (in estuarine environments), respectively. O_{do}, O_{se}, O_{dr}, O_{gr}, O_{fl}, O_{po}, O_{ab}: sediment output to the downstream area, towards secondary channels, due to dredging, towards groyne fields, to floodplains, to ports or through abrasion, respectively.

Spatiotemporal analysis on three-dimensional morphology of coastal cliffs using terrestrial laser scanning and SfM-MVS photogrammetry

Y.S Hayakawa[1,2] and H Obanawa[3]

[1] Earth and Environmental Science, Hokkaido University, Sapporo, Japan. hayakawa@ees.hokudai.ac.jp
[2] The University of Tokyo, Kashiwa, Japan.
[3] National Agriculture and Food Research Organization, Sapporo, Japan, obanawah924@affrc.go.jp

1. Introduction

Although rapid, over 1 m per year of erosion rates of coastal cliffs has been reported in the outer Boso Peninsula, eastern Japan (Sunamura 1992), the modern work of coastal protection caused a notable decrease in the erosion rates. The decrease in cliff erosion also affected the nearby long sand beach where sand supply had been from the formerly eroded rocky coast. Quantitative evaluation of erosion rates by natural processes would therefore be necessary to assess the dynamics, i.e., relationships between erosion and protection, in both rocky and sandy coasts.

2. Method and results

A small coastal island in the outer Boso Peninsula named Suzume-Jima Island is an ideal site for the assessment. This island is located outside of the artificial coastal protection and natural erosional processes can still be observed. Here we conducted repeated morphological measurements of the entire island using structure-from-motion multi-view stereo (SfM-MVS) photogrammetry based on an unmanned aerial system (Hayakawa et al. 2016). We also carried out terrestrial laser scanning out for the accuracy assessment.
The high-frequency (2 or 3 times a year) and high-resolution (at a centimeter scale) measurements of the small island for 5 years revealed spatially variable rockfalls and concentrated wave cuts.

Figure 1: Study site: Suzume-Jima island. Note that the island is located outside of protection along the coast.

3. Discussion and conclusions

The 3-D point cloud data series quantitatively revealed the volume of lost mass. The short-term modern measurements are also compared with the long-term historical 2-D topographic changes in the island by aerial photographs for 50 years (e.g., Gomez et al. 2015).
According to the results, the erosion rate of the bedrock cliffs is on the order of decimeters. Although the modern erosion rate is lower than the previously reported cliff retreat rates, this suggests that the small island will disappear in decades. Three-dimensional structural analysis will also help understand the dynamic processes of the erosion of the island.

Acknowledgments

This work is a part of the Joint Research by the Center for Spatial Information Science (CSIS), The University of Tokyo. This work was supported by JSPS KAKENHI Grant Numbers JP25702014, JP25750148, JP17H02031 and JP16KK0012.

References

Gomez, C., Hayakawa, Y.S., Obanawa, H. (2015) A study of Japanese landscapes using Structure from Motion derived DSMs and DEMs based on historical aerial photographs: New opportunities for vegetation monitoring and diachronic geomorphology. *Geomorphology*, 242, 11-20. doi:10.1016/j.geomorph.2015.02.021

Hayakawa, Y.S., Obanawa, H., Saito, H., Uchiyama, S. (2016) Geomorphological applications of Structure-from-Motion Multi-View Stereo photogrammetry: A review. *Transactions, Japanese Geomorphological Union*, 37 (3), 321-343. (in Japanese with English abstract)

Obanawa, H., Hayakawa, Y.S., Gomez, C. (2014) 3D modelling of inaccessible areas using UAV-based aerial photography and Structure from Motion. Transactions, Japanese Geomorphological Union, 35 (3), 283-294. (in Japanese with English abstract)

Obanawa, H., Hayakawa, Y.S. (2018) Variations in volumetric erosion rates of bedrock cliffs on a small inaccessible coastal island determined using measurements by an unmanned aerial vehicle with structure-from-motion and terrestrial laser scanning. *Progress in Earth and Planetary Science*, 5, 33. doi:10.1186/s40645-018-0191-8

Sunamura T (1992) Geomorphology of rocky coasts. Wiley, Chichester

Simulation for the transtion of fish habitat in rivers

H.J. Hung[1], W. C. Lo[2], C. N. Chen [3*] and C. H. Tsai[4]

[1] National Cheng-Kung University, Tainan, Taiwan. hsuanjuhung@gmail.com
[2] National Cheng-Kung University, Tainan, Taiwan. lowc@mail.ncku.edu.tw
[3]National Pingtung University of Science and Technology, Taiwan, ginrochen2mail.npust.edu.tw
[4] National Cheng-Kung University, Tainan, Taiwan. jht581212@gmail.com

1. Introduction

A river habitat is affected by hydraulic conditions (water depth, velocity, discharge and water quality) and riverbed evolution (bed material conditions and bed form). Bed evolution from runoff and soil erosion does not only affect flow conditions, but also render an impact on the habitat in the alluvial river. The two-dimension river habitat transition model was developed combining the alluvial river-movable bed-two dimensional model (ARMB-2D Model) with the habitat model of the physical habitat simulation. Tsengwen River in southern Taiwan is used as an illustrative example in this study. The hydraulic conditions of Tsengwen river during the ordinary-flow condition and the period of flood rising and recession were simulated by the alluvial river-movable bed-two dimensional model. The flow conditions and the habitat model can be combined to calculate the combined suitability factor (CSF), weighted usable area (WUA), and percent usable area (PUA) by habitat suitability curve of depth, velocity, and substrate of the target species. The fish habitat distribution and transition of the Tsengwen river during the ordinary-flow condition and the period of flood rising and recession were simulated the two-dimensional river habitat transition model.

2. Results and Discussion

The simulation area is from the No.59 cross-section to the No.73cross-section. The computed cells are squared with $\Delta x = \Delta y = 25m$. The total cells are 11,953 and the time step (Δt) is 0.05 second. The Manning′s roughness coefficient is 0.035. The river is under ordinary flow for the most days of a year. Moreover, flooding occurs several times in a year. The flood flow is completely different from the ordinary flow and may change in the river bed. Hence, the ordinary flow (average annual discharge 44.08 cms, average discharge in dry periods is 3.38cms, average discharge in rainy periods is 84.57cms) and the flood of 2, 5, 10, 25, 50 and 100 return-period years are selected for simulation cases. Acrossocheilus paradoxus (Cyprinidae) is the target fish. Figures 1 and 3 show the distribution of the CSF in the river for the average annual discharge, average discharge in dry periods is 3.38cms, average discharge in both dry and rainy periods, respectively. Table 1 and Table2 show WUA and PUA for the average discharge in the dry and rainy periods, and six different return periods.

3. Conclusions

The simulation results indicate that the WUA distribution in the main channel under ordinary discharge. During flood process, WUA were distributed in the floodplain of the river and WUA in the floodplain was found to be greater than that in main channel. The habitat distribution ordinary flow and rainy periods flow is significantly different. WUA and PUA decrease as the flood flow discharge increases.

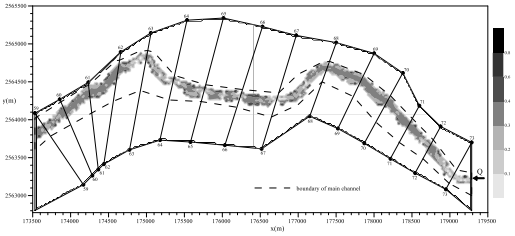

Figure 1: CSF during average annual discharge (44.08 cms) for Cyprinidae

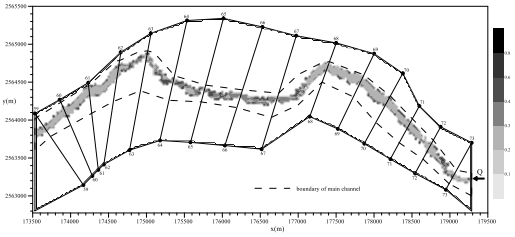

Figure 2: CSF during average discharge in dry periods (3.38 cms) for Cyprinidae

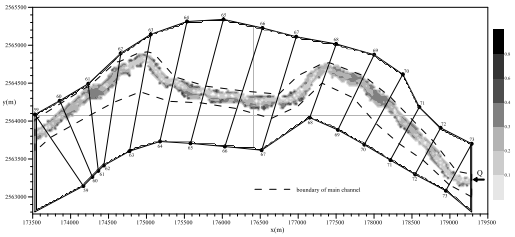

Figure 3: CSF during average discharge in rainy periods (84.57 cms) for Cyprinidae

Table1 WUA and PUA during average annual discharge, average discharge both in dry rainy periods.

Discharge (cms)	3.38	44.08	84.57
WUA (m^2)	234485	280534	267305
PUA(%)	33.35	32.36	27.33

Table 2 WUA and PUA during different return periods.

Discharge (cms)	2yr	5yr	10yr	25yr	50yr	100yr
WUA ($10^3 m^2$)	638.7	630.9	607.5	608.1	597.7	596.9
PUA(%)	12.90	10.22	9.25	8.75	8.37	8.18

References

Midcontinent Ecological Science Center(2001), PHABSIM for Windows ─ User's Manual and Exercises, USGS Open File Report, 01-340.

Tsai C.H. (2000) Numerical Simulation Flow and Bed Evolution in Alluvial River with Levees, Ph.D. Thesis. Department of Hydraulics and Ocean Engineering. National Cheng-Kung University: Taiwan.

Experiments on the Longitudinal Profile of Water Level Influenced by Dunes in Backwater Section

Yu Inami[1] and Satomi Yamaguchi[1]

[1] Civil Engineering Research Institute for Cold Region, Sapporo, Hokkaido, Japan. inami-y@ceri.go.jp

1. Introduction

In river engineering, it is important to be able to predict when and where water levels will rise. At the lower reaches of the Toyohira River in the City of Sapporo, Hokkaido, Japan, the water level is higher in sections affected by the backwater, as shown in Figure 1. Yoshikawa and Watanabe performed a calculation of one-dimensional unsteady flow in compound channels and suggested that the elevated water levels could be a result of flow resistance associated with dune shapes. In river sections affected by the backwater, water level rises caused by the formation of sand waves at reaches above or below those sections have a dominant influence on changes in the energy gradient; thus, it is possible that points in the river that satisfy the conditions for sand wave formation change in a complex way and that the longitudinal profile of the water level also undergoes complex changes. It has not been clarified how the characteristics of the longitudinal water level profile relate to the flow resistance associated with dune shapes in backwater sections. For the purpose of understanding the relationship between the characteristics of the longitudinal water level profile and the flow resistance associated with dune shapes in backwater sections, hydraulic experiments were conducted and the effects of sand waves on the kind of water level rises that are observed at the lower reaches of the Toyohira River were investigated.

2. Outline of Flume Experiments

The experiments were conducted in an experimental flume with a length of 34 m and a width of 0.5 m. Two cases were assumed in the experiments. In both cases, silica sand with a median diameter of 0.515 mm was used, and the discharge was 30 L/s. In Case 1, the bed gradient was 0 and the water level at the downstream end was the critical depth. In Case 2, the bed gradient was 1/500, and the water level at the downstream end was the critical depth.

3. Results

Figure 2 shows the longitudinal profiles of water levels and riverbed elevations in Case 1. Up to the 10.33-m point, the water level was the same as the initial water level and had not risen markedly in the 30 or 60 minutes after the start of the experiment. The water level had risen in the section upstream of this 10.33-m point. Sand waves formed throughout the flume within 30 minutes. In the section between the downstream end and the 4-m point, the sand waves disappeared within 60 minutes from the start of flow. Figure 3 shows the relationship between dimensionless total shear force and dimensionless effective shear force as proposed by Kishi and Kuroki (1973). The data for the first 30 minutes of the experiment indicate that flow resistance associated with dune shapes

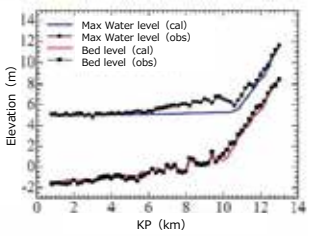

Figure 1. Water level and bed elevation

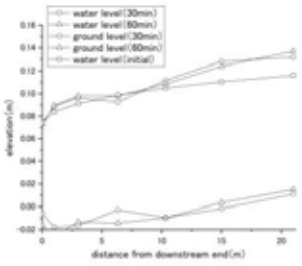

Figure 2. Water level and ground level（Case 1）

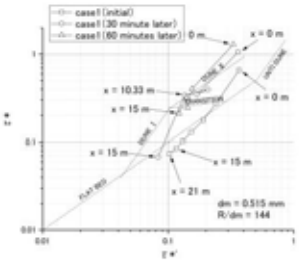

Figure 3. The τ* and τ*' relation （Case 1）

developed at the 10.33-m point but not at the 15-m point. This suggests that the water level rise at the 10.33-m point was caused by flow resistance associated with dune shapes, and that the water level rose at the 15-m point due to the water level rise at the 10.33-m point.

4. Conclusions

This study was conducted in order to examine the relationship between the characteristics of the longitudinal water level profile and the development of sand waves in backwater sections by addressing drop-down. The results help us to understand the development of sand waves in backwater sections and the process of water level rises at upper reaches which are caused by sand wave formation.

References

Yoshikawa, Y., WATANABE, Y. (2008). Examine of Manning's coefficient and the Bed-load layer for One-dimensional Calculation of Bed Variation.

kishi, T., kuroki, M. (1973). Bed Forms and Resistance to Flow in Erodible-Bed Channels (I).

Characterizing channel kinematics in the Ganges Brahmaputra Meghna Delta from remotely sensed imagery

T.M. Jarriel[1], L.F. Isikdogan[2,3], A. Bovik[2], and P. Passalacqua[1]

[1] Department of Civil, Architectural and Environmental Engineering and Center for Water and the Environment, The University of Texas at Austin, Austin, TX, USA. teresa.jarriel@utexas.edu, paola@austin.utexas.edu
[2] Department of Electrical and Computer Engineering, The University of Texas at Austin, Austin, TX, USA. leo@isikdogan.com, bovik@ece.utexas.edu
[3] Intel Corporation, Santa Clara, CA, USA.

1. Introduction

River deltas are one of the environmental ecosystems most threatened by climate change and increasing anthropogenic activity. One particularly large and threatened delta is the Ganges-Brahmaputra-Meghna Delta (GBMD) on the southern coast of Bangladesh/West Bengal India. This delta is home to hundreds of millions of people, hosts the largest continuous mangrove forest in the world, contains important marine and fluvial navigation pathways inland, and produces agricultural resources required for the maintenance of the rest of the region. Although this delta is very important, because of its size and complex network of constantly evolving channels, characterizing channel kinematics across different scales has been an issue that remains to be adequately addressed. In this study, we apply a new method for the automatic extraction of distributary channel networks, RivaMap, to obtain channel maps for kinematic analysis of the GBMD from 1989-2017. We first validate the method by applying it to a set of imagery of a physical experimental delta basin where the changes in forcings are explicitly known. We then apply the method to the imagery of the GBMD to characterize how different zones of the delta respond to changing forcings over the time period of observation.

2. Methods

2.1 RivaMap Method

RivaMap is an image processing-based method consisting of three major components (i) curvilinear structure detection using a multiscale singularity index, (ii) channel centerline extraction and delineation, and (iii) channel width estimation (Isikdogan et.al, 2015; Isikdogan et.al. 2017). The multiscale singularity index is a combination of first and second derivatives of the Gaussian kernel that is applied at different scales to extract the channel network. It responds strongly to curvilinear structures and weakly to edges. The outputs from this method are a non-binary singularity index response map representing channel locations, a skeleton of the channel centerline network, and a file containing data on channel center point location and width.

2.2 Variance Method

Once the singularity index response maps for each image have been produced, we calculate the variance of each pixel's singularity index through time. High variance values indicate that the pixel has experienced a large change in channelization. Small variance values indicate that there has been relatively low change in channelization. The variance map allows us to identify hot spots of change.

In addition to the variance map, to add directionality to the variance, we conduct a linear regression analysis on the time series of singularity index response. Positive slopes indicate that the pixel became more channelized, negative slopes indicate that the pixel became less channelized, and slopes near zero indicate that either the channel experienced no change or that the channel experienced an oscillatory pattern of change. By overlaying the linear regression slope map on the singularity index variance map, we can make inferences about what morphological changes occurred in the system (lateral migration, avulsions, bifurcations, widening, narrowing, etc.) (Jarriel et.al, in revision*)*.

Additionally, we track the migration of channel centerlines by applying particle image velocimetry (PIV) techniques to the centerline skeletal network output by RivaMap. The PIV method tracks centerlines from time step to time step and produces a vector field of migration rates that can be interpolated to create a map of the spatial distribution of the channel migration rates.

3. Conclusions

We find the RivaMap method can accurately extract channel locations and centerlines from the experimental delta imagery and that the variance analysis can distinguish between the different forcings on the experimental system. When the method is applied to the GBMD, there is a clear distinction in the variance of the singularity index response between the anthropogenically modified region and the Sundarban National Forest. High values of variance in the anthropogenically modified region suggest that the embankments are causing acceleration of morphological change.

Acknowledgments

We would like to acknowledge support from the National Science Foundation, grants OCE-1600222 and EAR-1350336.

References

Isikdogan, F., Bovik, A., and Passalacqua, P. (2015), Automatic channel network extraction from remotely sensed images by singularity analysis, IEEE *Geosci. Remote Sensing Letters*, 12 (11), 2218-2221.

Isikdogan, F., Bovik, A., and Passalacqua, P. (2017), RivaMap: An automated river analysis and mapping engine, *Remote Sensing of Environment*, 202, 88-97.

Jarriel, T., Isikdogan, F., Bovik, A., and Passalacqua, P., Automatic extraction of distributary networks and their variation through time, *Journal of Geophysical Research - Earth Surface*, in revision.

Understanding Global Motu Morphometrics

F. M. Johnson[1] and A. C. Ortiz[1,2]

[1] Dept. of Civil, Const., and Env. Engineering, North Carolina State University, Raleigh, USA. fmjohnso@ncsu.edu
[2]Department of Geology, Colby College, Waterville, ME USA.

1. Introduction

Atolls are carbonate reef systems found in subtropical and tropical oceans composed of a reef flat, motu (also known as reef islands, cays, and islets), and an inner lagoon (McLean and Kench, 2015) (Fig. 1). They may be particularly vulnerable to climate change including increasing ocean temperatures (causing coral die-off), ocean acidification (decreasing coral resiliency), and increasing sea level rise (Duvat et al., 2017). Accelerated rates of sea level rise is expected to increase significantly, with a global average increase of at least 1 m by 2100. Our goal is to automate the analysis of atolls morphometrics and apply it globally utilizing open-source cloud-based geospatial analysis coupled with freely-available Landsat satellite imagery.

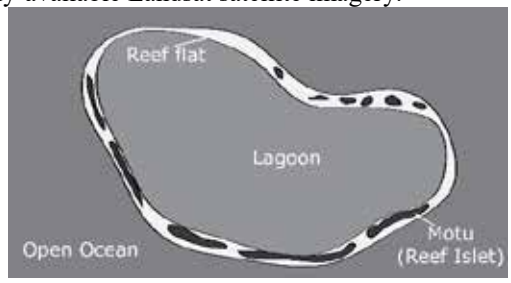

Figure 1. Characteristic atoll morphology.

2. Approach

Certain atolls and motu may be resilient to climate change (McLean and Kench, 2015). Motu form and respond to changes in the environment quickly, with motu formation on the scale of decades to millennia and evolution of motu on as short as time scale as weeks. However, we lack comprehensive understanding about the primary processes driving motu evolution within the paradigm of rising sea levels, changing sediment supply, and varying storm and wave climate. We must understand how motu respond and evolve with changing environmental forcings on a global scale.

2.1 Methods

Cloud-free temporal Landsat composites are created and automatically classified into three components: reef flat, motu, or water using methods developed by Ortiz et al. (2017). K-means clustering are applied to create a classified image to separate reef flat, motu, and water (Fig. 2a-b). The different Landsat bands will used together to identify each component of the atoll, automatically thresholding to achieve maximum separation of populations.

Previous work by Stoddart (1965) compiled a list of 99 atolls and found that there was a wide range of atoll size and shape, but that they clustered around a mean shape approximately 1.5-3 times long as they are wide. I am extending this analysis globally, automating it, and examining a wider range of motu morphometrics, including average width of the reef flat in front of the motu (Fig. 2f).

Modelled wave climate (from WaveWatch III) data over the time period of each temporal composite will be collated and reduced to representative offshore wave conditions for each atoll. I plot wave height squared (as a proxy for wave energy and proportional to bed shear stress driving sediment transport and ultimately motu evolution) vs. motu area and reef-flat width in front of motu (Ortiz & Ashton, 2019).

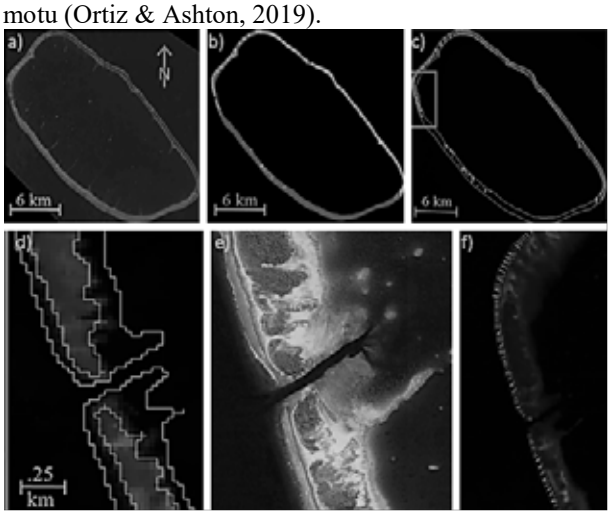

Figure 2. Landsat 8 satellite imagery of Katiu Atoll, French Polynesia. a) 2017 temporal composite; b) k-means classified atoll components; c) outlined components; e) Google Earth image; f) reef-flat width

3. Conclusions

This project will determine if wave climate and storms are the primary driver of motu evolution. Additionally, a global database of atolls and their morphometrics will be created and used for further analysis. This will increase our understanding of processes driving landscape change on atoll islands (locations highly vulnerable to changing climate impacts). Moreover, it will provide us with the tools to analyse globally which drivers of atoll island evolution dominates.

References

Duvat, V.K.E., Salvat, B., and Salmon, C., 2017, Drivers of shoreline change in atoll reef islands of the Tuamotu Archipelago, French Polynesia: GPC, doi: 10.1016/j.gloplacha.2017.09.016.

McLean, R., and Kench, P., 2015, Destruction or persistence of coral atoll islands in the face of 20th and 21st century sea-level rise? Wiley Interdisciplinary Reviews: Climate Change, v. 6, p. 445–463, doi: 10.1002/wcc.350.

Ortiz, A.C., and Ashton, A.D., 2019, Exploring carbonate reef flat hydrodynamics and potential formation and growth mechanisms for motu: Marine Geology, v. 412, p. 173–186, doi: 10.1016/j.margeo.2019.03.005.

Stoddart, D.R., 1965, The shape of atolls: Marine Geology, v. 3.

Study on Driftwood Deposition Patterns and Bed Morphology on an Alternating Bar

T. Kang[1], I. Kimura[2] and S. Onda[3]

[1] River System Engineering and Management Laboratory, Kyoto University, Japan. Kangxodns@gmail.com
[2] University of Toyama, Japan. ichiro@sus.u-toyama.ac.jp
[3] Kyoto University, Japan. onda.shinichiro.2e@kyoto-u.ac.jp

1. Introduction

Driftwood motions with wood deposition and jam formation affect to change the configuration of the water flows and channel bed in rivers. Therefore, the studies related to driftwood have been actively conducted to understand the mechanism of the driftwood dynamics. In particular, bed morphology by driftwood is one of the challenging issues in the numerical simulation. This is because the calculation for the morpho-dynamics with driftwood requires numerically refined physical interaction among the sediment transport, the water flow and the motion of driftwood. Thus, this study conducted the numerical simulation considering the bed morphology with large wood and tried to simulate the flume experiment. An alternating bar is considered as a bed shape in this study because it is useful to make clear the comparisons between bed morphology with/without driftwood and to easily reproduce the channel patterns in the simulations.
We discussed the experimental results and the simulation results, and the simulated bed morphology patters as well as the model limitation were clarified.

2. Experiment and computation

The flume experiment was set as shown in Table 1. We have two types of flow discharge to generate or not generate the alternating bar. The threshold the discharge of generating the alternating bar is 0.0023 m3/s and if flow discharge increases, the alternating bar is swept away by larger water flow. We considered several types of driftwood considering diverse length, diameter, and the absent/present of root wad. The time interval of wood supply is 5 sec, and initially, the angle between trunk wise and stream wise directions is 90 degree to be easily moved by large projection area to downstream when driftwood is supplied at the upstream region.
As for the computation, we used the 2D (two-dimensional) shallow water flow model, called Nays2DH (Shimizu et al., 2014) of the iRIC software (2019) to simulate the flow phase. Nay2DH is an Eulerian model to calculate the water flow on the generalized coordinate. A Lagrangian type driftwood model, which expresses the driftwood as connected sphere shape particles, was employed. We considered root wad effect by using larger diameter for a particle at a head of driftwood. In addition, an anisotropic bed friction was considered for the sliding motion dependent on stemwise, streamwise and motion directions (Kang and Kimura, 2018). We particularly considered changeable draft at each particle and projection area by an angle between stemwise and flow directions to precisely reproduce the wood motions. DEM (Discrete Element Method) was employed to reproduce the wood collision. Zero equation model is used for the turbulence flow. To solve the advection term in the water flows, we used the third order TVD MUSCL scheme. The first order forward Euler scheme is used for the wood motion. For the computational efficiency, we used the Open Multi-Processing (Open MP) in the solver. The simulation results were compared with experimental results to verify the model.

Table 1: Experimental setup

Type	Value (approximated)
Channel slope	0.005 m/m
Flow discharge	0.0023 – 0.0046 m^3/s
Grain size (d_{50})	0.51 mm
Channel width	0.4 m
Channel length	12.14 m
Diameter of driftwood	0.01 – 0.03 m
Length of driftwood	0.1 – 0.3 m
Diameter of root wad	0.02 – 0.05 m
Density of driftwood	670 – 700 kg/m^3
Interval time of driftwood supply	5 – 10 s
Wave length of alternating bar	3 m
Height of alternating bar	0.03 m
Initial angle of driftwood	90 [deg]

3. Conclusion

We conducted both experiment and computation, then the results were compared. The experimental results showed the driftwood deposition patterns by the alternating bars. The computation could visually reproduce them (Figure 1). However, some of limitations in the computation were indicated (e.g., jam formation of driftwood), so it should be refined in a further study.

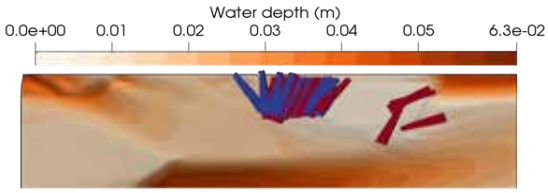

Figure. 1 Example of simulation result at upstream region (Blue and red trapezoids indicate driftwood with and without root, respectively.)

Acknowledgments

We are thankful to Japan Society for the Promotion of Science (JSPS) for providing funding for this research.

References

Kang, T., and Kimura, I. (2018). Computational modeling for large wood dynamics with root wad and anisotropic bed friction in shallow flows. Advances in Water Resources, 121: 419-431.

International River Interface Cooperative (iRIC). (2019). homepage, http://i-ric.org/en.

Shimizu, Y., Takebayashi, H., Inoue, T., Hamaki, M., Iwasaki, T., and Nabi, M. (2014). Nays2DH solver manual. Available Online: http://i-ric.org/en.

Numerical experiment on river meandering

Shigekazu Masuya [1], Takuya Inoue [2], Toshiki Iwasaki [2] and Yasuyuki Shimizu[3]

[1] DoconCo.,Ltd. sm1536@docon.jp
[1] Dr. of Eng., Researcher, Civil Engineering Research Institute for Cold Region, Sapporo, Hokkaido
inoue-t@ceri.go.jp , iwasaki-t@ceri.go.jp
[3] Department of Field Engineering for Environment, School of Engineering, Hokkaido University, Sapporo, Hokkaido
yasu@eng.hokudai.ac.jp

1. Introduction

The evolution of the meandering rivers is controlled by a mutual interaction among in-channel bed morpho-dynamics, bank erosion and deposition as well as channel planform dynamics. In spite of a number of previous researches, it is still challenging research topic to understand the morphodynamics of river meandering. In this study, we perform a sensitivity analysis of the simulated meandering channel dynamics by using a numerical model to understand how the model predicts the coevolution of the in-channel geometry and channel planform.

2. Method

We use a numerical model proposed by Asahi et al. (2013) to simulate the morphodynamcis of single-thread meandering channels. This model consists of a 2D unsteady shallow water flow model, the bedload-dominated in-channel morphodynamic model and channel planform model, which considers the interactions between outer bank erosion and inner bank deposition. The model can reasonably simulate the development of highly-sinuous meandering channel including the cutoffs.

We perform 30 numerical runs to understand the characteristics of modelled meandering channel dynamics. For this sensitivity analysis, we changed the water discharge, which is constant in time, and initial channel width for each run, but the grain diameter of 75 mm and initial channel slope of 0.01 are fixed. We herein focus on relatively short-time scale meandering development so that the effect of cutoff on the meandering development is neglected.

3. Results and Conclusions

Figure 1 shows the temporal changes of channel sinuosity and width-depth ratio simulated in the series of numerical runs. Figure 1 demonstrates that the channel sinuosity starts increasing at 8 hours, indicating the incipient of channel meandering. Within this early stage of meandering development, the channel width-depth ratio changes significantly as shown in Figure 1b. In the later stage, the channel sinuosity keeps varying in time, however, the channel width-depth ratio asymptotically approaches to constant value around 20. This result might indicate that the model can predict an equilibrium state in term of in-channel geometry of meandering rivers. In other words, under the given water discharge and grain size, the model selects their channel width and depth although the channel sinuosity is highly varied in time.

Another important result is that the model simulates two different types of channel planforms as shown in figure 2. These two computations were performed under same computational setting except the initial channel width. The meandering development shown in figure 2a indicates that the characteristics of the channel bends (e.g., wavelength) are likely well-organized in space. On the other hand, as shown in figure 2b, some combination of the model parameters generates an irregular pattern of meandering channel. The results suggest channel that the planform development is highly sensitive to the initial condition and selected model parameters, so that the location of the highly amplified meandering bends may be unpredictable in the context of deterministic point of view.

The implication of the results above needs to be further discussed by performing many computational runs with a large parameter space.

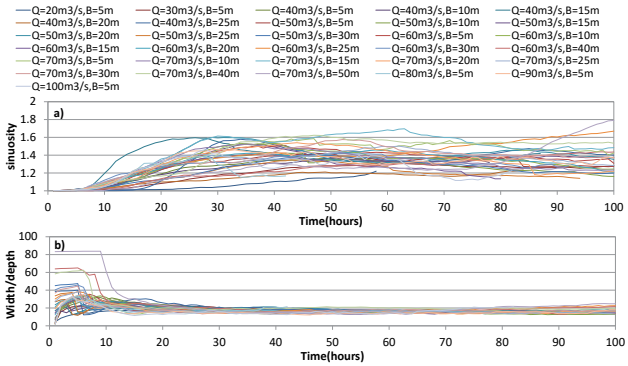

Figure 1. Temporal change of the a) channel sinuosity and b) width-depth ratio in the series of numerical runs.

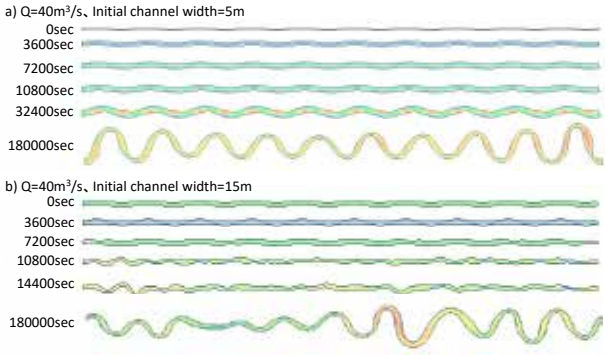

Figure 2. Two examples of the channel planform development.

References

Asahi, K., Shimizu, Y., Nelson, J. and Parker, G. (2013) Numerical simulation of river meandering with self-evolving banks, *J. Geophys. Res.*: *Earth Surface*, 118(4).

Effects of sand supply on gravel mobilization and channel formation in gravel beds

H. Miwa[1] and Keitaro Yamada[2]

[1] Department of Social Systems and Civil Engineering, Tottori University, Tottori, Japan. miwa-h@tottori-u.ac.jp
[2] Public Works Management Department, Kyoto City Office, Kyoto, Japan.

1. Introduction

Cut off the sediment supply to rivers downstream of dams may cause not only the channel degradation and bed-surface armoring but also the channel immobilization. Therefore, many works have been conducted in order to make restoration of such rivers. Since the existence of fine sediment (i.e. sand) in streambeds composed of coarse sediment (i.e. gravel) causes the reduction of the friction angle of coarse sediment (e.g. Miwa and Parker, 2017), fine sediment supply to the gravel bed may cause channel evolution through the gravel mobilization. In this study, we investigate the effects of sand supply to the armored gravel bed associated with sand-covering on gravel mobilization and channel formation.

2. Experimental setup and Procedures

Experiments were conducted in a straight open channel with a length of 16 m and a width of 0.5 m. Three kinds of uniform sediments, Gravel A of grain size d_g = 7.1 mm, Sand A of d_s = 1.4 mm and Sand B of d_s =0.52 mm, and the mixture which was made from Gravel A and Sand B were used for the experiment. The ratio of Sand B to Gravel A in the mixture was regulated so as to be 4:1. A box was used as a mobile-bed area with a length of L = 1.8 m and a width of B = 0.5 m. The upstream and downstream sides of the box was provided with a fixed bed of the Gravel A. The mobile-bed area was an armored bed which was made by supplying a low-flow rate without sediment feeding to the mobile bed composed of the mixture. The longitudinal right half of the mobile-bed area was covered with Sand A before commencing experiment. Five kinds of the thicknesses of the cover layer was provided. The amounts of Gravel A and Sand B which moved from their original positions were measured sequentially during the experiment. The bed surface elevations were measured in a prescribed timing. In order to clarify the effects of the sand-covering and subsurface sediment on the gravel mobilization and channel formation, the experiments without the sand-covering and/or without Sand B as subsurface sediment (only Gravel A) were also conducted.

3. Experimental results and discussions

Figure 1 shows the masses in grams of Gravel A and Sand B removed from the mobile-bed area under the condition of flow rate Q = 0.03 m^3s^{-1}. The mass of Gravel A that was removed in the experiment for which Sand A was supplied as a sand-covering (Case 2 and Case 3) was considerably larger than that for the experiment without sand-covering (Case 1). Moreover, the mass of Gravel A in the experiment with armored bed (Case 3) was the largest among the three experiments. This may be caused by the low friction angle of Gravel A engendered by the exposure of Sand B, which was originally in the subsurface layer, to the flow after removing gravel from the subsurface layer.

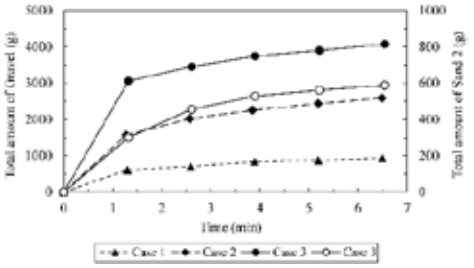

Figure 1: Masses of gravel and sand from mobile-bed.

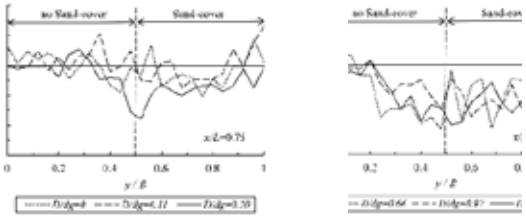

(a) D/d_g = 0～0.3 (b) D/d_g = 0.66～1.31

Figure 2: Transverse profiles in the end of experiments.

Figure 2 shows the transverse profiles in the end of the experiments with sand-covering to the armored bed (Case 3). The index of D/d_g means the ratio of the sand-covering thickness to the gravel size. The streambed erosion can be identified for all experiments. In particular, the bed erosion area is extended to the area without sand-covering in case of D/d_g is over approximately 0.6. This means that the sand-covering to the armored bed may cause channel formation through the gravel mobilization.

4. Conclusions

1. Gravel in streams with armored beds can be relatively easily mobilized by supplying sand as a sand-covering. The fraction of sand in the subsurface layer in the bed can also play a role in the reduction of the fraction angle of gravel.
2. The amount of gravel run-off increases with increasing the thickness of the sand-covering layer, whereas the efficiency of the sand-cover decreases when the height of surface of sand-cover exceeds the height of gravel bed surface.
3. Sand supply to the armored beds can produce the bed variation and channel formation through the gravel mobilization. In particular, the bed variation area is extended to the area without sand-covering in case of the value of D/dg is over approximately 0.6

References

Miwa, H. and Parker, G. (2017). Effects of sand content on initial gravel motion in gravel-bed rivers, *Earth Surface Process and Landforms*, Vol.42(9): 1355-1364.

Modification of the Wang-Lin River Reach and its impacts on the channel stability of the Huaihe River

Jin NI [1], Bangyi YU [1], Jueyi SUI [2] and Hui ZHANG [1]

[1] Anhui Province Key Laboratory of Water Conservancy and Water Resources (Anhui and Huaihe River Institute of Hydraulic Research), Bengbu, Anhui, China.
[2] University of Northern British Columbia, Prince George, Canada.

1. Introduction

The Wangjiaba-Linhuaigang River Reach (Wang-Lin Reach) of the Huaihe River has a length of 111 km. Along this river reach, several large branch rivers join the Huaihe River. Some large flood detention zones are located along this river reach. As a consequence, it is one of the most important and complicated river reaches of the Huaihe River. Since the main channel of the Wang-Lin reach is narrow, its discharge capacity during flooding season does not meet the requirement. The modification of this river reach has been carried out by dredging the main channel to increase the discharge capacity. Table 1 lists the existing methodologies for flood management (Yu and Yang, 2013; Chen et al., 2017).

Table1 Dredging Schemes

Scheme Name	Dredging Line	Dredging Volumn(10^4m^3)
A	North diversion channel	1901
B	North diversion channel	5000
C	South main channel	3000

Wherein, the two different dredging schemes of the north diversion channel refer to the dredging of flood diversion channel, namely the Menghe River (See Fig. 1).

The cross section at Wangjiaba is the boundary between the upper reach and middle reach of the Huaihe River. The Wang-Lin reach is located in the transition zone from the upstream mountainous region to the Huaihe plain. Due to the obvious decrease in slope of the riverbed, flow velocity in the Wang-Lin reach decreases clearly. Additionally, a secondary channel of the Huaihe River appears along the river reach. Thus, this river reach is the main sediment deposition zone of the Huaihe River. Under this specific condition, there are two questions: Whether the main channel lead to serious siltation after dredging process? Will this cause the current main stream to shrink and even cause the unfavorable translocation between main and diversion channels? Obviously, it is necessary to study the impact of modification scheme on the stability of riverbed, flow discharge and water level in the main channel of the Huaihe River.

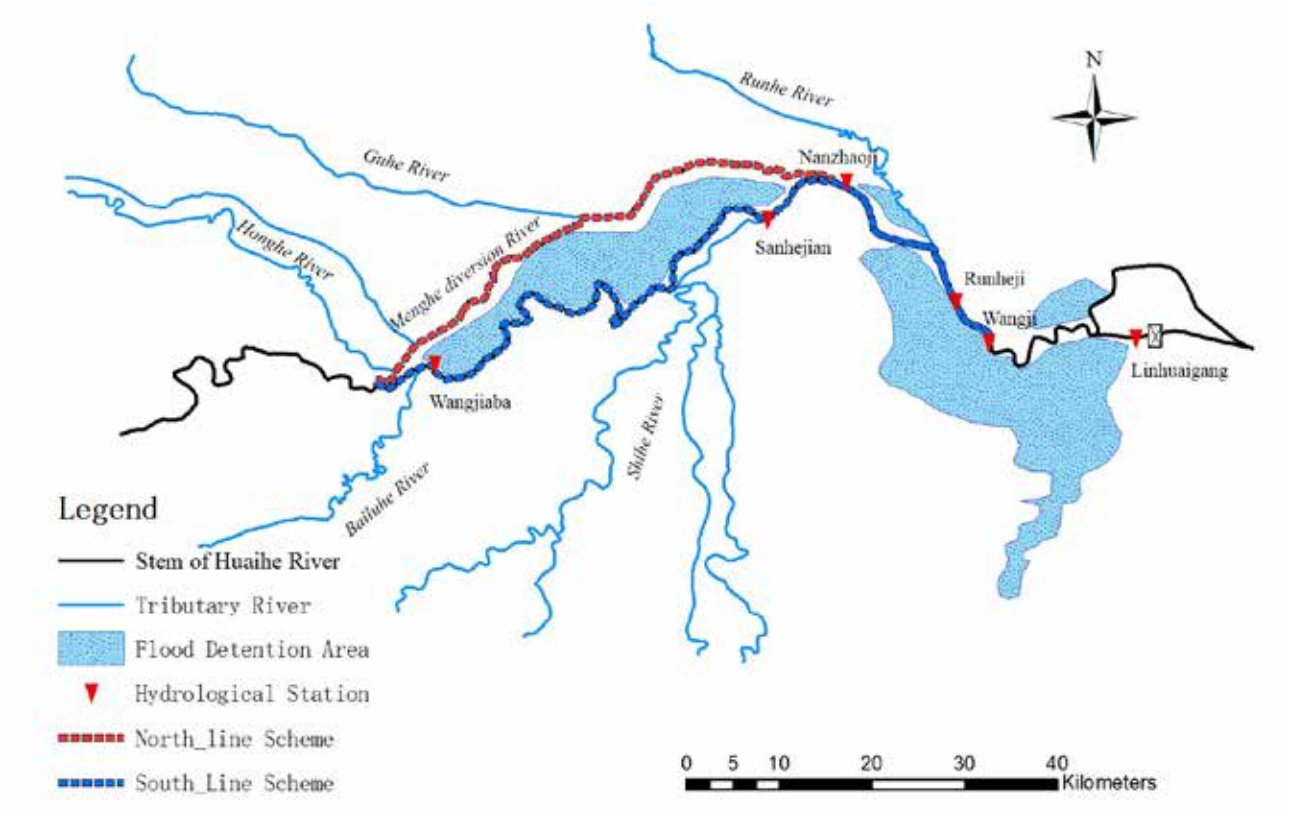

Fig. 1. River regime and modification schemes of the Wang-Lin reach of the Huaihe River

2. Research methods

2.1 Mathematical Model

Based on the theory of non-equilibrium transport of non-uniform suspended sediment proposed by Han (2013), the 1D water and sediment mathematical model has been developed to simulate sediment transport and flow along the Wang-Lin river reach including the flood detention zones and branch rivers. Following aspects have been considered on this model: 1) the input of water and sediment from tributaries, 2) the diversion radios for both flow and sediment at the Wangjiaba cross-section, 3) the operation of flood detention zones, and 4) the operation of the Linhuaigang gate. This model has been verified by the measured data of flow and sediment from 1999 to 2008.

2.2 Quantitative Analysis

The work selected the data series representing the typical characteriscs of the recent changes in water and sediment along this river reach. The verified water and sediment model was used to determine the river discharge capacity and the riverbed deformation (erosion and deposition) patterns under the un-modified condition. Besides, we demonstrated the impacts of those three modification schemes on the improvement of discharge capacity and the changes in riverbed and water level in the next 30 years. Afterward, the preferred scheme for the modification of the Wang-Lin river reach was proposed.

3. Results

Table 2 shows the river deposition-erosion amount of un-modified situation and three dredging schemes in the next 30 years.

Table2 River deposition-erosion amount(10^4 m^3)

Reach Name	un-modified	Scheme		
		A	B	C
Wangjiba-Sanhejian	162	289	557	179
Sanhejian-Nanzhaoji	258	245	195	236
Menghe river	374	485	646	309
Nanzhaoji-runheji	197	174	13	309
Runheji-Wangji	-15	76	42	103
Wangji-Linhuaigang	477	260	206	296
Wangjiba-Linhuaigang	1453	1529	1658	1432

Under the un-modified situation and schemes, sediment deposition process continues along the Wang-Lin reach. The deposition speed is slow due to the low sediment concentration of the Huaihe River. It can be seen from table 2 that the average deposition volume ranges from 48×10^4 m^3 to 55×10^4 m^3. The largest is the dredging scheme B, followed by dredging scheme A, and the smallest is dredging scheme C and un-modified. Calculation results indicate that more deposition occurs downstream of the Nanzhaoji station if the Wang-Lin river reach is kept un-modified or conducted with dredging scheme C. After the implementation of those two schemes of dredging process of north diversion channel(Schemes A and B), sediment is mainly deposited in the branch sections upstream of the Nanzhaoji station. Wherein, with the large amount of dredging scheme of north diversion channel, the deposition volume of sediment in the main channel of the Huaihe River is large. This may cause the risk that the mainstream of the Huaihe River gets shrinked.

Once the channel is modified with north line or south line dredging scheme, the erosion-and-deposition adjustment process will start. After 30 years, there will be no significant change in the discharge capacity of the channel. However, with the large amount of dredging scheme of north diversion channel, the water level of along the Wang-Lin reach will be uplifted, which is not beneficial to flood control.

4. Conclusions

The results showed that all three schemes for modifying the Wang-Lin river reach can significantly improve the discharge capability. However the dredging scheme C has a good effect on reducing channel's deposition and stabilizing the river regime. Based on the above analysis, the dredging scheme of south channel is the optimal choice.

Acknowledgments

The work was supported by the National Key Research and Development Program of China (Grant No.: 2017YFC0405602), and the Special Funds Under the Leadership of the Central Government of China - Science and Technology Projects for Benefiting the General Public (Grant No.: 2016080802D118).

References

Yu, Y.Q. and Yang, X.M.(2013). Regulation project of Wangjiaba-Linhuaigang reach of the Huaihe River. Water Resources Planning and Design, 2013(11), pp. 62-65.

Chen, X.P., et al.(2017). Suggestion for regulation of Wangjiaba-Wangjieliu reach of the Huaihe River. Jianghuai water resources Sciences and Technology, 2017(3), pp.13-14.

Han, Q.W. (2013). Non-equilibrium transport of non-uniform suspended load, Science Press, pp.136-170, Beijing, China.

Study on Riverbed Variation Management by Groin at the Confluence of Kakogawa and Mino River

Junta Nishio[1], Yoshihiro Okamoto[1], Keiichi Kanda[2], and Fuminori Nakamura[3]

[1] National Institute of Technology, Akashi College, Advanced Course of Architecture and Civil Engineering, Hyogo, Japan. ac1808@s,akashi.ac.jp
[2] National Institute of Technology, Akashi College, Civil Engineering, Hyogo, Japan. ac1705@s.akashi.ac.jp
[3] Nagaoka University of Technology, Department of Civil and Environmental Engineering, Niigata, Japan. fnakamura@nagaokaut.ac.jp

1. Introduction

The Kakogawa River flows through Hyogo Prefecture in Japan. At the confluence of Kakogawa and Mino River, due to the meander in the river upstream, barrage water from the large barrage on the Kakogawa River (Kakogawa Barrage) and the Mino River tributary, has promoted the development of the sandbars on the right bank. The sandbars, which have enlarged and become fixed, currently deflect the passage of water back to the left bank and have decreased the usable water surface area. To wash away the sandbars, the groin was installed at the left bank in 2015. The purpose of this study was to survey the river topography near the Mino River confluence and identify the factors responsible for sandbar development by using model experiments.

2. Method of the model experiment

Figure 2 shows the model experimental channel of this study. The channel is rectangular, and it reproduces the river channel of the site by a scale of 1/250. The slope of the channel is set as 1/850 and this is similar to the site. The water surface is controlled by the movable barrage of the rise and fall system that was installed the downstream of the main channel. For the upstream conditions, a board with a width of 0.2m is installed at the right bank of the main channel to reproduce the influence of the meander. For the riverbed material, we use the coal powder, which density ρ_s is 1.47(g/cm^3) and average particle diameter is 0.9mm.

The conditions are shown in Table 1. Case1 targets the flood flow rate and Case2 targets the normal flow rate in the site. Furthermore, we install the groin at right angle to the flow direction before the confluence at the left bank of the main channel(X=2.35m). And the height of the barrage is 0cm. The experiment time is 1 hour. This time is conditioned by the time it takes for the riverbed variation to reach an equilibrium state in the preliminary experiment.

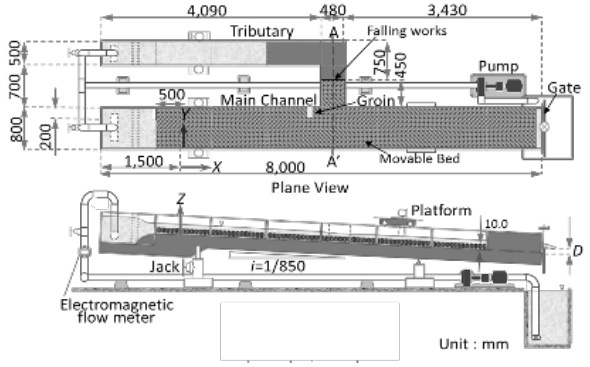

Figure 1 Experiment channel

Table 1 Conditions

No.	Time T(h)	The rate of Main Flow Q_M(l/s)	The Rate of Tributary Flow Q_T(l/s)	The Target Flow Rate	Groin
Case1	1.0	3.0	1.0	flood	Yes
Case2		0.8	0.27	normal	Yes

3. Results and considerations

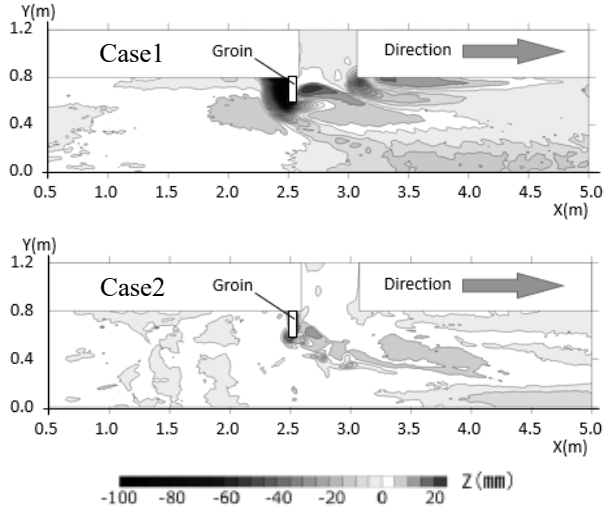

Figure 2 Riverbed Variation

Figure 2 shows the results of riverbed variation. In Case1, riverbed degradation occurs near the right bank after the confluence because the flow is deflected in the right bank by the groin. Because the flow is sharply deflected by the groin, deep scouring occurs in front of the groin, and the deposition occurs behind the groin, preventing the flow of the tributary.

In comparison with Case1 and Case2, the amount of riverbed variation decrease. And the tendency near the right bank is similar. But deep scouring in front of the groin is not observed; however, the deposition occurs there.

Acknowledgments

For this study, we used a grant for a joint study from the College of Technology and Nagaoka University of Technology. We express thanks to them.

References

Shoya, T., Keiichi, K., Kouji, M., Hiroki, K., Yoshihiro, O.,(2017)
Bed Variation and Its Control at a River Confluence Associated with the Upstream River Topography and Release of the Barrage *Annual Journal of Hydraulic Engineering, vol.61.*

Understanding the Impacts of Wave Converters on the Hydrodynamics and Morphodynamics

H. Moghadam[1] and A. C. Ortiz[1,2]

[1] Dept. of Civil, Const., and Env. Engineering, North Carolina State University, Raleigh, USA. hmohama@ncsu.edu
[2]Department of Geology, Colby College, Waterville, ME USA.

1. Introduction

Marine Hydrokinetic (MHK) devices provide an opportunity to expand renewable energy by harnessing waves and currents power and converting it to electricity. However, most MHK devices are in the developmental stage requiring research to understand their impacts on the environment, including the abiotic processes such as the wave field and sediment transport. We need to know whether these devices will be buried or excavated over time and the impact of the MHK devices on the hydrodynamics (the wave and current) and morphodynamics (the ocean floor evolution) to minimize operational costs. In this study, we use SNL-SWAN model (Chang et al., 2016) to investigate the wave field response to various MHK devices and then couple the MHK module from the SNL-SWAN model into Delft3D to obtain MHK impact on wave, flow, and sediment conditions driving long-term morphologic evolution.

The challenge for MHK devices is accurately modelling the response of the marine environment to the placement of these MHKs. Addressing this challenge requires the following considerations: (i) the MHK device extracting energy from the system as an energy sink, (ii) spinning turbines acting as a local energy source (Neill et al., 2009; Chen and Lam, 2014), (iii) effects of the sediment transport (due to waves, currents, and tides) such as scour or burial, and (iv) dynamically coupling all of these feedbacks within the system. Previous work has focused primarily on the response of the wave field around MHK devices as energy sinks, in particular, the SNL-SWAN model created by Sandia National Lab simulates the impact of wave energy converters (WECs) on the wave (hydrodynamics) field (Chang et al., 2016). However, it is necessary to understand the long-term impact of these devices on not just the wave field but also the sediment field and subsequent morphologic evolution of the coastal system.

2. Approach

Our overall goal is to develop a dynamically coupled model for the response and impact of the MHK device under waves, currents, tides, sediment transport, and energy production by the MHK structure. The specific objectives are: (i) simulate the wave field response to various MHK devices using the SNL-SWAN model, (ii) couple the WEC module from the SNL-SWAN model into Delft3D, (iii) simulate MHKs as both a source and sink of energy within Delft3D, and (iv) dynamically couple MHK impact on wave, flow, and sediment conditions driving long-term morphologic evolution.

2.1 Methods

Utilizing the Sandia National Lab (SNL) SWAN model (Chang et al., 2016), we investigated the various methods that MHKS can withdraw energy from the wave model (dependent on wave frequency, wave height, etc). We then implemented a simple analyses within Delft3D to investigate the morphodynamic impact of wave energy converters on sediment transport depending on how the MHKS are represented (Fig. 1).

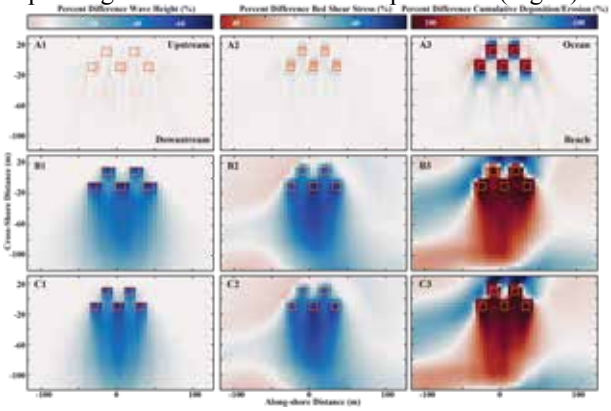

Figure 1. Comparison of different methods for representing MHK devices in Delft3D: method A – MHK only represented as bathymetric lump in Delft3D, method B – MHK only represented as obstacle in waves (no bathymetric change), and method C – MHK represented both as bathymetric lump in Delft3D flow and as obstacle in waves. Investigating the impact of MHK arrays on the wave height (column 1), bed shear stress (column 2), and cumulative bed level change (column 3) relative to the control (percent change).

3. Conclusions

We find that using the thin-dam obstacle inbuilt into the SWAN module of Delft3D seems to represent the wave climate and subsequent sediment transport reasonably. Moreover, it is important to also represent the devices physically within our model (method C) versus purely within SWAN (method B). We find significant near-field impacts on wave height and deposition under our large storm event (deposition exceeding several meters on the MHK devices over a storm) (Fig. 1).

4. References

Chang, G., Ruehl, K., Jones, C.A., Roberts, J., and Chartrand, C., 2016, Numerical modeling of the effects of wave energy converter characteristics on nearshore wave conditions: Renewable Energy, v. 89, p. 636–648, doi: 10.1016/J.RENENE.2015.12.048.

Chen, L., and Lam, W.-H., 2014, Methods for predicting seabed scour around marine current turbine: Renewable and Sustainable Energy Reviews, v. 29, p. 683–692.

Neill, S.P., Litt, E.J., Couch, S.J., and Davies, A.G., 2009, The impact of tidal stream turbines on large-scale sediment dynamics: Renewable Energy, v. 34, p. 2803–2812.

Influence of fluvial bar morphodynamics on seedling survival during floods

S. Rodrigues[1,2], C.L. Wintenberger[3], S. Greulich[1,2], P. Juge[4], M. Tal[5], M. Villar[6]

[1] UMR CNRS CITERES 7324, Université de Tours, 35 Allée Ferdinand de Lesseps, 37200 Tours, France. srodrigues@univ-tours.fr, greulich@univ-tours.fr
[2] Ecole Polytechnique de l'Université de Tours, 64 Avenue Jean Portalis, 37200 Tours, France
[3] Unité Risques Hydrauliques et Surveillance des Ouvrages et des Milieux - CEREMA Normandie-Centre - Laboratoire de Blois, France. coraline.wintenberger@cerema.fr
[4] CETU Elmis Ingénierie, Université de Tours, 11 quai Danton, 37500 Chinon, France. juge@univ-tours.fr
[5] CEREGE UMR 6635, Aix-Marseille Université, Europôle de l'Arbois, BP 80, 13545 Aix-en-Provence cedex, France tal@cerege.fr
[5] UMR 0588 INRA-ONF BioForA - 2163 Avenue de la Pomme de Pin CS 40001 Ardon, France. F-45075 ORLEANS Cedex 2, France. marc.villar@inra.fr

1. Introduction

During floods, seedlings endure three stresses: (i) drag force exerted on the stem induced by flowing water (Type I of Edmaier et al. 2011), (ii) substrate erosion combined with the drag force exerted on the plant (Type II), and (iii) burial. Several experimental studies highlighted the local disturbances exerted on plants (e.g., drag force exerted by the flow) and their ability to withstand these disturbances (Edmaier et al. 2011). Mechanistic studies integrating the complexity of sediment dynamics at the scale of the bar unit in natural rivers remain rare and local sedimentary processes involved in seedling mortality are poorly understood (Wintenberger et al., 2019).

Because of their relative stability in river channels, we assume that non-migrating bars of sandy-gravel bed rivers provide better conditions for recruitment and survival of woody pioneer trees (e.g., *Populus nigra*) in comparison with free migrating bars. This study relates survival patterns of *Populus nigra* seedlings to bar dynamics across flood phases on a non-migrating (forced) bar of the Loire River located near Orleans (France).

2. Methods

Sediment dynamics was assessed from bathymetrical, topographical, flow velocity (aDcp), scour chains, and sediment grain size surveys carried out on the same bar unit and related to seedling survival (see Wintenberger et al., 2019 for details).

Bathymetric and flow velocity surveys were conducted during two floods, that occurred after recruitment of *P. nigra* seedlings in November 2013 and January 2014. Surveys were done using a monobeam echo-sounder coupled with a Differential Global Positioning System (DGPS). Topography was surveyed at low flows using a Terrestrial Laser Scanner (TLS). Active sediment layer during floods was measured using scour chains and sieving was performed to analyze sediment grain size. At the end of the growing season of years 2013 and 2014 the density of *P. nigra* seedlings was measured at 48 plots georeferenced using a DGPS. Results were analysed using the Hill Smith analysis.

3. Results and discussion

Morphodynamical analysis of the bar highlighted contrasted sediment mobility according to the location on the bar. Namely a fixed area (presence of armor layers [D506.10-3 m]) and a spreading area (mixture of sands and gravels [2.10-3 m <D50< 6.10-3 m]) were identified (Wintenberger et al., 2015). Statistical analyses suggest that sediment texture and elevation influence initial seedling densities (high densities for higher elevation and finer sediment grain size). On the bar studied more than 90% of the seedlings present before the floods died. Stresses of Type I, II and III were responsible for 0.1%, 28% and 13.6% respectively. Finally, combination of Types II and III led to 50.6% of the mortality observed. This combination was the dominant parameter influencing seedling mortality at the bar scale but at different levels according to the area considered (15.9% on the fixed area *vs.* 34.7% on the spreading area). This combination complicates the determination of survival thresholds. The results suggests that seedlings tend to survive on more plots and at higher (survival) rates in the fixed area than in the spreading area.

4. Conclusions

The study highlights (i) the influence of flood succession and flood stages on seedling survival after establishment, (ii) the spatial distribution of fluvial processes at the bar scale and their relative contribution to seedling mortality, (iii) threshold values for each process. The relative contribution of each process depends on the combination and phasing of erosion and deposition processes, sediment supply (quantity and grain size), and flow velocity governed by hydrological variations. Based on the results of this study we hypothesize that the survival of seedlings during floods may be a function of local processes involved in bar dynamics.

References

Edmaier, K., Burlando P., Perona P. (2011). Mechanisms of vegetation uprooting by flow in alluvial non-cohesive sediment. Hydrology and Earth System Sciences 15:1615–1627.

Wintenberger C.L., Rodrigues S., Greulich S., Breheret J.-G., Jugé P., Tal M., Dubois A., Villar M. (2019) - Control of Non-migrating Bar Morphodynamics on Survival of *Populus nigra* Seedlings during Floods. Wetlands, in press. 10.1007/s13157-018-1121-7.

Wintenberger C.L., Rodrigues S., Claude, N., Breheret, J.-G., Villar M. (2015) - Dynamics of nonmigrating mid-channel bar and superimposed dunes in a sandy-gravelly river (Loire River, France). Geomorphology, 248, 185-204. DOI: 10.1016/j.geomorph.2015.07.032

A Tale of Two Deltas: Comparative Studies on the Effects of Dam Regulation On Deltaic Morphological Evolution

Weilun Gao[1], Dongdong Shao[2], Mawusi Amenuvor[3] and Yao Tong[4]

[1] State Key Laboratory of Water Environment Simulation & School of Environment, Beijing Normal University, Beijing, China. wl.gao@mail.bnu.edu.cn
[2] State Key Laboratory of Water Environment Simulation & School of Environment, Beijing Normal University, Beijing, China. ddshao@bnu.edu.cn
[3] State Key Laboratory of Water Environment Simulation & School of Environment, Beijing Normal University, Beijing, China. m.amenuvor_kfi@yahoo.com
[4] State Key Laboratory of Water Environment Simulation & School of Environment, Beijing Normal University, Beijing, China. 516709304@qq.com

1. Introduction

Deltas are the most populous areas and are among the most productive ecosystems on the planet. Despite their importance for human society and coastal ecosystems, the world's deltas are "sinking" to the ocean partly due to substantial decrease of sediment supply (Syvitski et al., 2009). Hydrological alteration induced by dam regulation has been recognized as one of the key factors affecting deltaic morphodynamics.

In this study, a comparative study on two wave-influenced deltas, namely, the Yellow River Delta in China and the Volta River Delta in Ghana, was conducted to illustrate the effects of dam regulations on delta morphological evolution. The implications of the results for the prediction of delta evolution under increasing human-induced hydrological alteration worldwide are also discussed.

2. Methodology

2.1 Study area

The Yellow River Delta is located at the coast of the Bohai Sea (Figure 1a), covering an area of 5,375 km^2. The Volta River Delta is located at the interface between the Volta River and the Atlantic Ocean (Figure 1b), covering a total area of approximately 5,000 km^2. Both deltas are classified as wave-dominated delta according to Galloway's diagram.

Figure 1. Remote sensing images of: (a) the Yellow River Delta and (b) the Volta River Delta.

Both rivers are subjected to significant dam regulations. The sediment flux to ocean for the Yellow River and Volta River were 1.3 and 2.6 Gt/a, respectively, before dam construction. Since the construction of the Xiaolangdi reservoir in 2002 in the Yellow River and the Akosombo reservoir in 1964 in the Volta River, the sediment supply to the two deltas has decreased substantially by 90%. As a result, both deltas have experienced severe coastal erosion.

2.2 Data analyses

The inter- and intra-annual alterations of the river discharge and sediment load were analysed and compared between pre- and post-dam periods. Mann-Kendall trend analyses were performed to reveal the impacts of dam regulations on hydrological alterations. Following Li et al. (2011), nonuniformity coefficient, C_y and regulated coefficient, C_r were adopted to quantify the intra-annual variations of the river discharge and sediment load.

Deltaic morphological characteristics including delta area and plan shape were extracted from remote sensing images and historical maps. The skewness quantifying the asymmetry of the delta following Wright and Coleman (1973) was adopted to assess the evolution of the delta plan shape. Finally, the relationship between river discharge (sediment load) and deltaic morphological characteristics were analysed.

3. Conclusions

Both nonuniformity coefficient, C_y and regulated coefficient, C_r decreased significantly with the dam construction in the two rivers. The annual sediment load to the deltas also decreased substantially after the dam construction. The decrease of sediment load resulted in erosion of both deltas and affected the plan shape of the deltas significantly.

Acknowledgments

This work was supported by the Key Project of National Natural Science Foundation of China (grant 51639001), the Key Project of NSFC-Shandong Joint Fund (grant U1806217) and the Interdisciplinary Research Funds of Beijing Normal University.

References

Li, D., Wang, W., Hu, S., and Li, Y. (2011). Characteristics of annual runoff variation in major rivers of China. *Hydrological Processes*. 26(19), 2866-2877.

Syvitski, J. P. M., Kettner, A. J., Overeem, I., Hutton, E. W. H., Hannon, M. T., Brakenridge, G. R., et al. (2009). Sinking deltas due to human activities. *Nature Geoscience*, 2(10), 681-686.

Wright, L. D. and Coleman, J. M. (1973). Variations in Morphology of Major River Deltas as Functions of Ocean Wave and River Discharge Regimes. *American Association of Petroleum Geologists Bulletin*. 57(2), 370-398.

A New Approach for Bathymetric Video-Inversion: Field Study

G. Simarro[1], D. Calvete[2], P. Luque[3], A. Orfila[4] and F. Ribas[5]

[1] Institute of Marine Sciences (ICM-CSIC), Barcelona, Spain. simarro@icm.csic.es
[2] Universitat Politecnica de Catalunya, Barcelona, Spain. daniel.calvete@upc.edu
[3] Coastal Ocean Observing and Forecast System Balearic Islands (SOCIB-CSIC), Palma de Mallorca, Spain.
[4] Mediterranean Institute for Advanced Studies (IMEDEA-CSIC), Esporles, Spain. aorfila@imedea.uib-csic.es
[5] Universitat Politecnica de Catalunya, Barcelona, Spain. francesca.ribas@upc.edu

1. Introduction and Methods

Scientists and managers of the coastal zone need to know the coastal bathymetry to understand the behaviour of the beaches and be able to predict their evolution. Intensive monitoring programs through campaigns of direct measurements of the bathymetry are excessively expensive, so that in the last decades alternative methodologies have been developed. Many of them are based on video monitoring stations, and among the different existing algorithms, cBathy (Holman et al., 2013) is the algorithm that achieves the best results.

In a first step, cBathy gets the dominant frequencies and their corresponding wave numbers from the Cross Spectral Matrices (CSMs) of a given set of frequency bands. An estimation of the local water depth is then obtained from the dispersion equation. In the second step, the estimated bathymetries obtained for each video are smoothed through a Kalman filter to obtain the final hourly estimates. This algorithm, which has been used in a number of studies (e.g., Bergsma et al., 2016; Rutten et al., 2017) to obtain 2-D bathymetries, presents however some limitations and/or known problems that have been reported in the literature (Rutten et al., 2017).

The work being presented here is an alternative to the first step of cBathy. It consists of performing a Principal Component Analysis (PCA) to the matrix made of pixel intensities from a series of snaps. The result of the PCA is the decomposition of the video into a set of modes associated with the components of the wave field. The spatial part (the Empirical Orthogonal Function, EOF), is associated with the spatial phase of the wave from which a wave number can be derived. The amplitude of the mode (Principal Component, PC) is associated with the frequency of the wave component. To facilitate the decomposition of the videos in modes of travelling waves, a Hilbert transformation in time of the matrix of intensities has been carried out.

The objective of this work is to apply the PCA of video images to obtain beach bathymetries. To this end, videos from different camera/field sites have been used and the bathymetry derived from videos has been compared with direct measurements. It has been studied the influence on the results of: the image lighting, the camera position, wave characteristics and study area size.

2. Results

The proposed methodology is applied to video images obtained at Castelldefels and Barcelona beaches (Spain), in the NW Mediterranean (coo.icm.csic.es). These beaches, open and embayed respectively, are exposed to relatively small dominant periods, in the order of 6s. The video snaps are first projected into a horizontal plane (plan-views) prior to apply the PCA. Further, it is analysed how the subdivision of the spatio-temporal domain influences the quality of the retrieved bathymetry.

For illustrative purposes, Figure 1 shows the bathymetry estimated for Castelldefels beach using the proposed algorithm.

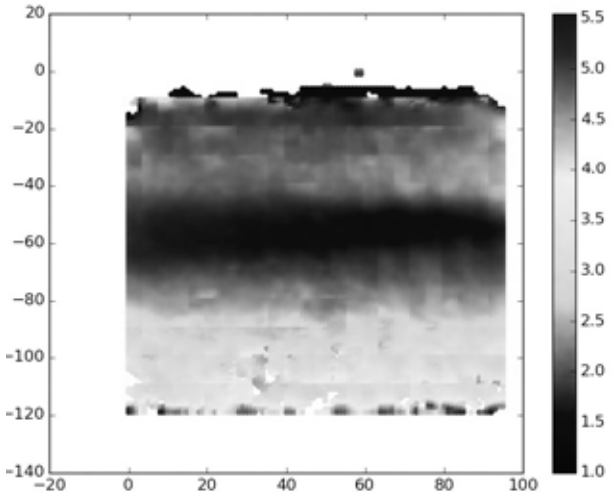

Figure 1. Bathymetry obtained from Castelldefels station. The shoreline is above. It is observed a bar at ≈ -50 in the vertical axis. All the units are meters.

3. Conclusions

The implementation of a simple and promising methodology for bathymetry inversion from video images is presented, and the results are satisfactorily compared to field data.

Acknowledgments

This research was partly funded by the Spanish Government projects CTM2015-66225-C2-1-P, and CTM2015-66225-C2-2-P (MINECO/FEDER).

References

Bergsma, E., Conley, D., Davidson, M., and O'Hare, T. (2016). Video-based nearshore bathymetry estimation in macro-tidal environments. *Marine Geology*, 374:31–41.

Holman, R., Plant, N., and Holland, T. (2013). Cbathy: A robust algorithm for estimating nearshore bathymetry. *JGR: Oceans*, 118(5):2595–2609.

Rutten, J., De Jong, S., and Ruessink, G. (2017). Accuracy of nearshore bathymetry inverted from x-band radar and optical video data. *IEEE Transactions on Geoscience and Remote Sensing*, 55(2):1106–1116.

The morphological response of a steep-slope channel to check dam adjustments, a numerical study

Su-Chin Chen[1] and Samkele Tfwala[2*]

[1] Department of Soil and Water Conservation, National Chung Hsing University, Taichung, Taiwan.
scchen@nchu.edu.tw
[2] Department of Geography, Environmental Science and Planning, University of Eswatini, Kwaluseni, Eswatini.
samkelet@gmail.com

1. Introduction

The frequency and magnitude of extreme events in Taiwan have soared over the years (Chen and Tfwala, 2018). These have seen accelerated rates of landslide formation, debris flow and channel bed erosion. In the wake of such natural disasters, engineering measures such as the installation of check dams have increased. Despite their wide adoption, most have become inactive as they are rapidly filled up by accumulating sediments (Figure 1).

Figure 1. Concrete check dam filled with sediments

This study applies a full 2D shallow water equation model resulting from the vertical integration of the Navier-Stokes equation and the 2D Exner equation, RiverFlow2D QGIS (GPU) by Hydronia to evaluate the channel morphological impacts of modifying the check dam shown in Figure 1 and 2. Upstream there was a single adjustable column while downstream there were 3. Triangular-cell flexible-mesh is applied in this model, in our case adopting 0.2 m cell size for the channel, with a much finer cell size where the check dam was located. Time step was dynamically computed. The bed load formula proposed by Ashida and Michiue (1972) was used to compute sediment transport rates. The check dams are fitted with blocks, 0.5 high × 3.4 wide. The studied river is Dongmen river, spanning 17.6 km with a catchment area of 68.6 hectares. The river is located in southern Taiwan and receives on average 2500 mm per annum.

Figure 2. Adjustable blocks fitted in the concrete dam

2. Results and discussion

Three simulation cases were conducted; one without any adjustments, with two blocks (1 m, vertically) removed and finally four blocks. An example of velocity distribution for the two blocks removed is shown in Figure 3. For illustrative purposes, the elevation changes of the unmodified check dam and two blocks removed is shown in Figure 4. The results suggest that RiverFlow2D may be applied to optimize the efficiency of check dams, within a short period of time. Block removal enhanced sediment transfer downstream.

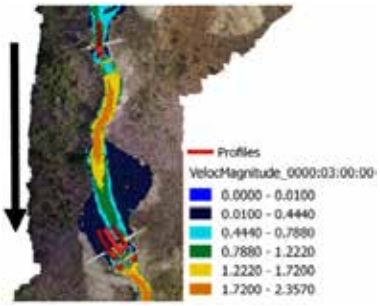

Figure 3. Velocity distribution in the simulated reach together with sampled longitudinal profiles. The arrow represents flow direction

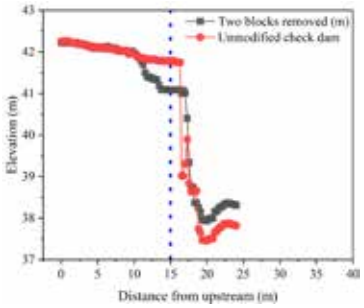

Figure 4. Longitudinal changes at upstream profile

.

3. Conclusions

The high-performance GPU algorithms in Riverflow2D supports engineers and river engineering works through better informed engineering decisions. From this study, optimum adjustments while obtaining results quicker is illustrated

References

Chen, C.N., and Tfwala, S.S. (2018). Impacts of Climate Change and Land Subsidence on Inundation Risk. *Water* 10(2): 157.

Ashida, K., and Michiue, M. (1972). Studies on bed-load transport rate in open channel flows, in *IAHR Int. Symp. River Mech*., Bangkok, 1, pp. 407.

Assessing particle travel distances in gravel-bed rivers

D. Vázquez-Tarrío[1,2] and R.J. Batalla[3,4,5]

[1] Department of Geology (University of Oviedo), Oviedo, Spain. vazquezdaniel@uniovi.es
[2] INDUROT (University of Oviedo), Mieres, Spain.
[3] Fluvial Dynamics Research Group (RIUS), University of Lleida, Lleida, Catalonia, Spain. rbatalla@macs.udl.cat
[4] Catalan Institute for Water Research (ICRA), Girona, Catalonia, Spain
[5] Facultad de Ciencias Forestales y Recursos Naturales, Universidad Austral de Chile, Valdivia, Chile

1. Introduction

Particle travel distances in Gravel-Bed Rivers (GBR) is a very relevant topic for many scientific and applied issues, which include river habitat, channel design and river restoration. For example, the estimation of travel lengths provides interesting clues for the smart design and/or implementation of the increasingly common dam removal and gravel augmentation operations. Fluvial geomorphologists have traditionally explored this question using the particle tracking method. However, due to the strong scatter in the available tracer data (Hassan and Bradley, 2017; Vázquez-Tarrío et al., 2019), the development of predictive tools remained elusive. The present research focus on the analyses of tracer data with the aim to examine the links between particle travel length, flow strength and riverbed characteristics, and advance in the prediction of travel lengths in GBR.

2. Methods

The event-based bed load transport volumes (Q_S) can be estimated from the active layer dimensions and the mean travel distance of bed sediments (L):

$$Q_S = L \cdot Wa \cdot h \cdot (1 - p) \quad (1)$$

where W_a is the mean active channel width, h is the average depth of the active layer and p is the fractional porosity of channel sediment. Q_S could be computed from the average bed load rate of the transport event (q_s) times the time-duration of the competent flow (t):

$$Q_s = q_s \cdot t \quad (2)$$

Meanwhile, bed load rates can be formulated as a power function of the transport stage ratio (τ^*/τ^*_c). On the other hand, we could postulate that active channel width scales with channel dimensions and total channel width (W_T), where the depth of the active layer does so with the grain-size (D) of the streambed surface (at a given hydraulic conditions). Based on all this, and eqs. 1 and 2, we hypothesized:

$$L = A \cdot {W_T}^{-\alpha} \cdot D^{-\beta} \cdot \left(\frac{\tau^*}{\tau^*_C}\right)^{\gamma} \cdot t^b \quad (3)$$

This expression relates travel lengths to channel width, surface grain size, flow strength and competent flow duration. We used multiple regression analysis in order to test this approach with a data set of tracer observations from fourteen study reaches compiled from the literature.

3. Results

Expression 3 explains the available tracer data in a strong and statistically significant way (Figure 1).

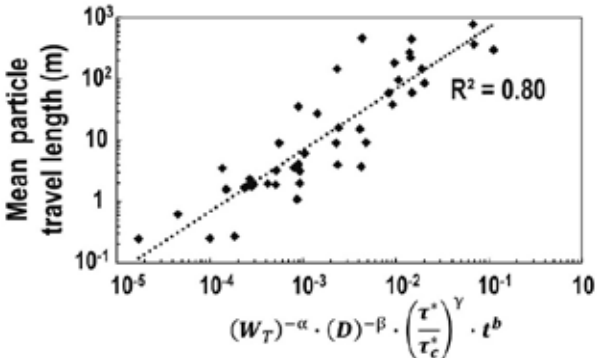

Figure 1: Results from the multiple regression analysis.

Additionally, we observed differences on model performance according to channel morphology (i.e. step-pool, riffle-pool). This may reflect the existence of morphological influences on gravel displacements.

4. Conclusions

Using a large data set of published tracer data, we observed that particle travel lengths are strongly and significantly correlated to channel width, surface grain size, Shields stress and competent flow duration. This approach provides a useful tool for investigating and predicting the distances of gravel movement in relation to several physical and morphological controls.

Acknowledgments

The present work has been possible thanks to: i. the grant ACB17-44, cofunded by the post-doctoral 'Clarin' program-FICYT (Principality of Asturias) and the Marie Curie Cofund; ii. the MorphPeak (CGL2016-78874-R) project funded by the Spanish Ministry of Economy and Competiveness and the European Regional Development Fund Scheme; and iii. the support from the Economy and Knowledge Department of the Catalan Government through the Consolidated Research Group 'Fluvial Dynamics Research Group' -RIUS (2017 SGR 459).

References

Hassan, M. and Bradley, D. N. (2017). Geomorphic controls on tracer particle dispersion in gravel-bed rivers. In Tsutsumi, D. & Laronne, J. B. (Eds.), Gravel-bed rivers. Processes and disasters, pp. 439-466.

Vázquez-Tarrío, D., Recking, A., Liébault, F., Tal, M., and Menéndez-Duarte, R. (2019). Particle transport in gravel-bed rivers: revisiting passive tracer data. *Earth Surface Processes and Landorms*, 44 (1), 112-128.

Geomorphological process of the Wujiadu - Hongshantou Reach of the Huaihe River

Bang-yi YU[1],Jue-yi SUI[2], Jin NI[1] and Hui ZHANG[1]

[1] Anhui and Huaihe Institute of Hydraulic Research, Bengbu, Anhui, China
[2] University of Northern British Columbia, Prince George, Canada.

1. Introduction

The Huaihe River originates from the Tongbo Mountain in Henan Province, which has a drainage area of 1.87×10^5km^2. This river has a main channel length of 1000 km and flows from west to east through Henan, Anhui and Jiangsu provinces. After regulated by the Hongze Lake, the Huaihe River joins the Yangtze river at the Sanjiangying Cross Section (CS). Based on channel characteristics, the Huaihe River can be divided into three sections: the upper river reach upstream from the Honghekou Station, the middle reach from the Honghekou Station to the Hongze Lake, and the lower river reach from the Hongze Lake to the Sanjingying CS. Since both the middle reach and lower reach of the Huaihe River flows in the plain region with rich precipitation, this river is notoriously vulnerable to flooding, expecially along the river reach from Wujiadu CS to Hongshantou CS. Thus, to regulate flow in the Huaihe River and prevent the Huaihe River from flooding, it is very important to investigate the geomorphological process along the river reach from Wujiadu CS to Hongshantou CS.

The river reach from Wujiadu CS to Hongshantou CS (W-H Reach) belongs to the Middle Reach of the Huaihe River (MRHR). The main channel length of the W-H reach is 145 km, the drainage area of the Huaihe River at the Hongshantou CS is 1.38×10^5km^2. The river bed of this river reach to the Hongze Lake has a negative slope. Based on the geomorphological features of the W-H reach, this river reach can be divided into following sections: a quasi-straight section, a bend section, and a braided section (Qian, 1987).

In this paper, several parameters are used to assess the geomorphology of the W-H reach. Statistical analyses are performed to establish relationship between the span length "*L*" and the bankfull channel width "*B*" for different channel patterns. The relationship between the length of the meandering channel "S" and the bankfull channel width "B" has also been derived. Results indicate that the bankfull channel width "B", the bankfull cross sectional area "A" and the average flow depth "H" are mainly dependent on the dominant discharge "Q" in the channel. The relationship has been established to describe the dependency of the curvature radius "R" on the dominant discharge "Q", water surface slope "J" and the turning angle "α". Finally, the river geometry coefficient "ζ" is calculated.

2 Methods

According to YU (2005,2008), following variables are normally used to describe the channel morphology, bankfull channel width (*B*), span length (*L*), meandering length of a channel (*S*), and the turning angle of river bend (*a*), as showed in Figure 1.

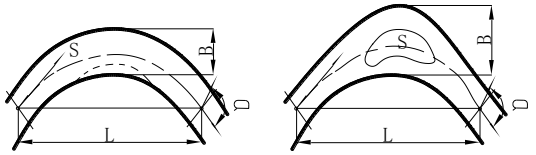

(a) A single channel (b) A braided channel

Figure 1: Variables describing channel geomorphology

According to Xie (1997), a single channel is referred to a asquasi-straight channel if following criteria are met:

$$\frac{L}{B} > 6.0 \qquad K = \frac{S}{L} \le 1.15 \tag{1}$$

where *K* is the bend coefficient, and is used to describe the sinuosity of a channel.

3 Results and Discussion

Both geomorphological data and Hydro-geometric data have been collected from some key gaging stations along this W-H reach, and used to assess the geomorphological process of the W-H reach, as presented in Tables 1 to 2.

Table 1 Geometric parameters of bend sub-sections of the W-H reach

Sub-sections of the W-H Reach		*L/B*	*S/B*	*K*
Quasi-straight sub-section	Range	6.0 ~ 20.4	6.1 ~ 20.8	1.01 ~ 1.09
	Average	9	9.3	1.03
Bend sub-section	Range	4.1 ~ 9.6	4.8 ~ 11.2	1.15 ~ 1.27
	Average	6.8	8.1	1.19
Braided sub-section	Range	2.9 ~ 4.2	3.0 ~ 4.9	1.02 ~ 1.15
	Average	3.6	4	1.09

Table 2 Curvature radius "R" and the turning angle "α" of the W-H reach

	R (m)	*R/S*	α (°)
Range	1270 ~ 5380	0.47 ~ 1.37	38 ~ 119
Average	2852	0.72	83

3.1 Hydro-geometric features of the Wujiadu-CS and the Xiaoliuxiang-CS

For natural rivers, there are the following relationships between hydro-geometric parameters and discharge.

$$B = \alpha_1 Q^{\beta_1} \quad H = \alpha_2 Q^{\beta_2} \quad U = \alpha_3 Q^{\beta_3} \quad A = \alpha_4 Q^{\beta_4} \tag{2}$$

where, *H* is average water depth, *U* is flow velocity, *A* is bankfull cross section area and Q is discharge. Coefficeints $\alpha_1, \alpha_2, \alpha_3, \alpha_4, \beta_1, \beta_2, \beta_3, \beta_4$ are determined

based on data collected from these two stations during a period from 1950 to 2007, and in Tables 3.

Table 3 The coefficient of Hydraulic geometry of Wujiadu-CS and Xiaoliuxiang-CS

Sub-sections	α_1	α_2	α_3	α_4
Wujiadu-CS (before removing the dike)	140.21	1.592	0.0045	223.33
Wujiadu-CS (after removing the dike)	120.31	8.812	0.0009	1060.2
Xiaoliuxiang-CS	315.76	3.086	0.001	974.59
Sub-sections	β_1	β_2	β_3	β_4
Wujiadu-CS (before removing the dike)	0.144	0.174	0.682	0.318
Wujiadu-CS (after removing the dike)	0.155	0.0165	0.828	0.171
Xiaoliuxiang-CS	0.056	0.09	0.854	0.146

Results show that the bankfull cross sectional area "A" along the section from Wujiadu-CS to Xiaoliuxiang-CS is smaller, the anti-scourability of riverbed and riverbank is stronger, normal and erosion is slow.

3.2 Relationship between hydro-geometric parameters and dominant discharge of the W-H reach

Sediment transport is an important process of channel morphology. Conceptually, the channel hydro-geometric parameters affect the dominant discharge of the channel - also called "channel-forming discharge" (Q_d) which has a magnitude of the 1–2 year flood. In the mean time, the dominant discharge of the channel results in the changes of channel hydro-geometric parameters. Yu et al (2010) developed a method to determine the dominant discharges of this river reach. Based on results of Yu et al (2010), following relationships have been established to assess the dependency of the hydro-geometric parameters on the dominant discharge.

$$A = 0.67{Q_d}^{1.05} \qquad r=0.97 \tag{3}$$

$$B = 1.48{Q_d}^{0.71} \qquad r=0.94 \tag{4}$$

$$H = 0.46{Q_d}^{0.35} \qquad r=0.98 \tag{5}$$

$$R = 82.27{Q_d}^{0.65}J^{0.09}a^{-2.31} \qquad r=0.95 \tag{6}$$

where, R is curvature radius of bend sub-sections, J is the hydraulic slop, a is turning angle of river bend, Q_d is dominant discharge.

Results show that there exists obvious relationships between the channel dominant discharge and all hydro-geometric parameters. One can see from the relationship, the larger the dominant discharge and the larger the hydraulic slope, the larger the curvature radius. However, the larger the turning angle of the bend channel, the less the curvature radius.

It is also found that the river geometry coefficient (ζ) does not change mauch, namely,

$$\zeta = \frac{\sqrt{B}}{H} = 2.7\sim3.0 \tag{7}$$

The features of the W-H reach which is characterized as a narrow and deep section have been proved by the calculated results.

4. Conclusions

Using data of discharge and hydro-geometric parameters collected along the the the W-H river reach and some key gaging stations of the Huaihe River, the hydro-geometric parameters of this river reach has been systematically analysed. Results show that there exists obvious relationships between the channel dominant discharge and all hydro-geometric parameters. The larger the dominant discharge and the larger the hydraulic slope, the larger the curvature radius. However, the larger the turning angle of the bend channel, the less the curvature radius. Findings from this research can benefit the flow regulation and flood protection of the Huaihe River.

Acknowledgments

The research work was supported by the National Key Research and Development Program of China (2017YFC0405602), and the Special Funds Under the Leadership of the Central Government of China - Science and Technology Projects for Benefiting the General Public (2016080802D118).

References

Qian, N., 1987, "Riverbed deformation", Science Press, Page, 123-220, Beijing, China.

Yu, W., 2008, "Bank collapse and bank protection of the Yangtze River", Water Resources and Hydropower Press, Page, 53-63, Beijing, China.

Yu, W., 2005, "Riverbed deformation and river engineering of the Yangtze River", Water Resources and Hydropower Press, Page, 67-89, Beijing, China.

Xie, J., 1997, "Riverbed deformation and river engineering", Water Resources and Hydropower Press, Page, 8-12, Beijing, China.

Yu, B., Yu, Y. and Zhao, K., 2010, "Calculation of dominant discharge of the Middle Reach of the Huaihe River", Journal of Hohai University, 38 (2), 210-214.

Effects of Tidal Range and Initial Basin Morphology on the Evolution of Experimental Tidal Channel Networks

A. Finotello[1], M.Ghianssi[1], C. Paola[2], N. Lentsch[2,3], A. Cantelli[4] and A. D'Alpaos[1],

[1] Department of Geosciences, University of Padua, Padua, Italy. alvise.finotello@unipd.it
[2] Dept. of Earth Sciences, St. Anthony Falls Laboratory, University of Minnesota, Minneapolis, MN 55414, USA.
[3] ExxonMobil Upstream Research Company, 22777 Springwood Village Parkway, Spring, TX 77389, USA
[4] Shell Technology Center Houston, 3333 Highway 6 South Houston, TX 77082-3101, USA

1. Introduction

Tidal embayments are characterized by the widespread presence of branching and sinuous tidal channel networks (TCN) (D'Alpaos et al., 2005; Coco et al., 2013). The control that TCN exert on the hydrodynamics of coastal areas, as well as on the ecology and sediment dynamics, is of primary importance for both the short- and long-term morphodynamic evolution of these environments (Coco et al., 2013). Worldwide-increasing anthropogenic pressures on coastal wetlands, combined with changes in the relative sea level, further emphasizes the critical importance of TCN on coastal morpodynamic, thus calling for new insights on the processes governing their evolution. During the last decade, laboratory experiments have been developed in order to pursue a complete characterization of the long-term evolution of TCN (Stefanon et al., 2010; Vlaswinkel and Cantelli, 2011). Even though these experiments proved that TCN can successfully be reproduced in small-scale experimental settings, the effects of the initial basin morphology (flat in the existing experiments) and shoreline configurations have escaped closer scrutiny thus far (Van Maanen et al., 2013). Here we present results of laboratory experiments aimed at assessing the influence of initial basin morphology and tidal range on the inception and morphodynamic evolution of TCN.

2.Methods and Results

The experiments were carried out in the "DeltaBasin2" experimental facility at St. Anthony Falls Laboratory (University of Minnesota), using a 2.5 by 2.5 m three-sided wood platform placed within the main basin and filled with well sorted crushed walnut shells (D_{50}=250 μm, ρ=1350 kg/m^3) (Figure 1a). Sediments were initially mixed with water up to the saturation point and poured into the basin forming a 20 cm thick layer. Capillary forces provided the wet sediments with a slight cohesion, sufficient to maintain channel-bank morphology during the experiment. A significant effort was required to ensure that the elevation of the platform at the shoreline perfectly tied the mean sea level by maintaining the desired slope. A 10 cm wide berm was built along each side of the platform in order to prevent localized scour along the platform walls. The system was purely erosional, because no sediment supply was provided. During the experiments, water was dyed blue to allow for channel identification from time-lapse photos taken by an overhead camera. A cart-mounted scanner recorded topography using a 3D SICK™ camera with millimetric horizontal and vertical resolution. In all the experiments we considered a sinusoidal tide with fixed tidal period of 1.5 minutes which produced reversing quasi-steady flow. Water levels were regulated and adjusted by means of a computer-controlled weir. Each experiment lasted 10 hours (400 tidal cycles). All the experimental TCN exhibited an initial, relatively rapid, growing stage followed by a period of slow morphological adaptation toward a final quasi-equilibrium configuration. Continuous monitoring of the basin hypsometry indicated that the evolution of TCN occurred more rapidly in the presence of a sloped basin and for higher tidal ranges. Flat basin (i.e., 0% slope) and sustained tidal ranges favour the development of more branching TCN, while channel sinuosity is enhanced when wide breaches (manmade in this case) favoured the initial flooding of the basin. Conversely, the evolution of the network and its final branching character appeared to be quite insensitive to the initial number of breaches along the shoreline, thus suggesting an autogenic behaviour that depends primarily on the characteristics of the tidal forcing.

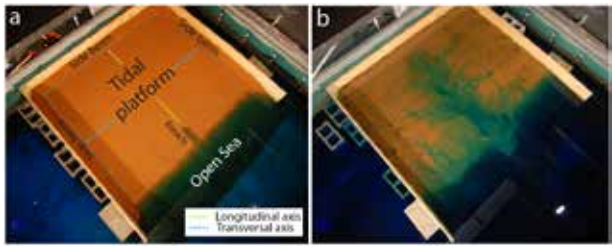

Figure 1: Experimental tidal networks. a) Experimental setup. b) Final network morphology obtained from an initial transversal slope equal to 0.8%.

References

Coco G, Zhou Z, van Maanen B, Olabarrieta M, Tinoco R, and Townend IH. 2013. Morphodynamics of tidal networks: Advances and challenges. *Mar. Geol.* 346 : 1–16.

D'Alpaos A, Lanzoni S, Marani M, Fagherazzi S, and Rinaldo A. 2005. Tidal network ontogeny: Channel initiation and early development. *J. Geophys. Res.-Earth Surface* 110 : 1–14.

Van Maanen B, Coco G, and Bryan KR. 2013. Modelling the effects of tidal range and initial bathymetry on the morphological evolution of tidal embayments. *Geomorphology* 191 : 23–34.

Stefanon L, Carniello L, D'Alpaos A, Lanzoni S, D'Alpaos A, and Lanzoni S. 2010. Experimental analysis of tidal network growth and development. *Cont. Shelf Res.* 30 : 950–962.

Vlaswinkel BM, and Cantelli A. 2011. Geometric characteristics and evolution of a tidal channel network in experimental setting. *Earth Surf. Proc. Land.* 36 : 739–752.

A retrospective numerical modelling analysis of the Seine Estuary (France) morphodynamics over the last 50 years

F. Grasso[1], B. Mengual[1,2], P. Le Hir[1], M. Caillaud[1] and B. Thouvenin[1]

[1] Ifremer, DYNECO/DHYSED, Centre de Bretagne, CS 10070, 29280 Plouzané, France. florent.grasso@ifremer.fr
[2] now at UMR 7266 LIENSs CNRS-Université de La Rochelle, Institut du Littoral et de l'Environnement, 2 rue Olympe de Gouges, La Rochelle 17000, France.

1. Introduction

The Seine Estuary (France) represents a dynamic area influenced by hydro-meteorological forcing (e.g., tides, wind, waves, river flow) that has undergone considerable changes through engineering works, such as dredging activities, dike construction and harbour extensions. It resulted in significant channel deepening and estuary narrowing (e.g., Grasso and Le Hir, 2019; Figure 1). Predicting the morphological changes of such mixed sediment (mud and sand) environments over few decades (around 50 years) is still challenging. Before simulating prospective scenarios to investigate the estuarine morphological responses to climatic and human pressures, it is necessary to assess the numerical modelling skill and ability via a morphodynamic retrospective analysis. Therefore, based on a process-based numerical model of the macrotidal Seine Estuary, the objective of this study is to investigate the model ability to simulate the estuarine morphodynamics for 10 to 50 years, through the influence of hydro-meteorological forcing and human-induced changes.

2. Methods

The numerical modelling strategy is based on a realistic hydrostatic model (MARS3D) forced by wind, tidal components and river flow (Grasso and Le Hir, 2019). It is coupled to a wave model (WAVEWATCH III®) and an advection-diffusion multi-layer sediment module (MUSTANG) taking into account mud and sand mixtures (Le Hir et al., 2011; Mengual et al., 2017). Dredging is simulated by releasing over real dumping sites the simulated deposition of sediments above the reference level in the navigation channels. The simulation of the estuarine morphodynamics was firstly analysed and validated in the 2009-2016 period, comparing annual bathymetry changes and dredged sediment amounts and classes (i.e. mud/sand ratio). The retrospective simulations started from a dominantly natural system in 1960 and ran toward a anthropogenically-controlled system in 2010 (Figure 1), vastly altered by human activity (i.e. dredging activities, channel deepening, dike constructions and harbour extensions). Sequencing of engineering works in the model were aimed at mimicking the real-time interventions, but scenarios with absence of engineering works were also considered.

3. Results and discussion

Over the 8-year recent period (2009-2016), the simulated morphological changes are of same order of magnitude as the observations. Erosion and accretion patterns are relatively well captured by the model, although the model struggles to properly simulate the mouth bank progradation seaward. The suspended sediment concentration, and especially the turbidity maximum

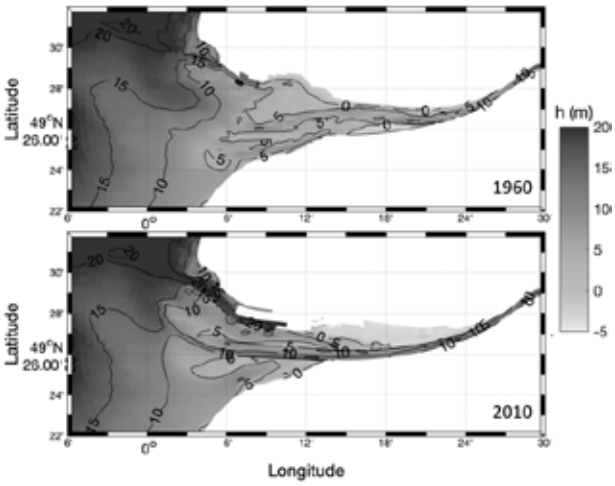

Figure 1: Bathymetries (rel. mean sea level) of the Seine Estuary in 1960 (top panel) and 2010 (bottom panel).

mass is slightly lower than in previous studies (e.g., Grasso and Le Hir, 2019), but the dredged sediment masses and classes are fairly well simulated. Encouragingly, the model presents a robust trend over the 8 years without significant suspended sediment decrease. Attention is also paid to simulate the right mud/sand ratio, without long term variation, despite seasonal changes. In addition, results from simulations using morphological factors (4 in this study) were similar to the reference one, providing confidence for further practices. The numerical model, calibrated over the recent period, is then applied in the 1960 configuration. This study investigates the simulated morphodynamics convergence or divergence in regards to observed bed level changes in order to assess the model relevance for prospective simulations.

Acknowledgments

This study is conducted in the framework of the MORPHOSEINE project funded by the Seine-Aval 6 scientific research program.

References

Grasso, F., and Le Hir, P. (2019). Influence of morphological changes on suspended sediment dynamics in a macrotidal estuary: diachronic analysis in the Seine Estuary (France) from 1960 to 2010. *Ocean Dynamics*, 69(1) :83-100.

Le Hir, P., Cayocca, F., and Waeles, B. (2011). Dynamics of sand and mud mixtures: a multi process-based modelling strategy. *Continental Shelf Research*, 31(10):S135-S149.

Mengual B., Le Hir P., Cayocca F., and Garlan T. (2017). Modelling Fine Sediment Dynamics: Towards a Common Erosion Law for Fine Sand, Mud and Mixtures. *Water*, 9(8):564.

The role of three-dimensional shape on tidal asymmetry in estuaries

L.Y.Chen[1, 2], Z.Zhou[1, 2], I.Townend[1, 3], C. Friedrichs[4] and C.K. Zhang[2]

[1]State Key Laboratory of Hydrology-Water Resources and Hydraulic Engineering, Hohai University, Nanjing, China
[2]College of Harbour, Coastal and Offshore Engineering, Hohai University, Nanjing, China
[3]Ocean and Earth Sciences, University of Southampton, Southampton, UK
[4]Virginia Institute of Marine Science, William &Mary, Gloucester Point, VA, USA

1. Introduction

Tidal asymmetry, the inequality of flood and ebb duration, is generated by the distortion of tidal wave when it propagates from offshore to shallow estuary. Flood dominance, which means shorter flood duration and faster flood velocity, favors landward sediment transport, while ebb dominance favors seaward sediment transport (Dronkers, 1986). The three-dimensional (3D) shape of estuaries plays a key role on the condition of tidal asymmetry and hence the equilibrium state of estuaries, which has not been well examined.

One of the most widely used equilibrium relationships between tidal asymmetry and estuarine morphology is developed by Friedrichs and Aubrey (1988) based on the 1D shallow water equations. They identified two key non-dimensional parameters a/h (the ratio between the offshore tidal amplitude and the mean water depth) and Vs/Vc (the ratio between the volume of tidal flat and channel). If the values of a/h and Vs/Vc satisfy the stability condition, the tide is considered symmetrical and the residual sediment transport is zero, suggesting that the estuary is in equilibrium.

An idealized 3D form model is integrated by Townend, (2010) who combined the equilibrium tidal flat profile and channel description, as follows:

$$z = a \cdot \sin\left(\frac{2y - W_{lw}}{W_0 - W_{lw}} - 1\right) \quad \text{for } a \geq z > 0$$

$$z = a \cdot \left(\frac{n_{bk}y - W_{lw}}{W_0 - W_{lw}} - 1\right) \quad \text{for } 0 \geq z > -a$$

$$z = -a - \frac{\mu W_{lw}}{4}\left[1 - \left(\frac{2y}{W_{lw}}\right)^n\right] \quad \text{for } z \leq -a$$

$$W(x) = W_m \cdot \exp\left(\frac{-x}{L_w}\right)$$

where, a is the offshore tidal amplitude; W_{lm} is the width at low water level; W_0 is the width at mean water level; n_{bk} is the a factor that has a value of 2 for a channel is symmetric about the centreline and 1 if the width relates to a half channel; W_m is the width at mouth and L_w is the rate of width convergence.

This study is focused on the effect of various 3D forms on tidal asymmetry while the key hydraulic and geometric parameters are kept unchanged. The specific objectives include: (1) to set up an idealized 3D estuary model based on Townend (2010) and check if it agrees with the classic equilibrium relationship of Friedrichs and Aubrey, and (2) to assess the influence of different shapes on tidal asymmetry given the same a/h and Vs/Vc as the idealized 3D form.

2. Method

Based on the equations above and the data of Humber estuary, we can set up the 3D form morphodynamic model using Delft3D (Figure 1a-c). Under the premise that a/h and Vs/Vc remain unchanged, different cross-sections (shown in Figure1 d-f), plan forms (such as various convergence rates) and slopes are considered.

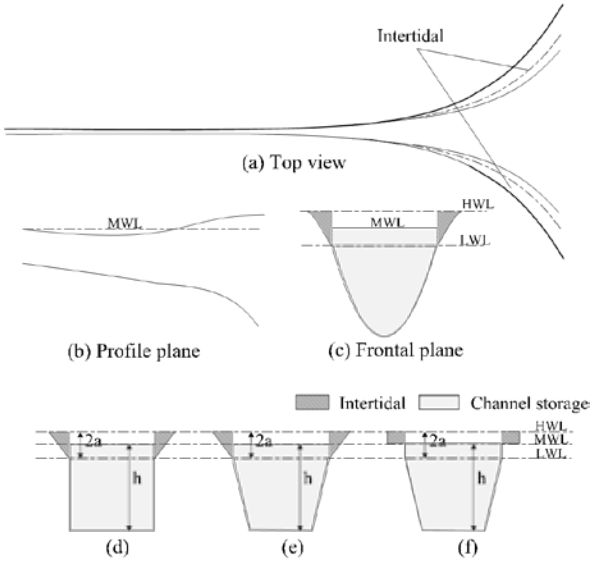

Figure 1: the idealized model based on Humber estuary and different cross-sections

3. Preliminary results and discussion

Although the key parameters a/h and Vs/Vc are the same, the state of tidal asymmetry varies with the 3D forms. Different 3D forms cause changes in bottom friction and cross-section areas, which is important to the distortion of tidal waves. This implies that using the hydraulic and geometric parameters a/h and Vs/Vc may not be enough to justify the state of tidal asymmetry and the 3D shape of estuaries plays an important role. Ongoing studies are being conducted to gain more in-depth insight into this topic.

References

Dronkers, J. (1986). Tidal asymmetry and estuarine morphology. Netherlands Journal of Sea Research **20** (2): 117-131.

Friedrichs, C. T. and D. G. Aubrey (1988). Non-linear tidal distortion in shallow well-mixed estuaries: a synthesis. Estuarine Coastal & Shelf Science **27** (5): 521-545.

Townend, I. (2010). An exploration of equilibrium in Venice Lagoon using an idealised form model. Continental Shelf Research **30** (8): 984-999.

Flow measurements in a tidal flat: field campaign and results

E. Santirosi[1], L. Schippa[2]

[1] Department of Engineering, University of Ferrara, Ferrara, Italy. elena.santirosi@student.unife.it
[2] Department of Engineering, University of Ferrara, Ferrara, Italy. Leonardo.schippa@unife.it

1. Introduction

Since the 13th century, in The Netherlands the inhabitants started to reclaim lands, creating a large number of polders. This process has caused the loss of natural intertidal areas, essential for the safeguard of the dikes from the rising sea level, caused from the climate change. For this reason, the European governments started to boost the protection of the existing intertidal areas and the creation of new ones. One of these projects refers to depoldering the Perkpolder area, in the Western Scheldt (NL) to develop a natural intertidal zone (ca. 70 ha). To characterize the hydrodynamic field in the new wetland, a velocity measurement campaign has been carried out.

2. Velocity measurements

An acoustic velocity profiler also equipped with a pressure cell was installed on different representative locations on the study area, measuring continuously water velocity along the vertical and water level. Tide level was registered in Walsoorden station, located on the Wester Scheldt, nearby the area inlet. The period of measurements has extended by 21 days between April and May 2018, to cover almost an entire tidal cycle. The flow field was characterized both in the channels network and in the mudflat. By combining the observed data with the DEMs of the Perkpolder obtained from available Lidar and Multi-Beam echosounder measurements, it has been possible to compare the direction of the water flow with the channel one.

3. Velocities profiles on the vertical

By observing the velocity profiles on the vertical it can be affirmed that, comparing the profiles corresponding to measurements collected in a small time interval (3 minutes), their trends are quite similar. Although the profiles are similar to each other, in the vertical direction the velocities do not increase or decrease uniformly but they have an irregular behaviour, especially in the instants corresponding to the maximum velocity.

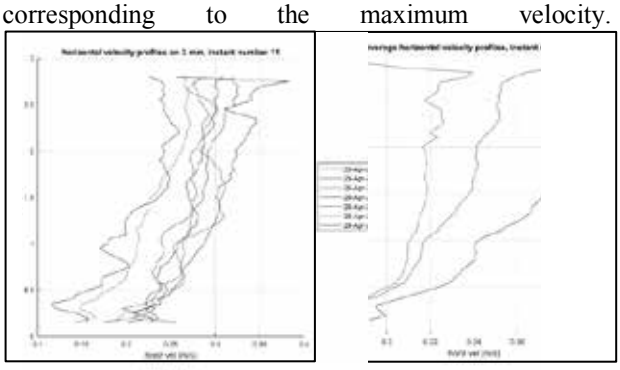

Figure 1: on the left the velocity profiles on the vertical measured in a time interval of three minutes, on the right three average profiles (from left to right: profile averaged on 15 minutes, 6 minutes and 3 minutes).

4. Plan view representation

From the velocity data collected in the Perkpolder basin it has been possible to obtain a representation of the velocity in the East-North plan.

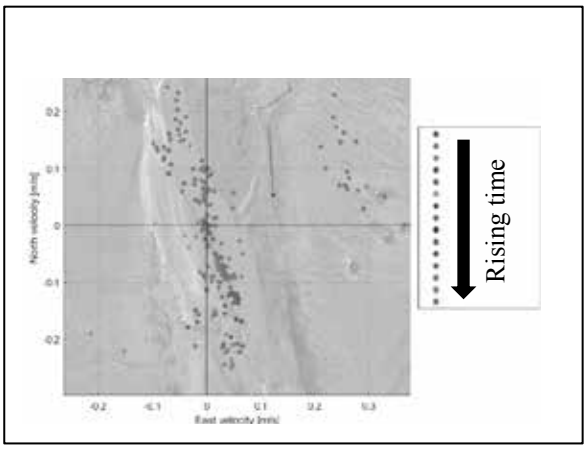

Figure 2: plan view representation of the horizontal velocity

From this representation it is clear that the water flow mainly follows the channels direction.

4. Conclusions

By analysing the flow velocity data, it can be stated that the prevalent velocity components are the East and the North components. In the channels, the general velocity trend is consistent with the tidal phase; in fact, it is positive during the flood phase and negative during the ebb phase. The most regular profiles on the vertical can be found in correspondence to the peaks of the water level measured by the instrument, probably due to the presence of lower values of the horizontal velocity. By looking at the plan view representation of the horizontal velocities, it can be observed that, in the channels, the water flow is ducted. In the channels, the average value of the maximum velocity reached in the flood phase is, in general, higher than the averaged minimum velocity (in absolute value) reached in the ebb phase. This underlines a flood dominant behaviour that is consistent with the sedimentation process highlighted in Perkpolder. In fact, according to (Friedrichs and Aubrey, 1988), "Flood-dominant lagoons and estuaries (having shorter duration, higher velocity floods) tend to infill their channels with sediment. Ebb-dominant systems (having shorter, higher velocity ebbs) tend to flush bed-load sediment seaward more effectively and may represent more stable geometries".

References

Friedrichs C. T., Aubrey. D. G. (1988). *'Non-Linear Tidal Distortion in Shallow Well-Mixed Estuaries: A Synthesis'. Estuarine, Coastal and Shelf Science* 27(5):521–45.

Do wind-generated currents affect tidal asymmetry in tidal basins with varying geometries?

P.J. de Ruiter[1], J.C. Mullarney[1], K.R. Bryan[1] and C. Winter [2]
[1] Coastal Marine Group, University of Waikato, Hamilton, New Zealand. pd31@students.waikato.ac.nz
[2] Institute of Geosciences, Christian-Albrechts University Kiel, Kiel, Germany

1. Introduction

Tidal basins worldwide vary in shape and size. The geometry of a tidal basin regulates the shape of the tidal wave and the associated hydrodynamic processes. The astronomical tide may become strongly distorted inside a basin, resulting in asymmetries in the surface tide (vertical tide) and the velocity field (horizontal tide) (De Ruiter et al., 2019). Distortion of the horizontal tide affects sediment transport potential by enhancing asymmetries in peak tidal velocities (TVA) (Dronkers, 2016). Previous research has shown that divergent and infilled meso-tidal basins are characterised by flood-directed horizontal tidal asymmetry, whereas more convergent and less infilled basins display greater ebb-dominance (e.g. de Ruiter et al., 2019). In addition tidal basin hydrodynamics and sediment transport potential can be altered by currents induced by wind events. In our paper we investigate how wind-generated currents modulate horizontal tidal velocity asymmetry in shallow tidal basins with divergent geometries.

2. Methods

Two hydrodynamic models of idealised shallow basins were developed in Delft3D, based on the hypsometric parameters methodology used by De Ruiter et al. (2019). The resulting intertidal morphologies represent an infilled constricted tidal basin and a less-infilled unconstricted basin. Consequently, three-dimensional model runs were undertaken forced by varying wind speeds and directions as well as varying wind event timing (relative to low tide) and duration.

3. Results and Conclusions

Horizontal tidal asymmetry patterns induced by a combination of tide- and wind-generated currents inside the idealised geometries were resolved by analysing modelled peak flood- and ebb current velocities over a tidal cycle. In general, our results show that effects of wind-generated currents on tidal asymmetry depend on wind characteristics, basin geometry, local water depth and the magnitude and residual direction of tide-generated currents.

Tidal velocity asymmetry (TVA) ratios indicate that currents generated for wind speeds of 6 m/s and greater can significantly affect hydrodynamics within a tidal basin. Overall TVA patterns within both basins were relatively similar, with locations and absolute values of maximum flood- and ebb dominance modulated by basin geometry. In shallow intertidal regions (flats) within the basins, winds generate currents that are aligned with the wind direction, resulting in an associated downwind-directed increase in TVA. Deeper subtidal regions (channels) are characterised by currents in the opposite direction of the wind, promoting TVA patterns that contrast with the intertidal asymmetry. This depth-dependent modulation of tidal asymmetry is most evident for wind directions parallel to the main axes of the tidal channel. Winds blowing directly into the idealised tidal basins from the open ocean, for example, increase flood dominance throughout the intertidal, whereas the subtidal is distinctly more ebb dominant. These particular TVA patterns are shown in Figure 1 for three transects inside a constricted basin (6 m/s winds). The figure also shows tide-only TVA ratios for one transect.

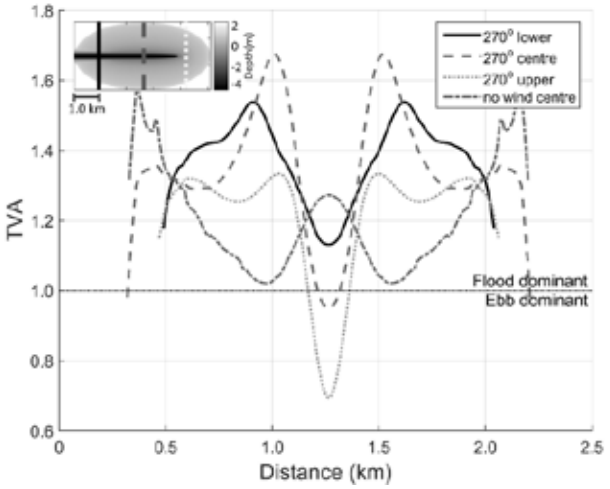

Figure 1: Tidal velocity asymmetry (TVA) inside the idealised constricted basin bathymetry (overview in top left inset) for three transects (lines on inset). Wind characteristics: 270° (west to east), 6 m/s

Our results suggest that an increase in wind speed promotes more extreme TVA ratios without substantially changing overall asymmetry patterns. We also show that timing and duration of a wind event can have important implications for associated TVA patterns. Wind events coinciding with flooding tide result in the most noteworthy differences between peak flood- and ebb dominant asymmetry ratios, for wind event durations of both three and six hours.

Consequences for sediment transport potential within both basin geometries will be discussed.

Acknowledgments

We thank the Bay of Plenty Regional Council for funding this research.

References

De Ruiter, P.J, Mullarney, J.C., Bryan, K.R., and Winter, C. (2019). The links between entrance geometry, hypsometry and hydrodynamics in shallow tidally-dominated basins. *Earth Surface Processes and Landforms,* Accepted.

Dronkers, J. (2016). *Dynamics of Coastal Systems (Second Edition).* World Scientific Publishing Co Pte Ltd.

The Role of Reclamation and Restoration on Tidal Flat-Channel Morphodynamics: A Modelling study

L. Chen[1,2], Z.Zhou[1,2], Fan Xu[3], C.K. Zhang[2]

[1] State Key Laboratory of Hydrology-Water Resources and Hydraulic Engineering, Hohai University, Nanjing, China
[2] College of Harbour, Coastal and Offshore Engineering, Hohai University, Nanjing, China
[3] State Key Laboratory of Estuarine and Coastal Research, East China Normal University, Shanghai, China

1. Introduction

Since the last century, land reclamation has been one of the major anthropogenic activities on coastal area for the demand of land resource. Land reclamation projects have pronouncedly changed the coastline worldwide and have caused morphological and ecological problems due to the lack of effective management, such as the sharp loss of intertidal flats and wetlands (Spencer et al., 2017). This have motivated the program of de-reclamation, which aims to return the coastal land to nature for more rational and sustainable development of coastal land resources.

Notwithstanding the researches about restorations have achieved great advances, the tidal network developing under the influence of land de-reclamations has received considerably less attention. These anthropogenic projects not only directly affect the hydrodynamic and sedimentary environments, but also lead to much more complicated geomorphic reworking of topography in adjustment. In the present study, a state-of-the-art numerical model (Delft3D) is employed to (1) explore the variations of the tidal flow and sediment transport, and (2) the long-term morphodynamic evolution of the tidal networks in response to reclamation and de-reclamation projects. By addressing these objectives, this study aims to provide scientific basis for the sustainable development and protection of coastal resources.

2. Method

An open-source morphodynamic model (Delft3D) is employed in this study. The 2D shallow water equations are solved for the tidal flow fields, which are utilized to calculate the sediment fluxes. Then the bed level change is calculated through the bed continuity equation. The descriptions of these governing equations have been detailed in previous studies (Zhou et al., 2014).

In order to analyse the morphodynamic evolution of tidal networks in response to reclamation and de-reclamation projects, a three-stage simulation is designed. In the first stage, the natural development of tidal networks is modelled without anthropogenic interventions. At the beginning of the second stage, parts of the computational domain are enclosed by sea dikes, which implementation of reclamation project (Figure 1d, 1e). These sea dikes are removed or opened in the third stage to simulate the recovery of the tidal networks after de-reclamation (Figure 1f, 1g, 1h, 1i). Each stage lasts for 100 years (i.e., 300 years in total). An additional run denoted without anthropogenic interventions throughout the simulation is performed for comparison.

3. Preliminary Results

Model results indicate that land reclamation decreased the landward sediment supply and the residual current in front of the dikes. For partly enclosed case, only channels near the corner of the dikes diverted because of the convergence and dispersal of flow.

For the case of de-reclamation, the method of removing all dikes to restore the tidal flats to the original natural condition, but the hydrodynamics do not seem to be able to reshape an identical tidal flat as the original one; the method of opening breaches altered the distribution of tidal channels seaward of the dikes.

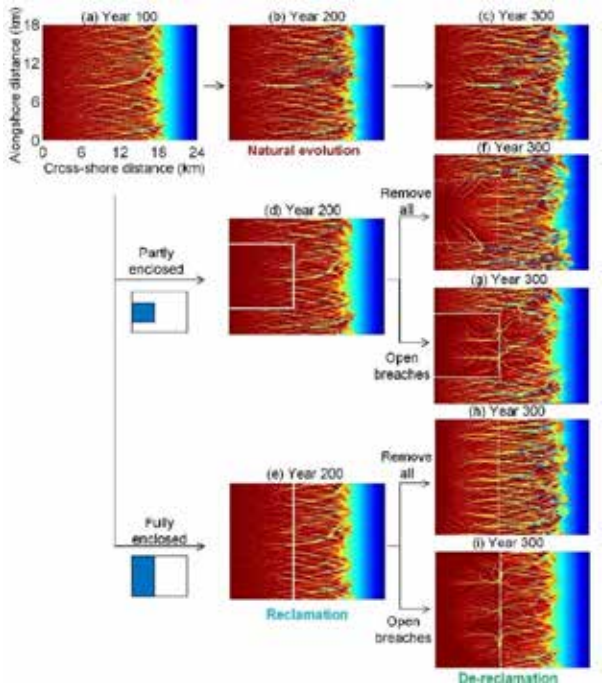

Figure 1: The morphological results of all cases. (a), (b) and (c) show natural evolution. (d) and (e) show reclamations. (f), (g), (h) and (i) show de-reclamations.

Overall, model results suggest that land reclamation hindered the development of tidal channel systems and the most pronounced influence was on the surrounding area of the dikes. De-reclamation projects can promote or restore part of the tidal flats and their effectiveness is dependent on the specific methods of breaching.

References

Spencer, K.L., Carr, S.J., Diggens, L.M., Tempest, J.A., Morris, M.A. and Harvey, G.L. (2017). The impact of pre-restoration land-use and disturbance on sediment structure, hydrology and the sediment geochemical environment in restored saltmarshes. Science of The Total Environment, 587-588: 47-58.

Zhou, Z., Olabarrieta, M., Stefanon, L., D'Alpaos, A., Carniello, L. and Coco, G. (2014). A comparative study of physical and numerical modeling of tidal network ontogeny. Journal of Geophysical Research: Earth Surface, 119(4): 892-912.

Formation mechanisms for rhythmic morphology on a low-energy beach. Trabucador beach (Ebro delta) case.

A. Falqués [1], F. Ribas[1], A. Mujal-Colilles[2] and M.Grifoll[2]

[1] Physics Department, Universitat Politècnica de Catalunya, Catalonia, Spain. albert.falques@upc.edu
[2] Laboratori d'Enginyeria Marítima, Universitat Politècnica de Catalunya, Catalonia, Spain. anna.mujal@upc.edu

1. Geographical setting and observations

The Trabucador is a long (6 km) narrow (125 m) barrier beach at the SW side of the Ebro delta (Catalonia). Its inner side facing the Alfacs bay is a low energy beach with a sandy shallow terrace featuring an intricate alongshore rhythmic morphology (see Fig. 1). Sixteen aerial orthophotos from 1946 to 2014 have been analysed and complemented with field observations from 1986 to present. This morphology is dynamic but it is usually characterized by: a) long transverse finger bars (LTFB) (Ribas et al., 2015) and b) large scale shoreline undulations (LSSU) (Arriaga et al., 2018) . The LTFB are thin and elongated, with lengths that are comparable to their alongshore spacing, which is in the range $15-25$ m. Spectral analysis shows peaks in this range and sometimes additional peaks in the range $30-65$ m that correspond to the spacing between the largest bars. They commonly open an anti-clockwise angle of $10^\circ-40^\circ$ with the shore normal and typically attach to the shoreline by a megacusp. The LSSU typically have wavelengths in the range $150-250$ m. Although they might interact, the LTFB and the LSSU are clearly two distinct morphological unitsMujal-Colilles et al. (2019).

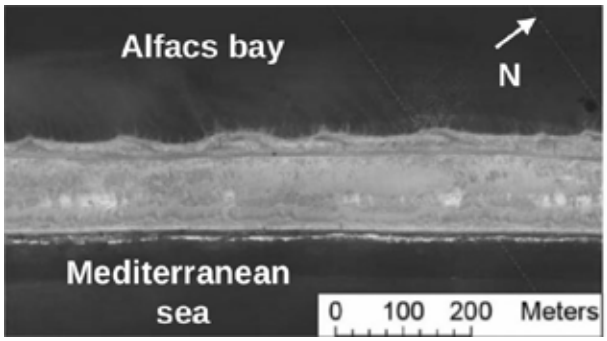

Figure 1. Aerial photo of the Trabucador barrier beach in 2013 showing the large scale shoreline undulations (LSSU) and the transverse bars (LTFB) facing the Alfacs bay.

2. Modelling results

We investigate the hypothesis that both the LTFB and the LSSU would emerge from positive feedbacks between the wave-driven hydrodynamics and the evolving morphology. A full 2DH morphodynamic model should be able of reproducing both LTFB and LSSU. However, because of the very different space and time scales such a model does not exist yet and LSSU are usually described with shoreline models based on averages in space and time. For large wave incidence angles with respect to the shore normal a rectilinear shoreline can become unstable and give rise to LSSU (Arriaga et al., 2018). SW breezes are very frequent during fair weather and can easily reach 8 m/s. Numerical simulations for these conditions show that they can generate waves of 0.4 m significant height with large incidence angles with respect to the Trabucador beach. We apply a one-line shoreline model to investigate shoreline instability. The dominant wavelengths range around $200-300$ m and the growth time (constant wave conditions) is about 30 days.

Regarding the LFTB a full 2DH surfzone morphodynamic model is applied. The model is forced with random initial perturbations of an alongshore uniform bathymetry and constant wave conditions corresponding to SW wind. As can be seen in Figure 2, it reproduces the formation of transverse bars with a spacing of about 30 m reaching an amplitude (from crest to trough) of about 10 cm within 34 h. Their spacing is in the range of the observed wavelength and their orientation is consistent with observations with an angle with the shore-normal of about 50°, i.e., somewhat larger than the observed one. We therefore conclude that both the LTFB and the LSSU could be originated by positive feedbacks between wave-driven currents and morphology during SW wind events.

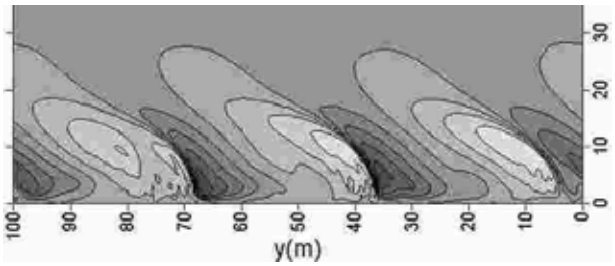

Figure 2. Morphodynamic modelling of transverse bars from random initial bathymetric perturbations: contour lines of the bathymetric perturbation, for $t = 34$ h. Dark greys represent deep and light colours represent shallow.

Acknowledgments

This research is part of the project CTM2015- 66225-C2-1-P funded by the Spanish Government and cofunded by the E.U. (FEDER). Funding from the research group LIM/UPC is also gratefully acknowledged.

References

Arriaga, J., FalquÃl's, A., Ribas, F., and Crews, E. (2018). Formation events of shoreline sand waves on a gravel beach. *Ocean Dynamics*, 68(6):735âĂŞ748. doi.org/10.1007/s10236-018-1157-5.

Mujal-Colilles, A., Grifoll, M., and Falqués, A. (2019). Rhythmic morphology in a microtidal low-energy beach. *Geomorphology*, 334:151âĂŞ164. doi.org/10.1016/j.geomorph.2019.02.037.

Ribas, F., Falqués, A., de Swart, H. E., Dodd, N., Garnier, R., and Calvete, D. (2015). Understanding coastal morphodynamic patterns from depth-averaged sediment concentration. *Rev. Geophys.*, 53. doi:10.1002/2014RG000457.

Transfer of sediment from fluvial to marine conditions: some processes that are changing

C.A. Nittrouer[1], A.S. Ogston[1], A.T. Fricke[1], D.J. Nowacki[2], E.F. Eidam[3], R.L McLachlan[1], N.E. Asp[4], P.W.M. Souza Filho[5], T.T. Nguyen[6], and H.P.Vo-Luong[7]

[1]School of Oceanography, University of Washington, Seattle, USA. nittroue@uw.edu
[2]U.S. Geological Survey, Santa Cruz, USA.
[3]Department of Marine Sciences, University of North Carolina, Chapel Hill, USA.
[4]Instituto de Estudos Costeiros, Universidade Federal do Para, Braganca, Brazil.
[5]Instituto de Geociencias, Universidade Federal do Para, Belem, Brazil.
[6]VAST Institute of Marine Geology and Geophysics, Hanoi, Vietnam.
[7]Vietnam National University, Ho Chi Minh City, Vietnam.

1. Introduction

Important sedimentary processes have recently been documented for the fluvial-to-marine portions of the Amazon and Mekong systems. Future environmental changes will impact sediment dispersal, by affecting sediment entrapment in the tidal river and by altering landward sediment return from the continental shelf to tropical deltas and mangrove shorelines.

2. Amazon tidal river

The Amazon tidal river contains only freshwater, but is modulated by tidal forces that extend 800 km upstream from the Atlantic Ocean. This region still remains in a relatively natural condition, and as much as a third of the sediment reaching the tidal river is trapped there (~300-400 Mt/y). Potential sinks include tributary mouths, tidal floodplains, and adjacent rivers.

The Tapajos and Xingu tributaries enter the Amazon tidal river, and contribute much water but negligible sediment. A range of processes cause entrapment of Amazon sediment in their mouths. Seasonally higher elevation of the Amazon water surface can cause barotropic flow into the Tapajos mouth, where quiescent conditions allow sediment to accumulate. For the Xingu tributary, tidal fluctuations cause the dominant barotropic flows, and strong tidal flood currents pump sediment into its mouth. Seasonally, Amazon water is cooler and enters the Xingu mouth as a dense, turbid bottom flow. Both tidal and density flows deliver sediment to quiescent conditions where sediment accumulates.

Flow of water into the tidal floodplain is controlled by changes in the elevation of the Amazon water surface that occur on seasonal and tidal time scales. In the upper 250 km of the Amazon tidal river, levees are high (as much as 7-8 m) and transfer to the floodplain is limited to seasonal flood conditions, when diffuse overbank flow dominates. The central 200 km of the tidal river experiences overbank currents driven by substantial tidal fluctuations (1-2 m). Consequently, levees are much lower and turbid river water is advected far into the floodplain, effectively trapping Amazon sediment. The lower 350 km of the tidal river experiences greater tidal processes, but sediment has largely filled the floodplain to high water levels. A complex network of tidal channels connects the lower tidal river with river systems south of the Amazon river mouth, and some of the Amazon sediment is transported to and likely trapped in estuarine seabeds and shorelines there.

3. Mekong deltaic system

The majority of the sediment received by the Mekong Delta is transferred through distributary channels to the adjacent continental shelf during high flow of the river (Jul-Nov). Some of the sediment is returned to channels and to mangrove shorelines during low flow (Dec–Apr). This coincides with the most energetic conditions on the shelf, when strong winds from the northeast cause relatively large surface waves and wind-driven currents to propagate landward and southwestward.

Turbid bottom water reaching the mouths of distributary channels can be transported into the channels by baroclinic estuarine flows. Observations in the southernmost distributary channel, Song Hau, indicate that the mass of sediment returned during Dec-Apr is about 30% of that discharged seaward in Jul-Nov. The sediment re-entering the channel is mud that is trapped by estuarine processes, and temporarily deposited on the channel bed. Most of this sediment and new sediment are transported seaward with the return of high-flow conditions during the following Jul-Nov.

During Dec-Apr, turbid water is also brought landward to ocean shorelines of the delta. Detailed observations were made of the shoreline at the mouth of the Song Hau distributary channel, where sediment is trapped in a mangrove forest. Deposition is dominant during the Dec-Apr period, and landward transport into the mangrove forest is enhanced by tidal flows. Sediment accumulation rates reach 5 cm/y, and cause seaward progradation of the mangrove shoreline. The bulk of Mekong sediment builds a shelf clinoform, but the complex landward flows also provide sediment that can nourish the shorelines of the ocean and of distributary channels.

4. Recent and future changes

In the future, the processes described above will operate under different conditions. Enhanced dam construction and climate change will severely affect the amount and timing of water and sediment discharge. Accelerated sea-level rise will flood land surfaces and create new accommodation space to trap sediment. Transgression will bring secondary effects from erosion of shorelines and seabeds, and from saltwater intrusion and upstream migration of estuarine processes. Predictions of future changes to Amazon and Mekong sediment dispersal are difficult, but would be impossible without knowledge of processes that have recently been documented.

The importance of spatially variable climate on sediment mobilisation in the south-central Argentine Andes

R.M. Harries[1, 2], B. Gailleton[1], L.A. Kirstein[1], M. Attal[1], A.C. Whittaker[3] and S.M. Mudd[1]

[1] University of Edinburgh, Edinburgh, United Kingdom. linda.kirstein@edinburgh.ac.uk
[2] Research Centre for Integrated Disaster Risk Management (CIGIDEN), Santiago, Chile. rebekah.harries@cigiden.cl
[3] Imperial College London, United Kingdom. a.whittaker@imperial.ac.uk

1. Introduction

Sediment transport dynamics in mountainous source regions have a direct impact on the morphology of river systems downstream (Baartman et al., 2013). Understanding the controls on sediment mobilisation in these regions is critical for predicting the evolution of flooding and mass flow hazards under future global climate change scenarios. It is also key to being able to interpret the sensitivity of rivers to past climatic change from their sedimentary records (Harries et al., 2019).

Here we present a quantitative analysis of the controls on long-term sediment dynamics in the arid Argentine Andes, 30-31°S. We first test the fundamental geomorphic principle that the sediment exported from a catchment is representative of catchment-wide rates of bedrock erosion (Dietrich et al. 2003). We then investigate to what extent precipitation rates, bedrock lithology and glaciation have modulated channel steepness and the potential for sediment mobilisation across the mountain range.

2. Methods

For seven river catchments, which feed three alluvial fans in the Iglesia basin, we map the spatial distribution of slope and normalised channel steepness (k_{sn}). Here k_{sn} is calculated as a function of the spatial distribution of discharge:

$$k_{sn,i} = Q_i^{\theta_{ref}} S_i \quad (1)$$

where Q_i and S_i are effective discharge and channel slope at any point i on the river network, and θ_{ref} is a reference concavity index. Effective discharge is calculated by accumulating the average precipitation rate in the wettest month (Fick and Hijmans, 2017) upstream of point i. These metrics are analysed as a proxy for erosion and sediment mobilisation in the cordillera.

Based on the observed erosional trends, we test the hypothesis that the upper reaches of the catchments, which have experienced higher rates of erosion due to glaciation, contribute a larger proportion of sediment to their alluvial fans. As the upper glaciated reaches have a bedrock lithology that is distinct from the lower fluvially dominated reaches, the relative contribution of sediment from these areas can be inferred from our extensive dataset of pebble lithologies.

3. Results

While there is clear geomorphic evidence for enhanced glacial erosion in the upper reaches of the Cordillera, we find in all three catchment-alluvial fan systems that sedimentary clasts sourced from the upper Cordillera are under-represented with respect to their source area exposure. In examining the relationship between clast size and lithology, we deduce abrasion has not had an important role in modulating sediment export. We hypothesise that the storage of large volumes of glacial sediments in the glaciated reaches is the dominant control on sediment composition on their alluvial fans.

We observe that the driest catchments to the north export clasts that are predominantly sourced from the lower Cordillera. Southwards, as precipitation rates increase, the bias towards clasts sourced from the lower Cordillera is significantly reduced. This pattern correlates with a latitudinal gradient in the distribution of k_{sn} across the Cordillera. Our analysis therefore implies that spatial variations in rainfall and steepness strongly influence the potential for sediment mobilisation, in particular with regards to upper cordillera glacial sediments.

4. Conclusions

The spatial distribution of precipitation within mountain regions is important for modulating the storage or mobilisation of sediment in post-glacial catchments. As storm intensity and frequency is set to increase in the arid Andes, this finding has important implications for predicting where sediment will be mobilised from in flood events. It is also fundamental for understanding the completeness of the sedimentary record downstream of complex mountain ranges.

Acknowledgments

This work was funded by NERC E[3] DTP Studentship NE/L002588/1 and the School of Geosciences at The University of Edinburgh.

References

Baartman, J.E.M., Masselink, R., Keesstra, S.D., Temme, A. J. A. M. (2013). Linking landscape morphological complexity and sediment connectivity. *Earth Surf. Process. Landf.*, 28:1457–1471.

Dietrich, W.E., Bellugi, D.G., Sklar, L.S., Stock, J.D. (2003). Geomorphic transport laws for predicting landscape form and dynamics, *Prediction in Geomorphology, Geophysical Monograph Series*, editors Wilcock, P. and Iverson, R., 136:103-123, AGU, Washington, D.C.

Fick, S.E. and Hijmans, R.J. (2017) Worldclim2: New 1-km spatial resolution climate surfaces for global land areas, *International Journal of Climatology*, 37(12):4302-4315.

Harries, R., Kirstein, L., Whittaker, A., Attal, M., Main, I. (2019) Impact of recycling and lateral sediment input on grain size fining trends - implications for reconstructing tectonic and climatic forcings in ancient sedimentary systems, *Basin Research*, DOI: 10.1111/bre.12349.

Numerical Investigation of the Geomorphic Processes Controlling Neck Cutoffs on the White River, Arkansas, USA

J.G.F. Rivera[1], K.M. Konsoer[2] and E.J. Langendoen[3]

[1] Juarez Autonomous University of Tabasco, Villahermosa, Tabasco, Mexico. jgfabianrivera@gmail.com
[2] Louisiana State University, Baton Rouge, Louisiana, USA. kkonsoer@lsu.edu
[3] Agricultural Research Service, U.S. Department of Agriculture, Oxford, Mississippi, USA, eddy.langendoen@usda.gov

1. Introduction

Neck cutoffs of elongated meander bends on the White River, Arkansas, USA, are prominent (Figure 1). Neck cutoffs occur when upstream and downstream channels of a meander bend migrate into each other. This process is different from chute cutoffs where a new channel is eroded through the point bar or floodplain, thereby connecting the upstream and downstream channels of a meander bend.

Figure 1: Two neck cutoffs occurred on the White River, Arkansas, USA, immediately downstream of the city of De Valls Bluff in the early to mid 2010s.

Both qualitative and quantitative descriptions of chute and neck cutoff processes and the subsequent evolution of the river and the abandoned channel (or oxbow lake) have been presented in literature (e.g., Gagliano and Howard, 1984; Hooke, 1995; Constantine and Dunne, 2008; Zinger et al., 2013). However, detailed field data sets of river morphodynamics, e.g. using acoustic Doppler current profilers (aDcp) and multi-beam echo-sounders (MBES), during and after cutoff are particularly limited (Zinger et al., 2013, for chute cutoffs; Richards, 2018, for neck cutoffs).

Gagliano and Howard (1984) conceptualized the neck cutoff process as a four-stage process: 1) Active meander bend stage; 2) Neck cutoff stage; 3) Lacustrine stage; and 4) Terrestrial stage. For the Lacustrine stage, channel diversion angle, that is the angle between the channel approaching the bend and the abandoned-channel entrance, and sediment load were identified as important parameters that control the rate of post-cutoff planform dynamics and oxbow lake alluviation (e.g., Shields and Abt, 1989). Sediment plug formation at the abandoned-channel inlet and outlet is typically established within 10 years.

The comprehensive field data set of Richards (2018) shows that the neck cutoffs on the White River generally follow the four-stage conceptual model of Gagliano and Howard (1984). However, the rate of sediment plugging at the entrance and exit of the abandoned bends is negligible. Richards (2018) hypothesized this to be caused by: 1) the deep incision of the channel bed perching the exit of the abandoned bend; and 2) the observed strong helical motion of flow producing near-bed flow oriented away from the exit of the abandoned bend promoting transport of bedload sediment in the downstream direction.

The limited availability of comprehensive field data sets of neck-cutoff morphodynamics and the difficulty to produce neck cutoffs experimentally in the laboratory inhibit a complete understanding of neck cutoff processes.

2. Approach

The river morphodynamics computer model Telemac-2D/Sisyphe/Meandre (Langendoen et al., 2016) is used to conduct a systematic analysis of the role of diversion angle and sediment load on post neck-cutoff river morphodynamics and oxbow lake alluviation. The model is validated against the observations of Richards (2018).

References

Constantine, J.A. and Dunne, T. (2008). Meander cutoff and the controls on the production of oxbow lakes. Geology, 36(1):23–26.

Gagliano, S.M. and Howard, P.C. (1984). The neck cutoff oxbow lake cycle along the Lower Mississippi River. In Elliott, editor, *River Meandering*, pages 147–158, New York, NY. American Society of Civil Engineers.

Hooke, J.M. (1995). River channel adjustment to meander cutoffs on the River Bollin and River Dane, northwest England. *Geomorphology*, 14(3):235–253.

Langendoen, E.J., Mendoza, A., Abad, J.D., Tassi, P., Wang, D., Ata, R., El kadi Abderrezzak, K., and Hervouet, J.-M. (2016). Improved numerical modeling of morphodynamics of rivers with steep banks. *Advances in Water Resources*, 93(Part A):4–14.

Richards, D.A. (2018). Three-dimensional flow, morphologic change, and sediment deposition and distribution of actively evolving neck cutoffs located on the White River, Arkansas. Ph.D. Thesis, Louisiana State University, Baton Rouge, LA.

Shields, F.D., Jr., and Abt, S.R. (1989). Sediment deposition in cutoff meander bends and implications for effective management. *Regulated Rivers: Research & Management*, 4(4): 381–396.

Zinger, J.A., Rhoads, B.L., Best, J. L., and Johnson, K. K. (2013). Flow structure and channel morphodynamics of meander bend chute cutoffs: a case study of the Wabash River, USA. *J. Geophys. Res. Earth Surf.*, 118(4):2468–2487.

The evolution of low-energy meandering planform in loess landscape (Transdanubia, central Europe)

M. Słowik[1], J. Dezső[2], J. Kovács[3] and M. Gałka[4]

[1] Adam Mickiewicz University, Faculty of Geographic and Geologic Sciences, Poznań, Poland slowikgeo@poczta.onet.pl
[2] University of Pécs, Institute of Geography, Department of Environmental and Physical Geography, Pécs, Hungary, dejozsi@gamma.ttk.pte.hu
[3] University of Pécs, Szentágothai Research Centre, Environmental Analytical and Geoanalytical Research Group, Pécs, Hungary, jones@gamma.ttk.pte.hu
[4] University of Lodz, Faculty of Biology and Environmental Protection, Department of Geobotany and Plant Ecology, 12/16 Banacha Str., Lodz, Poland, gamarga@wp.pl

1. Introduction

We present the first study that describes a spatial and temporal evolution of low-energy meandering river systems formed in a loess landscape of central Europe, in Transdanubia (south Hungary). The main objectives were to: i) identify the lithology, sedimentary structures, and age of the former channels and floodplain, ii) determine the evolution of low-energy meandering rivers of Transdanubia, and iii) propose a general model of meander bends evolution in various geomorphic settings.

2. Study area

The research was conducted in the Kapos and Koppány River valleys that belong to the Danube River drainage basin. The site has been selected for field research as traces of a complex system of palaeomeanders have been preserved in the floodplain (fig.1). A complex system high-curvature bends were formed by the Koppány River. Compound and large-scale meanders were formed in the course of the Kapos River.

Figure 1: Palaeochannels in the Koppány and Kapos valley floor.

3. Research methods

The internal structure of former channels and floodplain was studied by means of GPR (ground-penetrating radar), ground-truthed by sedimentary information from 30 boreholes and corings. Radiocarbon dates were determined for 20 samples of terrestrial plant macrofossils and charcoal pieces using the AMS technique to estimate the age of the palaeomeanders.

4. Results

Low-energy meanders replaced a braided river system in the Koppány valley at least 14000 cal. BP. The meandering system was characterized by elongated, compound bends with widened channel cross-sections near apexes. Silts constituting the river bed, oblique accretion within the inner banks, cutoffs formation between 14000 and 11300 cal. BP, and flow discontinuation after 3900 cal. BP, after which the river was turned into wetlands, were specific features of this river course.

The meandering system was formed due to the domination of suspended load originating from loess constituting the mantle of the surrounding hills. With the low-energy conditions, in which sands from the older braided system could not be entrained to transport, deposition of fines created a 2.0-2.5 m thick cohesive layer of floodplain sediments. A spatial transition from multi-headed compound bends to downstream migrating large-scale bends in the Kapos valley could have been caused by the formation of a tectonic fault.

5. Model of meander formation

We propose a general model of meander bends evolution for both high- and low-energy rivers evolving in various geomorphic settings. Large-scale meanders are formed by high discharges with a significant content of bed-load in convective regimes characterized by perturbations propagating downstream. Large meanders can also be formed in low-energy rivers e.g. owing to the formation of tectonic faults. The second type are bends with cutoffs. They occur both in low- and high-energy rivers. These meanders represent convective conditions, when sediments from a single chute cutoff are moved downstream, and cause downstream changes. Absolute conditions appear when, owing to multiple-cutoffs, and counter-migration of neighboring bends, perturbations are propagated in both directions. The occurrence of circular pools allows for distinguishig low- from high-energy courses. The third type are meanders formed in low-energy conditions, in a variety of sedimentary environments (tidal, peatlands, glacial-inherited valleys). In the loess landscape of Transdanubia, the absolute conditions were induced by the downstream base-level rise that, in turn, limited sediment delivery to fines from loess hills. As a result, the low-energy river evolved over a coarser layer inherited from the activity of a high-energy braided river system.

Acknowledgments This research work is part of the research project 2016/23/B/ST10/01027 supported by the National Science Centre, Poland.

Thermodynamic sediment-transport theory applied to the Tsangpo – Brahmaputra River

Jaia Syvitski[1], Sagy Cohen[2], Ariel Miara[3], Jim Best[4]

[1] CSDMS, University of Colorado, Boulder CO, USA. Jai.syvitski@colorado.edu
[2] Department of Geography, University of Alabama, Tuscaloosa, AL, USA. sagy.cohen@ua.edu
[3] Advanced Science Research Center at the Graduate Center of the City University of New York, NY, USA. ariel.miara@asrc.cuny.edu
[4] Departments of Geology, Geography & GIS, Mechanical Science & Engineering & Ven Te Chow Hydrosystems Laboratory, University of Illinois at Urbana-Champaign, Urbana, IL, USA. jimbest@illinois.edu

1. Introduction

A 25°C increase in water temperature, due to some combination of river elevation descent, or flow to warmer latitudes, or seasonal increases, can increase grain settling velocities by 7.3%, 42%, 85%, 90% for a 1000-µm, 250-µm, 62.5-µm, or a 10-µm grain respectively, and reduce sediment transport by 90% for a grain size population centred at 62.5 µm, or 300% if centred at 10µm (Syvitski et al., in press). To augment these findings, we apply thermodynamic transport theory to a day in the life of the Tsangpo – Brahmaputra River.

2. Theory of river temperatures

The one-dimensional heat-advection model of flowing water is:

$$A\frac{\partial T}{\partial t} + \frac{\partial QT}{\partial x} = \frac{WS_f}{\rho_f c_p} \quad (1)$$

where T is temperature across a reference volume wherein energy is exchanged vertically over the flow cross-sectional area, A (m^2) per unit time, t (s), Q is discharge (m^3/s), x is distance (m) in the flow direction, W is average river width (m), S_f is the sum of heat fluxes across the air-water and sediment-water interfaces (W m^{-2}), and c_p is the heat capacity of water (kg m^2 $K^{-1}s^{-1}$).

The atmospheric-water heat flux S_f is:

$$S_f = H_{ns} + H_{la} - H_{lw} - H_e + H_c - H_p \quad (2)$$

where H_{ns} is net solar radiation, H_{la} is atmospheric longwave radiation, H_{lw} is long-wave radiation from the water surface, H_e is evaporative heat flux, H_c is convective heat flux, and H_p is heat flux due to precipitation. Employing the thermal equilibrium concept of Edinger et al. (1968), a method appropriate for macro-scale water balance models, then:

$$S_f = K_e\,(T_e - T) \quad (3)$$

where K_e is the bulk coefficient of heat transfer that is a function of air temperature, dew point temperature, and wind velocity, T_e is the hypothetical equilibrium temperature that water reaches under constant atmospheric heating or cooling, wherein $S_f = 0$ across the air-water interface. Thus,

$$T = T_e + (T_0 - T_e)\exp\left(\frac{K_e x}{\rho_f c_p q}\right) \quad (4)$$

where q is flow per unit width of the river (m^2/s). The in-river equilibrium temperature T_e (°C) requires knowledge of local wind speed, air temperature, humidity, and incoming solar radiation to predict water temperatures (Edinger et al., 1968). The incoming upstream temperature T_0 (°C), requires a flow routing model that tracks non-point source thermal loadings into and out of each grid cell, including surface and groundwater sources, precipitation inputs, and snowmelt.

3. Modeling river temperatures

We use the model *WBM-TP2M* to calculate global stream temperatures (Miara et al., 2018), as based on the in-river equilibrium temperature model (Edinger et al., 1968). River temperature is a function of hydrologic flows and climate variables including wind speed, air temperature, humidity, and incoming solar radiation. The model's framework calculates surface runoff based on grids of precipitation, evapotranspiration, infiltration, soil moisture, irrigation, reservoirs and diversions. Flow routing uses a cell-tree topology (*HydroSHEDS*) and a semi-implicit finite-difference solution to the Muskingum–Cunge equation. Precipitation data is from the Global Precipitation Climate Centre. The temperature of precipitation differs from river temperature, and uses the approximation of runoff temperature as wet-bulb temperature plus 2°C. Spatial resolution is 6 arc-min (~11km x 11km). For a complete description with model validation, see Cohen et al. (2014) and Miara et al. (2018).

4. Thermodynamic sediment-transport theory

The density of river water ρ_f (kg/m^3) varies with river water temperature T (°C) as ρ_T, and as modified by the dissolved mineral concentration $\Delta\rho_{sal}$ (kg/m^3), and particulate concentration $\Delta\rho_{Cs}$ (kg/m^3):

$$\rho_f = \rho_T + \Delta\rho_{sal} + \Delta\rho_{Cs} \quad (kg/m^3) \quad (5)$$

where ρ_T is:

$$\rho_T = 1000\frac{1-(T+288.9414)}{508929.2(T+68.12963)}(T-3.9863)^2 \quad (6)$$

Kinematic viscosity, ν decreases as fluid temperature increases:

$$\upsilon = \frac{\frac{1.7910^{-3}}{1+0.03368T+0.00021T^2}}{\rho_f} \quad (m^2/s) \quad (7)$$

where the numerator represents the dynamic viscosity (N s/m^2), and ρ_f is the effective fluid density (Eq. 5).

The settling velocity ω of sedimentary grains (e.g. Julien 1995) is:

$$\omega = \frac{8\upsilon}{d_s}[(1 + 0.0139d^3)^{0.5} - 1] \quad \text{(m/s)} \quad (8a)$$

$$d = d_s \left[\frac{(\frac{\rho_{sed}}{\rho_f} - 1)g}{\upsilon^2}\right]^{1/3} \quad \text{(m)} \quad (8b)$$

where ν is kinematic viscosity (m^2/s) (Eq. 7), d_s is grain diameter (m), ρ_{sed} is grain density and ρ_f is fluid density (kg/m^3, Eq. 5, 6), and g is acceleration due to gravity (m/s^2).

The Bagnold (1966) method for estimating the suspended bed-material transport Q_{sbm} in fully turbulent flows and larger transport rates, is:

$$Q_{sbm} = \left(\frac{\rho_s}{\rho_s - \rho_f}\right)\rho_f \overline{Q}^{\beta} S \left(0.01\frac{\overline{u}}{\omega}\right) \quad \text{[kg/s]} \quad (9)$$

where $\overline{Q}$ is river discharge (m^3/s) averaged over turbulence, β is a load rating term (-) set to 1 for this study, S is the energy slope (m/m) that powers the discharge, $\overline{u}$ is the transport velocity of suspended particles and approximated by average river velocity (m/s), and ω is the settling velocity (m/s) of the bulk suspended particles, or for each size fraction being separately tracked. The method balances the available power of the flow, with the kinetic energy required for sediment transport.

The total suspended load of a river, Q_s, combines the suspended bed-material load, Q_{sbm}, with the wash load of a river, Q_w, such that:

$$Q_s = Q_{sbm} + Q_w \quad \text{(kg/s)} \quad (10)$$

Q_s is the product of Q *and* C_s, Q is water discharge (m^3/s) and C_s is suspended-sediment concentration (kg/m^3). Q_w represents the finer-grained portion of a river's suspended load, typically fine sand, silt and clay-sized grains, and sourced from a landscape affected by the land cover, land use, disturbances, character of the soil and bedrock, precipitation intensity, basin relief, tectonics, and air temperature. The wash load reflects the different types of runoff that enters a river (snowmelt, rainfall wash, glacier melt, and groundwater). A dimensionless stochastic model to capture this complexity (adapted from Morehead et al., 2003) is:

$$\frac{Qw_{[i]}}{\overline{Qw}} = \psi_{[i]} m \frac{\omega_{20C}}{\omega_{T_{[i]}}} \left(\frac{Q_{[i]}}{\overline{Q}}\right)^{c_{[a]}} \quad \text{(-)} \quad (11)$$

where $Qw_{[i]}$ is suspended sediment load, $Q_{[i]}$ is discharge, on the i^{th} day of the a^{th} year. $\overline{Qw}$ and $\overline{Q}$ are long-term mean suspended load and discharge, respectively. $\psi_{[i]}$ describes a lognormal random distribution having a variance scaling with $\overline{Q}$. Here, $\psi_{[i]}$ is set to 1. $c_{[a]}$ is a normally distributed annual rating exponent. m conserves mass. ω_{20C} is the settling velocity of wash load particles at a fluid temperature of 20°C, and $\omega_{T[i]}$ is the particle settling velocity at the relevant daily river temperature and grain size.

5. The Tsangpo – Brahmaputra Model Domain

The Yarlung Tsangpo (Zangbo) – Brahmaputra River warms by 23°C, from the headwaters in the Himalayas and Tibetan Plateau, to the river mouth. Drainage area increases linearly with river distance (R^2 = 0.977). The first half of the river length has no latitudinal effect, the latter half has a linear increase in southerly latitudes (Fig. 1). The river has three distinct zones– a highland Tibetan Plateau with moderate slopes, a steep (Tsangpo) Gorge, and a flat lowland Brahmaputra floodplain (Fig. 1).

We model the river's daily discharge using a 31-y climatology (1980-2010), and focus our thermodynamic transport theory to flow conditions on August 15, 2010, in the middle of the high-flow monsoon season. On that day, a water droplet entering the main headwater river takes 7.2 d to reach the Tsangpo Gorge, 1.5 days through the Gorge, and 2.9 days to cross the Brahmaputra floodplain. During the 4470 m descent, river temperatures warm at 1.6°C/km of elevation descent.

The river encounters three orders-of-magnitude of river gradients; a 15-fold range in discharge; a factor of 2 range in flow velocity; and a 134% range in river temperatures (Fig. 1). Findings for the August 15, 2010 model day are:

- The range in fluid densities is quite small when considering just thermal effects (0.2%), and only slightly larger (0.4%) when the dissolved and particulate concentrations are added (Fig. 1).
- The range in river viscosities is 42.8% (Fig. 1).
- The range in the settling velocity of a 50µm grain population is 42.5%, 23.7% for a 100µm population, and 6.5% for a 600µm size population. Compared to a simulation using a T=20°C standard, the largest particle settling differences (39%) occur in the cold alpine reaches, with decreasing differences downstream (Fig. 1).
- Mean grain size (d_s, mm) of the bed-material load is modelled as a function of river slope (S, -) (Fig. 1). Six grain size regions are defined: gravel (coarse, medium and fine) along the Yarlung Tsangpo River, cobbles through the Tsangpo Gorge, and 600µm sand along the Brahmaputra river bed (see Subramanian and Ramanathan 1996) (Fig. 1).
- Suspended bed-material load (Eq. 9) grows in magnitude, from headwaters at 0.1 t/s, to peak fluxes in the Gorge at 5.5 t/s. Loads decrease from the mouth of the Tsangpo Gorge at 3.5 t/s, to 1.9 t/s just 80 km further downstream. The remaining 800 km of the Brahmaputra River sees the bed-material load fluctuate from a low of 0.9 t/s to 3.2 t/s, as new tributaries join the river (Fig. 1).

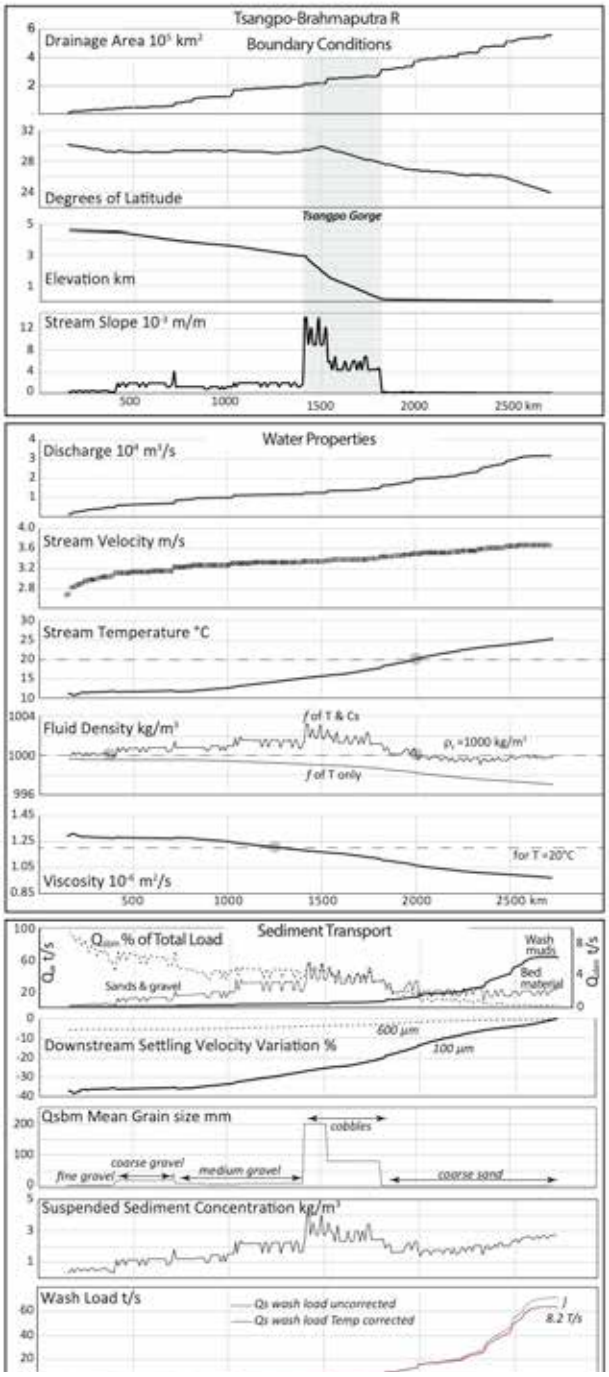

Figure 1: ***River boundary conditions*** *(upper panels): drainage area, degrees of latitude, river elevation, and river slope with flow distance.* ***Modeled water properties*** *(middle panels): discharge (WBM-TP2M simulation), river velocity ($\overline{u} = 1.3Q^{0.1}$), river temperature (WBM-TP2M simulation), fluid density (Eq. 5 & 6), and fluid viscosity (Eq. 7).* ***Modeled transport properties*** *(lower panels): along-river settling velocity of 100µm and 600µm particles (Eq. 8), suspended bed-material load (Eq. 9), total suspended load (Eq. 10), mean grain size of suspended bed-material ($d_s = 29911{*}S^{1.1867}$); total suspended concentration (Cs = Qs/Q); wash load, with and without a correction for river temperature variability (Eq. 11).*

- Wash load grows continuously downstream, from 0.007 t/s at the river's source, to 9.1 t/s at the exit of the Tsangpo Gorge, and then rapidly gains mass across the Brahmaputra Plain, to reach 63.3 t/s at its mouth (Fig. 1). Wash load is modelled with a mean grain size of 50µm (the river predominantly carries coarse silt to sand-size particles; see Subramanian and Ramanathan 1996).
- If we use a constant river temperature of T=20°C, the river-mouth wash load is overpredicted by 8.2 t/s (Fig. 1).
- The suspended load at the river mouth has a bed-material component of 3.5% (Fig. 1).
- When comparing suspended bed-material transport rates, between a model run with $\rho_f = 1000$ kg/m^3, T = 20°C, and a simulation using free variables, small differences (5.9%) exist for a 600µm particle population, with the differences becoming magnified for smaller sized particles: a 100 µm particle population is underpredicted by, ~20% in the cold alpine environment, to ~12% overprediction for the lowland river environment (Fig. 1). The transport discrepancy grows to 137% for 10µm particle populations.
- The total suspended sediment concentration begins at 0.09 kg/m^3 at the source waters of the river, and grows to a river mouth concentration of 2.1 kg/m^3 (Fig. 1).

6. Conclusions

Fluvial-transport theory supports efforts to: 1) include thermal-dynamic algorithms in fluvial fluid-dynamic models, 2) include planetary forces, such as weather and climate that simulate river discharge and river temperature, and 3) embed modelling approaches within geographically-based frameworks.

A 25°C change in river temperature can influence the wash load of a river from 70% for 100µm particles, to 320% for a suspended population 10µm in size. With both thermal and mechanical controls at play, our study suggests that river temperature controls on sediment transport should be accounted for. The use of thermal-dynamic models of particulate transport holds many significant applications within environmental management for predicting the flux of both natural and artificial sediments and organic particles from the world's rivers.

Acknowledgments

SC is supported by the National Science Foundation - Geography Spatial Sciences Program grant 1561082.

References

Cohen, S., Kettner A.J., and Syvitski, J. (2014). Spatio-temporal dynamics in riverine sediment and water discharge between 1960-2010 based on the WBMsed v.2.0 Distributed Global Model. *Global & Planetary Change* 115:44-58.

Edinger, J.E., Duttweiler, D.W., and Geyer, J.C. (1968). The response of water temperatures to meteorological conditions. *Water Resources Res*. 4(5):1137–1143.

Julien, P. (1995). *Erosion and sedimentation*. Cambridge University Press, Cambridge UK, 280 pp.

Miara, A., Vörösmarty, C.J., Macknick, J.E., Tidwell, V.C., Fekete, B., Corsi, F., and Newmark, R. (2018). Thermal pollution impacts on rivers and power supply in the Mississippi River watershed. *Environmental Res. Letters* 13: 034033.

Morehead, M.D., Syvitski, J.P.M., Hutton, E.W.H., Peckham, S.D., 2003. Modeling the inter-annual and intra-annual variability in the flux of sediment in ungauged river basins. Global and Planetary Change 39 (1/2), 95-110.

Subramanian V. and Ramanathan A.L. (1996). Nature of Sediment Load in the Ganges-Brahmaputra River Systems in India. In: Milliman J.D., Haq B.U. (Eds.) *Sea-Level Rise and Coastal Subsidence. Coastal Systems and Continental Margins*, v2. Springer, Dordrecht, Ch7:151-168

Syvitski, J., Cohen, S., Miara, A., and Best, J. (in review). River temperature and the thermal-dynamic transport of sediment. *Global & Planetary Change.*

Are salt-marsh meandering channels stable landscape features?

A. D'Alpaos[1], M. Ghianssi[1], A. Finotello[1], and M. Marani[4]

[1] Department of Geosciences, University of Padova, Padova, Italy. andrea.dalpaos@unipd.it
[2] Department ICEA, University of Padova, Padova, Italy

1. Introduction

Tidal channels branching and meandering through salt-marsh platforms exert a fundamental role on the eco-morphodynamic evolution of marsh ecosystems (Hughes, 2012). Despite of their prominence and wide occurrence, the characteristics and dynamics of meandering channels shaped by the periodically reversing tidal flows, lack the detailed scrutiny that has been devoted to their fluvial relatives (Ikeda and Parker, 1989; Seminara, 2006). To improve current understanding of the origins and evolution of salt-marsh meandering channels, together with their morphological characteristics, and the sedimentary structures emerging from their evolution, we studied a meandering channel cutting through the San Felice salt marsh, in the Venice Lagoon (Italy). Towards this goal we carried out morphometric and sedimentological analyses, together with mathematical modelling, that allowed us to provide a detailed picture of the evolution of such channel.

2.Methods

We adopted a multidisciplinary approach which combines field observations, analysis of remotely sensed data, mathematical modelling, and sedimentary facies analysis. The planimetric configuration of a network of saltmarsh channels (determined through the use of high resolution O(1cm) images obtained through UAV) was analyzed on the basis of mathematical models that allowed us to quantitatively define relevant geomorphic indicators, such as the drainage density and the distribution of the bottom shear stresses (D'Alpaos et al., 2005) and the morphological characteristics of the meandering channels (Marani et al., 2002). High-resolution sedimentological analyses were focused on a small winding channel, where 100 cores across 16 transects were collected. Repeated DGPS surveys in time (2002 and 2015) allowed us to describe channel migration and changes in channel morphology.

3.Results and Conclusions

The distribution of the bottom shear stresses, which controls the erosion processes, showed that network development occurred via headward growth. This was also confirmed by the analysis of sediment cores that emphasized the presence of an erosive trend in proximity of the channel tips, whereas a depositional trend was found to dominate the portion of the channel towards the outlet section.

The occurrence of a lateral migration of the meanders that characterize the small channel was also observed from the sedimentological structures, in agreement with the results obtained from the analysis of remotely sensed images and from the comparison of DGPS surveys at different times. Although tidal meandering channels are usually recognized as quite stable landscape features, here we show that channels display non negligible migration rates and rapidly adapt to changes in the landscape-forming discharges.

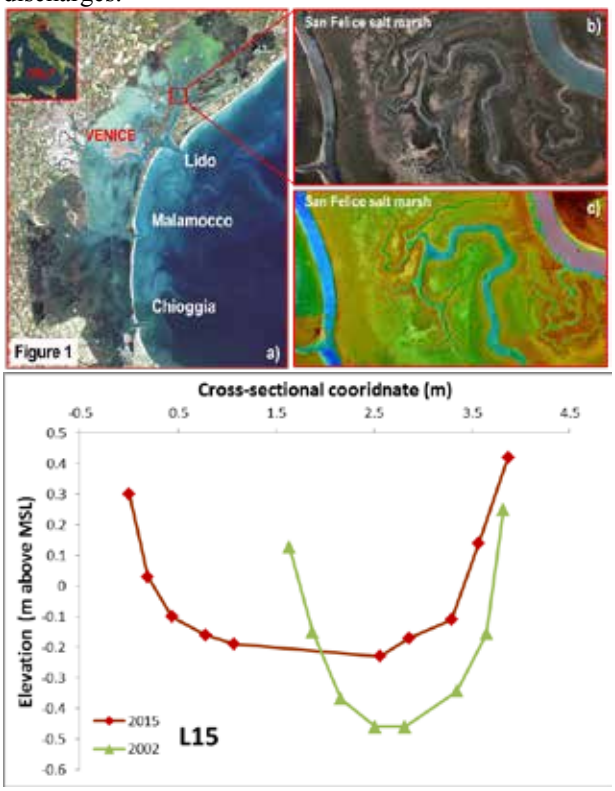

Figure 1: Study site within the San Felice salt marsh in the Venice Lagoon (a). Detailed image of the meandering channels considered in the study (b) together with a representation of marsh topography (c); d) example of a surveyed cross section in 2002 and 2015.

Our results show limited similarities between meandering fluvial and tidal channels, and suggest that the study of tidal meanders requires the development of specific theories and modelling frameworks, challenging the possibility of applying models developed for fluvial settings.

References

D'Alpaos, A., Lanzoni, S., Marani, M., Fagherazzi, S., and Rinaldo, A. (2005). Tidal network ontogeny: Channel initiation and early development. *J. Geophys. Res.-Earth* 110: 1–14.

Hughes, Z.J. (2012). Tidal Channels on Tidal Flats and Marshes. In: *Principles of Tidal Sedimentology* (Davis Jr., Richard A., Dalrymple, Robert W. Eds.), Springer Dordrecht Heidelberg London New York, pp 269-300.

Ikeda, S., Parker, G. (1989). River Meandering. Water Resources Monograph, 12.

Marani, M., Lanzoni, S., Zandolin, D., Seminara, G., Rinaldo, A. (2002). Tidal meanders. Water Resour. Res. 38, 1225.

Seminara, G. (2006). Meanders. *J. Fluid Mech*. 554, 271–297.

Sensitivity of a long-term coastal wetland evolution model to weekly variations in sediment inputs

A. Breda[1], P. Saco[2] and J. Rodriguez[3]

[1] School of Engineering, University of Newcastle, Newcastle, Australia. angelo.breda@uon.edu.au
[2] School of Engineering, University of Newcastle, Newcastle, Australia. patricia.saco@newcastle.edu.au
[3] School of Engineering, University of Newcastle, Newcastle, Australia. jose.rodriguez@newcastle.edu.au

1. Introduction

The suspended solids concentration (SSC) in the waters of an estuary is one of the main factors that contributes to soil accretion in coastal wetlands. Therefore, it is a key driver for the stability of coastal wetlands, especially in the face of sea level rise (SLR). The SSC over the tidal flats is affected by local hydrodynamic, terrain and vegetation, and is needed to model its spatial distribution, as local measurements are rarely available. Sediment transport models (STM) used for this task might be simple linear relationships fitted on observed data, or it can also be represented by complex physical relationships based in the interaction between wind, hydrodynamic, erosion and sediment settling/trapping. However, most applications assume a constant value of SSC as a boundary condition, thus representing an average situation. This may not represent the fact that severe events can lead to substantial change in the accretion rates due to the increased availability of sediment after storms. This work aims to compare the effect of using a dynamic condition for the input SSC when simulating eco-geomorphological processes. Many scenarios where simulated regarding different levels of average SSC and water levels. Analyses were conducted about how a dynamic fluctuation of sediment, instead of a static approach, may change soil accretion and vegetation distribution over the years.

2. Methods

A similar modelling framework used in Rodriguez et al. (2017), calibrated for SE Australia conditions, was applied in this study. The original constant STM was replaced by a quasi-2d advection model with sediment settling, as described in Garcia et al. (2015). The simulation area is a hypothetical tidal flat with a gentle slope of 1/1000 and a small inner tidal channel.

The 2010-2012 time series of water levels were obtained for the Hunter estuary region through the Australian Bureau of Meteorology, while the SSC data came from a MERIS satellite data derived product. We selected 13 one-month periods to represent different water level conditions and sediment load. We used this data to simulate wetland evolution from 2010 to 2050, using the IPCC AR5 PCP8.5 forecast for SLR rates. We simulated wetland evolution first using the time-average SSC value through the entire simulation (Static) and then using the SSC time series (Dynamic) and averaging the results over the year.

3. Results

The charts in Figure 1 show the results of static and dynamic SSC for a given scenario. Likewise, the accretion profiles and vegetation maps for each input type were compared for all the other scenarios.

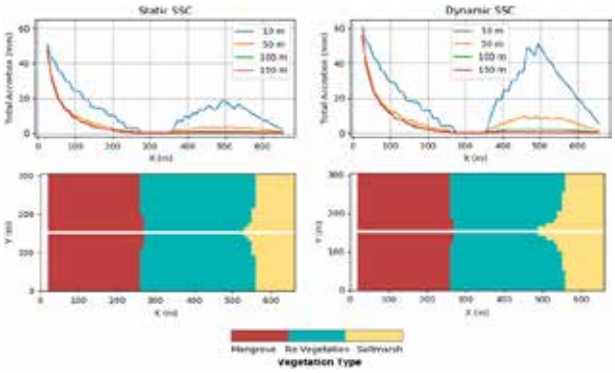

Figure 1: Example of accretion profiles (top) and vegetation maps (bottom) in 2050 for one of the scenarios (high water levels and high sediment load). Each line represents a longitudinal profile at a different distance from the inner channel. The maps show the suitable area for each vegetation type in the tidal flat.

The majority of the simulations showed higher accretion values when using a dynamic SSC. Comparing local values, the maximum differences varied from 2 mm up to 34 mm, or from 52% to 263% in relative terms. Analysing the spatial average the change ranged from 0.2 to 4.4 mm. It was noticed that the dynamic SSC resulted in higher accretion when high values of SSC were associated with high tides. Regarding simulations of the vegetation distribution, the greatest differences occurred in the saltmarsh areas closer to the inner channel. These were the only areas where a minor change in vegetation was found. For mangrove, the occupied area differ from -2% to 0.5% when adopting the dynamic SSC. For saltmarsh areas the changes were about of -0.8% to 9%.

4. Conclusions

This study showed that the adoption of a fluctuating SSC in the boundary condition might change the modelled accretion values significantly, compared to simulations using a constant SSC value. This variation is linked to hydrodynamic factors and the average sediment load available. However, no significant changes in the vegetation were found within the simulated period.

References

Garcia, M., Basile, P., Riccardi, G., A. and Rodríguez, J. (2015). Modelling extraordinary floods and sedimentological processes in a large channel-floodplain system of the Lower Paraná River (Argentina). *Int. J. of Sediment Res.*, 30(2), 150-159.

Rodríguez, J., Saco, P., Sandi, S., Saintlian, N., and Riccardi, G. (2017). Potential increase in coastal wetland vulnerability to sea-level rise suggested by considering hydrodyn. *Nat. Comm.*, 8, 16094, 1-12.

Sediment deposition patterns on salt marshes: the role of standard conditions and storm events

D. Tognin[1], M. Pivato[1], A. D'Alpaos[2] and L. Carniello[1]

[1] Department of Civil, Environmental and Architectural Engineering, University of Padova, Italy.
davide.tognin@phd.unipd.it, mattia.pivato@unipd.it, luca.carniello@unipd.it
[2] Department of Geosciences, University of Padova, Italy. andrea.dalpaos@unipd.it

1. Introduction

Salt marshes are worldwide affected by relative sea-level rise (RSLR), caused by both subsidence and eustatism. If vertical accretion is sufficient, salt marshes can keep pace with RSLR; otherwise, lack of sediment input can eventually lead to marsh drowning and plant death, transforming these landforms into tidal flats and subtidal platforms.

However, it is not yet clear what is the mutual role and relative contribution of intense storm events and standard hydrodynamic conditions in terms of sedimentation. Indeed, in tidal environments with no fluvial sediment input, resuspension due to intense meteorological events can represent the major source of sediment for salt marsh accretion (Day et al., 1998). Here we present field observations and related analyses aiming at describing sediment deposition dynamics and vertical accretion rates of salt marshes, revealing the role of intense storm events.

2. Methods

We selected three different sites in the Venice Lagoon, Italy: San Felice (SF), Sant'Erasmo (SE), and Conche (CO) salt marshes (Figure 1a). Subsidence at all these study sites ranges between 1.0 and 2.0 mm yr^{-1}, and the rate of sea level rise is of about 2.0 mm yr^{-1}, for a total rate of RSLR of about 3.0-4.0 mm yr^{-1} (Carbognin et al., 2004; Strozzi et al., 2013). For similar salt marshes in the Venice Lagoon, the accretion rate between 1993 and 1995 was estimated to be about 3.0 mm yr^{-1} by Day et al. (1998).

The SF study site is a sandy-rich soil salt marsh in the northern part of the lagoon, close to the Lido inlet. The SE and CO salt marshes, located in the northern and southern part of the lagoon, respectively, are more rich in silt and organic matter and they are both exposed to the action of wind-waves generated by the Bora wind, the most intense and morphologically significant wind in the Venice lagoon, blowing from North-East.

At each study site, we considered different transects (Figures 1b, c, and d) and for each of them we installed three measurement stations located respectively at 2.5 m, 7.5 m, and 27.5 m from the salt marsh margin. We equipped each station with an artificial marker horizon laid down on the marsh surface to measure the vertical accretion, and two sediment traps for measuring the short-term sedimentation (Figure 1e). The material deposited in the first sediment trap is collected monthly or after any single storm, meanwhile sediments deposited in the second one are collected once a year, in order to compare sediment deposition dynamics at short (single storm event) and annual time scales. Following the approach proposed by Roner et al. (2016), we measure accretion rate, grain size distribution, organic and inorganic content.

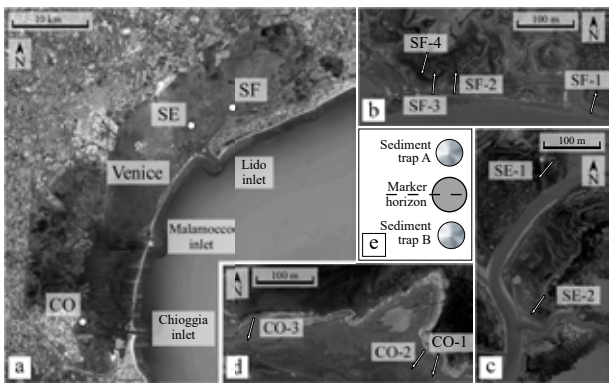

Figure 1. (a) Location of the study sites in the Venice lagoon, Italy. Position of the transects in (b) San Felice (SF), (c) Sant'Erasmo (SE), and (d) Conche (CO) study areas. (e) Sketch of a measurement station.

3. Results and Conclusions

The field campaign is still ongoing, and, since the beginning in October 2018, already two intense storm events occurred at the end of October 2018 and in December 2018. A preliminary analysis of our field data suggests that during intense storm events sediment deposition over the marsh surface can exceed the deposition occurring in several months characterized by standard hydrodynamic conditions. Furthermore, sedimentation seems to increase in the inner part of the marsh during storm events otherwise it mainly concentrates close to the margin. The analysis of sediments deposited on the traps will help us to relate sedimentation patterns to the eco-morphological salt-marsh characteristics and to further understand the relative contribution of severe storms.

References

Carbognin, L., Teatini, P., and Tosi, L. (2004). Eustacy and land subsidence in the Venice Lagoon at the beginning of the new millennium. *Journal of Marine Systems*.

Day, J. W., Rismondo, A., Scarton, F., Are, D., and Cecconi, G. (1998). Relative sea level rise and Venice lagoon wetlands. *Journal of Coastal Conservation*.

Roner, M., D'Alpaos, A., Ghinassi, M., Marani, M., Silvestri, S., Franceschinis, E., and Realdon, N. (2016). Spatial variation of salt-marsh organic and inorganic deposition and organic carbon accumulation: Inferences from the Venice lagoon, Italy. *Advances in Water Resources*.

Strozzi, T., Teatini, P., Tosi, L., Wegmüller, U., and Werner, C. (2013). Land subsidence of natural transitional environments by satellite radar interferometry on artificial reflectors. *Journal of Geophysical Research: Earth Surface*.

Ecogeomorphic modelling of coastal wetland evolution under climate and anthropogenic pressures.

J. Rodriguez[1], P. Saco[1], S. Sandi[1], N. Saintilan[2], G. Riccardi[3]

[1] School of Engineering, The University of Newcastle, Newcastle, Australia. jose.rodriguez@newcastle.edu.au
[2] Department of Environmental Sciences, Macquarie University, North Ryde, Australia. neil.saintilan@mq.edu.au
[3] Department of Hydraulics & Research Council, University of Rosario, Rosario, Argentina. riccardi@fceia.unr.edu.ar

1. Introduction

Models of vegetation evolution on coastal wetlands responding to expected sea-level rise scenarios are common in landscape simulation studies and coastal management plans. These modelling tools consider that wetland vegetation depends on the prevailing hydrodynamic conditions based on empirical evidence collected both on saltmarsh and mangrove studies.

Vegetation preference to hydrodynamic conditions has been described as a function of local values of depth below mean high tide (D), tidal range, hydroperiod or elevation with respect to the tidal frame. In previous models the hydrodynamic simulation of the flooding attenuation effects is extremely simplified or ignored. Vegetation roughness in tidal flats reduces depth and maximum inundation extent but increases ponding, so it affects both inundation depth and hydroperiod. Local man-made flow restrictions in tidal flats and channels also contribute to flood attenuation in a similar way. Hydrodynamic attenuation effects due to levies, culverts and other man-made tidal modifications are not considered in detail in any of the existing models.

2. Methods

Our simulation approach (Rodriguez et al., 2017; Sandi et al., 2018) couples a hydrodynamic model with vegetation rules based on preference to hydrodynamic conditions. It also includes soil accretion in vegetated areas for the long-term simulations. The model incorporates attenuation effects due to vegetation resistance using Manning's coefficient, and due to man-made restrictions using discharge coefficients. We then use the time series of local water levels to compute inundation depths and hydroperiods required by the vegetation rules. Hypoxia limits establishment for saltmarsh for values of D>30 cm. Oxygen availability and accumulation of phytotoxins in soils determine a suitable hydroperiod range for mangrove from 0.1 to 0.5. Once the vegetation cover is determined, a new run of the hydrodynamic model is performed on the modified domain.

3. Results

We present some results from a sub-tropical coastal wetland located in the Hunter estuary of SE Australia presented in Fig. 1a. The flow is heavily controlled by infrastructure, which includes 10 active culverts and bridges over an area of 1.2 km^2. Vegetation comprises mudflats, tidal pools, *A. marina* mangroves and *S. virginicus – S. quinqueflora* mixed saltmarsh (Fig. 1b). We first verify the model accuracy comparing vegetation measurements (Fig. 1b) with our model results (Fig. 1c). In order to assess sea level rise effects, we run continuous simulations for 60 years. We incorporate wetland surface elevation gain based on local measurements, and consider a sea-level rise rate that corresponds to the IPCC AR5 PCP8.5 scenario.

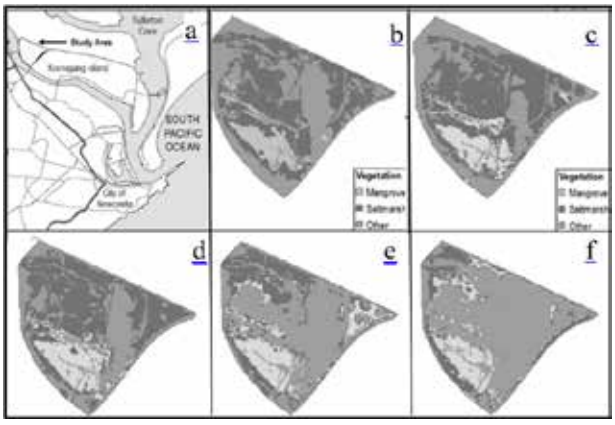

Figure 1: Simulation results a) study site, b) measured vegetation 2004, c) predicted vegetation 2004, d,e,f) predicted long-term vegetation at 2024, 2044, 2064.

By 2024 there is a minor migration to higher ground in both mangrove and saltmarsh communities as a result of increasing depths and hydroperiods (Fig 1d), which compensates vegetation losses due to the increase in the size of tidal pools. The next two snapshots at 2044 and 2064 show more pronounced vegetation losses due to an increase in permanently inundated areas that have long hydroperiods and are also becoming deeper (Fig. 1e,f).

4. Conclusions

By incorporating hydrodynamic attenuation effects, our model is able to predict an initial vegetation distribution that closely matches observations. As a result of sea level rise, mangrove is adversely affected by the increasing hydroperiods, while saltmarsh is displaced by mangrove and by the increasing depths. The final distribution of vegetation consists of mangroves fringing a large central tidal pool with remnant saltmarsh in the periphery, which agrees with the typical pattern observed in sub-tropical wetlands.

References

Rodríguez, J.F., Saco, P.M., Sandi, S., Saintlian, N., and Riccardi, G. (2017). Potential increase in coastal wetland vulnerability to sea-level rise suggested by considering hydrodynamic attenuation effects. *Nature Communications*, 8, 16094, 1-12.

Sandi, S., Rodriguez, J.F., Saco, P.M., Saintilan, N., Riccardi, G. (2018). Rising tides, rising gates: the complex ecogeomorphic response of coastal wetlands to sea-level rise and human interventions. *Advances in Water Resources*, 114, 135–148.

A large-scale field experiment on salt marsh construction in the Ems estuary, the Netherlands

M.J. Baptist[1], P. Dankers[2], J. Cleveringa[3], L. Sittoni[4,8], P. Willemsen[4,5,6,7], K. Elschot[1], M. van Puijenbroek[1], M. Hendriks[6]

[1] Wageningen Marine Research, Den Helder, Netherlands. martin.baptist@wur.nl
[2] Royal HaskoningDHV, Nijmegen, Netherlands
[3] Arcadis, Zwolle, Netherlands
[4] Deltares, Delft, Netherlands
[5] Royal Netherlands Institute for Sea Research, Yerseke, Netherlands
[6] Utrecht University, Utrecht, Netherlands
[7] University of Twente, Enschede, Netherlands
[8] EcoShape, Dordrecht, Netherlands

1. Introduction

Salt marshes provide important natural habitats, mitigate effects of subsidence and sea level rise and help in coastal defence (Temmerman et al. 2013). Commissioned by the municipality of Delfzijl, the EcoShape consortium obtained the opportunity to carry out a large-scale field experiment on salt marsh construction as part of their Living Lab for MUD. Through testing of different initial conditions and sowing glasswort seedlings valuable new knowledge on salt marsh biogeomorphology is obtained.

2. Material and methods

2.1 Study area

The city of Delfzijl, the Netherlands is located to the west of the middle part of the Ems estuary. It has a mean semi-diurnal tidal range of 2.99 m and a mean annual suspended sediment concentration of 90 mg/l. Near Delfzijl are large areas of sandflats and mudflats, but land-water boundaries consist of rock protected dikes. A medium-sized port is protected from wave attack by a 4 km alongshore dam. The municipality of Delfzijl started a project to enhance the environment and economy in the region, named Marconi. As part of this project a pioneer salt marsh is constructed attached to the longshore dam bordering the port.

2.2. Design of the salt marsh test site

Local conditions prevent a salt marsh of growing naturally because the bed level is too low and there is too much wave energy. In 2018 the bed level was raised with sand obtained from capital dredging in the estuary and a rockfill dam was built to provide shelter. The new bed height for the projected salt marshes was set around Mean High Water level from 1.65 m to 1.05 m in a gradient of 1:140. In the 15 ha salt marsh site we created test plots delineated with brushwood groynes, Fig. 1. Three plots to the west differ in shape but all have a surface area of 2.3 ha. These plots have one opening in the groynes. They differ with respect to the percentage of clay and silt particles that were mixed through the top 1 m of the sandy bed resulting in 5, 20 and 50% silt. Three plots to the south have equal shapes, slopes and sizes. These plots are 1.8 ha (216 x 85 m) in size and have two openings in the groynes. They also differ in clay and silt percentage and in half of each of these plots seedlings of glasswort (*Salicornia europaea*) were sown. A total of 13,500 glasswort plants were manually collected and cut into about 100 pieces each. The 1,350,000 plant pieces were mixed with sawdust and put in freshwater to germinate. In May 2019 in each of the 9,000 m^2 test plots seedlings were sown with a density of 50 m^{-2}.

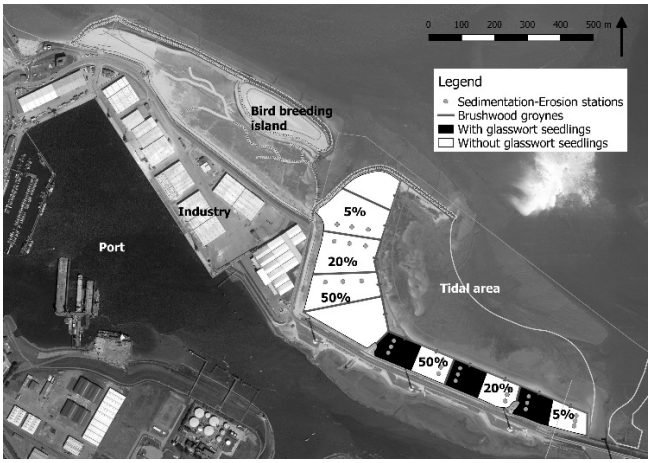

Figure 1: Design of the salt marsh test site.

2.4. Monitoring

A two year monitoring programme in 2019 and 2020 will determine sedimentation-erosion rates, development of drainage channels, bed height, flooding frequency, and density & condition of the glasswort seedlings. The biogeomorphodynamic developments will be analysed with respect to a.o. heights, slopes, silt percentages, and vegetation cover. Instruments include a.o. LiDAR drone, RTK-DGPS, Sedimentation-Erosion Bars, and Acoustic Surface Elevation Dynamics (ASED) sensors.

3. Conclusions

The presentation will elucidate preliminary results of the ongoing research.

Acknowledgments

This work was supported by the Dutch Waddenfonds. Cash and in-kind co-funding was received from the consortium partners of EcoShape. Manuscript writing is supported by the Wageningen UR Knowledge Base programme KB-36-003-009.

References

Temmerman, S., Meire, P., Bouma, T.J., Herman, P.M., Ysebaert, T., De Vriend, H.J. (2013). Ecosystem-based coastal defence in the face of global change. Nature 504, 79–83.

Self-organisation of saltmarsh-mudflat interfaces: An exploratory model of the interplay between hydrodynamic, biological and sedimentary processes

Z. Zhou[1], I. Möller[2], J. van Belzen[3], I. Townend[1,4], G. Coco[5], F. Xu[6], B. Evans[2], H. Li[1], Z. Gong[1], C.K. Zhang[1]

[1] State Key Laboratory of Hydrology-Water Resources and Hydraulic Engineering, Hohai University, Nanjing, China
[2] Cambridge Coastal Research Unit, Department of Geography, University of Cambridge, UK
[3] Department for Estuarine and Delta Systems, Royal Netherlands Institute for Sea Research (NIOZ) and Utrecht University, Yerseke, the Netherlands
[4] School of Ocean and Earth Sciences, University of Southampton, UK
[5] School of Environment, University of Auckland, Auckland, New Zealand
[6] State Key Laboratory of Estuarine and Coastal Research, East China Normal University, Shanghai, China

1. Introduction

Saltmarsh-mudflat interfaces around the world show different morphological patterns and evolutionary behaviour, depending on local environmental conditions such as sediment supply, tidal regimes, wave climates, sea level variations, marsh species and soil properties (Allen, 2000). Many European and North American saltmarshes are characterized by marsh-edge cliff erosion which can show either cyclic behaviour or irreversible marsh deterioration (van de Koppel et al., 2005). In contrast, some Asian saltmarshes are under continuous progradation without the formation of evident marsh-edge cliffs. Although many authors suggest that marsh-edge cliffs are erosional features as a result of wave action, there are also studies that demonstrate that they can be formed in accretional environments. As a transitional feature between smooth and cliffed marsh-edges, saltmarsh ramps of ridges and grooves have also been widely observed. Recent studies highlight that the fate of saltmarsh wetlands over the long term is critically dependent on the marsh-edge dynamics at the interface between the vegetated and the bare flats. Therefore, the geomorphology of saltmarsh edges is an important indicator for wetland stability, providing potentially useful information to probe regime shifts and assess the resilience of saltmarsh ecosystems. However, our understanding on marsh-edge dynamics is still limited, particularly the regime shift from one type of marsh margin to another. By developing an exploratory model, this study aims to gain more in-depth insight into the physics governing marsh-edge morphologies and hence predict their bio-morphodynamic evolution under sea level rise and human interventions.

2. Methods

Taking the interplay between sedimentary, biological and hydrodynamic processes into account, we developed a two-dimensional exploratory model by modifying and extending the one-dimensional model proposed by van de Koppel et al. (2005), to simulate the formation of different bio-morphologies at the saltmarsh-mudflat interface. We refer the reader to van de Koppel et al. for the detailed equations. The coupled equations governing marsh biomass change and bed level change are solved. The two coupled equations were extended by adding bed slope terms in the bed level change equation and marsh expansion terms in the biomass change equation. The sediment deposition and erosion terms in the bed level equation were also modified to facilitate a more physically representation of tidal flat morphodynamics.

3. Results and discussion

Model results indicate that the model is able to simulate the formation from marsh patches to marginal cliffs. The geometric parameters of the simulated marsh patches are statistically comparable to the ones observed along the Jiangsu coast (Figure 1). The marsh patch-size distribution follows a power law, suggesting the presence of self-organised processes (Taramelli et al., 2018). When waves are stronger and sediment supply is reduced, the simulated marsh edge is characterised by cliffs which may be further enhanced by sea level rise. Model results suggest that the marsh-edge morphology is self-organised via vegetation engineered biophysical feedbacks. The biomorphology and associated equilibrium of saltmarsh-mudflat interfaces are dependent on the delicate balance between various factors. Ongoing studies are being conducted to probe the condition for regime shifts from marsh patches to cliffs.

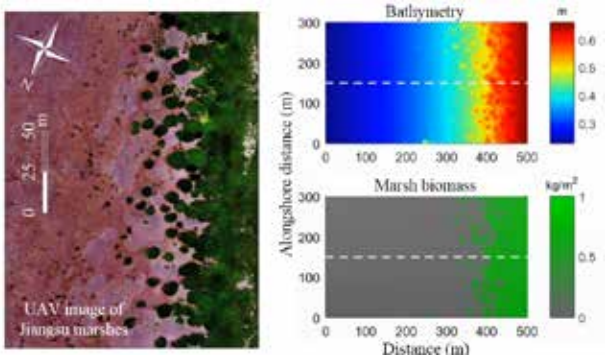

Figure 1. Comparison between the observed and simulated marsh patches. Left panel: the Jiangsu marsh patches; right panel: model result.

References

Allen, J., 2000. Morphodynamics of Holocene salt marshes: A review sketch from the Atlantic and Southern North Sea coasts of Europe. Quaternary Science Reviews, 19(12): 1155-1231.

Taramelli, A., Valentini, E., Cornacchia, L., Monbaliu, J. and Sabbe, K., 2018. Indications of Dynamic Effects on Scaling Relationships Between Channel Sinuosity and Vegetation Patch Size Across a Salt Marsh Platform. Journal of Geophysical Research: Earth Surface, 123(10): 2714-2731.

van de Koppel, J., van der Wal, D., Bakker, J.P. and Herman, P.M.J., 2005. Self-Organization and Vegetation Collapse in Salt Marsh Ecosystems. The American Naturalist, 165(1): E1-E12.

Flow Resistance Coefficient Measurement in Big Rivers

Bateman, A. and Sosa, R.

[1]Sediment Transport Research Group GITS-UPC. Civil and Environmental Department. Barcelona Tech. Jordi Girona 31-34 Barcelona-639217557 allen.bateman@upc.edu.

1. Abstract

A methodology to measure the flow resistance coefficient is presented. Different Colombian rivers and an estuary were studied, the results suggest interesting values for energy slope, bed stress and other factors whose values are intriguing.

2. Introduction

Photography, tables and other empirical systems were used to assess the flow resistance factor, engineering documents do not take deep care to this factors. The resistance factor is relevant because from its knowledge permits to evaluate the depth, velocity, energy slope, bed stress and sediment transport. All those values are closer connected through the Flow resistance factor. Manning value is one of them and its value is connected directly to the state of turbulence throughout the Von Karman-Prandtl law velocity.

2.1 Study zone

Figure 1 shows the Colombian map and studied rivers.

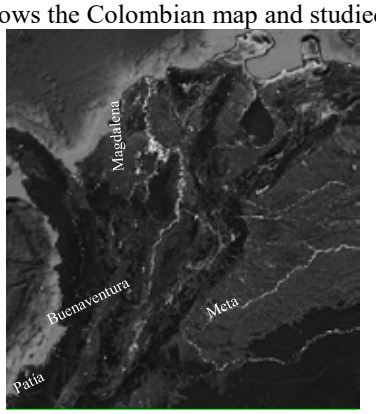

Figure 1 Colombian river zone study

3. Methodology

The velocity profile, from an ADCP, in a cross section of a river can be near the Von Karman distribution velocity law, as:

$$\frac{u}{u^*} = \frac{1}{k} ln\left(30\frac{z}{k_s}\right) \quad (1)$$

In which u is the velocity at the z level, u^* is the denominated shear velocity, k_s is the roughness height and k the KarmanPrandtl coefficient equal to 0.41, this law is provoked by a linear distribution of the Reynolds stresses, and at the bottom its value τ_b is

$$\tau_b = \rho g h S_f \quad (2)$$

In which ρ is the water density, g gravity acceleration and S_f the energy slope, also bottom stress can be expressed as:

$$\tau_b = \rho u_*^2 \quad (3)$$

An optimization analysis from the experimental velocity profile and the theoretical profile, constructing an objective function as,

$$F(u^*, k_S) = \sum_{i=1}^{n}\left(\frac{u_i}{u^*} - \frac{1}{k}\ln\left(30\frac{z_i}{k_S}\right)\right)^2 \left(\forall z_i, u_i\right) \quad (4)$$

Optimization process of (4) give us the shear velocity and the roughness height, given an entire velocity profile. By using (2) and (3) it is possible to get the friction slope, the shear stress knowing the water depth at the profile position. Manning coefficient can be solved by using Keulegan formula or other relationships. k_s, depends on the riverbed forms, Manning value is controlled by the roughness height and of course by bed forms and skin friction. Manning value is a measure also of the turbulent condition and then is intrinsic to the sediment transport process.

4. Results

	Q(m^3/s)	h_{max} (m)	u* (m/s)	Ks(m)	τ_0(N/m^2)	S_f(-)	n(s/$m^{1/3}$)
Patía	1240	4.40	0.110	0.180	12.3	$2.85\cdot10^{-4}$	0.036
Meta, Cabuyaro	450	5.3	0.0807	0.50-	6.51	$1.9\cdot10^{-4}$	0.030
Meta, Cabuyaro	1500	12.0	0.09	0.51	8.09	$1.7\cdot10^{-4}$	0.034
Meta, Humapo	1000	6.5	0.08	0.36	6.47	$3.8\cdot10^{-4}$	0.032
Meta, Humapo	2000	7.9	0.13	1.17	16.8	$3.5.10^{-4}$	0.034
Meta, Puerto Texas	1000	5.9	0.084	0.08	7.10	$1.5\cdot10^{-4}$	0.028
Meta, Puerto Texas	3000	9.8	0.089	0.49	7.88	$2.1\cdot10^{-4}$	0.032
Magdalena	7400	7.72	0.13	1.15	15.58	2.05.10-4	0.042
Buenaventura	Lowtide	9.66	-	3.83	4.04	$1.95.10^{-5}$	0.054
Buenaventura	Hightide	11.18	-	0.07	0.84	$7.62.10^{-6}$	0.028

5. Conclusions

The results obtained are encouraging and allow much closer to what happens in the channel. Also involve the possibility to modify the Karman Coefficient due to the influence of the sediment transport.

References

Bateman, A. 2017. Asesoría para la modelación numérica de la Bahía de Buenaventura en Colombia. Realizada para HMV.

Bateman, A. 2015. Monitoreo del río meta (136 km desde Cabuyaro hasta bocas del Manacacías). Weg Ingeniería.

Bateman, A. 2008. Estudio en el Río Patía para Solucionar la Problemática Generada por el Cambio de Curso del Río Patía Ocasionado por la Construcción del Canal Naranjo. Proyecto realizado para Universidad del Pacífico.

Pope, Stephen. 2000. Turbulent Flows. Cambidge University Press

Nezu,I; Nakagawa,H. 1991. Turbulence in Open Chanel Flows. Balkema

Investigating the dynamics of suspended sediment concentration and particle size grading during flood events

A. Haddadchi[1], M. Hicks[2], Y. Agrawal[3]
[1] National Institute of Water and Atmospheric Research, Christchurch, New Zealand. arman.haddadchi@niwa.co.nz
[2] National Institute of Water and Atmospheric Research, Christchurch, New Zealand. murray.hicks@niwa.co.nz
[3] Sequoia Scientific, Inc., Bellevue, Washington, USA, yogi.agrawal@sequoiasci.com

1. Introduction

Variation in the relationship between water discharge and suspended sediment concentration (SSC) during floods is well documented, but much less is known about the dynamics of the suspended sediment particle size distribution (PSD) – which exerts important control on the environmental effects of the suspended load. Here, we report on PSD and SSC data collected during flood events on the Oreti River on South Island, New Zealand, using in-situ instrumentation.

2. Methods

The LISST-SL2 (Laser In-Situ Scattering and Transmissometry, Stream-Lined version 2) instrument was employed to profile the SSC and PSD in the Oreti River. The LISST-SL2 is a laser-diffraction particle-size analyzer mounted in a weighted, streamlined "bomb" that is deployed into the river from a cable (Czuba et al. 2015).

It was deployed during three flood events (Q_{max} = 404 - 623 m^3 s^{-1}) at two monitoring sites using a jet boat. At the upstream site at Wallacetown, the river was confined to a single channel but was mainly braided further upstream. The Taramoa site was ~ 5km downstream along a meandering reach experiencing severe bank erosion. The LISST-SL2 instrument was traversed between the water surface and the bed, sampling for 1 second bursts at intervals of depth, with this repeated at five verticals located at the centroids of sub-sections each conveying 20% of the total discharge (as determined by a prior discharge gauging using an ADCP). Manual depth-integrated samples were collected from the same verticals using a D-49 isokinetic sampler. Two depth-integrated samples were collected from each vertical; one analyzed in the laboratory for SSC by filtering technique, the other analysed for PSD using a Beckman-Coulter laser diffraction particle size analyser.

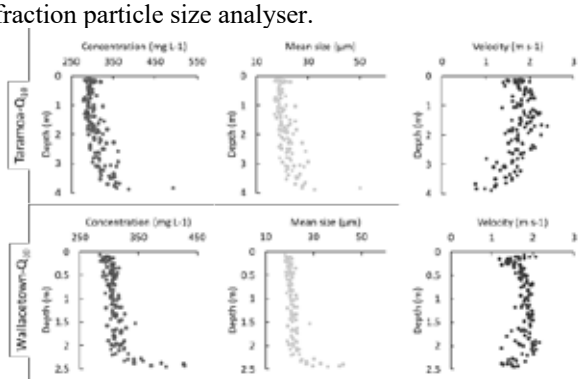

Figure 1: Real-time samples of the concentration, mean particle size, and velocity measured by the LISST-SL2 in 20% discharge verticals of the Wallacetown and Taramoa sites with 212.9 m^3 s^{-1} and 233.9 m^3 s^{-1} flows, respectively.

3. Results

As theoretically expected, SSC and mean particle size increased with depth on all measured verticals (similar to the example verticals shown in Figure 1), while the velocity distribution generally showed a logarithmic profile but not always. Measurements during the recession of the largest gauged event (Q_{max} =623 m^3 s^{-1}) indicate that the SSC changed from 298 mg l^{-1} near the water surface to 317 mg l^{-1} near the river bed in first vertical of the Taramoa site with 233.9 m^3 s^{-1} discharge. The mean PSD increased from 19.5 µm to 22.3 µm through the depth profile. At the Wallacetown site with 212.9 m^3 s^{-1} discharge, the SSC ranged between 297 mg l^{-1} to 368.5 mg l^{-1} through the water depth profile with mean size ranging from 19.5 µm to 30.7 µm.

The PSDs from the two monitoring sites during the 404 m^3 s^{-1} flood event showed tri-modal distributions, with a dominant silt mode and lesser clay and sand modes (Figure 2). The clay mode showed no change with depth; the silt mode showed a minor increase with depth; while the sand fractions increased markedly towards the bed, particularly at the Wallacetown site. The different sand mode behaviour at the two sites was probably due to the greater depth and different at the Wallacetown sampling vertical shown.

The manually sampled SSC and PSD remain under analysis and will be compared with the LISST-SL2 results in the presented paper.

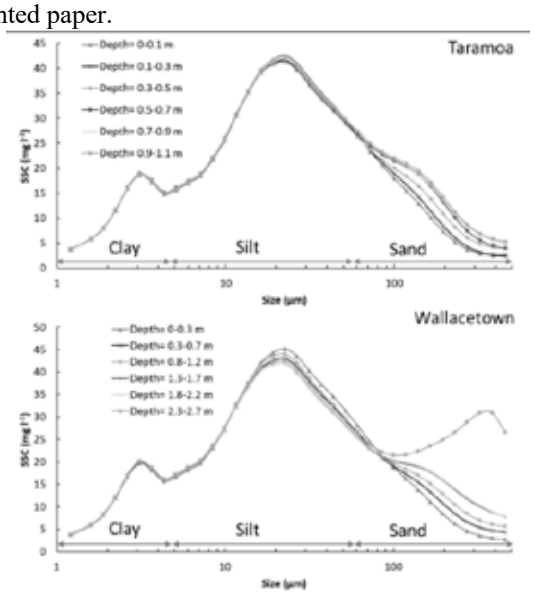

Figure 2: Particle size distributions at different depths measured by the LISST-SL2 at example verticals at the Taramoa and Wallacetown sites during the 404 m^3 s^{-1} flood.

4. Conclusion

The LISST-SL2 provided "on-the-fly" measurements of the variation in SSC, PSD and velocity distribution with water depth (as shown in Figure 1) that align with theoretical expectations. After calibration to establish apparent sediment density, it offers an expedient alternative to manual isokinetic sampling and laboratory analysis for making accurate measurements of the suspended sediment load and its PSD over a cross section.

Acknowledgments

This work was funded by NIWA's Managing Mud SSIF Programme.

References

Czuba, J. A., T. D. Straub, C. A. Curran, M. N. Landers and M. M. Domanski (2015). Comparison of fluvial suspended-sediment concentrations and particle-size distributions measured with in-stream laser diffraction and in physical samples. *Water Resources Research* 51(1): 320-340.

Discovering Small Scale Controls on Bedload Flux through Lagrangian Simulations

Cristián Escauriaza[1], Christian González[1] and Wernher Brevis[1]

[1] Hydraulic and Environmental Engineering, Pontificia Universidad Católica de Chile, Santiago, Chile.
cescauri@ing.puc.cl

1. Introduction

The dynamics of sediment particles moving in close contact with the bed has important implications for many physical and ecological processes in river channels. The analysis of the collective motion of particles is typically carried out from an Eulerian perspective, using formulas based on empirical relationships that estimate the bedload flux as a function of bulk sediment and flow properties.

These analytical expressions, however, do not capture the complexity of the transport dynamics at small scales, which is driven by nonlinear interactions of the sediment grains with the turbulent boundary layer, producing transport intermittency (Escauriaza and Sotiropoulos, 2011; González et al., 2017).

The integration of scales of bedload transport and investigations on the emergence of sedimentary patterns require an answer to two important questions: (1) Does the small-scale mechanics of sediment motion have an influence on the flux observed at larger time scales? (2) Can we improve the prediction of bedload transport formulas using high-resolution simulations?

To improve our understanding of the dynamics of bedload transport processes, we carry out Lagrangian particle simulations that capture the details of sediment motion, and use the results to study the impact on bedload flux at larger time scales as a function of the Shields parameter.

2. Lagrangian Model of Bedload Transport

We perform direct numerical simulations (DNS) of the turbulent flow in a rectangular channel with periodic boundary conditions, using the model developed by González et al. (2017). The solver of the incompressible Navier-Stokes equations is coupled in a two-way manner to a discrete-element model (DEM) for particles, which computes collisions between grains using a point-particle approach (see González et al., 2017, for details).

We carry out simulations for six different Shields parameters τ_*, maintaining the particle Reynolds number constant, $Re_p^* = 7.0$, to retain the statistical properties of the forcing exerted by turbulence on sediment grains.

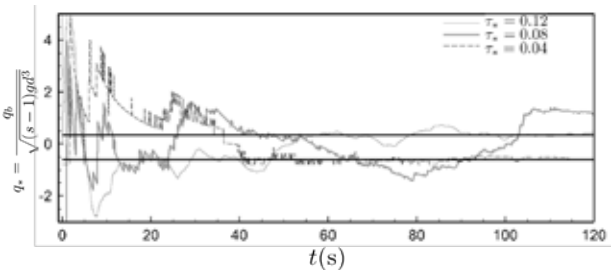

Figure 1. Standardized bedload flux for different Shields numbers τ_* as a function of the measurement time.

3. Upscaling the Bedload Transport Flux

The DNS results are used to compute the evolution of the bedload flux in time, integrating the sediment mass that exits the computational domain. As shown in Fig. 1, for short time scales, the fluctuations of particle transport produce a significant variability on the standardized non-dimensional bedload flux. At longer time scales, cases with lower and higher stresses converge to a constant flux and the effects of intermittency are averaged out. For intermediate cases, however, the variability persists and fluctuations are propagated across scales. A transport law based on a 3/2 exponent overpredicts transport in the cases that show this irregularity controlled by fluctuations, as shown in Fig. 2 .

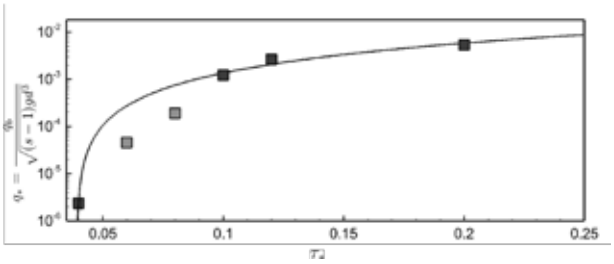

Figure 2. Results show that a bedload transport formula with a 3/2 exponent overpredicts the transport rate in cases when fluctuations control transport.

4. Conclusions

In this investigation we employ DNS Lagrangian simulations to investigate the effects of small scale processes on the bedload transport flux. The results show that there is a critical window, for which fluctuations of particle transport appear at longer time scales, producing an irregular bedload flux, as observed in plots of standardized transport. In the presentation, we will focus on the statistical analysis of this critical regime, to propose a new perspective on the prediction of bedload transport, based on the insights provided by the high-resolution Lagrangian particle model.

Acknowledgments

This work has been supported by Fondecyt grant 1191785 and Conicyt/Fondap grant 15110017.

References

Escauriaza, C. and Sotiropoulos, F. (2011). Lagrangian model of bed-load transport in turbulent junction flows. *Journal of Fluid Mechanics*, 666:36–76.

González, C., Richter, D. H., Bolster, D., Bateman, S., Calantoni, J., and Escauriaza, C. (2017). Characterization of bedload intermittency near the threshold of motion using a Lagrangian sediment transport model. *Environmental Fluid Mechanics*, 17:111–137.

Improving bedload rate prediction in gravel-bed rivers accounting for bed stability and large bedforms

E. Perret[1], C. Berni[1] and B. Camenen[1]

[1] Irstea, UR RiverLy, Lyon-Villeurbanne center, 5 rue de la Doua CS 20244, 69625 Villeurbanne, France

1. Introduction

Alpine gravel-bed rivers are complex systems associated with specific morphologies (bars, riffles/pools, poorly sorted sediments, possible armouring). They are often subjected to anthropogenic activities and connected to ecological and economic issues. Their bedload dynamics have received much attention these past decades. Many bedload formulae have been proposed but they often fail to reproduce the dynamic of such rivers, especially when assessing low transport rates (Gomez and Church, 1989). In this paper, we focused on the low transport rate regime which is mainly driven by bed roughness using laboratory experiments. Our objective is to better estimate bedload rate q_s at low bed shear stress using detailed information about bed morphology, which is the key factor to better understand gravel transport processes.

2. Experimental set-up and Methods

Eighteen tests were performed in the tilting flume of HH-Lab located at Irstea Lyon-Villeurbanne, France. Sediment transport experiments were carried out on different beds: loose (L), hybrid (H), packed (P), hybrid packed (HP) and water-worked (WW) beds. Beds were designed to mimic those found in Alpine rivers (i.e. with diverse degree of arrangements and bedforms at different scales). For details about bed formations, please refer to Perret et al. (2018). Tests consist in operating the flume with a flow hydrograph while collecting transported gravel at the flume's downstream end. Bedload rate, water slope and detailed bed surface topography were measured during these tests.

Total bed shear stress τ_t was computed using the well-known depth-slope equation. Criteria that describe bed surfaces were deduced using statistical tools and Bertin et al. (2018) method to isolate different scales of roughness from bed elevation measurements (grain, bed structures and large bedform scales).

3. Toward a new bedload formula

The analysis of bed surface criteria showed that beds can be divided into two categories: the quasi-flat beds (L, H, P and HP) and the beds with large bedforms (WW) (i.e. higher than 10% of the water depth). τ_t was assumed equal to the effective bed shear stress (used for gravel transport) for quasi-flat beds since no large bedforms are present. Among quasi-flat beds, non-organized beds (L) differs significantly from the arranged and imbricated beds (H, P, HP) in terms of gravel dynamics. Figure 1 shows the dimensionless bedload rate q_s^* as a function of the dimensionless effective bed shear stress τ_e^* for each tests and highlights the importance of considering bed stability in bedload studies. We suggest a new bedload model accounting for bed stability through two key parameters, namely the dimensionless reference bed shear stress τ_{ref}^* (inducing gravel incipient motion) and a parameter n describing bed reactivity to a change in bed friction: $q_s^* = q_{s,ref}^* (\tau_e^* / \tau_{ref}^*)^n$, where $q_{s,ref}^*$ is the dimensionless reference bedload rate reached at gravel incipient motion, and τ_{ref}^* and n are function of bed stability that is characterized here by a combination of bed surface criteria informing about bed arrangements at the grain and bed structure scales (i.e. size and magnitude of longitudinal and transverse bed structures, respectively, parameters reflecting anisotropy in terms of length and magnitude between transverse and longitudinal bed structures and index assessing grain imbrication).

Bedload rate of WW bed was estimated locally considering the distribution of local bed shear stresses assumed equal to the effective bed shear stresses and assuming the mechanisms governing q_s^* are the same as for quasi-flat beds. We use the new model and account for bed stability by computing τ_{ref}^* and n using criteria of the WW bed surface. Results of computed q_s^* for all tests are presented in Figure 1 and classified by types of bed configurations. q_s^* computed with Recking (2010) model is added to show the interest of using the new model.

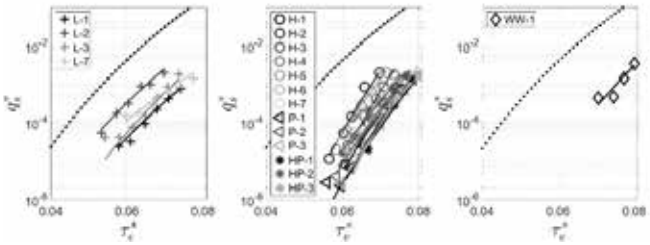

Figure 1: Comparison between measured and predicted dimensionless bedload rates. Solid and dotted lines refer to the new and Recking (2010) model, respectively.

3. Conclusions

We show that bed morphology acts at different scales on diverse factors (energy dissipation, bed stability) impacting directly q_s. Bedload formula accounting for the bed stability and the effective bed shear stress distribution is developed using flume tests carried out at low transport regime. We succeed in evaluating gravel dynamics over complex beds such as arranged beds with large bedforms.

References

Bertin, S., Groom, J., and Friedrich, H. (2017). Isolating roughness scales of gravel-bed patches. *WRR*, 53:6841-6856.

Perret, E., Berni, C., Camenen, B., Herrero, A., and El kadi Abderrezzak, K. (2018). Transport of moderately sorted gravel at low bed shear stresses: the role of fine sediment infiltration. *ESPL*, 43(7):1416-1430.

Recking, A. (2010). A comparison between flume and field bedload transport data and consequences for surface based bedload transport prediction. *WRR*, 46(W03518):1-16.

Gomez, B. and Chruch, M. (1989). An assessment of bed load sediment transport formulae for gravel bed rivers. *WRR*, 25(6):1161-1186.

Riverbed evolution and sediment sorting during flood

Robin K. Biswas[1], D. Harada[2], Y. Nakamura[3] , H. Ito[4] and S. Egashira[5]

[1]International Centre for Water Hazard and Risk Management (ICHARM), Public Works Research Institute (PWRI), Tsukuba, Japan. robin-k177bt@pwri.go.jp
[2]ICHARM, PWRI, Tsukuba, Japan. d-harada55@pwri.go.jp
[3]ICHARM, PWRI, Tsukuba, Japan. y-nakamura44@pwri.go.jp
[4]ICHARM, PWRI, Tsukuba, Japan. hi-itoh@pwri.go.jp
[5]ICHARM, PWRI, Tsukuba, Japan. s-egashira77@pwri.go.jp

1. Introduction

River channels are composed of non-uniform sediment. The size distribution of sediment particles influences the riverbed evolution process and stage-discharge relationship. Simultaneously, riverbed evolution, flood flow and longitudinal variations in cross-sections have significant effect on temporal-spatial sediment sorting. Thus, the present study aims to investigate the sediment sorting process, river bed evolution and the stage-discharge relationship during floods in a reach of Seri River, Shiga, Japan.

2. Methodology

Channel bed evolution, sediment sorting and stage-discharge relation during floods can be evaluated by means of numerical computation based on a 2-d depth averaged flow model and corresponding sediment transport model (e.g. Ashida and Michiue, 1972; Egashira et al., 1997), in which thickness of exchange layer is one of the most important factors. Most of the researchers treated the thickness of exchange layer as constant although it changes corresponding to bed shear stress; i.e. the exchange layer thickness is proportional to the non-dimensional bed shear stress (τ_*) (Egashira et al., 1997). Present study employs two methods for exchange layer thickness for comparison; one is the variable thickness proposed by Loc et al. (2006) and the other is constant thickness. In addition, in order to investigate dependencies of sediment sorting process on the functional form of bed-load formula, two different formulas are employed; a type of $\tau_*^{1.5}$ (Ashida and Michiue, 1972) and a type of $\tau_*^{2.5}$ (Egashira et al., 1997). The details of the numerical model are explained in Shimizu and Takebayashi (2011).

3.1 Computation condition

The computational domain of study reach is about 4.2 km long and its bed slope is about 0.006. The reach is divided into 10521 computational grids with resolution of about 4m, part of which is shown in Figure 1(A). Figure 1 (B) shows a flood hydrograph employed in present simulation, which is reproduced artificially using a single flood hydrograph computed by 2013 flood event to investigate a relation between temporal and spatial changes of bed surface elevation and sediment particle size distribution around these equilibrium mean values.

3.2 Results

Figure 1(C) and (D) show sediment sorting at (a) and (b) during T1 and T2 for bedload transport rate proportional to $\tau_*^{1.5}$ and $\tau_*^{2.5}$ respectively. (a) is located on deposition zone while (b) is on channel centreline as indicated in

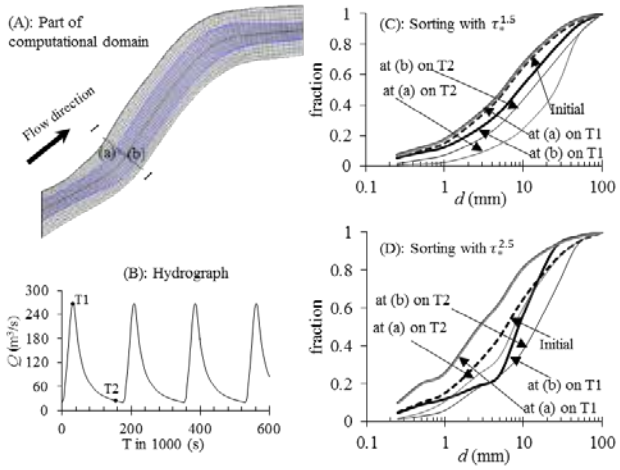

Figure 1: Spatial and temporal sediment sorting (T1, T2: timing in hydrograph).

Figure 1(A). T1 and T2 are peak and low flood time in Figure 1(B). Figure 1(D) indicates very active sediment sorting for computation with exchange layer thickness is proportional to non-dimensional bed shear stress.

4. Conclusion

The sediment sorting, riverbed evolution and stage-discharge relationship during flood are discussed based on data from numerical simulation. This abstract include part of the results. Sediment sorting depends on the choice of the bedload transport formula as well as on treatment of exchange layer. We will verify the results by conducting field observations.

Acknowledgments

We would like to thank Y. Shimizu and H. Takebayashi for generously proving us with the source code of the numerical model which has been used in this study.

References

Ashida, K. and Michiue, M. (1972). Study on hydraulic resistance and bed-load transport rate in alluvial rivers. *Transactions of JSCE*, Vol. 206, pp. 59-69.

Egashira, S., Miyamoto, K. and Itoh, T. (1997). Constitutive equations of debris flow and their applicability. *Debris-Flow Hazards Mitigation: Mechanics, Prediction and Assessment, Water Resources Engineering Division, ASCE*, pp. 340-349.

Loc, X. L., Egashira, S. and Takebayashi, H. (2006). A new treatment of exchange layer thickness to evaluate sediment sorting and armouring. *Journal of Applied Mechanics*, Vol. 9, 1025-1030

Shimizu, Y. and Takebayashi, H. (2011). Nays2DH Solver Manual.

Influence of filter layer on the stability of man-made step-pool systems

F. Maager, B. Hohermuth, R.M. Boes, V. Weitbrecht

Laboratory of Hydraulics, Hydrology and Glaciology (VAW), ETH Zurich, Switzerland
maager@vaw.baug.ethz.ch, hohermuth@vaw.baug.ethz.ch, boes@vaw.baug.ethz.ch, wv@ethz.ch

1. Introduction

Mountain torrents are often heavily stabilized with massive concrete drop-structures to reduce bed incision and the amount of transported sediment during flood events. These structures lead to fragmented habitat conditions, need expensive maintenance and fail abruptly during overload conditions. The general idea of this research project is to replace these check-dams by boulder structures that are close to natural step-pool systems, in function and optical appearance. Flume experiments were conducted to determine the stability of man-made step-pool systems. The boulder arrangement was optimized to achieve maximum stability in terms of maximum bed slope during flood conditions. It turned out that the grain size distribution of bed material significantly influences step stability. Therefore, the effect of a filter layer (FL) is analysed herein.

2. Experimental setup

The experiments were conducted in a 13.5 m long and 0.3 m wide tilting flume (Kaspar, 2017). Figure 1 shows the parameters of the tested step-pool configurations, where the first test run (TR1) was conducted without FL and the second test run (TR2) included a FL (orange parts). A unit discharge of $q = 0.011$ m^2/s was applied to the bed until it stabilized. The discharge was then increased by $\Delta q = 0.011$ m^2/s and the procedure was repeated until a critical discharge q_c was reached.

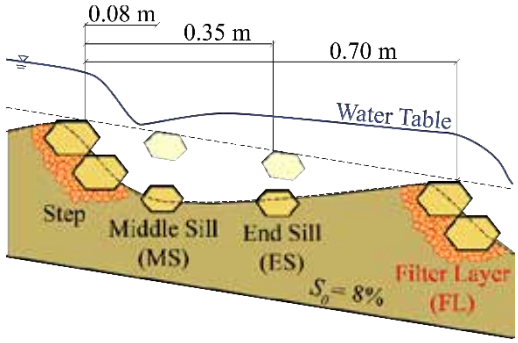

Figure 1: Side view of the tested step-pool configuration

The characteristic grain diameters of the bed material, filter material and the step-forming blocks are listed in Table 1. The large blocks are in the upper range of the criteria of Raudkivi and Ettema (1982) regarding the ratio between block diameter and grain size of the base material. The filter material was selected according to the criteria of Terzaghi and Peck (1948).

	d_{15} [mm]	d_{50} [mm]	d_{84} [mm]
Bed material	0.5	2.2	8.1
Filter material	11.1	13.3	15.1
Step-forming blocks	67.3	72.6	78.6

Table 1: Characteristic grain diameters.

3. Results and Discussion

Figure 2 shows TR1 and TR2 at unit discharges of $q = 0.034$ m^2/s each. Inner erosion occurs when the FL is absent and consequently the blocks are more exposed to the flow. The use of filter material reduces this internal erosion, leading to more stable steps. The step-pool sequences of TR1 remained stable up to a unit discharge of $q_c = 0.067$ m^2/s, whereas TR2 failed at $q_c = 0.089$ m^2/s.

Figure 2: a) TR1 without FL, b) TR2 with FL

The failure mechanisms of TR1 and TR2 were not recorded, because the steps failed almost instantaneously. It is assumed that the step-forming blocks slid into the downstream pools in both cases. The steps in TR1 tended to be less stable during lower discharges due to erosion of fine material. In case of a high flood following a smaller flood, the step-forming blocks in TR1 are more prone to be directly eroded.

4. Conclusions

The use of FL in man-made step-pool sequences reduces internal erosion thereby increasing the integrity and overall stability of the steps. Nevertheless, man-made step-pool sequences might not be able to self-stabilize after a failure, because the FL may not maintain its function after step failure.

Acknowledgments

The Project is funded by the Swiss Federal Office for the Environment (FOEN), contract No. 17.0093.PJ / Q422-0908.

References

Kaspar, P. (2017). Stabilität künstlicher Stufen-Becken Systeme. *Master's Thesis, unpublished,* ETH Zürich. [in German].

Raudkivi, A. J. and Ettema, R. (1982). Stability of Armour Layers in Rivers. *Proc. ASCE, J. of Hydr. Div.* 108(HY9), 1047-1057.

Terzaghi, K. and Peck, R. B. (1948). *Soil Mechanics in Engineering Practice*. John Wiley&Sons, New York.

Sorting waves in unidirectional shallow-water flows

M. Colombini[1] and C. Carbonari[2]

[1] Dipartimento di Ingegneria Civile, Chimica e Ambientale, Università degli studi di Genova, Via Montallegro 1, 16145 Genova, Italy. col@dicca.unige.it

[2] Dipartimento di Ingegneria Civile e Ambientale, Università degli studi di Firenze, Via di S. Marta 3, 50139 Firenze, Italy. costanza.carbonari@unifi.it

1. Introduction

River beds present heterogeneous sediment mixtures undergoing sorting processes during bed load transport and, as a consequence, the superficial concentration of the sediment fractions develops spatial patterns. Bedload sheets are sorting waves resulting in rhythmic alternations of finer and coarser sediments aligned across the flow, characterized by downstream migration and negligible amplitude. The present 1D linear stability analysis addresses the problem of sorting waves' formation by investigating the stability of a uniform shallow-water flow above an erodible bed composed by a bimodal sediment mixture.

2. Formulation of the problem

The model is composed of the governing equations of hydrodynamics, consisting in the 1D Saint-Venant and continuity equations, and the mass-conservation sediment model, consisting in a simple three-layer model which implement the concept of the 'active layer' of Hirano. A discrete grain size distribution composed by just two sizes in the same proportion is considered, whereby the finest and the coarsest grain diameters are, in the sedimentological phi-scale, equally distant from the average grain size of the mixture. By doing so, two Exner-like equations are obtained for the sediment phase. Once the equations are linearized, an algebraic eigenvalue problem is obtained. In the case of quasi-steady approximation the eigenvalue problem reduces to a quadratic eigenrelation, whereas in fully unsteady conditions (i.e. fully coupled equations) a rank-four eigenvalue problem is obtained.

The interaction between the flow and the erodible bed drives two distinct modes of instability, each one characterized by its own wavespeed, growth rate and longitudinal wavelength, each one involving spatial variations of both grain size density and bed elevation. We named the two modes of instability 'bed wave' and 'sorting wave', and the two related eigenvalues 'bed eigenvalue' and 'sorting eigenvalue'. The bed eigenvalue is associated with the formation of bed forms with a small amount of sorting along the unit wavelength, the sorting eigenvalue with the formation of sorting waves with a small variation of the bed elevation along the unit wavelength. The former is then related to the modifications of the bed form induced by the presence of the heterogeneous mixture, such as the accumulation of finer (coarser) material at the crests (troughs) or viceversa. The latter is associated with the formation of the low-amplitude sorting waves, namely bedload sheets.

3. Discussion of results

Only the sorting eigenvalue is found to be unstable, confirming that the 1D shallow-water model is unable to describe the formation of bed waves; indeed only a more refined rotational flow model can capture the dynamics of dunes and antidunes.

Sorting waves propagate downstream faster than bed waves, confirming both the mathematical analysis by Stecca et al. (2014) and the experimental observations on bedload sheets (Whiting et al., 1988; Nelson et al., 2009; Recking et al., 2009). Moreover, the order of magnitude of the ratio between bed wave celerity and sorting wave celerity depends on the nondimensional thickness of the active layer as in Stecca et al. (2014). Two regions of positive growth rate are found for the sorting eigenvalue, one for subcritical flows and one for supercritical flows; this outcome is in accordance with experimental studies which monitored bedload sheets in subcritical conditions (Kuhnle et al., 2006) as well as in supercritical conditions (Recking et al., 2009). Both the unstable regions ($Fr < 1$ and $Fr > 1$) are bounded, then the analysis encompasses an adequate mechanism of wavelength selection. This does no longer apply for macroroughness regime (very low values of the Chézy coefficient, namely large grain diameter with respect to water depth), neither for conditions where suspended sediment transport is likely to occur (very large values of the Chézy coefficient).

4. Conclusions

A 1D linear stability analysis of flow above an erodible bed composed by a bimodal sediment mixture is performed. Sorting waves resembling bedload sheets are found unstable. Results confirm that the perturbations associated with the sorting eigenvalue propagate faster than those associated with the bed eigenvalue.

References

Kuhnle, R. A., Horton, J. K., Bennett, S. J., and Best, J. L. (2006). Bed forms in bimodal sand-gravel sediments: laboratory and field analysis. *Sedimentology*, 53(3):631–654.

Nelson, P. A., Venditti, J. G., Dietrich, W. E., Kirchner, J. W., Ikeda, H., Iseya, F., and Sklar, L. S. (2009). Response of bed surface patchiness to reductions in sediment supply. *Journal of Geophysical Research: Earth Surface*, 114.

Recking, A., Frey, P., Paquier, A., and Belleudy, P. (2009). An experimental investigation of mechanisms involved in bed load sheet production and migration. *Journal of Geophysical Research*.

Stecca, G., Siviglia, A., and Blom, A. (2014). Mathematical analysis of the saint-venant-hirano model for mixed-sediment morphodynamics. *Water Resources Research*.

Whiting, P. J., Dietrich, W. E., Leopold, L. B., Drake, T. G., and Shreve, R. L. (1988). Bedload sheets in heterogeneous sediment. *Geology*.

Transport Processes of Plastic Particles in Rivers

S. Francalanci[1], E. Paris[2], F. Ruggero[3] and L. Solari[4]

[1] University of Florence, Department of Civil and Environmental Engineering, simona.francalanci@dicea.unifi.it
[2] University of Florence, Department of Civil and Environmental Engineering, eparis@unifi.it,
[3] University of Florence, Department of Civil and Environmental Engineering, federica.ruggero@unifi.it,
[4] University of Florence, Department of Civil and Environmental Engineering, luca.solari@unifi.it

1. Introduction

The knowledge of the main mechanisms governing the plastic transport by rivers to the sea is fundamental to develop appropriate measures to reduce the impact of plastics in the fresh and marine water environments.

Transport phenomena of plastic particles in the ocean have been fairly studied (e.g. Zeng, 2018), while little attention was devoted to plastic particle movement in rivers.

Transport processes of plastic particles in rivers are important to quantify the volumes of plastic delivered by the rivers to the sea. In order to better understand these processes, we need to quantify the effect of shape, size and density of plastic particles on fall velocity, which is naturally related to the transport processes of suspension, deposition and re-suspension.

For the above reasons, we conducted several laboratory and field experimental activities both for quantifying fall velocity of micro-plastic in a still water column, for separating plastic particles from natural sediment, and for monitoring the amount of plastic carried in suspension during flood events.

2. Preliminary results for settling velocity

We conducted laboratory experiments for measuring settling velocity of different source of plastic particles: mixed plastic pellets, PVC irregular fragments, PET irregular fragments, PET regular fragments.

The settling velocity W was measured via image analysis of falling particles in a water column. The drag coefficient Cd is calculated according to the procedure by Camenen (2007) and Song et al. (2017).

Plastic particles behave differently in accordance with shape, size and density. For each set of samples, the model develops a linear or exponential correlation between W and Cd with an error $R^2 \geq 0.98$.

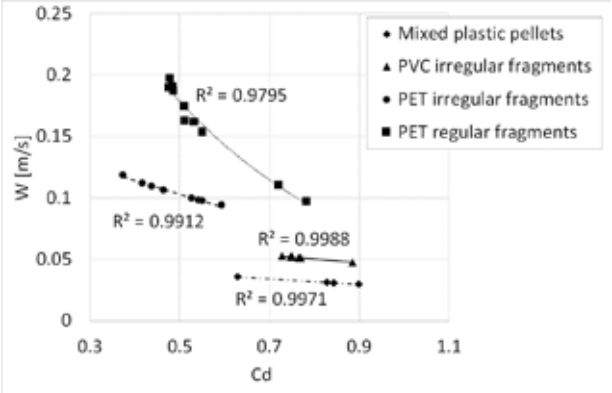

Figure 1: Predicted settling velocity versus drag coefficient, for 4 types of plastic particles.

Additional experiments are currently ongoing, regarding the settling dynamics of mixtures of plastic and natural sediments.

3. Monitoring of plastic particles in the Arno River

A monitoring activity was started at the water treatment plant for producing drinking water in Florence, which withdrawals the water directly from the Arno River. The main goal of this activity is quantifying the amount of plastic which is transported in suspension by the river.

The samples are collected in the withdrawal channel of the Publiacqua plant in Florence, by the use of sampling bags with a mesh opening of 250 μm.

3. Conclusions

This research summarized the results of the experimental and monitoring field activity conducted for a better understanding of transport processes of plastic particles in rivers. In particular, the experiments on settling velocity can help in defining the influence of particles shape, size and density on the suspension processes, including the effects of the presence of mixture with natural sediments, while the field activity can produce a sound estimate of the amount of suspended plastic particles during low and high flows.

Acknowledgments

The Authors would like to thank Publiacqua for the support in the monitoring activity.

References

Camenen, B. (2007). "Simple and General Formula for the Settling Velocity of Particles" Journal of Hydraulic Engineering 133 (2), 229–233. doi.org/10.1061/(ASCE)0733-9429(2007)133:2(229).

Xianzhi Song, Zhengming Xu, Gensheng Li, Zhaoyu Pang, Zhaopeng Zhu, 2017, A new model for predicting drag coefficient and settling velocity of spherical and non-spherical particle in Newtonian fluid, Powder Technology 321 (2017) 242–250, 0032-5910/© 2017 Elsevier B.V. All rights reserved, http://dx.doi.org/10.1016/j.powtec.2017.08.017

Zeng, E.Y. Editor (2018) "Microplastic Contamination in Aquatic Environments - An Emerging Matter of Environmental Urgency" Book. Elsevier. doi.org/10.1016/C2016-0-04784-8.

Connecting levee deposition to suspended-sediment concentration along a 90km river reach

H.J. Hassenruck-Gudipati[1], J. Mason[1], P. Passalacqua[2], and D. Mohrig[1]

[1] Department of Geological Sciences, The University of Texas at Austin. himghg@utexas.edu, jasminemason@utexas.edu, mohrig@jsg.utexas.edu
[2] Department of Civil, Architectural and Environmental Engineering, The University of Texas at Austin. paola@austin.utexas.edu

1. Introduction

Floodplain deposition is often assumed to occur throughout the duration of overbank floods. However, the constraints on sediment availability in the upper water column of a river in flood are limited. On the Trinity River, Texas, USA, a sand-bed meandering river, we constrained the volumes of deposited sediment on natural levees that flank the river cutbanks. Levee growth is captured using two elevation difference maps for 2015-2011 and 2017-2015 and compared to estimated volumes of suspended sediment advected onto the floodplain during extended floods. Exploring the link between in-channel sediment availability and levee deposition better constrains transfer processes from the channel to the floodplain.

2. Methods and Results

2.1 Change using repeat lidar surveys

Deposition on levees was measured using two lidar difference maps for time periods: 2011-2015 (47 flooded days in 1 event) and 2015-2017 (104 flooded days in 6 events). Natural levees were manually defined along the cutbank of each river bend and their extents (Figure 1 white lines) generally coincided with the areas covered by small levee channels. Deposition was observed to be focused at the distal ends of levee (Figure 1), indicating that overbank velocities were too large to deposit significant amounts of sediment along the levee crest closest to the main channel. The deposition amount during 2017-2015 was an order of magnitude larger than for 2011-2015.

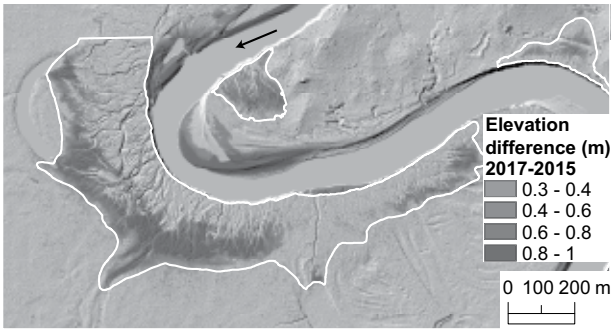

Figure 1. Levee deposition (levee extent outlined in white line) between 2017 and 2015 for one river bend. The deposition is focused at the distal levee, which coincides with the ends of levee channels.

2.2 Observed grain size variability on levees

A total of 117 sediment samples collected from six levees were collected, from the levee crest to its extent, and analyzed. The grain sizes of these levees neither fine away from the river nor downstream along the survey extent. The D_{50} on the levees is $123\mu m$ with a D_{90} of 224 μm and a D_{10} of 33 μm. Most levee deposits are composed of coarse silt – fine sand, preserving ripple stratification.

2.3 Estimating in-river available suspended sediment for levee sedimentation

River-bed samples and estimates of flood velocities were used to find sediment concentrations and volumes available for transfer out of the channel and onto levees. The grain size of the river bed (D_{10} = $194\mu m$, D_{50} = $322\mu m$, D_{90} = 532 μm) is significantly coarser than the levees such that the finest sediments on the levee are not observed on the river-bed. An estimate for suspended-sediment concentration by grain size was made throughout the floodwater column by calculating Rouse concentration profiles. The top 1m of the water column and its estimated sediment were allowed to inundate the floodplain. Estimates for the sediment volumes transferred from each river bend were made using the constant calculated sediment concentration, a measured flow velocity across the proximal levee, a cutbank length, and the known inundation duration.

3. Conclusions

Modeled estimates for the volumes and grain size of sediment transferred from the river to the floodplain were directly compared to levee measurements. The calculated sediment volumes overestimate measured levee additions by two to three orders of magnitude in a sample river bend. In addition, the sediment constructing levees was noticeably enriched in sand compared to the estimated distribution of fines moving out onto the floodplain.

Based on our field observations, deposition measurements, and modeling, we find that: 1. sediment concentrations are not constant during a flood period, given the overestimation of sediment volumes; 2. sand-sized sediment is supply-limited not transport-limited on levees; and 3. natural levees are composed of sediments that are coarse enough to have overbank transport restricted to levees, yet fine enough to have sediment concentrations in the uppermost portion of the flooded river water column sufficient to build levee deposits.

Acknowledgments

We acknowledge Gabriella Zegarra for grain size samples processing and The Trinity River Wildlife Refuge (USFWS), D. Aylward, B. Cardenas, B. Carlson, M. Daniller-Varghes, M. Day, T. Goudge, N. Hu, C. Kortyna, J. Molito, M. Velazquez, and W. Wagner for field assistance. HHG was funded through NSF GRFP and a GSA research grant. The 2015 NCALM airborne lidar survey was paid for by NSF EAR-1547200.

Sediment threshold of motion on rivers with steep slopes: impulse criterion

B. Marin-Esteve[1], A. Bateman[2] and C. Fernández[3], C. Lin[4]

[1]Universitat Politècnica de Catalunya, Catalonia. blanca.marin@upc.edu
[2] Universitat Politècnica de Catalunya, Catalonia. allen.bateman@upc.edu
[3] Universitat Politècnica de Catalunya, Catalonia. cfernandez.lop@gmail.com
[4] Universitat Politècnica de Catalunya, Catalonia, youngpope1024@gmail.com

1. Introduction

The hydraulics of mountain channels is still less studied and understood than in alluvial rivers. However, the turbulence produced by a highly energetic flow (steep slope) in a bed of coarse grain size with a low relative submergence causes deep erosions that often have to be alleviated by the hand of man.

The present study aims to shed light on the mechanism that triggers the initiation of the movement of these particles in steep slopes flows and highlights the importance of the turbulent parameters associated with the flow, for a stochastic treatment of the problem.

2. High slope streams

The hypothesis made in this investigation is that in mobile-bed rivers with steep slopes, channel hydraulics and bed morphology interactions avoid Froude number to exceed the unity. According to Grant (1997), competent, high-gradients streams with beds ranging from sand to boulders typically achieve an equilibrium adjustment between the flow, sediment transport and channel morphology at or near critical flow. Thus, critical flow condition itself may be both a threshold condition and a state of flow regime.

Most of researches use some form of Shields diagram to describe the threshold motion condition. However, the critical shear stress from Shields diagram does not consider the streamwise component of gravity acting on particles (Chiew y Parker 2010). In this study a new force balance model (Figure 1) is developed taking into account bed slope (α).

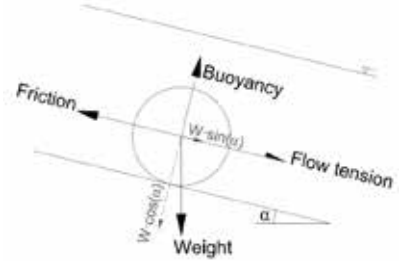

Figure 1: Conceptual balance model scheme

Furthermore, steep slope flows turn out to be highly turbulent; the variables of the flow suffer strong fluctuations. This generated turbulence has great implications; therefore the consideration of a constant dimensionless Shield coefficient might be no longer valid. Since the discovery of the so-called "Bursting events" by Kline (1967), an interest appeared in relating these coherent structures to the beginning of the movement. The concept is based on considering the pairs of instantaneous velocities (u', w'), longitudinal and vertical respectively. The latest findings have provided evidence that not only the magnitude of the turbulent forces acting on the grains is decisive, but also their duration of application Diplas et al., (2008).

3. Conceptual model

The conceptual model includes an energy scheme of the particles to evaluate the critical impulse (I_{cr}) necessary for their mobilization and the obtaining of the impulse signal exerted by the flow on the particles (I_i).As Fernandez (2019) defines, I_{cr} is the minimum impulse necessary to set the particle in motion, and is calculated from the new force balance. I_i is calculated considering the Reynolds shear stress (-ρu'w'), force per unit area, as responsible of sediment transport, it is possible to consider that whilst a bursting event remains inside a quadrant (pulse) the direction of the applied stress (τ_{xz}) is the same, this with the same sign (Fernández 2019).

Once I_{cr} and I_i have been obtained, they can be compared. An impulse rate (Imp.R) is defined as the probability that an impulse exceeds the critical value, thus each time that $I_i > I_{cr}$ is fulfilled, the particle (D_x) receives the necessary energy to be displaced, and therefore all D_x particles are mobilized, whereas if $I_i < I_{cr}$, they remain in its place.

4. Conclusions

A new conceptual model is developed in order to assess the threshold of motion in steep slope flows; it considers streamwise components of the forces applied in the particle and the concept of critical impulse, to consider the fluctuations of the Reynolds stress in the threshold of motion of the particles in steep slopes rivers.

Acknowledgments

This research is supported by FPI grant (FPI 2015) from Spanish Ministry of Science and Innovation (MCINN) and by Generalitat de Catalunya (FI-DGR 2015).

References

Cheng, N.-S. y Chiew, Y.-M., 1998. Pickup Probability for Sediment Entrainment. *Journal of Hydraulic Engineering*. Vol. 124, no. 2, p. 232-235.

Chiew, Y.-M. y Parker, G., 2010. Incipient sediment motion on non-horizontal slopes. *Journal of Hydraulic Research*. Vol. 32, no. 5, p. 649-660. ISSN 0022-1686. DOI 10.1080/00221689409498706.

Diplas, P. et al., 2008. The Role of Impulse on the Under Turbulent Flow Conditions. *Science*. Vol. 322, no. October, p. 717-720.

Fernández, C., 2019. *Experimental characterization of turbulence in steep rough streams*. Universitat Politècnica de Catalunya.

Grant, G.E., 1997. Critical Flow Constrains Flow Hydraulics in Mobile Bed Stream: A New Hypothesis. *Water Resources Research*. Vol. 33, no. 2, p. 349-358.

Kline, S.J. et al., 1967. The structure of turbulent boundary layers. *Journal of Fluid Mechanics*. Vol. 30, no. 04, p. 741-773. ISSN 0022-1120. DOI 10.1017/S0022112067001740.

Sediment Budget Uncertainty: Signal and Noise in the Sand Budget of a River with Episodic Supply and Transport

P.E. Grams[1], D. Buscombe[2], and D.J. Topping[1]

[1] U.S. Geological Survey, Southwest Biological Science Center, Grand Canyon Monitoring and Research Center, Flagstaff, Arizona, USA. pgrams@usgs.gov, dtopping@usgs.gov

[2] School of Earth and Sustainability, Northern Arizona University, Flagstaff, Arizona, USA. daniel.buscombe@nau.edu

1. Introduction

Sediment budgets, based on the laws of mass conservation, are essential tools in the analysis of geomorphic change and prediction of response to potential changes in streamflow sediment supply. Such changes may be caused by upstream water development, landscape change, or changes in climate.

Accurate sediment budgets are, however, difficult to construct because of issues associated with measurement error (Wheaton et al., 2010) and/or sampling design (Grams et al., 2019). These issues are particularly problematic when the signal of the sediment budget is small relative to the total flux of the river system.

We exploit temporally rich and spatially comprehensive measurements of sediment transport and morphological change to reveal the sampling effort that is required to estimate meaningful sediment budgets. We do this in the framework of a signal-to-noise ratio (SNR), wherein signal is the sediment budget and noise is the spatially or temporally propagated uncertainty. We provide examples from repeat measurements from over 140 km of the Colorado River in Grand Canyon collected spanning a period of six years.

2. Methods and Analyses

Flux-based sand budgets were computed from continuous measurements of stream flow and suspended-sediment concentration and grain size measured with acoustical instruments calibrated to conventional suspended-sediment samples. Morphological sand budgets were computed from repeat maps of river bathymetry and topography measured by multibeam and singlebeam sonar, and topographic surveys with total stations. We mapped approximately 70% of the active river channel within the study area, comprised of unvegetated sandbars, eddies, and channel segments. The remainder comprises areas of shallow, turbulent water in the channel and dense riparian vegetation, and rapids/riffles which are assumed to be stable.

The high temporal resolution flux data and the spatially extensive morphological measurements were downsampled to simulate "subsampling" noise that would arise by varying sample frequency and spatial extent. To evaluate the effect of sample frequency on the estimated flux-based sand budget, we resampled the 15-minute suspended-sand concentration record at a range of sample intervals, increasing from 15 minutes to more than 30 days, in 15-minute increments. The sand budget signal was taken to be the sand mass balance based on the original 15-minute record. Noise was computed as the difference in upper and lower envelope of the resampled sand mass balance per sample interval.

To evaluate how reductions in spatial coverage affects the morphologic sediment budget, we divided the maps of morphological change into 100-m long streamwise segments and subsampled the measured sand storage change from a random selection of those segments, incrementally increasing from one to all segments. The signal was computed from 1,000 iterations of the random subsample as the absolute value of the morphologic change, and the noise was the sum of unsigned morphologic changes in the segments not included in the subsample. The noise caused by measurement uncertainty was computed as the sum of uncertainty for each randomly selected subsample based on measurement method.

3. Conclusions

Uncertainty can severely limit the utility of computed sediment budgets. Uncertainty associated with measurement methods accumulates and, in the case of flux-based sediment budgets, often causes the budget to be indeterminate within a few years. In the case of morphological sediment budgets, measurement uncertainty accumulates spatially and may also overwhelm the signal. Uncertainty is also contributed by spatial and/or temporal sampling design. Analysis of signal-to-noise ratio of large datasets can be used to estimate the spatial and temporal sampling strategies necessary to compute meaningful sediment budgets, also accounting for measurement uncertainty. For the Colorado River in Grand Canyon, daily sampling of suspended-sand concentration is required to determine the sand budget with SNR $\geq$1, and sub-daily sampling is required to achieve SNR $\geq$2. We also show that repeat morphological measurements comprising at least 50% of a river segment are required to estimate the budget with SNR$\geq$1. Achievement of SNR$\geq$2 would require substantial reduction in measurement uncertainty and robust spatial sampling.

Acknowledgments

This work is funded by the Glen Canyon Dam Adaptive Management Program, administered by the U.S. Department of the Interior Bureau of Reclamation.

References

Grams, P. E., Buscombe, D., Topping, D. J., Kaplinski, M., & Hazel, Joseph E., J. (2019). How many measurements are required to construct an accurate sand budget in a large river? Insights from analyses of signal and noise. Earth Surface Processes and Landforms, 44. https://doi.org/10.1002/esp.4489

Wheaton, J. M., Brasington, J., Darby, S. E., & Sear, D. A. (2010). Accounting for uncertainty in DEMs from repeat topographic surveys: improved sediment budgets. Earth Surface Processes and Landforms, 35, 136–156. https://doi.org/10.1002/esp.1886

Modelling of fine sediment dynamics in an Alpine gravel-bed river reach: a reservoir flushing case in the Isère River, France

C. Bel[1], N. Claude[2], M. Jodeau[1,2], H. Haddad[2,3] and P. Tassi[1,2]

[1] Saint-Venant Hydraulics Laboratory (LHSV), ENPC, Cerema, EDF R&D, Chatou, France. coraline.bel@enpc.fr
[2] National Hydraulics and Environment Laboratory (LNHE), EDF R&D, Chatou, France.
[3] Institute for Geosciences and Environmental research (IGE), UGA, CNRS, IRD, INPG, Grenoble, France.

1. Context and objectives

Many mountain and piedmont regulated rivers present steady vegetated alternate bar systems responsible for the degradation of their ecological quality as well as the increase of flood risk because of channel obstruction. This mainly arises as a consequence of the anthropogenic modifications over the last two centuries (e.g. Serlet et al., 2018) which have impacted on both, the hydrologic regime and the sediment supply. During major floods, massive deposits of fine sediment occur on gravel bars, and favour the riparian vegetation growth and so the bar stabilization (Figure 1). In order to optimize river management strategies aiming at preventing bar colonization by plants, a better understanding of fine sediment dynamics (storage and re-suspension) on gravel bars during varying hydrologic events (natural flood and reservoir flushing) is necessary.

Figure 1: Fréterive gravel bar, Isère River. Fine sediment deposits, woody debris and vegetation development.

In 2018, a field campaign was performed during a reservoir flushing in the Isère River (France) in order to collect a comprehensive dataset which strongly benefits the calibration and validation procedure of hydro-morphodynamic model. The purpose of this investigation is to model the erosion, transport and deposition processes of fine sediment, at reach scale, during this flushing event.

2. Study site and field measurements

The Isère River is an Alpine regulated gravel-bed river located in South-Eastern France. Its flood regime is pluvio-nival and impacted by hydroelectric structures. The flow discharges for 2 and 10-year floods are 209 m^3/s and 345 m^3/s, respectively. The study reach is about 100-m wide between dikes, and extends over 3 km up to upstream of the Arc-Isère confluence. The bed slope is 0.0016 m/m. The D_{50} is approx. 24 mm, 180 µm, and 50 µm for coarse, non-cohesive (2-0.063 mm) and cohesive (<0.063 mm) sediments respectively. The average suspended sediment concentration (SSC) is less than 1 g/l but can reach up to about 10 g/l during major floods.

During the flushing event, time series of water discharges and SSC were recorded downstream the dam as well as point measurements of current velocities, settling velocities, grain size and bedload fluxes. In addition, pre- and post-event measurements were performed including aerial photography, topo-bathymetry, fine-sediment deposit characterisation, geomorphic observations and vegetation monitoring.

3. Numerical modelling

Flow and sediment transport simulations were computed using the open source TELEMAC-MASCARET suite of solvers (www.opentelemac.org) with the finite element method. Hydrodynamic is solved through the 2D depth-averaged shallow-water equations, with closure relationships for turbulence and roughness effects. Morphodynamic is accounted by solving both the sediment transport processes with semi-empirical relationships for sediment river capacity, and the bed evolution through the sediment mass balance equation (Villaret et al., 2013).

4. Conclusion and perspectives

The simulation of the 2018 reservoir flushing at the study reach was first performed to validate the hydro-morphodynamic model and its parameterization. The next stage consists in examining the effects of different environmental forcing (e.g. bed morphology, water and sediment supplies, macro-roughness elements) on the fine sediment dynamics. Finally, new scenarios of reservoir flushing will be tested, aiming at reducing the fine sediment deposit.

Acknowledgments

This investigation is supported by the ANR Dear project. Authors would like to thank colleagues from EDF-CIH for their technical contributions.

References

Serlet, A. J., Gurnell, A. M., Zolezzi, G., Wharton, G., Belleudy, P., and Jourdain, C. (2018). Biomorphodynamics of alternate bars in a channelized, regulated river: an integrated historical and modelling analysis. *EARTH SURF PROC LAND*, *43*(9), 1739–1756.

Villaret, C., Hervouet, J.-M., Kopmann, R., Merkel, U., and Davies, A. G. (2013). Morphodynamic modeling using the Telemac finite-element system. *COMPUT GEOSCI*, *53*, 105–113.

Sand settling through bedform-generated turbulence in rivers

B.T. Yuill[1] and Y. Wang[2]

[1] The Water Institute of the Gulf, New Orleans, U.S.A. byuill@thewaterinstute.org
[2] The Water Institute of the Gulf, Baton Rouge, U.S.A. ywang@thewaterinstute.org

1. Introduction

Fluvial bedforms generate a turbulent wake that may impact the settling rate of sediment particles suspended in the passing flow (Allen, 1965; Chang and Scotti, 2003). While the nature of this impact is not well understood, nor is it resolved in most models of river or bedform morphodynamics, it has been shown to influence the settling trajectories and the deposition patterns upon the proximal channel bed and therefore may play a role in river channel evolution. The objective of this study was to investigate how turbulence influences settling sand-sized sediment particles and assess how that influence may impact sediment deposition in a sand-bedded river channel.

2. Methods

We used one-dimensional (1D) and three-dimensional (3D) numerical modeling to quantify how turbulence modified the vertical velocity and settling rate of sand-sized particles. We employed a 1D model to investigate the impact of isotropic turbulence on particle settling and focused on quantifying the effect of non-linear drag on settling velocity. We employed a 3D model to investigate how realistic bedform-generated turbulence, which was simulated using detached-eddy simulation (DES) in OpenFOAM, impacted particle settling and deposition patterns. In the 3D modeling analysis, the model resolved the impact of a bedform that was based on a dredged borrow pit in a lower Mississippi River (USA) channel bar, which altered the flow field in a manner similar to a large natural dune. The 3D modeling scenarios varied bed morphology, inlet flow velocity, and the simulation of turbulent fluctuations in the flow field (i.e., turbulence was turned 'on' or 'off') to test the impact of a range of turbulence intensities on particle settling.

3. Results and Discussion

Our results from the 1D model show that isotropic turbulence, due to the non-linear drag effect, reduced sediment-particle settling velocity by up to 40 % for the range of turbulence intensities tested. However, (isotropic) turbulence intensities indicative of high Mississippi River discharges reduced settling velocities by less than 15 %, which was predicted to only have minor influence on sediment deposition patterns in a river channel (Fig. 1). In our 3D model, the bedform generated a turbulent wake that was predominately composed of eddies with significant anisotropic properties. Sediment particles entering the turbulent wake experienced mixing due to interaction with the eddies and became relatively diffuse throughout the flow column. Both bedform-generated turbulence and background turbulence contributed to the reduction of particle settling rates relative to the settling rates predicted in the absence of turbulence. The results of our 3D modeling predicted that the resolved turbulence reduced sediment deposition within the model domain by 21 % (17 % due to bedform-generated turbulence, 4 % due to background turbulence). Further, the 3D model predicted that turbulence reduced sediment deposition produced from the reduced flow velocities in the dredged borrow pit by nearly half. These results suggest that the turbulence created by the morphology of the dredged channel was a substantial control on the sedimentation occurring within it. Our results provide enhanced understanding between the interaction of suspended sediment and bedforms and how that interaction may influence the evolution of the downstream channel bed.

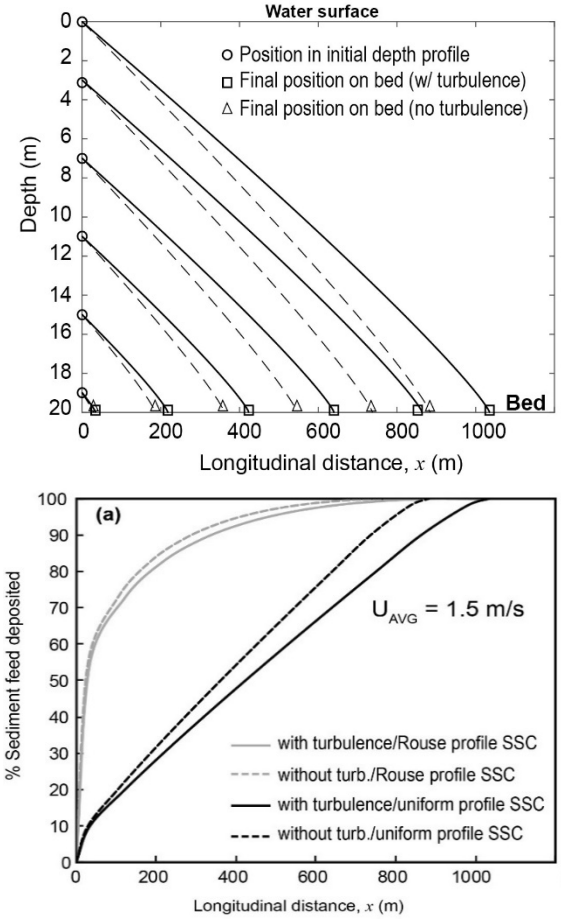

Figure 1: Predicted sediment (a) settling and (b) deposition with and without consideration of 1D isotropic turbulence. When anisotropic eddies were resolved using the 3D DES model, settling was further reduced.

References

Allen, J. R. L. (1965). Sedimentation to the Lee of Small Underwater Sand Waves: An Experimental Study. *The Journal of Geology*, 73(1), 95–116.

Chang, Y., & Scotti, A. (2003). Entrainment and suspension of sediments into a turbulent flow over ripples. *Journal of Turbulence*, 4. https://doi.org/10.1088/1468-5248/4/1/019.

Image-based fine sediment detection on gravel bars surface

L. Pénard[1], T. Drevet[1], T. Vergne[1], J. Deng[1] and B. Camenen[1]

[1] Irstea, UR RIVERLY, Lyon-Villeurbanne center, 5 rue de la Doua, CS 20244, F-69625 Villeurbanne Cedex, France
lionel.penard@irstea.fr

1. Introduction

Measurement of fine sediment stock within the river corridor is an essential step for sediment transport and river morphodynamics understanding. Fine sediments are indeed involved in several processes: bar stabilization through coarse matrix clogging and vegetation development, channel erosion and thus inundation risk increase... River managers need to reliably estimate the amount of fine sediments (clay, silt, sand). However, this requires tedious field work. Image-base method have been implemented to remotely make this estimation (Carbonneau et al., 2004; Camenen et al., 2013), but their application remains difficult and often site- and period-specific. This abstract presents a new method for determining fine sediment deposits on the gravel bar surface.

2. Data and preprocessing steps

Time-lapse cameras were installed on top banks, attached to tree trunks in order to observe temporal variation of surface characteristics of a gravel bar. A part of a gravel bar with fine sediment deposits lays within their field of view. The image ground resolution varies from 1 to a few centimeters, depending on the distance to the camera.
Preprocessing steps are carried out: (1) camera calibration (2) camera pose estimation, with Ground Reference Points (GRPs). The pose estimation has to be performed for each image since the trees appear to be slightly moving due to wind (3) orthorectification in the bar plane, to get equal ground pixels and display both image and segmentation results in QGIS. Figure 1 shows the resulting image.

3. Image processing methodology

The first step consists in removing the spatial low frequency part of the image to enhance the coarser parts of the bar. After converting the image in HSV color space, a fast Fourier transform is performed on the Value channel and a high pass filter is applied in the Fourier space. Back in the image space, a k-means clustering in 4 classes (3 for the sediment types, 1 for pixels outside the bar) is done along with a smoothing of region shapes.
Results are compared to a manually extracted ground truth map of the bar from the same image.

4. Results and conclusion

The obtained results (Figure 2) show very precise accordance with ground truth. More than 92% of fine sediments in the ground truth classification are correctly labelled as fine sediments by the presented method. Furthermore, it yields more natural segmented regions compared to square patches. This work will now be applied to get temporal evolution over more than 2 years of image acquisition, in order to understand the fine sediment dynamics during flood events. It is also planed to use UAVs imagery in order to extend the surveyed areas.

Acknowledgments

This work is supported by Agence de l'Eau Rhône Méditerranée Corse. The authors thank A. Buffet, L. Liger, D. Sigaud and F. Thollet for field work.

References

Camenen, B., Jodeau, M., and Jaballah, M. (2013). Estimate of fine sediment deposit dynamics over a gravel bar using photography analysis. *International Journal of Sediment Research*, 28(2):220–233.

Carbonneau, P., Lane, S., and Bergeron, N. (2004). Catchment-scale mapping of surface grain size in gravel bed rivers using airborne digital imagery. *Water Resources Research*, 40(7):W072021–W0720211.

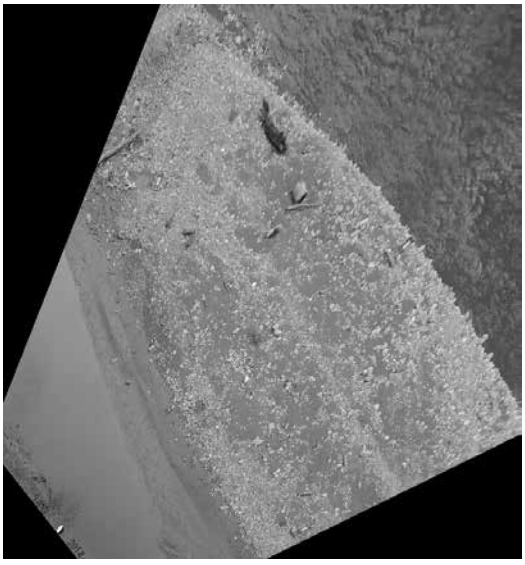

Figure 1. Orthorectified image

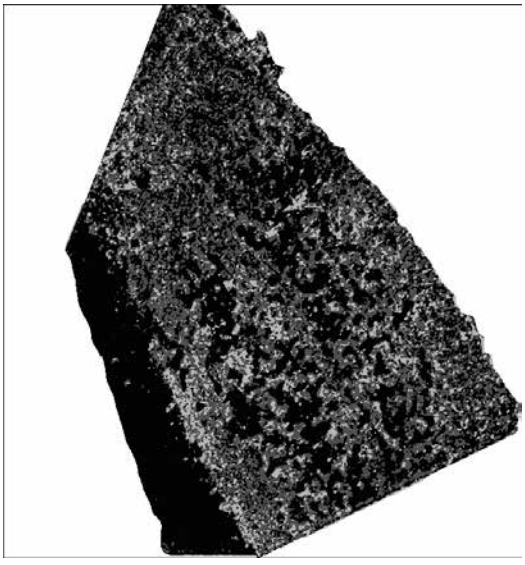

Figure 2. Sediment segmentation. Black: fine sed., dark grey: sed. mix, light grey: coarse sed., white: no sed.

Towards a channel morphology for optimal sediment transfer

C. Carbonari[1,2], A. Recking[2] and L. Solari[1]

[1] Dipartimento di Ingegneria Civile e Ambientale, Università degli studi di Firenze, Firenze, Italy.
costanza.carbonari@unifi.it luca.solari@unifi.it
[2] UR ETGR IRSTEA/Université Grenoble Alpes, Saint Martin d'Hères, France.
alain.recking@irstea.fr

1. Introduction

Gravel bed rivers are self-formed channels in coarse alluvial substrata; their dynamics results from the feedback between the flow and the morphology through sediment transport, which essentially occurs as bedload. Gravel bed rivers also present bed surface and subsurface sediment heterogeneity, these streams being typically characterized by poorly-sorted sediment grain size distributions and planimetric and vertical sorting patterns. In gravel bed rivers complex morphodynamic feedbacks have been identified between river morphologies and bedload transport (Francalanci et al., 2012; Recking et al., 2016), lateral confinement and river morphologies (Garcia Lugo et al., 2015), channel geometry and sediment sorting.
Through a physical modeling approach we investigated the effect of lateral confinement on gravel bed rivers morphology, sediment sorting dynamics, and bedload transport rates.

2. Material and Method

The experiments were conducted in a 6-m-long flume with a maximum width of 0.5 m. The slope of the flume was fixed at a value of 3.18%. The flume bed consisted of a layer of the bimodal sediment mixture used for the inlet solid discharge (coarse fraction (d_{50}= 1.8 mm) and fine fraction (d_{50}= 0.7 mm) 60% and 40% of the mixture, respectively). We performed constant feeding rate conditions both for water and solid discharge (Q = 0.55 l/s e Q_s = 8 g/s). We performed three long runs differing from one another in respect of the lateral constraint: the 1st, 2nd, and 3rd run had a width value of 0.5 m, 0.25 m, and 0.12 m, respectively. In run 1 and in run 2 the flow was low constrained: the channel could wander in the large alluvial bed, actually reproducing a self-formed channel; whereas in run 3 the flow was confined. For the whole duration of each run, we monitored the granulometric composition of the bed surface, the average bed slope, the outlet solid discharge, and the active channel width. Hydraulic measurements such as the flow depth and the flow velocity were performed as well.

3. Discussion of results

The observations from each individual run provided information concerning active channel and planform variations, both in the planimetric and altimetric directions, together with planimetric and vertical sorting; and a specific issue of run 3 alone was the occurrence of bedload sheets whose monitoring confirmed the observations by Recking et al. (2009).
All the configurations showed large fluctuations of the parameters characterising the bed system in terms of bed sediment composition, slope, active channel width, and sediment transport rate. The analysis of such parameters allowed for defining feedbacks among morphological variables.
Vertical sorting occurred only in the narrow-flume experiment, whereas in all the tests planimetric sorting took place, but in different ways depending on the flow confinement: in the narrow-flume experiment the planimetric sorting was only longitudinal and characterized by longer spatial scales with respect to low confined configurations. The comparison of the three runs revealed different mechanisms of bed storage and release of sediments: indeed the channel bed, and the planform in those cases where the channel wandered in the mobile layer of sediments, stocked and released sediments with different mechanisms, intensities, and characteristic periods. Moreover the sediment storage and release process was related to the variability of the bedload transport rate (in terms of amplitude and frequency of the fluctuations around the mean value). Precisely we identified the channel configurations with a relevant sediment storage and release coupled with an highly varying downstream sediment transfer; on the other hand, when the sediment storage and release was less important, the downstream sediment transfer was more constant. We extrapolated this argument to typical morphologies of gravel bed rivers towards a channel morphology for optimal sediment transfer.

4. Conclusions

In the context of gravel bed rivers' physical modeling, we carried out a set of flume experiments reproducing flows over a bimodal sediment mixture and considering three different flow confinements. The three different lateral confined flow configurations presented a different degree of bed complexity as well as differences in bedload transport rate fluctuations associated to different magnitude and mechanisms of bed storage and release of sediments.

References

Francalanci, S., Solari, L., Toffolon, M., and Parker, G. (2012). Do alternate bars affect sediment transport and flow resistance in gravel-bed rivers? *Earth Surface Processes and Landforms*, 37(8):866–875.

Garcia Lugo, G. A., Bertoldi, W., Henshaw, A. J., and Gurnell, A. M. (2015). The effect of lateral confinement on gravel bed river morphology. *Water Resources Research*, 51(9):7145–7158.

Recking, A., Frey, P., Paquier, A., and Belleudy, P. (2009). An experimental investigation of mechanisms involved in bed load sheet production and migration. *Journal of Geophysical Research*.

Recking, A., Piton, G., Vazquez-Tarrio, D., and Parker, G. (2016). Quantifying the morphological print of bedload transport. *Earth Surface Processes and Landforms*, 41(6):809–822.

Development of an ANN-based tool for sediment management at run-of-river reservoirs

M. Reisenbüchler[1], M.D. Bui[2] and P. Rutschmann[3]

[1] Technical University of Munich, Munich, Germany. markus.reisenbuechler@tum.de
[2] Technical University of Munich, Munich, Germany. bui@tum.de
[3] Technical University of Munich, Munich, Germany. peter.rutschmann@tum.de

1. Introduction

Reservoirs are needed for many fundamental tasks like agriculture, drinking water supply, flood protection, and energy production. For each of the listed demands, sustainable management of the reservoir is of great importance in designing the storage volume of water. However, sedimentation threatens this storage volume worldwide (Schleiss et al., 2016). In addition, a reduced retention volume due to sedimentation might also increase the danger potential of floods (Reisenbüchler et al., 2019).
Numerical models are widely accepted for designing new reservoirs and dams or to develop management strategies at existing dams to counteract sedimentation (Annandale et al., 2016). Such models can accurately represent reality and give reliable predictions. However, accurate and complex (e.g. two- or three-dimensional) models require great computational efforts. Furthermore, achieving an optimal design or evaluating different management strategies requires multiple long-term simulations for different scenarios. In that case, simplified 1D models were still applied. To provide an alternative, our work presents the application of a data-driven method for predicting bed level change along a river section including a hydropower plant.

2. Objective

The study's objective is to develop a data-driven, Artificial-Neural-Network (ANN) to predict future riverbed level changes only based on the available and measurable inputs. This approach can greatly reduce computational cost compared to conventional numerical models, without losing accuracy. Furthermore, the designed network can be considered as an easy-to-use-tool for stakeholders, unlike numerical models.

3. Methodology

This task can be classified as a time series prediction problem, where the future state of a system depends on its previous state and specified input. The training and testing data for the network are obtained from conventional numerical simulations for different flushing operations, see Figure 1. By selecting different, heterogeneous flushing schemes for training, ANN capable of predicting other untrained flushing schemes and the resulting riverbed.
While training the network, a so-called series-parallel or open loop architecture is selected, where the network states are adjusted in a way that the network outputs match the given data, see Figure 2 on the left. Here the external input u(t) contains information regarding the defined flow including the water depth and discharge. The additional input y(t) and output y(t+1) are the riverbed elevation. For further predictions, the best performing network architecture is applied and transferred to a so called

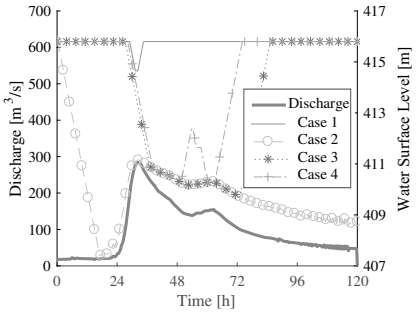

Figure 1. Four tested different flushing schemes during a flood wave.

parallel, or closed loop configuration, on the right side of Figure 2, where the network uses the predicted output y(t+1) as input for the next iteration.

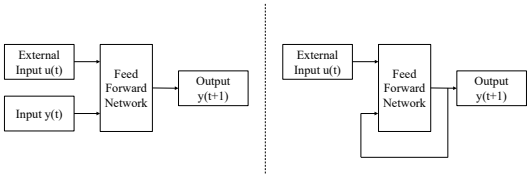

Figure 2. Training in open loop (left) and prediction in closed loop (right) architecture.

4. Conclusions

The proposed ANN-based tool is be a promising alternative to conventional methods for sediment managements at rivers. The advantages of this approach are that it performs with the accuracy of a state-of-the-art 2D hydromorphological model and has low computational requirements, as well as being able to work on standard computers.

References

Annandale, G. W., Morris, G. L., and Karki, P. (2016). *Extending the life of reservoirs : sustainable sediment management for dams and run-of-river hydropower*. Washington, D.C. : World Bank Group.

Reisenbüchler, M., Bui, M. D., Skublics, D., and Rutschmann, P. (2019). An integrative model improves predictive accuracy on floods: Hydromorphological analysis of a flood event in the saalach river. *Science of the Total Environment*, VSI:Effects global change floods.

Schleiss, A. J., Franca, M. J., Juez, C., and De Cesare, G. (2016). Reservoir sedimentation. *Journal of Hydraulic Research*, 54(6):595–614.

Effects of Adjusting Check Dam on Sediment Transport in the Landao Creek, Taiwan

Yu-Fang Chiu[1], Cheng-Wei Kuo[2] and Su-Chin Chen[3*]
[1]Department of Soil and Water Conservation, National Chung Hsing University, Taichung, Taiwan, tracyshet@gmail.com
[2]Sinotech Engineering Consultant, Taipei, Taiwan, cwkuo7215@gmail.com
[3*]Department of Soil and Water Conservation, National Chung Hsing University, Taichung, Taiwan,
Corresponding author: scchen1431@gmail.com

1. Introduction

Many check dams were built in the past to deal with the vast amounts of sediment. However, these check dams become threats to the long-term ecology and sediment transport continuity with the passage of time and reduction in sediment yield. The unchangeable check dam structure cannot easily cope with rapidly changing sediment transport, therefore, the effective adjustment of check dams is currently an important issue in Taiwan. This study integrated historical aerial images and topographic surveys by UAV were used to analyze the variation of sediment yield and channel bed elevation in the Landao Creek.

2. Study area

Landao Creek is a strongly erosion river. The length between the comb dam and the confluence of Landao Creek and Beigang River is about 700 m, average 10m wide channel, and the average slope of the channel bed is about 10°.

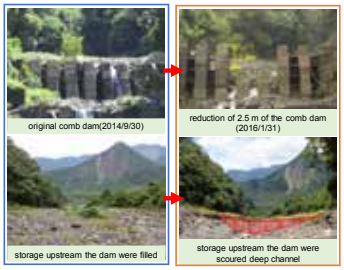

Typhoon Mindulle in 2004 and Typhoon Morakot in 2009 caused debris flow over the dam. The sediment supply from the upstream collapse has gradually decreased with time, decreasing the sediment transport to the downstream. In order to consider the balance of sediment transport along the river, the flume experiment and numerical simulation were conducted to choose the best case to execute in the field. The central two pillars were lowered down by 2.5m in 2015 for the balance of sediment transport.

3. Research method and analysis result

Using UAV aerial imagery with Agisoft PhotoScan to create an orthophoto and digital surface model (DSM). Through monitoring riverbed topography before and after the dam adjustment, observing the elevation of the riverbed and the variation of erosion and deposition.

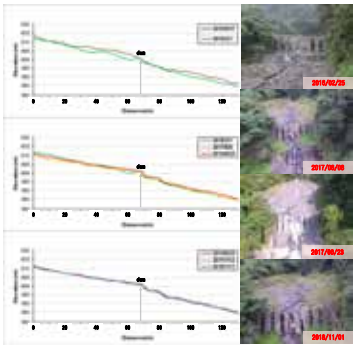

Longitudinal profile of the comb dam at upstream of Landao Creek

In 2010, the longitudinal profile showed significant sedimentation volume behind the comb dam. To increase storage upstream the dam, the central two pillars were lowered down by 2.5m in December 2015. The sediment deposited upstream of the dam moved to downstream obviously, and the elevation difference reached 3m in 2017, then heavy rain resulted in the sediment deposited upstream scour 1~2m in June.

In 2010, there was a narrow channel (<5 m) at the center. Due to the reduction of 2.5 m of the comb dam, the center developed a 10 m wide channel in 2016. Sediment transport was reworked after dam adjustment. In 2017 the main channel expanded to 15 m, and rainfall events gradually eroded the riverbed. The adjusted comb dam has gradually restored the natural sediment transport balance in the Landao River.

historical aerial imagery of Landao Creek

Historical satellite images were used to estimate changes in the area of the landslide area upstream. The landslide area was a sporadic distribution in only 5.5 ha in 2001. In 2005, several small landslide sites have combined into a big area about 9 ha, induced by the typhoon Mindulle in 2004. The total landslide area reached its peak in 2007 (13.8 ha). In 2014, it was reduced to 7.8 ha , that seem to have entered a period of decline.

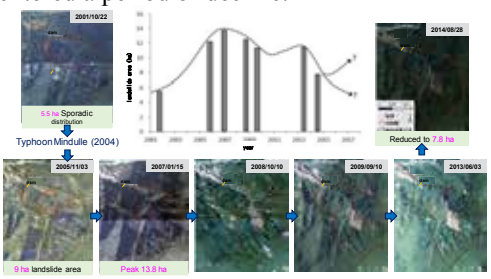

Historical satellite images of the landslide area upstream

4. Conclusions

Based on the debris flow scale and feature, the permeability of dams should be changed accordingly to promote sediment balance along rivers, and then to increase the ecological continuity of streams. During the period of low sediment yield, the beams of check dam can be adjusted to promote sediment transport downstream. The experimental adjustment of the dam has successfully proved the possibility of adjusting the check dam with the variation of sediment transport. However, the more positive thought is how to design a check dam that can be adjusted according to the variation of transported sediment before building the dam.

References

Chen, S.C. (2017) *Development and application of technology for adjustable check dams*, Soil and Water Conservation Bureau, Taiwan. (in Chinese))

Chen, S.C., An, S.P., and Kokuryo, H., Lin, Y.H.(2016). "Modular Check Dam Management in a High-Sediment-Disaster Torrent." *Journal of Chinese Soil and Water Conservation*, 47 (3), 111-121.

Static equilibrium state of riverbed with extremely wide range of sediment grain sizes

Y. Hiramatsu[1] and M. Sekine[2]

[1] Waseda Research Institute for Science and Engineering, Tokyo, Japan.
[2] Department of Civil and Environmental Engineering, Waseda University, Tokyo, Japan. sekine@waseda.jp

1. Introduction

We have conducted experimental investigation on sediment transport occurring on riverbed with extremely wide range of sediment grain sizes. Such riverbed can be seen in river reach just downstream of a dam. Riverbed materials are generally divided into three grain sizes groups of sediment; large particles that cannot move at all, medium particles that can move as bedload, and small particles that can move as suspended load. We have called these groups L-, and M- and S-particles respectively, and carried out fundamental experiments in which each group is represented by only one particle size. Based on the experimental results, a riverbed of actual river has a continuous grain size distribution, so the experiment was conducted under the condition that M-particle group consists of various grain sizes.

It is important to consider hiding effect of L-particles in understanding such sediment transport phenomena. When M-S particles are transported, an exposure degree of L-particles increases. As a result, the shear force acting on M-S particle becomes smaller. With reference to the research of Ashida and Fujita (1986), we proposed an equation for evaluating this hiding effect. In this paper, we summarize the results of the static equilibrium state when sand or gravels are not supplied from upstream.

2. Experimental Materials

Experimental materials are as follows. Alumina balls with a grain size of 50 mm (specific weight is 3.98) are used for L-particles. Glass beads with a sediment diameter of 1 to 5 mm whose specific weight is 2.5 are used for M-particles, and silica sand having a diameter of 0.21 mm and a specific weight is 2.65 for S-particles. The dimensionless critical tractive force (critical Shields number) of M-particles is τ^*_{MC} = 0.050, 0.050, 0.047, 0.042, 0.066 in descending order of the sediment grain sizes, and the settling velocity of S-particles is w_{oS} = 0.025 (m/s).

3. Characteristic of riverbed with extremely wide range of sediment grain sizes

3.1 Hiding effect of cobbles

The hiding effect given by L-particles is expressed by the following equation by focusing on the static equilibrium state of riverbed which composed of two grain sizes groups; L-M and L-S bed.

$$\Delta_i / D_L = \alpha \times (H_i^{-2} - 1)^{0.5} \quad (1)$$

where Δ_i is the vertical distance from the top of L-particles to the center of M- or S-particles exposed on riverbed surface, and the hiding coefficient H_i is defined as the ratio of the friction velocity acting on M- or S-particles u^*_i to the average value u^* acting on the entire bed surface. Also, a proportional constant α is 0.3.

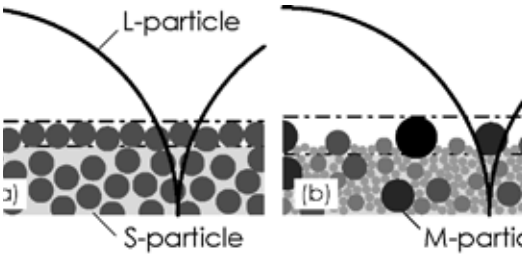

Figure 1: Schematic diagram of riverbed structure from side (bedload gravel group consists of (a) only 3mm and (b) 1-5 mm particles).

3.2 Vertical structure of riverbed

Furthermore, we briefly explain the vertical structure of L-M-S bed. Firstly, when M-particle group consists of one grain size, it was found that a layer composed of M-particles (M-particle layer) only was formed on the surface of riverbed as shown in Figure 1 (a). The quadrants in this figure represent L-particles, the circles correspond to M-particles, and the light grey portion are S-particles and the void space. Based on this, when conducting another experiment set in the case where M-particle group consists of various grain sizes, M-particle layer similarly appeared. In addition, when we see the bottom elevation of M-particle group with different particle sizes, it was found that vertical sorting as roughly equal level occurred as shown in Figure 1 (b).

4. Conclusions

We conducted fundamental experiments focusing on sediment transport phenomena in riverbed which contains cobbles that cannot move by water flow. As a result, we proposed an equation that shows the hiding effect of cobbles. Examination of the vertical structure of riverbed revealed that the bottom elevation of the particle is uniform when the sediment which can move as bedload has various sizes.

Acknowledgments

We would like to thank K. Hongo, Y. Nakagawa, Y. Kadoi, and N. Kenmotsu for conducting the experiments.

References

Ashida, K. and Fujita, M. (1986). Mechanism of particle suspension in an open channel. *Proceedings of JSCE*, 375(II-6), 79–88. (In Japanese.)

Peter R.Wilcock and Stephen T. Kenworthy (2002). A two-fraction model for the transport of sand/gravel mixtures. *Water Resour. Res.*, Vol.38, No.10, 1194.

Sekine, M. and Hiramatsu, Y. (2017). Gravel Sorting and Variation of Riverbeds Containing Gravel, Sand, Silt and Clay, *Gravel-Bed Rivers: Processes and Disasters*, pages 591-608, John Wiley & Sons, Ltd, 2017.

Experimental Study of Abrasion on Mixed Alluvial-Bedrock in Annular Flume.

M.R. Andriamboavonjy [1], A. C. Lima [2] and N. Izumi [3]

[1] Graduate School of Engineering, Hokkaido University, Sapporo, Japan.
andrymamyrija2@eis.hokudai.ac.jp
[2] Faculty of Engineering, Hokkaido University, Sapporo, Japan.
adriano@eng.hokudai.ac.jp
[3] Faculty of Engineering, Hokkaido University, Sapporo, Japan.
nizumi@eng.hokudai.ac.jp

1. Introduction

The Riverbed is commonly subjected to erosional mechanisms. One of the most important of them is abrasion by bed load (Sklar et al., 2004).

Analytical and experimental studies have already been undertaken related to abrasion by bed load, mostly on straight channel. Recently, studies have also been conducted in curved channel using annular flume. In annular flume, under equilibrium state of flow, the sediment forms transverse slope along the inner wall because of the secondary flow (Ikeda S., 1974). Instability leads gradually to regular deposition patterns of the sediment (Engelund F., 1975), and erosion mainly occurs in moderately covered bed portions (Taguchi et al., 2017). The bed near the outer bank is on the other hand exposed; erosion by abrasion occurs there as well, but has likely received few attention. even if curved channel constitutes most part of river course and even if abrasion on exposed bed also contributes to the bed erosion.

In this study, we focused on abrasions on the exposed bed along the outer bank in curved channel, here studied in annular flume.

2. Methodology

The actual study is composed of two main steps. First, experiment run, and then photogrammetry analysis.

The experiment was carried out using annular acrylic flume with rectangular cross-section. The experiment's run is similar to the one described in Engelund's paper (1975), the flume settings are alike as in Taguchi's work (2018) but with bedrock made of gypsum. The flume characteristics is as following: average radius - 45cm, width - 10cm, maximum depth - 18cm. The rotation of the top lid, also made of annular acrylic plate, on the water surface permitted to generate the flow within the flume. And the experiment settings are: bed thickness - 6cm, sand grain - 2.5kg - 2.62g/cm3, ø0.515mm, water depth - 5cm, and top lid rotation velocity - 40rpm.

The photogrammetry was mainly used for data processing: imaging the bed surface, images reconstruction using photo-coordinate system, vectorization and photo interpretation, and data analysis.

3. Preliminary results

Apart from the main bed incision around the boundary between covered and exposed bedrock, described in Taguchi's work (2017), erosion by abrasion on the exposed bed is observed (figure 1).

The present result is obtained after 48 hours of experiment run. The photo-interpretation permitted to highlight two forms abrasions on the exposed bed: smooth elongated and thin linear abrasions.

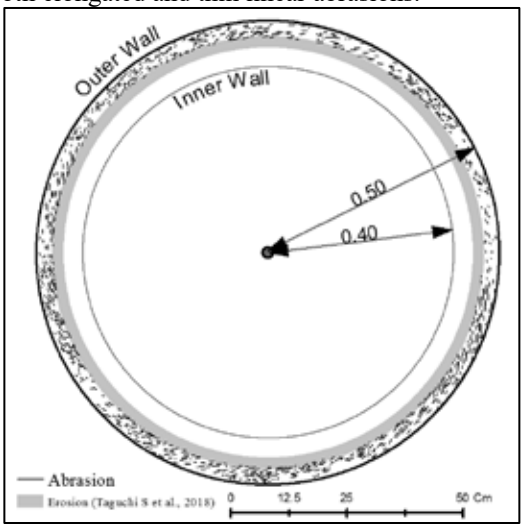

Figure 1: Abrasions on the exposed bed, near the outer wall.

3. Conclusions

Two forms of abrasions on the exposed bed are observed:

- Smooth elongated abrasions resulted from fluid flow and bed interaction
- Thin linear abrasions resulted from bed, sand grains, and fluid flow interaction

Both are directed toward the inner bank. In addition, the second type of abrasions increases from the outer to the inner bank, geometrical characteristics.

References

Ikeda, S. (1974). On secondary flow and dynamic equilibrium of transverse bed profile in alluvial curved open channle. *Proc. of JSCE*, No.229, Sept 1974 (in Japanese).

Engelund, F., (1975). Instability of flow in a curved alluvial channel. *Journal of Fluid Mechanics* 72, 145-160.

Sklar, L. S., & Dietrich, W. E. (2004). A mechanistic model for river incision into bedrock by saltating bed load. *Water Resources Research*, 40(6).

Taguchi, S., Ozawa, H., Lima, A.C. and Izumi, N. (2017). Experimental study of bedrock degradation in annular flume flow. In Lanzoni, Redolfi and Zolezzi, editors, *River, Coastal and Estuarine Morphodynamics: RCEM 2017 - Back to Italy*, page 63, Trento- Pandova.

Morphological effects of groundwater table variation on Bolivian meandering rivers

K.R. Arnez Ferrel[1], J.M. Nelson[2], Y. Shimizu[1] and T. Kyuka[1]
[1] Graduate School of Engineering, Hokkaido University, Sapporo, Japan. rubikraf@gmail.com
[2] U.S. Geological Survey, Golden, Colorado, USA. jmn@usgs.gov

1. Introduction

Wide seasonal water level fluctuations in rivers affect hydrologic, ecological and morphological processes (Alsdorf et al. 2000). One example of the importance of changes in riverine water-surface elevation is the role they play in bank erosion and associated channel migration. There are many observations that suggest that variations in groundwater elevation due to seasonal or flood-related stage changes produce seepage and pore pressure anomalies that can enhance or directly cause bank failures. The objective of this study is to develop a numerical model that considers groundwater table variations and to test and validate the modeling approach using data from a field survey.

2. Methodology

In this study, we present field observations on Bolivian rivers that are tributaries to the Amazon River. The study site is located in the city of Puerto Villarroel in the Department of Cochabamba, Bolivia. These rivers are characterized by very sinuous meandering shapes and active, rapid channel migration. The Ichilo and Sajta Rivers are considered in the work here.

2.1 Field Survey

Using Landsat Imagery from 1985 to 2016 from Google Earth Engine, we observed the meander migration rates of different rivers and decided to visit these two Bolivian rivers, which meet in a confluence near the city of Puerto Villarroel, as shown in Figure 1. River morphology of the reaches was mapped using images acquired by an unmanned aerial vehicle (UAV). The data was acquired during one-day field campaign during the rainy season on February, 2019. The data obtained from the UAV was processed and Digital Elevation Models (DEMs) and orthomosaics were created. Typical active river meander morphology such as river cut-off development and abandoned patterns of river channels were evaluated using the orthomosaics and the DEMs. Erodibility of the banks was measured using the pocket erodometer following the procedure described in (Bernhardt and Leclair 2012).

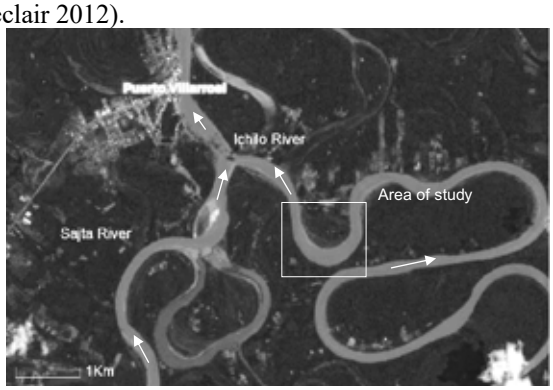

Figure 1: Location of the area of study Source: Modified Copernicus Sentinel data (2019)/Sentinel hub

In addition, one cross-section of velocity distribution and depths were measured using an Acoustic Doppler Current Profiler (ADCP) by the Laboratory of Hydraulics of the University Mayor of San Simon (LHUMSS). The intent of this initial data collection was to provide an assessment for a second, more intensive field campaign to be performed in May 2019.

2.2 Numerical model

The main focus of the model discussed here is to include the water table variation in the banks within an existing model for flow, sediment transport, and bed evolution in rivers (Nays2dh, Asahi et al. 2013). In our approach, the groundwater table is considered in terms of the continuity equation and Darcy's law. We use both 2-d and 3-d formulations to explore the importance of three-dimensional effects, such as the convergence of ground-water flow lines near concave banks. Using the time-varying flow and water-surface elevation field from the Nays2dh model, the groundwater model along with assumed diffusivity allows computation of the groundwater recharge as well as the effect of enhanced pore pressure on the river banks during falling discharges (and water levels). The importance of this effect is strongly dependent on location within a channel bend and the rapidity of discharge decrease relative to the bank permeability. For banks with very low permeability, the effect is negligible. Similarly, for banks with very high permeability (meaning ground water can "follow" the riverine stage changes), the effect is small. However, for an intermediate range of permeability and for reasonable stage changes, the effect can produce failure where a simple failure-plane type force balance would otherwise indicate stability. We compute the failure plane using the limit equilibrium method calculating the lowest safety factor. This analysis shows the potential importance of the groundwater pore pressure and also indicates the spatial extent of the greatest effect, which is in good agreement with observations of bank failure.

3. Conclusions and future work

For certain conditions, the water table variation can have an important effect on meandering migration rates. Our current efforts are directed at using the coupled groundwater/surface water model to reproduce long term meander migration including this effect.

Acknowledgments

We would like to thank to the Japanese government for the MEXT grant and the Nitobe School Advanced Program for funding. Also we would like to thank the Servicio Departamental de Cuencas-Cochabamba (SDC) in Bolivia, and LHUMSS for their cooperation during the field survey.

References

Alsdorf, Douglas E et al. 2000. "Interferometric Radar Measurements of Water Level Changes on the Amazon Flood Plain." *Nature* 404: 174. https://doi.org/10.1038/35004560.

Bernhardt, M, and M Leclair. 2012. "The Pocket Erodometer Test : Development and Preliminary Results." *Geol Testing J.l* 35(2): 342–52.

Asahi, K., Y. Shimizu, J. Nelson, and G. Parker (2013), Numerical simulation of river meandering with selfevolving banks, J. Geophys. Res. Earth Surf., 118, 2208–2229, doi:10.1002/jgrf.20150.

Multi-model comparison in long-term drainage evolution: introducing terrainbento 1.0

Katherine R. Barnhart[1,2], Rachel C. Glade[2,3], Charles M. Shobe[1,2], and Gregory E. Tucker[1,2]

[1] Cooperative Institute for Research in Environmental Sciences, University of Colorado at Boulder, Boulder, CO, USA.
katherine.barnhart@coloorado.edu
[2] Department of Geological Sciences, University of Colorado at Boulder, Boulder, CO, USA
[3] Institute for Arctic and Alpine Research, University of Colorado at Boulder, Boulder, CO, USA

Models of landscape evolution provide insight into the geomorphic history of specific field areas, create testable predictions of landform development, demonstrate the consequences of current geomorphic process theory, and spark imagination through hypothetical scenarios. While the last 4 decades have brought the proliferation of many alternative formulations for the redistribution of mass by Earth surface processes, relatively few studies have systematically compared and tested these alternative equations.

We present a new Python package, terrainbento 1.0, that enables multimodel comparison, sensitivity analysis, and calibration of Earth surface process models (Barnhart et al., 2018). Terrainbento provides a set of 28 model programs that implement alternative transport laws related to four process elements: hillslope processes, surface-water hydrology, erosion by flowing water, and material properties. The 28 model programs are a systematic subset of the 2048 possible numerical models associated with 11 binary choices. Each binary choice is related to one of these four elements—for example, the use of linear or nonlinear hillslope diffusion. Terrainbento is an extensible framework: base classes that treat the elements common to all numerical models (such as input/output and boundary conditions) make it possible to create a new numerical model without reinventing these common methods. For example, Figure 1 shows how alternative boundary conditions influence simulation results.

Terrainbento is built on top of the Landlab framework such that new Landlab components directly support the creation of new terrainbento model programs. Terrainbento is fully documented, has 100% unit test coverage including numerical comparison with analytical solutions for process models, and continuous integration testing (Barnhart et al., 2019b). We support future users and developers with introductory Jupyter notebooks and a template for creating new terrainbento model programs (Barnhart et al., 2019a).

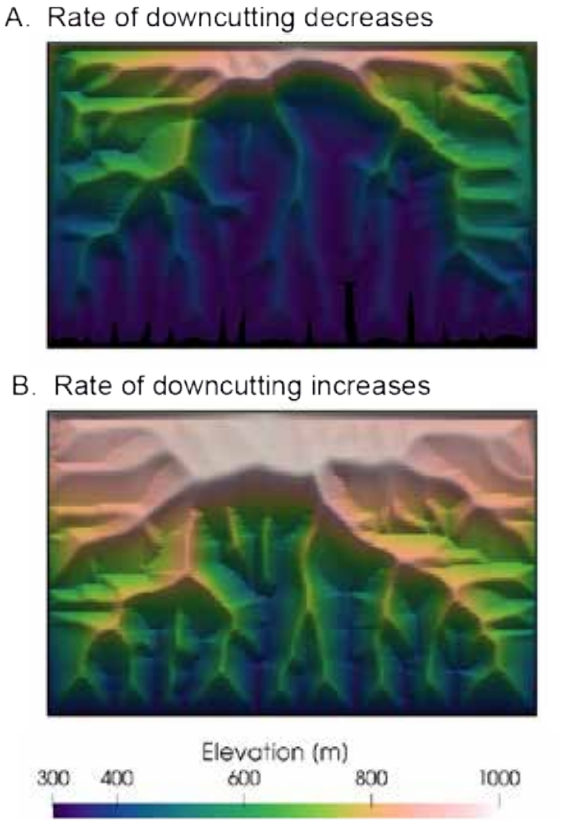

Figure 1. Example model output from terrainbento 1.0. Model domain is 1×1.6 km and uses 10 m grid spacing. Each panel represents topography at the end of a 200,000 year simulation run with the terrainbento model `Basic` (dt=500 years). Models were initialized with topography of 1000 m and open flux boundary conditions only to the south. The west, south, and east boundary elevations were progressively dropped during the simulation. In the upper panel (A), the boundaries drop more rapidly at the beginning of the simulation than at the end. In the lower panel (B), the reverse is true such that the boundaries drop more rapidly at the end of the simulation.

References

Barnhart, K., Shobe, C., Glade, R., and Tucker, G. (2019a). Terrainbento/examples_tests_and_tutorials: v1.0 soba.

Barnhart, K., Shobe, C., Glade, R., Tucker, G., and Hutton, E. (2019b). Terrainbento/terrainbento: v1.0 soba.

Barnhart, K. R., Glade, R. C., Shobe, C. M., and Tucker, G. E. (2018). terrainbento 1.0: a python package for multi-model analysis in long-term drainage basin evolution. *Geoscientific Model Development Discussions*, 2018:1–57.

Role of hydraulic-geomorphic interactions in controlling river morphodynamics following sudden sediment input

E.R.C. Baynes[1] and H. Friedrich[1]

[1] Department of Civil and Environmental Engineering, University of Auckland, Auckland, New Zealand.
edwin.baynes@auckland.ac.nz, h.friedrich@auckland.ac.nz

1. Background

The presence of thresholds and non-linear processes between sediment transport regimes have the potential to lead to catastrophic change in the river morphology (Baynes et al., 2018). Recent analogue model experiments identified that the morphodynamic response of an alluvial river to a change in the balance of the input sediment supply and river sediment transport capacity was generated by above threshold supercritical flow (Froude number > 1) (Baynes et al., 2018). The potential importance of interactions between flow hydraulics and erosion processes have also been inferred in bedrock canyon settings. Constrictions in the canyon morphology can generate vertically plunging flow fields that focus energy onto the canyon floor (Venditti et al., 2014; Hunt et al., 2018), potentially leading to a localised areas of erosion. However, the quantitative understanding of the generation, interactions and feedbacks between hydraulic and geomorphic processes is currently limited, especially during the response of a river system to a high magnitude event, such as a large flood or landslide (e.g., An et al., 2017). Here, we present a suite of physical modelling experiments that aim to identify and quantify the processes that drive the evolution of river morphodynamics in response to a sudden input of a large volume of sediment (e.g., a landslide) under a variety of hydraulic conditions. The study highlights the interactions between the flow hydraulics and the morphodynamics.

2. Physical modelling approach

Experiments were performed in a fixed width (450 mm; Fig. 1) flume in the Water Engineering Laboratory at the University of Auckland, set up to replicate conditions in a reach of a bedrock-constrained river channel (i.e., a canyon). Gravel was fixed to the flume floor to provide bed roughness, while the flume walls were clear plastic, simulating smooth bedrock canyon walls and allowing visualisation of the flow and sediment from the side.

Initially, a large volume of sediment relative to the water depth was placed in a single location in the flume to simulate a landslide deposit, and the subsequent pattern and rate of removal of the sediment from this pile was monitored using cameras and particle tracking software.

A variable valve at the upstream end of the flume allowed a range of different hydrograph scenarios to be tested, exploring the impact of variable flow regimes on the rate and pattern of sediment transport.

Dye was introduced to the water flow at the sediment pile to allow visualisation of the impact of the sediment pile and the sediment transport on the evolving flow dynamics. This evolution provides evidence for the co-evolution of flow hydraulics and geomorphic processes during the response of the system to the large sediment input, including the identification of vertically plunging flow around the initial sediment pile, and whether the different hydrograph regimes had a significant impact on the flow conditions. The characteristics of the initial sediment pile included a non-uniform grain size distribution, replicating the true nature of possible landslide deposits in a natural environment.

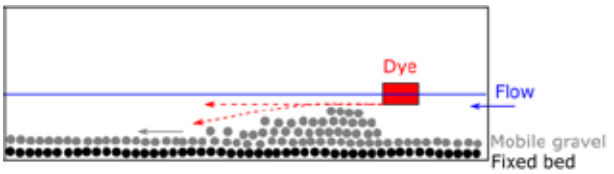

Figure 1: Schematic diagram of the experimental set up, with dye highlighting the flow hydraulics around the sediment pile.

3. Conclusions

The preliminary experiments presented here show the potential for physical modelling experiments for highlighting the role of hydraulic-geomorphic interactions in driving the potentially non-linear response of river morphodynamics to extreme perturbations (e.g., a landslide).

Acknowledgments

This research was funded by the George Mason Centre for the Natural Environment, University of Auckland.

References

An C., Cui, Y., Fu, X., Parker, G. (2017) Gravel-bed river evolution in earthquake-prone regions subject to cycled hydrographs and repeated sediment pulses. *Earth Surface Processes and Landforms* 42, 2426-2438.

Baynes, E.R.C., Lague, D., and Kermarrec, J-J. (2018) Supercritical terraces generated by hydraulic and geomorphic interactions. *Geology* 46 (6), 499-502

Hunt, B., Venditti, J.G., Kwoll, E. (2018) Experiments on the morphological controls of velocity inversions in bedrock canyons. *Earth Surface Processes and Landforms* 43, 653-668

Venditti, J.G., Rennie, C.D., Bomhof, J., Bradley, R.W., Little, M., Church, M. (2014) Flow in bedrock canyons. *Nature* 513, 534-537

Spatio-Temporal Drag Variations in a Mangrove Creek System

E.M. Horstman[1,2], K.R. Bryan[2,3] and J.C. Mullarney[2]

[1] Water Engineering & Management, University of Twente, Enschede, the Netherlands, e.m.horstman@utwente.nl
[2] Coastal Marine Group, University of Waikato, Hamilton, New Zealand, julia.mullarney@waikato.ac.nz
[3] Environmental Research Institute, University of Waikato, Hamilton, New Zealand, karin.bryan@waikato.ac.nz

1. Introduction

Above-ground root structures are ubiquitous in mangrove forests and provide substantial drag to currents and waves propagating through these systems. Creeks can improve the hydraulic conductivity of mangrove systems, providing low-resistance conduits for the tidal prism to propagate into and out of the intertidal area. Consequently, the presence of creeks in mangroves may reduce the total attenuating capacity of the system, while improving the transport of suspended and dissolved matter. In this work we address the effect of mangrove vegetation on the tidal hydrodynamics in an ephemeral creek catchment with no terrestrial fresh water input, located in the Whitianga estuary in New Zealand (Fig.1).

Figure 1: Low tide at the creek entering the study site.

2. Data collection

A series of acoustic instruments was deployed throughout the creek channel (800 m long) and within the mangrove forest, to monitor spatial changes in the velocity profiles over a 10-day period covering spring and neap tides. Co-located elevation, vegetation and sediment data were collected to provide insight into the drivers of the observed tidal dynamics.

3. Results

3.1 Tidal asymmetry

Tidal stage-velocity curves show that, during flood tide, peak (depth-averaged) velocities occur at increasing water levels for higher tides; whereas during ebb tides velocity maximums occur when water levels are just above bank-full stage regardless of the tidal amplitude (Fig.2a). These differences between tidal phases are caused by (i) decreasing impact of vegetation roughness for deeper inundations of the surrounding mangroves on flood tide and (ii) the impact of delayed drainage from the mangrove platform on ebb tide.

2.2 Drag coefficients

Examination of the forcing terms in the momentum equation shows that inertia is insignificant. The depth-averaged momentum balance in the along-creek direction is:

$$g\frac{d\eta}{dx} = -C_D u|u|/h \qquad (1)$$

where η is water surface elevation, x is along-creek distance, u is depth-averaged velocity, h is water depth and C_D is the bulk drag coefficient. Accordingly, C_D is computed by fitting linear trends to measurements of $gd\eta/dx$ and $u|u|/h$.

Obtained drag coefficients show significant variations with tidal stage (Fig.2b). During flood, C_D shows a slight decrease with water levels exceeding the bank level. When the tide reverses, the drag coefficient increases rapidly, reaching a maximum as the water level drops to the bank level. Observed C_D-values for overbank stages range between 0.01-0.05 during flood, but can reach ~0.15 during ebb. These drag coefficients agree with values approximated from collected vegetation densities on the creek banks (cf. Baptist et al., 2007) and reflect C_D values found in previous studies (Mullarney et al., 2017).

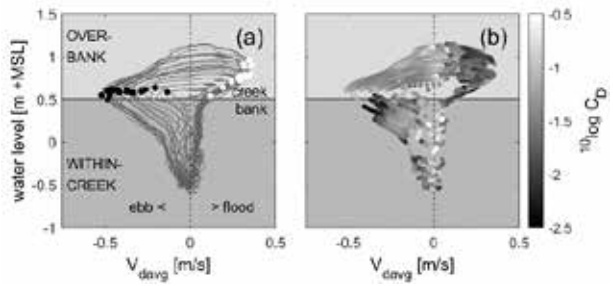

Figure 2: (a) Stage-velocity curves with maximum tidal flood and ebb velocities (white and black dots) and (b) drag coefficients, 300 m inland from the creek mouth.

3. Conclusion

We resolve temporal variations in the drag coefficients observed at 7 stations along the full length of the creek. Linking these spatio-temporal variations to both the geometry and vegetation of this mangrove creek system –parameters that can also be easily obtained/extracted for other mangrove creek systems– enhances our understanding of hydrodynamic feedbacks between intertidal mangrove forests and their creek systems.

Acknowledgments

We thank Dean Sandwell, Steve Henderson, Hieu Nguyen and John Montgomery for their contributions and for field assistance. This research is funded by the Royal Society of New Zealand's Marsden Fund (UOW1402).

References

Baptist, M.J., et al. (2007). On inducing equations for vegetation resistance. *Journal of Hydraulic Research*, 45(4):435-450.

Mullarney, J.C., Henderson, S.M., Reyns, J.A.H., Norris, B.K. and Bryan, K.R. (2017). Spatially varying drag within a wave-exposed mangrove forest and on the adjacent tidal flat. *Cont. Shelf Res.*, 147:102-113.

Continuous sand-transport estimation on the Colorado River

B. Camenen[1], G. Dramais[1,2], J. Le Coz[1] and D. J. Topping[2]

[1] Irstea, RiverLy Research Unit, 5 rue de la Doua, BP 32108 - 69616 Villeurbanne, France. benoit.camenen@irstea.fr
[2] U. S. Geological Survey 2255 N. Gemini Dr. Flagstaff, Arizona 86001, USA

1. Introduction

The estimation of sand transport in large rivers is a complex task since bedload or suspended load may prevail depending on hydrodynamic conditions and because sediment transport capacity may be affected by an insufficient sediment supply. A challenge is first to sample suspended load due to strong vertical and lateral gradients and such direct sampling, though necessary, has a prohibitive cost and cannot provide high frequency estimates. Topping and Wright (2016) developed a physically based method for high frequency measurement of suspended-sand concentration and grain size based on side-looking acoustic-Doppler profilers (HADCP) deployed at different sites on the Colorado River. We propose here to use a sediment rating curve to evaluate sand-transport capacity and validate its potential use for long-term sediment budget in comparison to field experiments and as a complement to the acoustical approach.

2. Material and methods

We study the U.S. Geological Survey gaging station of the Colorado River above Diamond Creek, AZ, USA, where side-looking acoustic-Doppler profilers were installed to estimate continuous sand fluxes and grain size characteristics (`https://www.gcmrc.gov/discharge_qw_sediment/station/GCDAMP/09404200`). Calibration and validation of the methodology is presented in Topping and Wright (2016). As a comparison, a simple sediment rating curve was set for the Diamond Creek station following Camenen et al. (2014). A stage-discharge relationship has been calibrated using a set of discharge measurements. All hydraulic parameters (such as bed shear stress) were deduced from this stage-discharge relationship using measured bathymetry, sand grain-size distribution, etc., with the only calibration parameter the bedform-related roughness length set here as $k_s = 0.1$ m. Using an average grain-size distribution (GSD), results are in reasonable agreement with sediment flux measurements (direct sampling) available at Diamond Creek though over- or underestimation occurs when GSD differs from that used in the calculations.

This sediment rating curve was applied to the main events observed during 2002-2016. Example results are presented in Fig. 1 where sand concentration based on the sediment rating curve is compared with the data obtained from acoustical measurements. Similar observations can be made from these results, i.e. an underestimation of the sand concentration by the model during the rising phase of the flood and overestimation during the rest of the flood. This confirms previous observations that grain size of suspended sediment is finer during the first phase of the flood (Topping et al., 2000), likely due to the remobilization of fine deposits accumulated during the low flow period and/or coming from upstream tributary floods. Based on acoustical measurements, one can observe a clear sensitivity of the measured sand flux to the grain size.

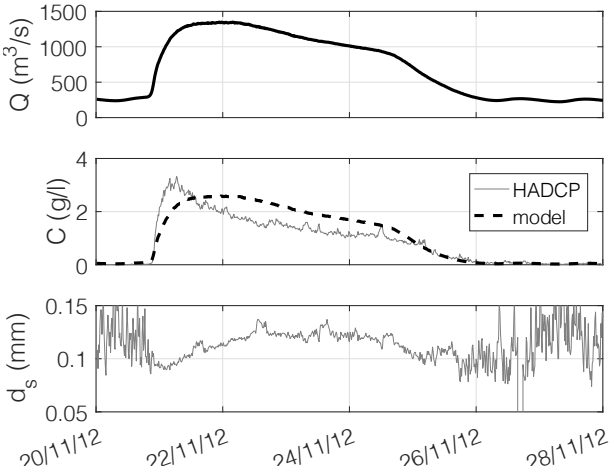

Figure 1. Discharge, sand concentration, and suspended-sand grain size measured and estimated during the November 2012 flood on the Colorado River above Diamond Creek.

3. Conclusions

The comparison of a sand-transport rating curve and direct measurements using HADCP confirmed a clear fining of the grain size in most initial parts of flood events arising from enriched supplies of finer sand. Physically based sediment rating curves, though difficult to apply in reaches subjected to sediment-supply limitation, can provide some interesting results for understanding the sediment dynamics. We would like to apply this method using the measured grain size to evaluate periods that are supply-limited.

Acknowledgments

We would like to thank USGS, Irstea, and CNR for their support of this project.

References

Camenen, B., Le Coz, J., Dramais, G., Peteuil, C., Fretaud, T., Falgon, A., Dussouillez, P., and Moore, S. A. (2014). A simple physically-based model for predicting sand transport dynamics in the Lower Mekong River. *River Flow, Proc. 7th Int. Conf. on Fluvial Hydraulics*, pages 2189–2197, Lausanne, Switzerland.

Topping, D. J., Rubin, D. M., Nelson, J. M. ., Kinzel III, P. J., and Corson, I. C. (2000). Colorado River sediment transport 2 - Systematic bed-elevation and grain-size effects of sand supply limitation. *Water Resources Research*, 36(2):515–542.

Topping, D. J. and Wright, S. A. (2016). Long-term continuous acoustical suspended-sediment measurements in rivers - Theory, application, bias, and error. Professional Paper 1823, U. S. Geological Survey.

Optimization theory applied to the modeling of sandy beach dynamics : Application to linear seabed

M. Cook[1,3], F. Bouchette[1,3] and B. Mohammadi[2,3]

[1] GEOSCIENCES-M, Univ Montpellier, CNRS, Montpellier, France, megan.cook@umontpellier.fr, frederic.bouchette@umontpellier.fr
[2] IMAG, Univ Montpellier, CNRS, Montpellier, France, bijan.mohammadi@umontpellier.fr
[3] GLADYS, Univ Montpellier, CNRS, Le Grau du Roi, France

1. Introduction

The processes that connect the hydrodynamics and morphodynamics in the coastal zones are both numerous and complex. We propose a new approach in the description of coastal hydro-morphodynamics, based on optimization theory. The latter refers to the evolution of a system, while systematically searching for the minimum of a certain physical quantity. Optimization theory applied to coastal dynamics has previously been developped by Mohammadi and Bouchette (2014); Isebe et al. (2008); Bouharguane et al. (2010). Here, we present the approach by optimization using a linear seabed in a 1D configuration, and the simplest wave-driven hydrodynamics.

2. Hydrodynamic model

The morphodynamic model is based on the assumption that the seabed evolves in order to minimize a certain type of wave energy. We therefore need a hydrodynamic model providing the required wave-related data, in this case, the wave height H. We have chosen a simple model based on the following shoaling equation :

$$H_S = H_0 \left(\frac{1}{2n} \frac{C_0}{C} \right)^{1/2} \tag{1}$$

where H_0 is the incoming wave height, C the wave velocity, C_0 the incoming wave velocity, and $n = \frac{C_g}{C}$ where C_g is the group velocity. We set the wave height H as :

$$H(x) = \begin{cases} H_S(x) & \text{if } \frac{H_S(x)}{h(x)} < \gamma \\ \gamma\, h(x) & \text{otherwise} \end{cases} \tag{2}$$

where h is the water depth and γ a wave breaking index.

3. Morphodynamic model by wave energy minimization

The wave-based function to be minimized is debatable, and depends on what we consider to be the driving force behind coastal morphodynamics. We have chosen :

$$J := \frac{1}{8} \int_0^{x_B} \rho_w g H(x)^2 dx \quad [J.m^{-1}] \tag{3}$$

where ρ_w is the water density, g is gravitational acceleration and H is the wave height provided by the previously described hydrodynamic model. This choice implies that the seabed ψ evolves in order to minimize the energy of the waves preceding breaking. We use the following descent method, which yields the evolution over time of the seabed ψ_t by following the direction of descent $\vec{d}$:

$$\psi_t = -\rho \Lambda \vec{d} \tag{4}$$

where ρ represents the mobility of the seabed and Λ the impact the waves have on the seabed. The direction $\vec{d}$ is driven by the vector $\nabla_\psi J$ and indicates the optimal direction to follow in order to find the minimum of J. Constraints have been included in order to incorporate additional physics into the morphodynamic model. This alters, among other things, the direction of descent $\vec{d}$.

4. Results

Taking a linear seabed and a simplified storm profile yields the following results :

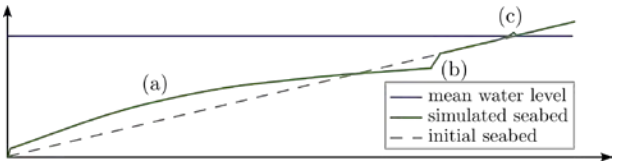

Figure 1. Simulated seabed by wave energy minimization

Two natural phenomena can be observed : the shoreline has advanced, displaying accretion and the previously linear seabed has curved, depicting the formation of a sandbar (a), a beach step (b) and a berm (c) at the shoreline.

5. Conclusion

In spite of the complex coupling of hydrodynamics and morphodynamics and the simplicity of the chosen hydrodynamic model, we can observe that the numerical simulation by wave energy minimization reproduces certain natural coastal mechanisms. A more realistic seabed may be obtained by experimenting with the choice of J and/or adopting a more complex hydrodynamic model, as well as introducing additional constraints to the configuration.

Acknowledgments

We are grateful to GLADYS for funding associated projects as well as BRLi and ANRT for funding M. Cook's PhD.

References

Bouharguane, A., Azerad, P., Bouchette, F., Marche, F., and Mohammadi, B. (2010). Low complexity shape optimization and a posteriori high fidelity validation. *Discrete and Continuous Dynamical Systems*, 13. 10.3934/dcdsb.2010.13.759.

Isebe, D., Azerad, P., Mohammadi, B., and Bouchette, F. (2008). Optimal shape design of defense structures for minimizing short wave impact. *Coastal Engineering*, 55. 10.1016/j.coastaleng.2007.06.006.

Mohammadi, B. and Bouchette, F. (2014). Extreme scenarios for the evolution of a soft bed interacting with a fluid using the value at risk of the bed characteristics. *Computers and Fluids*, 89. 10.1016/j.compfluid.2013.10.021.

Evaluation of Mitigation Measures for Channel Bed Degradation in Highly-Engineered Rivers

Matthew J. Czapiga[1], Michelle Rudolph[2], Enrica Viparelli[3] and Astrid Blom[4]

[1] Department of Hydraulic Engineering, Delft University of Technology, M.J.Czapiga@tudelft.nl
[2] Department of Hydraulic Engineering, Delft University of Technology, michelle.rudolph@rwth-aachen.de
[3] Department of Civil and Environmental Engineering, University of South Carolina, VIPARELL@cec.sc.edu
[4] Department of Hydraulic Engineering, Delft University of Technology, Astrid.Blom@tudelft.nl

1. Introduction

As economic thoroughfares, rivers have been engineered to reduce flooding and ensure navigation. Some rivers have been engineered for centuries. For example, channel modifications on the Dutch Rhine River over the last 150 years and have led to a continued channel degradation rate of 1-2 cm per year (Sieben, 2009).

Channel incision can lead to the deterioration of floodplain ecosystem due to the reduced floodplain inundation frequency, reduced navigability via unequal degradation in less mobile regions, and a potential for long-term destabilization of flow partitioning between distributaries. As such, it is necessary to comparatively evaluate available mitigation measures.

The study is focused on the Rhine River, but the findings are relevant toward reducing undesired degradation in any highly-engineered river.

Mitigation Measures

Common practices to control negative impacts of channel bed incision include: channel naturalization, channel lengthening (via re-attachment of oxbow lakes), sediment nourishments, and construction of side channels, longitudinal dams, or bendway weirs. Here, we evaluate three of these measures to reduce or reverse channel incision:

- side channels
- longitudinal dams
- sediment nourishments

2. Methodology

Our analysis is twofold, including an evaluation of field scale implementations and a numerical investigation of the relative efficacy for each mitigation measure.

A longitudinal dam pilot study in the Waal River is evaluated based on repeated measurements of bed elevation and bed surface grain size sampling. A pilot study of a sediment nourishment in the Bovenrijn, just upstream of the Pannerdens Kop bifurcation, is also evaluated using results of a bed tracer study and repeated measurements of bed surface material grain size.

The construction of side channels and longitudinal dams, as well as sediment nourishments, are then studied with a 1D morphodynamic model that explicitly accounts for the non-uniformity of the bed material grain size. To evaluate the effectiveness of each measure we compare changes in bed elevations and bed surface grain size associated with different implementation scenarios. In addition, we compare morphodynamic changes relative to various dispersal schemes for sediment nourishments, e.g. placing all sediment in the sediment feed versus dispersing it evenly across the reach.

3. Preliminary Results

Both field sites are recently implemented and, therefore, most changes are local. At the longitudinal dam, results show some upstream aggradation, but the most pronounced changes occur at junction points between dams, or just downstream of the last dam. The tracer particles of the sediment nourishment are quickly lost as the deposit disperses downstream, but the nourishment itself has not yet reached the downstream bifurcation.

All three implementations are modeled to understand the magnitude of changes to water flux Q_w, sand/gravel flux Q_s, Q_g, and/or channel width B necessary to attain a specified slope change. For example, a 25% increase in bed slope can be accomplished by doubling the mean-annual gravel feed, or by diverting 20% of water and 10% of sand flux to a system of side channels (thus removing these quantities from the main channel).

Morphodynamic changes relative to sediment nourishment dispersal scheme are tested by introducing the same volume of sediment nourishments in a variety of spatial and temporal patterns. Adding all sediment at the upstream boundary is the most effective long-term strategy for reducing bed degradation, but is ineffective across the entire domain within engineering timescales.

4. Conclusions

Altogether, our analysis details the performance of these measures in a relative context. It is useful to understand the scale and practicality of necessary changes to reduce bed degradation. Short term changes are observed in the analysis of field data and further projections can be made via numerical modeling.

Acknowledgments

This study is carried out as part of the Water2015 project 14508 ”Long-term bed degradation in rivers: causes and mitigation”, which is funded by the NWO Domain Applied and Engineering Sciences (AES).

References

Sieben, J. (2009). Sediment management in the dutch rhine branches. *Intl. J. River Basin Management*, pages 43–53.

Experimental observations on the generation of turbulent structures in tidal forced compound channels

A. De Leo[1], N. Tambroni[1] and A. Stocchino[1]

[1] DICCA - Dipartimento di Ingegneria Chimica, Civile e Ambientale, University of Genoa, Italy.

annalisa.deleo@edu.unige.it, nicoletta.tambroni@unige.it, alessandro.stocchino@unige.it

1. Introduction

Environmental fluid dynamics has the aim to provide the tools to assess the flow of nutrients required for the life of the ecosystems, to limit toxic pollutants and to minimize the anthropic impact. In particular, we focus on what are the so-called passive tracers, i.e., those substances that do not produce any change in the dynamics of fluid motion. In the last twenty years, scientific researchers have been widely interested in the study of the processes governing the dynamics of uniform and non-uniform flows in compound channels (e.g., Stocchino et al., 2011; Stocchino and Brocchini, 2010). Since the river mouth is a transition environment in which different ecosystems meet, it is interesting to understand how the mixing processes in compound channels may be affected by the presence of a tide.

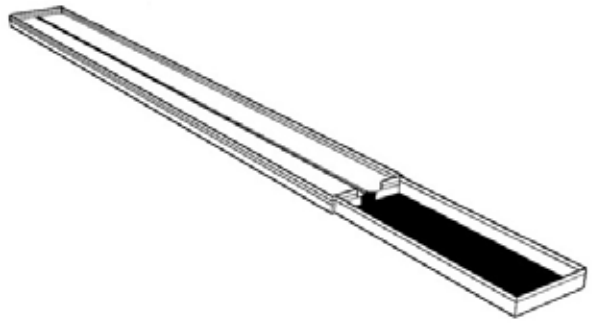

Figure 1. 3D view of the experimental compound channel.

2. State of the art

In the last twenty years, many efforts have been done by researchers in modelling the mixing processes associated with uniform flows in compound channels. In particular, the experiments performed by Stocchino et al. (2011) and Stocchino and Brocchini (2010) have shown that, despite the three-dimensional character of the flow, the main contribution to the transport processes is associated with the quasi-bidimensional macro vortices generated in the transition area, and that the mixing processes in fluvial compound channels are mainly controlled by the exchange of mass and momentum between the main channel and the lateral floodplains. Moreover, in a more recent theoretical analysis (Enrile et al., 2018), it has been found that secondary flows are confined to small regions, close to the bottom of the main channel, suggesting that a 2D approach, based on the shallow water approximation, may adequately describe the main involved processes.

Mixing processes in estuarine systems are driven by a variety of further mechanisms, including density-driven flows and tidal transport. Moreover, the complex time- and space-varying nature of estuarine hydrodynamics makes quantifying and analysing mixing process in estuaries challenging (a.o., **?**). Here we focus on the processes involving the dispersion in an unstratified tidal channel of finite length.

3. Methods and results

The most common way to analyse mixing processes is from a Lagrangian point of view. For this reason, the problem will be approached experimentally, performing a series of empirical observations in the physical model of the Laboratory of the University of Genova (Figure 1). The experimental apparatus consists of a 29 m long tidal channel, closed at one end and connected to a rectangular basin, representing the sea, at the other end. The main channel has a rectangular cross section with a landward decreasing width, and it is bounded laterally by two tidal flats (overall model width= 2.42 m). A specific tidal forcing is provided to the compound tidal channel through the sea, by the periodic motion of an oscillating cylinder inside an adjacent feeding tank. These first series of experiments are performed with a fixed bed. Bed roughness will be scaled in order to correlate the mixing processes with the characteristics of the sediments eventually lying on the bed. Free surface velocity fields in the basin and in the compound channel are acquired through PIV measurements (particle image velocimetry): an optical method consisting in the measurement of the velocity field by means of tracer particles. Particles trajectory measurements on the surface will be analysed in order to obtain information on the dispersion rates and on the effect of the unsteadiness of the flow on the Langragian coherent structures. A systematic and detailed study of the picture emerging from these experiments together with the possible implications in the modelling of estuarine environments will be presented at the meeting.

Acknowledgments

The authors would like to thank the University of Genova staff taking part in the project.

References

Enrile, F., Besio, G., and Stocchino, A. (2018). Shear and shearless lagrangian structures in compound channels. *Advances in Water Resources*, 113:141–154.

Stocchino, A., Besio, G., Angiolani, S., and Brocchini, M. (2011). Lagrangian mixing in straight compound channels. *Journal of Fluid Mechanics*, 675:168–198.

Stocchino, A. and Brocchini, M. (2010). Horizontal mixing of quasi-uniform straight compound channel flows. *Journal of Fluid Mechanics*, 643:425–435.

Geostatistical analyses of fluvial deposits in valleys: a lever for the restoration large river systems.

B. Deleplancque[1], S. Rodrigues[1,2], A. Lacoste[3], G. Le Loc'h[4]

[1] UMR CNRS 7324 CITERES, University of Tours, Tours, France. deleplancque@univ-tours.fr
[2] Graduate School of Engineering Polytech Tours, University of Tours, Tours, France. srodrigues@univ-tours.fr
[3] EA 6293 GéHCO, University of Tours, Tours, France. lacoste@univ-tours.fr
[4] Mines ParisTech, Center of geosciences, Fontainebleau, France. gaelle.le_loch@mines-paristech.fr

1. Introduction

Detritic sediment supply delivered to rivers is composed of two components. The first is related sediments coming from upstream (tributaries, erosion of the catchment area) and participating to the present fluxes. The second is composed by ancient fluvial deposits present in the valley and subject to potential erosion by the river. In several large river systems of NW Europe, channels flow in alluvial plains built by sediments deposited since the Pleistocene. This sediment storage can be considered as a lever for the restoration of sediment transport continuity in modern fluvial systems affected by bed degradation, specifically if the sediment supply coming from upstream is reduced (e.g. due to the presence of dams).

In the Loire catchment the weak sediment production suspected in the upstream reaches raises questions related to the use of the alluvial deposits (alluvial channel, flood plain and terraces) to restore the system. In function of river sediment transport capacity, grain size and spatial distribution of these deposits, one can use geostatistical analyses to prioritize restoration projects and manage river incision. This study presents a methodology for the analysis of fluvial deposits based on geostatistics and applied on the Loire and its main tributaries. This allows to localize and quantify sediment storage areas available for sediment erosion and transport at the basin scale.

2. Geostatistical Methods

The study of the potential sediment supply in the bottom of the valley is based on the analysis of alluvial formations.

The geometry of the incised valley was obtained through geostatistical analyses of depth values extracted from the BRGM (French National geological Bureau) core drill database. The new database represent extraction and homogenization of more than 3400 core drills. Several interpolation methods exist, kriging-estimators, semi-variance and variogram, simple kriging (SK), ordinary kriging (OK), universal kriging (UK), co-kriging (CoK, CoOK) and empirical bayesian kriging (BK) form part of the most common methods. The depth of the bedrock contact is considered as a continuous regional variable that ranges from zero to fifteen meters. For this study we applied OK, UK and CoK. For the co-kriging method, additional surface elevation data was included (Ohmer et al., 2017) for optimal selection of interpolation methods for groundwater contouring. All model parameters were optimized and we choose to assess the accuracy of the intepolation with cross validation. Cross validation consist to measure each point wich is sequentially omitted, and the value at this point is predited by using the rest of the data.

In the extension of Donsimoni (2008) works on the Loire catchment we applied the methods proposed by Deleplancque (2016) to estimate the initial topography and the thickness of alluvial deposits. This procedure was applied on several large tributaries of the Loire: the Cher river from Tours to Vierzon, the Allier river from the Loire confluence (Nevers) to Brioude and the Loire river from Nervers to Roanne.

3. Conclusion

This study presents an original combination of database and a geostatistical numerical modelling. The estimate of the interface between the substratum and alluvium terrace is useful to evaluate the volumes of potentially erodible sediments present in the valley.

This results will be compared with soil occupation database and with the sediment transport capacity of the river to guide restoration works of the river quality (space of river mobility, sediment refilling, channel reopening and widening of embanked areas).

Acknowledgements

This work is a part of the COSAL project funded by "l'Agence de l'Eau Loire-Bretagne (dossier n°170158601 ; n° RIC 135383)" and the European Union (convention n°2017-EX001782).

References

Deleplancque, B., (2016). *Caractérisation des hétérogénéités sédimentaires d'une plaine alluviale : Exemple de l'évolution de la Seine supérieure depuis le dernier maximum glaciaire*. PhD Thesis, Université de recherche Paris Sciences et Lettres / PSL Research University; 282 pp.

Donsimoni, M. M. Berthier H. Martin J.C. Nachbaur A. Bourgine B. Garcin, (2008). *Determination de la résence de karsts sous les levées domaniales du bassin de la Loire et reduction du risque d'effondrement de la digue lié à la présence de ces conduits souterrains naturels*, BRGM.

Ohmer, M. et al., (2017). On the optimal selection of interpretation methods for groundwater contouring: An example of progradation of uncertainty regarding inter-aquifer exchange. *Advances in water resources*, 109, pp.121–132.

Long-Term Analysis of Sediment Yield in Ogouchi Watershed

C.J.C. Gunay[1], M.A. Duka[2] and K. Yokoyama[3]

Tokyo Metropolitan University. [1]ccgunay@up.edu.ph; [2]mauriceduka@gmail.com; [3]k-yoko@tmu.ac.jp

1. Introduction

The increasing amount of sediment yield in a reservoir is a serious problem as this could drastically decrease the storage capacity of this water body. With changing land use and intense rainfall events, catchments are subject to accelerated erosion rates and the transport of the eroded soil becomes highly possible towards the streams and eventually the reservoir.

Rainfall is identified as one primary factor affecting erosion, which through time leads to sedimentation. Catchments receive varying amount of precipitation each year and therefore, it is of great significance to analyse the temporal effect of rainfall on sediment yield. Thus, this study aims to analyse the long-term effect of rainfall on sediment transport in Ogouchi Reservoir.

2. Methodology

The study area is the Ogouchi Reservoir, which has a storage capacity of 185 million m^3 and was completed on 1957. Its 262.9-km^2 catchment, has a maximum elevation of 2,017 m and is dominated by forest cover. It receives a mean annual rainfall of 1,530 mm.

The 57-year daily rainfall data was obtained from six weather stations and it was averaged by using Thiessen method. The annual sediment yield in the watershed was generated from the reservoir sedimentation data.

To estimate the sediment load transported from the watershed to the reservoir, Meyer-Peter and Müller (MPM) formula in (1) is applied. MPM is used for quantifying bedload transport in open channels.

$$q_b^* = 8(\tau^* - \tau_c^*)^{1.5} \quad (1)$$

where q_b^* is the estimated bedload volume, $\tau^*$is shear stress, and τ_c^* is critical Shields stress.

This equation was modified assuming that sediment transport in a catchment is driven by rainfall, provided by:

$$q_b^* = \alpha\{\rho g S(R - R_c)\}^{1.5} \quad (2)$$

where α is the adjusted coefficient, ρ is fluid density, S is catchment slope, and $(R - R_c)$ is effective rainfall i.e. difference between actual and critical depth that will cause sediment transport.

A correlation between actual sediment yield and MPM estimates was then established using lagging and moving average methods.

3. Results and Discussion

Figure 1 shows a decreasing trend of sediment yield from years 1959 to 1965, which cover the early period after dam construction. The case is reversed for 1966 to 1991 where an increase in sedimentation rate from 180 to 460 m^3/km^2 was observed over the course of 26 years. Afterwards, the sedimentation rate remained relatively constant until 2015. No significant relation is found between rainfall and sediment yield from Figure 1, therefore the MPM equation was applied.

Figure 2 provides the relationship between actual sediment yield and MPM estimates for each decadal group. Using a critical rainfall depth of 30 mm, it was established that the two-year moving average method would give a better correlation as against using the actual data and lagging methods.

Figure 1: Time series of annual rainfall and sediment yield in Ogouchi Reservoir.

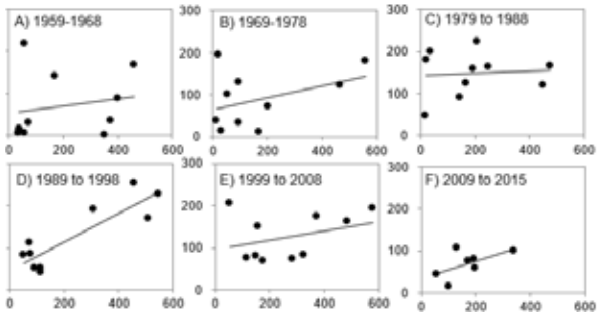

Figure 2: Correlation of computed and actual sediment yield in Ogouchi Reservoir every 10 years.

These 10-year correlation plots expressed the difference in soil erodibility. Since erodibility coefficient, α, of MPM is fixed, if actual sediment yield becomes high for a certain MPM value, actual erodibility increases.

Plot of period A is distributed because the topography survey has relatively larger error just after the construction of dam and therefore sedimentation data was not stable. Periods C and D, on the other hand, showed high erodibility, and then decreased when it reaches period E. Minimum erodibility was found in period F, as the Tokyo Metropolitan Bureau of Waterworks had been intensifying their afforestation efforts. This means that the soil in the watershed achieved better condition and its resistance against erosion by rainfall increases.

4. Conclusions

No direct relation was found in time series of rainfall and sediment yield from 1959 to 2015 for the Ogouchi Reservoir. However, employing the modified MPM equation considering two-year moving average method showed a positive correlation between the two parameters but relationship is not the same for each decade.

5. References

Meyer-Peter, E. and Müller, R., 1948, Formulas for Bed-Load Transport, Proceedings, 2nd Congress, IAHR, Stockholm: 39-64.

Bedload discharge measurement in actual river with MBES and ADCP

M. HASHIBA [1], A. YOROZUYA[2], H. KOSEKI [2] and K.TSUCHIDA [1]

[1] Fukuda Hydrologic Centre, SAPPORO, JAPAN, hashiba@f-suimon.co.jp, k-tsuchida@f-suimon.co.jp
[2] Hydrologic Engineering Research Team, Hydraulic Engineering Research Group, Public Works Research Institute, Ibaraki, JAPAN, yorozuya@pwri.go.jp, h-koseki@pwri.go.jp

1. Introduction

Bedload discharge is important to understand the sediment dynamics in the basin and to verify to numerical analysis of riverbed fluctuation. The bedload sampler was developed since 1960's. However, because it was difficult to install the sampler on the riverbed during high flow, there was involved uncertain data. In this study, the authors conducted the field measurement with the MBES (Multi-Beam Echo Sounder) and ADCP(Acoustic Doppler Current Profiler) mounted on a manned-control boat. By using measured data which were bed wave form, bed migration, we evaluated bedload discharge measurement methods in actual river.

2. Field observation

The authors conducted to measure the riverbed by MBES and ADCP at the 3 samples area and 3 times repeatedly between upstream and downstream.

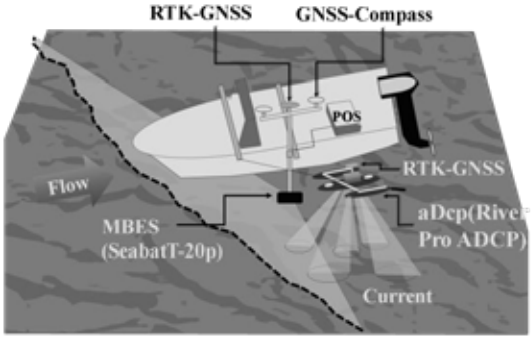

Figure 1: Measurement system

3. Result

3.1 Riverbed wave form

The measured shape of the bed wave, the averaged wave height was 0.30-0.49 m, while the averaged wave length was 4.4-6.7 m, which gives the height/length of 0.07.

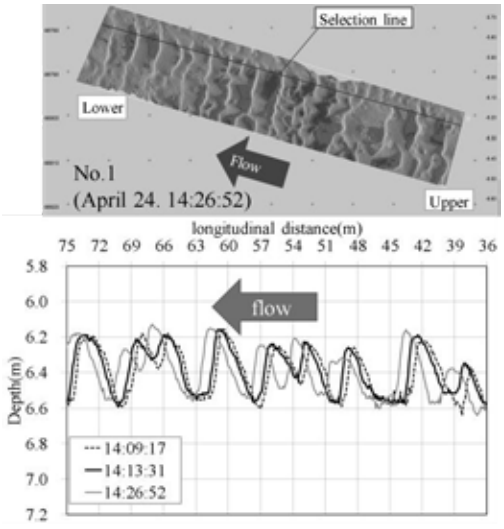

Figure 2: Riverbed wave form and bed migration

3.2 Bed wave migration

The riverbed migration, 0.05 m/min to 0.08 m/min was estimated as moving speed of the sand waves using the space-time image.

4. Bedload discharge

Regarding the bedload discharge, two different methods were compared. First one is the bed form migration, which is the function of the wave height and the wave migration speed proposed by Kikkawa (1985). Second one is the method using bedload velocity(u_b) of ADCP proposed by Koseki et al. (2016) shown in Eq(1) and (2).

$$q_b = \int_0^{h_s} c \cdot u \cdot dz \cong \alpha_{bs} \cdot u_b \cdot h_s \cdot c_s \quad (1)$$

$$\frac{h_s}{d} = \frac{1}{c_s \cos\theta\{\tan\varphi_s - \tan\theta\}}\tau_* \quad (2)$$

where q_b=bedload discharge; α_{bs}=correction coefficient for calculating u_s from u_b (=0.65); u_b=bedload velocity by ADCP; h_s=bedload thickness; c_s=averaged sediment concentration by bedload thickness (h_s); d= sediment particle size(=d60); φ_s=interparticle friction angle; θ=bed slope; τ_*=dimensionless shear stress

As shown in Table 1, the both of bedload discharge was the same order.

Table 1: Bedload discharge

Sample	Kikkawa(1985) ($\times 10^{-3}m^3/s/m$)	Koseki(2016) ($\times 10^{-3}m^3/s/m$)
No.1	0.24	0.13
No.2	0.18	0.04
No.3	NG	0.07

3. Conclusions

Regarding to sand wave behaviour, it was able to measure the sand wave form and wave migration in time series using MBES.

The authors measured the bedload discharge by bedload velocity of ADCP without sediment samplers in the actual river using the method of Koseki et al.(2016).

References

Yalin, M.S. and Karahan, F. (1978). Steepness of sedimentary dunes, Proc. ASCE, Vol.105, HY4, pp.381-392.

S. Egashira, K. Miyamoto, T. Itoh (1997). Constitutive Equations of Debris-Flow and Their Applicability, Proc. of 1st International Conference on Debris-flow Hazards Mitigation, C. L. Chen (Eds.), ASCE: NewYork; pp. 340-349.

H.Koseki,A.Yorozuya,S.Kudo,Y.Iwami, Development of a system to measure bed forms and vertial velocity profiles in a river channel,River Flow 2016.

Geomorphological Meaning of Discontinuous Levee System on the Kurobe Alluvial Fan, Japan, in the early 19th century

T. Ishikawa[1]

[1] Professor Emeritus, Tokyo Institute of Technology, Tokyo, Japan. workishikawa0612@yahoo.co.jp

1. Introduction

In early-modern age of Japan (from the 17th to the mid19th century), when strong, continuous levees were not built, discontinuous levee system was commonly employed. The system often functioned well to control floods exceeding a channel capacity (e.g., Ishikawa and Akoh, 2018). However, the extent of knowledge for levee openings design in those days has not been fully clarified.

This study discussed a possibility that the knowledge for discontinuous levee design had covered even a long term geomorphological movement, by taking the case of levee system on the Kurobe Alluvial Fan.

2. Topography of the Kurobe Alluvial Fan

The Kurobe River flows down a stretch of 85 km from the central mountain range of 3,000 meters high to the Japan Sea Coast. Large volume of sediment yielded in the canyon formed a coastal alluvial fan having a radius of 13 km and an average slope of 1/100 (see Figure 1).

The grey bands represent the old river courses, which tend to branch in the middle of the fan as well as near the top of fan. Short solid lines bounding the present river course represent the levee locations measured at the end of the 19th century. The upstream section has a lot of simple levee openings, whereas the downstream has a series of funnel shape levees which open upstream. This fact suggests that the engineers of those days noticed some difference between the two sections.

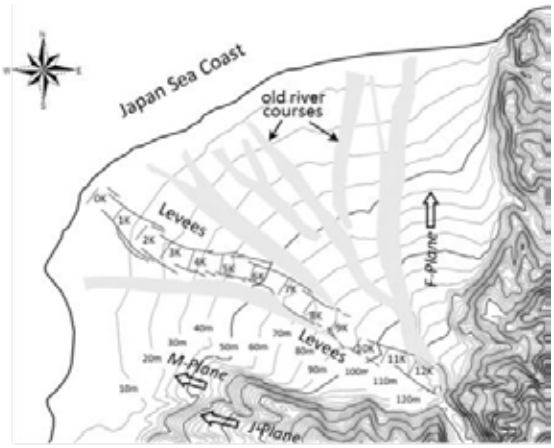

Figure 1: Topography of Kurobe Alluvial Fan.

3. Long term geomorphological motion

The *J*, *M* and *F-planes* with open arrows in the figure are remains of old fans. Their radial profiles from the present fan top are plotted in Figure 2, where *P-plane* is the present one. Carbon-14 dating showed that the order of fan plane ages is $J > M > F > P$ just the same order as slopes, which means that the ground of this area has been tilting with time. According to various field data, such as the rate of ground rising/sinking, the sea surface change after the Ice Age and the unconformity under the seabed, the variation from *F*-plane to *P*-plane has continued for the last 10,000 years, though those data are not presented here for lack of space. The two lines intersect in the middle of the present fan, which means that erosion occurred on the upper and deposition on the lower half of fan. This geomorphological movement was the cause of the river course changes in the "intersection zone" located in the middle of present alluvial fan.

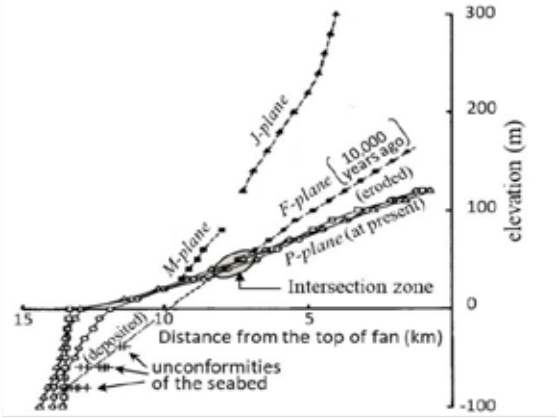

Figure 2: Radial profiles of alluvial fans.

4. Flood flow through levee openings

One possible method to mitigate the river course change in the middle of fan was to allow an excess water flow diverge from the channel before the intersection zone, and return to the channel after the zone. Figure 3 shows a numerical simulation result for a flood exceeding the channel capacity. A part of river water overflowed from an upstream levee-opening, and returned to the channel through the funnel-form levees with a time lag.

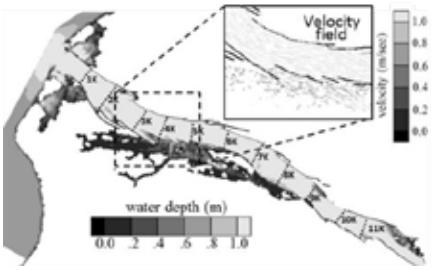

Figure 3: Flood flow control by discontinuous levees.

5. Conclusions

Engineers of early-modern age didn't have technology to build large levees. Instead, they perhaps collected geomorphological evidences outside of river channel as much as possible, and tried to control the flood flow not only in a river channel but also on the floodplain.

References

Ishikawa, T. and Akoh, R. (2018). Assessment of flood risk management in lowland Tokyo areas in the seventeenth century by numerical flow simulation. *EFM*, https://doi.org/10.1007/s10652-018-9616-6.

Effective artificial sediment supply to a river channel disturbance

Ayaka Ito[1], Yasuharu Watanabe[2], Kazusige Odagaki[2] and Tamaki Akiyama[3]

[1] Kitami Institute of Technology, Kitami city, Japan. m1852200025@std.kitami-it.ac.jp
[2] Kitami Institute of Technology, Kitami city, Japan. y-watanb@mail.kitami-it.ac.jp
[3] Kitami Institute of Technology, Kitami city, Japan, m1952200090@std.kitami-it.ac.jp
[4] Hokkaido Regional Development Bureau, Japan, akiyama-t22ad@mlit.go.jp

1. Introduction

In rivers where dams are built at upstream, the frequency of disturbance in rivers decreases. The Satsunai River is a branch of the Tokachi River in Hokkaido. This river used to be a braided channel and a gravel bed river. Forest zones were increasing in the river channel after dam construction at the upstream. Trees in the river progressed remarkably, and gravel bars were covered by the trees. The river environment of the Satsunai River was changed completely.

Under such circumstances, a large flood attacked this basin in 2013. Bank erosion and channel shift occurred in large numbers at the flood, but especially along old channels (distributary), disturbances occurred. Based on this result, the Hokkaido Development Bureau planned to restore old channels in order to cause the river channel disturbances at the time of floods. In areas where old channel had already completely disappeared, the development of rods with artificial sediment supply made plans to cause river disturbances. However, it was unknown how to effectively supply artificial sediment to the disturbance of the river channel. Therefore, we conducted hydraulic experiments and numerical experiments to clarify the method of setting the sediment effectively promoting the development of bars which is considered effective for the river disturbance. As a result, it was found that the bank erosion due to the development of bars would be increased by placing the sediment on the upstream side of the scouring section of bar. Using this result, a demonstration field experiment was conducted in the Satsunai River. During artificial flood in June 2018, bank erosion in about 10 m occurred at the place where the setting of sediment was applied. In this research, it is verified by using numerical calculation method whether this bank erosion was due to the installation of sediment.

2. Outline of field experiment results

In the site, approximately 100 m^3 of sediment replenishment was installed on the left bank at the middle reach of the Satsunai River. When an artificial flood occurred in 2018, bank erosions and channel shifts and wash out of trees were observed. It is thought that gravel bars were formed because trees were washed out as the channel was shifted. Also, bar development and bank erosion occurred at the downstream of the artificial sediment supply area. And, the area of bars formed during this artificial flood in 2018 was larger than those formed during any of the previous artificial flood. It was found that the bar development by the artificial sediment supply promoted the fluctuation of the river channel.

3. Outline of numerical calculation

Nays2DH (http://i-ric.org/) was used in this study. Reproducibility is confirmed by field observations before and after the artificial flood from a Satunai-gawa Dam implemented at the installation of sediment at the middle reach of the Sataunai River in June 2018. We decided to understand the impact on the disturbance of the river by the presence of sediment replenishment. The longitudinal calculation range was about 1 km including the location of sediment replenishment. The size of calculation grid is 10 m in the longitudinal direction and 5 m in the transverse direction. The time step is set to 0.1 seconds and the Manning roughness factor is set to 0.025.

4. Results

The calculation results show how the degree of development of bars and the degree of bank erosion differ depending on the presence or absence of the sediment replenishment. As a result, bank erosion became more active by bar development and new gravel bars were formed in the presence case. Artificial sediment supply promotes the development of bars and activates channel shifts caused by bank erosion.

5. Conclusions

This study focuses on bank erosion caused by bars. And we have investigated effective artificial sediment supply method using numerical calculation. It has been shown that it is possible to effectively cause channel shift

References

Hokkaido Regional Development Bureau. (2008). Technical study meeting document in the Satsunai River

Ministry of Land, Infrastructure, Transport and Tourism River Bureau. (2011). Downstream river sediment reduction manual (draft)

Kazuo Asida. (1982). Three-dimensional structures of river flood and channel process

Tamaki Akiyama and Yasuharu Watanabe. (2018). Study on effective artificial sediment supply to a river channel disturbance. The 63rd Conference on Hydraulic Engineering.

Morphological and ecological response of a coastal dune to experimental notches: Truc Vert, SW France

Q. Laporte-Fauret[1], B. Castelle[1], R. Michalet[1], V. Marieu[1], D. Rosebery[2], S. Bujan[1]

[1] CNRS, Université de Bordeaux, UMR 5805 EPOC, Pessac, France. quentin.laporte-fauret@u-bordeaux.fr
[2] Office National des Forêts, Paris, France.

1. Introduction

Sandy coastlines are vulnerable environments, particularly in the context of climate change and increasing anthropogenic pressure. Most of the world's sandy beaches are backed by dunes acting both as a buffer against the ocean onslaught and providing many ecosystem services (Nordstorm, 2015). However, most coasts in the world are highly managed to reduce the impact of marine and wind erosion, often at the detriment of vegetation dynamics and natural community diversity. Coastal dunes in SW France have been reprofiled by stakeholders in the 70s and 80s, with subsequent vegetation planting to fix the dune and protect the adjacent forest from silting. In recent years, the doctrine of coastal dune environments management has gradually evolved towards more flexible management restoring natural dynamic processes. In addition, many managers suggest that in some coastal dune environments, dunes maintained as dynamic systems could be more resistant to marine and wind erosion than fixed dunes, although this hypothesis has never been studied quantitatively.
Thus, the objective of this study is to better understand the interactions between physical and biological processes in coastal dunes.

2. Material and methods

An original experiment was set up on a 4-km alongshore dune stretch at Truc Vert beach (SW France), where eight experimental transverse notches (ETNs) were dug in pairs every 1 km in December 2017. Each pair consists of one ETN in the incipient foredune and one ETN in the foredune, in order to stimulate natural dynamics and restore sedimentary exchanges between the beach and the dune as coastal blowouts (Hesp, 2002). The high-resolution morphological evolution of the ETN and the 4-km of dune has been monitored quarterly using UAV photogrammetry, with additional pre/post storm surveys in winter. In addition, 260 measurement points were placed in 20 transects of 13 survey points. Each transect extends from the beach to the back of the dune, in line with the ETN and in a control situation in order to monitor vegetation composition and abundance, elevation variations, organic matter decomposition rate, wind speed and grain size.

3. Results

The first results show a significant erosion of the beach with a lowering from 1.5 m to 2.5 m locally, driven by the high-energy waves during the 2017-2018 winter. The foredune shows an average vertical accretion from 0.4m to 1.1m locally between the crest and the lee side, with a slight landward migration (Figure 1). Finally, large sand deposition fields, with a thickness between 0.1 and 0.3m driven by aeolian processes, were measured over several tens of meters on the grey dune, greatly affecting the vegetation present. Indeed, the abundance and composition of plant species shows significant seasonal discrimination based on their resistance to disturbance. Environmental measures highlight significantly higher wind speeds, sand deposits and organic matter decomposition rates behind the ETN in the foredune compared to ETN in the incipient foredune and undisturbed areas.

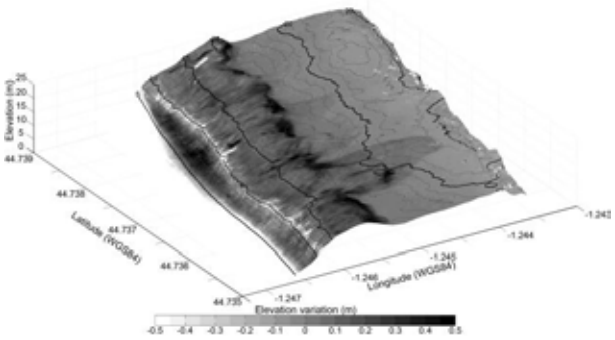

Figure 1: Zoom onto the 0.5-km alongshore DSM difference between October, 9 2017 and March, 13 2018. The color bar indicate the elevation difference. DSM was performed using UAV photogrammetry.

4. Conclusion

The implementation and monitoring of experimental mechanical disturbances in the Truc Vert beach-dune system highlights that notches impacted the morphological and ecological behaviour of the coastal dune. Longer term monitoring will provide more insight into the potential benefit of artificial notches in the region, with implications from the perspective of coastal dune monitoring.

References

Hesp, P.A. (2002). Foredunes and blowouts: Initiation, geomorphology and dynamics. *Geomorphology*, 48, 245–268.

Nordstrom, K.F. (2015). *Coastal dunes*. In: Masselink, G., Gehrels, R. (Ed.), Coastal Environments and Global Change. John Wiley & Sons, Ltd., pp 178–193.

Measuring sediment suspensions in rivers using bi-frequency acoustic inversion

J. Le Coz[1], A. Vergne[1], C. Berni[1] and G. Pierrefeu[2]

[1] Irstea, UR RiverLy, River Hydraulics, Lyon, France. jerome.lecoz@irstea.fr
[2] Compagnie nationale du Rhône (CNR), Lyon, France. g.pierrefeu@cnr.tm.fr

1. Introduction

Hydro-acoustic profilers have emerged as a promising technology for measuring suspended sediment concentration (SSC) in rivers. Especially, side-looking Acoustic Doppler Current Profilers (ADCPs) have been used to monitor river sediment fluxes, assuming the suspension is homogeneous along the horizontal profile. Down-looking ADCPs would be useful for exploring sediment transport throughout river cross-sections but the inversion of vertical backscatter profiles is more difficult as the suspension usually varies vertically. We set up an acoustic signal inversion strategy and applied it to data acquired at various river sites using a down-looking multi-frequency Acoustic Backscatter System (ABS).

2. Inversion method

A bi-frequency inversion method was modified from that proposed by Hurther et al. (2011) with a number of assumptions that are usually met in river applications with sufficiently high concentrations. The water attenuation was assumed to be constant throughout the cross-section. The suspension was approximated as the mixture of a fine (silt and clay) sediment population and a coarse (sand) sediment population with variable concentrations but constant grain size distributions. Such conditions were observed by several authors in various rivers. As the respective concentrations of fines and sand vary, the combined, bimodal grain size distribution vary throughout the cross-section.

As a reasonable approximation, backscatter and attenuation can be assumed to be governed by, respectively, the sand only and the fines only. The related backscatter and attenuation constants are therefore homogeneous throughout the cross-section and can be estimated using point water samples distributed over a vertical profile with substantial near-bed sand suspended load. The backscatter constant was modelled from the sand grain size distribution while the attenuation constant was measured from observed acoustic energy losses. Once these backscatter and attenuation constants have been estimated, the bi-frequency inversion method can be applied to deduce the spatial distribution of sediment backscatter and attenuation, and finally obtain an estimation of sand and fine SSCs throughout the river cross-section.

3. Results

Figure 1 presents the results obtained at a high SSC ($\sim$ 10 g/l) river site, the confluence of the Isère (on the left) and Rhône (on the right) as the Isère dams were flushed. The grain size distributions and acoustic constants were estimated using water samples taken in the Isère since its concentration was much higher than that of the Rhône. The bi-frequency inversion method was applied to 0.3 MHz and 1 MHz records to compute the sediment backscatter and attenuation throughout the cross-section and finally estimate the sand and fine SSCs.

For both sediment populations, the acoustically-derived concentrations appear to be in acceptable agreement with the concentrations observed in the water samples, in spite of the strong assumptions made. Due to total attenuation of the acoustic signal, measurements are missing in near-bed areas: acoustic attenuation increases with range, concentration of fines and emitting frequency. Near-surface vertical plumes of higher fine SSC are thought to be spurious results due to the presence of air micro-bubbles, which have powerful backscatter and attenuation properties. Nonetheless, these backscatter data provide a high-resolution view of this complex hydro-sedimentary system, comparable to a turbidity current.

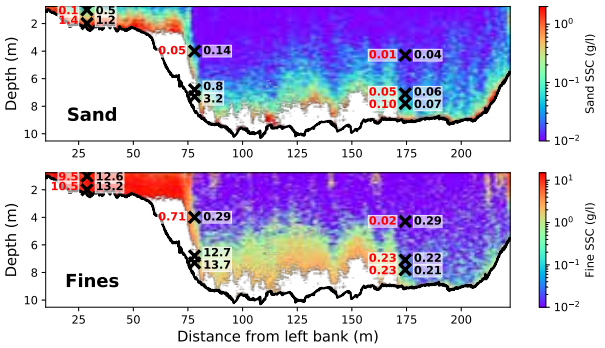

Figure 1. Fine (top) and sand (bottom) suspended sediment concentrations (SSC) inverted from 0.3 MHz and 1 MHz backscatter records at the confluence of the Isère (on the left) and Rhône (on the right) during Isère dam flushing. SSC data (g/l) from water samples (crosses) and from acoustic inversion are shown in black and red, respectively. White areas are missing data.

4. Conclusions

These promising results suggest that multi-frequency acoustic backscatter inversion can provide spatially-distributed measurements of bimodal sediment suspensions in rivers. However, the inversion failed at low SSC ($\sim$ 30 mg/l) sites likely because the suspended solids were not the main sound scatterers in the medium.

Acknowledgments

Adrien Vergne's PhD was partly funded by CNR. This study was supported by the Rhône Sediment Observatory (OSR), a multi-partner research program partly funded by the Plan Rhône and by the European Regional Development Fund (ERDF) allocated by the European Union.

References

Hurther, D., Thorne, P. D., Bricault, M., Lemmin, U., and Barnoud, J.-M. (2011). A multi-frequency Acoustic Concentration and Velocity Profiler (ACVP) for boundary layer measurements of fine-scale flow and sediment transport processes. *Coast. Eng. J.*, 58:594–605.

Numerical Study on Organic Sediment Deposition in Brackish Water Reach of Nomi River in Tokyo Metropolis

S. Miura[1], T. Ishikawa[2], T. Nakamura[3] and T. Kotajima[4]

[1] CTI Engineering Co. Ltd, Tokyo, Japan, miura@ctie.co.jp
[2] Tokyo Institute of Technology, Tokyo, Japan, workishikawa0612 @yahoo.co.jp
[3] Tokyo Institute of Technology, Tokyo, Japan, tnakamur@depe.titech.ac.jp
[3] CTI Engineering Co. Ltd, Tokyo, Japan, Tokyo, Japan, ttk-kotajima@ctie.co.jp

1. Introduction

In the downstream reach of urban rivers flowing from the uptown Tokyo, water quality problems such as scum generation and offensive odor often occur after the rain runoff. The cause of problems is considered as follows: Organic sediment is flushed from the combined sewer pipes to the downstream river section during a storm, and it is reduced to anaerobic gas under the saline stratification condition.

In this study, the sedimentation process of organic matter was simulated numerically using models of sediment runoff from combined sewer system as well as of deposition in a stratified water flow. Calculation result was verified with field data that authors collected.

2. Study site and field data collection

Study site is the Nomi River which has the main channel length of 14.4 km and the catchment area of 17.7 km^2. The watershed is highly urbanized and covered with combined sewer system. The most upstream 5 km reach is now a culvert as a part of the sewer line.

Figure 1 shows the longitudinal river bed profile of open channel part. The segment-1 is a steep slope, concrete lining channel, and the segment-2 is an almost zero slope, movable bed channel. Based on the pilot survey, sediment traps were installed on the channel bed at three locations where sedimentation was remarkable (see Figure 2). Sedimentation for five rainfall events was obtained from July 18 to August 15, 2017. The sediment weight and ignition loss were analysed for each event.

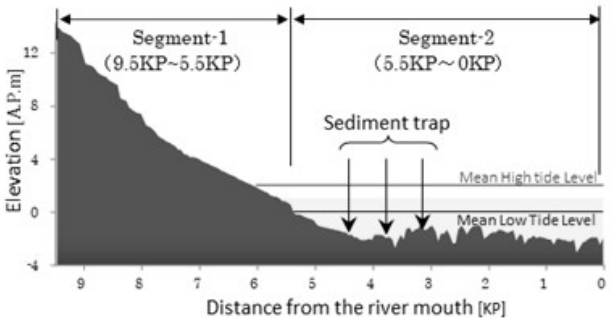

Figure 1: Longitudinal channel bed profile

3. Numerical simulation model

Considering sewer pipes with an inner diameter ≥ 600 mm, a drainage system map was prepared for the whole watershed. MIKE URBAN (DHI, 2017) was used by applying gully pot module to manhole pots where domestic waste water flows into the rainwater drainage pipes. Model parameters were calibrated using field data collected in sewer pipes.

The SS transport and deposition process in the downstream stratified water body was simulated using TITECH WARM (Xu et al., 2013) in the laterally average 2-D form. Deposition/ suspension rate of sediment particles at the river bed was estimated using the following equation.

$$F_b = (C_b - C)w_0 \qquad (1)$$

where F_b is the net suspension rate, C_b is the critical sediment concentration proposed by Lane and Kalinske, C is sediment concentration just above the channel bed obtained from the TITECH WARM and w_0 is sediment settling velocity.

4. Results and discussion

According to the calculation results, most of sediment was flushed out from the sewer pipes to the river channel in the first stage of each storm, and deposited just downstream from the segment-1 (see Figure 1). The sediment was re-suspended around the time of flood peak, transported to the section from 4.5KP to 3KP where sediment traps were located, and settled there.

Figure 2 shows the correlation between the calculated and observed organic sediment (ignition loss of trapped sediment) for the five runoff events, where ignition loss of deposit in the sewer pipe system was assumed as 70 % from the pilot survey result.

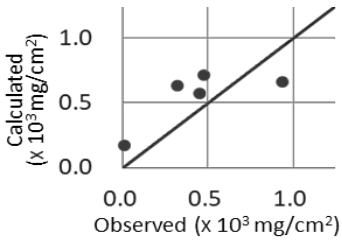

Figure 2: Calculated and observed Ignition loss

5. Conclusions

Sedimentation of organic matter discharged from the combined sewer system to the downstream saline stratified water section can be roughly estimated by the method presented here. The method will be used to predict the water quality problems by combining a model for anaerobic reduction of organic matter.

References

DHI (2017). MIKE URBAN Manual. http://mikepoweredbydhi.com/products/mike-urban

XU, X., Ishikawa, T. and Nakamura, T. (2013): Three-dimensional modeling of hydrodynamics and dissolved oxygen transport in Tone River Estuary, *Journal of JSCE*, Vol.1, 194-213.

Shoreline changes at Tairua Beach at different temporal scales.

J. Montaño[1], G. Coco[1], K.R. Bryan[2], and E. Lazarus[3]

[1] School of the Environment, University of Auckland, New Zealand. jmon177@auckland.ac.nz, g.coco@auckland.ac.nz
[2] School of Science, University of Waikato, Private Bag 3105, Hamilton, New Zealand. karin.bryan@waikato.ac.nz
[3] School of Geography and Environmental Science, University of Southampton, UK E.D.Lazarus@soton.ac.uk,

1. Introduction

Predicting shoreline evolution is one of the key challenges in coastal studies. In general terms, during storms, the shoreline rapidly moves landward (erosion), while during calm periods the shoreline slowly moves seaward (accretion). These changes may be intensified by longer time scale (e.g. inter-annual fluctuations) and/or regional climatic patterns (e.g. ENSO).

We analyzed 18 years of daily shoreline evolution and wave characteristics at Tairua Beach to identify shoreline changes at different temporal scales and link them with waves and regional weather patterns.

2. Methods

2.1 Study area and data acquisition

Tairua Beach is located in the Coromandel peninsula, on the east coast of the North Island of New Zealand. Tairua is a 1.2 km long pocket beach and is classified as an intermediate beach (Blossier et al., 2016) The beach is located in a microtidal environment with a tidal range varying between 1.2 and 2 m. Eighteen years of daily shoreline evolution (1999-2017) were obtained using a camera system. Wave characteristics (1999-2017) were obtained from a SWAN model (wave height, peak period, and direction). Additionally, pressure and pressure gradients fields during this period were analysed.

2.2 Complete Ensemble Empirical Mode Decomposition Method (CEEMD)

We used the Complete Ensemble Empirical Mode Decomposition (CEEMD) to decompose the time series into a finite set of "intrinsic mode functions" (IMFs). This method overcomes limitations of Fourier-based methods for time series analysis (e.g. FFT and wavelet techniques) since the method was designed to analyse non-linear and non-stationary phenomena, identifying also processes and patterns characterised by small amplitudes (Hunag et al., 1998; Flandrin, 2011).

3. Initial Results

Energy distribution of the shoreline spectrum displayed energy concentrated at annual and bi-annual frequencies. Pressure gradients (PG) fields and wave height spectra showed similar inter-annual fluctuations and also significant energy at higher frequencies (20-60 days) which was not observed in the shoreline spectrum. The incoherence between drivers (e.g. waves) energy distribution and shoreline response has been reported in previous studies (e.g. Lazarus et al., 2019) However, CEEMD analyses captured oscillations at intra-annual frequencies (e.g. 20-60 days, blue line Figure 1c) which may cause large shoreline changes (black line, Figure 1c). Significant cross-correlation between shoreline and wave height IMFs at these frequencies (blue lines, Figure 1) was found ($R_{xy} = 0.6$). Additionally, some of the IMFs at inter-annual scales could be related to regional weather patterns, pressure fields and storms.

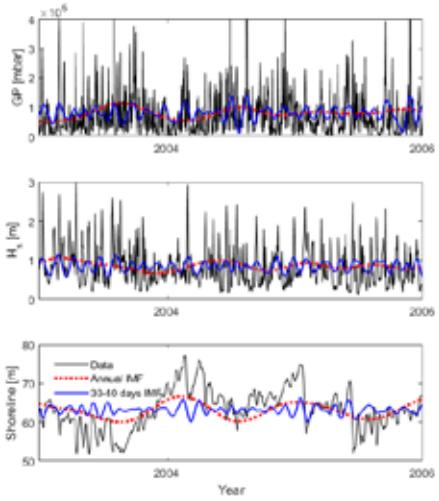

Figure 1. Annual IMF (red line) and 30-40 days IMF (blue line) for: a) Pressure Gradients fields (PG) b) Significant wave height (Hs) c) Shoreline position.

4. Summary

Power density spectra for the three time-series displayed a strong energy at annual frequency. PG and Hs also displayed energy at higher frequencies (monthly scale). CEEMD allowed us to capture such "hidden" oscillation at different frequencies (intra and inter annual) and relate them with regional patterns.

Acknowledgments

Thanks to Waikato Regional Council and NIWA for providing the video images, to R. Bell (NIWA) for tide data, and to MetOcean for the wave hindcast.

References

Blossier, B., Bryan, K. R., Daly, C. J., and Winter, C. (2016). Nearshore sandbar rotation at single-barred embayed beaches. *Journal of Geophysical Research: Oceans*, *121*(4), 2286-2313.

Huang, N.E., Shen, Z., Long, S. R., Wu, M.C., Shih, H. H., Zheng, Q& Liu, H.H. (1998). The empirical mode decomposition and the Hilbert spectrum for nonlinear and non-stationary time series analysis. *Proc. Royal Society of London. Series A,*, 454(1971), 903-995.

Lazarus, E., Harley, M. D., Blenkinsopp, C. E., & Turner, I. L. (2019). Environmental signal shredding on sandy coastlines. *Earth Surface Dynamics*, 7, 77-86.

Torres, M. E., Colominas, M. A., Schlotthauer, G., & Flandrin, P. (2011, May). A complete ensemble empirical mode decomposition with adaptive noise. In 2011 *IEEE,* 4144-4147.

Validation of a Morphodynamics Model in a Coastal Area based on a Statistical Reduction applied to in-situ measurements

Rem-Sophia Mouradi[1, 2], Olivier Thual[2, 3], Cédric Goeury[1], Pablo Tassi[1, 4], Fabrice Zaoui[1]

[1]LNHE, EDF R&D, 6 quai Watier, 78400 Chatou, France
[2]CECI, CERFACS – CNRS, 42 avenue Gaspard Coriolis, 31820 Toulouse, France
[3]Université de Toulouse, INPT, CNRS, IMFT, Toulouse, France
[4]Laboratoire d'Hydraulique Saint-Venant, Chatou, France
E-mail: rem-sophia-r.mouradi@edf.fr

1. Introduction

Water intakes are used to ensure the cooling process of power plants via a pumping system. They can be subject to sediment accumulation, which requires costly dredging operations. The latter can be optimized if a robust prediction of the involved sediment dynamics is possible.

The presented methodology is applied within the context of a coastal water intake monitoring. The interest intake is subject to sediment arrivals, implying fast bathymetric changes. Due to the monitoring needs, bathymetric measurements of the channel are performed on a regular basis, along with meteorological and hydrodynamic surveys (waves, wind, tidal levels, etc.). One of the challenges is to predict the morphodynamics using a numerical model, which assumes that the latter provides results within a reasonable confidence interval.

We propose an approach to assess the accuracy of a numerical model regarding the prediction of the sediments dynamics involved in the intake of interest, using statistical reduction.

2. Methodology

When a fairly large set of measurements is available, an opportunity for numerical model validation arises. The choice of the best strategy to adopt in order to exploit all the available measurements is not trivial. Typically, the data-based validation procedure is to simulate each measured scenario, which implies calibrating the model's parameters in order to fit the observed data.

We hereby propose an alternative approach of validation using Proper Orthogonal Decomposition (POD) [1]. The POD consists of decomposing a field that depends on time and space variables (in this case the bathymetric data) into a finite sum of functions with separate variables. This allows first to isolate the spatial patterns, called the POD basis. The POD basis terms, when added, explain the observed dynamics. They are each multiplied by a coefficient that varies in time, which amplifies their contribution to the resulting field.

The idea of model validation using POD would be to launch a Monte Carlo like sampling of the input space, and to produce corresponding numerical solutions. These solutions can be post-processed using POD. The latter helps deducting the dynamical patterns of bathymetric evolutions. These patterns can be compared to patterns deduced from in situ measurements, presented in the following section.

3. Application on in-situ measurements

The POD has been applied to the intake's bathymetry measurements, recorded each 2 weeks, for a 10 years duration. The resulting spatial patterns are presented in **Figure 1**, and are associated to temporal coefficients.

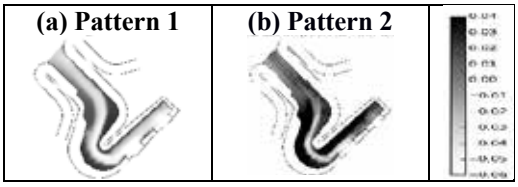

Figure 1: First two elements of the POD basis applied to the bathymetry history of the studied water intake.

Pattern 1 indicates a uniform siltation inside the channel, whereas Pattern 2 corrects the geographical distribution of the latter, with respect to the flow and to the geometry of the channel. For a numerical model to be accurate, its resulting solutions must be projectable on this same basis deduced from measurements. That would imply that, on the analysed temporal and spatial scales, the model has the same nature of response as the in-situ observations.

The temporal coefficients deduced from POD represent the variations in time due to the influence of the external forcings. We propose a statistical modelling of this causality using Polynomial Chaos Expansion method (PCE) [2]. The aim here would be to compare the statistical models resulting from the numerical scenarios and from the in-situ measurements analysis. This would allow to conclude about the importance of each parameter in both the real configuration and the numerical model.

4. Conclusion

The results of a numerical model are compared to in-situ measurements via a spatial patterns deduction, using POD. The temporal variations are modelled using PCE, taking the forcings as inputs. The differences of ranking of the forcings contribution on the temporal responses between the numerical model and the in-situ measurements are confronted.

References

[1] Lumley, J. L. *The Structures of Inhomogeneous Turbulent Flow.* Proc. Int. Colloq. Fine Scale Structure of the Atmosphere and Its Influence on Radio Wave Propagation, (Nauka, Moscow, 1967), pp. 166–178.

[2] Blatman, G., 2009. *Adaptive sparse polynomial chaos expansions for uncertainty propagation and sensitivity analysis.* Ph.D. thesis, IFMA/Université Blaise Pascal.

Feasibility of 100-year estuarine geomorphology prediction

H. Muller[1], P. Le Hir[1], P. Tandeo[2], F. Dufois[1], F. Grasso[1] and R.Verney[1]

[1]IFREMER, Centre de Bretagne, 29280 Plouzane, France. heloise.muller@ifremer.fr, pierre.le.hir@ifremer.fr, francois.dufois@ifremer.fr, florent.grasso@ifremer.fr, romaric.verney@ifremer.fr
[2]IMT Atlantique, Lab-STICC, UBL, Brest, France. pierre.tandeo@imt-atlantique.fr

1. Introduction

Estuaries are areas with high ecological and economic stakes. Characterized by the mixing of fluvial and marine waters, they are complex ecosystems with a high spatio-temporal variability. They play a key role in the life cycle of many species: they host different habitats (including shallow open areas, salt marshes, tidal flat, oyster reefs, seagrass beds...) and are important feeding, spawning and nursery grounds. Estuaries also host significant anthropic activities, such as shipping and fishing, and are affected by urbanisation and industrialisation. Within a sustainable development approach and the context of climate change, long-term predictions of estuaries morphology and sediment composition under different forcing conditions (natural and anthropic) would be a valuable decision-making tools for coastal area management. While process-based sediment dynamics models can provide relevant information, they are extremely computationally expensive to predict long-term evolutions. Besides, the development of improved measurement techniques, like LIDAR or hyperspectral grants access to large amounts of topographic and bathymetric data with a very high spatial resolution (of the order of magnitude of meters), which paves the way to new data-based modelling methods under the heading of machine learning. Indeed, machine learning covers algorithms used to develop predictive relationships using a set of input data (Goldstein et al., 2018).

The overarching idea is to predict the geomorphology of estuaries at century scale using increasingly available historical topographic and bathymetric data (e.g. 30 years of data for the Seine estuary) with machine learning approaches. In addition, the open access to worldwide data will undoubtedly improve the learning and lead to more accurate predictions.

2. Approach

With this goal in mind, a first objective has been set to test the feasibility of the approach. Here, instead of in situ topographic-bathymetric data, we used model-based maps. A set of 150 topographic-bathymetric maps was generated using a hydro-sediment process-based model (MARS-3D numerical model of coastal hydrodynamics (Lazure and Dumas, 2008) and its sediment module MUSTANG (Le Hir et al., 2011)) computed under different forcing conditions (tidal range, river flow and upstream sediment concentration). The model configuration is an idealized muddy estuary. The final bathymetries issued from 150 runs performed over 100 years (using the Morphological Acceleration Factor (MORFAC) approach (Roelvink, 2006)) for which the forcing are taken uniform, provide the data set (see Figure 1) to build a data-driven prediction method for this idealized estuary. After the analysis of the different 100-year bathymetries according to the different forcing, a Support Vector Machine algorithm is implemented to study the relationship between the estuary geomorphology and the environmental variables.

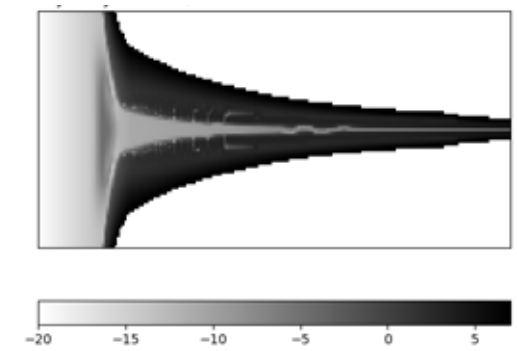

Figure 1: Bathymetry (in m) after 100 years subject to semi-diurnal tide (tidal range 4m), river flow about $600 m^3/s$ and with an upstream mud concentration of $0.1 kg/m^3$

3. Conclusions

Using statistical tools, we inferred some relationship between forcing, morphological changes and estuary typology. The application of the Support Vector Machine method gives promising results, allowing to predict the main morphological trends. Moreover recent advances in deep learning machine learning algorithms open up some interesting paths for this issue. Thus, the use of conditional Generative Adversarial Net (Huang et al., 2018) could enable to predict the snapshot of the bathymetry of whatever estuary in 100 years according to the environmental forcing.

References

Huang, H., Yu, P. S., and Wang, C. (2018). An introduction to image synthesis with generative adversarial nets. *arXiv preprint arXiv:1803.04469*.

Goldstein, E. B., G. Coco, and N.G. Plant. (2018) A Review of Machine Learning Applications to Coastal Sediment Transport and Morphodynamics. *in revision at Earth Science Reviews, available as an EarthArXiv Preprint*, https://dx.doi.org/10.31223/osf.io/cgzvs

Lazure, P. and Dumas, F. (2008). An external-internal mode coupling for 3D hydrodynamical model for applications at regional scale (MARS). *Adv. Water Resssour.*, 31, 233-250.

Le Hir, P., Cayocca, F. and Waeles, B. (2011). Dynamics of sand and mud mixtures: a multiprocess-based modelling strategy. *Continental Shelf Research*, 31, 134-149.

Roelvink, J. A. (2006). Coastal morphodynamic evolution techniques. *Coastal Engineering*, 53(2), 277-287.

A General Lagrangian Tracking Methodology for Riverine Flow and Transport

J.M. Nelson[1], Y. Shimizu[2], T. Kyuka[2], and S. R. Charlton[1]

[1] U.S. Geological Survey Geomorphology and Sediment Transport Laboratory, Golden, Colorado USA. jmn@usgs.gov
[2] Hokkaido University Department of Civil Engineering, Sapporo, Japan. yasu@eng.hokudai.ac.jp

1. Introduction

Most problems in rivers requiring computational solutions are treated using Eulerian methods, in which the primary objective is to predict flow characteristics at each point in the flow. However, there are many riverine problems that benefit from the use of Lagrangian methods that track specific information through the flow field. For example, pollutant dispersal is a commonly desired prediction that requires tracking some constituent through the flow field to understand where the material goes and how long it stays in various regions. Similarly, the passive movement of biological agents like drifting fish nutrients or larvae as a function of source areas and other characteristics is best treated in a Lagrangian framework. To treat these problems, we developed a completely new Lagrangian particle-tracking code that incorporates both advection and dispersion by turbulence or other unresolved details of the flow field. Unlike previous efforts, our method is flow solver independent, works for one, two, and three-dimensional applications, and has a unique particle cloning technique that allows high spatial resolution without high computational expense.

2. Model Development

The basis of the approach follows standard methods in that it combines advection by the flow with a dispersion calculation formulated as a random walk. Thus, given some population of particles in a known flow field, the position **r** of each particle a small time step, Δt, in the future can be written as:

$$\mathbf{r}(t+\Delta t) = \mathbf{r}(t) + \mathbf{u}(\Delta t) + \mathbf{L}\sqrt{2\mathbf{K}\Delta t} \qquad (1)$$

where **u** is the vector velocity, K is the (presumed isotropic) diffusivity taken from the flow model, and **L** is a vector, each component of which is randomly chosen from a Gaussian distribution with a mean of zero and a standard deviation of one. This equation represents passive movement of a particle through a turbulent flow; if the particle has some active behavior, such as swimming or maintaining position at a certain depth, an active component of velocity or position can be added to this equation. If the flow model yields anisotropic diffusivities, the last term in Equation (1) can be replaced using a direction-dependent diffusivity.

This method is well known, and we have used it before (e.g., Nelson et al, 2018). However, in the current approach, the algorithm is built as a solver in the iRIC public-domain suite of flow and morphodynamics models (Nelson et al, 2016), and can be applied with various iRIC solvers. We also include user-selected treatments for particle-boundary interactions, complete treatment of vertical velocities in 3-dimensional flow fields, user-specified active particle behavior, and particle cloning.

In past work, computations of concentration and residence times in important storage areas, like lateral separation zones, has been well treated only by using very large particle populations, which leads to high computational demand. We circumvent this issue with particle cloning, in which an individual particle splits into a group of n particles, each of which has 1/n of the weighting of the original particle. Users can specify the cloning process either spatially by selecting polygonal high-resolution areas or by particle density thresholds that can include several levels to allow recursive cloning. This provides very high resolution where particles may be sparse (but spend more time) such as near banks and in areas of flow separation. The method gives similar spatial resolution in these areas but requires a much smaller number of tracked particles, thus replacing brute force computation with an elegant recursive solution.

Figure 1: Instantaneous particle distribution for a continuous upstream line source in the Ishikari River.

3. Application and Conclusions

Figure 1 shows a simple application of the particle-tracking approach for the Ishikari River upstream of Sapporo, Japan using the Nays2dh two-dimensional flow solver in iRIC with a continuous upstream line source. Our presentation includes several such examples illustrating the utility of the approach for surface and bed larval drift, well-mixed pollutant dispersal, oil dispersal, and sediment movement. The method is freely available in the iRIC software found at www.i-ric.org.

References

Nelson, J.M., McDonald, R.R., Legleiter, C.L., Kinzel, P.J., Terrell-Ramos, T., Higashi, Y., Seo, I.W., Baek, D., Lee, D. H., Ryu, Y., 2018, New methods for predicting and measuring dispersion in rivers, Proceedings of River Flow 2018, Lyon, France, 8 p.

Nelson, J.M., Shimizu, Y., Abe, T., Asahi, K., Gamou, M., Inoue, T., Iwasaki, T., Kakinuma, T., Kawamura, S., Kimura, I., Kyuka, T., McDonald, R.R., Nabi, M., Nakatsugawa, M., Simoes, F., Takebayashi, H., and Watanabe, Y., 2016, The international river interface cooperative: Public domain flow and morphodynamics software for education and applications, Advances in Water Resources, 93, p. 62-74.

Revisiting Flocculation Dynamics

R. Fernández[1], A.J. Manning[2], and D. Parsons[3]

[1] Energy and Environment Institute, University of Hull, Hull, United Kingdom. R.Fernandez@hull.ac.uk
[2] Energy and Environment Institute, University of Hull, Hull, United Kingdom; HR Wallingford, Coasts & Oceans Group, Wallingford, United Kingdom, andymanning@yahoo.com
[3] Energy and Environment Institute, University of Hull, Hull, United Kingdom. D.Parsons@hull.ac.uk

1. Introduction

Flocculation of cohesive sediments occurs in both natural and engineered environments, and is affected by biotic and abiotic factors alike (e.g. Mehta, 2013; Partheniades, 2009). Initial studies on fine sediment dynamics conducted at the University of California, Berkeley last century (see R. Krone, H.A. Einstein; in Mehta et al., 2014 for details), were mostly based on samples extracted from the San Francisco Bay area (Garcia, 2008) and to this day, the vast majority of studies have also focused on sediment extracted from specific sites.

Our goal is to revisit the issue of flocculation following a systematic approach, and extend it to include related issues that have received little or no attention in the past, including the impact of clay type, the effect of ocean acidification (increasing pH), and the role of micro-plastics in flocculation dynamics. This contribution describes our proposed methodology (introduced below) and our research hypotheses.

2. Objectives and Proposed Methodology

Our systematic approach studies the flocculation dynamics of three different clay minerals, namely, kaolinite, illite, and montmorillonite.

The first objective of the study is to quantify the shear stresses in a mixing jar over a shaker in the laboratory, to guarantee that the clay minerals are subjected to realistic shear rates commonly observed in natural environments.

Initial tests are conducted with deionized water defining the simplest baseline scenario. Following this the concentrations of minerals, and salinity, will be systematic increased to assess how the flow and flocculation dynamics and characteristics change based on deionised water conditions. The experiments are repeated but with a different water pH to assess the effect of ocean acidification on flocculation dynamics.

To determine the floc characteristics, samples are extracted from the shaker with a pipette and with negligible transferal interference, allowed to settle in the LabSFLOC settling column. Settling velocities and floc characteristics are measured with image processing techniques. Figure 1a shows the LabSFLOC equipment (e.g. Manning, 2006; Manning et al., 2007, 2017) used to measure the floc settling velocities and Figure 1b shows an image of settling particles acquired with it.

3. Expected Outcomes

The expected outcomes from our proposed systematic approach are:

- Quantification of settling velocities. It is hypothesised that the three different clay minerals will be different. Montmorillonite, having the largest cation exchange capacity, will form the largest flocs, thus settling faster.
- Settling velocities will change with different ambient water conditions. It has been shown that increased salinity leads to increased floc sizes. However, above 10 ppt, salinity no longer plays a role in the size of the flocs.
- Low turbulence in the mixing jar will lead to floc aggregation, whereas high turbulence will limit the size of the flocs.
- Higher pH values in the mixing jar will lead to larger and stronger flocs. Settling velocities will be faster than under baseline pH conditions.

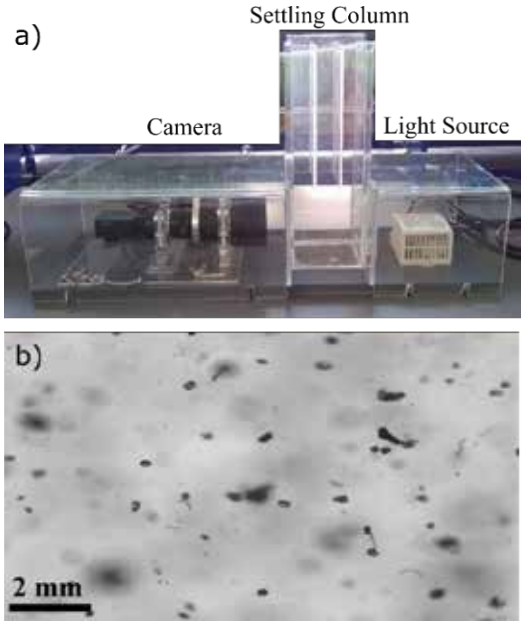

Figure 1: a) LabSFLOC Settling column and camera; b) Image acquired with equipment.

References

Garcia, M.H. (2008) ASCE Manual of Practice 110 - Sedimentation Engineering: Processes, Measurements, Modeling, and Practice. 1155pp.

Manning, A.J. (2006). LabSFLOC – A laboratory system to determine the spectral characteristics of flocculating cohesive sediments. HR Wallingford Tech. Report, TR 156.

Manning, A.J., Friend, P.L., Prowse, N. and Amos, C.L. (2007). Preliminary Findings from a Study of Medway Estuary (UK) Natural Mud Floc Properties Using a Laboratory Mini-flume and the LabSFLOC system. *Cont.Shelf Res.*, doi:10.1016/j.csr.2006.04.011.

Manning, A.J., Whitehouse, R.J.S. and Uncles, R.J. (2017). Suspended particulate matter: the measurements of flocs. In: R.J. Uncles and S. Mitchell (Eds), ECSA practical handbooks on survey and analysis methods: Estuarine and coastal hydrography and sedimentology, Chapter 8, pp. 211-260, Pub. Cambridge University Press, DOI: 10.1017/9781139644426.

Mehta, A.J. (2014) An Introduction to the Hydraulics of Fine Sediment Transport. World Scientific Publishing Co. USA. 1038pp.

Mehta, A.J., Manning, A.J. and Khare, Y.P. (2014). A Note on the Krone deposition equation and significance of floc aggregation. *Mar. Geology*, 354, 34-39, doi.org/10.1016/j.margeo.2014.04.002.

Partheniades, E. (2009) Cohesive Sediments in Open Channel Flows. Elsevier. 358pp.

Wave-induced scour around a complex pier foundation

M. Qi[1], P. Shi[2]

[1] School of Civil Engineering, Beijing Jiaotong University, Beijing, P. R. China. mlqi@bjtu.edu.cn
[2] Shanghai Municipal Engineering Design Institute (Group) CO., LTD. Shanghai, P.R.China. shipochen@smedi.com

1. Introduction

A complex structure, a pile group on top of which a pile cap and a column (or pier) are superimposed, hereafter called PCP for short, is commonly used as foundation of bridge or marine structures. Wave-induced seabed scour around PCP possibly leads the structure to be vulnerable. Most of the previous studies concerned wave scour with a monopile (Larsen, et al., 2017; Qi, et al., 2015; Tonkin, et al., 2003) or a pile group (Ahmad, et al., 2018). However, the pile cap of the PCP element touching wave surface alters the wave flow regime, which therefore increases seabed scour depth around the PCP structure. Other scholars studied the scour around PCP under current by experiments. This work focused on solitary wave-induced scour at complex piers located on a sloped beach. Comparisons were conducted for the scour depth and flow structure between piles with and without the superior pile cap and pier. The effects of the parameters related to the pile cap and wave's characteristics on the scour depth were analyzed.

2. Methods

Numerical simulation method was used to modeling wave generation, propagation, and bed scouring at PCP mounted vertically on a sloping beach. The unsteady Reynolds-Averaged Navier-Stokes (RANS) equations coupling with k-ε, sediment transport including bedload and suspended load, and morphological (e.g., Exner formula) equations were solved. Wave free surface was captured with volume of fraction at air-water interaction surface. The models were firstly validated under the same computational setup and conditions with that of the experiments conducted by Tonkin, et al. (2003). Solitary wave generation and propagation was tested by the theoretical resolution.

3. Results

The model was used to simulate the wave-induced scour at PCP and 2 piles side-by-side under the following conditions: the ratio of wave height and water depth is 0.3; the KC number is 6.0; the pile spacing, G, is 1.5D

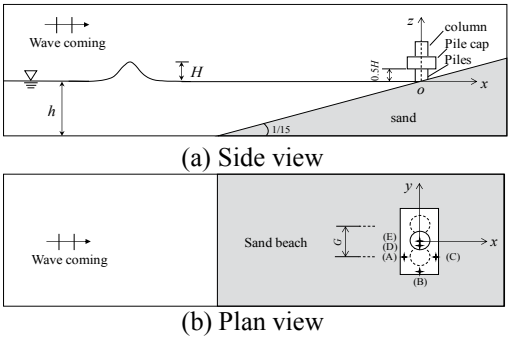

Figure 1: Sketch of the simulation domain and structure arrangement.

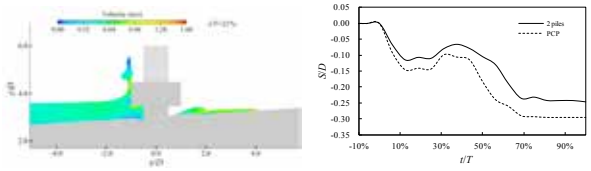

Figure 2: Wave flow pattern at PCP wave flow pattern at the moment of t/T =21% (a) and scour depth variation with time at point A for PCP comparing with 2 piles side-by side (b).

(the pile diameter); and the sand diameter is 0.35 mm. The configuration of PCP and the calculation setup are shown in Figure 1. When the wave propagates to the beach and approaches the structure, the flow pattern is disturbed more dramatically by the PCP than that by the 2 piles without cap. Therefore, larger shear stress on bed and scour depth appear for PCP than that for 2 piles only, as shown in Figure 2, in which t is the time, T is the period of time from wave climbing up the sloped beach to flowing down, S is the maximum scour depth around structure. The relatively maximum difference of scour depth caused by one solitary wave between the two structures reaches almost to 26%. Fast scouring occurs in the duration of t/T = 40% to 70% when the wave runs down the sloped beach.

4. Conclusions

Scour depth at complex structure with pile cap mounted on a sloped beach is larger than that without the cap by solitary wave. When the wave runs down the sloped beach, faster scouring experiences. It is the pile cap that intensifies the wave's hydrodynamic effect on bed shear stress around the structure, which therefore increases the bed erosion or scour depth. Multiple solitary waves certainly increase larger scour depth beyond this work.

Acknowledgments

This research was financially supported by the National Natural Science Foundation of China [Grant No. 51578062].

References

Ahmad, N., Bihs, H., Myrhaug, D., et al. Three-dimensional numerical modelling of wave-induced scour around piles in a side-by-side arrangement. (2018). *Coastal Eng.*, 138(2018): 132-151.

Larsen, B.E., Fuhrman, D.R., Baykal, C., et al. (2017). Tsunami-induced scour around monopile foundations. *Coastal Eng.*, 129(2017):36-49.

Qi, M., Li, J. and Kuai, Y. (2015). Solitary wave scour around a cylinder in shoaling conditions. *J. Hydraul. Eng.*, 46(7):783-791 (in chinese).

Tonkin, S., yeh, H., Kato, F., et al. (2003). Tsunami scour around a cylinder. *J. Fluid Mech.*, (496):165-192.

Offshore Wave Climate and River Mouth Bypassing affect the Avulsion Timescale of River Deltas

Weilun Gao[1], Jaap Nienhuis[2], William Nardin[3], Zheng Bing Wang[4] and Dongdong Shao[1]

[1] State Key Laboratory of Water Environment Simulation & School of Environment, Beijing Normal University, Beijing, China. wl.gao@mail.bnu.edu.cn, ddshao@bnu.edu.cn
[2] School of Geosciences, Utrecht University, Utrecht, the Netherlands, j.h.nienhuis@uu.nl
[3] Horn Point Laboratory, University of Maryland Center for Environmental Science, Cambridge, MD, USA. wnardin@umces.edu
[4] Faculty of Civil Engineering and Geosciences, Delft University of Technology & Deltares, Delft, the Netherlands zheng.wang@deltares.nl

1. Introduction

Deltaic channel avulsion controls the abandonment and creation of delta lobes, and thus plays an important role in predicting delta evolution. Swenson (2005) showed that the removal of sediment from the river mouth due to wave energy reduces the seaward progradation and aggradation rate of a deltaic channel and thus increases the avulsion timescale. However, sediment accumulation at the river mouth and hence the progradation of deltaic channels in wave-influenced deltas are affected by the directional wave climate and alongshore sediment bypassing of the river mouth.

Among those factors, sediment bypassing at river mouth correlates negatively with river flow jet momentum and fluvial sediment input and positively with wave momentum (Nienhuis et al., 2016), such that high and low sediment bypassing tend to occur during periods of low and high flows, respectively.

To better quantify the effect of waves on the avulsion timescale of deltaic channels, a coupled model of channel avulsion and coastline dynamics was developed in this study, which considers the distribution of wave-angle and time-varying sediment bypassing. The interaction between wave climate, sediment accumulation at the river mouth, and avulsion timescales of deltaic channels was explored using this coupled model.

2. Methodology

The coupled avulsion model developed in this study consists of two modules: (1) the module simulating the evolution of the shoreline under waves; and (2) the module for the evolution of the profile of the deltaic channel. The Coastline Evolution Model (CEM) is adopted in this study to simulate the evolution of the shoreline under waves. We consider channel orientation and time-varying sediment bypassing in the model. The Deltaic Channel Profile Model (DCPM) is developed by solving the 1-D non-uniform shallow water flow equations, Engelund and Hansen's formula and Exner equation.

River discharge is schematized as pulse waves (Figure 1). A set of high flows and low flows together with constant wave heights and wave periods is adopted in this study, resulting in different combinations of sediment bypassing during periods of high and low flows.

Sediment accumulation and evacuation at the river mouth during periods of high and low flow is calculated to show the relative strength between blocking of sediment during periods of high flow and adjustment of sediment distribution during periods of low flow and illustrate how wave-angle distribution and time-varying sediment bypassing control the progradation of deltaic channels.

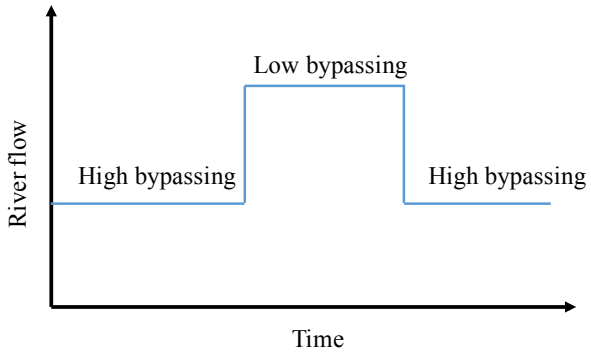

Figure 1. Schematic of river discharges adopted in DCPM.

3. Conclusions

The progradation of deltaic channels depends on the cumulative effects of wave-angle distribution and time-varying sediment bypassing at the river mouth, which is found to significantly affect the avulsion timescale of deltaic channels. Improved understanding of the effects of waves on the progradation of deltaic channel helps to quantify avulsion timescales.

Acknowledgments

This work was supported by the Key Project of National Natural Science Foundation of China (grant 51639001), the Joint Funds of the National Natural Science Foundation of China (grant U1806217) and the Interdisciplinary Research Funds of Beijing Normal University.

References

Nienhuis, J. H., Ashton, A. D., Nardin, W., Fagherazzi, S. and Giosan, L. (2016). Alongshore sediment bypassing as a control on river mouth morphodynamics. *Journal of Geophysical Research: Earth Surface*, 121(4): 664-683.

Swenson, J. B. (2005). Relative importance of fluvial input and wave energy in controlling the timescale for distributary-channel avulsion. *Geophysical Research Letters*, 32(23).

Achieving large-scale braided-river training by porcupine fields

C.J. Sloff[1], and F. Schuurman[2]

[1] Deltares and Delft University of Technology, Delft, Netherlands. kees.sloff@deltares.nl
[2] Royal HaskoningDHV, Amersfoort, Netherlands. filip.schuurman@rhdhv.com

1. Introduction

For a century various cost-effective approaches have been developed for training large braided sand-bed rivers. Most promising and sustainable has been a blend of more or less 'fixed' or 'stable' points, and flexible adaptive measures that are used to guide and direct channels to a desired path. The measures need to be designed in such a way that they do not resist natural processes, but instead use and enhance the natural forces of flow and sediment transport.

Following this approach, to improve navigability in the Ayeyarwady River in Myanmar, it has been proposed to place fields of 'porcupines' in major secondary channels. This needs to prevent avulsion of the main channel to these secondary channels. Porcupines are permeable frames made of wooden or concrete bars, mostly in a tetrahedron shape. They impact the flow, and depending on the layout of porcupine groups they are used to reduce velocity (provide roughness), enhance sedimentation, and force flow away from eroding river banks. Porcupines are not yet applied on large scale and application is limited to only a few locations in the world (e.g., USA, India, Bangladesh), mostly for protecting river banks. The scientific basis of these structures is rather poor, and their performance on modifying large-scale morphology of braiding rivers has not been studied. This study aims to improve the understanding of the effect of these structures on flow and sediment, and develop an approach for modelling their large-scale influence on braided rivers.

2. Laboratory experiments

Laboratory experiments were carried out in a 12 m long, 0.8 m wide flume at the Fluid Mechanics Laboratory of TUDelft by Nientker (2018). Porcupines made of 10 centimetre long brass square beams with a diameter of 7 millimetres were placed on a sand bed with grain size D_{50} = 260 µm, see figure 1.

Figure 1: Flume experiment with porcupines

Experiments with and without sediment have been carried out for a range of submergence and porcupine placement. The results show how the porcupine fields generate trailing vortices and a wake downstream that causes flow retardation over a distance up to 30 times the porcupine height. Deposition occurs even over longer distances. A staggered placement enhances deposition. If porcupines are placed only on one side of the flume, the flow is redistributed, and an alternating-bar pattern develops downstream.

3. Morphodynamic modelling

In the large-scale quasi-3D models used for simulating large braided rivers, the porcupines have to be introduced through sub-grid parametrization. It has been found that the method of Baptist et al (2007) developed for inclusion of vegetation, does approximate the impact of the porcupine field on flow resistance and sediment transport reasonably well. The concept considers the effect of blockage and energy loss by a group of vertical elements (stems of trees or bars of a porcupine). The approach has been tested using the Delft3D software.

4. Application to Ayeyarwady River, Myanmar

In the Ayeyarwady River near Mandalay, the proposed porcupine fields need to be long enough, and cover the full width of the channels. Based on the model, an area of 322,000 m^2 needs to be covered with about 25,000 porcupines with heights of about 2 m. Model results show that that a reduction of the porcupine density has less effect than reducing the area of the porcupine fields. Flood conditions account for flow water depths up to 15 m and velocities up to 1.5 m/s (see Figure 2). The fields are presently constructed (2019).

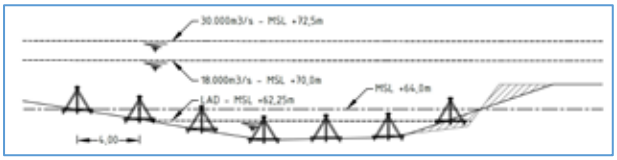

Figure 2: Cross-section placement Sagaing channel

3. Conclusions

Fields of porcupines can be used as flexible and sustainable river-training solutions in braided rivers. This study provides understanding in placement of the porcupines, and methods to predict their impact using large-scale quasi-3D models for braided rivers.

Acknowledgements

Gustav Nientker is acknowledged for his experimental work and analysis. The application for Myanmar is part of the AIRBM project, component 3 (www.airbm.org).

References

Baptist, M., Babovic, V., Rodríguez U, J., Keijzer, M., Uittenbogaard, R., Mynett, A., Verwey, A. (2007). On inducing equations for vegetation resistance. J. Hydr. Res., IAHR, 45(4).

Nientker, G.E. (2018). Porcupines for river training. A study on the near-field effect of porcupines. MSc thesis, Delft University of Technology, Jul 2018.

Effect of Current Velocity on Riverbed Fluctuations based on Long–Term (12 years) Topographic Surveys in a Macrotidal Estuary

K. Somsook[1], G. Azhikodan[2] and K. Yokoyama[3]

[1] Tokyo Metropolitan University, Tokyo, Japan. amp.kirana@gmail.com
[2] Tokyo Metropolitan University, Tokyo, Japan. gubash@gmail.com
[3] Tokyo Metropolitan University, Tokyo, Japan. k-yoko@tmu.ac.jp

1. Introduction

Estuaries are important regions for both humans and animals. In order to protect the high commercial and ecological values of an estuary, it is necessary to understand the long–term changes in bed topography. Many studies have focused on the erosion and deposition dynamic of cohesive sediment in a small scale on short periods. However, the impact of current velocity on riverbed fluctuations on long periods are rarely studied. This study analysed the variation of bed topography for 12 years and the effect of current velocity on change in bed elevation.

2. Study Site

The Chikugo River estuary, Japan is a macrotidal estuary with a tidal range from 1.5 m (neap tide) to 5 m (spring tide). The total length of the river is nearly 143 km and it drains to the Ariake Sea. The salt water intrusion in the estuary reaches until the barrage located 23 km upstream from the river mouth. The bottom sediments in the estuary consist of sand from the river mouth until 8 km, consist of silt and clay in the section from 10 km to 20 km, and consist of sand in the region upstream of 20 km.

3. Methods

The field measurements of the riverbed topography were conducted on every one to four months in the period from 2005 to 2017 at a location 14 km landward from the river mouth using a digital sonar system (Eagle, Fishstrike–2000C). The acoustic transducer, having a frequency of 200 kHz, obtained image data below the water surface including the horizontal positions which were recorded onto a SD card. Water level and the freshwater discharge data were continuously monitored and recorded in hourly interval by Japan government. The mean river bed elevation (MBE) at the middle part of cross section was estimated from the water level data and the raw acoustic image data. The change in bed elevation (Δh) was calculated between two consecutive surveys and the current velocity was computed using Manning's equation.

4. Results and Discussion

The mean freshwater discharge was 54 $m^3 s^{-1}$ during the dry season and the mean annual storm discharge was 2,800 $m^3 s^{-1}$ during the rainy season (Figure 1). During the dry season, MBE was stable with an approximate elevation of –3 m. A rapid decrease in MBE was observed during rainy season. This was caused by the erosion of approximately 1 m thick sediment layer which made the channel deeper for a time span of 1–2 months. Similar fluctuations of mud bed occur every year and it relate to the strong flood discharge which affect to the fluctuations of the current velocity.

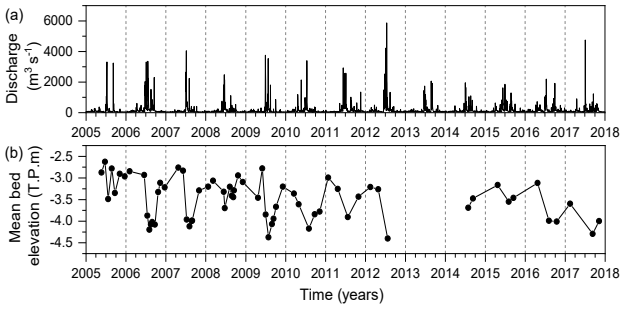

Figure 1: Time series of (a) river discharge and (b) MBE of channel cross section during 2005 to 2017

The effect of current velocity on the riverbed fluctuations for dry and rainy seasons was studied (Figure 2). During the rainy season, primary erosion occurred when the velocity exceeds 0.8 m s^{-1} and Δh was increased with increase in velocity. On the contrary, secondary erosion occurred when the maximum velocity exceeds 1.0 m s^{-1}. Because the riverbed was hard due to the removal of top layer of the deposited sediment by primary erosion. Both erosion and deposition was occurred when the maximum velocity became lower than 0.8 m s^{-1}, especially the deposition occurred even though the velocity was high. This was due to high concentration of suspended sediment and its cohesiveness which resulted the flocculation and thereby accelerated deposition.

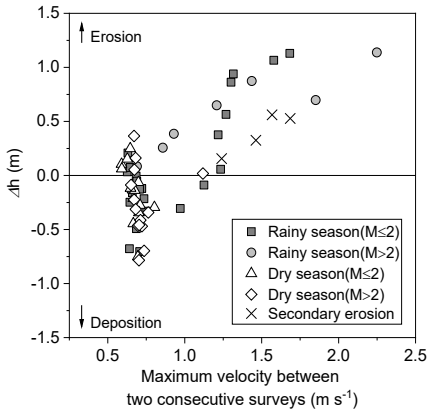

Figure 2: Relationship between change in bed elevation (Δh) and maximum velocity between two consecutive surveys in the period from 2005 to 2017 (M is number of months between two consecutive surveys).

6. Conclusions

The effect of current velocity on bed topography in a macrotidal estuary was studied. Both erosion and deposition occurred during dry season when the velocity was lower than 0.8 m s^{-1}. During the rainy season, erosion occurred when the current velocity exceeds 0.8 m s^{-1}.

Application of Quadtree Mesh to a Finite Volume 2D SWE Scheme

W.J. Syme[1], Dr G.R. Collecutt[3], P. A. Ryan[2]

[1] BMT. bill.syme@bmtglobal.com; [2] BMT. greg.collecutt@bmtglobal.com; [3] BMT. phillip.ryan@bmtglobal.com

1. Introduction

Finite difference schemes are commonly implemented on Cartesian grids with uniform grid-point spacing. The benefits of doing so are simplified math (and therefore faster solution time per cell) and ease of model construction. However, the user is forced into applying the same resolution for the entire model, with sometimes large areas or volumes of the model having a resolution that is significantly smaller than the features of the solution at those locations, in which case the model uses more memory and floating-point operations (FLOPS) than necessary to represent the significant features of the solution. The most common alternative to the uniform Cartesian grid is an arbitrary flexible mesh, typically used with finite volume schemes. Such schemes are more mathematically intensive, but the savings in total memory and FLOPS are very significant. However, a commonly noted drawback of the arbitrary flexible mesh is the effort required to create the mesh. Although the mesh generation is usually mostly automated, the user must still guide the process indicating desired mesh type, resolution and alignment to primary flow paths throughout the domain.

A possible approach that maintains most of the benefits of each of the above approaches is the Quadtree mesh (note that the term Quadtree is specific to 2D domains, with Octree being the equivalent for 3D domains). With this method reduced grid resolution is possible where appropriate, and the associated savings on memory and FLOPS are achieved, but less effort is required on behalf of the user to define the mesh. The paper focuses on the implementation and performance of the TUFLOW HPC scheme (Collecutt and Syme, 2017) on Quadtree meshes.

2. Quadtree rectilinear grid

The concept of recursively dividing rectilinear cells into four sub-cells is not new and has roots in the science of data compression. An example of a Quadtree mesh is shown in Figure 1.

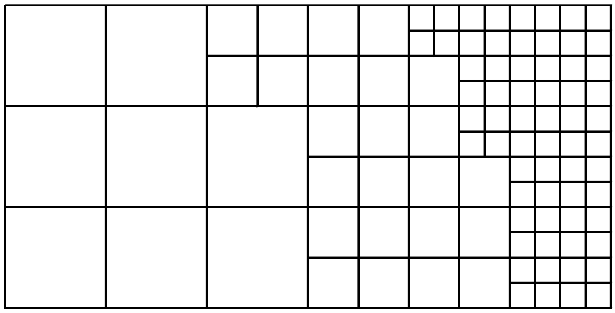

Figure 1: Quadtree mesh

While other division factors are possible, dividing cells into four appears to be the most common. It is possible for a cell to have up to eight neighbouring cells and associated boundary faces across which volume fluxes are computed. Here one of the other advantages of the Quadtree mesh becomes apparent: the cell faces are orthogonal and aligned with the coordinate system, meaning the mathematics is significantly simpler than for an arbitrary mesh. The HPC scheme utilises cell centred mean depth and face centred velocity data, as shown in Figure 2. The black dots represent cell centred mean depth data, the red crosses the face centred u-velocity data, and the green pluses the face centred v-velocity data.

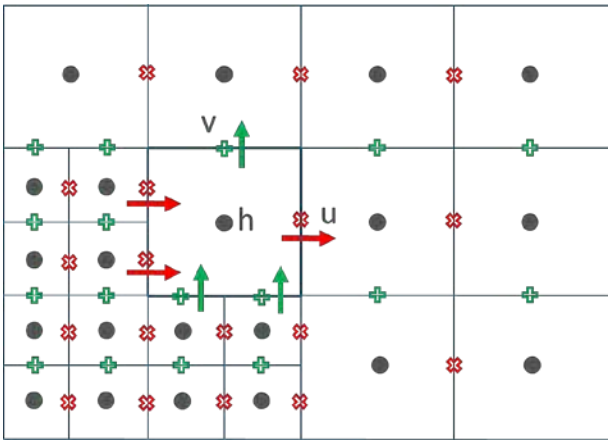

Figure 2: HPC scheme on Quadtree mesh

The main difference in the implementation of the scheme on a Quadtree mesh as opposed to uniform grid is the computation of the water surface gradient across faces that straddle a transition in mesh size: this required the interpolation of water surface elevation to ghost integration points.

The paper presents and discusses: (1) the implementation of the Quadtree mesh within a 2nd order 2D SWE finite volume scheme; and (2) benchmarking to a range of model resolutions and types from flume tests to calibrated real-world models to ascertain the authenticity and pros and cons of the Quadtree approach.

3. Conclusions

The implementation thus far has demonstrated: (1) reduced memory requirements compared to uniform fixed grid; (2) reduced solution times compared to uniform fixed grid; (3) ability to achieve higher spatial resolution where needed; (4) for direct rainfall rain-on-grid models, the ability to better resolve tributary flow and calibrate hydrologic response times; and (5) successful benchmarking to a range of model resolutions and types.

References

Collecutt, G., and Syme, B. (2017). Experimental benchmarking of mesh size and time-step convergence for a 1st and 2nd order SWE finite volume scheme. *Proceedings of the 37th IAHR World Congress, Kuala Lumpur*.

Basic Experiment and Optimum Computational Mesh Size for High Accuracy Analysis of Bank Erosion of Low Water Channel

Ryuji TANAKA[1], Ryosuke Akoh[2] and Shiro MAENO[3]

[1] Wesco Co., Ltd, Okayama, Japan. r-tanaka@wesco.co.jp
[2] Okayama University, Okayama, Japan. akoh@okayama-u.ac.jp
[3] Okayama University, Okayama, Japan. maeno@okayama-u.ac.jp

1. Introduction

In the flow analysis of the rivers, it is difficult to reproduce bank erosion of low water channel with high accuracy because of mesh size restriction due to computational memory size and time consuming.

In this research, model experiments and numerical analyses were conducted aiming to obtain basic data for developing a simulation model using a dynamically moving mesh that tracks bank erosion.

2. Experimental investigation

To clarify bank erosion characteristics along the low water channel with or without flow on the flood channel, model experiments were conducted using experimental channel shown in Fig. 1.

2.1 Experimental condition

The experimental channel is a 14 m long, 0.6 m wide. Its slope is 1/500. The movable bed was installed as shown in Fig. 1. The movable part was filled with silica sand and mean diameter is 0.88 mm.

Case	Discharge	Angle of spur dike	Slope	Uniform flow depth
1-1	6.0 L/s	30°	1/500	5.9 cm
1-2		60°		
2-1	1.5 L/s	30°		2.9 cm
2-2		60°		

Table 1: Model Case.

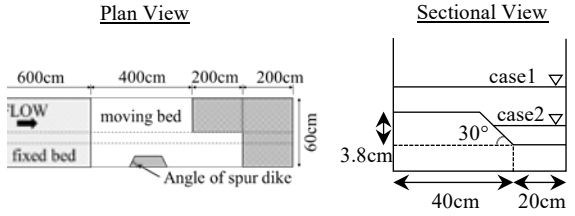

Figure 1: Experimental Channel.

2.2 Experimental Results

Erosion area becomes larger for the submerge case on the flood channel. And the sand on the flood channel was scoured and delivered to the low water channel, eventually the cross sectional slope becomes mild.

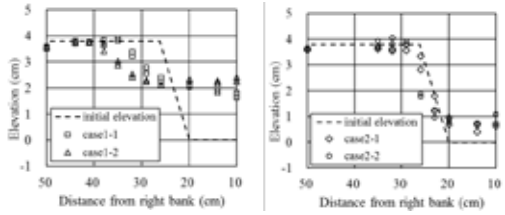

Figure 2: cross-section profile

3. Numerical Analysis

Numerical simulations were conducted using iRIC Nays 2DH. Three different mesh sizes 1.5 cm, 2.5 cm and 5 cm were used in the numerical analysis.

3.1 Result

Fig. 3 shows non-dimensional bed level difference between numerical and experimental values. As the numerical mesh size becomes coarser, numerically obtained elevation difference between flood channel and low water channel differs more than 20% from the experimentally observed values.

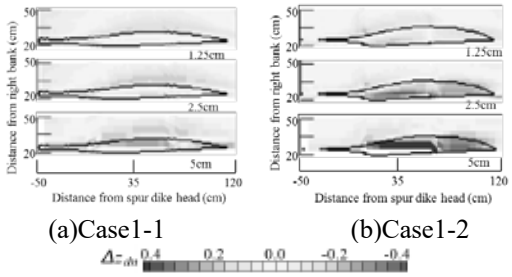

Figure 3: Non-dimensional bed level difference normalized by 3.8 cm. (black line is 35% area of maximum scoured depth in the experiment)

4. Conclusions

In order to reproduce bank erosion with high accuracy, it is necessary to use a small mesh that can resolve riverbanks.

The area requiring a small mesh size for accurate simulation is local to the entire numerical domain, and it is quantitatively confirmed that this area moves with the progress of the bank erosion.

The results obtained by this study contribute to the creation of a dynamic mesh to analyse bank erosion accurately.

References

Yasutaka, H., Shiro, M., Keisuke, Y., Syunsuke, F., and Ryosuke A. (2016). Examination of Physical Environmental Changes After Gravel Bar Restoration Using a Simulation Model with Vegetation Growth and Disappearance. Annual *Journal of Hydraulic Engineering*, Vol.72: 1063-1068.

Nobuhisa, N., Takashi, H., Yoshio, M. and Md. Munsur RAHMAN. (1996). Numerical Analysis of Channel Processes with Bank Erosion by Means of Moving Boundary Fitted Co-ordinate System. *Annual Journal of Hydraulic Engineering*, Vol.40: 927-932.

Masato, S. (2003). Numerical Simulation of Braided River with The Aid of Slope-Collapse Model. Annual Journal of Hydraulic Engineering, Vol.47: 637-642.

iRIC Software, <http://i-ric.org/ja/>.

Two counterintuitive findings on channel bed incision in engineered alluvial rivers

M. Siele[1], A. Blom[2] and E. Viparelli[3]

[1] Delft University of Technology, Delft, the Netherlands, m.s.tewolde@tudelft.nl
[2] Delft University of Technology, Delft, the Netherlands, Astrid.Blom@tudelft.nl
[3]University of South Carolina, Columbia, USA, VIPARELL@cec.sc.edu

1. Introduction

Channel bed incision occurs (1) when a channel, due to changes in the controls, tends towards a smaller equilibrium slope, (2) upstream from a (bend) cut-off, or (3) under conditions of sea level fall. Here we focus on channel bed incision of type 1, and distinguish between two types of changes in the controls: incision caused by changes in domain-wide controls (e.g., domain-wide channel narrowing and an increase of the representative water discharge) and incision caused by changes in the upstream controls (e.g., a decrease of the total sediment supply and a fining of the sediment flux).

2. Method

We make simulations using a one-dimensional numerical research code based on the backwater-Hirano equations. The schematic base case is 100 km long, 300 m wide, and consists of gravel of 16 mm and sand of 1 mm. The water discharge is constant and floodplains are absent.

3. Incision accompanied by surface fining

Channel bed incision is typically assumed to be accompanied by bed surface coarsening. Yet, analysis of the equilibrium states shows that, as the channel width decreases, the equilibrium slope decreases while the bed surface becomes finer (Figure 1a,b). The same holds for a fining of the sediment flux (Figure 1c,d).

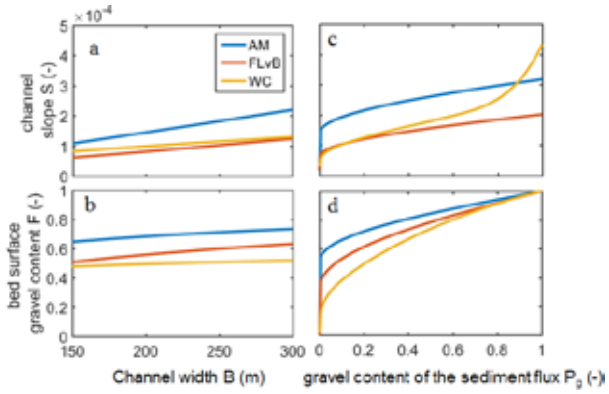

Figure 1: Equilibrium states as a function of changes in (a,b) channel width and (c,d) gravel content of the sediment flux. We use sediment transport relations of Wilcock and Crowe (2003, WC), Fernandez-Luque and Van Beek (1976, FLvB), Ashida and Michiue (1972, AM).

The fact that a finer sediment flux leads to a finer bed surface can be understood: for a finer sediment flux the bed surface does not need to coarsen as strongly to have the sediment transported downstream. The fact that a narrower channel requires a finer bed surface is less trivial: in a narrower channel the equilibrium flow velocity is higher and therefore the bed surface does not need to coarsen as strongly to transport the sediment downstream.

4. Time scale of channel response

The time scale of channel response surprisingly appears to be inversely related to the extent of domain-wide channel narrowing (Figure 2a). This is because the associated increase in sediment transport capacity (which reduces the time scale of channel response) overcompensates the effect of the extent of the change (which increases the time scale). This finding also applies to channel bed incision due to an increase in the representative water discharge. The overcompensating effect is absent in case of changes in upstream controls such as an increase of the fining of sediment flux (Figure 2b).

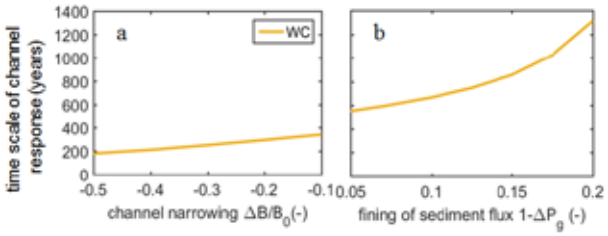

Figure 2: Time scale of channel response for (a) domain-wide narrowing and (b) fining of the sediment flux.

5. Conclusions

Counterintuitively (a) channel incision is not always accompanied by bed surface coarsening and (b) the time scale of channel response decreases with increasing change of the control for changes in domain-wide controls (e.g., domain-wide narrowing or an increase in the representative water discharge).

Acknowledgments

This research is part of project 14508 funded by the Netherlands Organization for Scientific Research (NWO), TTW-Water 2015.

References

Ashida, K. and Michiue, M. (1972). Study on hydraulic resistance and bed-load transport rate in alluvial streams. Trans. Japan Soc. Civil Eng., 206, 59–69.

Fernandez-Luque, R. and R. van Beek, 1976, Erosion and transport of bedload sediment, *J. Hydr. Res.*, 14(2).

Wilcock, P. R., & Crowe, J. C. (2003). Surface-based transport model for mixed-size sediment. J. Hydr. Eng., 129(2), 120–128.

Control of bed erosion at river confluence using piles and a horizontal cylindrical setup

S. T. Kalathil[1], R. N. Jagtap[2] and V. Chandra[3]

[1]Indian Institute of Technology Madras, Chennai, India. tk.sruthi@gmail.com
[2] SECON Private Limited, Bangalore, India. rishinjagtap48@gmail.com
[3]Indian Institute of Technology Madras, Chennai, India.vc@iitm.ac.in

1. Introduction

A river confluence is the coalescence of two different rivers resulting in a complex hydro-morpho dynamic phenomenon (Ali et al., 2019). At the confluence, centrifugal forces lead to the generation of a separation zone near the inner bank, and erosion near the outer bank of the main river. This causes a scour-hole formation at the confluence accompanied by point bar deposition resulting in various problems (Ullah et al., 2015). Several measures have been attempted to control erosion with the use of piles and vanes (Wuppukondur and Chandra, 2017 and 2018). In the present study, the authors tried a horizontal rotating cylinder in combination with pile arrangement to tackle the issue of sediment erosion.

2. Experiments

Physical model study of a mobile bed confluence has been carried out at the Hydraulics Laboratory of Indian Institute of Technology Madras, India. The median diameter d_{50} and geometric standard deviation σ_g of the bed sediment is 0.28 mm and 1.66, respectively. A lateral channel (0.60 m wide) joins with the main channel (0.90 m wide) at a confluence angle of 90^0. A width of 1.20 m, flow depth (d) of 5 cm and a combined discharge of 0.01 m^3/s were maintained at the downstream of the confluence. The discharge ratio (Q_r) between the lateral and main channel discharge is fixed as 0.33. Also, a sediment feed of 0.0083 kg/min is introduced at the upstream of the main channel to generate live bed conditions in the model.

Piles of diameter (ϕ) 8 mm are arranged in a single row perpendicular to the lateral flow intercepting the mixing layer. The piles are tested at different pile spacing (S) such as d, $2d$, and $3d$, respectively at 15 cm downstream of a horizontal cylindrical setup (HCS). The HCS consists of hollow cylinders (18 mm diameter) that rotate along an axial rod. It is stationed at the water surface level ahead of the mixing layer, to alter the flow dynamics at the confluence. Scour depth measurements are collected from a test section of size 130 cm x 140 cm with 10 cm x 10 cm size grids.

2.1 Bed topography

Analysis of bed topography is essential to identify the pattern of scour-holes under different scenarios. The initial bed topography consisted of a large scour-hole concentrated towards the outer bank of the confluence which may lead to intense bank erosion and possible collapse. The aforementioned HCS-pile arrangements were installed in the middle of the confluence in an attempt to mitigate this bank erosion. Based on experimental results, the best arrangement was found with piles spaced at $2d$, and the bed topography is shown in Figure 1. The contour levels of the bed elevation are normalized using their maximum value. The HCS dampens flow velocity at the entrance to the confluence, and the piles undergo sacrificial scouring to protect the banks. The erosion gets restricted to a localized scour-hole around the pile array with a 59.5% reduction in the maximum scour depth. The separation zone near the confluence inner bank also reduces in width due to this arrangement.

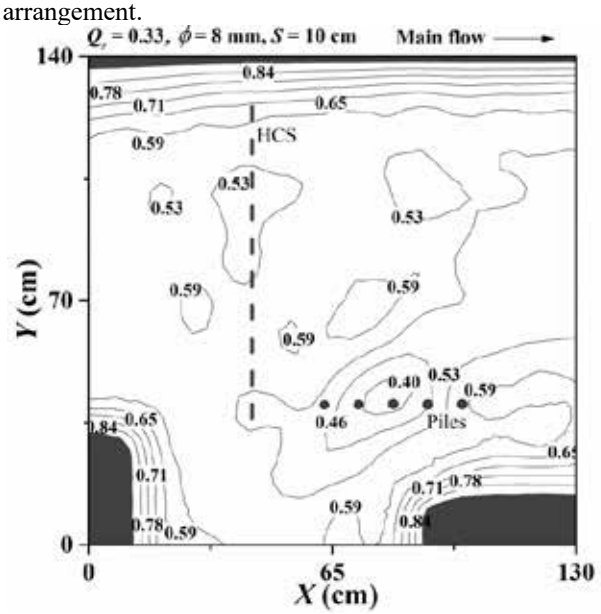

Figure 1: Bed topography of the test section with the best HCS-pile arrangement

3. Conclusions

Sediment control at river confluences is imperative since the eroded sediment gets deposited in the downstream canals and reservoirs reducing the water quality. The addition of a horizontal cylindrical setup improves the performance of piles in reducing the bed erosion at the confluence.

References

Ali, H.L., Yusuf, B., Mohammed T.A. et al. (2019). Improving the hydro-morpho dynamics of a river confluence by using vanes. *Resources*, 8(1), 9.

Ullah, M.S., Bhattacharya, J.P., and Dupre, W.R. (2015). Confluence scours versus incised valleys: Examples from the cretaceous ferron notom delta, Southeastern Utah, USA. *J. Sediment Res.*, 85(5): 445–458.

Wuppukondur, A. and Chandra, V. (2017). Methods to control bed erosion at 90° river confluence: An experimental study. *Int. J. River Basin Manag.*, 15(3): 297–307.

Wuppukondur, A. and Chandra, V. (2018). Control of bed erosion at 60° river confluence using vanes and piles. *Int. J. Civ. Eng.*, 16(6): 619–627.

Sediment supply and surface coarsening in gravel-bed rivers

D. Vázquez-Tarrío[1, 2] and R. Menéndez-Duarte[1, 2]

[1] Department of Geology (University of Oviedo), Oviedo, Spain. vazquezdaniel@uniovi.es; ramenendez@uniovi.es
[2] INDUROT (University of Oviedo), Mieres, Spain.

1. Introduction

Streambed texture in gravel-bed rivers adjusts to the dominant balance between water and sediment supplies. For instance, reductions in sediment feed promote active-channel narrowing, bedload fining and surface coarsening in gravel-bed rivers (GBRs) (Dietrich et al., 1989). Understanding these linkages is a keypoint in river morphodynamics. In this research, we explore this topic using a large dataset of bedload and grain size distribution (GSD) measurements from 49 natural gravel-bed streams compiled from the scientific literature.

2. Surface versus subsurface GSD in GBRs

Surface grain size parameters are coarser than in the subsurface GSD for the compiled data. This situations has been commonly reported in GBRs: surface sediment is very often coarser than the underlying bed material. It is very typical in river-reaches lacking sediment supply (e.g. below dams), but non-degrading GBRs with considerable sediment supplies may also exhibit surface coarsening.

On the one hand, we can consider subsurface GSD as a proxy for the GSD of the average annual bedload, or the average sediment inputs into a given reach. On the other hand, the top of the streambed represents the sediment in direct contact with the flow and actively involved in bedload transport. This points out what the major controls on surface GSD in GBRs are.

3. Controls on surface GSD in GBRs

The grain size of sediment inputs should exert an obvious control on the grain size of surface sediment. In this regard, we observed some statistically significant and moderate correlation between surface and subsurface GSD parameters in the compiled data (R^2~0.3, *p-value* <0.05, *N=49*). However, we also observed a moderately significant and negative power correlation between the surface median size and the ratio between bedload fluxes (q_s) and stream power (ω) at bankfull (R^2 = 0.51; p-value < 0.05, *N=49*).

The previous findings highlight together how surface GSD at a given reach depends on two different constraints: i. the grain size of the sediment inputs into the channel that defines the GSD of the available bed material; and ii. the capacity of the channel to mobilize and export the available bed sediment, which is size-selective.

In order to go further, we performed a multiple regression analysis considering the surface and subsurface median size of GSD (D_{50s} and D_{50ss}, respectively) and the q_s/ω ratio at bankfull, so we could obtain a relation in the following form:

$$D_{50_s} = a \cdot \left(\frac{q_s}{\omega}\right)^b \cdot D_{50_{ss}}^c \quad (1)$$

The multiple linear regression analysis confirmed that both variables were significant in explaining the surface median size (p-values< 0.05), with a negative (b~-0.26) and a positive power dependence (c~0.52) on the q_s/ω ratio and D_{50ss}, respectively (Figure 1). In addition, the q_s/ω ratio is able to explain twice the amount of variance in data explained by D_{50ss}.

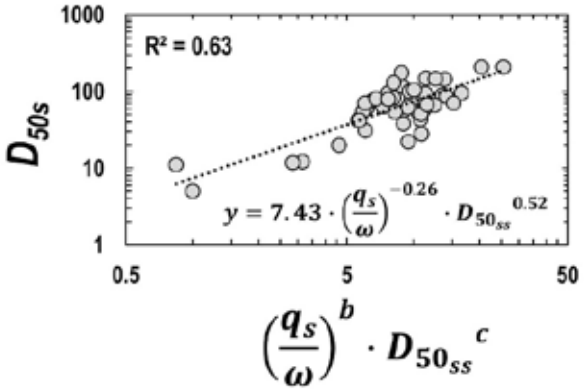

Figure 1: Results from multiple regression analysis.

4. Conclusions

In this research, we re-analyzed a large dataset of bedload and grain size measurements from natural examples. Our analysis highlights:

- GSD of sediment inputs influences the surface GSD of a giver reach: the coarser the subsurface GSD is, the coarser the surface GSD is.
- Surface grain size exhibits a negative dependence on the q_s/ω ratio, suggesting that streambed surface coarsens with decreasing bedload supplies.
- Trends in surface GSD with sediment supply blunt and overimpose the signal in surface grain size linked to subsurface GSD.

In summary, our main outcome is documenting how the balance between sediment yields and transport capacities has a quantifiable reflect on the surface coarsening observed in field data.

Acknowledgments

The present work has been possible thanks to the financial support provided by the grant ACB17-44, cofunded by the post-doctoral 'Clarín' program-FICYT (Government of the Principality of Asturias) and the Marie Curie Cofund.

References

Berni,C., Perret, E. and Camenen, B. (2018). Characteristic time of sediment transport decrease in static armour formation. *Geomorphology*, 317, 1-9.

Dietrich, W.E., Kirchner, J.W.,Ikeda,H. and Iseya, F. (1989). Sediment supply and the development of the coarse surface layer in gravel-bedded rivers. *Nature*, 340, 215–217.

A Theoretical Hydrodynamic Model For Very Shallow Water Stages on the Muddy Flats

Beibei XU[1], Zheng GONG[2], Qian ZHANG[1] and Changkuan ZHANG[1,2]

[1] College of Harbour, Coastal and Offshore Engineering, Hohai University, No.1 Xikang Road, Nanjing 210098, China. bbxu@hhu.edu.cn

[2] Jiangsu Key Laboratory of Coast Ocean Resources Development and Environment Security, Hohai University, No.1 Xikang Road, Nanjing 210098, China. gongzheng@hhu.edu.cn

1. Introduction

Muddy flats are submerged and exposed periodically under the action of tides. At the early stage of flood, tidal flows are very shallow with a water depth in order of 20 cm. During these shallow water stages, velocity and resulting sediment surge have been observed (Zhang *et al.*, 2016). What's more, field observation suggests that very shallow water stages accounted for only 11% of the duration of the entire tidal cycle, but accounted for 35% of the bed-level changes (Shi *et al.*, 2017). However, for large scale flow and sediment simulation, hydrodynamic processes during very shallow water stages is neglected due to a small critical water depth in wet and drying scheme in depth-averaged model (van Rijn, 1993; Hsu *et al.*, 2013). Different from large water depth at which depth the resistance can be neglected, hydraulic resistance, the controlling factor in the propagation of the tide along dry muddy flats, caused by stream bed friction and turbulence dominates the flow during shallow water stages(Dressier, 1952). Therefore, it is of great value to explore hydrodynamic conditions during very shallow water stages.

2. Methods

2.1 Field observations

Field observations were conducted on mudflats of Jiangsu coast (China) during spring tide periods (Dec 23-26, 2015, and July 21-24, 2016). Three typical stations at intertidal zone were chosen(Gong *et al.*, 2017). Water levels, high-resolution near-bed velocities, wave parameters, intratidal bed-level changes and stratified suspended sediment concentration (SSC) were measured simultaneously by a self-designed measuring system (Zhang et al., 2016).

2.2 Theoretical model

The moment and continuity equations used are as follows,

$$\frac{\partial u}{\partial t} + u\frac{\partial u}{\partial x} + g\frac{\partial h}{\partial x} + R\frac{u^2}{h} = 0$$

$$\frac{\partial h}{\partial t} + u\frac{\partial h}{\partial x} + h\frac{\partial u}{\partial x} = 0$$

Where u is depth-average velocity, t is time, x is the distance from the tip of tidal front, h is water depth, R is the Chezy resistance coefficient.

The asymptotic expressions of solutions u and c are as follows (Dressier, 1952),

$$u(x,t,R) \sim \frac{2}{3}\left(\frac{x}{t}+1\right) + U(x,t)R$$

$$c(x,t,R) \sim \frac{1}{3}\left(2-\frac{x}{t}\right) + C(x,t)R$$

3. Outlook

A theoretical hydrodynamic model for shallow water stages is built and utilized to explore the effect of bed roughness, bed slope and the rate of change of water level. The results will be coupled the depth-averaged flow model to resolve the hydrodynamic processes at the early stage of flood with very shallow water depth.

Acknowledgments

We would like to thank Peter Nielsen and Kaili ZHANG for their help in the model. Special thanks to Geng Liang, Jin Chuang, Yan Jiawei, Kun ZHAO and Li Huan for their concerted efforts in the field investigation.

References

Dressier, R.F. (1952). Hydraulic resistance effect upon the Dam-Break functions. *Journal of Research of the National Bureau of Standards*, 49 (3),217-225.

Gong, Z., Jin, C., Zhang, C., Zhou, Z., Zhang, Q. and Li, H. (2017). Temporal and spatial morphological variations along a cross-shore intertidal profile, Jiangsu, China. *Continental Shelf Research*, 144,1-9.

Hsu, T., Chen, S. and Ogston, A.S. (2013). The landward and seaward mechanisms of fine-sediment transport across intertidal flats in the shallow-water region—a numerical investigation. *Continental Shelf Research*, 60, Supplement,S85-S98.

Shi, B., Cooper, J.R., Pratolongo, P.D., Gao, S., Bouma, T.J., Li, G., Li, C., Yang, S.L. and Wang, Y. (2017). Erosion and accretion on a mudflat: The importance of very Shallow-Water effects. *Journal of Geophysical Research: Oceans*.

van Rijn, L.C. (1993). *Principles of Sediment Transport in Rivers, Estuaries and Coastal Seas*: Edition 1993 / L.C. Van Rijn. Morfologie Morf.

Zhang, Q., Gong, Z., Zhang, C., Townend, I., Jin, C. and Li, H. (2016). Velocity and sediment surge: What do we see at times of very shallow water on intertidal mudflats? *Continental Shelf Research*, 113,10-20.

The formation and evolution of the erosional cuspate shape in tidal channels

Kun Zhao[1], Giovanni Coco[2], Zheng Gong[3], Keyu Wang[1], Changkun Zhang[1]

[1] Jiangsu Key Laboratory of Coast Ocean Resources Development and Environment Security, Hohai University, Nanjing 210098, China. zk1357@hhu.edu.cn, keyu_wang97@163.com, zhangck@hhu.edu.cn
[2] School of Environment, University of Auckland, Auckland, New Zealand. g.coco@auckland.ac.nz
[3] State Key Laboratory of Hydrology-Water Resources and Hydraulic Engineering, Hohai University, Nanjing 210098, China. gongzheng@hhu.edu.cn

1. Introduction

Tidal channels are one of the most distinctive features of tidal systems (Perillo, 2009). They are characterised by significant flow-induced bank erosion and consequently gravity-induced bank collapse (Gong et al., 2018). Erosional cuspate shapes, reported by Ginsberg and Perillo (1990), are a common phenomenon along tidal channels, possibly even leading to channel meanders. Although extensive studies have been conducted on the morphodynamic evolution of tidal channels (Xu et al., 2019), few of them attempt to consider bank erosion and collapse from the combined perspectives of geotechnics and soil mechanics, and to investigate the formation and evolution of erosional cuspate shapes in tidal channels. Here, we propose a process-based numerical model, taking into account hydrodynamics, bank erosion and collapse, and sediment dynamics, to explore the effects of bank erosion and collapse on erosional cuspate shapes.

2. Methodology

We build on the Gong et al. (2018)'s bank retreat work to develop a more general morphodynamic model. To trigger erosional cuspate shapes, initial perturbations at one (or two) side of the channel are added by means of changing soil properties (e.g., critical shear stress for bank erosion). Four series of numerical experiments on channel evolution are performed with different distributions of initial perturbations (regular or random), with the value of initial perturbations ranging from 10% to 50% (Table 1).

Run ID	Initial perturbations	One/two side
Run A	none	none
Run B	regular	one
Run C	regular	two
Run D	random	one
Run E	random	two

Table 1: The distribution of initial perturbations added in numerical experiments.

3. Results

As preliminary runs, only flow-induced bank erosion is taken into account. In the context of homogeneous channel bank (Run A), both channel depth and width decrease gradually landward according to the 0/-1m contour line (Fig. 1). Contrary to Run A, several significant erosional cuspate shapes are observed in Run B, as a consequence of regular initial perturbations (50%) added at one side of the channel. The cuspate depth, defined in Fig.1, increases gradually with time and undergoes a landward decrease resulting from the decrease in bed shear stress. As expected, the occurrence of the cuspate shape remarkably changes the topography of the opposite bank of the channel. The existence of cuspate shapes affects flow properties and morphodynamics. For example, the bed shear stress increases along the opposite bank leading to patterns of bank erosion and deposition that almost resemble an incipient meandering channel. Also, at locations neighbouring the ones with a lower critical shear stress, bank erosion decreases.

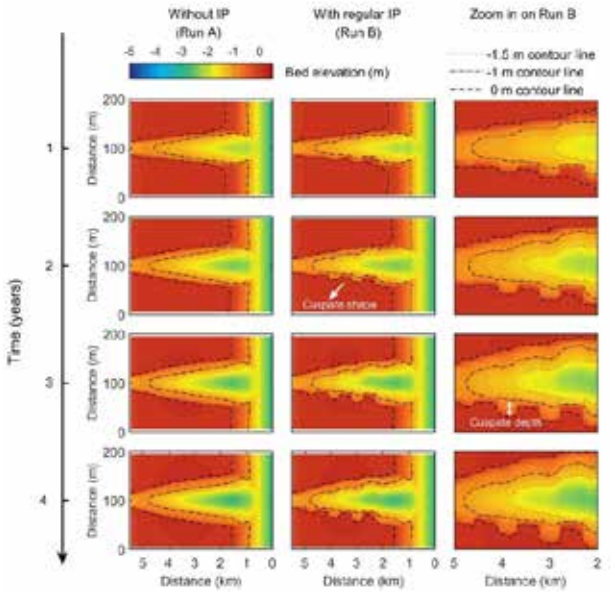

Figure 1. The morphodynamic evolution of the tidal channel and adjacent tidal flats without initial perturbations (IP), with regular IP on one channel bank, and zoom in on Run B, respectively.

Acknowledgments

National Natural Science Foundation of China (No. 51620105005, No. 51879095) and funding from the Graduate Student Innovation Project (No. 2018B638X14) is gratefully acknowledged.

References

Ginsberg, S.S., and Perillo, G.M., 1990, Channel bank recession in the Bahía Blanca estuary, Argentina: Journal of Coastal Research, p. 999-1009.

Gong, Z., Zhao, K., Zhang, C., Dai, W., Coco, G., and Zhou, Z., 2018, The role of bank collapse on tidal creek ontogeny: A novel process-based model for bank retreat: Geomorphology, v. 311, p. 13-26.

Perillo, G.M., 2009, Tidal courses: classification, origin and functionality: Coastal Wetlands: An Integrated Ecosystem Approach. Elsevier, p. 185-209.

Xu, F., Coco, G., Tao, J., Zhou, Z., Zhang, C., Lanzoni, S., and D'Alpaos, A., 2019, On the morphodynamic equilibrium of a short tidal channel: Journal of Geophysical Research: Earth Surface.

Exploring Controls on Barrier Spit Autodecollation

A.D. Ashton[1] and R. Palermo[1,2]

[1] Department of Geology and Geophysics, Woods Hole Oceanographic Institution, Woods Hole, USA. aashton@whoi.edu

[2] Joint Program in Oceanography/Applied Ocean Science and Engineering, Massachusetts Institute of Technology/Woods Hole Oceanographic Institution, Woods Hole, USA. rpalermo@mit.edu

1. Introduction

As spits extend their planform shapes off of eroding headlands, they develop two constitutive parts, the accreting "hook" typically composed of recurved depositional beach ridges and an erosive "neck" that connects the hook to the headland (Figure 1; Ashton et al., 2016). Alongshore transport gradients initially drive erosion of the neck; however, as the spit extends, to maintain a continuous shoreline a growing portion of the spit neck must move landwards by overwash. Here we investigate how limitations (or lack thereof) on onshore overwash fluxes affect spit extension and the stability of the eroding neck shoreline. Our focus is on the criteria for the overwashing neck shoreline to disappear completely—under what conditions do spits cut their own necks off (e.g. autodecollate), creating an island?

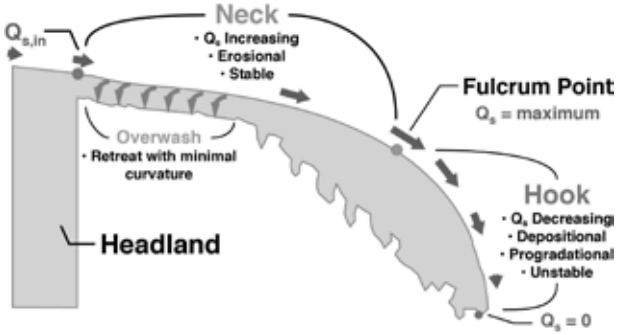

Figure 1: Morphodynamic spit components. After Ashton et al., 2016.

2. Modelling Spit Breakup

Using the Coastline Evolution Model (CEM), which has previously been applied to model the wave climate and headland controls on spit formation (Ashton et al., 2016), we explore how different rates of maximum potential overwash flux affect the stability of the neck shoreline. We do not investigate the effect of tides, focusing on alongshore transport and overwash processes. We find that, as expected, as gradients in alongshore sediment transport begin to erode the neck, if overwash fluxes are too low, the neck shoreline thins and the hook disconnects from the headland shoreline. However, we also find another criteria for shoreline instability, whereby excessive overwash fluxes can cause the neck shoreline to retreat faster than the rest of the spit. In this case, the shoreline is only stable if alongshore transport gradients are strong enough to smooth the retreating shoreline.

These two modes of functional planform breakdown of a a growing spit bear a similarity to previously identified modes of barrier island disappearance, one from insufficient overwash ("height drowning") and one from excessive overwash ("width drowning") (Lorenzo-Trueba and Ashton, 2014). However, in the case of a spit, we identify how local alongshore diffusivity on the neck as well as the rates of headland and neck retreat affect the beheading process. We also make comparisons to both natural spits and locations where sandy islands appear to have been separated from the mainland (in the absence of vigorous tidal flows).

3. Conclusions

Previous modelling studies have suggested that the shaping of spits as they grow off of a headland is continuous—spits do not attain a steady-state geometry (Ashton et al., 2016). Here, we demonstrate how, for certain overwash and wave climate regimes (and for different headland erosion rates), extension can lead a spit to detach itself from the mainland. This breaching process is of great interest as spit necks are often utilized as corridors for transportation and infrastructure to the larger hook region. These corridors may be subjected to more rapid overwash as sea levels rise, which could separate hooks from the mainland. Furthermore, this process of autodecollation provides a means whereby spits transform to barrier islands even in the absence of inlet breaching, adding a twist to a long-hypothesized mechanism of barrier formation.

Acknowledgments

This research has been supported by NSF grants EAR-1424728 and EAR-1518503.

References

Ashton, A.D. and Lorenzo-Trueba, J. (2018). Morphodynamics of Barrier Response to Sea-level Rise. In Moore, L.J. and Murray, A.B., editors, *Barrier Dynamics and Response to Changing Climate* Springer: pp 277-304, https://doi.org/10.1007/978-3-319-68086-6_9.

Ashton, A.D., Niehnuis, J.H., and Ells, K. (2016). On a Neck, On a Spit: Controls on the Shape of Sandy Spits. *Earth Surface Dynamics*, 4, 193-210, doi:10.5194/esurf-4-193-2016.

Lorenzo-Trueba, J., and Ashton, A.D. (2014). Rollover, Drowning, and Discontinuous Retreat: Distinct modes of barrier response to sea-level rise produced by a simple morphodynamic model. *J. Geophys. Res. Earth Surf.*, 119, 779-801, doi:10.1002/2013JF002941.

On the behaviour of a morphologically forced rip current

P.S. Pereira[1], P.S. Lins[2] and C.A.F. Schettini[3]

[1] Federal University of Santa Catarina, Laboratory of Coastal Oceanography, Brazil, pedro.pereira@ufsc.br
[2] Federal University of Pernambuco, Laboratory of Geological Oceanography, Brazil, pedrols.oc@gmail.com
[3] Federal University of Pernambuco, Laboratory of Coastal Hydrodynamics, Brazil, guto.schettini@gmail.com

1. Introduction

Rip currents are part of the surf zone circulation and have been found worldwide on beaches dominated by waves. This common element of the nearshore circulation is essentially forced by the waves and modulated by tides (Dalrymple et al., 2011). However, due to specific beach characteristics several types exist, with the coastal morphology playing an important whole on the rip type (Castelle et al., 2016).

Despite the great occurrence of rips on open ocean sand beaches, rips whose occurrence are related and controlled by morphology, specially by reefs, are no so well documented. In this context, the aim of the present work is to describe the behaviour of a rip current forced by a morphological feature as sandstone reef.

2. Methodology

2.1 Study area

The beach object of this study is Boa Viagem located at the northeast of Brazil in the city of Recife (8°07'05" S and 34°53'36" W). This tide modified tropical beach has several reef lines made by sandstone along its coastline which were formed thousands of years ago during the quaternary period (Fig. 1). Due to gaps in the reef line rip currents occurs as a result of the returning flux.

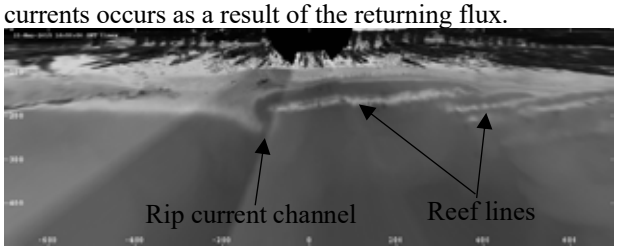

Figure 1: Long exposure mosaic of a strength of Boa Viagem beach, northeast of Brazil.

The wave climate in this area is mostly from SE with the mean wave height between 1-1,5m and a peak wave period from 8 to 9 seconds been generated by the SE trade winds.

2.2 Methods

To achieve the goal of the present work two approaches were used: i) sediment plumes were analysed in to two minutes exposure images captured by a local Argus video station; ii) an experiment during five days was deployed at the surf zone of Boa Viagem. Three ADCPs were deployed in different locations across the surf zone to characterize wave and currents. Also, during the first experiment day, dolls similar to human in size and weight were used as drifters. Each doll had a GPS unit connected with his body providing speed and position.

3. Results

From the video images, it was possible to determine the rip current head position in which the offshore edge position was digitalized. By comparing a set of different images apart by a time span of 2 minutes it was possible do determine the average speed of the sediment plume at the rip.

Over 34 rip currents pulsation events were observed in the images where the permanent rip current is. The average value found for the current speed was 0.21 m/s with the values ranging from a minimum of 0.09 m/s to a maximum of 0.5m/s. The plume edges had different propagation directions with some going towards the southeast (diagonal to the image center) and some towards the south/southwest (alongshore direction).

The data from the ADCP deployed in the rip neck during the experiment had a strong tidal modulation of the cross-shore component toward open waters. Applying an one our average window, the current had a maximum of approximately 0.55m/s during low tide and a minimum of zero at high tide.

From the thirteen drifters launched only one was effectively caught by the rip current while other four had longitudinal flow and the last seven were pushed towards the shore by the incoming waves. The drifter that was caught by the rip presented a circular pattern where it exits the surf zone using the reef and then crossed the reef to get back in to the rip feeder and once again go out. The average circulation speed was 0.24 and 0.48m/s for each one of the circulation event measured which still within the speed range found by video image observations.

4. Conclusions

From the data analyzed in here a morphologically forced rip current has a similar behaviour of those found on open sandy beaches. A cell circulation pattern was observed, even tough was not the main detected pattern. The video images used in here are showing to be a feasible technique to study rip current pulsation. For the present case study at Boa Viagem beach, the rip current average speed was shown to be modulated by the tide, where it can reach a maximum during the low tide and a minimum during high tide periods.

Acknowledgments

The authors would like to thank FACEPE for supporting the deployment of the Argus video station (contract number APQ-1312-1.08/10) and also CNPq for supporting PSL scientific initiation scholarship and the Rip Current Dynamics Project (contract number 484180/2012-6).

References

Castelle, B., Scott, T., Brander, R.W., McCarroll, R.J. (2016). Rip current types, circulation and hazard. *Earth Science Reviews*, 163, 1-21.

Dalrymple, R. A., MacMahan, J.H., Reniers, Ad J.H.M., Nelko, V. (2011). Rip Currents. Annu. Rev. Fluid Mech. 2011. 43:551–81

Optimization theory applied to the modeling of sandy beach dynamics : Validation of the model

M. Cook[1,3], F. Bouchette[1,3] and B. Mohammadi[2,3]

[1] GEOSCIENCES-M, Univ Montpellier, CNRS, Montpellier, France, megan.cook@umontpellier.fr, frederic.bouchette@umontpellier.fr
[2] IMAG, Univ Montpellier, CNRS, Montpellier, France, bijan.mohammadi@umontpellier.fr
[3] GLADYS, Univ Montpellier, CNRS, Le Grau du Roi, France

1. Introduction

Optimization theory is the study of the evolution of a system, while systematically searching for the minimum of a physics-based function. We have applied this approach to coastal dynamics, with our primary objective to simulate the interactions between the waves and the seabed. Describing coastal dynamics using optimization theory has previously been developped by Mohammadi and Bouchette (2014); Isebe et al. (2008); Bouharguane et al. (2010). We have designed an algorithm that describes the evolution of the seabed based on the assumption that the seabed adapts in order to minimize a wave-related function. The aim here is validate our morphodynamic model in a 1D experimental configuration, using the hydro-morphodynamic model Xbeach.

2. Configuration

We applied our morphodynamic model by optimization in an experimental setting, for the purpose of later comparing the simulated and experimental results. The initial seabed and forcing is provided by the COPTER 2D project, an experiment conducted in a 35m long wave flume.

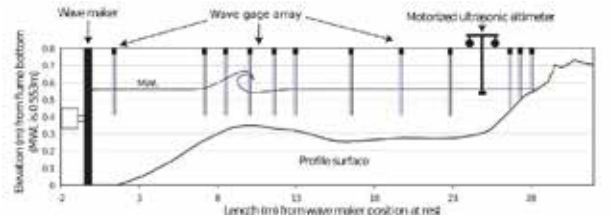

Figure 1. Diagram of the COPTER 2D experiment, including wavemaker, gages and altimeter

Computing the morphodynamic response requires a hydrodynamic model. We have chosen Xbeach (Roelvink et al. (2009)), an open-source hydro-morphodynamic model for the nearshore and coast.

3. Morphodynamic model by wave energy minimization

Our morphodynamic model is based on the assumption that the seabed ψ adapts to the oceans waves by minimizing a certain energy-based function J. The choice of J is debatable and depends on what we consider to be the driving factors behind coastal morphodynamics. We have chosen :

$$J := \frac{1}{8}\int_0^{x_B} \rho_w g H(x)^2 dx \quad [J.m^{-1}] \tag{1}$$

where ρ_w is the density of the water, g is gravitational acceleration and H is the height of the wave provided by the hydrodynamic model Xbeach. The evolution of the seabed ψ_t is given by the following descent method :

$$\psi_t = -\rho\Lambda\vec{d} \tag{2}$$

where ρ is the mobility of the sand, Λ is the impact of the waves on the seabed and the vector $\vec{d}$ is the direction of descent, that is the vector we follow in order to reach the minimum of J. This direction is driven by the vector $\nabla_\psi J$. A certain number of constraints have been included, adding more physics to the morphodynamic model. For example, the slope of the seabed cannot exceed a certain threshold and the waves have more impact on the seabed close to the shore than in deeper waters. These constraints change the way the seabed evolves over time; they modify the direction of descent $\vec{d}$ and the parameter Λ.

4. Validation of the model

In order to validate this model, we compare the results of the simulation with those produced by Xbeach's morphodynamic model. Both models are given the same hydrodynamic data, and comparaisons have been carried out between the two numerical models as well as the results of the experimental simulation. By comparing both models, we wish to establish the potential of morphodynamic modeling by wave energy minimization, bearing in mind that this model has the advantages of being fast, robust and of low complexity.

Acknowledgments

We are grateful to GLADYS for funding associated projects and providing the experimental data. We also thank BRLi and ANRT for funding M. Cook's PhD.

References

Bouharguane, A., Azerad, P., Bouchette, F., Marche, F., and Mohammadi, B. (2010). Low complexity shape optimization and a posteriori high fidelity validation. *Discrete and Continuous Dynamical Systems*, 13. 10.3934/dcdsb.2010.13.759.

Isebe, D., Azerad, P., Mohammadi, B., and Bouchette, F. (2008). Optimal shape design of defense structures for minimizing short wave impact. *Coastal Engineering*, 55. 10.1016/j.coastaleng.2007.06.006.

Mohammadi, B. and Bouchette, F. (2014). Extreme scenarios for the evolution of a soft bed interacting with a fluid using the value at risk of the bed characteristics. *Computers and Fluids*, 89. 10.1016/j.compfluid.2013.10.021.

Roelvink, D., McCall, R., Mehvar, S., Nederhoff, K., and Dastgheib, A. (2009). Modelling storm impacts on beaches, dunes and barrier islands. *Coastal Engineering*, 56. 10.1016/j.coastaleng.2009.08.006.

Direct Rainfall and Traditional Hydrology Aproaches: Case Studies

M Pinto[1], S Lohani[2]

[1] Camden Council, Oran Park, NSW, Australia. maria.pinto@camden.nsw.gov.au
[2] Cardno Pty Ltd (NSW / ACT), Sydney, NSW, Australia. Sabina.lohani@cardno.com.au

1. Introduction

The application of rainfall directly onto the 2D domain is known as Direct Rainfall approach or Rainfall on Grid (RoG). Traditional hydrologic models are lumped rainfall – runoff models. In traditional hydraulic modelling, the inflows are derived from hydrologic models, rather than from direct rainfall. This paper presents the results of four case studies conducted in order to compare RoG and traditional hydrology approaches in flood modelling. These case studies are based on three separate flood modelling undertaken in lower part of Upper Nepean River catchment, at four different locations. The research on RoG hydrology approach is limited even though the method is in use for some years (ARR 2016). The objective of this study is to assess some advantages of RoG hydrology approach in some situations and add to the existing literature on this methodology.

2. Methodology

In each case study, a 1D/2D TUFLOW hydraulic model was used for RoG hydrology approach and traditional hydrology approach. For the latter XP-RAFTS hydrologic model was used. Case studies 1, 2 and 4 were to test the appropriateness of RoG hydrology approach in providing detailed flood data for the entire urbanised catchment, compared to traditional hydrology approach. With traditional hydrology, sub catchment discretisation can be difficult in flat terrain, and case study 3 is such a situation. The resulting flood behaviours from RoG and traditional hydrology approaches in this flat terrain catchment were compared. Both hydraulic models were calibrated, and volume checks were undertaken for all case studies.

3. Results

Case studies 1, 2 and 4 showed that the traditional hydrology approach does not provide flood data upstream of the inflow hydrograph input locations, whereas the RoG approach captures flood data from the furthest upstream point of the catchment. Also due to the different approaches in two methods, the RoG hydrograph approach provided higher flood levels than the traditional hydrology at the inflow hydrograph input locations and lower flood levels at the upstream of the catchments. Case study 3 showed the advantage of RoG hydrology approach, as it is difficult to decide the point of application of upstream inflow hydrograph to the hydraulic model with the traditional hydrology approach. With RoG hydrology approach, no assumptions are made in either inflow hydrograph input locations or catchment delineation as in traditional hydrology.

4. Conclusions

Case studies 1, 2 and 4 showed the appropriateness of RoG hydrology approach in detailed urban flood studies, as it captures flood data from the furthest upstream point of the sub catchment. RoG hydrology approach provides higher flood levels at the inflow hydrograph input locations and lower flood levels at upstream of the catchments, due to flow distribution and timing of surface runoff movement. Case study 3 showed that the location selected to apply discrete catchment inflows can significantly influence the hydraulic model results. With RoG hydrology, flow movement is determined by 2D terrain topography and hydraulic principles. This demonstrates the advantage of ROG hydrology, as no assumptions are required on catchment inflow input locations. However, due to the complications associated with RoG hydrology approach, a series of checks including mass balance, and comparison to traditional modelling techniques and quality assurance procedures are required, if RoG hydrology approach is undertaken.

Acknowledgments

Authors would like to thank S. Mortimer, Cardno for extracting model results and Camden Council staff for reviewing the abstract.

References

Caddis, B. M., Jempson, M. A., Ball, J. E. and Syme, W. J. (2008). Incorporating Hydrology into 2D Hydraulic Models - the Direct Rainfall Approach. *9th National Conference on Hydraulics in Water Engineering: Hydraulics 2008*, pp 57-64, Barton, ACT.

Cardno. (2019). Draft Nepean River Floodplain Risk Management Study & Plan. Interim Report. Internal report prepared for Camden Council, Sydney, Cardno.

Engineers Australia. (2012). Two Dimensional Modelling in Urban and Rural floodplains. *Australian Rainfall & Runoff Revision Project 15*, Stage 1 & 2 Report, Australia.

Johnson, P. (2015). Comparison of Direct Rainfall and Lumped-Conceptual Rainfall Runoff Routing Methods in Tropical North Queensland - A Case Study of Low Drain, Mount Low, Townsville. *2015 Floodplain Management Association National Conference*, Brisbane.

Rehman, H. (2011). Rainfall-on-Grid Modelling – A Decade of Practice. *34th IAHR World Congress: 33rd Hydrology and Water Resources Symposium and 10th Conference on Hydraulics in Water Engineering, June 26-July 1*, pp. 372-379, Australia.

Swan, R and Thomson, R. S. D. (2011). Direct Rainfall – Verifying the Technique Across Two States. *34th IAHR World Congress: 33rd Hydrology and Water Resources Symposium and 10th Conference on Hydraulics in Water Engineering, June 26-July 1*, pp. 3992-3999, Australia.

WorleyParsons. (2015). Nepean River Flood Study, prepared for Camden Council, Sydney, WorleyParsons Pty Ltd.

Headland Influence on Sandbar Migration at an Embayed Beach

Thomas E. Fellowes[1,3], Karin R. Bryan[2,3], Shari L. Gallop[3,1] and Ana Vila-Concejo[4].

[1]Department of Environmental Sciences, Macquarie University, Sydney, Australia. thomas.fellowes@mq.edu.au
[2]Environmental Research Institute, University of Waikato, Hamilton, New Zealand. karin.bryan@waikato.ac.nz
[3]School of Science, University of Waikato, Tauranga, New Zealand. shari.gallop@waikato.ac.nz
[4]School of Geosciences, University of Sydney, Sydney, Australia. ana.vilaconcejo@sydney.edu.au

1. Introduction

Sandbars are sedimentary bodies that characterise the surf zone of wave-dominated beaches (Blossier et al., 2016). Their morphology is commonly used to define morphodynamic beach state and they are an important influence on wave dissipation and surf zone currents (Wright and Short, 1984). On embayed beaches (i.e., beaches with headlands), alongshore sandbar migration is impacted by complex headland–induced processes such as boundary currents, wave shadowing and wave deflection (Castelle and Coco, 2012). Few studies have looked at sandbar migration on wave-dominated embayed beaches to understand how headland control impacts beach morphodynamic states. Additionally, vorticity (i.e., spinning motion) has been used in many studies to describe flow (e.g., rip currents) (MacMahan et al., 2010), but it has never been extracted from changes in sandbar morphology. In this study, we use an approach typically used to study flows to quantify daily sandbar migration and vorticity from video imagery.

2. Study site and methods

Our study location is Bondi Beach (Sydney, Australia), a 950 m-long embayed beach that faces SSE relative to the typical SE swell waves. It has an exposed south and protected north, caused by its asymmetrical headland geometry (McCarroll et al., 2016). Images were collected daily over a 6-year period (2012–2018) and were pre-processed (rectified, rotated and time-merged) to highlight light areas where waves break over the sandbars from dark rip channels (Figure 1a). Timestacks are an image product whereby a line of pixels at a known location (in both x and y domain) is extracted from each daily image and stacked (days, *n=2205*) across the surf zone (timestacks, *n=4633*). Maximum pixel intensity positions in each line are the sandbar location, allowing us to track migration through time. A smoothed curve was fitted, and migration rates were calculated from the curve slope. Sandbar vector directions were defined, and vorticity quantified following MacMahan et al. (2010).

3. Sandbar migration

We show that sandbar migration is directly linked to wave energy, with more movement evident during winter when wave energy is higher than in other seasons. Sandbar migrations were recorded up to 10 m/day but were typically <1 m/day. Two areas were identified, the south area which migrates south (with wave direction) and the north which migrates north (against wave direction) (Figure 1b). Vorticity was observed to be more frequent in the south area spinning sandbars in both directions (clockwise and anticlockwise), whereas in the north area it was less frequent and only clockwise (Figure 1c). Vorticity was shown to increase during reset events.

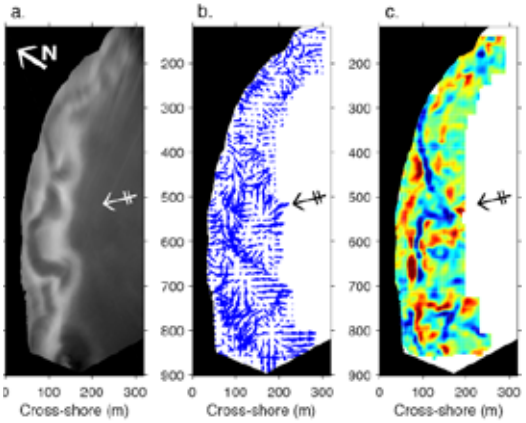

Figure 1: (a) Bondi sandbars (white pixels) with arrows showing typical wave direction, (b) migration, and (c) vorticity clockwise (red) and anti-clockwise (blue).

4. Conclusions

Sandbar migration is driven by wave energy and headland–induced processes. Higher energy equals more sandbar movement, seen in the south area, from a strong headland boundary current and wave deflection. Vorticity increased during reset events, which may indicate it is a component in shifts between beach morphodynamic states. This study provides new insight into sandbar morphodynamics on embayed beaches, highlighting different migration processes and their controls.

Acknowledgments

Camera installed by Rob Brander (UNSW), study funded by the MQRTP and MQPGRF and Re-Entry Fellowship from Women in Science at the University of Sydney.

References

Blossier, B., Bryan, K.R., Daly, C.J., and Winter, C., 2016. Nearshore sandbar rotation at single-barred embayed beaches. *J. Geophys. Res.*, 121, 2286-2313.

Castelle, B., and Coco, G., 2012. The morphodynamics of rip channels on embayed beaches. *Cont. Shelf Res.*, 43, 10-23.

MacMahan, J., Brown, J., Brown, J., Thornton, E., Reniers, A., Stanton, T., Henriquez, M., Gallagher, E., Morrison, J., Austin, M.J., Scott, T.M., and Senechal, N., 2010. Mean Lagrangian flow behavior on an open coast rip-channeled beach: A new perspective. *Marine Geol.*, 268, 1-15.

McCarroll, R.J., Brander, R.W., Turner, I.L., and Van Leeuwen, B., 2016. Shoreface storm morphodynamics and mega-rip evolution at an embayed beach: Bondi Beach, NSW, Australia. *Cont. Shelf Res.,* 116, 74-88.

Wright, L.D., and Short, A.D., 1984. Morphodynamic variability of surf zones and beaches: A synthesis. *Marine Geol.*, 56, 93-118.

Swash zone morpho-sedimentary dynamics on a megatidal mixed sand-gravel beach

T.B. Guest[1], A.E. Hay[1]

[1] Department of Oceanography, Dalhousie University, Halifax, Nova Scotia, Canada. tristan.guest@dal.ca

1. Introduction

Swash zone sediment transport on mixed sand and gravel beaches is complicated by interactions between flow, morphology, and textural properties determined by the grain size distribution (Carter and Orford, 1993; Buscombe and Masselink, 2006). However, few observations of the coevolution of morphology and bed texture exist in the literature. This is due in large part to the difficulty in obtaining sedimentological data with temporal resolution commensurate with timescales of morphological change. Often-energetic shorebreaks capable of entraining gravel- and cobble-sized grains limit the utility of in situ instrumentation, also contributing to the scarcity of observational data. Non-intrusive remote sensing methods provide logistically appealing alternatives. In particular, digital grain sizing techniques allow for the acquisition of grain size distributions with previously unattainable temporal resolution. Field observations are presented of swash zone morpho-sedimentary evolution at a megatidal mixed sand-gravel beach. The principal objective is to investigate linkages between grain size sorting processes and swash zone morphologic change using a combination of video and aero-acoustic sensors for coincident bed level and sedimentological observations, and Lagrangian cobble tracking.

2. Methods

The field site is a steep (1:10 slope), mixed sand-gravel beach in Advocate, Nova Scotia, Canada. Located near the head of the Bay of Fundy, the tidal range at the site ranges from 8-12 m. A longshore array consisting of four pairs of bed-facing ultrasonic range sensors and cameras was deployed during selected high tides over a two week period. The array elements were mounted on a mobile frame and cantilevered over the swash zone. The range sensors provided time series of swash tongue thickness during instances of runup, and beach surface elevation when the bed was exposed. Images captured by the cameras while the bed was exposed were processed with a wavelet-based digital grain sizing algorithm (Buscombe, 2013), providing estimates of mean grain size and sorting at the beach surface, at sampling intervals on the order of the swash period. Video from an overhead camera mounted on a separate frame was used to track the movement of painted gravel- and cobble-sized tracer stones in the swash. Both frames were moved with the incoming and outgoing tide in order to remain positioned over the swash zone.

3. Results

Results from selected tides, all characterized by low energy wave conditions and the formation of a high tide berm, are examined. In general, data from the range sensor and camera array show that bed accretion during berm formation was accompanied by coarsening and poorer sorting of beach surface sediments (Figure 1). Video of tracer cobble movement was collected during high tide and early ebb. During at least one tide, the cobble trajectories indicated net shoreward displacement during and immediately following high tide, while the substrate consisted, wholly or in part, of the coarse berm material. During ebb, seaward fining of the substrate coincided with net cobble displacement that diverged to seaward and landward from the mid-swash zone, having a mean of near zero. Cumulative cobble displacement increased with offshore distance, the greatest mobility being seen where the substrate was fine. Cobble transport occurred predominantly in the cross-shore direction.

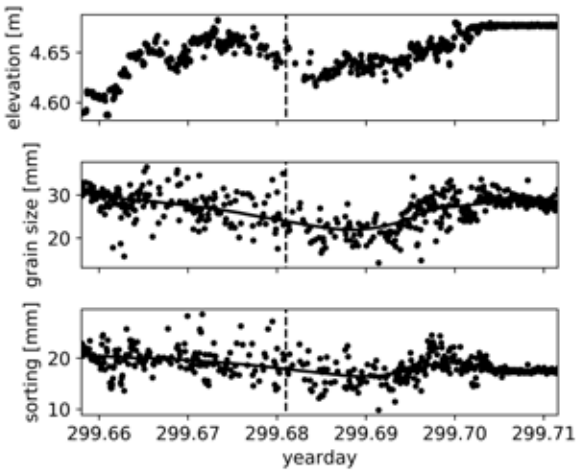

Figure 1. Swash zone bed elevation (upper), mean grain size (middle), and sorting (lower) registered by one range sensor and camera pair during a period of berm evolution. The berm formed beneath the sensors during late flood tide, then migrated shoreward. More material accumulated beneath the sensors during early ebb tide. The dashed black line indicates high tide. Solid black lines are loess regressions of the grain size and sorting data.

References

Buscombe, D. (2013). Transferable wavelet method for grain-size distribution from images of sediment surfaces and thin sections, and other natural granular patterns. *Sedimentology*, 60(7):1709–1732.

Buscombe, D. and Masselink, G. (2006). Concepts in gravel beach dynamics. *Earth-Science Reviews*, 79(1-2):33–52.

Carter, R. and Orford, J. (1993). The morphodynamics of coarse clastic beaches and barriers: a short-and long-term perspective. *Journal of Coastal Research*, pages 158–179.

Nonlinear process-based sand wave model: a comparison with North Sea field observations

G.H.P. Campmans[1], T.A.G.P. van Dijk[2,3], N.R. van der Sleen[4], A. Stolk[4], P.C. Roos[1] and S.J.M.H. Hulscher[1]

[1] Water Engeneering and Management, University of Twente, Enschede, the Netherlands. g.h.p.campmans@utwente.nl
[2] Dept. of Applied Geology and Geophysics, Deltares, Utrecht, the Netherlands
[3] Dept. of Geology, University of Illinois, Urbana-Champaign, USA
[4] Rijkswaterstaat Zee en Delta, Rijswijk, the Netherlands

1. Introduction

Tidal sand waves are rhythmic bed patterns observed in sandy tidally-dominated shallow seas all around the world. They have wavelengths of hundreds of meters, reach heights of several meters and can migrate several meters per year. They interfere with various human activities, such as navigation, construction and maintenance of wind farms and pipelines. Thus knowledge on their behavior is required.

Sand waves have been studied both via observational studies and modeling studies. Recently, Damen et al. (2018) performed a large scale data analysis of sand waves. This resulted in detailed maps of sand wave characteristics in the entire North Sea. Campmans et al. (2018) developed a nonlinear idealized process-based sand wave model that, next to tidal currents, also includes storm-related processes such as wind-driven currents and wind waves.

2. Methodology

In this research the sand wave characteristics in the North Sea (Damen et al., 2018) are compared to model results of the newly developed sand wave model (Campmans et al., 2018). Seven locations are chosen, for which mean water depth, grain size (d50), tidal current amplitudes (M2 and M0) and average surface wave height from the data analysis study are used as model input. For each of the model simulations the same randomly perturbed seabed was used as initial condition on a 4 km long horizontally periodic model domain. The model solves the depth-dependent (2DV) shallow-water equations. Sediment transport is modeled by a bed load formula that accounts for slopes in the seabed. The seabed evolution is modeled via the Exner equation. After 40 years of simulation, the sand wave characteristics; height H, wavelength L and asymmetry A, are compared with those observed by Damen et al. (2018). Here asymmetry is defined as $A = |L_1 - L_2|/L$, where L_1 and L_2 are the lengths from the crest to the troughs on either side.

3. Results

Figure 1 shows the seabed evolution of one of the simulations, and the comparison of observed and modeled sand wave characteristics. For each of the characteristics a least squares fit is drawn through the datapoints. The model quantitatively overpredicts sand wave height, wavelength and asymmetry. Qualitatively the predicted sand wave height shows the best match of the three characteristics. Asymmetry shows a slightly negative correlation. Here it should be noted that direction of asymmetry is correct for each of the simulations, and thus the model has difficulties to predict the magnitude of asymmetry.

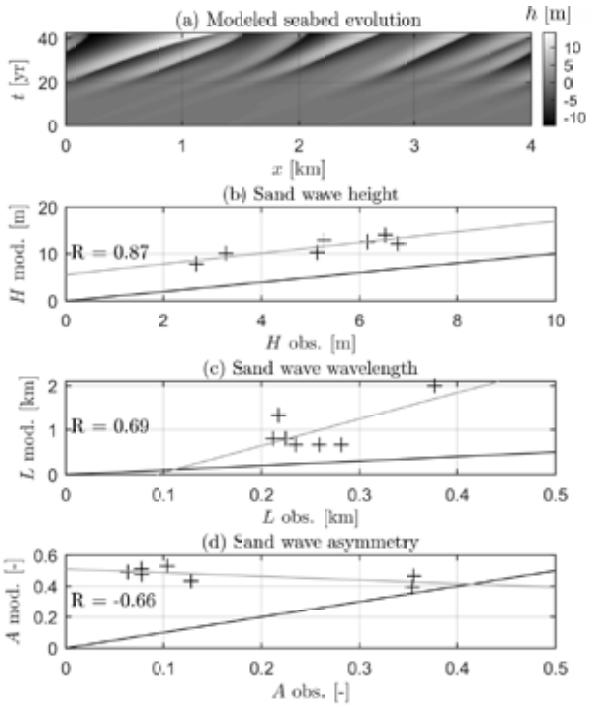

Figure 1. Panel (a) shows the seabed evolution of one of the simulations. The panels (b-d) show observed v.s. modeled characteristics: (b) height, (c) wavelength and (d) asymmetry. The lines indicate a linear fit (grey) and one to one comparison (black).

4. Conclusions

Preliminary results lead to the conclusions that quantitatively the characteristics are overpredicted. However, qualitatively the height (and to a lesser extend wavelength) is correctly modeled.

Acknowledgments

This work is part of the research programme SMARTSEA with project number 13275, which is (partly) financed by the Netherlands Organisation for Scientific Research (NWO).

References

Campmans, G. H. P., Roos, P. C., De Vriend, H. J., and Hulscher, S. J. M. H. (2018). The influence of storms on sand wave evolution: a nonlinear idealized modeling approach. *Journal of Geophysical Research: Earth Surface*, 123(9):2070–2086. doi:/10.1029/2018JF004616.

Damen, J. M., Van Dijk, T. A. G. P., and Hulscher, S. J. M. H. (2018). Spatially varying environmental properties controlling observed sand wave morphology. *Journal of Geophysical Research: Earth Surface*, 123(2):262–280. doi:/10.1002/2017JF004322.

Dune bed-form contribution to flow resistance in sand river

L. Schippa[1]

[1] Department of Engineering, University of Ferrara, Ferrara, Italy. Leonardo.schippa@unife.it

1. Introduction

One of the more relevant feature of alluvial sediment-laden channels concerns flow resistance, which depends on many factors, mainly including grain resistance and form drag. A possible approach consists of separate the global flow resistance into two contributions, due to the surface roughness and to the macro roughness. In terms of energy gradient it leads to $S=S'+S'$, where S' refers to the dune surface and S'' to a cumulative losses due to a sudden flow expansion just downstream the dune crest. Based on momentum and energy balance equations, and accounting for hydrostatic pressure distribution, a semi empirical approach is herein proposed to estimate dune bed contribution to flow resistance.

2. Dune bed contribution to flow resistance

Two dimensional steady fully developed turbulent flow in a sediment laden channel is considered (Figure 1). Energy balance equation are applied to the reference control volume of a portion of 2-D dune bed bounded between cross section 1 (i.e., the crest of the dune), and cross section 2 (i.e., the stagnation point on the lee side of the dune) where the streamlines are assumed to be parallel

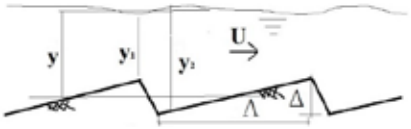

Figure 1: Sketch of 2-D dune bed

Considering a vertical lee side of the dune, and accounting for hydrostatic pressure distribution over the cross section 1 and 2, and after mean water depth y has been introduced, we obtain:

$$S'' = \kappa_{\Delta/y} \frac{\Delta H''}{\Lambda} = \kappa_{\Delta/y} F^2 \frac{y}{\Lambda} \Gamma_{\Delta/y} \quad (1)$$

$$\Gamma_{\Delta/y} = \frac{2\left(\Delta/2y\right)}{\left[1-\left(\Delta/2y\right)^2\right]^2} \quad (2)$$

where empirical correction coefficient $\kappa_{\Delta/y}$, which is function of the relative dune height Δ/y, is introduced in order to account for energy losses at negative steps are higher for inclined steps than for abrupt vertical steps (Tokyay and Altan-Sakarya, 2011), and for the actual pattern of stream flow and dune bed geometry. Once the measured energy slope S and the measured bed dune geometry are known, and after S' is calculated assuming logarithmic stream velocity profile and Nikuradse equivalent roughnes $k_s'=2.5d_{50}$ (being d_{50} the mean diameter), it is possible to determine the empirical coefficient $\kappa_{\Delta/y}$. Based on a selection of 122 field data collected on different sand rivers in presence of dune, the best fitting equation results:

$$\kappa = 0.14 \cdot e^{-1.2\Delta/y} \quad (1)$$

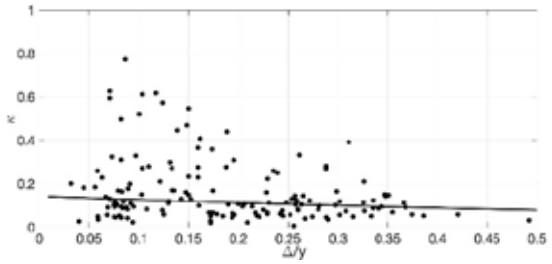

Figure 2: Fitting of empirical coefficient $\kappa_{\Delta/y}$

2. Model validation

The proposed model (Equations 1-3) has been validated, considering 524 field data observed in 15 rivers (Brownlie 1981). To this aim, the relative dune height Δ/y and the relative dune length Λ/y was chosen following Karim (1999) and Yalin (1964) respectively, in order to calculate S'' (Eqs. 1-3). Hence, the contribution due to skin roughness S' and eventually the total energy grade $S=S'+S''$ has been estimated. Figure 2 shows the comparison between predicted and measured S.

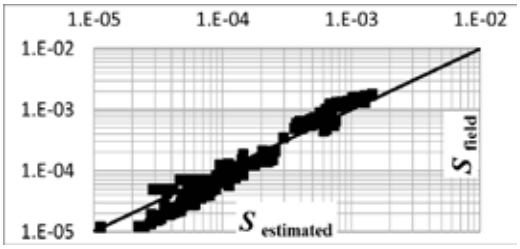

Figure 3: Model validation (303 field collected data)

3. Conclusions

Dune bed contribution to flow resistance is derived accounting for semi-empirical relationship based on momentum and energy balance equations applied to free surface flow over undulated bed, assuming hydrostatic pressure distribution. Comparison with large field dataset of sand rivers shows a satisfactorily agreement.

References

Brownlie, W. R. (1981). Compilation of fluvial channel data: Laboratory and field. Res. Report. KH-R43B, W. M. Keck Lab. of Hydraul. and Water Resour., Calif. Inst. of Technol., Pasadena

Karim, F. (1999). Bed-form geometry in sand-bed flows. *J. Hydraul. Eng.*, 125(12):1253-1261

Tokyay, N.D., Altan-Sakarya A B. (2011). Local energy losses at positive and negative steps in subcritical open channel flows. *Water SA*, 37(2):237-244

Yalin, M.S., 1964. Geometrical properties of sand waves. Jour. Hyd. Div., ASCE, 90(HY5)105-119 part I.

The Sedimentary Record of Bedform Disequilibrium

K.C.P. Leary[1] and V. Ganti[1,2]

[1] Department of Geography, UC Santa Barbara, Santa Barbara, CA, USA. learykcp@ucsb.edu
[2] Department of Earth Science, UC Santa Barbara, Santa Barbara, CA, USA.

1. Introduction

The migration of bedforms (i.e. dunes, unit bars) results in the development of cross-stratification, which is an ubiquitous sedimentary feature on Earth and other planets. Cross-set geometry is directly related to the kinematics of the evolving bedforms that created them and provides a unique opportunity to invert for their formative fluvial environments. Existing work has primarily focused on connections between bedform kinematics and cross-stratification under steady-state conditions; however, sediment and water discharge vary continuously in natural rivers. Field observations suggest that bedforms are seldom in equilibrium with prevailing flow conditions—a phenomenon called 'bedform disequilibrium' (Myrow et al., 2018)—indicating that cross-strata may dominantly record the bedform disequilibrium dynamics. Here we develop quantitative linkages between flood discharge variability, bedform disequilibrium dynamics, and cross-stratal geometries.

2. Theory and Methods

We analyzed existing experimental data of bedform evolution to assess the effects of unsteady flows on the preservation of fluvial strata. Martin and Jerolmack (2013) conducted a series of bedform experiments under abrupt, step increases in water discharge, and slow and fast triangular flood hydrographs. For each of these unsteady flow runs, we quantified the bedform kinematics in terms of their migration (horizontal velocity of topographic change, V_c) and deformation rates (vertical velocity of topographic change, π; McElroy and Mohrig, 2009). We then also constructed synthetic stratigraphy using high-resolution topographic evolution data, and tracked the time recorded in stratigraphy.

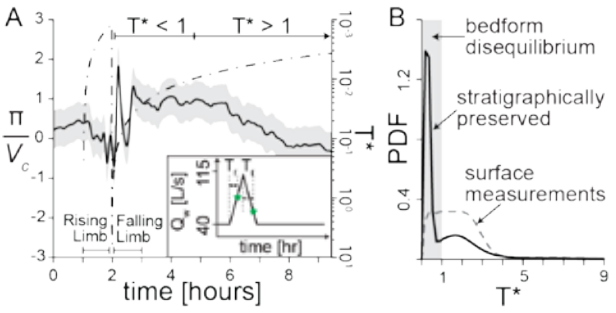

Figure 1. A) Temporal evolution of π/V_c and T^* for the fast flood experiment. Inset: imposed water discharge. B) Probability distributions of stratigraphically preserved T^* compared to surface T^* observed during experiment.

Reesink et al. (2015) and Paola et al. (2018) argued that the preservation of surface dynamics is directly related to the ratio of the local sedimentation rate to the migration rate of topography, i.e., π/V_c. For π/V_c«1, bedform deposits get repeatedly reworked by migrating topography, resulting in a fraction of bedforms being preserved in stratigraphy. In contrast, for $\pi/V_c \sim 1$ and higher, the local bedform climb angle is high, which leads to the majority of the bedform features to be stratigraphically preserved. Flow variations are expected to affect π and V_c, which control the stratigraphic preservation.

Following previous work (Myrow et al., 2018), we parameterized bedform disequilibrium using a dimensionless number $T^* = T_f/T_t$, where T_f is the duration of the prevailing flow conditions and T_t is a bedform turnover time, which is a function of the bedform size and bed material flux. Within this framework, a bedform disequilibrium number of $T^* > 1$ indicates that the bedforms are equilibrated with prevailing flows, whereas $T* < 1$ corresponds to the prevalence of bedform disequilibrium.

3. Results and Discussion

Across all unsteady flow experiments, we find that (1) bedform disequilibrium is characterized by elevated variability in local sedimentation rates, which leads to the enhanced stratigraphic preservation of bedform disequilibrium dynamics (Fig. 1), and (2) the variability of cross-set thickness, parameterized by its coefficient of variation, provides a reliable indicator of the formative T^*. Field observations indicate that T_t is on the order of months to years for dunes in large rivers (Myrow et al., 2018), suggesting that cross-stratification can house information of the formative flood discharge variability.

4. Conclusions

Theoretical considerations and experimental results indicate that cross-stratification preferentially records disequilibrium, rather than equilibrium, bedform dynamics. Our results provide a quantitative tool for reconstructing the nature of flood discharge variability in deep time.

References

Martin, R. L. and Jerolmack, D. (2013). Origin of hysteresis in bed form response to unsteady flows. *Water Resour. Res.*, 49:1314–1333.

McElroy, B. and Mohrig, D. (2009). Nature of deformation of sandy bed forms. *J. Geophys. Res. Earth Surf.*, 114(F3).

Myrow, P. M., Jerolmack, D. J., and Perron, J. T. (2018). Bedform disequilibrium. *Journal of Sedimentary Research*, 88(9):1096–1113.

Paola, C., Ganti, V., Mohrig, D., Runkel, A. C., and Straub, K. M. (2018). Time not our time: Physical controls on the preservation and measurement of geologic time. *Annual Review of Earth and Planetary Sciences*, 46:409–438.

Reesink, A., Van den Berg, J., Parsons, D. R., Amsler, M. L., Best, J. L., Hardy, R. J., Orfeo, O., and Szupiany, R. N. (2015). Extremes in dune preservation: Controls on the completeness of fluvial deposits. *Earth-Science Reviews*, 150:652–665.

The effect of forced bars on dunes in lowland rivers

T.V. de Ruijsscher[1], S. Naqshband[1] and A.J.F. Hoitink[1]

[1] Hydrology and Quantitative Water Management Group, Department of Environmental Sciences, Wageningen University, Wageningen, The Netherlands. ton.hoitink@wur.nl

1. Introduction

Bed forms have been studied extensively for decades, amongst others for their relation to bed roughness. As dunes can exist superposed on larger scale bed forms in rivers, the question arises whether dune dynamics is influenced by the underlying morphology, contradicting the assumption of a spatially homogeneous roughness coefficient. Here we focus on testing whether dunes and forced bars can be treated independently, with the Dutch Waal River as our research area (Figure 1).

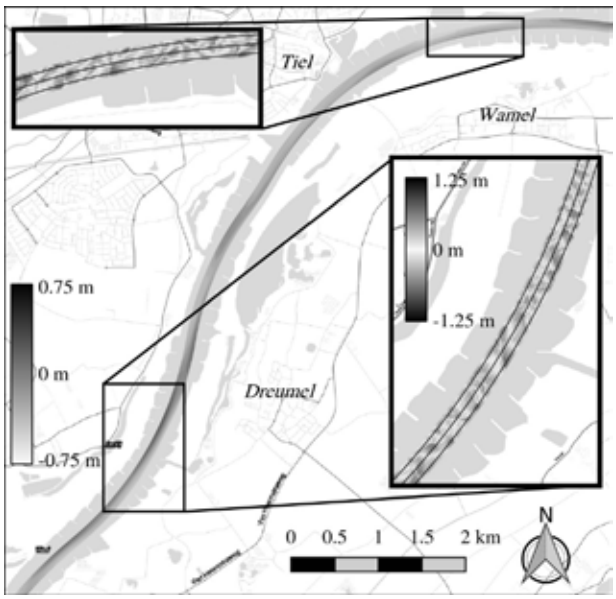

Figure 1. Bars and dunes (inset) on a 10 km stretch of the Waal River on 23 March 2011. Flow is from top right ($s = -24$ km) to bottom left ($s = -14$ km).

2. Methods

The bed level in the fairway of the Waal River is monitored on a biweekly basis using Multi-Beam Echo-Sounding. Three parallel profiles are defined, located on the river axis and 41 m on either side. Those profiles are used for a 2-D analysis of dune characteristics following van der Mark and Blom (2007). Dune characteristics of interest are height Δ, length λ, steepness ψ, and lee side slope S_{lee}, which are analysed in relation to the spatially varying underlying forced bar pattern. In addition, a qualitative analysis of the 3-D dune pattern is performed.

3. Results

Time-averaged detrended deviations of dune steepness from the spatial average ($\psi_{\text{detr}}/\langle\psi\rangle$) show a large spatial variation. However, when a LOESS algorithm is used to filter those out, the remaining variations in ψ correlates with the forced bar pattern (Figure 2). Correlations are also observed for Δ, λ and S_{lee}, although less pronounced. Spatial analysis of the full three-dimensional dune pattern shows that the part of a dune crest line on a bar crest is ahead of the part in a bar trough (Figure 3). This agrees with the effect of changing dune characteristics on dune celerity, both from field studies and from theory.

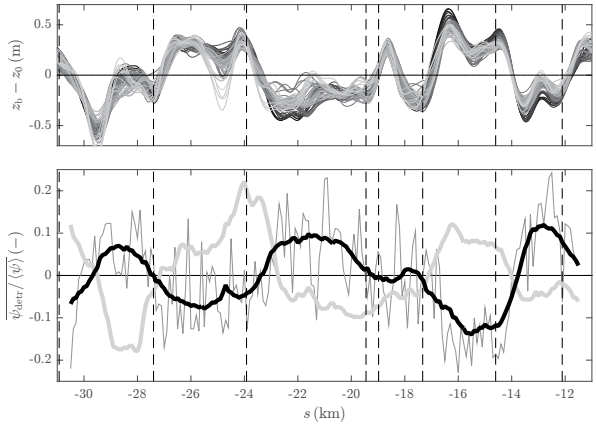

Figure 2. Top: Bars along the northern profile, during two years (dark to light). Dashed lines denote inflection points. Bottom: Deviations of steepness ψ from its spatial average, for the northern profile (dark, with and without spatial filtering) and the southern profile (light).

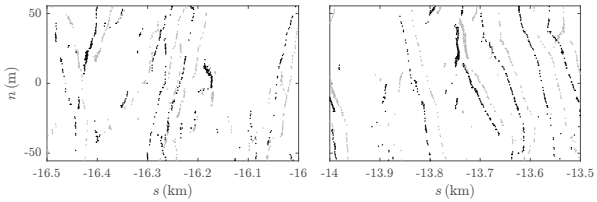

Figure 3. Dune crests on 21 (black) and 27 (grey) Sept. 2011, for bar crests at $n > 0$ (left) and at $n < 0$ (right).

4. Conclusions

- Despite large spatial and temporal variations, influence of forced bars on dunes is eminent, and most noticeable for dune steepness.
- On bar crests, dunes are on average longer, lower, less steep and have a smaller lee side angle.
- Dune fronts are obliquely oriented, with the part on the bar crest ahead of the part in the bar trough.

Acknowledgments

This research is part of the research programme Rivercare, supported by the Netherlands Organization for Scientific Research (NWO), which is partly funded by the Ministry of Economic Affairs under grant number P12–P14 (Perspective Programme).

References

van der Mark, R. and Blom, A. (2007). A new and widely applicable tool for determining the geometric properties of bedforms. Civil Eng. & Man. Res. Reports 2007R-003/WEM-002 1568-4652, University of Twente: Water Engineering & Management.

The fluid dynamics of barchan dunes and their interactions

N.R. Bristow[1], G. Blois[1], J.L. Best[2] and K.T. Christensen[1]

[1] University of Notre Dame, Notre Dame, IN, USA. nbristow@nd.edu; gblois@nd.edu; kchrist7@nd.edu
[2]University of Illinois at Urbana-Champaign, Urbana, IL, USA. jimbest@illinois.edu

1. Introduction

Barchan dunes are formed in sediment supply limited conditions and often occur when mobile sediment is transported over an unerodible substrate. The celerity of barchans is dictated by their volume, with smaller barchans migrating faster, and thus interacting with larger downflow bedforms. Although the morphology of barchan dunes has been widely studied, the interactions between turbulent flows and barchans is limited to a few recent studies (Palmer et al., 2012; Bristow et al., 2018). Indeed, "minimal" models of bedform interactions do not possess an adequate simulation of the wake flow structure induced by dunes (Parteli et al., 2014), and struggle to predict the morphodynamics of barchans accurately when they come in close proximity, including dune-dune collisions. Our research goal has been to use innovative experimental methods to investigate the turbulent flow structure associated with isolated barchan dunes, and highlight the changes to these flow fields at various stages of barchan interactions.

In this paper, we detail an experimental study of flow fields on the stoss side and in the wake of an isolated barchan and in the interdune space of interacting barchans, using a combination of low and high frame-rate measurements with both two-component planar particle imaging velocimetry (PIV) and three-component stereo-PIV. This allows us to propose models for flow associated with barchans and how the flow structure is influenced by bedform proximity.

2. Methods

Experiments were conducted in a specially designed refractive index matching (RIM) flow facility, which enables optical access to geometrically complex bedform configurations. Transparent models of barchan dunes, whose shape was based upon previous work (Palmer et al., 2012), were fabricated by 3D printing positive models, which were used to create negative silicone molds, which in turn were used to cast transparent acrylic models. The models were fixed in the RIM flume that employs an aqueous solution of sodium iodide (~63% by weight) as the working fluid, and rendered invisible, thus facilitating unimpeded data collection around the entire bedform configuration. The RIM approach also minimizes reflections of the laser sheet off the model and floor surfaces, allowing for higher accuracy measurements in these critical regions.

3. Results

Flow over the barchans is dominated by establishment of a horseshoe vortex system on the stoss side of the dunes, and a complex wake structure in the leeside. These two vortex systems determine the distribution of Reynolds stresses around the barchans (Figure 1). This paper will describe the nature of these turbulent flow fields, the lengthscales of the turbulent flow structures and discuss the implications for both the entrainment of sediment and transport pathways associated with isolated and interacting barchan dunes.

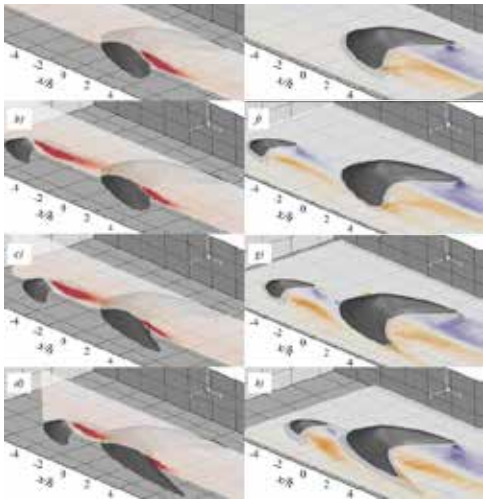

Figure 1: Contour maps of in-plane Reynolds shear stress: (*a-d*) in the up-flow barchan dune centerline plane and (*e-h*) 0.25h elevation (h = large barchan height) wall-parallel planes. (*a,e*) isolated barchan, (*b-h*) different stages of barchan collision.

4. Conclusions

The RIM approach allows unique insight into the fluid dynamics of barchan dunes and their interactions. This work demonstrates both the changing fluid dynamics of the wake zone as barchans become increasingly closely spaced, and the role of the stoss side dynamics in influencing sediment transport pathways and sediment dispersal.

Acknowledgments

This work was supported by National Science Foundation collaborative grants CBET-1603211 (Notre Dame) and CBET-1604155 (Illinois).

References

Bristow, N. R., Blois, G., Best, J. L., Christensen, K. T., (2018). Turbulent flow structure associated with collision between laterally offset, fixed-bed barchan dunes. *Journal of Geophysical Research: Earth Surface*, 123, 2157-2188.

Palmer, J. A., Mejia-Alvarez, R., Best, J. L., Christensen, K.T., (2012). Particle-image velocimetry measurements of flow over interacting barchan dunes. *Experiments in Fluids*, 52, 809–829.

Parteli, E. J. R., Kroy, K., Tsoar, H., Andrade, J. S., Pöschel, T., (2014). Morphodynamic modeling of aeolian dunes: Review and future plans. *European Physical Journal Special Topics*, 223, 2269–2283.

3D dune analysis: deformation of dune crests during migration and associated sediment fluxes

R.C. Terwisscha van Scheltinga[1], G. Coco[2] and H. Friedrich[1]

[1] Civil and Environmental Engineering, University of Auckland, Auckland, New Zealand.
rgal477@aucklanduni.ac.nz, h.friedrich@auckland.ac.nz
[2] School of the Environment, University of Auckland, Auckland, New Zealand. g.coco@auckland.ac.nz

1. Introduction

A planar riverbed, composed of sediment with particle size < 2mm, will deform into a wavy morphology for a range of flow conditions. The self-organized dune field is made up of individual dunes that are limited in height by water depth, whilst displaying similar height/length ratios (Yalin, 1979). Dunes can have different shapes and previous studies have described the interaction between adjacent dunes (e.g. Kocurek et al., 2010). Dune interaction can also be regarded as a limiting factor on individual dune size. Smaller sand waves travel at faster speed than larger sand waves (Guala et al., 2014), resulting in interaction: e.g., a small wave will catch up with a large wave and subsequently 'cuts off' sediment supply from the large wave. During this process the large wave (temporarily) destabilizes, as the sediment load is no longer saturated at its crest (brink point). Additionally, dunes are shown to compete for space as they grow or decay in response to changing flow depth and velocity (Reesink et al., 2018). Instabilities (sources or sinks of sediment) are created on top of, and between, dunes. Reesink et al. (2018) conclude that dune adaptation happens from multiple interacting dunes (spatially- and temporally- variable response). Questions remain to be answered. For example: 1) do individual dunes persist in shape (and steepness) or are they in continuous transformation? And 2) how do sediment fluxes vary during the transformation stages of individual dunes? By using high-resolution digital elevation models (DEMs) at frequent time scales we can quantify the local sediment flux, whilst also tracking dune migration and deformation.

2. Method

Laboratory flume experiments are performed in a 0.44 m wide flume with a water depth of 0.15 m and an average flow velocity of 0.5 m/s. The natural sand has a median diameter of 0.85 mm and the sediment bed consists of self-formed dunes (Figure 1b). Images of the submerged bed are collected at 8-minute intervals and processed into 40 DEMs using the Structure from Motion technique. An example of a DEM is provided in Figure 1c, at a grid-resolution of 2 by 2 mm.

3. Outlook

For our experimental conditions, the formation of a regular dune crest is observed 2-4 times in a period of 5 hours, alternating with occurrence of irregular crests. It suggests that crests and troughs of individual dunes deform continuously while migrating. Sediment fluxes are unsteady for individual dunes and the fluxes associated with the dune crest deviate with a factor 1-3 around a mean flux, indicating acceleration and deceleration phases of dune migration ('breathing'). The process of cannibalization is associated with the highest flux.

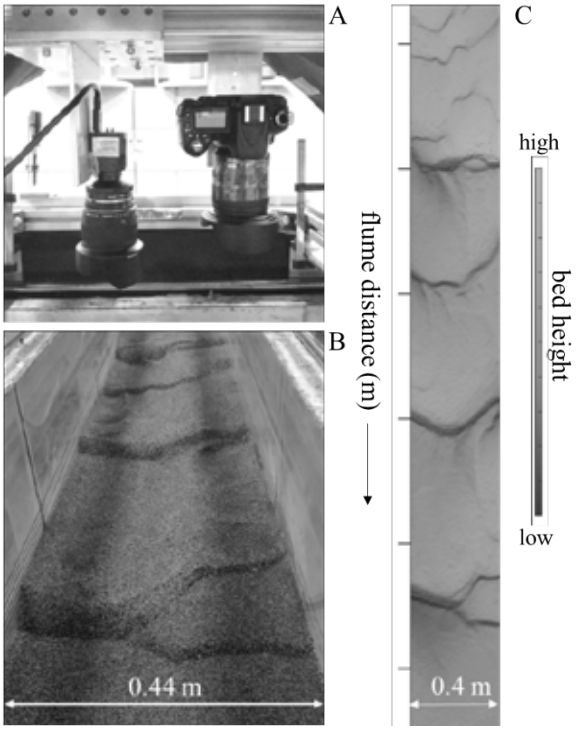

Figure 1: a down looking camera is used to record through-water images of the sand bed (a) which is covered with self-formed dunes (b). The images are processed into detailed DEMs (c).

References

Guala, M., A. Singh, N. Badheartbull, and E. Foufoula-Georgiou (2014), Spectral description of migrating bed forms and sediment transport, *J. Geophys Res.,* 119(2), 123-137.

Kocurek, G., R. C. Ewing, and D. Mohrig (2010), How do bedform patterns arise? New views on the role of bedform interactions within a set of boundary conditions, *ESPL,* 35(1), 51-63.

Reesink, A. J. H., D. R. Parsons, P. J. Ashworth, J. L. Best, R. J. Hardy, B. J. Murphy, S. J. McLelland, and C. Unsworth (2018), The adaptation of dunes to changes in river flow, *Earth-Sc. Rev.,* 185, 1065-1087.

Yalin, M. S. K., E. (1979), Steepness of Sedimentary Dunes, *J. of the Hydr. Division,* 105(4), 381-392.

Evaluation of estuarine sediment dynamics in response to tide-variable hydraulic flow resistance induced by asymmetric dunes

G. Herrling[1], M. Becker[2], K. Krämer[3], A. Lefebvre[4], A. Zorndt[5] and C. Winter[6]

[1] University of Kiel, Germany. gerald.herrling@ifg.uni-kiel.de
[2] University of Kiel, Germany. marius.becker@ifg.uni-kiel.de
[3]University of Kiel, Germany. knut.kraemer@ifg.uni-kiel.de
[4] MARUM, University of Bremen, Germany. alefebvre@marum.de
[5] BAW, German Federal Waterways Engineering and Research Institute, Germany. anna.zorndt@baw.de
[6]University of Kiel, Germany. christian.winter@ifg.uni-kiel.de

1. Introduction

Bedforms (dunes and ripples) constitute a form roughness, i.e. hydraulic flow resistance, which has a large-scale effect on hydrodynamics, sediment transport and morphodynamics of rivers, estuaries and coastal seas. Flow separation behind the dune crest and recirculation on the downstream side result in turbulence and energy loss (Vanoni and Hwang, 1967). Since the energy loss is related to the dune lee slope angle (Best and Kostaschuk, 2002), asymmetric dune shapes induce variable flow resistance during ebb and flood in tidal environments (Lefebvre and Winter, 2016).

Bedform induced flow resistance must be considered in coastal-scale numerical hydro- and morphodynamic model simulations and is parameterized by (bed-)form friction coefficients, since dune dimensions (lengths of tens to 100 meters) are typically of 'sub-grid-scale'. It is common practice to calibrate models adjusting bed roughness coefficients, irrespective of the actual bedform size, shape and orientation. In our idealized approach, we apply a non-calibrated numerical model to analyze the large-scale effect of dunes on estuarine circulation and sediment dynamics. Thereby, we focus on the intratidal variability of roughness, induced by dune asymmetry.

2. Methodology

Dune size and asymmetry (orientation and slope angles) were obtained from high-resolution bathymetric data of the Weser estuary (length of 120 km), southern North Sea, Germany. Mean values of dune parameters were determined for the dune fields, located along the channel. For each dune field, two roughness coefficients were calculated, one for each tidal flow direction (Lefebvre and Winter, 2016).

These coefficients were used as bed roughness in a 3D process-based morphodynamic model with graded sediment fractions (Delft3D, Deltares). Consequently, in each dune field in the model domain, the bed roughness varies between ebb and flood tide in case of asymmetrical dune parametrizations. Scenario simulations have been performed with bed roughness coefficients parameterizing the hydraulic flow resistance of symmetric and asymmetric dune shapes.

3. Results, conclusions and outlook

Weser dunes are asymmetric with gentle stoss sides and steep lee sides in downstream (ebb-)direction. In relation to symmetric dunes, the tidal wave propagates faster up-estuary when imposing (realistic) asymmetric dunes, i.e. higher bedform roughness during ebb than during flood (Figure 1). The flood dominance increases for asymmetrical dunes with increasing current velocities along the entire estuary. During flood, the bed shear stress shows spatially varying dependencies since it is also a function of the locally (imposed) dune roughness. While flood dominance increases, bed shear stress can decrease for asymmetrical dunes (Figure 1). This has an immediate effect on spatiotemporal sediment transport and dynamics.

The ongoing project evaluates and discusses simulated sediment and morphodynamics in response to distinct dune roughness configurations: shifting of the turbidity zone, residual suspended and bed load transports along the estuarine channel and associated morphological and sedimentological changes.

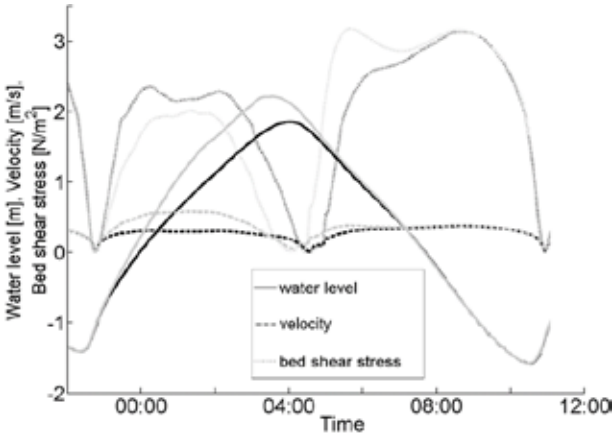

Figure 1: Simulated water level, near-bed velocity and bed shear stress at Nordenham in the Lower Weser estuary using roughness parametrizations of symmetric (black) and asymmetric (grey) dunes, respectively.

Acknowledgments

This study is funded by the research project FAUST financed by and in cooperation with the German Federal Waterways Engineering and Research Institute (BAW). AL is funded by the German Research Foundation (DFG), project number 345915838.

References

Best, J., Kostaschuk, R.A. (2002). An experimental study of turbulent flow over a low-angle dune. *J. Geophys. Res,* 107, 3135. doi:10.1029/2000jc000294.

Lefebvre, A., Winter, C. (2016a). Predicting bed form roughness: the influence of lee side angle. *Geo-Marine Letters*, 36:121-133. doi:10.1007/s00367-016-0436-8.

Vanoni, V.A., Hwang, L.-S. (1967). Bed forms and friction in streams. *J. Hydraul. Div.*, 93, 121–144.

On the dynamics of vegetated alternate bars by means of flume experiments

G. Calvani[1], S. Francalanci[1] and L. Solari[1]

[1] Department of Civil and Environmental Engineering, University of Florence, Florence, Italy. giulio.calvani@unifi.it

1. Introduction

Alternate bars are large-scale bedforms, scaling with channel width, and develop in fully transporting straight channels as a result of riverbed instability. Colombini et al. (1987) proposed a linear theory and a weakly nonlinear formulation to investigate the threshold conditions for the formation (i.e., width-to-depth ratio above a critical value) and the dynamics (e.g., the migration rate) of unvegetated alternate bars with uniform grain size. Additionally, Lanzoni and Tubino (1999) accounted for mixed sediment composition and found that grain sorting reduces the downstream migration rate of alternate bars. However, none of the available mathematical models of alternate bars accounts for the presence of vegetation. Nevertheless, there are strong evidences that vegetation significantly alters the dynamics of alternate bars in straight channels but such alterations were investigated by numerical simulations only (e.g., Bertoldi et al., 2014), whereas flume experiments on alternate bars were carried out either without vegetation (e.g., Lanzoni, 2000) or in fixed bed conditions (e.g., Bennett et al., 2002). In this work, we investigate the effects of added rigid vegetation on the dynamics of freely migrating alternate bars in a straight channel.

2. Materials and methods

We performed laboratory experiments in a straight, 0.43m wide and 10.5m long flume using poorly graded sand ($D_{50} = 1.25$mm, $C_u < 0.6$) as bed material. Sediment feeding at the inlet of the flume was provided using the same bed material and adjusted according to Wong and Parker relation. We involved different setup of bed slope and flow discharges to let unvegetated alternate bars freely develop and downstream migrate in the flume, according to the linear theory of Colombini et al. (1987) (see Table 1 for experimental conditions). At the downstream outlet, we measured sediment transport rate by weighting sediment using a collecting net. We ran each experiment until dynamic equilibrium (i.e., equal sediment transport rate at the inlet and outlet and constant bar wavelength and migration rate) was achieved. At the end of the first phase (achievement of dynamic equilibrium), we deployed 1mm diameter metal rods on the most elevated areas of the bars to simulate presence of rigid vegetation. For each setup in Table 1, we employed three different densities of vegetation (m=0.125, 0.1875, 0.25 cm^{-2}), for a total of twelve experiments. We then kept running the experiments for at least 20 hours after deployment and monitored bed evolution using Structure-From-Motion technology. The analysis of the outcome Digital Elevation Models of the flume bed showed the effects of adding vegetation on the dynamics of already formed alternate bars in terms of celerity (i.e., migration rate) and length (see Figure 1 for some results for the experiments ID=1).

ID	s [-]	Q [l/s]	F_r [-]	β [-]	β_{cr} [-]
1	0.008	3	0.89	11.7	5.0
2	0.008	4	0.92	9.9	6.0
3	0.009	3	0.95	12.2	5.2
4	0.009	4	0.97	10.2	6.1

Table 1. Different setup involved in the flume experiments. s is bed slope, Q is the flow discharge, F_r is the Froude number and β is width-to-depth ratio. The critical width-to-depth ratio β_{cr} was calculated according to Colombini et al. (1987).

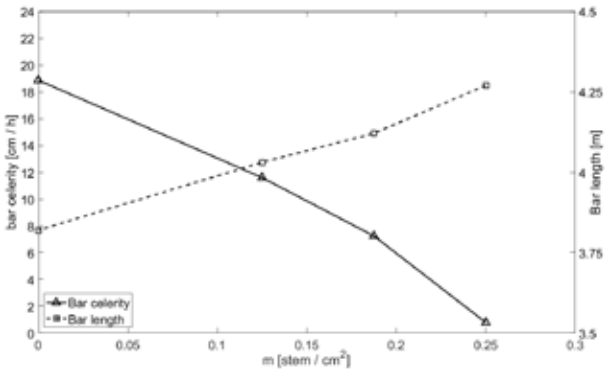

Figure 1. Comparison of the results for the experiment with bed slope $s = 0.008$ and flow discharge $Q = 3l/s$ (ID=1 in Table 1) in terms of bar celerity and length for the unvegetated (w/o) and vegetated configurations with respect to vegetation density.

3. Conclusions

The results of the performed experimental activities showed that vegetation reduces wave speed (celerity) of alternate bars and enhances their length and amplitude. The analysis demonstrated that vegetated alternate bars behave more similarly to forced than to free migrating bars, when vegetation density is higher than a critical value.

References

Bennett, S. J., Pirim, T., and Barkdoll, B. D. (2002). Using simulated emergent vegetation to alter stream flow direction within a straight experimental channel. *Geomorphology*, 44(1-2):115–126.

Bertoldi, W., Siviglia, A., Tettamanti, S., Toffolon, M., Vetsch, D., and Francalanci, S. (2014). Modeling vegetation controls on fluvial morphological trajectories. *Geophysical Research Letters*, 41(20):7167–7175.

Colombini, M., Seminara, G., and Tubino, M. (1987). Finite-amplitude alternate bars. *Journal of Fluid Mechanics*, 181:213–232.

Lanzoni, S. (2000). Experiments on bar formation in a straight flume: 2. graded sediment. *Water Resources Research*, 36(11):3351–3363.

Lanzoni, S. and Tubino, M. (1999). Grain sorting and bar instability. *Journal of Fluid Mechanics*, 393:149–174.

Centennal sea-level rise impact on fluvio-deltaic morphodynamics

L.C. Guo [1, *], Q. He [1], F. Xu [1]

[1] State Key Lab of Estuarine and Coastal Research, East China Normal University, Shanghai, China
* lcguo@sklec.ecnu.edu.cn

Global climate change has led to accelerated sea-level rise (SLR), which is a worldwide concern as regards to the consequent coastal flooding and erosion risk. It is of particular interest to understand how coastal and estuarine morphodynamics will respond and adjust to SLR, and whether their inter-tidal flats can survive SLR at the century time scale.

Field data is not readily available to assess SLR impact in the future. Long-term morphodynamic modelling provides an effective tool to evaluate SLR impact on coasts. Previous knowledge of SLR impacts on open coasts include the Brune rule. More recently, Dissanayake et al. (2012), van Maanen et al. (2013), van der Wegen (2013) had employed morphodynamic models to explore SLR impact on tidal inlets and basins. It was reported that tidal flats in those systems were highly likely to be drowned under SLR. But it remains insufficiently understood to what degree and how system dynamics may adapt to SLR of different rates.

In this work we use a long-term morphodynamic model to explore large-scale morphodynamic evolution of a schematized tide-dominated estuary-delta system based on Delft3D software. We first run a simulation for 500 years starting from a schematized initial bathymetry. Based on that, we continued simulations considering SLR of 0 to 2.0 m in 100 years. The erosion and deposition pattern and the sediment flux at the estuary mouth were estimated.

Model results show that a tide-dominated estuary exhibits ebb dominance and net sediment export due to the hypsometric effects of tidal flats. Rising sea levels inundate high land and convert them into tidal flats, leading to subsequent hypsometry changes which will enhance the ebb dominance and enlarge sediment export. Erosion of the high land provides extra sediments to the system.

We see that tidal flat accretion may match a SLR < 0.25 mm yr^{-1}, but fails to keep pace of SLR larger than that. Moreover, lateral expansion under SLR increases tidal flat area inside the estuary. We conclude that tidal estuary-delta system has a buffering capacity that alleviates the drowning impact of SLR by sediment redistribution and morphodynamic adjustment within the system. These results suggest that preserving tidal flats in estuaries, instead of reclaiming them, sustains the natural resilience to SLR.

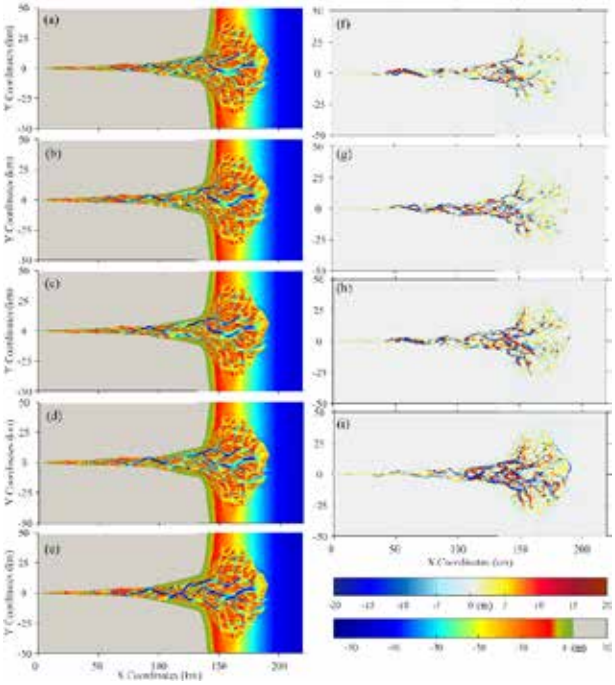

Figure 1. The morphology after 100 years considering (a) no SLR, SLR of (b) 0.25 m, (c) 0.5 m, (d) 1.0 m, and (e) 2.0 m, and accordingly the bathymetry differences between the SLR scenarios and the reference scenario with SLR of (f) 0.25 m, (g) 0.5 m, (h) 1.0 m, and (i) 2.0 m. The morphology in panel (b) to (e) was adjusted to the rising of the sea level, and the elevation was positive above mean sea level. The green shading in panels (a) to (e) roughly indicates the inter-tidal zone. Positive values in panels (f) to (i) indicated accretion and negative indicated erosion in the SLR scenarios compared to the reference case.

Acknowledgments

Ministry of Science and Technology of China (No. 2016YFE0133700; 2017YFE0107400), and Natural Science Foundation of China (No. 51739005, 41876091).

References

Dissanayake D.M.P.K., Ranasinghe R., Roelvink J.A., 2012. The morphological response of large tidal inlet/basin systems to relative sea level rise. *Climate Change* 113(2), 253–276, doi: 10.1007/s10584-012-0402-z.

van Maanen B., Coco G., Bryan K.R., Friedrichs C.T., 2013. Modeling the morphodynamic response of tidal embayments to sea-level rise. *Ocean Dynamics*, doi: 10.1007/s10236-013-0649-6.

van der Wegen M., 2013. Numerical modeling of the impact of sea level rise on tidal basin morphodynamics. *Journal of Geophysical Research: Earth Surface* 118, 447-460.

Numerical simulation of sand bar formation in Sittaung River Estuary, Myanmar

T. S. Ahmed[1], S. Egashira[2], D. Harada[3], A. Yorozuya[4] and B.B.Srestha[5]

[1] PhD Student, National Graduate Institute for Policy Studies, and
[1]International Centre for Water Hazard and Risk Management, Public Works Research Institute, Japan.
[1]tanjirsaifahmed@gmail.com
[2,3,4,5] International Centre for Water Hazard and Risk Management, Public Works Research Institute, Japan.
[2]s-egashira77@pwri.go.jp [3]d-harada77@pwri.go.jp [4]yorozuya@pwri.go.jp [5]shrestha@pwri.go.jp

1. Introduction

The Sittaung River estuary is 220km long southwards, 270km wide and it opens to Gulf of Martaban. Due to a trumpet shape of the estuary, tidal bores and associated strong currents take place in spring and autumn, and sand bars form and migrate actively. In addition, silt-clay material is dominant in the bank and bed material. The bank erosion, thus takes place severely (Ahmed 2019). This study aims to reproduce tidal currents and sand bar behaviour by means of numerical methods in order to obtain some ideas for countermeasures against the bank erosion.

2. Methodology

Depth averaged governing equations for tidal currents and corresponding sediment transportation and channel changes are employed to reproduce tidal currents and sand bar deformation. To treat bed erosion and sediment transportation over the bed composed of very fine material, new formulas for erosion rate and bed-load rate (Egashira et.al 2019) are introduced into the governing equations. The International River Interface Cooperative (iRIC) software is employed (Nelson et.al. 2016) to conduct numerical simulation for tidal currents and associated bed deformation.

3. Computation condition and numerical results

Reference grain size of bed material is specified as 0.03 mm referring to the result of field survey (Ahmed 2019). The computational domain covers the estuary area which is 220km long and 270km wide, involving the upstream river channel. Two different discharges of 1000 m^3/s and 3000 m^3/s are employed as upstream boundary conditions. A cyclic tidal motion which has the amplitude of 2m and the period of 12 hours are specified as the downstream boundary condition. A general grid system is employed, in which Δx (south-north direction) and Δy in the upstream side are about 100 m. Computation time step is 0.2 s.

Figure 1(A) shows a recent photo of Sittaung river estuary. Figure 1(B), (C) and (D) shows simulated results on bed morphology produced after 2, 3 and 4 days of computation respectively with 1000 m^3/s constant inflow discharge. Computed results show severe erosion tendency near the Mamauk village area where maximum active bank erosion experienced almost 1 km bank line retreat in one year (Ahmed 2019). Moreover, simulated deposition areas illustrated by circles agree well with sand bars identified by recent satellite image.

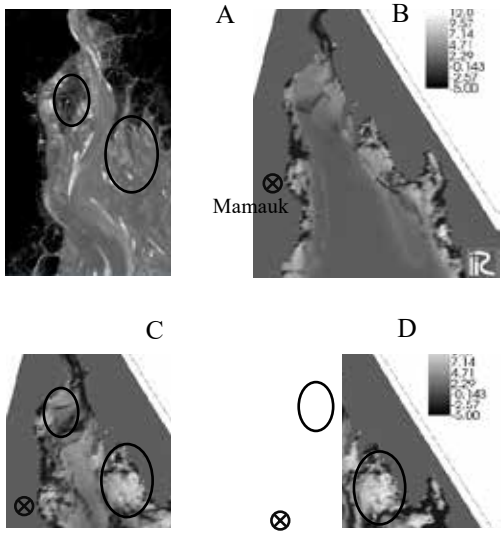

Figure 1 (A) Recent Landsat image of Sittaung estuary, (B) Computed bed morphology after 2 days, (C) after 3 days and (D) after 4 days.

4. Conclusions

Simulated results suggest that tidal currents and corresponding sediment transport processes including active bed evolutions can be reproduced in the estuary area where very fine sediment such as silt-clay material is dominant. Such method and simulated results would be very much helpful for river administrators to determine vulnerable locations in the estuary due to active channel change.

References

T. S. Ahmed, S. Egashira, D. Harada, A. Yorozuya, Y. kwak, B.B. Shrestha, D. Kuribayashi, H. Sawano & T. Koike (2019). On bank erosion in estuary of sittaung river in Myanmar. *Scour and Erosion IX-Keh-Chia (Ed.) Taylor & Francis Group, London, ISBN 978-0-367-07467-8.*

S. Egashira, D. Harada and T. S. Ahmed. Entrainment of very fine sediment in treating the estuary bed evolution. *River, Coastal and Estuarine Morphodynamics: RCEM 2019*, (submitted).

J. M. Nelson, Y. Shimizu, T. Abe, K. Asahi, M. Gamou, In oue, T & T. Kyuka, 2016. The International River Interface Cooperative: Public domain flow and morpho-dynamics software for education and applications. Advances in Water Resources, 93, 62-74.

Vegetation age (size) reduces the morphological impact of river flooding

Rocio Luz Fernandez[1], Daniel R. Parsons[2], Stuart J. McLelland[1,2] and Bas Bodewes[1]

[1] Department of Geology and Geography, University of Hull, Hull, United Kingdom. r.l.fernandez@hull.ac.uk
[2] Energy and Environment Institute, University of Hull, Hull, United Kingdom.

Introduction

Flow-stage variation is known to impact braided channel pattern parameters more than single thread channels, because braided rivers are characterized by higher width/depth ratios and are strongly dependent on exposure of bar-scale topography (Bridge, 1993). As future variability in hydro-climate is set to increase over large parts of the globe due to the impacts of climate change, variability in flow stage will likely disproportionately alter the morphodynamics of braided channel systems. It is also now widely accepted that fluvial process cannot be well understood without considering biological influences. Changes in vegetation as a result of climate and land use change will also likely impact river systems and their longer-term response. Indeed, scaled flume studies have shown how changes in vegetation density can have a significant control on hydrogeomorphic processes (Gran and Paola, 2001). The interactions of changing flood frequency, drought and alterations in vegetation growth patterns on fluvial system response remain very poorly understood. This study addresses this gap in understanding with the main research question: how do the channel planform and channel dynamics in a braided river reach respond to a flood sequencing during vegetation growth stages? We modelled the hydro-morphodynamics of a river reach subjected to a periodic change of the discharge (flood sequence) whist simultaneously growing vegetation on bar surfaces, to address this research question. The experimental procedure tested the impact of timescales on recovery and explored how multiple perturbations impacted morphodynamic responses to flood sequences.

Experimental Set-up

The experimental data was collected in the Total Environment Simulator (TES), University of Hull. The TES was divided into two mobile bed flumes (2.5 m wide, 10 m long) with constant longitudinal slope (0.015) and uniform grain size (d_s = d_{50} = 0.45 mm). The flow discharge was controlled at the source point upstream and was adjusted for changes in time to simulate a flood sequence of low and high floods. Two sediment supply conditions were considered: equilibrium (balance between transport capacity and supply) and deficit. For the vegetation, alfalfa seeds were uniformly spread on the bed (1 seed cm^{-2}) and allowed to grow before the release of the sequential floods. Four different age stages of the vegetation were investigated along with a vegetation dying phase. Above the flume, a 3D laser scanner enabled us to produce 1 mm precision digital elevation maps (DEMs) of the morphology after each flood event.

Results

Channel changes and sediment dynamics were identified by differencing of sequential DEMs. Statistical properties, such as the reach-scale braiding indexes (BI) were computed through the experiment sequence. The cross-sectional mean bed elevation was used as threshold to discriminate between bars and channels. Figure 1 suggests that on average bar height (h_b) increased with plant size (l_v). BI increased for the vegetated runs relative to the bare bed condition. By defining a BI difference for the different floods relative to the bare situation as $\Delta BI = (BI_{post\text{-}flood} - BI_{pre\text{-}flood})/\Delta BI_0$, where ΔBI_0 is the difference no vegetation condition. Figure 2 shows that ΔBI was less sensitive to flood sequence as plant age and size increased. The same trend was observed for the width/depth ratios along the reach lengths analysed, though, plant topographic effects decreased for the runs in which the sediment balance within the supply was shifted to deficit.

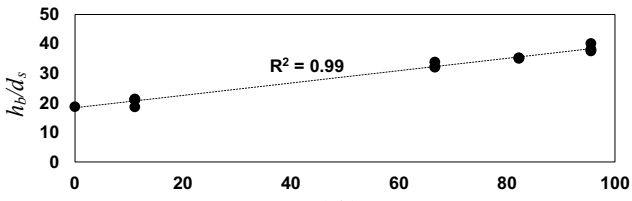

Figure 1: Bar height increased with plant size.

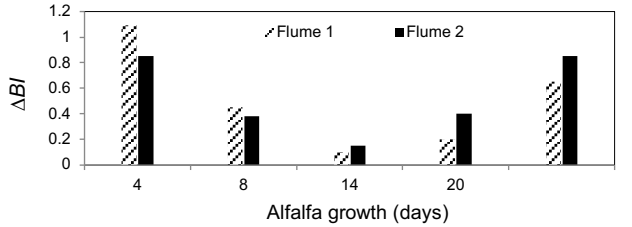

Figure 2: Response of the vegetated runs as evaluated by ΔBI.

Conclusions

Results allowed for the characterization of bed morphology changes in response to the growth of vegetation. In particular, it was found that river's morphological and topographic response was less sensitive to a given flood sequence as the plant age and size increased, until a threshold value where the vegetation began to die back. This study aids the long-term understanding of river dynamics and the importance in including the effects of flood sequencing in long-term characterization, particularly in relation to sediment supply conditions and size and age profile of riparian vegetation.

References

Bridge, J.S. (1993). The interaction between channel geometry, water flow, sediment transport and deposition in braided rivers. In: Braided Rivers (Best, J., and Bristow, C.0, No.75, London, 13-71.

Gran, K. and Paola, C. (2001). Riparian vegetation controls on braided stream dynamics. Water Resources Research, 37(12), pp. 3275–3283.

Co-evolution of alternate gravel bars and vegetation: the role of vegetation traits

F. Caponi[1] and A. Siviglia[1]

[1] Laboratory of Hydraulics, Hydrology and Glaciology (VAW), ETH Zurich. caponi@vaw.baug.ethz.ch

1. Introduction

Riparian vegetation is widely recognized to influence gravel bed river morphology modifying flow and sediment transport characteristics. Alternate gravel bars represent preferential areas for vegetation development, displaying alternate stable states (i.e. vegetated and bare) that depends on flow regime and vegetation characteristics. However, it has been recently suggested that specific plant traits, e.g. how plants allocate biomass to their above and below-ground structures, can strongly mediate biogeomorphic feedbacks (Hortobágyi et al., 2018). Moreover, plant root-related feedbacks has been showed to represent a key factor for determining river trajectories, controlled by the ratio between erosion dynamics and vegetation anchoring resistance (ω_v, Caponi and Siviglia, 2018). Quantitative tools that incorporate specific plant traits and investigate their effect on alternate bar morphology are limited. Our aim is to present a novel model for including above and below-ground vegetation dynamics and their related feedbacks into a numerical morphodynamic model and study the co-evolution of alternate bars and vegetation. We perform 2D numerical simulations in a straight channel with alternate bars and showed how morphological trajectories can be influenced by specific vegetation traits under different flow regimes and the ratio ω_v.

2. Vegetation Model

We consider vegetation as biomass density partitioned into an above-, B_a, and below-ground part, B_r, linked by an allometric function, $B_r = c(B_a)^m$, where c and m are two constant parameters depending on the vegetation allometric characteristics. B_r is further described by a rooting depth, ζ_r, and a vertical distribution, b_r, over the bed depth, ζ. The latter is obtained using the root model developed by Tron et al., (2014), which links root dynamics with water table fluctuations.

The above-ground vegetation is assumed to grow with a logistic function with a rate σ_a, that depends on the amount of water available to roots through the function:

$$\sigma_a \propto F(t) = \frac{B_r(t)}{\zeta_r(t) B_{ref}} \qquad (1)$$

representing the ratio between the root biomass and a reference root biomass ($\zeta_r(t)B_{ref}$). ζ_r is the rooting depth that is considered to grow over time following an exponential function with specific growth rate σ_r until a maximum value that is limited by the position of the groundwater. The function F(t) (Eq. 1) allows to include the effect of the root dynamics, which is controlled by physically-based parameters describing the water table regime, on above-ground vegetation growth. This in turn impacts morphodynamic processes assuming that (i) B_a changes the flow resistance and the shear stress at the bottom, thus reducing sediment transport; (ii) $b_r(\zeta)$ modifies the threshold for sediment motion and (iii) B_r controls the uprooting mechanism, which occurs when scour erodes a critical root biomass.

3. Alternate bar dynamics

We tested how different vegetation traits influence bar morphodynamics. The initial conditions for our numerical runs is an alternate bar pattern generated in a straight channel. In Figure 1, we show how fast-growing vegetation, characterized by greater σ_a and σ_r, is able to stabilize the bar creating a distinct erosion/deposition pattern, while slow-growing vegetation only slightly impacts river morphology, allowing for bar migration.

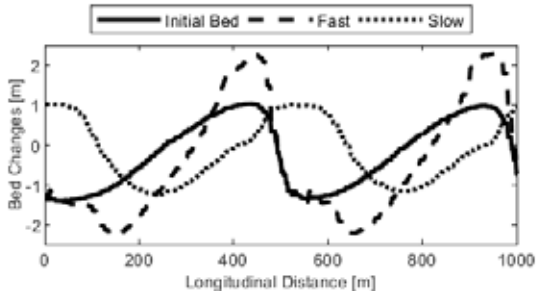

Figure 1: Side view of riverbed changes after a flood for Fast and Slow vegetation, exhibiting different growth rates, σ_a (Eq. 1) and σ_r.

4. Conclusion

We present the results from the application of a novel model accounting for above and below-ground vegetation dynamics and their related biogeomorphic feedbacks on alternate bar dynamics. Our current and future work aims at fully exploring the capabilities of the model to reproduce the co-evolution of alternate bars and vegetation under different scenarios of flow regime in term of the ratio ω_v (Caponi and Siviglia, 2018).

References

Caponi, F., & Siviglia, A. (2018). Numerical Modeling of Plant Root Controls on Gravel Bed River Morphodynamics. Geophysical Research Letters, 45(17), 9013-9023.

Tron, S., Laio, F., & Ridolfi, L. (2014). Effect of water table fluctuations on phreatophytic root distribution. Journal of Theoretical Biology, 360, 102–108.

Hortobágyi, B., Corenblit, D., Steiger, J., & Peiry, J. L. (2018). Niche construction within riparian corridors. Part I: Exploring biogeomorphic feedback windows of three pioneer riparian species (Allier River, France). Geomorphology, 305, 94-111.

Numerical modelling of rivers, dynamic riparian vegetation and climate change

J.T. Dijkstra[1], Y.Bossenbroek[1,2], M. van Oorschot[1], C.J. Sloff[1,2], L. Javernick[3], R.L. Fernandez[4] and B. Smits[1]

[1] Deltares, Delft, the Netherlands, jasper.dijkstra@deltares.nl
[2] Delft University of Technology, Delft, the Netherlands
[3] River Science and Lotic Hydrological, Canon, Colorado, USA
[4]University of Hull, Hull, United Kingdom

1. Introduction

The biogeomorphological development of river planforms is governed by both short-term (flood) interactions, such as bank erosion and vegetation removal and processes on the long-term (years-decades), such as riparian vegetation growth (Corenblit et al., 2014). To assess how rivers will respond to changes in forcing as a result of climate change, both timescales need to be represented in numerical models.

Anticipating the response of rivers is relevant to managers to deal with changes in e.g. flooding risks or natural value. The uncertainties involved in development over decadal timescales ask for envelopes of likely development rather than a single deterministic solution.

So far, the role of changing vegetation in rivers has received considerably less attention than the purely physical processes, whereas the planform of rivers is definitely co-determined by riparian vegetation. In part, this is due to the fact that the inclusion of vegetation dynamics in physical and numerical models has been limited.

2. Approach

To address the issues above, we developed a Dynamic Vegetation model based on Basic Model Interface (BMI) technology and the Delft3D Flexible Mesh Suite. The model for riparian vegetation dynamics is based on the work of Van Oorschot et al. (2014) but set up along more generic lines of plant development processes (establishment, growth, stress, mortality and competition) to also allow for other plant species such as described by Temmerman et al. (2007). BMI allows for direct and quick communication of parameters between the morphodynamic and vegetation models, and bookkeeping of key variables for plant growth such as inundation time. Moreover, the timing of morphodynamic and vegetation updates is more flexible as these can be set to occur when a relevant threshold has occurred, rather than at pre-defined moments in time.

The model has been compared against observations by Javernick et al. (2016) of morphological and vegetative change induced by a flood. Subsequently, a limited Monte Carlo simulation or a series of runs with minor variations in parameter settings was used to generate an envelope of likely river developments, with and without vegetation.

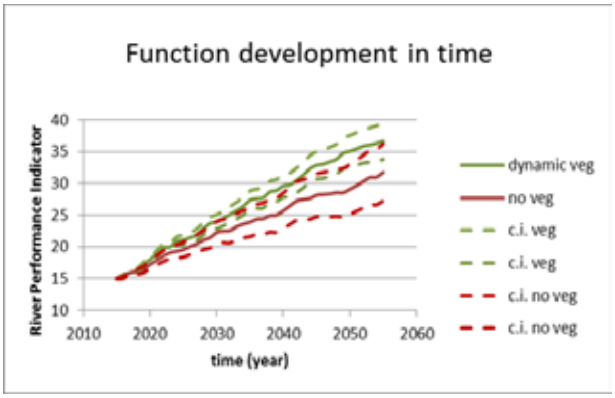

Figure 1: River development with and without dynamic vegetation. The dashed lines indicate confidence intervals or development envelopes.

3. Conclusions

Inclusion of dynamic vegetation in numerical morphological models enables studies of floodplain developments.

Computationally efficient simulation methods allow for multiple model runs, which permit development envelopes.

The developed model system is not only applicable to rivers but also to tidal environments with strong biogeomorphological feedbacks such as saltmarsh and mangrove coasts.

References

Corenblit, D., Steiger, J., González, E., Gurnell, A. M., Charrier, G., Darrozes, J., … Voldoire, O. (2014). The biogeomorphological life cycle of poplars during the fluvial biogeomorphological succession: a special focus on Populus nigra L. Earth Surface Processes and Landforms, 39(4), 546–563. http://doi.org/10.1002/esp.3515

Javernick, L., Hicks, D. M., Measures, R., Caruso, B., and Brasington, J. (2016). Numerical Modelling of Braided Rivers with Structure-from-Motion-Derived Terrain Models. River Research and Applications, 32(5), 1071–1081. http://doi.org/10.1002/rra.2918

Temmerman, S., Bouma, T. J., Van de Koppel, J., Van der Wal, D., De Vries, M. B., & Herman, P. M. J. (2007). Vegetation causes channel erosion in a tidal landscape. Geology, 35(7), 631. http://doi.org/10.1130/G23502A.1

van Oorschot, M., Kleinhans, M., Geerling, G., & Middelkoop, H. (2015). Distinct patterns of interaction between vegetation and morphodynamics. Earth Surface Processes and Landforms, 18. http://doi.org/10.1002/esp.3864

Effects of meander cutting on macroinvertebrates in the high plateau peat-substrate meandering rivers

Mengzhen Xu[1], Fakai Lei[2] and Xiongdong Zhou[3]

[1] Department of Hydraulic Engineering, Tsinghua University, Beijing 100084, China. mzxu@tsinghua.edu.cn
[2] Department of Hydraulic Engineering, Tsinghua University, Beijing 100084, China
[3] Department of Hydraulic Engineering, Tsinghua University, Beijing 100084, China

1. Introduction

As one of the largest high plateau peat swamps around the world, the Yellow River Source, has gain much attention due to its rapid deterioration (Zhou et al., 2018). Meandering rivers are the major flowing water systems on the peat-substrate plateau. Along with climate change and human activities, these meandering river are experiencing active evolution, e.g. meander cut-off and oxbow lake formation. Due to these facts, the aquatic ecosystem has also been influenced. Change in hydrological connectivity of meandering rivers associated with meander cutoff had an important impact on macroinvertebrate assemblages, followed by physical and chemical factors, and nutrition factors (Gallardo et al., 2008).

However, how macroinvertebrate assemblages were influenced by hydrological connectivity and its associated environmental variables in the meandering river-oxbow lake systems on the unique peat-substrate plateau might differ from the previous studies, and requires careful study for statutory habitat protection. In this study, we investigated the macroinvertebrate assemblages in the Lanmucuo River, a typical peat-substrate meandering river in the Yellow River Source Region, in attempt to show the characteristics of the assemblages and their aquatic habitats. In addition, the effects of meander cutoff on the habitat suitability and community structure of macroinvertebrates were predicted with assistance of a model coupled with hydrodynamic and sediment transport and macroinvertebrate suitability to the hydraulic conditions.

2. Study area and methods

The Lanmucuo River is located in the northeast Qinghai-Tibet Plateau (Figure 1 a). This is a small second tributary of the Yellow River with a total length of 55 km and a watershed area of 357 km^2, and the river width is 3 - 10 m. Wide and flat valleys enable free meandering of the Lanmucuo River along most of its reaches. Figure 1 b shows a typical tributary of the Lanmucuo River, where detailed investigations of macroinvertebrate assemblages and their habitat conditions were carried out (Figure 2).

Bio-indices including taxa richness, density, biomass, and improved Shannon-Wiener Index, were determined for each sampling site. Morphological and hydraulic variables were measured correspondingly. The suitability curves of each species to the habitat physical variables were plotted based on the field investigation and the database from our previous study. The species that were very sensitive to changes of physical variables were recognised as the specific indicator for ecological effects of meander cutoffs. Changes in physical variables and their ecological effects were modelled for both of the neck cutoff and chute cutoff patterns.

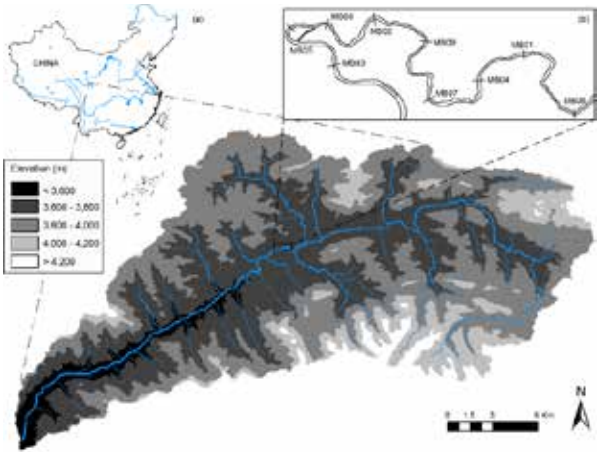

Figure 1 (a) the Lanmucuo River; (b) macroinvertebrate sampling sections on the Lanmucuo River.

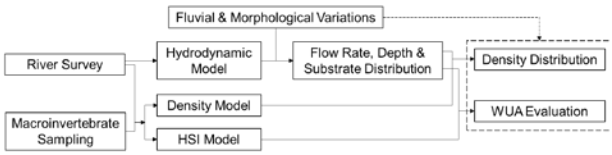

Figure 2 Flow diagram of field investigation and modelling

3. Conclusions

As the flow discharge increased significantly in the channel or even triggered meander cutoff simultaneously, the total abundance of macroinvertebrate assemblages and the abundances of the specific indicator species for physical variations, Polypedilum, Brachycentrus and Limnophila all increased significantly. To be specific, effects of meander cutoff on the macroinvertebrates are much stronger than the discharge increase but without cutoff occurrence.

Acknowledgments

The study was financially supported by the National Science Fund (91547204, 51779120).

References

Zhou X. D., Xu M.Z., Wang Z.Y., Yu B.F., Shao X.J. Responses of macroinvertebrate assemblages to environmental variations in the river-oxbow lake system of the Zoige wetland (Bai River, Qinghai-Tibet Plateau) . *Science of the Total Environment*, 2019, 659: 150~160

Gallardo B, García M, Cabezas Á, González E, González M, Ciancarelli C, Comín F A (2008). Macroinvertebrate patterns along environmental gradients and hydrological connectivity within a regulated river-floodplain. *Aquat Sci*, 70(3): 248-258

Impact of vegetation on bank erosion in a planform braided physical model

Bas Bodewes[1], Rocio L. Fernandez[1] and Stuart J. McLelland[1] and Daniel R. Parsons[2]

[1] Department of Geology and Geography, University of Hull, Hull, United Kingdom. b.bodewes@2016.hull.ac.uk
[2] Energy and Environment Institute, University of Hull, Hull, United Kingdom

Introduction

In fluvial systems, vegetation is considered to be one of the most significant factors influencing the behaviour of river morphology (Gurnell, 2014). Vegetation increases bank stability and therefore can reduce bank erosion; However the interrelationship between vegetation and bank erosion throughout a river reach is poorly understood. This lack of understanding can be attributed to a number of complexities in the system, for example the variability of vegetation over time; both in terms of seasonality as well as growth and decay of vegetation. Such complexities in the behaviour of the system, over different hydrodynamic and morphological time scales, make field research a challenge. Moreover, it makes it difficult to predict inter-relationships between vegetation and bank erosion under future climate change scenarios.

It may be possible to improve our understanding of this from modelling; and although numerical modelling can be used to investigate future scenarios, there is still a need for validated vegetation parameters to improve the accuracy and robustness of such predictions. Physical modelling has the potential to both improve parameters and also validate change over longer periods of simulated time. In the laboratory scaled surrogate vegetation can be used to induce similar effects on sediment stability as vegetation at the field scale, but can be grown much faster than prototype examples. Physical modelling therefore offers a route to parameterise vegetation in numerical models, particularly under a range of forcing scenarios.

The use of surrogate vegetation in flume experiments has previously been demonstrated by Tal and Paola (2007) to stabilise fluvial systems. However, there is limited research on the impact of vegetation age and complexity on the behaviour of fluvial systems. Research presented in this paper addresses this through a focus on identifying the effect of vegetation age (linked to its stabilising influence), on bank erosion rates in a braided system.

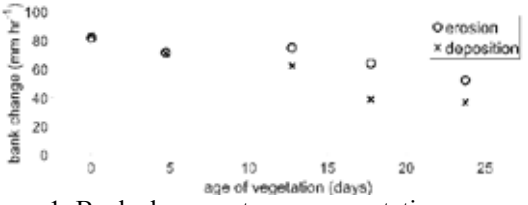

Figure 1: Bank change rates over vegetation age.

Experimental Set-up

For this research, we used a physical model of a braided fluvial system at the Total Environment Simulator, University of Hull. Two parallel mobile channel beds, each 10 m long and 2.5 m wide, were constructed with a bed slope of 0.015. Initially, a constant water and sediment discharge allowed the river system to evolve towards an equilibrium state. Then we seeded vegetation (Alfalfa) and allowed it to grow for up to 24 days. At regular intervals, we released a succession of hour long flood events. Each event was separated from the next by a break to collect terrestrial laser scans, sediment output and imagery. As a reference condition, we conducted a similar sequence of measurements on a bare braided river.

Results

As expected, analysis of the digital elevation models (DEMs) between each run indicate a negative relation between vegetation and erosion rates in the braided system. A novel method to examine bank erosion rates, based on each individual channel in the DEM, allowed us to collect bank erosion rates over small (1 cm) stretches of each channel, totalling several thousands of data points per individual flood event. Distributions of these datasets allowed us to compare different planform geometries to each other to identify the impacts of vegetation on bank erosion rates. Moreover, by comparing distributions of different vegetative settings we were able to identify the relative impact of different stages and ages of vegetation on bank erosion rates. The results show that older vegetation decreases bank erosion rates by over 50% compared to our bare reference (Figure 1).
A similar approach for deposition rates not only allowed us to identify a decrease in deposition rates for vegetation presence. It also permitted, through comparison of erosion and deposition rates, a decrease in channel width.

Summary and Conclusions

This research correlates with present day expectations on the reduction of bank erosion rate with vegetation presence and the age of the vegetation, it also highlights the possibility to deliver a dataset to correlate and test numerical modelling parameters of vegetation modulated morphodynamics. Moreover, the techniques used to explore spatial distributions of bank erosion should also be transferable to numerical modelling, field data and providing a comparison over different fluvial and scientific methods.
The outcomes of our experiments reveal bank erosion rates are decreased by adding vegetation; older, more complex vegetation decreases bank erosion rates even further; and channels become narrower and deeper with older vegetation.

Acknowledgements

Experiments supported by funding from European Union's Horizon 2020 research and innovation programme, grant agreement No654110, HYDRALAB+.

References

Gurnell, A. (2014). Plants as river system engineers. *Earth Surface Processes and Landforms,* 39: 4-25.

Tal, M., Paola, C. (2007) Dynamic single thread channels maintained by the interaction of flow and vegetation. *Geology*, 35(4): 347-350.

Seeds entrainment due to capillarity by a vegetation canopy

P. Peruzzo[1], W. Shi[1] and A. Defina[1]

[1] Department of Civil, Environmental and Architectural Engineering, University of Padova Padova, Italy.
paolo.peruzzo@dicea.unipd.it, wei.shi.1@studenti.unipd.it, andrea.defina@dicea.unipd.it

1. Introduction

The classical scheme of the morphodynamic evolution of wetlands relies on the mutual interactions between the hydrodynamics, vegetation and sediment. More recently the efforts in this field focused also on the development of vegetative areas coupled with the morphology of the watercourses as well as the tidal environments.

The physical processes involved in the so-called biomorphodynamic are manifold. Among the others, the hydrochory, namely the dispersion of plants seeds by the water, plays a pivotal role in the restoration as well as the colonization of new regions (Nilsson et al., 2010). Such a process strictly depends on the seeds and vegetation (plants features, pattern, and density), as well as the hydrodynamic regime, in particular as far concerning for the fate of floating particles. On the other hand, the preservation of vegetative areas is possible as long as the plants are able to retain an adequate amount of seeds and organic matter. This latter aspect is rather unexplored and a robust theory explaining reciprocal interactions between the plant and the generated seeds still lacks in the literature. In this perspective, the present contribution aims at determining the retention capability of floating particles within a canopy of emerging vegetation.

2. Methods

The fate of particle flowing within the canopy, which can be approximated as an array of rigid cylinders, depends on its probability to interact with the stem and on the result of this potential interaction. Both these events are mainly governed by the counterposed forces due to the capillarity and flow dragging. However, the estimation of the drag force acting on the particle is hardly feasible deterministically, because of the heterogeneity of the velocity field (Peruzzo et al., 2012). Consequently, only a stochastic approach can be incisive to model the retention of floating particles. Specifically, a seed with floating time T_F traveling within a canopy can encounter a cylinder in average any $\Delta s=1/\sqrt{n_s}$, where Δs is the mean centre-to-centre spacing between adjacent cylinders and n_s is the stem density. Let P_i be the probability that a particle interacts with the stem, on average, a particle interacts with one cylinder over a path whose length is $\Delta s/P_i$. On assuming that each interaction results in random temporary trapping whose time distribution follows a negative exponential with mean retention time T_R, in uniform flow condition of velocity U, the distance travelled L by the seeds before being capture, i.e. before its travel time exceeds T_F, is

$$P(x > L) = \sum_{k=0}^{n} \binom{k}{n} (1 - P_i)^k P_i^{n-k} [1 - \Gamma] \qquad (1)$$

where n=int($x/\Delta s$) is the number of the potential interactions travelling the distance L, and $\Gamma = \Gamma$ (k, T_R, $T_F - L/U$) is the Gamma cdf distribution of the seed residual time $T_F - L/U$.

3. Results and Discussion

The comparison between the probability distribution predicted by Equation 1 and the literature data for calamus seeds released into a wooden rods array (Liu et al., 2019) provides a preliminary assessment of the proposed model. The results are summarized in Figure 1a. The distance covered by the particles in T_F= 600 s increases with U. The increasing of the flow and hence of the drag acting on the particles entails a plummeting of both the capacity of the stem to interacts and to retain the particle, as clearly visible by the exponential decreasing of the parameters T_R and P_i with U reported in Figure 1b.

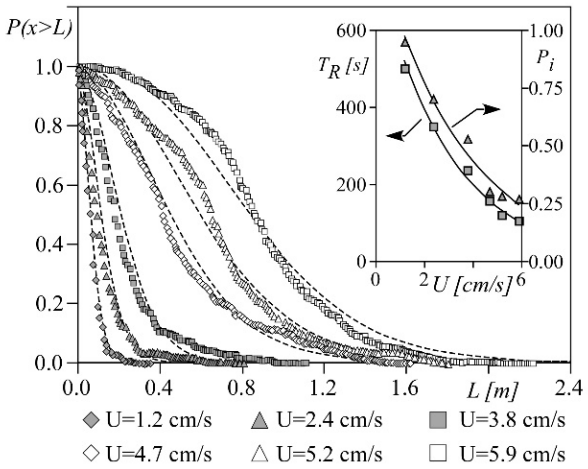

Figure 1. a) The probability a particle has of travelling a distance x greater than L in the experiments of Liu et al. (2019). Dotted line represents the model prediction. b) T_R and P_i as function of the bulk velocity U.

4. Conclusions

Although the role of the hydrodynamics in the particles retention is well established, the proposed model also allows us to properly quantify the seeds entrainment. This aspect is crucial towards the definition of a more complex model able to describe the evolution in time of the vegetative region including the process of hydrochory.

References

Liu, X., Zeng, Y., & Huai, W. (2019). Floating seed dispersal in open channel flow with emergent vegetation. *Ecohydrology*, 12(1), e2038.

Nilsson, C., Brown, R. L., Jansson, R., & Merritt, D. M. (2010). The role of hydrochory in structuring riparian and wetland vegetation. *Biological Reviews*, 85(4), 837-858.

Peruzzo, P., Defina, A., & Nepf, H. (2012). Capillary trapping of buoyant particles within regions of emergent vegetation. *Water Resources Research*, 48(7).

Three-dimensional distribution of vegetation-induced turbulence and its effect on suspended sediment concentration profiles in oscillatory flows.

J.E. San Juan and R.O. Tinoco

Ven Te Chow Hydrosystem Laboratory, Department of Civil and Environmental Engineering, University of Illinois at Urbana-Champaign, Urbana, USA. snjnbln2@illinois.edu, tinoco@illinois.edu

1. Introduction

Changes in coastal morphology at the regional-scale result from the summation of nonlinear processes that take place at the micro- and mid-scales [Perillo and Piccolo (2011)]. As aquatic vegetation grows, it modifies the flow and sediment transport rates locally around it. Aquatic plant's drag (canopy drag) drains energy from currents and waves into canopy-scale and stem-scale turbulence. Such vegetation-induced hydrodynamic conditions affect sediment transport as a function of vegetation morphology, which modifies turbulence dynamics in terms of dissipation and production [Norris et al. (2017)]. Thus, a dual bed erosion–protection behavior for aquatic vegetation is commonly found in literature and yet not well understood [Tinoco and Coco (2018)]. We identify and characterize the fundamental mechanisms controlling suspended sediment transport in coastal vegetated environments, conducting an extensive experimental series to measure suspended sediment concentrations within vegetation patches in an oscillatory tunnel.

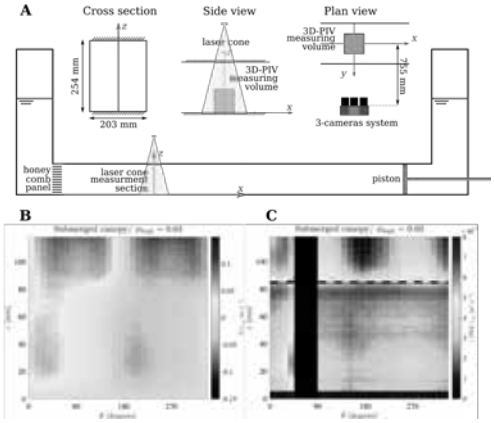

Figure 1. Setup in oscillatory tunnel (A) and temporal distribution of long. velocity and TKE (B-C) for submerged dense vegetation on a vertical x-z plane.

2. Experimental Setup

Experiments are conducted in a U-shaped 0.20 m-wide 0.25 m-high cross-section oscillatory tunnel (see Figure 1A as shown in San Juan et al. (2019)). The tunnel is provided with an actuator-piston system that drives a sinusoidal flow in a range of 3 to 10 s-period and 25 to 100 mm-piston stroke. We used crushed walnut shells (D_{50} = 1.26 mm and ρ_s = 1,300 kg m^{-3}) as mobile bed to ensure sediment resuspension. Arrays of randomly distributed acrylic 6.35 mm-diameter cylinders simulate emergent and submerged vegetation at 3 different patch densities (sparse, intermediate, and dense conditions). Instantaneous velocity fields are measured using a 3-dimensional 3-component Particle Image Velocimetry system (3D PIV – TSI V3V system from TSI, Inc). It uses a coplanar array of 3 PowerView, 4MP (2048 × 2048), 180 fps cameras, and an Nd:YAG, 100 mJ, 532 nm, 100 Hz, dual cavity PIV laser with a maximum sampling frequency of 80 Hz. We measure suspended sediment concentration using the backscatter intensity signal from an Ultrasonic Velocity Profiler (UVP – UVP-DUO system from Met-Flow SA). A 1 MHz probe allows us to take suspended sediment concentrations profiles at 1 mm-resolution.

3. Results

A first series without sediment was conducted to focus solely on hydrodynamics of both emergent and submerged arrays with no sediments. The spatial distribution of Turbulent Kinetic Energy (TKE) and coherent flow structures caused by the vegetation is measured in a 120×120×100 mm^3 measuring volume at a 2 mm spatial resolution. Our data shows both canopy-turbulence structures at the water-canopy interface as well as wake-generated turbulence inside the array (see Figure 1B-C). Our studies with sediment will show the relative dominance of these two processes to properly characterize the vegetation effect on enhancing or suppressing sediment transport within vegetation patches.

4. Conclusions

Using calibrated ultrasonic backscatter intensity and 3D-PIV, we are able to measure suspended sediment concentration profiles and correlate it with their vegetation-induced hydrodynamics. Characterizing suspended sediment transport in vegetated oscillatory flows will lead to better understanding of the physical mechanisms that bring and keep sediments in suspension, to improve fundamental sediment transport relationships for near-shore environments, and ultimately enhance our understanding of the role of aquatic vegetation in the morphological development of coastal systems.

References

Norris, B. K., Mullarney, J. C., Bryan, K. R., and Henderson, S. M. (2017). The effect of pneumatophore density on turbulence: A field study in a sonneratia-dominated mangrove forest, vietnam. *Continental Shelf Research*, 147:114–127.

Perillo, G. and Piccolo, M. (2011). *Global Variability in Estuaries and Coastal Settings*, volume 1, pages 7–36. Waltham: Academic Press.

San Juan, J. E., Carrillo, G. V., and Tinoco, R. O. (2019). Experimental observations of 3d flow alterations by vegetation under oscillatory flows. *Environmental Fluid Mechanics*, pages 1–29.

Tinoco, R. and Coco, G. (2018). Turbulence as the main driver of resuspension in oscillatory flow through vegetation. *Journal of Geophysical Research: Earth Surface*, 123(5):891–904.

The interaction between vegetation patches and tidal creeks in salt-marsh system

L. Geng[1], S. Lanzoni[1], A. D'Alpaos[2], Z. Gong[3], Y. Zhang[3]

[1] Department ICEA, University of Padova, Padova, Italy. liang.geng@dicea.unipd.it, stefano.lanzoni@dicea.unipd.it
[2] Department of Geosciences, University of Padova, Padova, Italy. andrea.dalpaos@unipd.it
[3] State Key Laboratory of Hydrology-Water Resources and Hydraulic Engineering, Hohai University, Nanjing, China. gongzheng@hhu.edu.cn, ying.zhang95@hhu.edu.cn

1. Introduction

The interaction between the expansion of vegetation patches and the growth of tidal creeks plays an important role on the evolution of tidal flats and salt marshes, driving the eco-morphodynamic evolution of the system. On the one hand vegetation distribution and biomass strongly depends on the local elevation. On the other hand, vegetation patches influence the hydrodynamic and sediment transport (Temmerman et al., 2005; Van Oyen et al., 2015), determining the evolution of the topography and the development of tidal creeks. However, the processes that control the formation of an efficient tidal channel network remain unclear (Kearney and Fagherazzi, 2016).

2. Method

Based on the model introduced by Van Oyen et al. (2015), we set up a new model to simulate a tide-dominated salt marsh and study the interaction between the expansion of vegetation patches and the growth of tidal creeks. The flow field is calculated by solving the depth-averaged momentum and mass conservation equations. The local annually-averaged biomass production is expressed through a fitness function (D'Alpaos and Marani, 2016). The roughness on the bed surface is assumed as a linear function of local biomass. Three vegetation species with the same optimal elevation are compared, in which species 1 can survive within the broadest range of elevations, while the suitable range of elevations for species 3 is the narrowest.

3. Results and Conclusions

The simulation begins with a flat topography with initial randomly-distributed roughness. The tidal current propagates into the salt marsh through a deep channel. After several tides, two distinct tidal creeks initiate between vegetation patches, and extend into the salt marsh through headward erosion. As the bed elevation increases, vegetation patches also expand towards the area far away from the channel. Vegetation growth is restrained at the area much higher than the optimal elevation. Figure 1 shows the bed elevation and the distribution of biomass on the salt marsh with species 2 after 730 tidal cycles.

At the beginning of evolution, the sediment deposition is much stronger than erosion (see Figure 2). The magnitude of deposition decreases with the rising elevation and increasing flow shear stress. After the first vegetation patches formed, more sediment deposits and the erosion between the vegetation patches becomes intense. After the creeks grow much deeper, the erosion begins to weaken. On the anther hand, as the elevation continually increases, some areas near the channel become higher than the optimal elevation for vegetation, the vegetation patches there degenerate and a further decrease in

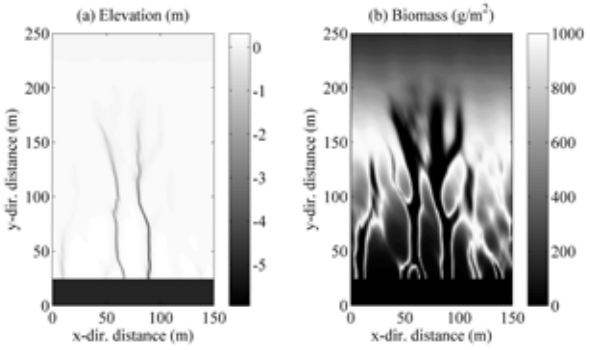

Figure 1. Bed elevation and distribution of biomass on the salt marsh with species 2 after 730 tidal cycles.

deposition happens. If one only considers the influence of roughness induced by vegetation, the luxuriant vegetation which can survive in a board range of elevation (e.g. species 1, solid lines in Figure 2) will lead to more erosion and less deposition at the beginning of the evolution, and the variation in erosion and deposition on the salt marsh is much faster, generating deep creeks much earlier than in other cases.

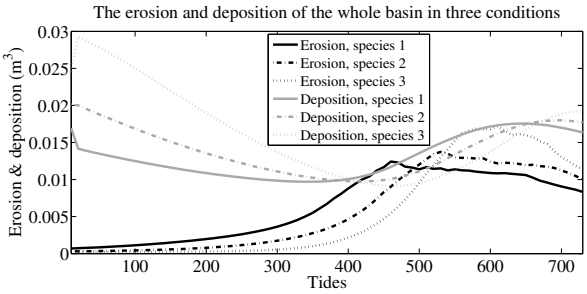

Figure 2. Erosion and deposition of the whole basin in three conditions with different vegetation species.

References

D'Alpaos, A. and Marani, M. (2016). Reading the signatures of biologicgeomorphic feedbacks in salt-marsh landscapes. *Advances in Water Resources*, 93:265–275.

Kearney, W. S. and Fagherazzi, S. (2016). Salt marsh vegetation promotes efficient tidal channel networks. *Nature Communications*, 7:12287.

Temmerman, S., Bouma, T. J., Govers, G., Wang, Z. B., and Herman, P. M. J. (2005). Impact of vegetation on flow routing and sedimentation patterns: Three-dimensional modeling for a tidal marsh. *Journal of Geophysical Research Earth Surface*, 110(F4):–.

Van Oyen, T., Carniello, L., D'Alpaos, A., Temmerman, S., Troch, P., and Lanzoni, S. (2015). An approximate solution to the flow field on vegetated intertidal platforms: Applicability and limitations. *Journal of Geophysical Research Earth Surface*, 119(8):1682–1703.

Wave-dominated or current-dominated? A study on turbulence-driven sediment resuspension on combined flows through aquatic vegetation

R.O. Tinoco

University of Illinois at Urbana-Champaign, IL, USA, tinoco@illinois.edu

1. Introduction

Aquatic vegetation controls various physical, chemical, and biological processes in coastal areas, estuaries, and wetlands (e.g., Nepf 2012 and references therein). Sediment transport is one of the processes affected by the presence of vegetation, and various studies have advanced our understanding on the dynamics driving initiation of motion, resuspension, and deposition within and around vegetation patches subjected to unidirectional currents or waves (Tinoco and Coco 2016, 2018). Insight from these studies allows us to study more complex scenarios closer to the conditions found in estuaries, wetlands, and tidal areas, where the interaction between waves and currents drives the sediment dynamics.

We present results from a series of laboratory experiments using rigid cylinders to mimic submerged vegetation on a sand bed. Dense, sparse, and null (no vegetation) arrays were subjected to waves, currents, and combined flows. Synchronous measurements of velocity, free surface elevation, and suspended sediment concentration, were collected to investigate the effect of wave-current interactions on sediment dynamics within and around the submerged arrays.

2. Experimental setup

The experiments were conducted in a 2 m wide wave-and-current flume. An 18 m long, 0.2 m thick sand bed was built at the center of the flume. A 6 m long array of rigid cylinders, with diameter d = 0.02 m was placed at the center of the sand bed, protruding 0.21 m from the bed. Four array densities were investigated: n = {0, 25, 150, 250} cyl / m^2, to represent flat bed, sparse, intermediate, and dense conditions. A submergence ratio h / D = 2 was used, where h = height of the array and D = water depth. Currents up to Uc = 0.2 m/s following and opposing the direction of propagation of waves with wave heights up to H = 0.12 m and wave periods of T = 2.5 s were tested.

Velocities were recorded with arrays of Acoustic Doppler Velocimeters (ADV), synchronous with Optical Backscatter Sensors (OBS) to monitor suspended sediment concentration at elevations z/D = {0.12, 0.33, 0.50, 0.63, 0.76} at the mid-length of the cylinder array, and an array of capacitive wave gages along the length of the flume to monitor free surface elevation. In addition, top- and side-view pictures (Figure 1) were collected to visualize the changes in bed morphology within the arrays before and after each experiments series. The sand bed was manually flattened before each series to ensure repeatability by starting each test with similar initial conditions.

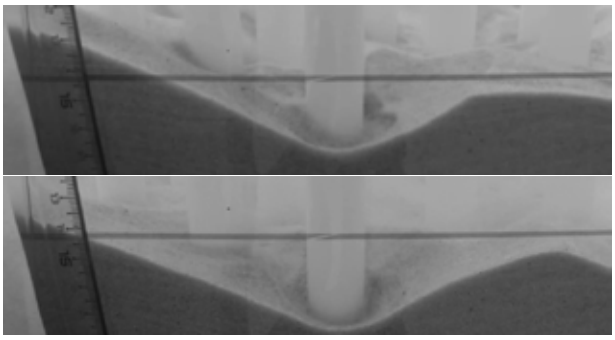

Figure 1: Current (top) and wave (bottom) erosion patterns within a dense (n=250 cyl/m^2) array of rigid cylinders.

3. Results

The series with only waves, and with only currents, show that velocities within the array decrease due to vegetated drag. However, more sediment is lifted onto suspension with denser arrays using the same forcing, indicating that vegetation-generated turbulence, rather than mean speed or orbital velocities, drives sediment resuspension.

The findings with waves- and current-only scenarios allowed us to compare against the results from combined flows, to identify whether the various combinations investigated can be treated as wave-dominated or current-dominated flows. Stem-scale turbulence was clearly identified for all combined flows, but not the canopy-scale eddies, generated by shear at the top of the canopy. We use our turbulence data with existing models (Zeller et al. 2015, Yang et al. 2018) to clearly identify the main parameters to predict suspended sediment dynamics under various flow combinations.

References

Nepf, H.M. (2012). Flow and transport in regions with aquatic vegetation. Annual review of fluid mechanics, 44, pp.123-142.

Tinoco, R.O. and Coco, G. (2016). A laboratory study on sediment resuspension within arrays of rigid cylinders. Advances in Water Resources, 92, pp.1-9.

Tinoco, R.O. and Coco, G. (2018). Turbulence as the main driver of resuspension in oscillatory flow through vegetation. Journal of Geophysical Research: Earth Surface, 123(5), pp.891-904.

Yang, J.Q. and Nepf, H.M. (2018). A Turbulence-Based Bed-Load Transport Model for Bare and Vegetated Channels. Geophysical Research Letters, 45(19), pp.10-428.

Zeller, R.B., Zarama, F.J., Weitzman, J.S. and Koseff, J.R. (2015). A simple and practical model for combined wave–current canopy flows. Journal of Fluid Mechanics, 767, pp.842-880.

On the Dynamics of Turbulence within Aquatic Vegetation Canopies

R. C. Houseago[1], L. Hong[2], J. L. Best[2,3], D. R. Parsons[1], L. P. Chamorro[2]

[1] Energy and Environment Institute, University of Hull, HU6 7RX, UK (r.houseago@hull.ac.uk)
[2] Mechanical Science and Engineering Department, University of Illinois, Urbana, IL, 61801 (lpchamo@illinois.edu)
[3] Departments of Geology, Geography & GIS and Ven Te Chow Hydrosystems Laboratory, University of Illinois, Urbana, IL, 61801 (jimbest@illinois.edu)

1. Introduction

Aquatic vegetation significantly influences the hydrodynamics of many riverine and coastal environments, which subsequently affects sediment transport and broader-scale morphodynamics. Present flume-based research has investigated vegetation flow dynamics around surrogate rigid and flexible canopies; however, the physical obstruction has limited continuous spatial assessment of flow inside canopies, thus relying on point measurements using ADV or LDA techniques.

Preliminary efforts by the team (Hong *et al*, 2019) characterised the flow field and blade dynamics of a staggered flexible canopy (see Figure 1). The research presented herein builds upon, and applies these findings, through an investigation of a dynamically scaled vegetation canopy, providing knowledge of flow-biota dynamics and the associated importance of turbulence within such environments.

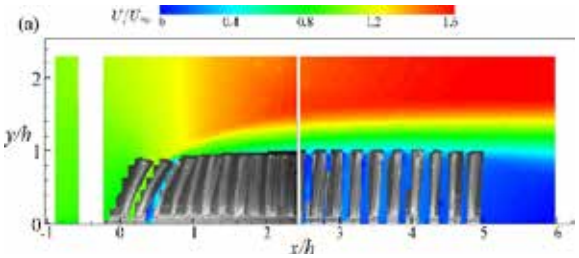

Figure 1: Example of PIV time-averaged streamwise velocity flow field around a flexible canopy illustrating the shear layer evolution. From Hong et al. (2019).

Although the shear layer at the top of canopies has been quantified in detail (Ghisalberti and Nepf, 2006), the dynamics, transport and evolution of coherent structures across scales from flow over the canopy to the bed is not well understood. This work provides new insight on the spatiotemporal momentum fluxes and associated blade motions on in-canopy hydrodynamics, an essential process zone in terms of near-bed turbulence and associated sediment entrainment and mixing.

Using a unique Refractive Index Matched (RIM) flume facility, this research provides continuous spatial coverage of flow dynamics within and above a dynamically scaled surrogate flexible seagrass vegetation canopy. These data are complimented by comparative assessment of a rigid canopy to provide broader application of this research to a diverse range of biota-flow environments, including coral reef, saltmarsh, and mangroves. Results detail the fundamental understanding of complex flexible blade motions and associated in-canopy hydrodynamics.

2. Experimental Methods

A flexible canopy of length 1.4 m, height 0.12 m, and width 0.45 m, and a rigid counterpart were placed in a recirculating Refractive Index Matching (RIM) flume that is 2.5 m long, 0.45 m wide, and 0.45 m high, at the University of Illinois. The flume was operated in a free surface mode with a flow depth of H = 0.36 m. The flexible canopy was dynamically scaled using the Cauchy Number (Ca) in comparison to *Zostera marina,* a common seagrass species, at a canopy density of 566 stems m^{-2}. The RIM flume provided an undistorted optical view throughout the interior of the geometrically and dynamically scaled flexible vegetation canopy. This enabled the acquisition of mean and time resolved Particle Image Velocimetry (PIV) measurements at various planes within the developed flow of each canopy. Measurements of the flow allowed characterisation of the unsteady, three-dimensional motions of the vegetation blades using 3D Particle Tracking Velocimetry (PTV). The ability to obtain in-canopy instantaneous velocity vectors, and coherent flow structure evolution, has been unobtainable previously due to optical impingement, and is only achievable though this novel non-intrusive methodological approach.

3. Research Outcomes

The results quantify the differences in turbulence processes present when dynamic scaling of vegetation flexural rigidity is suitably considered, in comparison to rigid canopies. Research outputs provide new insight into the understanding of hydrodynamics and coherent flow structure generation and transport within vegetation canopies, along with the associated potential implications for sediment entrainment and transport. Results also offer new understanding of flow-biota interactions, which in turn influence broader scale morphodynamics.

Acknowledgements

This work was supported by a British Society for Geomorphology Postgraduate Research Grant, awarded to R. C. Houseago. The experiments were performed in a facility built under the NSF Grant Award CBET-0923106. This work was supported by the MechSE Dept, UIUC, as part of the start-up package of L. P. Chamorro.

References

Ghisalberti, M. and Nepf, H. (2006). The Structure of the Shear Layer in Flows over Rigid and Flexible Canopies. *Env. Fluid Mech.*, 6(3), pp.277-301.

Hong, L., Houseago, R.C., Best, J.L., Parsons, D.R. and Chamorro, L.P. (2019). On the unsteady dynamics of a fully submerged, flexible canopy. Manuscript in Preparation.

Whakarongo ki nga taniwha – Listen to the taniwha: Decoding Indigenous Knowledge to enable Intercultural River Management

D.C.H. Hikuroa [1]

[1] Te Wānanga o Waipapa, University of Auckland, Auckland, New Zealand. d.hikuroa@auckland.ac.nz

1. Introduction

Hitherto mostly ignored or disregarded by the science and engineering community because it seemed to be myth or legend, fantastic and implausible, mātauranga, the knowledge of the indigenous people of New Zealand, is generated using techniques consistent with the scientific method, but also includes culture and values and is explained according to a Māori world view (Hikuroa 2017). Pūrākau are a traditional form of mātauranga, in narrative form, containing philosophical thought, epistemological constructs, cultural codes and world views. Pūrākau are an integral part of mātauranga. They are explanations of landscapes, seascapes and associated phenomena, consistent with a Māori world-view, deliberately constructed to encapsulate and condense into easily understood forms, Māori views of the world, of ultimate reality and the relationship between the atua (deities), the universe and humans. Pūrākau explained as 'myths' invalidate Māori ontological and epistemological constructs of the world, and pūrākau understood as just 'stories' is an inadequate explanation of the importance and efficacy of pūrākau in teaching, learning and the intergenerational transfer of knowledge (Lee, 2009; Hikuroa 2017. There is a commonly held view that indigenous knowledge is static and only relevant and applicable in the past (Hikuroa et al. 2008). Pūrākau can be accurate and precise (Hikuroa 2017). Pūrākau are codified forms of knowledge – once the 'code' is known, useful empirical information regarding river, coastal and estuarine morphodynamics can be revealed.

2. Taniwha

Taniwha are supernatural creatures in Māori tradition, similar to serpents and dragons in other cultures. They could also take the shape of animals such as sharks, whales, octopuses, or even logs. Some taniwha could change their shape, moving between different forms. They were said to reside in the ocean, rivers, lakes or caves. Exploits of taniwha include eating and killing people, kidnapping women and eating or inundating land. One example is Karu-tahi, whom Ngāti Naho inform, has a number of lairs along the banks of the Waikato River.

Taniwha are a form of pūrākau, that can have varied meanings to different whānau (families), hapū (groups of families) and iwi (tribal nations). Another common widespread but less well known understanding is that taniwha are our kaitiaki – our guardians. One example is Tuhirangi, whom Kupe the legendary explorer left in the Te Moana a Raukawa (Cook Strait), who guided and protected canoes in the area.

However in contemporary New Zealand society, taniwha, and those who know and speak of them, are at best widely misunderstood, at worst ridiculed. Practically, taniwha can be explanations for the observations of how rivers, coasts and estuaries change through time and serve to reduce disaster risk, acting simultaneously as warning signs and guardians (Hikuroa 2017).

3. Intercultural decision-making

While there are many similarities between mātauranga and science, it is important that the tools of one are not used to analyse and understand the foundations of the other (Hikuroa 2017). Te Mana Rauhī Taiao – the Environmental Protection Authority is developing a new and comprehensive approach to bringing mātauranga into its regulatory practice (Jenkins 2018).

This talk will discuss taniwha and their role in contemporary Aotearoa New Zealand, how they provide temporal components of river behaviours that extend back through centuries, how in turn that can influence our work to better understand river, coastal, and estuarine morphodynamics, their emergent intercultural use in decision-making, and how they continue to keep us safe.

3. Conclusions

Some indigenous knowledge has been generated according to the scientific method.

Pūrākau are codified forms of knowledge, that can have an empirical basis.

In the de-coding process, it is critical that the once prevalent practic of appropriating knowledge is not continued, and that ethical and moral considerations are met.

Indigenous knowledge and its role in intercultural management of rivers, coasts and estuaries is not only relevant today but also in the future.

Acknowledgments

The author would like to thank Anthony Olsen, Frontiers Abroad and its alumni, Te Mana o Ngāti Rangitihi Trust, Ngā Kaihautū Tikanga Taiao, Kaupapa Kura Taiao, Te Mana Rauhī Taiao, all of whom have contibuted in some way to the work being presented herein.

References

Hikuroa, D., Morgan, K., Durie, M., Henare, H. 2011. Integration of Indigenous Knowledge and Science. The International Journal of Science in Society 2:1-14.

Hikuroa, D. 2017. Mātauranga Māori – the ūkaipō of knowledge in New Zealand. Journal of the Royal Society of New Zealand 47(1): 5-10.

Jenkins, K. 2018. Remember the flicking tail of the lizard: How mātauranga Māori is being woven into place-based regulatory decisions in Aotearoa 15(2): 55-61.

Lee J. 2009. Decolonising Māori narratives: Pūrākau as method. MAI Review 2(3):1–12.

Turbulent Oscillatory Flow Through Random Array of Emergent Vegetation

S. Dutta[1], P. Ranjan[2], K. Mittal[2], P. Fischer[2] and R.O Tinoco[2]

[1] CSI, City University of New York (CUNY), New York, USA. somdutta.mail@gmail.com
[2] University of Illinois at Urbana-Champaign, Urbana, USA

1. Introduction

Aquatic vegetation are commonly referred to as "ecosystem engineers" due to its ability to modify and stabilize its environment, and are a fundamental component of the near-shore ocean ecosystem (Nepf, 2012b). They not only improve water-quality and help create habitat, they also play a major role in protecting coastal environment from erosion. Most of the studies in the past have focused on unidirectional flows (Nepf, 2012a), and a few that have focused on oscillatory flows have primarily relied on laboratory experiments (Tinoco and Coco, 2018). These experiments provide ambient conditions closer to nature, though they often lack the spatial and temporal resolution required to fathom the fundamental details. On the other hand, most of the numerical studies till date have primarily used CFD models based on temporal averaging of the Navier-Stokes equations (RANS), which approximates the turbulence in the system rather than accurately calculating it. And a few studies which conducted Large Eddy Simulations (LES), did it for relatively small number of vegetation elements (cylinders). The current study is a geared to bridge the above-mentioned gap in knowledge, with numerical simulations being conducted at unprecedented scale. The simulations are at the scale of laboratory experiments, but at a spatio-temporal resolution that is able to resolve all the important scales of turbulence. Flow through array of cylinders with different arrangements like random, regular and staggered have been conducted, to understand the effect of spatial heterogeneity of the vegetation on the flow. Eventually, better understanding of the flow structure and turbulence within the array has been used to gain insight into transport of sediment within the vegetation array.

2. Numerical Model

High-resolution Large Eddy Simulations (LES) of the flow at different configurations of the idealized vegetation have been conducted using the open-source, spectral element based higher-order incompressible Navier-Stokes solver Nek5000 (Fischer et al., 2008). The Spectral Element Method (SEM) combines the accuracy of spectral methods and the flexibility of Finite Elements Method (Deville et al., 2002). The simulated domain contain an array of around 200 rigid-cylinders, and the have been resolved using around 200 million computational points. A portion of the computational domain has been shown in fig. 1.

3. Results and Conclusions

Here we provide a glimpse of the flow results. Instantaneous velocity magnitude at different distance from the bottom have been plotted in fig. 2, and it shows that the length of the vortex being shed increases with distance from the bottom. Due to the unsteady nature of the flow (oscillatory), the flow shows significant variation in time.

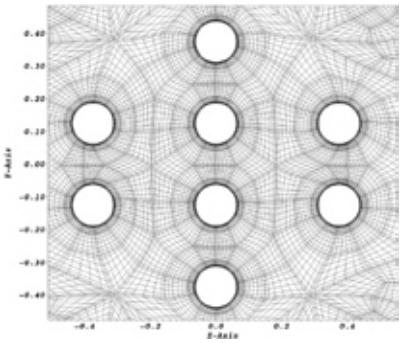

Figure 1. Part of the computational domain, zoomed in to illustrate the resolution of the mesh.

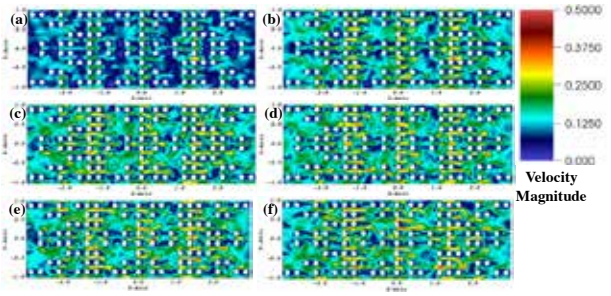

Figure 2. Instantaneous velocity magnitude at different distance from the bottom. Slices at (a) 0.5 % height (b) 1 % height (c) 10 % height (d) 50 % height (e) 75 % height (f) 95 % height. The length of the vortex being shed increases with distance from the bottom.

Additionally, the flow is highly 3D in nature, and often the local and global flow and dissonant. Part of the analysis, turbulent kinetic energy (tke) and vorticity has also been calculated. The highly three-dimensional flow not only aids vertical mixing, it also has significant effect on transport of sediment.

Acknowledgments

Major part of the research was conducted my the first author while he was post-doc at UIUC.

References

Deville, M. O., Fischer, P. F., and Mund, E. H. (2002). *High-order methods for incompressible fluid flow*, volume 9. Cambridge university press.

Fischer, P. F., Lottes, J. W., and Kerkemeier, S. G. (2008). nek5000 web page, 2008. *https://nek5000.mcs.anl.gov/*.

Nepf, H. M. (2012a). Flow and transport in regions with aquatic vegetation. *Annual review of fluid mechanics*, 44:123–142.

Nepf, H. M. (2012b). Hydrodynamics of vegetated channels. *Journal of Hydraulic Research*, 50(3):262–279.

Tinoco, R. and Coco, G. (2018). Turbulence as the main driver of resuspension in oscillatory flow through vegetation. *Journal of Geophysical Research: Earth Surface*, 123(5):891–904.

Aggradation and degradation in the upper Rhine-Meuse Delta in response to climate change

Clàudia Ylla Arbós[1], Francesca Soci[1,2], Ralph M.J. Schielen[3,4] and Astrid Blom[1]

[1] Delft University of Technology, Delft, the Netherlands. c.yllaarbos@tudelft.nl; astrid.blom@tudelft.nl
[2] Università degli Studi di Firenze, Florence, Italy. francesca.soci@stud.unifi.it
[3] Rijkswaterstaat Water, Traffic and Environment, Lelystad, the Netherlands. ralph.schielen@rws.nl
[4] University of Twente, Enschede, the Netherlands

1. Introduction

The upper Rhine-Meuse Delta (RMD) is not in equilibrium (Blom, 2019). On one hand, the river bed is incising, and by that decreasing its slope. Degradation rates vary depending on the location, and can reach up to 2 cm/yr. On the other hand, the bed surface is rapidly coarsening. In the Bovenrijn, the median grain size has increased an order of magnitude (from 1 to 10 mm) in the past 20 years. The decrease of channel slope is associated with extensive channel narrowing in the 19th and 20th centuries. The bed surface coarsening seems to be related to a coarsening of the sediment supply from upstream, which is due to both ongoing bed degradation and nourishment of coarse sediment in the German Rhine. Climate change affects these trends, as it affects several controls of the river system. Here we consider changes in the probability distribution of water discharge and sea level rise, in order to gain insight on the response of the upper RMD to climate change.

2. Method

In a first approach, we use a 1D hydro-morphodynamic model for unisize sediment, in a simplified reach of the Waal. Due to future-related uncertainty, we use climate scenarios, as done by Verhaar et al. (2010). We consider the sea level rise scenarios of the KNMI (2015) and the water discharge scenarios of Sperna Weiland et al. (2015).

3. Preliminary results

3.1 Sea level rise

For simplification, we apply sea level rise at the current rate of 3 mm/yr (KNMI, 2015) for 25 years, starting from an equilibrium state. This variation of the downstream boundary condition triggers a morphodynamic response towards a new equilibrium state, which consists of an increase of bed level equal to the total rise of sea level. The slope is the same in the two equilibrium states. Indeed, higher water levels imply smaller flow velocities, reduced sediment transport capacity, and thus aggradation.

First results show an important increase of the aggradation rate in the first years, tending to a value of 2.5 mm/yr at the mouth (Figure 1).

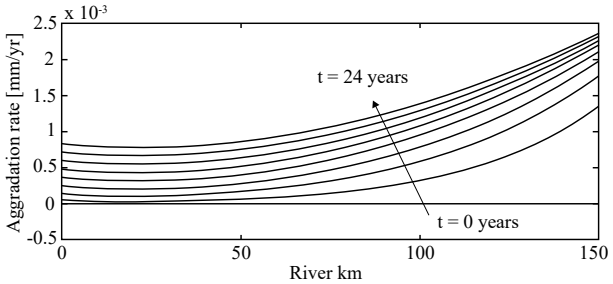

Figure 1. Aggradation rate for 25 years of sea level rise.

The morphodynamic response does not proceed as fast as sea level rise, i.e. the river bed cannot keep pace with the base level change. This results in an aggradational wave that migrates upstream, far beyond the backwater zone. This idea is contrary to the common misconception that the morphodynamic response is confined to the backwater-affected reach.

3.2 Changes in water discharge

Climate change affects the probability distribution of water discharge through 1) higher winter peak flow rates; 2) lower summer base flow rates; and 3) increased duration of low flow periods (Sperna Weiland et al., 2015). Higher peak discharges have a stronger effect in the resulting dominant discharge, making it increase. So do the flow velocity and sediment transport capacity, which results in a decrease of the equilibrium slope and therefore a downstream-migrating degradational wave. Further research is needed in order to study the interaction between the degradational and the aggradational waves.

4. Conclusions and outcome

Preliminary conclusions from these first results are:

- Current morphodynamic trends in the upper RMD proceed fast. Climate change influences these trends, with important consequences for the river functions.
- Enhanced bed aggradation develops in response to sea level rise. The resulting aggradational wave migrates upstream, beyond the backwater zone.
- A higher dominant discharge causes a downstream-migrating degradational wave.

In the next step, the models used for these predictions will be improved to account for mixed-size sediment, larger spatial scales, and eventually include 2D features for complex processes such as bifurcations or floodplain effects. Other upgrades include accounting for human interventions, which can have major morphological impacts.

References

Blom, A. (2019). Effects of climate change on the Dutch Rhine branches. https://goo.gl/M7AE8G.

KNMI (2015). KNMI'14 Climate Scenarios for the Netherlands. http://www.climatescenarios.nl/.

Sperna Weiland, F., Hegnauer, M., Bouaziz, L., and Beersma, J. (2015). Implications of the KNMI'14 climate scenarios for the discharge of the Rhine and Meuse. Technical report, Deltares, Delft.

Verhaar, P. M., Biron, P. M., Ferguson, R. I., and Hoey, T. B. (2010). Numerical modelling of climate change impacts on Saint-Lawrence River tributaries. *Earth Surface Processes and Landforms*, 35(10):1184–1198.

A morphological investigation of marine transgression in estuaries

I.H. Townend[1,2], Z.Zhou[1], G. Coco[3], L. Chen[1], C.K. Zhang[1]

[1] College of Harbour, Coastal and Offshore Engineering, Hohai University, Nanjing, China
[2] School of Ocean and Earth Science, University of Southampton, UK
[3] Faculty of Science, University of Auckland, New Zealand

1. Introduction

The landscape setting for an estuary varies widely and the primary origin is an important component of any estuary classification (Hume and Herdendorf, 1988). The origin is determined by the antecedent landform of which there are three broad classes, namely: surface deformations of the hard geology (tectonic, volcanic and glacial), marine derived embayments, and fluvial/glacial river valleys (Townend, 2012). our research has focussed on estuaries in river valleys and how they may adjust in response to sea level rise, or, in other words, the marine transgression of the estuary system.

2. Brief Background

Under conditions of marine transgression, such as those experienced over the Holocene, river valleys are areas of excess accommodation space. Provided a sediment supply exists, then estuaries in such settings have a tendency for sedimentary infilling (e.g. Rees, 2006). It is generally believed that this infilling continues, supply permitting, until the estuary form achieves a dynamic equilibrium in relation to the incident hydrodynamic forces (Pethick, 1994). Observations in the Severn Estuary, have led to the suggestion that once an estuary system reaches this dynamic equilibrium, then infilling ceases and the estuary form begins to migrate landwards (Allen, 1990). The role of limiting factors in this process, such as sediment supply, is not wholly understood, but it appears that under conditions of rising sea level, estuary forms have the potential to maintain their positions relative to the tidal frame (Townend and Pethick, 2002). To do this the estuary form must move landwards and upwards, a process which has been referred to as "estuary rollover", or 'stratigraphic rollover' (Allen, 1990).

3. Method

A simple 3D geometric representation of an idealised estuary form is used to capture the dominant longitudinal and cross-sectional variations. Whilst this ignores meanders it does include a 3D representation of the surrounding hinterland - the antecedent valley. The resultant representation is then used to explore the implications of translating the 3D estuary form. This enables the changes that might be expected under conditions of sea level rise and marine transgression to be explored. This is a morphological analysis to examine the characteristics of accommodation space. It is distinct from a morphological process model, which predicts the changes in form in response to hydrodynamic forcing conditions but rarely considers the landscape setting. To examine which of the various possible morphological changes are more likely, a simple aggregated model (ASMITA) is used to represent the ability of the channel and tidal flats to adapt.

5. Preliminary Results

If the estuary system does not translate (e.g. because it is fixed by geology or sea walls) this generates a sediment demand and the available sources of sediment become critical in determining the system response. However, if the system is able to migrate landward, whilst also warping-up the sediment demand reduces. In a manner akin to the so-called 'Bruun' rule for beaches, there is a translation distance that requires zero sediment input, Figure 1. This is achieved by spatially varying accretion and erosion, which is dependent on the shape of the estuary.

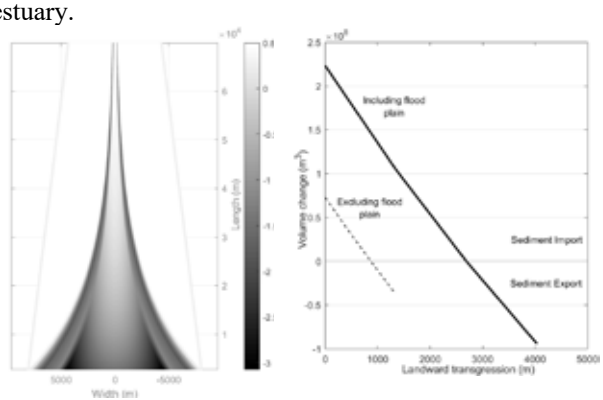

Figure 1: (a) plan view contour plot of change in elevation (dark-erosion, light-accretion); (b) volume change as function of transgression distance

5. Conclusions

For the estuaries examined, sediment budgets suggest net import is small and historical records of change suggest systems close to equilibrium. This implies that landward transgression is an integral part of the response to sea level rise, with clear management implications. Furthermore, the greater the lateral constraint the higher the sediment demand to avoid "drowning".

References

Allen, J.R.L., 1990. The Severn Estuary of southwest Britain: its retreat under marine transgression, and fine sediment regime. Sedimentary Geology, 66(1-2), 13-28.

Hume, T.M., Herdendorf, C.E., 1988. A geomorphic classification of estuaries and its application to coastal resource management. Journal of Ocean and Shoreline Management, 11, 249-274.

Pethick, J.S., 1994. Estuaries and wetlands: function and form. In: R.A. Falconer, P. Goodwin (Eds.). Wetland Management. Thomas Telford, pp. 75-87.

Rees, J.G., 2006. Sea-level, topographical and sediment supply controls on Holocene sediment composition in the Humber Estuary. Phil.Trans.R.Soc.Lond.A., 364, 993-1008.

Townend, I.H., 2012. The estimation of estuary dimensions using a simplified form model and the exogenous controls. Earth Surface Processes and Landforms, 37, 1573-1583.

Townend, I.H., Pethick, J., 2002. Estuarine flooding and managed retreat. Phil.Trans.R.Soc.Lond.A, 360(1796), 1477-1495.

Projections of 21st century global river delta change in response to sediment supply and sea-level rise

J.H. Nienhuis[1], H. Middelkoop[1] and R.S.W. van de Wal[1,2]

[1] Physical Geography, Utrecht University, Utrecht, NL, j.h.nienhuis@uu.nl, h.middelkoop@uu.nl
[2] Marine and Atmospheric Research, Utrecht University, Utrecht, NL, r.s.w.vandewal@uu.nl

1. Introduction

Aside from "bath-tub" style inundation models, the effects of sea-level rise (SLR) on global river delta change remains elusive. Coincidentally, decreased sediment loads are likely to influence the response of deltas to SLR, but this is poorly quantified.

From theory and physical experiments it is well-known that the balance between sediment supply and sea-level rise exerts a first-order control on delta change (Parker & Muto, 2003; Lorenzo-Trueba et al., 2013). Here we assess this balance for 10,848 river deltas and predict global deltaic land area change for SLR rates expected in the 21st century.

2. Methods

We use the USGS HydroSheds and ETOPO1 to retrieve global river and offshore elevation for 10,848 rivers (Fig. 1, Fig. 2A). For these rivers, we estimate the fluvial sediment flux (Cohen et al., 2013), regional SLR (Church et al., 2004), and estimate the ratio of the fluvial to bedrock slope (Lorenzo-Trueba et al., 2013), an important non-dimensional ratio that determines the response of the fluvial profile to SLR. We apply a simple scaling for delta width based on empirical relations of Syvitski and Saito (2007). We estimate the proportion of fluvial sediment retained within the deltaic profile based on a calibration obtained from observed delta change (Donchyts et al., 2016).

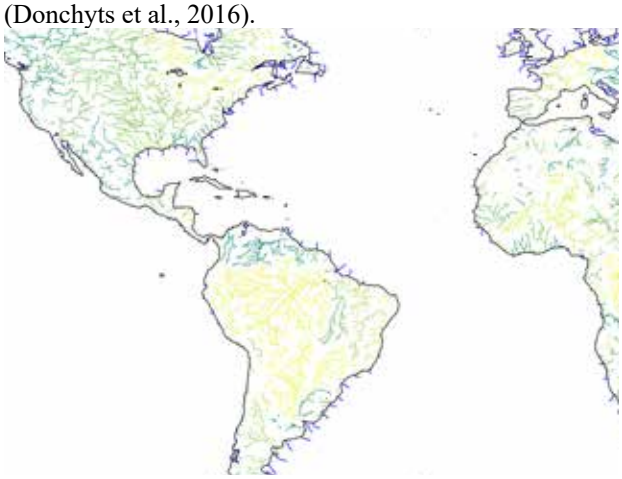

Figure 1: Global fluvial and shelf profiles

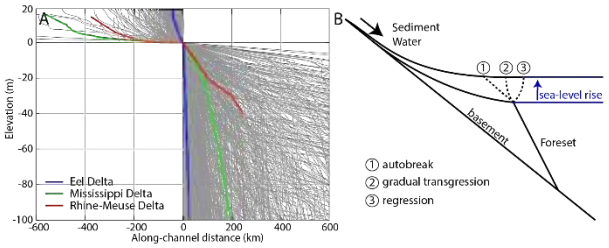

Figure 2: (**A**) fluvial and shelf profiles, and (**B**) potential responses of river profiles to sea-level rise.

3. Results and Conclusions

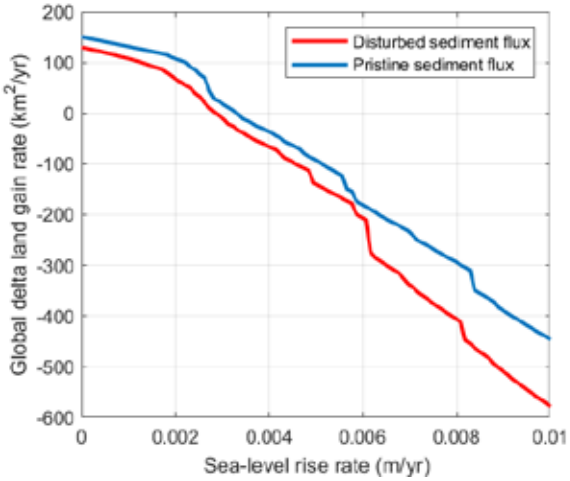

Figure 3: Expected global deltaic land area change.

We find that the range of potential future SLR rates exerts an important control on future deltaic change (Fig. 3). Modern global delta growth, based on an average SLR rate of ~2.5 mm/yr, is ~50 km^2/yr. Net global delta loss ensues at about 3 mm/yr. For SLR rates of 10 mm/yr, deltas are expected to lose 500 km^2/yr. A similar calculation assuming deltas would still carry pre-dam ('pristine') sediment fluxes highlights the effects of dams on global river delta change.

5. References

Church, J. A., White, N. J., Coleman, R., Lambeck, K., & Mitrovica, J. X. (2004). Estimates of the Regional Distribution of Sea Level Rise over the 1950–2000 Period. *Journal of Climate*, *17*(13), 2609–2625. https://doi.org/10.1175/1520-0442(2004)017<2609:EOTRDO>2.0.CO;2

Cohen, S., Kettner, A. J., Syvitski, J. P. M., & Fekete, B. M. (2013). WBMsed, a distributed global-scale riverine sediment flux model: Model description and validation. *Computers & Geosciences*, *53*, 80–93. https://doi.org/10.1016/j.cageo.2011.08.011

Donchyts, G., Baart, F., Winsemius, H., Gorelick, N., Kwadijk, J., & van de Giesen, N. (2016). Earth's surface water change over the past 30 years. *Nature Climate Change*, *6*(9), 810–813. https://doi.org/10.1038/nclimate3111

Lorenzo-Trueba, J., Voller, V. R., & Paola, C. (2013). A geometric model for the dynamics of a fluvially dominated deltaic system under base-level change. *Computers & Geosciences*, *53*, 39–47. https://doi.org/10.1016/j.cageo.2012.02.010

Parker, G., & Muto, T. (2003). 1D numerical model of delta reponse to rising sea level. In *3rd IAHR Symposium on River, Coastal and Estuarine Morphodynamics* (pp. 1–10). Barcelona.

Syvitski, J. P. M., & Saito, Y. (2007). Morphodynamics of deltas under the influence of humans. *Global and Planetary Change*, *57*(3–4), 261–282. https://doi.org/10.1016/j.gloplacha.2006.12.001

Modelling response of the Wadden Sea tidal basins to relative sea-level rise

Z.B.Wang[1,2]

[1] Deltares, Delft, The Netherlands. zheng.wang@deltares.nl
[2] Delft University of Technology, Delft, The Netherlands. z.b.wang@tudelft.nl
[3]

1. Introduction

The Wadden Sea contains the world largest coherent tidal flats and spans a distance of nearly 500 km along the northern coasts of the Netherlands and the North Sea coast of Germany and Denmark. It is separated from the North Sea by a series of barrier islands, and characterized by a wide variety of channels, sand and mud flats, gullies and salt marshes.

Climate change and especially the associated acceleration of sea-level rise forms a serious threat to this ecologically valuable system. Subsidence of seabed due to e.g. gas and salt extraction contributes to additional relative sea-level rise.

The intertidal flat in the Wadden Sea can be drowned when the sea-level rise rate exceeds a critical limit (Van Goor et al., 2003). This means that the intertidal flats are then permanently inundated seriously affecting the ecological functioning of the system. However, the determination of this critical limit and the modelling of the transient process of how a tidal basin respond to accelerated sea-level rise is still a subject of research.

For the tidal basins in the Dutch Wadden Sea Wang et al. (2018) evaluated the critical sea-level rise rate and projected the impact of the relative sea-level rise in 2030, 2050 and 2100 using the sea-level rise scenario's presented by Vermeersen et al. (2018) and the predictions for seabed subsidence by Fokker et al. (2018). However, the evaluation is based on the then available models and the future projections are mainly based extrapolation of the observed morphological development in the tidal basins.

In this contribution we revisit the modelling of the response of the Wadden Sea tidal basins to sea-level rise. The main questions we want to address are: what are the possibilities and restrictions of the various models? How can the different types of models be applied in combination with (restricted) field data for reliable future predictions?

2. Approach

Two types of morphodynamic models are considered, the process-based models e.g. Delft3D and the aggregated models e.g. ASMITA (see e.g. Van Goor et al., 2003). The relations between the two types of models are made clear by analysing the model formulations. The analysis reveals the essential differences between the two types of models and makes clear their possibilities and restrictions.

A problem for modelling impact of relative sea-level rise is the model verification / validation. Direct validation of the model concerning e.g. drowning of tidal flats due to sea-level rise is practically impossible as it would require field observations of at least centuries. Analysis based on the ASMITA model provides insight on how the long-term morphodynamic modelling for response to sea-level rise can be validated using shorter-term field observations and process-modelling using complex models.

3. Results & Conclusions

Comparison between Delft3D and ASMITA reveals that the only essential differences between the two types of models is the level of (spatial and temporal) aggregation and the type of empirical knowledge implemented in the model. In ASMITA the empirical relations defining morphological equilibrium are used instead of the empirical sediment transport formulas in Delft3D. The high level of aggregation makes ASMITA capable to relate e.g. the critical rate of sea-level rise explicitly to the model parameters, but on the other hand the parameter setting of ASMITA needs careful consideration as the model parameters are less directly measurable than those in Delft3D.

Theoretical analysis on the ASMITA model reveals that the critical sea-level rise rate is determined by the morphological equilibrium state and a time scale. Surprisingly, this time scale is not the same as the morphological time scale for a disturbance to the morphological equilibrium to decay in time. The power in the relation between sediment transport capacity and flow velocity does not influence the time scale determining the critical sea-level rise rate but it does influence the decaying time scale of a disturbance to morphological equilibrium. This insight can be used for better guiding the analysis of the (limited available) field data concerning morphological development for determining the parameters in morphodynamic models for simulating the response to sea-level rise.

This makes the modelling of the response of the Wadden Sea to future sea-level rise, based on the combined use of different type of models and available field data, more reliable.

References

Van Goor, M.A., Zitman, T.J., Wang, Z.B. & Stive, M.J.F., 2003. Impact of sea-level rise on the morphological equilibrium state of tidal inlets. Marine Geology 202: 211–227.

Fokker, P.A., Van Leijen, F., Orlic, B., Van der Marel, H. & Hanssen, R., 2018. Subsidence in the Dutch Wadden Sea. Netherlands Journal of Geoscience, Netherlands Journal of Geosciences, 97-3: 129-181.

Vermeersen, L.L.A., Slangen, A.B.A. et al., 2018. Sea level change in the Dutch Wadden Sea. Netherlands Journal of Geoscience, Netherlands Journal of Geosciences, 97-3: 79-127.

Wang, Z.B., Elias, E.P.L., Van der Spek, A.J.F. & Lodder, Q.L., 2018. Sediment budget and morphological development of the Dutch Wadden Sea - impact of accelerated sea-level rise and subsidence until 2100. Netherlands Journal of Geosciences, 97-3: 183-214.

Mesh Size Independent Turbulence Closure for the Shallow Water Equations

Dr G.R. Collecutt[1], Dr S. Gao[2] and W.J. Syme[3]

[1] BMT. greg.collecutt@bmtglobal.com; [2] BMT. shuang.gao@bmtglobal.com; [3] BMT. bill.syme@bmtglobal.com

1. Introduction

In the vast majority of fluid flows involving water, turbulent eddies are the principle mechanism for the diffusion of momentum, heat and mass. Computational solutions for fluid flows fall into two broad categories: (1) steady state, in which the mean velocity field is solved, or (2) transient (or unsteady), in which turbulent eddies of sizes larger than the grid size are represented within the velocity field. In the first case, a turbulence closure model representing all scales of turbulence must be chosen, whereas for the second case the turbulence model needs only represent the scales of turbulence that are not resolved – i.e. sub-grid-scale.

Consider the two-dimensional (2D) depth averaged incompressible Navier-Stokes equations, i.e. the Shallow Water Equations (SWE). Historically, many SWE solvers utilised 1st order spatial schemes, which exhibit (mesh size dependent) numerical diffusion. Software developers would often forgo the complexity of a turbulence closure model on the assumption that it was approximately included via the diffusivity of the 1st order scheme. However, due to inaccuracies inherent with 1st order solutions (Collecutt and Syme, 2017), SWE solvers need to be 2nd order spatial schemes, which exhibit little numerical diffusion, to model complex flows. Modellers are also using increasingly finer spatial resolutions, sometimes approaching or smaller than the water depth. However, turbulence closures in use (e.g. Smagorinsky) are not necessarily applicable and can show inconsistent results across different mesh sizes. Therefore, there is a pressing need for a SWE turbulence closure approach that is mesh size independent.

2. Turbulence Closure for the SWE

The kinetic energy associated with turbulent eddies cascades from larger to smaller physical scales. In the case of shallow flows, the turbulent energy cascade becomes bi-modal as shown in Figure 1, which is based on a similar figure from Nadaoka and Yagi (1998).

For spatial scales similar to and smaller than the water depth (right side of the figure), the turbulence is 3D with the energy source primarily bed friction. However, for spatial scales much larger than the water depth the turbulence becomes 2D, with bed friction representing an energy sink (wherein it is converted to smaller scale 3D turbulence). The bi-modal nature of the turbulence has significant implications with regard to turbulence modelling for shallow flows.

For the 2D sub-grid-scale turbulence the zero-equation, widely used, Smagorinsky model was considered. For the 3D sub-depth-scale turbulence two models were considered. The first was a zero-equation model (Wu 2004) based on depth averaged vertical diffusion coefficient and Prandtl's mixing length theory. The second was a one-equation transport model known as the Prandlt model. Three benchmark case studies of widely varying spatial scale were used to assess the utility of these models: a right-angled flume bend, a dam breach flume into a channel with obstacle, and a deep, fast flowing river with sharp bends. In each case mesh-size sensitivity studies are performed and results compared with available calibration data. The TUFLOW HPC solver (Collecutt and Syme 2017) was used, and the primary assessment criterion was the prediction accuracy of energy/head losses derived from flume measurements or recorded field data.

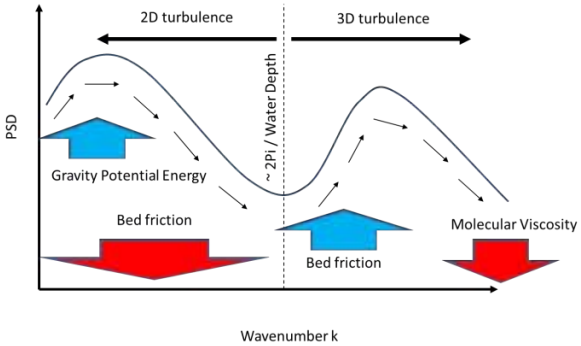

Figure 1: Shallow Flow Turbulent Energy Cascade

3. Conclusions

Findings show that including only the 2D sub-grid-scale turbulence leads to unphysical solutions as the mesh size is reduced to values significantly less than the water depth. Further, for the cases studied (in which mesh size was typically not significantly greater than water depth) modelling the 2D sub-grid-scale turbulence was found to be unnecessary when the 3D sub-depth-scale turbulence is included. In this regard, both Wu's zero-equation model and the Prandtl one-equation model performed equally well. However, it was also found that using only the depth averaged vertical diffusion coefficient of Wu's equation performed equally well over the range of mesh sizes and physical scales studied. Should further testing of Wu's approach produce the similar conclusions, we will make Wu's formulation available in future releases of TUFLOW.

References

Nadaoka, K., and Yagi, H. (1998). Shallow Water Turbulence Modelling and Horizontal Large Eddy Computation of River Flow. *J. Hydraulic Engineering*, pages 493–500.

Wu, W., Wang, P., Chiba, N. (2004), Comparison of Five Depth Averaged 2D Turbulence Models for River Flows, *Hydro-Engineering and Environmental Mechanics*, Vol. 51, No 2, pages 183-200.

Collecutt, G., and Syme, B. (2017). Experimental benchmarking of mesh size and time-step convergence for a 1st and 2nd order SWE finite volume scheme. *Proceedings of the 37th IAHR World Congress, Kuala Lumpur*.

Sensitivity of River Flooding to Coastal Bar Morphology

M.J. Smith[1], M.P. Barnes[2] and T.J. Devlin[3]

[1] BMT, Brisbane, Australia. mitchell.smith@bmtglobal.com
[2] BMT, Brisbane, Australia. matthew.barnes@bmtglobal.com
[3] BMT, Brisbane, Australia. toby.devlin@bmtglobal.com

1. Introduction

Low-lying floodplain and coastal regions adjacent to river mouths are often densely populated due to historical settlement, as well as the aesthetic and recreational values they provide. These regions are typically susceptible to periodic inundation from both riverine floods and storm tides, and combined with low topographic relief, small changes in inundation level can have a pronounced impact on the number of properties and infrastructure affected.

Bar and spring tide delta formation is a common feature at river mouths and act as a hydraulic control to tidal or river flows. The morphology and bathymetry of these areas can be highly dynamic and experience rapid changes during periods of high flows, significantly affecting the flood behaviour. Understanding the morphological changes and the consequential hydraulic effects can meaningfully benefit risk management of floods and storm tides.

The river entrance investigated naturally migrates in response to the prevailing coastal and fluvial processes. Hydraulic modelling undertaken as part of a previous flood hazard assessment adopted a static entrance condition representative of the available bathymetry and topography datasets at the time. From a review of historical imagery and surveys there are episodic scour events that provide a wide range of possible river mouth configurations that can profoundly affect flood behaviour and upstream inundation.

This paper addresses the uncertainty related to variable bathymetry and entrance conditions via a coupled hydrodynamic-morphological numerical model scour analysis. They key objectives include:

- Quantifying the sensitivity and changes in flood behaviour and tidal intrusion with respect to the entrance configuration and channel bathymetry.
- Defining the most appropriate entrance configuration and channel bathymetry for design flood events.

2. Numerical Modelling

A 'river mouth' model encompassing the lower reach of the estuary and offshore was developed using TUFLOW FV (BMT, 2019). The model was calibrated and validated to ADCP-derived flows and currents, as well as surveyed water levels at key locations adjacent to the mouth and upstream for astronomical tide conditions. The 5, 100 and 2,000 year return period flood events were sourced and applied from an existing calibrated catchment flood model of the system that overlapped with the 'river mouth' model. Outflows, velocities and bed shear stresses from the models were shown to be in good agreement for each flood event.

Multiple-layer non-cohesive sediment modelling utilised the TRANSPOR model (Van Rjin et al., 2004). With advances in computational power, and an innovative hydrodynamic-morphological coupling of the whole system from lower estuary to offshore, a continuous feedback loop between bed scour/deposition was achieved to more accurately quantify currents and dynamically changing sediment transport processes.

Flood levels and velocities using a static bed (i.e. without morphology enabled) were compared with the coupled hydrodynamic-morphological modelling to quantify the sensitivity on inundation levels caused by scour during flood events. Sensitivity testing of key parameters was carried out to help quantify uncertainty.

3. Conclusions

Substantial redistribution of sand is predicted to occur from the river mouth to offshore during flood events with average scour depths ranging between 0.5 to 1.5 m depending on the event's severity. The deepening of the entrance acts to increase flood conveyance through the river mouth causing lower flood levels. The deeper entrance also increases tidal inflows following the event, increasing the risks from storm tide inundation. The study concludes that it is beneficial to incorporate variable river mouth bathymetry into the modelling to better quantify design flood levels, hazards and uncertainties for planning and flood risk management.

References

BMT (2019). *TUFLOW FV Flexible Mesh Hydrodynamic Finite Volume Manual*. BMT, Brisbane.

Van Rijn, L.C., D.J.R. Walstra and M. van Ormondt (2004). Description of TRANSPOR2004 and Implementation in Delft3D-ONLINE. Z3748.10 – report prepared by Delft Hydraulics for DG Rijkswaterstaat.

Sediment delivery from post-earthquake landslide reactivation caused by Cyclone Gita, February 2018, Kaikoura, New Zealand

B. Rosser[1], C. Massey[1], S Dellow[1], J. K. Jones[1,2]

[1]Geological and Nuclear Science GNS Science, Te Pū Ao, Lower Hutt, New Zealand. b.rosser@gns.cri.nz
[2]School of Geography, Environment and Earth Sciences, Victoria University of Wellington, Wellington, New Zealand

1. Introduction

At 12.03 am local time on 14th November 2016 (UTC: 11.03 am 13th November 2016) a shallow magnitude 7.8 earthquake, with an epicentre located near Waiau in North Canterbury, struck the North Canterbury and Marlborough regions of New Zealand. The earthquake produced one of the most complex fault ruptures observed in the historical period, with at least 23 on-land and submarine fault surface ruptures mapped. The most visible consequence of the strong ground shaking was widespread landslides. More than twenty-nine thousand landslides were triggered over a total area of about 10,000 km^2 with the majority concentrated in a smaller area of about 3,600 km^2 (Massey et al 2018). Notably, 196 landslide dams were identified and posed the greatest post-earthquake risk to downstream communities.

In February 2018, ex-tropical Cyclone Gita bought 270 mm of rain to the earthquake impacted area in 12 hours causing significant reactivation of existing landslides triggered by the Kaikoura earthquake, as well as remobilisation of landslide debris stored on slopes and in the channel network causing debris flows. The Annual recurrence interval (ARI) of the storm rainfall was between 20-40 years, with isolated areas experiencing rainfall with an ARI of 100-200 years (Rosy Morn).

2. Study area

The study area is located in the coastal catchments of the Kaikoura Front ranges, covering parts of the Clarence, Hapuku and Kowhai River catchments. The geology of the study area is dominated by three main rock types: 1) Quaternary alluvial deposits comprising active floodplains and river terraces; 2) erodible Neogene limestone, sandstone and siltstone underlying the hill country, and 3) basement sandstone, predominantly greywacke, forming the coastal slopes and the steep inland Kaikoura ranges. The landslide type was controlled by the geology, with each lithology exhibiting distinct mechanism, deposits and reactivation styles. The slopes are generally steep and highly coupled to the river channels.

3. Methods

Airborne LiDAR was captured in November 2016, immediately after the earthquake, and in March 2018, following Cyclone Gita. A (1 m resolution) difference model was developed by subtracting the 2018 DEM from the 2016 DEM. The difference model identified areas of negative (erosion) and positive (deposition) ground surface change. New landslides as well as reactivation and reworking of existing landslides and their deposits were mapped using the difference model and checked using high resolution aerial photography. Sediment delivered to the channel network by post-earthquake landslides were assessed and quantified.

4. Results

Rainfall associated with Cyclone Gita triggered many landslides in the earthquake affected area. Preliminary results from the LiDAR differencing suggest that most sediment was generated by reactivation or enlargement of existing earthquake-induced landslides or from reworking of landslide debris stored on hillslopes or already in the channel network (from co-seismic landslides). Most of the landslides triggered during Cyclone Gita were highly mobile debris flows that were highly coupled to the channel network leading to a high degree of sediment delivery. The rainfall threshold for triggering landslides on these highly cracked and dilated slopes has reduced from pre-earthquake thresholds so more sediment is generated at lower rainfall and delivered to the already overloaded post-earthquake river systems.

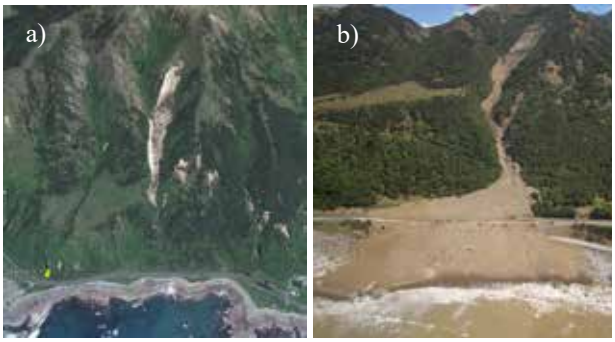

Figure 1: a) Co-seismic landslide triggered by the M7.8 Kaikoura earthquake. Note significant material that is stored on the slope and in the channel. b) Debris flow at the same site triggered by Cyclone Gita. Landslide debris was remobilised during the storm and inundated SH1 below.

5. Conclusions

The rainfall threshold for triggering landslides in the earthquake affected area has reduced and sediment generation rates from landslides has increased following the earthquake through both the triggering of new landslides on weakened slopes and reactivation and reworking of landslide debris stored on the landscape. Data from LiDAR differencing will help to quantify rates of post-EQ sediment generation and delivery to the river system thus improving our understanding of post-earthquake landscape recovery.

References

Massey, C., Townsend, D., Rathje, E., Allstadt, K. E., Lukovic, B., Kaneko, Y., ... & Horspool, N. (2018). Landslides triggered by the 14 november 2016 M w 7.8 Kaikōura earthquake, New Zealand. *Bulletin of the Seismological Society of America*, 108(3B), 1630-1648.

Design of Channel Capacity Improvements Using Physical Hydraulic Model Studies of Two Critical Locations on Water of Leith, Dunedin, New Zealand

M.G. Webby[1], C. Whittaker[2], B.W. Melville[2], J-L.Payan[3], B. Shrestha[3] and A. Shamseldin[2]

[1] Damwatch Engineering, Wellington, New Zealand, grant.webby@damwatch.co.nz
[2] University of Auckland, Auckland, New Zealand, c.whittaker@auckland.ac.nz
[3] Otago Regional Council, Dunedin, New Zealand, Jean-Luc.Payan@orc.govt.nz

1. Introduction

The Water of Leith is a steep mountain stream which flows across an intensively developed floodplain at the north end of Dunedin City. A scheme concept was developed to enable the stream channel to pass the 1% annual exceedance probability (AEP) flood of 171 m^3/s. The existing stream channel provided some difficult challenges to achieve the design flood standard. This paper describes two physical hydraulic model studies undertaken at the University of Auckland to develop economic solutions for two critical locations.

2. Union Street to Leith Street Bend

The Union Street to Leith Street Bend has historically been the breakout point for floods on the Water of Leith with breakouts in 1923 (twice) and 1929 flooding much of Central Dunedin. The sharp 90 degree bend was modified in the 1930's with a series of grade control weirs and near vertical concrete walls lining the banks.
Figure 1 shows a view of the 26 April 2006 flood with a peak flow of 95 m^3/s (56% of the 1% AEP design flood) passing around the bend. The limited channel capacity is compounded by a standing wave pattern along the outer wall and the potential for scouring of the outer wall.

Figure 1: View looking upstream of 26 April 2006 flood (peak flow 95 m^3/s) at Union Street to Leith Street Bend.

A concept for improving the channel capacity at this location was originally developed using a 1:50 scale physical hydraulic model (Webby *et al*, 2006). This involved widening the channel, modifying the grade control weirs, reinforcing the streambed with large boulders and raising the height of the outer wall.
During detailed design, a second 1:25 scale physical model was used to develop an economical solution for the stream channel round the bend. Flood levels along the outside wall were very sensitive to the height of the weirs which were effectively designed as bed control elements. The model was also used to optimise the design of the boulder reinforcement of the streambed.

3. Dundas Street Bridge

The Dundas Street Bridge is skewed on an angle across the start of an S-shaped bend. It was originally designed to accommodate a proposed super-critical flow channel which has never been constructed. Figure 2 shows the 26 April 2006 flood passing under the bridge.

Figure 2: View looking upstream of 26 April 2006 flood (peak flow 95 m^3/s) at Dundas Street Bridge.

A 1:25 scale physical hydraulic model was constructed to assist with designing a culvert extension to the bridge. A 1-d numerical model indicated that the optimum culvert extension width was 4 m compared to the 12 m width of the existing bridge waterway. The physical model was used to refine the geometry of the upstream channel and a downstream wingwall, evaluate the super-elevated flood levels past the bridge, quantify streambed armouring needs, assess flow behaviour through the second part of the bend and test bridge blockages.

3. Conclusion

Physical hydraulic models successfully aided the design of channel modifications to achieve increased flood capacity at two critical locations on the Water of Leith which exhibit complex hydraulic behaviour.

References

Webby, M.G., Parsons, T.G., Coleman, S.E., Melville, B.W., Palmer. G. and Collings, G. (2006). Innovative aspects of design concept for comprehensive flood scheme for water of Leith, Dunedin, South Island, New Zealand. In Ferreira, Alves, Leal and Cardoso, editors, *River Flow 2006, Proc. Int. Conf. on Fluvial Hydraulics*, vol. 2, pages 2167-2178, Taylor and Francis Group, London.

Morphological modelling of the Waikato River between Hamilton and Port Waikato to assess the long term effects of sand extraction

H.L. MacMurray[1] and V.J. Henderson[1]

[1] Barnett & MacMurray Ltd, Hamilton, New Zealand. info@riversandfloods.co.nz

1. Introduction

The Waikato River is one of the largest in New Zealand, with a catchment area of 13701km^2 at Mercer (near the limit of tidal influence), 8230km^2 at Hamilton, and 3487km^2 at the outlet of Lake Taupo. Upstream of Hamilton, seven hydro power dams were built on the river. The furthest downstream of the dams (Karapiro) located about 30km upstream of Hamilton, was completed in 1947. Construction of the dams cut off the sediment flow from a large part of the catchment, and created a long term degrading trend in the river downstream. The lower Waikato River has a sand bed and a low gradient, of approximately 1 in 10,000 between Hamilton and the coast. Sand mining has been carried on in the Waikato River at various places over most of the 20th century, accentuating the tendency for the river bed to degrade. The Waipa River is a major tributary and source of sediment to the lower Waikato River, with a catchment area of approximately 3,000km^2 at the confluence with the Waikato River at Ngaruawahia. Average monthly flows in the Waikato just downstream of the Waipa confluence vary between about 250m^3/s in late autumn to about 450m^3/s in mid winter. The lower river remains an important source of sand for the construction industry. The purpose of the investigation reported here was to assess the long term effects of continued sand extraction on river bed levels.

2. Sand extraction proposal

Winstone Aggregates applied for resource consent to extract 200,000m^3 (bulk volume) of sand per year from a site near Tuakau, in the lower tidally influenced reach of the river. This reach of the river tends to aggrade if there is no sand extraction.

3. Morphological model

A one dimensional morphological model was constructed using DHI MIKE11 software, extending from Hamilton to the coast on the Waikato River, and from Whatawhata to Ngaruawahia on the Waipa River. The model was based on surveyed river cross sections with an average spacing of 600m, and was calibrated to reproduce observed changes in river bed volume between 1998 and 2007. It was verified by simulating river bed changes over the period from 1988 to 1998. The calibrated model was used to predict changes in river bed volume up to 2057. The hydraulic and morphological time steps were 5 minutes and 60 minutes respectively, thus satisfactorily resolving the tidal flow and level variation in the lower river.

4. Sediment inflow boundary conditions

The sediment supply from the Waikato River to the lower river at Ngaruawahia mainly comes from erosion of the river bed. A sediment inflow function was derived for Hamilton such that the observed river bed degradation was reproduced over the calibration period. For the prediction simulation, the sensitivity to a declining rate of river bed erosion was tested.

The sediment supply from the Waipa River to the lower Waikato was estimated to be approximately 60,000m^3/y by measuring sediment transport during a high flow event. The model satisfactorily reproduced the sediment flow rate by specifying a fixed bed level boundary condition.

5. Discharge and tidal boundary conditions

A tidal boundary condition reproducing the neap – spring cycle and with a gradually rising mean level of the sea (by 0.32m in 2050) was generated. Discharge time series were generated by processing the data from the river flow gauges at Hamilton, Ngaruawahia, and Rangiriri, and allowing for an increase in flood flows of approximately 20% by 2050.

6. Prediction simulations

The model predicted that the river bed between Ngaruawahia and the coastal delta would erode by about 2 million m^3 without the proposed sand extraction, and by about 8.6 million m^3 with the proposed extraction. The corresponding average lowering of the river bed in the extraction reach near Tuakau was approximately 0.95m, with the proposed extraction, and approximately 0.7m without any further sand extraction. The model also predicted that in the absence of sand extraction, two reaches in the lower river, upstream and downstream of the extraction site, would aggrade up to 2057, by approximately 0.5m, reducing the flood flow capacity.

7. Monitoring

A resource consent for sand extraction was granted. A condition of the consent is that river bed levels near the extraction site are monitored at 4 yearly intervals. To date the changes in river bed level have been somewhat smaller than the morphological model predicted.

8. Conclusions

The Waikato River has a long term tendency to degrade downstream of the hydro dams. That trend is exacerbated by the historical and continuing sand extraction. However the predicted differences in future bed levels due to the sand extraction are relatively modest.

References

Barnett & MacMurray Ltd 2010: Assessment of effects of Waikato River sand extraction. Report for Winstone Aggregates.

Shoreline evolution modelling for the Clifton to Tangoio 2120 Coastal Hazards Strategy: Southern Cell

J. F. Beya[1]

[1]Asset Management Group, Hawke's Bay Regional Council, Napier, New Zealand. jose.beya@hbrc.govt.nz

1. Introduction

The Clifton to Tangoio 2120 Coastal Hazards Strategy is a process started in 2014 which aims to respond to the anticipated future erosion and inundation risks. In the third stage of the strategy a preferred pathway for coastal adaptation was defined by a panel of community members with the advice of local government and technical experts (Bendall, 2018). The coast was classified in littoral cells and units (within cells) where short, medium and long term preferred pathways were defined.

In the present 4th stage of the strategy, a preliminary but more refined design is needed for the preferred short term pathways. The design involves wave modelling, shoreline evolution modelling and design of groyne fields and nourishment. The present work covers the shoreline evolution modelling part of this process.

2. Shoreline evolution modelling

The shoreline evolution modelling was undertaken with UNIBEST CL+ v. 7.1. Prior to this, a 37 year wave hindcast was generated with SWAN 41.20A for the Hawke's Bay with focus on the area on the present study area. Calibration was achieved by comparing model result to the Napier Port buoy measurements for year 2010. The wave model set-up included 3 nested rectangular grids of 1000 m, 250 m and 50 m and spectral wave boundary conditions and gridded wind forcing from MetOcean. A sensitivity test was also undertaken to assess variability showing that the sheltered zones north of the port and at Clifton and Tangoio had the greatest differences.

In the first part of the shoreline evolution model carried out with UNIBEST LT, several transport formulas (Van der Meer-Pilarczyk, 1988; Van Rijn, 2004; Van Rijn, 2014) input reduction settings and methods, grain size, profile lengths, wave parameters (mean, peak or peak from partitions) and position of the offshore wave boundary condition were assessed in a sensitivity test for 4 beach profiles distributed alongshore. This assessment indicated that the Van der Meer-Pilarczyk formula produced very high transport rates (~100,000 m^3/y) compared to what was expected from sediment balance estimates and previous studies (~30,000 m^3/y). The Van Rijn (2014) formula produced transport in the opposite direction from observations in the northern part of the littoral cell, and, Van Rijn (2004) appeared to produce better results, although this formula was not derived for gravel beaches unlike the previous two. In most cases, using a high number of wave classes (> 2,000), wave partitioned data, wave inputs closer to shore seemed to provide the most reasonable results.

In the second part of the shoreline modelling using UNIBEST CL, the above three transport formulas using wave partitioned and non-partitioned peak parameters and the closest to shore wave inputs were tested. Boundary conditions were initially set as zero transport at the northern boundary (Port) and 18,000 m^3/y at the southern end (Clifton). River sources and sinks were estimated from gravel extraction records at Awatoto and Marine Parade and sediment balance estimates from river cross section surveys. This first modelling results showed that the Van der Meer-Pilarzcyk formula was the only one able to reproduce the qualitative behaviour of the littoral cell where erosion is present south of Awatoto and accretion is occurring north of it. The other two formulas presented erosion at the norther part of the cell which is contrary to the observations. Further calibration of the model with this formula included increased extraction at Awatoto, source modification at the Tukituki river, adding a boundary condition of 32,000 m^3/y at the northern end (port dredging of fine sand material), decreasing sediment transport rates by a 0.7 factor, and, further decreasing the transport rates at the southern part of the cell due to identified hard sea bed structures (Met Ocean, 2011). Model calibration was carried out by comparing model shoreline change rates against measurements (Figure 1).

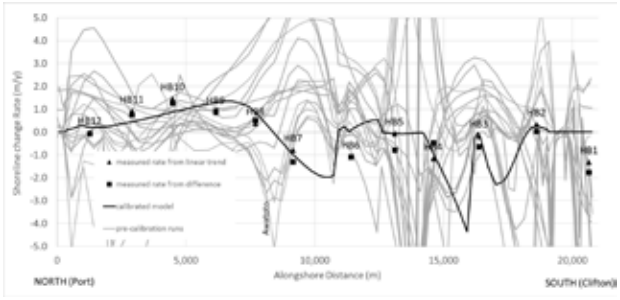

Figure 1: Modelled and measured shoreline change rates.

3. Conclusions

A one-line shoreline evolution model has been developed for the southern cell of the Clifton to Tangoio 2120 strategy. This model will be of use to assess the impact of proposed erosion mitigation alternatives such as groyne fields and nourishment.

Innovative use of wave partition data and a in number of wave classes in the input reduction has shown to produce better results.

There is a significant degree of uncertainty in the model and potential to undertake further studies to decrease it. The main uncertainties are related to the quantification of sediment sources and sediment transport rates.

References

Bendall, S. (2018). Report of the Northern and Southern Cell Assessment Panels – Clifton to Tangoio Coastal Strategy 2120. Final report.

MetOcean (2011). Hawke's Bay October 2011 Sidescan Sonar Survey Interpretation. MetOcean Solutions Ltd: Report P0088-01.

Badass gully morphodynamics and sediment connectivity in Waipaoa Catchment, New Zealand

I.C. Fuller[1], F. Strohmaier[2], S.T. McColl[3], J. Tunnicliffe[4], M. Marden[5]

[1] Physical Geography Group, Massey University, New Zealand. i.c.fuller@massey.ac.nz
[2] Institute of Geography, Friedrich Schiller University of Jena, Germany. florian.strohmaier@uni-jena.de
[3] Geosciences Group, Massey University. s.t.mccoll@massey.ac.nz
[4] School of the Environment, University of Auckland, New Zealand. j.tunnicliffe@auckland.ac.nz
[5] Manaaki Whenua Landcare Research, New Zealand. mardenm@landcareresearch.co.nz

1. Introduction

Large (> 10 ha) gully-mass movement complexes (badass gullies; Marden et al., 2018) are significant contributors to the sediment cascade in steepland East Coast Region catchments. The scale of change taking place in these gully systems allows significant evolution in morphology and sediment dynamics to be tracked at annual to decadal timescales. Here we document changes in two badass gullies in Waipaoa Catchment (Figure 1) to infer sediment connectivity processes using a morphological budgeting approach. This work extends that of Taylor et al. (2018) both spatially and temporally, whose focus was Tarndale from 2005-2011.

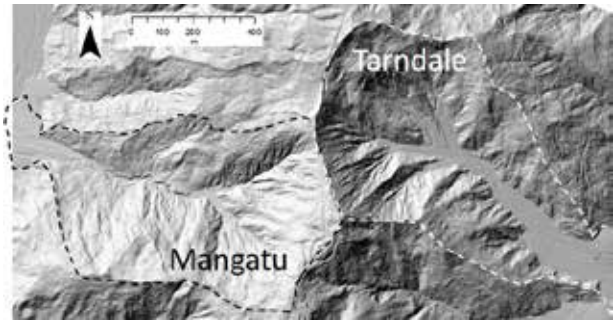

Figure 1: Mangatu and Tarndale gully-mass movement complexes, tributaries of Waipaoa Catchment, East Cape Region, New Zealand.

2. Methodology

A baseline dataset for this study is provided by a LiDAR-derived Digital Elevation Model (DEM) in 2005. We produced new DEMs and orthophoto mosaics using photogrammetry with aerial photographs collected by a remotely piloted aircraft system in 2017, 2018, and 2019. The DEMs and orthomosaics were compared to quantify volumes of erosion and deposition associated with gully morphodynamics in both systems. This approach provides an opportunity to develop assessment of sediment connectivity in two gully systems as they co-evolve.

3. Key findings and conclusions

Preliminary results indicate ongoing rapid development of both these gully mass movement complexes. Severe erosion is taking place at the gully heads with lowering and shifting of the topographic divide separating the two badass gullies (Figure 2). In places there is lateral expansion of the gully complexes, into established plantation forest (Figure 2), while in other places historically-active zones have temporarily stabilised. Key sediment generating processes at both gullies are identified to include surface erosion, shallow and deep-seated landslides, and debris flows. A strong degree of off-slope sediment connectivity is effected by debris flows which transport material from the steep slopes. At Mangatu there is little opportunity for sediment storage, which suggests a high degree of sediment connectivity between the hillslopes and the channel network. In contrast, a larger coalescing fan at Tarndale acts as a buffer, which modulates the sediment connectivity to the downstream receiving trunk valley. Regardless, transport-reaches below both sites periodically cut and fill in response to sediment supply fluctuations, but to differing degrees and timescales, highlighting the complexity of sediment connectivity processes in these systems.

Figure 2: Eroding drainage divide with lateral expansion of the headwall into plantation forest (Tarndale)

Acknowledgments

We would like to thank our field assistants Amy England, James Fay, and Michal Brezny.

References

Marden, M., Fuller, I.C., Herzig, A. and Betts, H.D., 2018. Badass gullies: Fluvio-mass-movement gully complexes in New Zealand's East Coast region, and potential for remediation. *Geomorphology*, 307, 12-23.

Taylor, R.J., Massey, C.I., Fuller, I.C., Marden, M., Archibald, G. and Ries, W., 2018. Quantifying sediment connectivity in an actively eroding gully complex, Waipaoa catchment, New Zealand. *Geomorphology*, 307, 24-37.

Role of sediment flux in setting the channel geometry of bedrock and mixed gravel-bedrock rivers

E.R.C. Baynes[1,2], D. Lague[2], P. Steer[2], S. Bonnet[3]

[1] Department of Civil and Environmental Engineering, University of Auckland, Auckland, New Zealand.
edwin.baynes@auckland.ac.nz,
[2] Univ Rennes, CNRS, Géosciences Rennes – UMR6118, Rennes, France
[3] GET, Université de Toulouse, CNRS, IRD, UPS (Toulouse), France

1. Background

The role of sediment supply is often overlooked in modelling studies of landscape evolution, despite sediment playing a key role in the physical processes that drive erosion and sedimentation in river channels (Turowski, 2018). In response to variations in climate or tectonic uplift rate, it has been shown that bedrock channels evolve dynamically through adjustments to both width and slope. However, landscape evolution models often assume that channel width scales simply with water discharge (Q) or drainage area (e.g. Whipple and Tucker, 1999) or with a constant ratio between the channel width and channel depth (e.g., Finnegan et al., 2005), failing to capture dynamic patterns of channel geometry driven by sediment supply.

2. Approach

This study presents a combined field and experimental study to identify the impact of sediment flux on the channel geometry of bedrock and mixed gravel-bedrock rivers, and the transition from bedrock and mixed gravel-bedrock channels to fully alluvial channels. We first explore trends in channel geometry of river channels in the Rangitikei catchment of the North Island of New Zealand, a natural laboratory where the impact of sediment flux on channel geometry can be isolated. We then used the Bedrock River Experimental Incision Tank at Geosciences Rennes (Baynes et al., 2018) to explore the processes and interactions between sediment dynamics and channel incision in a controlled laboratory setting, allowing the processes leading to small changes in channel geometry to be identified and quantified. Experiments were performed with a fixed water discharge (1.5 l/min) under different sediment supplies (between 0 and 20 g/l) allowing the quantification of the role of sediment in setting the width and slope of channels as well as the distribution of shear stress within channels

3. Results

In the Rangitikei catchment, channels receiving a supply of coarse-grained, hard, sediment are systematically (up to as much as an order of magnitude) wider than channels with no sediment input for a given discharge. During the experiments, increasing the sediment supply for a fixed discharge increased the width, slope and width to flow depth ratio of the channels (Fig. 1). Additionally, channels with low sediment supplies are characterised by simple in-channel morphologies with a uniform distribution of shear stress within the channel while channels with high sediment supplies are characterised by dynamic channels with multiple active threads and a non-uniform distribution of shear stress within the channel.

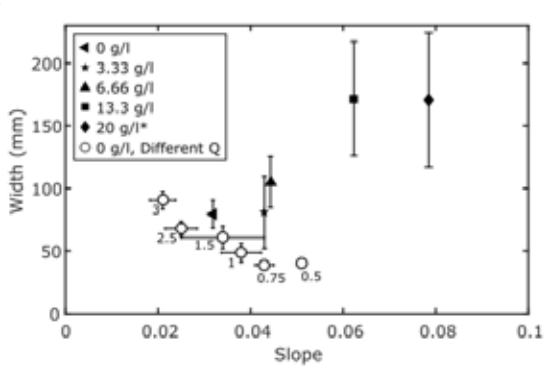

Figure 1: Impact of sediment supply on channel width and slope in experimental channel.

3. Conclusions

Sediment is a critical component of bedrock channel systems, with the supply of hard, coarse-grained, material having a direct impact on the width of channels in the Rangitikei river, New Zealand, and sediment supply having a significant impact on the morphology and dynamics of experimental channels. Given that multiple configurations of channel geometry can exist for a given discharge, solely due to the input sediment supply, we suggest that caution is required when using the channel geometry to reconstruct past environmental conditions such as discharge.

Acknowledgments

This research was funded by the EU Horizon 2020 programme through Marie Sklodowska-Curie Actions Individual Fellowship No. 703230 (to E.B), a British Society for Geomorphology ECR grant (to E.B) and the EROQUAKE project funded by the Agence Nationale de le Recherche No. ANR-14-CE33-005 (to P.S).

References

Baynes, E.R.C., Lague, D., and Kermarrec, J-J. (2018) Supercritical terraces generated by hydraulic and geomorphic interactions. *Geology* 46 (6), 499-502

Finnegan, N.J., Roe, G., Montgomery, D.R., Hallet, B. (2005) Controls on the channel width of rivers: Implications for modelling fluvial incision into bedrock. *Geology* 33, 229-232

Turowski, J. (2018) Alluvial cover controlling the width, slope and sinuosity of bedrock channels. *Earth Surface Dynamics* 6, 29-48

Whipple, K.X., Tucker, G.E. (1999)Dynamics of the stream-power incision model: Implications for height limits of mountain ranges, landscape response timescales, and research needs. *J. Geophys Res* 104, (B8), 17661-17674

A new approach to substrate mapping: supporting high resolution models

J. Hoyle[1], A. Haddadchi[1] and J. Bind[1]

[1] National Institute of Water and Atmospheric Research, Christchurch, New Zealand. Jo.Hoyle@niwa.co.nz

1. Introduction

Environmental flows are often designed based on predictions of the physical habitat that will provided by a given flow for key species (typically fish and aquatic invertebrates). A common approach used is the Instream Flow Incremental Methodology (IFIM), which involves using habitat suitability indices to calculate weighted usable area for key species based on depth, velocity and substrate composition (by areal proportion). With advances in modelling capability, velocity and depth for a given flow are now commonly predicted using high resolution 2-dimensional hydraulic models, creating a need for substrate composition to be mapped at an equivalent resolution. Mapping substrate across large study reaches (e.g. 1-2 m grid resolution over 1-2 km long reaches) presents a significant challenge and pushes the boundaries of what has been previously attempted. Developing a semi-automated substrate classification workflow is necessary to provide a cost-effective approach.

2. Aim

To develop a workflow which enables underwater and sub-aerial mapping of substrate over large reaches from imagery for ready integration with 2d hydraulic models.

3. Methods

The workflow developed involves six key steps:

1. Substrate image collection - using aerial photographs collected by UAV or underwater video.
2. Preparation of images for automated substrate classification – extracting image tiles over a regular grid, or extracting video frames, and discarding blurry/noisy images or those where substrate is obscured by vegetation, bubbles, algae etc.
3. Automatically classifying the proportion of substrate in each image that is sand, fine gravel, gravel, small cobble, coarse cobble, and boulder (Wentworth 1922) using batch-processing of the Morlett Wavelet approach developed by Buscombe (2013).
4. Non-automated classification (for locations where automated classification could not be run) - using either manual (visual) classification or synthetic classification based on facies mapping and the allocation of surrogate classifications.
5. Combining and checking substrate classification approaches for consistency (Figure 1).
6. Interpolating substrate grids for integration with hydraulic model grids.

4. Conclusions

There are limitations with the Morlett Wavelett approach, which will be described in our presentation, however, overall we consider that the automated classification performed very well and the workflow provided excellent results (Figure 2). This approach has substantial advantages over the commonly used approach of visually estimating grainsize proportions on site: it is more objective, more consistently reliable, and it can be applied over large areas.

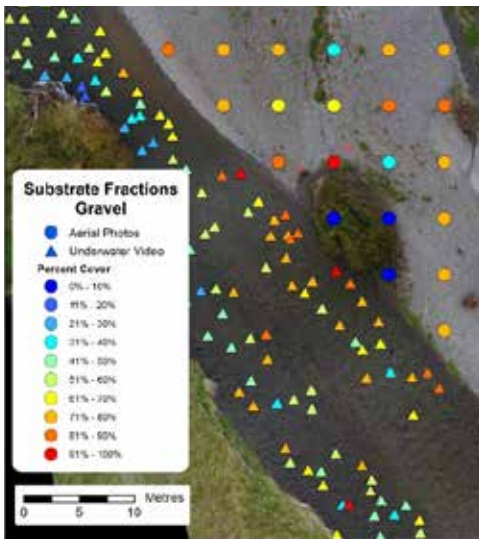

Figure 1: Example of substrate classification in a reach of the Aparima River, Southland, showing proportion of gravel in the substrate at locations where aerial/underwater imagery was classified (both automatic and manual classification).

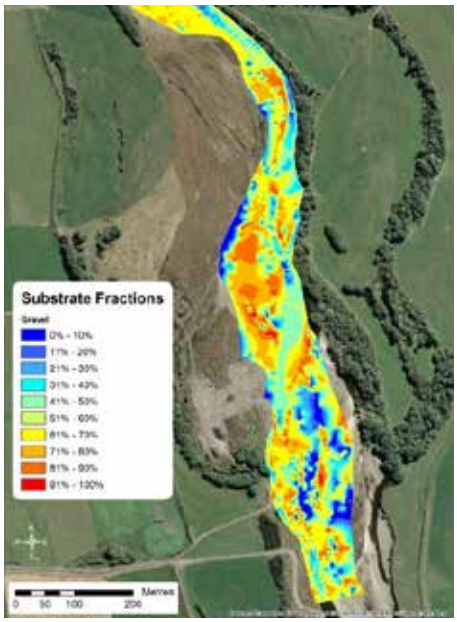

Figure 3: Example of final substrate classification in a reach of the Aparima River, Southland

References

Buscombe, D. (2013) Transferable wavelet method for grain-size distribution from images of sediment surfaces and thin sections, and other natural granular patterns. *Sedimentology* 60(7): 1709-1732.

Wentworth C.K. (1922) A scale of grade and class terms for clastic sediments. *The Journal of Geology* 30 (5). 377-392.

The longitudinal development of a coarse-grained sedimentary wave following a major landslide event, Kaikōura, New Zealand

J. Tunnicliffe[1], J. Howarth[2], D. Lague[3], P.Upton[4], K. Jones[2,4], and C. Massey[4]

[1] School of the Environment, University of Auckland, Auckland, New Zealand. j.tunnicliffe@auckland.ac.nz
[2] School of Geography, Environment and Earth Sciences, Victoria University of Wellington, Wellington, New Zealand
[3]Géosciences Rennes, Université de Rennes, Rennes, France
[4]Geological and Nuclear Science GNS Science, Te Pū Ao, Lower Hutt, New Zealand

1. Introduction

Following the Mw 7.8 earthquake of November 2016, tens of thousands of landslides impacted the steepland terrain surrounding Kaikōura, NZ. Many of these landslides reached the fluvial system, driving some rivers into a regime of buildup and rapid change. It is well known that the timing and transit dynamics of the sediment 'wave' will depend critically on the recurrence rate and severity of floods, as well as sediment texture and slope of the channel, but there has been less attention paid to varying longitudinal conditions that influence transit time, most notably breaks in slope, the valley's planform course, and the relative confinement of the river valley. Steep and confined canyons are able to convey most sediment loads, while wider valley sections may experience heightened rates of deposition. Intervening reaches may undergo complex cycles of accumulation and down-cutting to accommodate the transport gradient. Longitudinal development of the grain size distribution may further complicate estimates of transit times and predicting the signal that is ultimately recorded at the outlet of the mountain catchment.

2. Study Setting

The Hapuku River drains a 65 km^2 catchment in the Kaikoura Front Ranges, reaching the ocean roughly 8 km north of the town of Kaikoura. The largest coseismic landslide observed following the Kaikoura Event ('Hapuku 740'; Dellow et al., 2017, Massey et al, 2018) mobilised more than 20 M m^3 directly into the valley below. The river course was effectively blocked, and a lake was formed upstream of the deposit. Roughly 5 months later (April 2017), the dam had been incised and the river began to mobilise significant amount of coarse-grained sediment downstream.

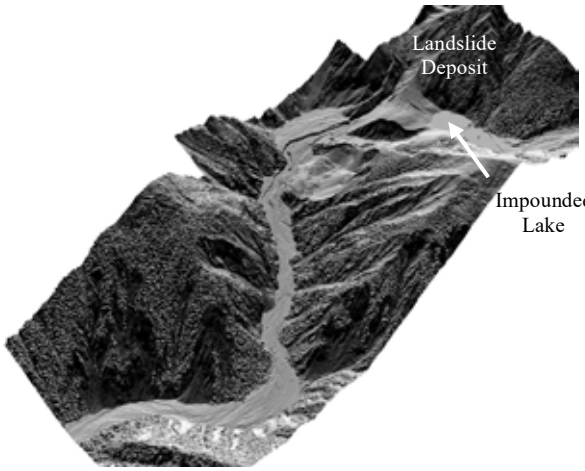

Figure 1: Airborne LiDAR derived Digital Surface Map (DSM), showing the aggraded Hapuku River, extending 2.5 km downstream from a major landslide deposit.

3. Methods

Five airborne LiDAR surveys and local SfM surveys between November 2016 and February 2019 have revealed the remarkable pace of change in the river valleys. In multiple field visits we have collected grain size information, including surface and subsurface distributions, to assess changes in river bed texture.

4. Results

Hapuku River has accumulated more than 315,000 m^3 of coarse-grained alluvium in the upper reaches, leading to over 25 m of aggradation of the riverbed. The time-series of landscape change provided by the LiDAR surveys shows that as of mid-2018, the bulk of landslide-derived material has not translated more than ~8 km downstream. Notably, there has been no vertical bed change within the steep, winding canyon, three km downstream of the primary deposit, as material is advected quickly through this confined river section. Downstream of the canyon aggradation resumed in the lower gradient channel. During aggradation phases, the river and floodplain widened significantly, where valley walls allowed. During degradational phases, the river tended to become lodged against the valley side, and carved narrow canyons and terraces within the coarse alluvium.

5. Conclusions

Coseismic landslide delivery to rivers represents a significant hazard to infrastructure and populated areas following an earthquake event. In order to improve numerical simulations of river re-equilibration following major sediment loading (e.g. Croissant et al., 2017), it is essential to collect observations from systems such as the Hapuku for model validation. In systems undergoing such extreme change, the transporting characteristics of rivers change radically, as morphology is profoundly transformed. In addition, the influence of valley confinement, lateral sediment sources, and evolving sediment texture lead to complex dynamics of recovery. Our initial findings from this work have already begun to inform new approaches to numerical modelling in seismically-active environments.

References

Croissant, T., Lague, D., Steer, P., & Davy, P. (2017). Rapid post-seismic landslide evacuation boosted by dynamic river width. *Nature Geoscience*, 10(9), 680.

Dellow, S., Massey, C. I., McColl, S. T., Townsend, D. B., & Villeneuve, M. 2017. Landslides caused by the 14 November 2016 Kaikoura Earthquake, South Island, New Zealand. *Proc. 20th NZGS Geotechnical Symposium*. Eds. GJ CY Chin, Napier.

Massey, C., Townsend, D., Rathje, E., Allstadt, K. E., Lukovic, B., Kaneko, Y., ... & Horspool, N. (2018). Landslides triggered by the 14 november 2016 M w 7.8 Kaikōura earthquake, New Zealand. *Bulletin of the Seismological Society of America*, 108(3B), 1630-1648.

Modelling lagoon dynamics at the mouths of New Zealand's gravel-bed rivers

R.J. Measures[1,2], T.A. Cochrane[2], D.E. Hart[2] and D.M. Hicks[1]

[1] National Institute of Water and Atmospheric Research (NIWA), Christchurch, New Zealand.
richard.measures@niwa.co.nz murray.hicks@niwa.co.nz
[2] University of Canterbury, Christchurch, New Zealand. tom.cochrane@canterbury.ac.nz deirdre.hart@canterbury.ac.nz

1. Introduction

Non-estuarine river mouth lagoons, known locally as hapua, are common on the East Coast of New Zealand's South Island. Hapua form where gravel-bed rivers emerge onto high wave energy, micro-tidal coasts. Hapua have highly dynamic outlet channels, which migrate rapidly along the shore in response to river flows and waves. These lagoons can be strongly influenced by anthropogenic changes to river flow and sediment supply. This paper presents developments with conceptual and numerical models for predicting the effects such changes.

2. Conceptual model

A detailed conceptual model of hapua morphology was developed following analysis of three years of monitoring data from the Hurunui Hapua including time-lapse imagery and concurrent river flow, lagoon level, sea level and wave data (Figure 1A). The model builds on earlier work by Patterson (2000) and Hart (2007).

2. Numerical model

A quasi-2D numerical model has been developed by combining simple 1D representations of different key processes including (Figure 1B):

- one-line shoreline modelling;
- 1D river hydraulics and morphology; and
- barrier overtopping and overwashing influences on barrier height and width.

These processes are combined in a model framework which accounts for their interaction. The model tracks the location of the outlet channel with respect to the shoreline, barrier and lagoon, such that the spatial links between the different processes are adjusted as the system evolves. These links capture processes such as: bedload delivery from outlet channel to coast, longshore transport into the outlet channel, barrier overwash into the outlet channel, and lagoon overtopping breaching new outlet channels.

3. Conclusions

The improved conceptual model identifies how river bedload plays an important role in driving 'primary breaching' of the barrier opposite the main river channel, as well as in initial constriction of the outlet channel. The numerical model's ability to reproduce the highly dynamic nature of the outlet channel, and the overall lagoon geometry, is evaluated using data from the time-lapse imagery. Whist the numerical model cannot yet replicate all the processes identified in the conceptual model, it allows a quantitative prediction of lagoon response to external changes.

Acknowledgments

This research has been funded by NIWA's Sustainable Water Allocation research programme.

References

Hart, D. E. (2007). River-mouth lagoon dynamics on mixed sand and gravel barrier coasts. Journal of Coastal Research, (SI 50), 927–931.

Paterson, A., Hume, T. M., & Healy, T. R. (2001). River Mouth Morphodynamics on a Mixed Sand-Gravel Coast. Journal of Coastal Research, (34), 288–294.

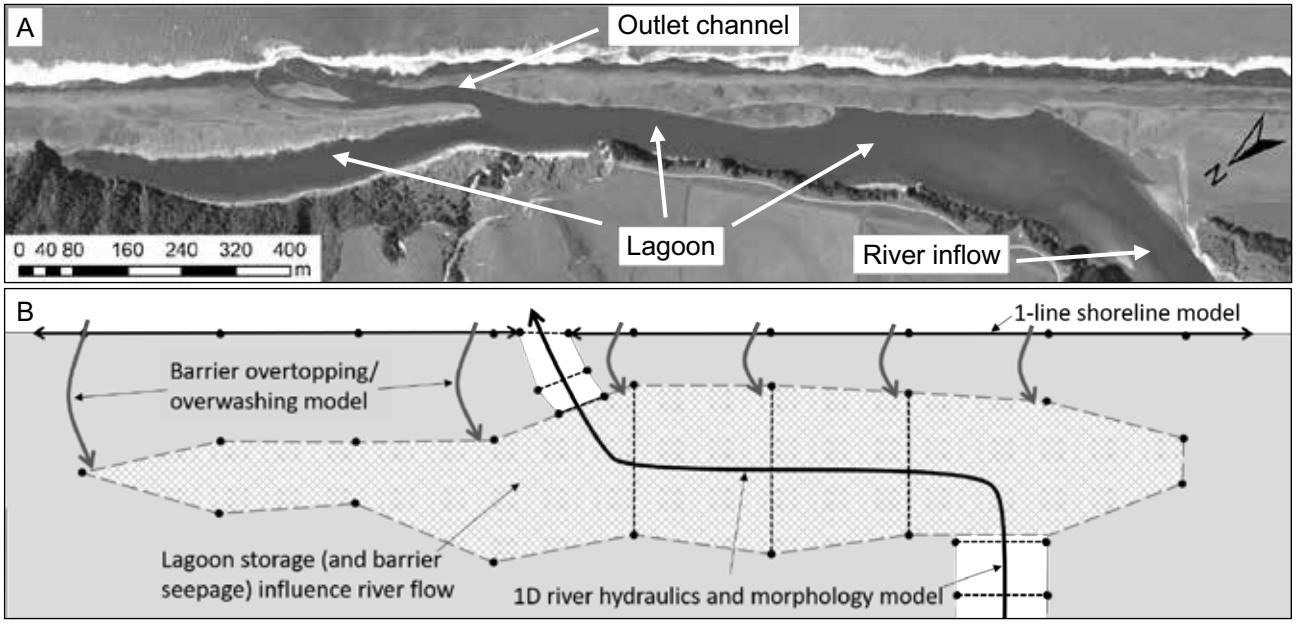

Figure 1. A: The Hurunui Hapua, B: Schematic showing key features of the quasi-2D numerical hapua model.

Morphodynamic Sensitivity of Anthropogenically-Forced Gravel-Bed Rivers: Wairarapa Region, New Zealand

W. Conley[1], I.C. Fuller[1], S.T. McColl[1], M. Macklin[1], J. Tunnicliffe[2]

[1] Geosciences Group, Massey University, New Zealand. fluviotect@gmail.com, i.c.fuller@massey.ac.nz, s.t.mccoll@massey.ac.nz, m.g.macklin@massey.ac.nz
[2] School of the Environment, University of Auckland, New Zealand. j.tunnicliffe@auckland.ac.nz

1. Introduction

Unconfined gravel-bed rivers draining steep catchments present a variety of management challenges globally. Such rivers near population centres of New Zealand's Wairarapa region are generally multi-thread (Figure 1) and, as is common globally, are managed for increased hydraulic capacity by reducing roughness and manipulating cross-sectional dimension. Though some levees/stopbanks are present, the broader management strategy is "fairway" based and tolerates small lateral movements within a predefined meandering planform. Fairway maintenance is achieved by frequent (often annual- to sub-annual) mechanical treatments that remove vegetation and modify channel position and volume.

Figure 1: Typical view of Waingawa River study segment looking downstream. Lineations on medial features are windrows from dozer-sidecast associated with routine vegetation clearance. Rock-barbs (left-bank) are a common erosion control technique.

Land-use intensification has increased demands for flood-protection managers to also constrain erosion related property losses as well as provide commercial aggregate sources. Collectively, routine treatments such as bar reduction/removal, armour ripping, riparian vegetation and large wood removal, and gravel extraction disrupt development and persistence of self-ordered fluvial features that otherwise provide a measure of stability. This talk presents analyses from high-resolution, sub-annual planimetric and morphological time-series to characterise increased system sensitivity that appears to correlate with management activities.

2. Methodology

To quantify morphometric changes, develop sediment budgets, and assess the effects of management interventions, we use a time-series of digital elevation models (DEMs) and orthoimagery derived from low-elevation aerial photographs. A remotely piloted aircraft system (RPAS) was used for seven collections between May 2017 and March 2019 that included RTK GNSS quality ground-control. DEMs and orthophoto mosaics were generated using AgiSoft Photoscan Pro and compared to quantify volumetric and planimetric erosion and deposition (Figure 2).

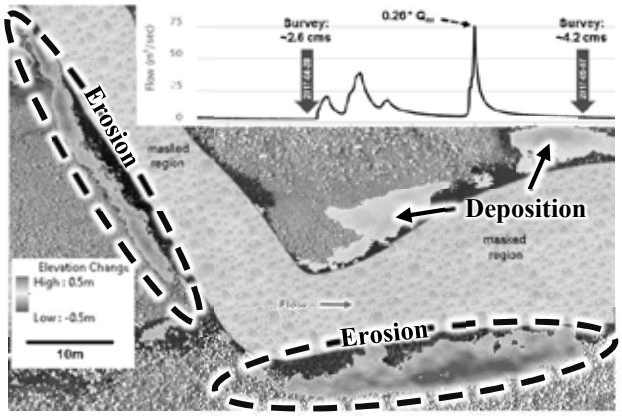

Figure 2: Example of unit-scale geomorphic change associated with a frequent peak-discharge event.

3. Key findings and conclusions

Preliminary results show highly frequent geomorphic effectiveness associated with routine discharge events (<< average annual flood (Q_{aa})). Local bank retreat up to 2 m has been observed following peak discharge magnitude less than 30% of the Q_{aa} (Figure 2). Medium to large gravel tracers have moved more than 50 m from inset bars during a single <0.1* Q_{aa} flow event.

Morphodynamic responses extend beyond the original footprint of treated areas. Channel incision is observed upstream and downstream of gravel extraction sites as local starvation and headward incision propagate (respectively). Primary channel aggradation (i.e. capacity reduction) is observed downstream of where misfit secondary channels erode due to flow diversions from the primary channel.

Frequent, local disruption of self-ordered fluvial forms coupled with translocation of fluvial processes seems to contribute to highly active channel behaviours and systems in constant adjustment. As reaches become more sensitized, process feedbacks may be resulting in reduced duration of treatment effects and/or driving the need for further mechanical interventions.

Acknowledgments

We would like to thank our field assistants James Fay, Amelia Horne, and Brent Vermolen.

Evaluation of driftwood behaviour in terms of convection-diffusion equation -In the Akatani reach at the flood disaster in July, 2017 -

D. Harada[1] and S. Egashira[2]

[1] International Centre for Water Hazard and Risk Management (ICHARM), Public Works Research Institute, Japan. d-harada55@pwri.go.jp

[2] International Centre for Water Hazard and Risk Management (ICHARM), Public Works Research Institute, Japan. s-egashira77@pwri.go.jp

1. Introduction

A huge amount of driftwood from upstream influences the flood flow in downstream areas when sediment runoff takes place at upstream areas. The present study proposes a method to simulate the behaviour of driftwood based on a convection-diffusion equation. A numerical simulation with the proposed method is conducted to simulate the flood flow with sediment and driftwood in the Akatani river flood disaster in July, 2017.

2. Methodology

A numerical simulation using a depth averaged 2-D flow model and a 2-D sediment and driftwood transport process model are conducted.

2.1 Governing equations of driftwood

Driftwood behaviour is simulated using following convection-diffusion equations with erosion / deposition terms as well as with an accumulation term.

$\partial z_b/\partial t>0$:

$$\frac{\partial C_{drf}h}{\partial t}+\frac{\partial C_{drf}uh}{\partial x}+\frac{\partial C_{drf}vh}{\partial y} = \frac{\partial}{\partial x}\left(\varepsilon_x h\frac{\partial C_{drf}}{\partial x}\right)+\frac{\partial}{\partial y}\left(\varepsilon_y h\frac{\partial C_{drf}}{\partial y}\right) - c_*\frac{\partial z_b}{\partial t}C_{drf}r(t,x,y) - v_n C_{drf}\delta(x-x_i,y-y_i) \quad (1)$$

$$\frac{\partial S}{\partial t}=\frac{\partial z_b}{\partial t}C_{drf}r(t,x,y)+v_n C_{drf}\delta(x-x_i,y-y_i) \quad (2)$$

where c_{drf} is the depth-averaged driftwood concentration, c_* is the sediment concentration of stationary bed, v_n is the inward velocity normal to the structure area such as the bridge, S is the storage of driftwood on the riverbed per unit area, D is the depth of tree's root. Dirac's δ-function is employed to evaluate the capture of driftwood at structures such as bridges and buildings, in which where a bridge exists ($(x,y)=(x_i,y_i)$), δ=1, otherwise δ=0. Other parameters are referred at Harada et al. (2017).

2.2 Target areas and computational conditions

Numerical simulations are conduted in the Akatani river reach, where severe flood disasters with sediment and driftwood occurred in July 2017. The drainage area of the Akatani River is approximately 20km^2. The computation area is approximately 3.5km long. Within the computational area, 7 bridges exist, which are defined as bridges ($(x,y)=(x_i,y_i)$) in Eq.(1).

As for bed materials, the sediment size distributions observed in the Akatani River is employed as initial sediment size distributions in the computation. In addition, as a lot of fine sediment supplied from upstream is considered to have influenced the flood flow, the conditions of fine sediment supply at the upstream boundary are determined based on Egashira et al. (2018), in which the fine sediment runoff is predicted as the sum of sediment erosion of a single debris cone.

3. Results and discussions

Fig.1 compares the computational results of cases between with driftwood transportation (Case1) and without driftwood transportation (Case2) in terms of velocity distribution. The velocity upstream of the bridge in Case 2 decreases compared to that of Case 1, though the velocity downstream of the bridge in Case 2 is much higher than that of Case1, which is caused by the driftwood deposition at around the bridge. Difference in velocity distribution between Case 1 and Case 2 results in difference in channel changes of the whole domains.

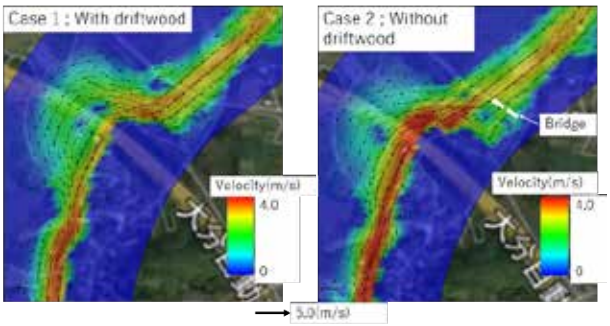

Figure 1: Comparison of computational results between cases with driftwood (Case1) and without (Case2)

3. Conclusions

The present study tries to evaluate driftwood behaviour in terms of convection-diffusion equation. The computational result suggested that consideration of driftwood behaviour in the flood flow is significantly important for the river management of mountainous rivers such as the Akatani River.

Acknowledgments

This work was supported by JSPS KAKENHI Grant Number 18K13842.

References

Harada, D. and Egashira,S. (2017). Flood flow characteristics with fine sediment supply and drift woods -analysis on the Akatani River flood hazards in july, *Journal of Japan Society of Civil Engineers, Ser. B1 (Hydraulic Engineering)*, 74, 2017 (In Japanese).

Shimizu, Y. (2002). A method for simultaneous computation of bed and bank deformation of a river. In: *River Flow 2002, Int'l Conf. on Fluvial Hydraulics Louvain-la-Neuve*, *Belgium.*

Flow and bed morphology response to the introduction of wood logs for sediment management

J.Y. Poelman[1], A.J.F. Hoitink[1] and T.V. de Ruijsscher[1]

[1] Hydrology and Water Management Group, Wageningen University, Wageningen, the Netherlands.
judith.poelman@wur.nl

1. Introduction

The implementation of wood logs in rivers is a promising method for sediment management and the improvement of aquatic biodiversity. Wood logs can be placed on the river bed, similar to submerged vanes. Submerged vanes are placed in a small angle with the approaching flow. The resulting pressure gradients induce a secondary circulation, through which the direction of sediment transport is altered, without significantly compromising the conveyance capacity of the river (Odgaard, 2009). Here, a laboratory study is conducted to investigate whether wood logs or tree trunks can be used to introduce a secondary circulation and with that, alter sediment transport.

2. Methodology

Through a series of experiments, the effects of a traditional vane field are compared to those of screens of stacked logs, and large individual trunks. Experiments are performed with a fixed bed to facilitate detailed 3D velocity measurements and with a movable bed to study morphological effects. The three types of objects--vanes, screens of stacked logs and trunks--are placed in eight rows of four objects. The angle of incidence is varied: $\alpha = 15^0$ and $\alpha = 25^0$.

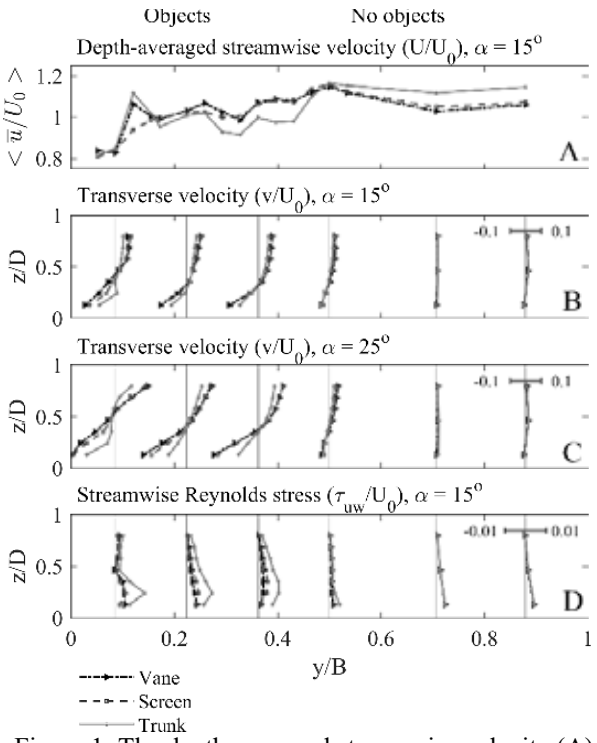

Figure 1: The depth-averaged streamwise velocity (A), profiles of transverse velocity (B-C), profiles of streamwise Reynolds stress (D). The objects were located between y/B = 0.1-0.5. Values are normalized with the mean streamwise velocity of an experiment.

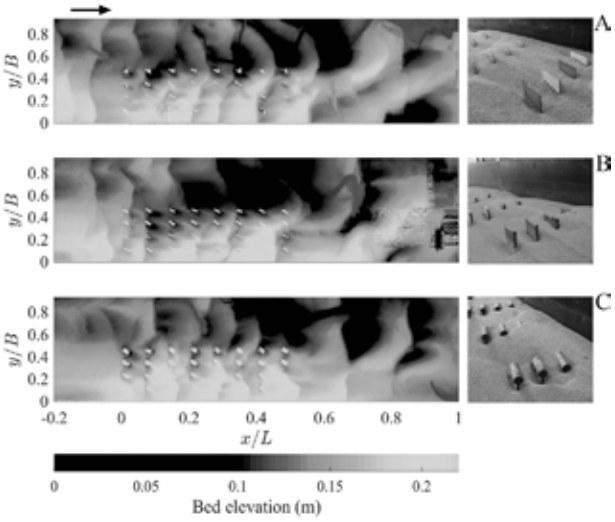

Figure 2: Bed morphology determined at the end of the experiment with vanes (A), screens (B) and trunks (C).

3. Results and conclusions

The results from the fixed-bed experiments indicate that the trunks are least effective in inducing a secondary circulation and cause higher turbulence and drag, which leads to a stronger decrease in the streamwise velocity (Figure 1). Screens of stacked logs, on the other hand, are almost as effective as traditional vanes. Results from the movable-bed experiments show that all three set-ups redistribute sediment (Figure 2). However, where the configuration of dunes in experiments with vanes and screens indicate a bottom current that is in line with the expected secondary circulation, dunes in the experiment with trunks do not show the same pattern.

We conclude that a field of trunks acts as a sediment trap because of strong reduction of the streamwise velocity, without a strong secondary flow such as dominant in the other configurations. Screens of stacked logs can be successfully implemented in rivers, as they are only slightly less effective than traditional vanes. The risk of piping underneath objects and the associated scour are points of concern.

References

Odgaard, A. J. (2009), River training and sediment management with submerged vanes, American Society of Civil Engineers (ASCE).

Poelman, J. Y., A. J. F. Hoitink, T. V. De Ruijsscher (2019), Flow and bed morphology response to the introduction of wood logs for sediment management. Manuscript under review.

The topographic signature of large wood and vegetation in braided rivers

L. Mao[1,2], D. Ravazzolo[3] and W. Bertoldi[4]

[1] School of Geography, University of Lincoln, Lincoln, UK. lumao@lincoln.ac.uk
[2] Centro de Investigación para la Gestión Integrada de Desastres Naturales (CIGIDEN) and Instituto de Geografía, Pontificia Universidad Católica de Chile, Chile
[3] Faculty of Engineering, University of Auckland, Auckland, New Zealand. diego.ravazzolo@gmail.com
[4] Department of Civil, Environmental and Mechanical Engineering, University of Trento, Trento, Italy. walter.bertoldi@unitn.it

1. Introduction

Rivers are in constantly changing as results of interaction among climate, sediment transport, flow, and also vegetation and large wood dynamics. Both vegetation and large wood (LW) contribute to shaping rivers, but they seem to exert opposite roles in conditioning river morphology. Bertoldi et al. (2015) reported that vegetation increases bank stability, reduces the braiding index, and increase the mean channel depth. Instead, LW alone tends to increase channel dynamics often creating pioneering islands. This study is based on the experiments reported by Bertoldi et al. (2014, 2015), and take advantage of the topographical surveys of the channels to explore the topographical signature left by vegetation and large wood using a physical modelling approach.

2. Flume experiments and topographical analysis

The experiments were conducted in three 1.7 m-wide flume channels, using homogeneous fine sand (Bertoldi et al., 2014; 2015). Experiments were designed to observe large wood and vegetation acting mutually and separately. Large wood was simulated using 8 cm-long wood dowels and logs were introduced from the upstream end of the flume channels at different rates. Vegetation was reproduced with alfalfa seeds. The experiments were designed to analyse four different scenarios: sand (S), large wood (SLW), vegetation (SV), and vegetation and large wood acting together (SVLW). A Terrestrial laser scanner was used to scan the entire flume facility at the end of each run. The scans were filtered and a digital elevation model (DEM) of each channel with cell size of 1 mm was created. Statistics information of the main characteristics of the bed elevations were extracted from the detrended DEMs. Also, two-dimensional second-order structure functions were used to assess the spatial correlation in bed elevation at various distance in different directions and to evaluate the complexity of the bed elevations.

3. Results and conclusions

Results show that vegetation growing on the bars of the flume channels reduced the braiding index (Bi) and the space available for the flowing water (W) resulting in fewer, wider and deeper channels (Figure 1). Deeper channels and localized sediment accumulations result in higher standard deviation of the bed elevations (δ). Large wood alone is not very effective if compared with the morphological effects of vegetation. Indeed, LW causes only a slight reduction of both the mean channel width and braiding index. The standard deviation of bed surface elevations is very comparable with the value measured for the experiments conducted with sand alone. Interesting, when LW is introduced in the flumes where vegetation is growing, this is not effective in changing the average channel width, or the braiding index, but the bed surface becomes relatively smoother if compared with the bed on flumes with only vegetation. The structure functions allowed to compare the flume channels in terms of the extent of their scaling region, also called the Hurst exponent (H). This is considered a measure of the complexity of bed elevations, with topographical complexity varying inversely with H. Results suggest that the surfaces with higher complexity are the flume channels with sand braided patterns and flumes with LW. This is somehow counterintuitive, as one could expect higher complexity in rougher surfaces as in flumes with vegetation. Instead, at the scale of the transition regions of the structure functions which ranges from 10 to 150 mm, the distribution of elevations of a sand braided surface appears intrinsically more diverse, as mesoscale topographical features like bars are more numerous. Instead, in the flumes with vegetation, at that particular spatial scale the surface is likely more homogeneous, as the morphological units as channels, islands, and floodplains tend to be larger.

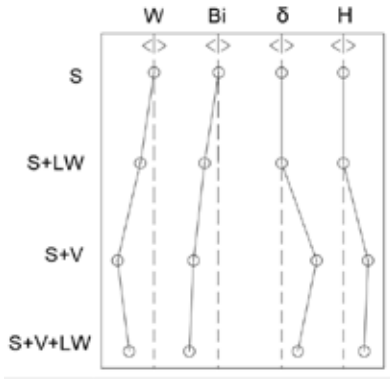

Figure 1: Width of channels in the flume (W), braiding index (Bi), standard deviation (δ), and Hurst exponent of structure functions of multithread rivers.

4. References

Bertoldi W, Welber M, Gurnell AM, Mao L, Comiti F, Tal M. 2015. Physical modelling of the combined effect of vegetation and wood on river morphology. Geomorphology 246: 178–187.

Bertoldi W, Welber M, Mao L, Zanella S., Comiti F. 2014. A flume experiment on wood storage and remobilization in braided river system. Earth Surf. Process. Landforms 39: 804–813.

Acknowledgments

The work was supported by projects HYDRALAB IV (HyIV-HULL-01) and Fondecyt Regular1170657.

Application of state-of-the-art measurement technologies for large wood (LW) research

G. Spreitzer[1], J. Tunnicliffe[2] and H. Friedrich[3]

[1] Faculty of Engineering, The University of Auckland, Auckland, New Zealand. gspr390@aucklanduni.ac.nz;
[2] School of the Environment, The University of Auckland, Auckland, New Zealand. j.tunnicliffe@auckland.ac.nz
[3] Faculty of Engineering, The University of Auckland, Auckland, New Zealand. h.friedrich@auckland.ac.nz

1. Introduction

The geomorphic impacts from flood events upon New Zealand's river environments and adjacent infrastructure are strongly exacerbated by the transport and jamming of large wood (LW). Our understanding of the interactions between LW and channel morphology is limited. Advancing our knowledge has been limited by a lack of applicable methodologies and technologies to track the mobilization, transport and interactions of woody elements in the river environment. In the Water Engineering Laboratory at the University of Auckland we are working on implementing two novel measurement methods that will provide novel insights into LW movement and accumulation processes. A 6.3 m long flume with conveyor-belt feeder, live gravel bed conditions, fixed embankments, a critical cross-section (bridge with central pier) and a sediment trap at the outlet was designed and prepared with the aim of testing LW mobilisation, transport and deposition behaviour at a variety of flow rates, with obstructions in the channel. Our hydraulic flume experiments are fully scaled at a ratio of 1:15 for geometric, kinematic and dynamic similarity.

2. Methodology

We used five high-resolution cameras, assembled in a multi-camera array (Figure 1a), installed at a height of 1 m and positioned on a mobile cart. Structure from Motion photogrammetry is used to generate precise 3D models of LW accumulations from 2D images. The 3D models are then used to assess accumulation volume and porosity.

We used custom-designed smart sensors, termed SmartWood (Spreitzer et al. 2019), which enable nine degrees of freedom (9-DoF) measurements, by means of a fully synchronized accelerometer, gyroscope and magnetometer. The smart sensors are installed into scaled wooden dowels (Figure 1b), representing prototype wood logs in their simplest form - without rootwads or branches. The wooden dowels from the laboratory setup are representative of standard wood logs used in timber production. Sensor data capture acceleration force, angular velocity and magnetic field strength at frequencies of up to 100 Hz, which enables data recording of rapidly occurring impacts on channel boundaries, river-crossing infrastructure or collisions of individual LW pieces during their journey downstream.

3. Conclusions and Outlook

A better understanding of LW movement processes helps to more efficiently predict impacts upon channel morphology, river-crossing infrastructure (Figure 1c) and the riparian environment. Results will contribute to more reliable risk assessment for wood prone stream systems, improved river management, with improved models of LW transport, and identification of accumulation processes, such as the critical role key-logs play in altering stream systems.

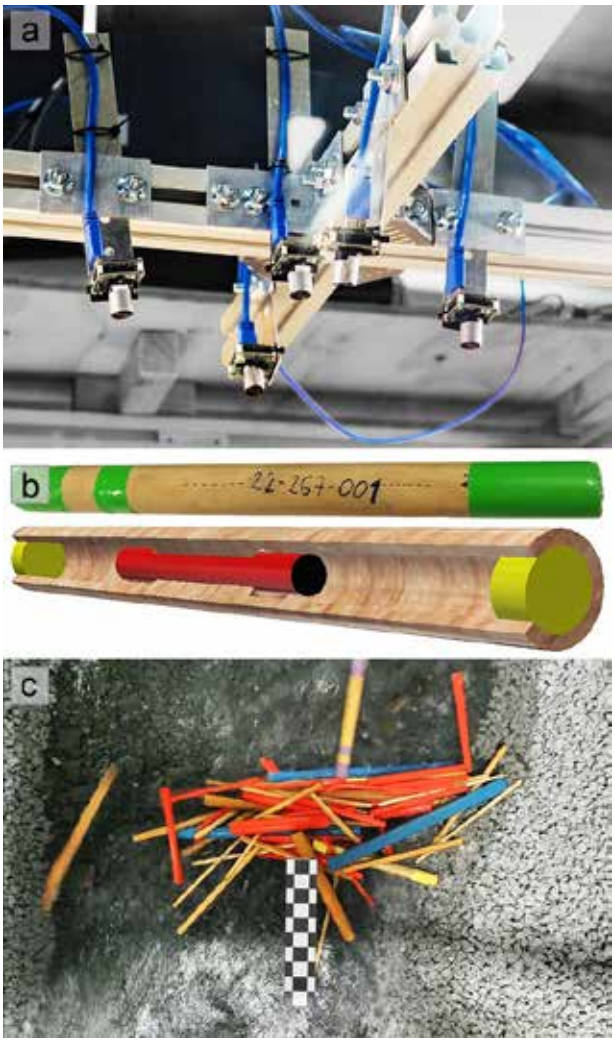

Figure 1: Camera array for Structure from Motion photogrammetry (a) and SmartWood (b) used for assessing the effect of LW accumulations on channel morphology (c).

Acknowledgments

The authors acknowledge funding from the George Mason Centre for the Natural Environment and the Engineering New Zealand Rivers Group.

References

Spreitzer, G., Gibson, J., Tang, M., Tunnicliffe, J., & Friedrich, H. (2019). *SmartWood: Laboratory experiments for assessing the effectiveness of smart sensors for monitoring large wood movement behaviour*. Catena, 182, 104145.

Investigations on levee piping induced by crayfish *Procambarus clarkii* burrows

G. Calvani[1], C. Carbonari[1], M. Bendoni[1], N. Savoia [1], E. Tricarico[2] and L. Solari[1]

[1] Department of Civil and Environmental Engineering, University of Florence, Florence, Italy. giulio.calvani@unifi.it
[2] Department of Biology, University of Florence, Florence, Italy. elena.tricarico@unifi.it

1. Introduction

River levees are fundamental structures for protection against flood risk. Stability of levees is ensured by their structural integrity, which can be compromised by animal activity when considering earthen levees (Michelazzo et al., 2018). In this kind of embankments, burrows are often dug by several animal species and affect the behaviour of the levee itself in terms of permeability and seepage processes. The presence of burrows shortens the filtration pathways, increases the filtration rate and promotes the internal erosion (i.e., piping). Piping induced by bioturbation can favor levee failure, even for minor flood events (Orlandini et al., 2015) (see Figure 1).

Figure 1. Levee piping triggered by animal burrowing during the flood event of 19^{th} January 2014 on the Panaro River, Italy. Picture from Orlandini et al. (2015).

The red swamp crayfish *Procambarus clarkii* is a widespread invasive animal species in freshwater ecosystems, responsible of habitat-changes and particularly active in levee burrowing. In literature, the effects of animal burrows on levee piping were investigated in field campaigns (e.g., Orlandini et al., 2015), laboratory experiments under controlled conditions (Saghaee et al., 2016) and 2D numerical simulations of an earthen riverbank (e.g., Palladino et al., 2018). Nevertheless, specific studies on *P. clarkii* burrowing effects on levee piping are scarce.

The present work addresses the influence of *P. clarkii* crayfish burrows on the filtration pathways and the triggered piping. Both the experimental and the numerical approaches are adopted.

2. Materials and methods

To assess shape, volume and structure of crayfish burrows, several laboratory experiments were performed in a water tank containing an artificial earthen levee. One side of the levee was filled with water to cover the 50% of its height (0.5 m) and four specimens of *P. clarkii* were placed inside the tank and left for around 100 hours. On the field side of the levee, measuring probes for water content in the soil were installed. After crayfish activity, we obtained casts of the burrows by injection of polyurethane foam. Then, 3D reconstruction of the casts was obtained through digital photogrammetry (Agisoft PhotoScan). We found average length of the burrows of about 50 cm on average and the excavated volume in the order of 4% the total volume of the levee. The geometry of reconstructed burrows was then used to model discontinuity in the soil matrix in 2D numerical simulations using GeoStudio Seep/W. The analysis revealed the burrows drastically altering bank hydraulics and increasing levee vulnerability to seepage flow. Ongoing activity is focused on the local hydrodynamics near the burrow using 3D numerical modelling (USGS Modflow).

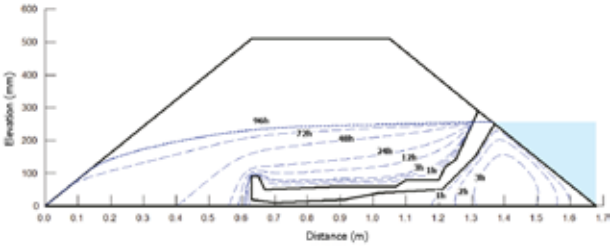

Figure 2. Saturation lines at different time steps for one of the simulated experiments with burrowed levee.

3. Conclusions

Based on the preliminary results of this work, levee vulnerability to piping appears to be enhanced by the burrowing activity of *P. clarkii*. Phreatic lines inside the burrowed levee reach the field side much faster with respect to the undamaged embankment, promoting an earlier occurrence of levee failure due to processes of internal seepage. In particular, the reduction of the time scale for the phreatic line to reach the field side appears to scale with the increased hydraulic gradients imposed by the burrows.

References

Michelazzo, G., Paris, E., and Solari, L. (2018). On the vulnerability of river levees induced by seepage. *Journal of Flood Risk Management*, 11:S677–S686.

Orlandini, S., Moretti, G., and Albertson, J. D. (2015). Evidence of an emerging levee failure mechanism causing disastrous floods in Italy. *Water Resources Research*, 51(10):7995–8011.

Palladino, M. R., Barbetta, S., Camici, S., Claps, P., and Moramarco, T. (2018). Levee body vulnerability to seepage and impact of animal burrows. *XXXVI Convegno Nazionale di Idraulica e Costruzioni Idrauliche,* Ancona, 12-14 September 2018.

Saghaee, G., Mousa, A. A., and Meguid, M. A. (2016). Experimental evaluation of the performance of earth levees deteriorated by wildlife activities. *Acta Geotechnica*, 11(1):83–93.

Storm Erosion and Recovery on Estuarine Beaches

S.L. Gallop[1,2], A. Vila-Concejo[3], T.E. Fellowes[2,3] and J.L. Largier[4]

[1] School of Science, University of Waikato, Tauranga, New Zealand. shari.gallop@waikato.ac.nz
[2] Department of Environmental Sciences, Macquarie University, Sydney, Australia. thomas.fellowes@mq.edu.au
[3] School of Geosciences, University of Sydney, Sydney, 2006, NSW, Australia. ana.vilaconcejo@sydney.edu.au
[4] Bodega Marine Laboratory, University of California, Davis, USA. jlargier@ucdavis.edu

1. Estuarine beaches

Estuarine beaches are particularly vulnerable to storm wave events and sea level rise, as they tend to be narrow and low-lying, and prone to coastal flooding. They can undergo severe erosion due to storms, where the eroded sand can be trapped flood-tide deltas and cannot return to the beach (Austin et al., 2018). Estuarine beaches typically lack morphological features such as breaker bars and rip channels, common in beach classification and conceptual models based on the open coast (Jackson et al., 2002). They are also generally protected from swell and have low longshore sediment supply. Most understanding of beach recovery after storms relates to oceanic sandy beaches, which accrete under long-period swell waves. However, for estuarine beaches, in the absence of swell, a key question is how these beaches recover after erosive events – and how long it takes. Our research focuses on tracking storm erosion and recovery rates and drivers on estuarine beaches.

2. Study sites and methods

We focus on 8 estuarine beaches around Sydney, Australia, with different exposure to ocean swells and prevailing winds, and varying relationships to a flood tidal delta. These sites are located in 2 contrasting estuaries: (1) the drowned river valley Pittwater estuary; and (2) the heavily-developed embayed Botany Bay estuary. Beach topography has been surveyed monthly since April 2016, and interannual–decadal trends in shoreline behaviour was analysed using aerial photos since 1940. In addition, wave/current-meter deployments have been undertaken in both estuaries to explore wave exposure along the various estuarine shorelines, and the influence of tidal currents.

3. 3–5 June 2016 storm erosion and recovery

In this paper, we track erosion and recovery after a severe East Coast Low (ECL) storm on 4-5 June 2016, where peak waves (up to 17.7 m offshore maximum wave height) coincided with spring tides. This storm was particularly damaging due to the unusual NE wave direction, when large waves generally come from the SE. At the estuarine beaches monitored, this storm caused severe erosion. The worst erosion (0.88 m^3/m) occurred at one of the most sheltered beaches with a westerly aspect, while accretion occurred on the eastern shore beaches. Simultaneously, the storm had negligible impact on the most exposed estuarine beaches. While the eroded volumes are relatively low compared to those experienced on the open coast, the percentages of beach volume are large considering the relatively small size of estuarine beaches. For example, in the Pittwater, typical subaerial volume loses ranged between 16% and 100%, and from 9% to 38% in Botany Bay. Since the 2016 storm, many beaches have not experienced significant recovery and some have eroded further (Figure 1). Recovery rates have been highly variable both between and within beaches. At one beach in the Pittwater on the eastern shore, one beach profile monitored had largely recovered 2 years after the storm, while another 2 profiles had regained half their sediment volume. This phenomenon is in stark contrast to recovery patterns on oceanic beaches in the region where typically beaches regain half of the sediment lost within 6 months (Harley et al., 2017).

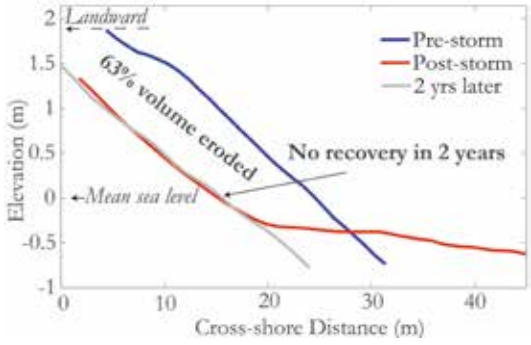

Figure 1: Example of storm erosion and lack of recovery at Pittwater Estuary, Australia after June 2016 storm.

4. Conclusions

Estuarine beaches are vulnerable to erosion under unusual wave angles. Erosion volumes can be a large proportion of the subaerial beach (up to 100%) and recovery can be extremely slow. It is unclear if all types of estuarine beaches are able to recover after severe erosion, and what the mechanism might be to allow this. Our preliminary analysis suggests ebb dominance, and the significantly stronger tidal current at the bottom suggest an important role of tidal currents in beach recovery. This study provides a fundamental understanding of the vulnerability of estuarine beaches to erosion.

References

Austin, P. T., Vila-Concejo, A., Short, D. A., and Ranasinghe, R. (2018). A Multi-Scale Conceptual Model of Flood-Tide Delta Morphodynamics in Micro-Tidal Estuaries. *Geosci.,* 8.

Harley, M. D., Turner, I. L., Middleton, J. H., Kinsela, M. A., Hanslow, D. J., Splinter, K. D., and Mumford, P. J. (2017). Observations of beach recovery in SE Australia following the June 2016 east coast low. *Australasian Coasts and Ports Conference.* Cairns.

Jackson, N. L., Nordstrom, K. F., Eliot, I., and Masselink, G. (2002). 'Low energy' sandy beaches in marine and estuarine environments: a review. *Geomorphol.*, 48**,** 147–162.

An in-situ device to measure the critical shear stress for sediment erosion in the intertidal zone

Gong Zheng[1], Gan Quan[2], Zhou Zeng[2], Zhang Qian[2], Zhao Kun[2]
1. State Key Laboratory of Hydrology-Water Resources and Hydraulic Engineering, Hohai University, Nanjing, China. gongzheng@hhu.edu.cn.
2. Jiangsu Key Laboratory of Coast Ocean Resources Development and Environment Security, Hohai University, Nanjing, China. ganquan@hhu.edu.cn, zhouzeng@hhu.edu.cn, zhangqian@hhu.edu.cn, zk1357@hhu.edu.cn.

1. Introduction

Incipient motion condition is one of the most important properties of sediment in the field of river, coastal and estuarine morphodynamics. The condition for sediment incipient motion is crucial for the research of morphodynamic evolution of tidal flats which are commonly characterized by fine sediment. Pelitic silty-sand, with complex structures and properties, is widely distributed on tidal flats. In-situ measurement of the critical shear stress for sediment erosion is more appropriate to obtain accurate data of intertidal sediment incipient motion without disturbing the original soil status. Most of existing devices measuring in situ cannot generate uniform horizontal bed shear stress, so it remains questionable whether they can measure the critical shear stress accurately (Moore and Masch, 2012; Watts et al., 2003). This study presents a newly-developed in-situ device to measure the critical shear stress for sediment erosion in the intertidal zone, with the advantage of generating a uniform bed shear stress.

2. Description of device

The invented device is shown in Figure 1. It consists of three parts: the supporting structure, the upper structure and the holder. The supporting structure is used to support the upper structure. The upper structure includes the inner cylinder, outer cylinder, shear ring, electrical machinery and transmission shaft. Its inner cylinder's radius is 210mm, outer cylinder's radius is 400mm and operating water depth is 260mm. The holder is inserted into tidal flats to stabilize the whole structure. After setting up the device, water is added into the device until water level reaches shear ring. Then the electrical machinery is switched on to activate the inner cylinder, outer cylinder and shear ring to rotate at the optimal speed ratio. When the measured turbidity in the device increases dramatically, the critical shear stress for sediment erosion can be calculated by the relation of the rotating speed and bed shear stress. It is critical that the device can generate uniform bed shear stress at the optimal speed ratio.

3. Methodology

This study builds a numerical model to simulate the flow field and bed shear stress of the device without shear ring and with shear ring in turn using the CFD software called Fluent, in order to explore whether the device can generate uniform horizontal bed shear stress and the optimal speed ratio of different parts. Bed shear stress is measured in the device without shear ring when the inner cylinder and outer cylinder rotate in the same direction, and outer cylinder's velocity is 24rpm. The simulated and measured bed shear stresses are compared in Figure 2, suggesting that this numerical model can be used to simulate bed shear stress for the invented device.

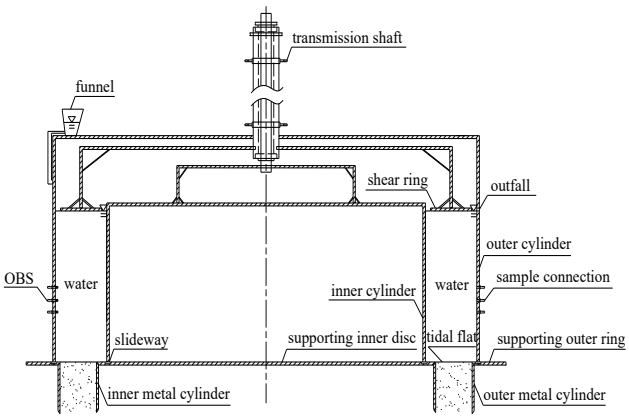

Figure 1: Schematic diagram of the invented device

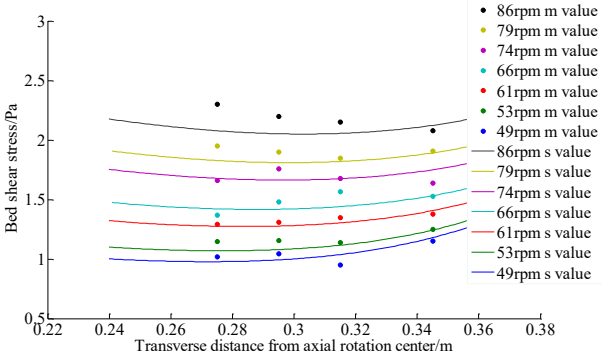

Figure 2: Simulated and measured bed shear stresses when the inner cylinder rotates at different velocities

4. Results and conclusions

The inner cylinder, outer cylinder and shear ring of the device rotating in the same direction at the speed ratio of 3.3:1:1 can generate the most uniform bed shear stress, and there is another quadratic function between bed shear stress and the rotating speed of inner cylinder If the dimensions of the device without shear ring change within a specific limits, there is a quantitative relation between the dimensions and the optimal speed ratio.

References

Moore W L, Masch F D. (2012). Experiments on the scour resistance of cohesive sediments. *Journal of Geophysical Research*. 67(4):1437-1446.

Watts C W, Tolhurst T J, Black K S, et al. (2003). In situ measurements of erosion shear stress and geotechnical shear strength of the intertidal sediments of the experimental managed realignment scheme at Tollesbury, Essex, UK. *Estuarine, Coastal and Shelf Science*, 58(3): 611-620.

Effect of cross-channel variation on the uncertainty of bed-load measurements: Universal guidelines for sampling bed-load in sand- and gravel-bed rivers

R.M. Frings[1] and S. Vollmer[2]

[1] Institute of Hydraulic Engineering and Water Resources Management, RWTH Aachen University, Aachen, Germany. frings@iww.rwth-aachen.de
[2] Department of River Morphology, Sediment Dynamics and Management, Federal Institute of Hydrology, Koblenz, Germany. vollmer@bafg.de

1. Introduction

The stability of river channels and their suitability as habitat for aqueous organisms is strongly controlled by the rate of bed-load transport. Quantification of bed-load transport rates in rivers is difficult, not only because of the temporal variation in transport, but also because of the cross-channel variation in transport. The objectives of this study were: (1) to determine the effect of cross-channel variation in bed-load transport on the uncertainty of width-integrated transport rates, and to use this knowledge (2) to improve guidelines for bed-load sampling.

2. Methods

To arrive at these objectives a thorough statistical evaluation of stochastic and systematic uncertainties involved in bed-load transport measurements was made.

3. Uncertainty of bed-load sampling

In the planning phase of a bed-load measurement, it is often desired to set up a measuring scheme that produces results with maximum accuracy at minimum efforts. To do so, an *a priori* estimate of the uncertainty of the outcomes is needed. Based on the statistical evaluation (Section 2) we arrived at a new expression for the sampling uncertainty. The expression relates to bed-load measurements made with pressure-difference (Helley-Smith type) samplers that require numerous bed-load samples of short duration at several, equally-spaced positions across the channel. The expression reads (Frings and Vollmer, 2017):

$$R = R_{stochastic} + R_{interpolation} \quad (1a)$$

$$R_{stochastic} = \frac{CV}{\sqrt{n_m}} + \frac{1}{(kn_s)^{z_1}} \quad (1b)$$

$$R_{interpolation} = z_2 e^{-kn_s} \quad (1c)$$

where R (-) is the relative uncertainty of the cross-channel integrated transport rate with $R_{stochastic}$ (-) its component due to stochastic uncertainties and $R_{interpolation}$ (-) its component due to systematic interpolation errors. It is assumed that other systematic sources of uncertainty are accounted for by calibration factors and appropriate sample durations. CV is a measure of the stochastic variability of bed-load transport (for which empirical estimates exist) and k represents the fraction of the river width in which bed-load transport occurs, z_1 (-) and z_2 (-) are theoretically derived coefficients, whereas n_s (-) and n_m (-) represent the number of sampling positions and the number of samples per sampling position, respectively. Efficient sampling schemes for bed-load measurements with a minimum number of samples required can be generated using Eq. 1 by minimizing the product n_s x n_m. Eq. 1 has a general character and can be applied to most alluvial rivers. Values for CV, k, z_1 (-) and z_2 (-) are provided by Frings and Vollmer (2017).

4. Guidelines for sand-bed and gravel-bed rivers

Because gravel-bed rivers typically have wider grain size distributions (and more variation in critical shear stress) than sand-bed rivers and because the prevailing shear stress is generally closer to incipient motion conditions, many gravel bed rivers show much stronger cross-channel variations in bed-load transport than sand-bed rivers. This also comes to expression in the fact that sand-bed rivers often show bed-load transport over the full cross section, whereas gravel-bed rivers (including sand-gravel bed rivers) often only show transport over a limited part of the cross section. Application of Eq. 1 shows that generally more sampling positions across the channel are required in gravel-bed rivers than in sand-bed rivers. For gravel-bed rivers with unknown cross-channel distribution of transport, at least 10 sampling positions are recommended, whereas for most sand-bed rivers 5 positions suffice. In addition, at least 12 short-duration samples are required at each position to obtain bed-load estimates with uncertainties below 20%. If the same level of uncertainty is desired in the case of high spatial and temporal variation in transport rates, the number of short-duration samples needed per sampling position increases to 40.

5. Conclusions

In gravel-bed rivers with bed-load transport concentrated in narrow (*a priori* unknown) lanes, more sampling positions across the channel are needed than in sand-bed rivers with bed-load transport occurring over the full river width. We presented a universal expression for the *a priori* assessment of sampling uncertainty to be used for optimizing bed-load sampling.

Acknowledgments

Christian Beckhausen, Kristin Bunte and Michael Church.

References

Frings, R.M. and Vollmer, S. (2017). Guidelines for sampling bed-load transport with minimum uncertainty. *Sedimentology,* 64(6), 1630-1645, https://doi.org/10.1111/sed.12366.

Sediment Transport and Flow Structure in Tojingawa River Estuary

Ryuichi Hirakawa[1] and Terunori Ohmoto[2]

[1] Maebashi Institute of Technology, Maebashi, Japan. hirakawa@maebashi-it.ac.jp
[2] Kumamoto University, Kumamoto, Japan. ohmoto@kumamoto-u.ac.jp

1. Introduction

Observations of suspended sediment concentration, salinity and current were made in the Tojingawa River estuary, Northern Kumamoto prefecture, Japan. The estuarine reaches are approximately 11 km in length, and are formed a compound channel by clay and silt. Flow measurements were undertaken in a straight part (Nezu and Rodi, 1986; Shiono et al., 1998; Ishigaki et al., 2001) to investigate the effect of stratification on secondary flow in well-mixed estuary. Flow velocity was measured using a ADCP. Salinity was also carried out using a water quality monitoring sensor.

2. Field observation result and consideration

2.1 Riverbed materials

The riverbed material on the flood plain surface and the low waterway surface was gathered, and the grain diameter was examined. . The median particle diameter is about 0.05mm, and the silt element has increased to either bottom sediment. It is understood that the transportation of the Suspended sediment by the tide similar to Kikuchi river (Ohmoto and hirakawa, 2012) is thought at the long-run average water flow, and there is a possibility of the sedimentation density is a high flowfield from this on ground for the observation.

2.2 Sedimentation flux

In the amount of the maximum passing sedimentation, the ebb was 33g/s against 400g/s at the flood tide. In the amount of the maximum passing sedimentation, the ebb was 33g/s against 400g/s at the flood tide. The day when the sea level corrugate became symmetry because of the ebb and the flood tide was chosen in the present study on the observation day. However, the amount of sedimentation was asymmetry at the flood tide and the ebb.

2.3 Sediment transport at the strongest tide

The sedimentation density goes up on the flood plain in the vicinity of the low waterway shoulder at the ebb though the change in the direction of the crossing is small. The perpendicular direction change in the sedimentation density has become small oppositely high by the vicinity of the surface of the water in the vicinity of the bottom. That is, it is thought that sedimentation on not low-water channel's sedimentation but the flood plain is rolled up, and it is floating in the surface of the water. It is understood that the sedimentation transportation in the direction of the crossing is predominant in the cross-section.

The sedimentation density at the flood tide becomes the maximum on the flood plain and it has been minimized in the center part of a low waterway. A perpendicular change in the sedimentation density rises in the vicinity of the surface of the water, and has become small oppositely in the vicinity of the bottom. It is thought that the sedimentation transportation in the direction of the crossing is predominant as well as the ebb. However, the change in the direction of the crossing is seen in the sedimentation density compared with the ebb at the rflood tide. A high density region exists in the upper part of the slope of the sidewall of the low waterway region.

2.4 Salinity concentration

Salinity lowers in the center part of a low waterway, and has risen from there to the flood plain at an ebb strongest tide. This is thought that it is because there are a lot of ratios of the fresh water in half depth from the surface. Moreover, it is thought that it is because there are a lot of ratios of seawater in the vicinity of the bottom layer. It is thought that a stable density stratification is formed at an ebb strongest tide.

3. Conclusions

The measured data shows that the position of maximum flow velocity in the low-water channel convected downward on flood tides. Suspended sediment concentration profiles were very well-mixed both vertically and laterally. Salinity profiles showed a cross-channel salinity gradient have a sharp inclination than flood tides. The salinity profiles produce an effective transverse flow velocity distribution for natural compound channels.

Acknowledgments

This work was supported by JSPS KAKENHI Grant Number JP18K04371.

References

Nezu, I and Rodi, W. : Open channel flow measurements with a Laser Dppler anemometer , Journal of Hydraulic Engineering , Vol.112 , No.5 , pp.335-355, 1986.

Shiono, K and Muto, Y : Complex flow mechanisms in compound meandering channels with overbank flow, J. Fluid Mech. Vol.376, pp.221-261, 1998.

Taisuke ISHIGAKI, Koji SHIONO, Tong FENG and Renato N.SIQUEIRA : EFFECT OF STABLE DENSITY STRATIFICATION ON SECONDARY FLOW IN COMPOUND CHANNEL , Annual Journal of Hydraulic Engineering, JSCE, VOL.45, pp.535-540, 2001.

Terunori Ohmoto, Ryuichi Hirakawa, FLOWS AND SEDIMENT TRANSPORT OVER SAND BAR OF MACROTIDAL ESTUARY IN THE KIKUCHI RIVER, Proceedings of 9th International Symposium on Ecohydraulics, 2012.09, No.14226.

Numerical Study on Flood Control Function of Levee Openings located along Valley Bottom Rivers in Japan

Y. Ito[1], T. Ishikawa[2], R. Akoh[3] and S. Maeno[4]

[1] CTI Engineering Co. Ltd, Japan. itou-yasushi@ctie.co.jp
[2] Tokyo Institute of Technology, Japan. workishikawa0612@yahoo.co.jp
[3] Okayama University, Japan, akoh@okayama-u.ac.jp
[4] Okayama University, Japan, maeno@okayama-u.ac.jp

1. Introduction

Traditional levees on valley bottoms in Japan often had openings to allow excess river water to flood into paddy area, but recently, they are being closed to reduce inundation area following the modern flood control policy. Although the continuous levee system is effective for ordinary floods, the damage from extra-ordinary floods might be increased by the uncertainty of levee collapse due to levee overtopping. In this study, the basic idea of past engineers on the hydraulic function of levee openings was investigated using numerical flow simulation based on shallow water equations to discuss application of their idea to future flood control policy.

2. Study Site

The study area was a narrow valley bottom in an upper reach of the Sayo River flowing in a low mountain area of Japan Main Island. Figure 1(a) shows the aerial photograph of the study area, which includes two levee openings (A and B), and Figure 1(b) shows a close view of the opening-A. The basin area upstream from the study site is 102.4km^2, the current design flow rate of river channel is 560m^3/s, and the corresponding flood return period is 17 years. The mean riverbed slope of the flow simulation reach is about 1 / 210.

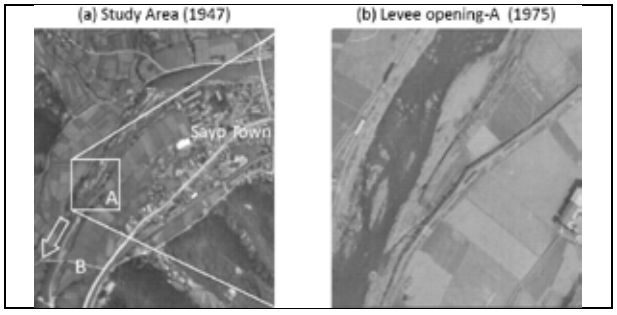

Figure 1: Aerial View of Study Site.

3. Methodology

Shallow flow model formulated on an unstructured triangular mesh system (Akoh et al., 2017) was used. Landform in the past was assumed based on GIS data (2015) and aerial photographs. Five flood hydrographs were prepared by applying a runoff model based on a rational formula using the 32 years rainfall data obtained at a nearby weather station. The corresponding flood return period (T_0) was 3, 5, 10, 15, 20 years, respectively.

4. Results and Discussion

The calculation result with the hydrograph of T_0 = 20 years are shown below. Figures 2(a)-(c) are the variation of inundation area and depth, and (d) shows the area of inundation caused by a 2004 flood, the T_0 of which was estimated as 17 years.

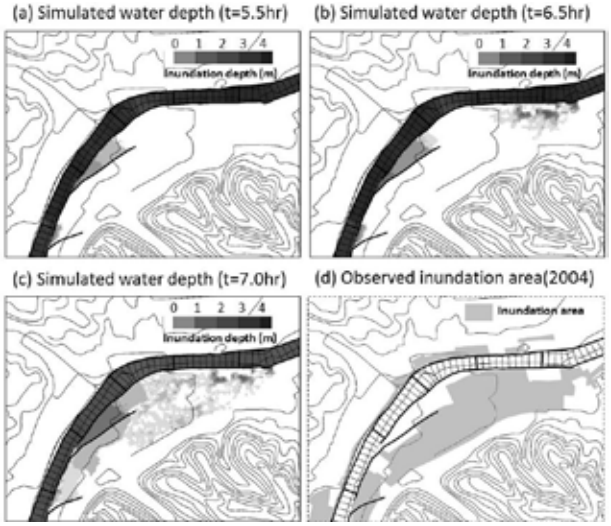

Figure 2: Inundation Area

At t = 5.5 hr, flooding occurred from two levee openings, but its areas were limited. On the other hand, overflow flooding from the upstream spread downstream, and merged to the flood water from the opening A at t = 6.5 hr, and also with flooded water from B at t = 7.0 hr (just at the flood peak). Flood area observed at the 2004 flood was similar to the simulation result at t = 7 hr.

Figure 3 shows the flood flow field near the levee openings at two elapse times. Inundated water was almost stagnated before flooding from the upstream arrived, and it flows into the levee openings after the arrival.

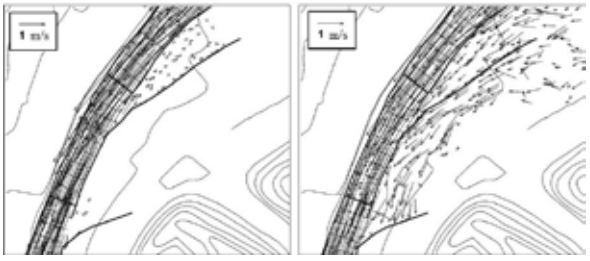

Figure 3: Velocity Field near levee openings

5. Conclusions

The purpose of setting the openings on the levee along the Sayo River was not to spread excess river water, but to drain flood water coming from the upstream. At the time of flood, paddy along the river channel is considered to have been utilized as a temporary divergent channel.

References

Akoh R et al. (2017) High-resolution modeling of tsunami run-up flooding: a case study of flooding in Kamaishi city, Japan, induced by the 2011 Tohoku tsunami. *Nat Hazards Earth Syst Sci* 17:1871-1883.

Defects, hysteresis and ripple morphodynamics

C. Jin[1], G. Coco[1], T. Perron[2], E. B. Goldstein[3], R. O. Tinoco[4], H. Friedrich[1] and Z. Gong[5]

[1] University of Auckland, Auckland, New Zealand. cjin987@aucklanduni.ac.nz, g.coco@auckland.ac.nz, h.friedrich@auckland.ac.nz

[2] Department of Earth, Atmospheric & Planetary Sciences, Massachusetts Institute of Technology, Cambridge, MA 02139, USA. perron@mit.edu

[3] Department of Geography, Environment, and Sustainability, University of North Carolina at Greensboro, Greensboro, NC 27412 USA. ebgoldst@uncg.edu

[4] Department of Civil and Environmental Engineering, University of Illinois at Urbana-Champaign, Urbana, IL 61801 USA. tinoco@illinois.edu

[5] State Key Laboratory of Hydrology-Water Resources and Hydraulic Engineering, Hohai University, Nanjing, China. gongzheng@hhu.edu.cn

1. Introduction

Wave-generated ripples are rhythmic bedforms present in subaqueous sandy environments subject to wave forcing. The presence of ripples leads to increases in both bed roughness and sediment suspension. Forcing conditions control the geometry of wave-ripples, but changes in ripple geometry lag the changes in wave forcing, a behaviour usually termed as hysteresis. Wave forcing is usually considered as the only factor determining the hysteresis (Soulsby et al., 2012). However, an alternate view is that defects (irregularities) in pre-existing ripple geometries also exert a significant impact on hysteresis (Huntley et al., 2008), but the relationship remains unclear. We investigate the role of defects in setting hysteresis using two lab experiments.

2. Laboratory experiments

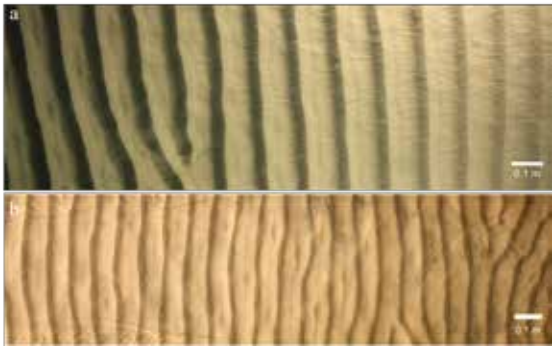

Figure 1. Photo of ripples before the changes in wave forcing in experiments of (a) Jin et al. (in review) and (b) Perron et al. (2018).

We use the ripple experiment datasets published by Perron et al. (2018) and Jin et al. (in review). The flumes were characterized by different length (7 m vs 54 m), sediment size (0.18 mm vs 0.31 mm). Water depth is 0.4 m in both experiments. All experiments are initiated from a flat bed with bed perturbations of variable size and subjected to a step change in wave forcing. Both increase and decrease in wave forcing are considered. Cameras were used to monitor the time-evolving ripple wavelength by applying spectral methods to each picture. We used images before the changes in wave forcing (Figure 1) to quantify defect density, (based on Huntley et al. 2008) and compared it to hysteresis time for increasing and decreasing changes in wave conditions.

3. Results

Our initial results show that the details of the change in wave forcing directly affects hysteresis. Also, when the change in wave forcing is limited, defect density has limited effect on hysteresis. However, when the increase in wave forcing is larger, defect density becomes important and faster ripple adjustment (i.e., shorter hysteresis) is observed. We also observed a marked difference depending on whether wave forcing increases or decreases.

Acknowledgements

C. Jin supported by China Scholarship Council.

Reference

Huntley, D. A., Coco, G., Bryan, K. R., Murray, A. B. 2008. Influence of “defects” on sorted bedform dynamics. *Geophys. Res. Letters*, *35*(2), L02601. https://doi.org/10.1029/2007GL030512

Jin, C., Coco, G., Tinoco, O. R., Goldstein B. E., Gong, Z. (in review). Laboratory experiments on the role of hysteresis, defect dynamics and initial perturbation on wave-generated ripple development. *Estuarine, Coastal and Shelf Sci.*

Perron, J. T., Myrow, P. M., Huppert, K. L., Koss, A. R., & Wickert, A. D. (2018). Ancient record of changing flows from wave ripple defects. *Geol.* https://doi.org/10.1130/G45463.1

Soulsby, R. L., Whitehouse, R. J. S., Marten, K. V. 2012. Prediction of time-evolving sand ripples in shelf seas. *Continental Shelf Research*, *38*, 47–62. https://doi.org/10.1016/j.csr.2012.02.016

The Victorian Coastal Monitoring Program: Predicting Future Geomorphological Change along Victoria's Coastline

C. Leach[1], D.M. Kennedy[1] and D. Ierodiaconou[2]

[1] School of Geography, Faculty of Science, The University of Melbourne, Parkville, VIC 3010, Australia.
chloe.morris@unimelb.edu.au, davidmk@unimelb.edu.au
[2] School of Life and Environmental Sciences, Deakin University, Warrnambool, VIC, Australia.
daniel.ierodiaconou@deakin.edu.au

1. Introduction

Coastal environments are increasingly at risk from the impacts of climate change, such as rising sea level and changing storm patterns. In Victoria, Australia, changing wave patterns associated with increasing intensity of Southern Ocean storms is inferred to be the greatest impact on the open coast. Understanding the geomorphic response to environmental changes is key to predicting their future evolution and therefore potential impact on socioeconomic factors.

On the theme of 'looking back, moving forward', this research aims to use our past and present understanding of coastal processes along the Victorian coastline, south east Australia, to predict its future geomorphic behaviour and response to climate change particularly changing wave directions associated with poleward shifts in subtropical atmospheric circulation systems.

2. The Victorian Coastal monitoring Program (VCMP)

The Victorian Coastal Monitoring Program (VCMP) was formed to address community concerns of present and future coastal risks by "providing communities with information on coastal condition, change, hazards, and the expected longer-term impacts associated with climate change that will support decision making and adaptation planning" (DELWP, 2019).

This research focuses on using coastal compartment modelling and visualisation to predict the future morphodynamics of the Victorian coastline. Modelling the entire coastline is a significant challenge given its spatial extent and the vast number of processes and environmental conditions that influence different parts of this system. For this reason, key sites of interest have been selected, based on stakeholder workshops and historical erosion records (Figure 1).

Figure 1: Location map of key sites of interest for the VCMP.

3. Methods

Numerical models provide powerful tools for understanding and predicting behaviours in coastal systems, although a compromise is often found between model complexity and scale. Each key site of interest (Figure 1) presents a different modelling challenge according to the scale and processes of interest and as such, a range of models have been selected to suit each location. These models include Delft3D, XBeach and CEM2D and are designed to simulate highly complex processes in coastal systems over relative short time periods (Delft3D), the impact of storm activity (XBeach) and the reduced complexity evolution of coastal systems over long time periods (CEM2D).

Data collected as part of the VCMP (such as repeat drone-based surveys, multibeam mapping of the seafloor and wave buoy data) will be used to drive these models to determine how each site behaves morphodynamically. The models will then be forced with future environmental conditions to determine how the coastal systems might respond to predicted environmental change. Initial modelling efforts have focused on the use of Delft3D at Port Fairy, investigating the role of key hydrodynamic wave and tidal conditions on the morphodynamics of this embayment along the Victoria coastline.

4. Conclusion

This study forms part of the wider VCMP and aims to use numerical modelling techniques to investigate the geomorphic behaviour of key sites of interest along the Victorian Coastline. At this preliminary stage, key sites of interest have been selected and numerical models have been assigned to address the specific research questions at each location. This research sets out to understand the past, present and future behaviours of these sites, under predicted changes in driving environmental conditions. Data available to calibrate and validate the models is a significant challenge particularly regarding more local hydrodynamic conditions, but efforts to address this data gap are underway through the deployment of a buoy network.

Acknowledgments

This project is funded from Department of Environment, Land, Water & Planning, as part of the Victorian Coastal Monitoring Program (VCMP) in partnership with Deakin University and the University of Melbourne.

References

DELWP. (2019). Victorian Coastal Monitoring Program. Retrieved from https://www.coastsandmarine.vic.gov.au/coastal-programs/victorian-coastal-monitoring-program

The channel bed responses to flood events and check dam construction in a mountain stream, Taiwan

Min-Chih Liang[1], Cheng-Wei Kuo[2] and Su-Chin Chen[3*]
[1]Department of Soil and Water Conservation, National Chung Hsing University, Taichung, Taiwan, minchih1126@gmail.com
[2]Sinotech Engineering Consultant, Taipei, Taiwan, cwkuo7215@gmail.com
[3*]Department of Soil and Water Conservation, National Chung Hsing University, Taichung, Taiwan, Corresponding author: scchen1431@gmail.com

1. Introduction

Many studies focused on erosion processes and recession rate of waterfalls and knickpoints (Ortega et al., 2013). However, the studies of effects of sedimentation upon morphology of waterfalls and downstream channel beds are less. Indeed, waterfalls play important roles in sediment transport and deposition. Kuo et al. (2017) explored the influence of check dam construction upon the development of the Meng-Gu Waterfall, Central Taiwan by historical photographs and terrain surveying by UAV. This study continues to trace the evolutionary processes of the channel bed downstream the waterfall.

2. Study site

The Meng-Gu Waterfall is located in the Nanshan Stream, Center Taiwan. The watershed area of the Nanshan Stream is 18.23 km^2 and the elevation ranged from 700 to 2,420 m with an average channel slope of 6%. The geology is mainly composed of grey-black thick slate with well-cleavage. According to historical photos, the Meng-Gu Waterfall was a waterfall with two steps in 2004. Then the study area has suffered two serious typhoon events (Mindulle in 2004 and Sinlaku in 2008) causing the accumulations up to 13 m height thus the lower step of waterfall had been buried (Kuo et al., 2017). The channel bed level experienced dramatic changes during the last decade. One heavy rainfall event occurred on 1st June 2017, produced a total rainfall of 863 mm within three days and induced the flood event. This removed most of the vegetation on the riverbed and greatly changed the morphology of the river.

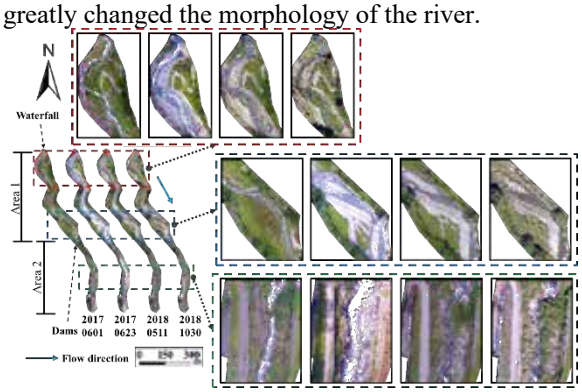

Figure 1: Orthophotos in different periods.

3. Material and Methods

This study used Unmanned Aerial Vehicle (UAV) to capture aerial images on 1st June 2017, 23rd June 2017, 11th May, 2018, and 30th October, 2018, respectively, and produced the Digital Elevation Model (DEM) for each time slices. The rainfall data was collected form the station Maple Forest near the Meng-Gu Waterfall. In terms of river bed changes, the difference of DEMs and the longitudinal profiles before and after the flood event are used. In terms of river planform morphology, four dates of orthoimages are used. The study area was divided into two sections: from the waterfall to the check dam (Area 1), and downstream the check dam section (Area 2).

4. Results

The results show that the invasion of 0601 flood event caused most of the vegetation on riverbeds in the Area1 and 2 to be removed (Fig1). Due to the construction of the check dam downstream, the slope of the upstream reaches was reduced, the river mainly shifted horizontally, and the removed vegetation is gradually recovered after one year. Thus the longitudinal change of the channel bed was small. The result showed that the 0601 flood event caused the scouring in the lower part of the waterfall, and sediment was transport to the downstream area of the check dam (Fig2 a). The slope reduced after the dam construction then lower the energy for scouring.

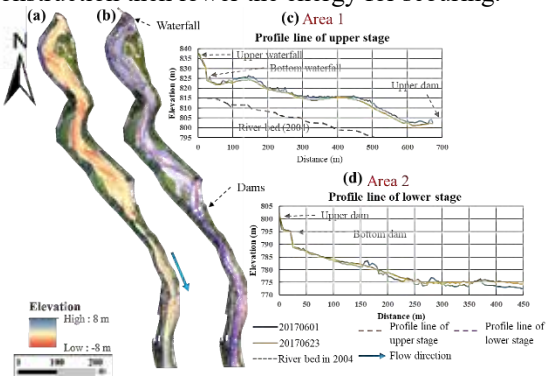

Figure 2: (a) The result of difference of the DEM on 0601 and 0623. (b) The position of the profile line. (c) & (d) the profile line of Area 1 and 2 before and after the flood event.

5. Conclusions

After the check dam was built in 2009, the changes of morphology of the river is limited, causing the river mainly shifting horizontally, and reducing the ability for floods to scour the channel bed. The accumulation of sediment upstream the check dam caused the original landscape unable to recover. In the future, if the sediment blocking capacity of the check dam can be adjusted, the sustainability of the natural landscape and the ecological environment could be increased.

References

Ortega, J.A., Wohl, E., and Livers, B. (2013). Waterfalls on the eastern side of Rocky Mountain National Park, Colorado, USA. Geomorphology, 198, 37-44.

Kuo, C.W., Chen, S.C., Chang, F.J., Su, K.X., Liang, M. C., Liu, Y. J., Huang, C. L. (2017). The influence of hydrological events and check dams upon the geomorphic changes of the Meng-Gu Waterfall. Journal of Chinese Soil and Water Conservation, 48 (3): 105-112.

Changes in flow distribution in a river bifurcation, case of study of the lowlands of the Grijalva Basin, Mexico

A. Mendoza[1,2], and M. Berezowsky[3], Y. Blas[4]

[1] Universidad Autónoma Metropolitana, Lerma, México. a.mendoza@uam.ler.mx
[2] Instituto de Ingeniería, Universidad Nacional Autónoma de México, México. amendozar@ii.unam.mx
[3] Instituto de Ingeniería, Universidad Nacional Autónoma de México, México. mberezowskyv@ii.unam.mx
[4] Universidad Autónoma Metropolitana, Lerma, México. 2142040615@uam.ler.mx

1. Introduction

The Grijalva basin, located in the southeast of Mexico starts in the highlands of Guatemala and drains toward the Gulf of Mexico. In the lowlands of the basin there is a record of constant avulsions in the last centuries; one of the products is such avulsions is the bifurcation of the Mezcalapa River into the rivers Samaria and Carrizal (Figure 1).

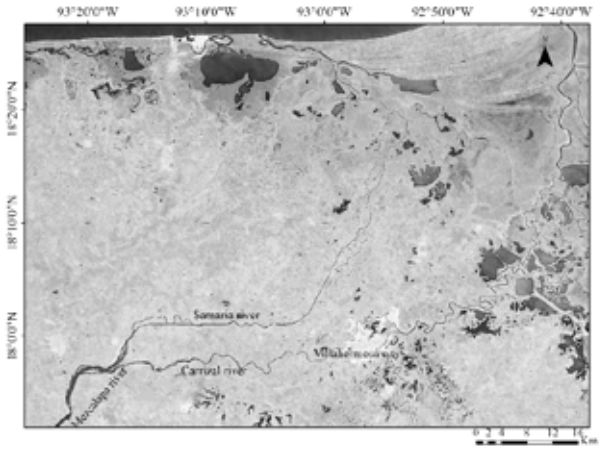

Figure 1. Bifucation of the river Mezcalapa in the lowlands of the Grijalva Basin.

At the end of the last century, the magnitude of the flow diverting to the Carrizal River increased the risks of floods in Villahermosa, city located downstream the bifurcation. It was alleged that the change of distribution of flow was caused by the extraordinary rains and river floods of the time, however, it has been found that the flow distribution started to raise several years before that (Mendoza et al., 2019). Figure 2 shows that the flow distribution in the bifurcation is changing since the 1960's, and the increasing pattern in the Carrizal River starts by 1983.

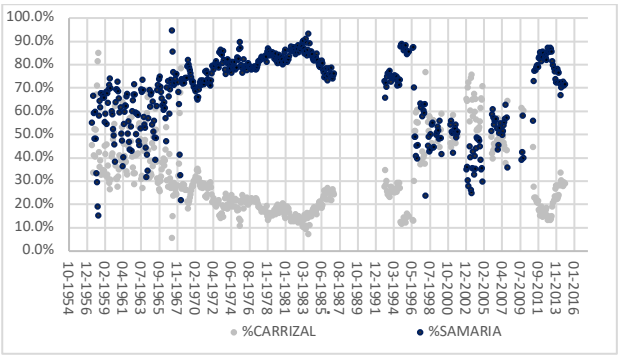

Figure 2: Historical distribution of flow in the bifurcation.

In 2005 a structure with gates was build in the entrance of Carrizal River to control the flow, the response was a significant reduction of the flow in that river as can be seen in Figure 2. However, before that date, it is unclear what drove the changes of the distribution of flow. It has been identified thee possible causes:

- The banks of the rivers on the bifurcation migrate constantly, they can change the flow pattern and consequently the flow distribution.
- The change of flow regime caused by the system of dams build upstream the bifurcation.
- The change in the sediment supply caused by the dams located upstream.

The effects of the first cause are addressed in this work by numerical simulation with Telemac-2D.

2. Methods

A bidimensional model of flow in the bifurcation was set up to simulate the distribution of flow considering the position of the river banks in different years. The position of the banks in the rivers surrounding the bifurcation were obtained from Landsat imagery and from archived aerial photography. Preliminary results were obtained for the position of the banks in 1972, 1980 and 1986.

Year	Carrizal/Mezcalapa flow distribution
1972	21% / 79%
1980	20.3% / 79.7%
1986	20.3% / 79.7%

Table 1: Flow distribution in the bifurcation from numerical simulations.

3. Conclusions

The simulations reproduce the general distribution of flow between 1972 and 1986, however, by 1986 the historical data shows a gradual increment in the flow diverting to the Carrizal River (25% of the flow), while the simulation indicates 20.3% (Table 1). It would be interesting to analyse the results for the position of the banks in the 1990's and 2000's, which are being computed. This will allow to identify if the magnitude of impact of the change of the geometry of the bifurcation on the flow distribution observed historically.

References

Mendoza, A., Soto-Cortes, G., Priego-Hernandez, G., Rivera-Trejo, F. (2019). Historical description of the morphology and hydraulic behavior of a bifurcation in the lowlands of the Grijalva River Basin, Mexico. *Catena.*, 176, 343–351.

Morphological and ecological effects of Mid-Barataria Sediment Diversion in Coastal Louisiana

Francesca Messina[1*], Brendan Yuill[1], Martijn Bregman[1], Hoonshin Jung[1], Melissa Baustian[1], Ehab Meselhe[1], Kazi Sadid[1]

[1]The Water Institute of the Gulf, Baton Rouge, Luisiana
**fmessina@ thewaterinstitute.org*

1. Introduction

The Mississippi River Delta is one of the most complex ecosystems in the world. Louisiana coastal area is among the most productive and dynamic eco-geomorphic systems in the world. However, this unique natural environment has been altered by human activities and natural processes such as sea level rise, subsidence, dredging of canals, levee systems, etc.

The Louisiana's Comprehensive Master Plan for Sustainable Coast proposed different large-scale restoration efforts for sustaining and creating new wetlands in Louisiana. Two major sediment diversions are being considered and analysed to reconnect the Mississippi River to the estuaries and to divert sediment, nutrients and fresh water to build new land, maintain existing marshes and increase habitat resiliency to sea level rise and storm events.

A comprehensive model which incorporates hydrodynamics, morphodynamics, nutrient dynamics, vegetation dynamics and their feedbacks has been developed (Baustian et al., 2018) and used to investigate and analyse the landscape evolution, the hydrodynamic and water quality changes, and the vegetation dynamic in the next 50 years considering different sediment diversion operations, and environmental scenarios such as sea level rise and subsidence.
Synergies with additional marsh creation projects in the diversion outfall area have also been considered and incorporated into the modelling efforts.

The model results will improve our understanding of the morphodynamic and ecological responses of the receiving basins. This analysis could assist in optimizing the planning and design one of the largest-scale restoration projects for coastal areas all over the world.

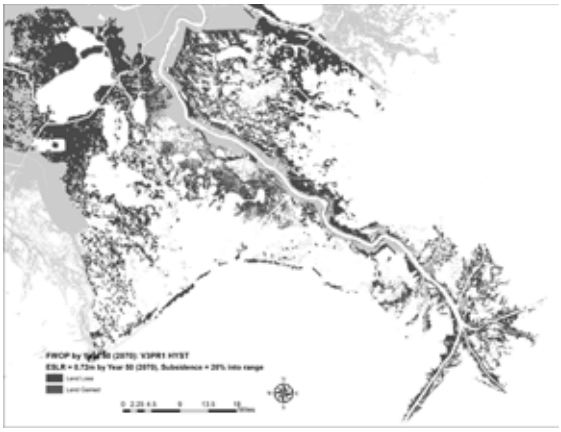

Figure 1. Predicted land change in the Mississippi River Delta in 50 years. Future without projects case.

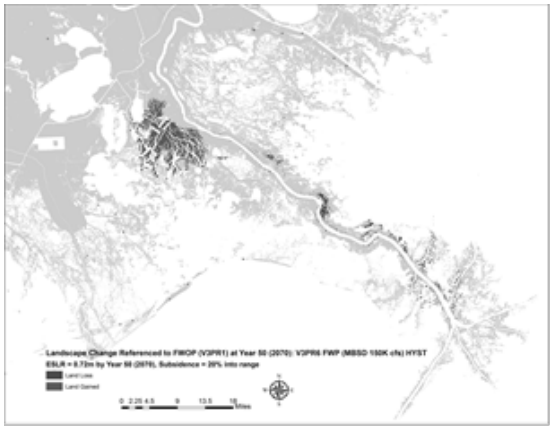

Figure 2. Predicted land change in the Mississippi River Delta in 50 years. Future with projects case: Mid-Barataria Sediment Diversion open, max discharge of 150,000cfs

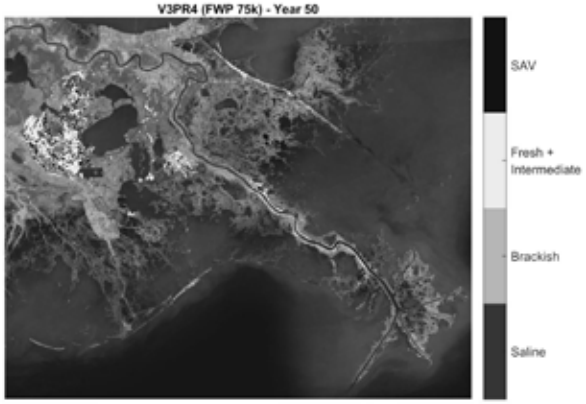

Figure 3. Predicted vegetation coverage in the Mississippi River Delta in 50 years. Future with projects case: Mid Barataria Sediment Diversion open with a max discharge of 75,000cfs

References

Baustian, M. M., Meselhe, E., Jung, H., Sadid, K., Duke-Sylvester, S. M., Visser, J. M., Allison, M. A., Moss, L. C., & Ramatchandirane, C. G. (2018). Development of an Integrated Biophysical Model to represent morphological and ecological processes in a changing deltaic and coastal ecosystem. *Environmental Modelling & Software*, 19.

Flood Attenuation Through Channelized Mangrove Forests

J.M. Montgomery[1], K.R. Bryan[2] and G. Coco[3]

[1] University of Waikato, Hamilton, New Zealand, jmontgom31@gmail.com
[2] University of Waikato, Hamilton, New Zealand, karin.bryan@waikato.ac.nz
[3] University of Auckland, Auckland, New Zealand. g.coco@auckland.ac.nz

1. Introduction

Mangroves can be an effective form of coastal flood protection and have been shown to reduce storm surge by up to 50 cm/km of forest width (Krauss et al., 2009). Mangroves reduce the flow of water and act as a water storage mechanism reducing peak flood levels (Montgomery et al., 2019). Channels efficiently convey water and reduce the capacity of mangrove forests to attenuate coastal floods (Krauss et al. 2009). Similarly, vegetation density influences the rate water is transported though a forest and has been shown to influence flood attenuation. Here we use a numerical model of a mangrove forest in Tauranga estuary, New Zealand to explore the role of channels and mangrove density in flood attenuation.

2. Parameterizing Vegetation Density

Drag exerted by vegetation has typically been parametrized by vegetation frontal area density (projected area of stems as seen by the oncoming flow, per unit volume) (Nepf, 2004). Often, homogenous forest density and rigid vertical stems are assumed allowing a flow resistance area to be estimated. Here, the study area is comprised of complex tree geometries and varying canopy heights that present a challenge to estimating vegetation properties (Fig. 1). We apply a method developed by Jarvela et al. (2004) based on the natural structure of branched trees to estimate plant characteristics of complex vegetation and therefore frontal area density and flow resistance.

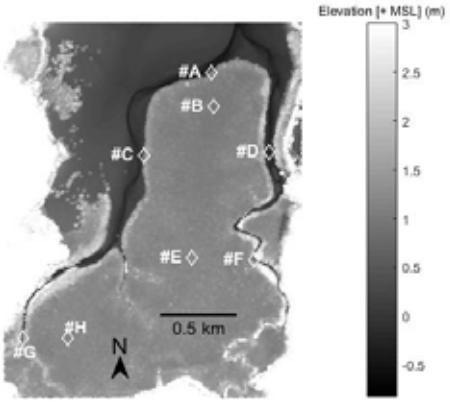

Figure 1: LiDAR data from Tauranga study site with instrument locations identified. Note higher elevations (larger mangroves) bordering creeks.

Tree surveys were conducted over a range of canopy heights obtaining a relationship between vegetation frontal area density and canopy height. In Pahoia, canopy heights and vegetation density are greatest along intertidal creeks and typically diminish with distance away from channels (Fig. 1). Tree heights are estimated as the difference between canopy elevations (peak LiDAR return for a discretized area) and surface elevation measured via an RTK GPS survey. Applying the previously obtained relationship between canopy height and vegetation density results in a spatially varying vegetation frontal area density which is modelled as rigid vertical cylinders with equivalent frontal area.

3. Results

Field data collected from an array of water level sensors deployed at the field site (Fig. 1) show no reduction of peak water level across the forest. This is attributed to water transport into the area being dominated by channelized flow. However, preliminary modelling results show attenuation of peak flood level occurs when vegetation density is increased.

4. Conclusions

When present, channels dominate the convenience of water through a mangrove forest reducing the flood attenuating benefit. However, sufficiently high vegetation density allows for some attenuation of peak water level due to reduced water transport into the region (via channels) and slow propagation of water from the channels into the forest.

Acknowledgments

The research was supported by the Natural Hazards Platform (contract C05X0907). The authors would like to acknowledge Dean Sandwell for field work contributions

References

Jarvela, J. (2004). Determination of flow resistance caused by non-submerged woody vegetation. *International Journal of River Basin Management, 2*, 61-70.

Krauss, K. W., Doyle, T. W., Doyle, T.J., Swarzenski, C.M., From, A.S., Day, R.H., &Conner, W.H. (2009) Water level observations in mangrove swamps during two hurricanes in Florida. *Wetlands, 29*, 142-149. https://doiorg/10.1672/07-232.1

McIvor, A., Spencer, T., Moller, I., & Spaldinga, M. (2016). 2|Coastal defense services provided by mangroves. *Managing Coasts with Natural Solutions,* 24.

Montgomery, J., Bryan, K., Mullarney, J., & Horstman, E. (2019). Attenuation of Storm Surges by Coastal Mangroves. *Geophysical Research Letters, 46*. https://doi.org/10.1029/2018GL081636.

Nepf, H. (2004). Vegetated flow dynamics. In *The Ecogeomorphology of Tidal Marshes* (pp. 137-163). Washington, DC: American Geophysical Union. https://doi.org/10.1029/59CE-0.

Turbulence, flocculation and sediment transport along a tidally influenced river: the Lagrangian transition from fresh to salt water

Julia C. Mullarney[1], Iain T. MacDonald[2], Bérengère S. Déjeans[1] and Glen M. Reeve[2]

[1] Coastal Marine Group, University of Waikato, Hamilton, New Zealand. julia.mullarney@waikato.ac.nz
[2] NIWA, Hamilton, New Zealand.

1. Introduction

Flocculation controls the size and settling velocity of fine sediments. Therefore, this process plays a key physical role in the dispersal and settling of muddy sediments within aquatic environments. Our understanding of the flocculation processes is often based on the assumption that sediment particles suspended in a moving water column are in equilibrium with the local environment. However, this assumption is not always correct as flocs can be affected by the environmental conditions to which they have previously been exposed (such as water column stratification and suspended sediment concentrations). Here, we explore physical controls on flocculation, by examining Lagrangian observations of floc size, hydrodynamics and water column properties along a heavily sediment-laden and tidally influenced river. We also compare observations to numerical model results.

2. Methods

In-situ observations of floc size, hydrodynamics and water column properties were measured along the Kaipara River, New Zealand using novel 'Lagrangian FlocDrifter' platforms (MacDonald and Mullarney, 2015). Up to three drifters were released at the start of the ebb tide at different locations along the river. In total drifters were released for around 4 hours and the total track length was around 11 km (from freshwater conditions upstream to the estuary). In each case, floc cameras provided particle size distributions up to an upper working limit of concentrations of 350 mg/L. Velocities and estimates of the dissipation rate of turbulent kinetic energy, ε, were obtained from a Nortek Aquadopp operating in pulse-to-pulse coherent mode.

Numerical modelling was undertaken using Delft 3D, in 3D mode with 10 levels in the vertical. The model was forced by time series of depth-averaged velocity and water levels at the upstream and seaward boundaries, respectively. The model was calibrated against Eulerian measurements from the centre of the domain.

3. Results

A time series of ε and observed median floc size (D_{50}) for a single drifter is shown in Figure 1. As the drifter progresses downstream, the dissipation rate of TKE fluctuates around $10^{-4.5}$ W/kg. The moving average of D_{50} (solid black line) displays a slow increase over the first 2.5 hr but roughly doubles to 200 μm over the last 1.5 hr. This slow upward trend likely represents the timescale of flocculation, whereas the higher frequency variability (grey points) could be associated with sources and sinks of sediment such as erosion from bed and deposition. To model changes in median floc size D_{50}, we use the flocculation model of Winterwerp (1998):

$$\frac{\mathrm{d}D_{50}}{\mathrm{d}t} = k_A c G D_{50}^2 - k_B G^{3/2} D_{50}^2 \left(D_{50} - D_p\right), \qquad (1)$$

where D_p is the diameter of the primary particles, c is suspended sediment concentration and $G = \sqrt{\varepsilon/\nu}$ is a dissipation parameter in which ν is the kinematic viscosity. The first and second terms on the right-hand size of (1) represent aggregation and break up, respectively. We fit data to determine the constants k_A and k_B. Preliminary model fits (dashed lines) are promising - clearly capturing the lower frequency variability.

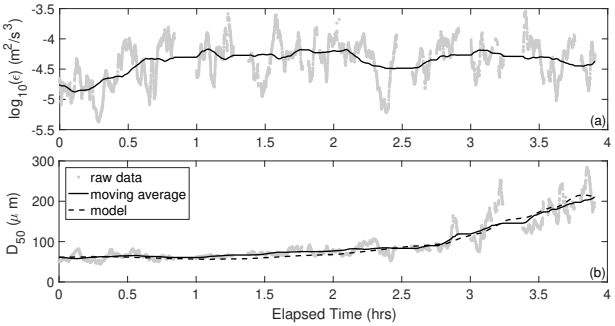

Figure 1. (a) Observations and moving average of the dissipation rate of trubulent kinetic energy along the river for a single drifter release. (b) Observations and model predictions for D_{50}. In this example, $k_A = 10.8$ and $k_B = 10,000$.

We will also present results from numerical modelling results of the system. In particular, we demonstrate reasonable agreement between modelled and observed TKE dissipation rates; however; the model generally underpredicts ε on bends. Moreover, dissipation rates appear to be predominantly controlled by the system geometry. Future work will explore the connection between environmental conditions (e.g. turbulence, SSC and salinity) and floc size, and will determine if the high frequency variability can be captured by accounting for source and sink terms.

Acknowledgments

We thank NIWA for funding and Dave Bremner, Rod Budd, Scott Edhouse, Sam Parkes and Mark Pritchard for their assistance with the field work.

References

MacDonald, I. T. and Mullarney, J. C. (2015). A Novel "FlocDrifter" Platform for Observing Flocculation and Turbulence Processes in a Lagrangian Frame of Reference. *Journal of Atmospheric and Oceanic Technology*, 32(3):547–561.

Winterwerp, J. C. (1998). A simple model for turbulence induced flocculation of cohesive sediment. *Journal of Hydraulic Research*, 36(3):309–326.

Anthromorphodynamics: Coastal case studies

Murray, A. B.[1], Gopalakrishnan, S.[2], Hutton, E.[3], Keeler, A. G.[4], Landry, C. E.[5], McNamara, D.[6], Moore, L. J.[7], Mullen, M.[1], Smith, M. D.[1], Williams, Z.C.[6]

[1] Nicholas School of the Environment, Duke University, USA. abmurray@duke.edu
[2] The Ohio State University, USA. gopalakrishnan.27@osu.edu
[3] University of Colorado, Boulder; Community Surface Dynamics Modeling System, USA. hutton.eric@gmail.com
[4] East Carolina University; UNC Coastal Studies Institute, USA. keelera@ecu.edu
[5] University of Georgia, USA. clandry@uga.edu
[6] University of North Carolina, Willmington, USA. mcnamarad@uncw.edu
[7] University of North Carolina, Chapel Hill, USA. laura.moore@unc.edu

1. Introduction

In morphodynamic systems, couplings between morphology, sediment flux patterns, and morphology change generate rich arrays of patterns and behaviors. In anthromorphodynamics, an additional set of couplings creates additional possibilities for interesting, emergent behaviors. When landscape changes related to large-scale morphodynamics spur human decisions to alter the landscape or landscape-forming processes, those alterations can in turn fundamentally change the large-scale morphodynamic behavior—and therefore affect future human risks and decisions. As distinguished from studies of how human actions alter morphodynamic systems—which address one direction of influence—in anthromorphodynamic studies, human actions are both the response to and the cause of morphodynamic changes. Human decision making is an integral part of anthromorphodynamic system.

In coastal landscapes, couplings between human dynamics and landscape dynamics are especially tight, for two reasons. First, coastal systems tend to change on timescales that are faster than those for many terrestrial landscapes; in undeveloped coastal environments, significant changes in location and elevation can occur over years to decades, corresponding with timescales of human decision making. In addition coastal landscape-change processes, ranging from storm impacts to chronic shoreline erosion, represent acute hazards for growing coastal populations, prompting the expenditure of significant resources to mitigate the hazards—i.e. alter the landscape-change processes

2. Case studies

Ongoing work couples economic models (analytical and agent based) with morphodynamic models to address two sets of questions. The first set involves patterns of plan-view coastline change that emerge from the coupling between large-scale coastline morphodynamics (Murray and Ashton, 2013) and communities making decisions about localized shoreline stabilization (e.g. beach nourishment projects; e.g. Murray et al., 2013; Smith et al., 2015). Even localized shoreline stabilization alters regional coastline-change patterns, which in turn changes the erosion pressures and resultant decision making in other coastal communities. When storm-climate oscillations tend to produce fluctuations in coastline shape (e.g. Antolinez et al., 2018), humans can prevent changes in coastline shape, but the costs of stabilization increase. As those costs exceed the benefits for some communities, and those communities cease to stabilize their shorelines, the patterns of coastline change and erosion pressures on other communities shift (e.g. McNamara et al., 2011). The second set of questions involve how developed barrier systems respond to sea-level rise and storm impacts—e.g. how maintaining artificial dunes and bulldozing overwashed sand after storms affect the feedbacks that tend to maintain barrier elevation relative to rising sea level, and how humans might respond to the resultant changes in storm and flood hazards.

3. Discussion

Plan-view coastline change arising from gradients in alongshore sediment flux, and long-term cross-shore-profile dynamics arising from cross-shore sediment fluxes and sea-level rise have been most often treated separately. Couplings with human dynamics in plan-view and profile contexts have been addressed separately. However, the plan-view and profile anthromorphodyanmics interact with each other, and we plan to couple the two sets of models

References

Antolinez, J. A. A., Murray, A. B., Mendez, F. J., Moore, L. J., Farley, G., and Wood, J., 2018, Downscaling changing coastlines in a changing climate, the hybrid approach, Journal of Geophysical Research: Earth Surface, 123. *https://doi.org/10.1002/2017JF004367*.

McNamara, D., Murray, A.B., and Smith, M.D., 2011, Coastal sustainability depends on how economic and coastline responses to climate change affect each other, Geophysical Research Letters, 38, L074, doi: 10.1029/2011GL047207.

Murray, A.B., S. Gopalakrishnan, D. E. McNamara, and M. D. Smith, 2013, Progress in Coupling Models of Human and Coastal Landscape Change, Computers and Geosciences, 53, 30-38, 10.1016/j.cageo.2011.10.010

Murray, A. B., and Ashton, A. D., 2013, Instability and finite-amplitude self organization of large-scale coastline shapes, Philosophical Transactions of the Royal Society of London A Math Phys Eng Sci, vol. 371:20

Smith, M. D., Murray, A. B., Gopalakrishnan, S., Keeler, A. G., Landry, C. E., McNamara, D., and Moore, L. J., 2015, Chapter 7 – Geoengineering Coastlines? From Accidental to Intentional, in *Coastal Zones, Solutions for the 21st Century*, Elsevier, doi: 10.1016/B978-0-12-802748-6.00007-3.

Dynamic Channel Shifting and Corresponding Formation and Destruction of Villages in the Sittaung River Estuary

N. Nagumo[1] and S. Egashira[2]

[1] International Centre for Water Hazard and Risk Management, Public Works Research Institute, Japan.
n-nagumo55@pwri.go.jp
[2] International Centre for Water Hazard and Risk Management, Public Works Research Institute, Japan.
s-egashira77@pwri.go.jp

1. Introduction

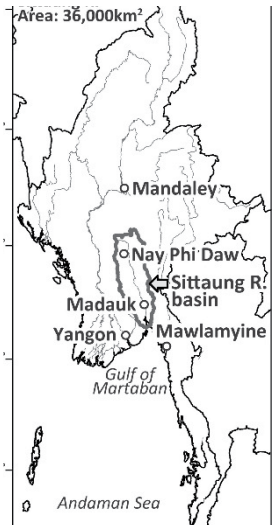

Figure 1: Study Area

The Sittaung River basin is located in the north of the Gulf of Martaban, and the river develops an estuary of 270 km wide and 220 km long in its mouth (Figure 1). Owing to the estuary topography with a maximum tide difference of 4 to 5 m, strong tidal currents reverse the river flow and cause tidal bores particularly in spring and autumn. Although these phenomena play an important role in sediment transport in the estuary, a severe bank erosion of c. 1km/yr threatens the livelihood of local people at the same time.

This paper explains how the main channel has shifted in the Sittaung estuary by interpreting maps, satellite images, and the results of field surveys and how the shifting has affected the formation and destruction of villages. The analysis will contribute not only to revealing bank erosion processes but also to identifying risks, planning efficient land use, and developing practical measures for protecting riverside areas.

2. Channel shifts and bank line changes

Figure 2 illustrates historical changes of the main flow route of the Sittaung River by interpreting satellite images captured after 1972 and topographic maps around the estuary in 1929, the 1940s, and 2013. Active channel shifts are observed downstream of the Sittaung bridge; for example, disappearance of a meander after 2002 (A) and change in shifting direction from right to left or left to right banks after 1977, 1994, and 2005 (B). The main channel had moved closer to the right bank by 2016, a large sand bar appeared along the bank in 2018, and the channel started moving toward the left bank again. The analysis found that the channel shifts in an area of c. 30 km wide every 10 to 15 years in the past 90 years, and that the shifts are closely related to sediment transport and the formation of sand bars caused by tidal currents and river flow.

The impact of bank erosion varies between both sides of the river. Bank erosion is limited in the left bank due to its upland topography while it is severe in the right bank where the area is lowland. As Reclus (1876) describes, the channel ran far west from the present location in the

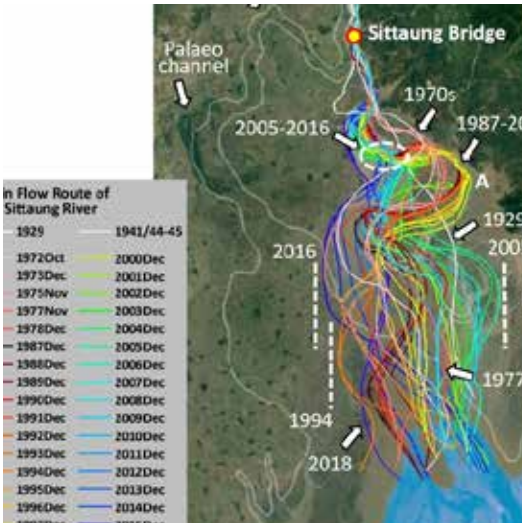

Figure 2: Historical changes of main flow route

19th century (Figure 2), which suggests that the expansion of lowland is quite recent and that more active erosion or flow route shifting may occur in millennial timescales.

3. Formation and destruction of villages

Our investigation in 1929, 2013 and 2018 found that most of the villages along the estuary had already established by 1929 and that the number has since been increasing. Several villages were newly established in the left bank due to sand bar development after 2013 while some in the main flow route completely disappeared because of erosion, which accelerated bank retreat. In order to adapt to environmental changes and eliminate erosion risk, several villages in the right bank moved inland after 1929.

4. Conclusions

This paper revealed spatio-temporal flow route changes in the Sittaung estuary and explained the formation and destruction of villages related to very active bank erosion enhanced by tidal bores. Finding in this study contributes planning practical solutions to protect the livelihood of people living around the estuary. For local sustainability, more research is necessary to clarify historical phenomena and future risks.

References

Reclus, E. (1876). *The universal geography: earth and its inhabitants,* vol. 8, London. J.S. Virtue & Co., Limited.

Monitoring temperature dynamics in shallow tidal lagoons combining in situ observations, satellite retrievals, and numerical modeling.

M. Pivato[1], S. Silvestri[2], D.P. Viero[1], C. Soranzo and L. Carniello[1]

[1] Department of Civil, Environmental and Architectural Engineering, University of Padova, Padova, Italy
mattia.pivato.1@dicea.unipd.it
[2] Department of Land, Environment, Agriculture and Forestry, University of Padova, Padova, Italy

1. Introduction

Water and sediment temperature plays a crucial role in many physical and biological processes driving the bio-morphodynamic evolution of aquatic environments, such as carbon sequestration , dissolved oxygen levels (Wetzel, 2001) and the growth of macroalgae and microphytobenthos. Therefore, the development of proper methods and tools for monitoring and estimating the temperature dynamics of water and bed sediment is of paramount importance. The aim of the present study is to present a numerical model for describing the time-space dynamics of the water temperature within shallow water environments, with a specific focus on the Venice Lagoon.

2. Methods

We implemented a temperature module into an already existing two-dimensional hydro-morphodynamic model (Carniello et al., 2012) solving for hydrodynamics, wind-waves, sediment transport and bed evolution. The temperature module is based on the solution of the advection diffusion equation of the water temperature and computes the energy fluxes at the atmosphere-water interface using the meteorological data as boundary conditions (Pivato et al., 2018).

Model calibration and validation are performed combining point measurements with information provided by satellite images (Fig. 1). Sequences of at least two satellite images taken a few days away one from the other have been selected in order to use the first one for initializing the thermal state of the system and the following ones for comparison with model results. In situ point measurements ensure useful information about the time evolution of the temperature dynamics, but their distribution within the water basins usually allows only a rough description of its spatial variability. Instead, satellite images provide a full description of the water temperature spatial distribution, but not of the time evolution of the process, being the time interval between two consecutive images typically of the order of days. Using a numerical model calibrated combining the information provided by point measurements and satellite images enables us to overcome the limitations of both the type of data, thus obtaining a much more complete description of the process we are interested in.

3. Results and Conclusions

We performed two 7 to 10-days-long simulations in Spring and Summer. For each run we compared model results with temperature data collected at 10 stations within the lagoon (Fig. 1) and at least one temperature map retrieved from satellite images. Our results highlight the capability of the model to correctly reproduce the temperature dynamics everywhere within the lagoon. In particular the agreement is good both at the inlets, where in situ measurements display a local temperature modulation in phase with the semi-diurnal tidal period highlighting the crucial role exerted by the advective fluxes driven by tidal current, and in the inner areas of the water basin, where tidal currents are low and water temperate variation is mainly affected by the day/night cycle. Also the comparison between the spatial distribution of the water temperature estimated by the model and the one retrieved using remote sensing techniques shows a good agreement. Using a point model for describing the local temperature dynamics of the water-sediment continuum we recently investigated the proliferation of microalgae and the related stabilizing effect on the bed sediment (Pivato et al., 2019). The temperature module presented herein represents the first step for extending at the the basin scale the analysis of the bio-morphodynamic feedback between microalgae growth and sediment transport processes affecting the morphological evolution of tidal environments.

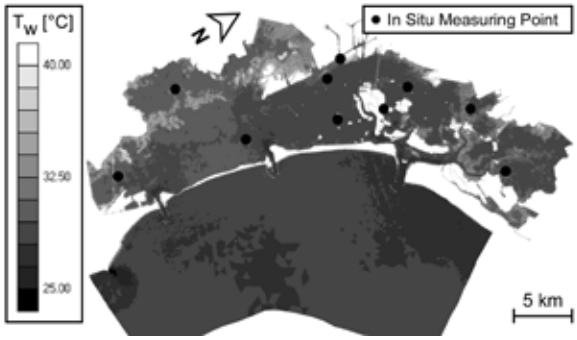

Figure 1. Water temperature spatial distribution within the Venice lagoon provided by a satellite image (22-Aug-2011 09:30).

References

Carniello, L., Defina, A., and D'Alpaos, L. (2012). Modeling sand-mud transport induced by tidal currents and wind waves in shallow microtidal basins: Application to the Venice Lagoon (Italy). *Estuarine, Coastal and Shelf Science*, 102-103:105–115.

Pivato, M., Carniello, L., Gardner, J., Silvestri, S., and Marani, M. (2018). Water and sediment temperature dynamics in shallow tidal environments: The role of the heat flux at the sediment-water interface. *Advances in Water Resources*, 113:126–140.

Pivato, M., Carniello, L., Moro, I., and D'Odorico, P. (2019). On the feedback between water turbidity and microphytobenthos growth in shallow tidal environments. *Earth Surface Processes and Landforms*.

Wetzel, R. G. (2001). The Phosphorus Cycle. *Limnology: Lake and River Ecosystems*, pages 242–50.

Utilisation of Sub-Grid-Scale Bed Elevation Data in Gridded 2D SWE Schemes

P.A. Ryan[1], S. Gao[2] and W.J. Syme[3]

[1] BMT phillip.ryan@bmtglobal.com [2] BMT. shuang.gao@bmtglobal.com [3] BMT. bill.syme@bmtglobal.com

1. Introduction

Solutions to the depth average (2D) Navier Stokes equations, known as the Shallow Water Equations (SWE), are typically computed on either uniform Cartesian grids, or flexible arbitrary meshes. In either case, it is often the case that the model mesh resolution is significantly coarser than the available bed elevation data (from a digital elevation model, or DEM), particularly with the advent of modern ground scanning techniques such as LiDAR. When sampling the DEM data at the grid cell centres, the three most common options are (1) discrete point sampling, (2) average elevation within cell, or (3) minimum elevation within cell. With all these options, knowledge of the terrain at sub-grid-scales is essentially lost, with an associated loss of model fidelity.

2. Why utilise sub-grid-scale DEM data?

The data degradation caused by not using or averaging sub-grid-scale bed elevation data potentially causes a loss in model accuracy, especially in areas of highly variable topography. In particular:

a) Channels that are less than one or two cells in width may become a disconnect series of pits that choke and retain water, causing a poor reproduction of the flow behaviour.
b) For rain-on-grid models, unrealistic water retention and flow responses will adversely affect the model's reliability.
c) The flow field along the wet-dry boundary can show artefact velocities and disproportionately steep water surface profiles where the mesh is not aligned with the wet/dry boundary.

The last point is very significant as the water surface gradient along a channel can be substantially over-predicted, especially where there are only a few cells across the waterway. Figure 1 illustrates an example of the flow field past steps in the wet/dry boundary for a gridded mesh causing a choke on the hydraulics.

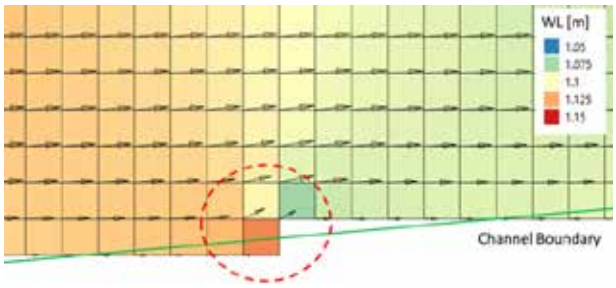

Figure 1 Artefact velocities near wet/dry boundaries

The significance of this problem lies in that the disturbance of the flow field causes artefact energy losses along the flow path. The severity of these unrealistic losses depends significantly on the number of 2D cells across the waterway and the degree of misalignment of the mesh to the wet/dry boundary. The authors have also observed that the type and spatial order of the numerical solution scheme can also have a bearing. Ultimately, the calibration and reliability of the model is not only dependent on mesh size, but also on grid rotation. Note that this problem is not limited to gridded schemes but may also occur in flexible arbitrary meshes where the mesh is not well aligned with the wet/dry boundaries.

Intelligent utilisation of sub-grid-scale DEM data has the potential to improve model fidelity and reduce model sensitivity to grid size and rotation.

3. Study

A simple approach to calculating water surface elevation within cells, and effective cell face areas as a function of face interpolated water elevation that utilises sub-grid-scale DEM data is presented.

The TUFLOW HPC solver (Collecutt and Syme, 2017) has been adapted to include the described sub-grid-scale DEM model, and benchmarking studies performed, including angled channelled flow, and rain-on-grid catchment models, to ascertain the validity and effectiveness of the approach.

4. Conclusions

Findings have shown that the approach of utilising the sub-grid-scale DEM data significantly addresses the issues identified in Section 2, in that the flow responsiveness of small tributaries is improved, water retention is reduced, and most importantly flow along narrow channels is substantially better resolved (Figure 2), with unrealistic head losses associated with misalignment between the mesh and the channel no longer an issue.

The results thus far indicate that channelled flow can be accurately modelled by a coarse resolution of gridded cells and the paradigm that a carefully constructed flexible mesh is preferable no longer applies.

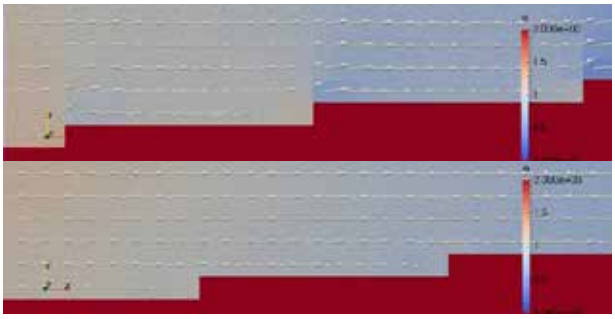

Figure 2 Above without sub-grid data, below with

References

Collecutt, G., and Syme, B. (2017). Experimental benchmarking of mesh size and time-step convergence for a 1st and 2nd order SWE finite volume scheme. *Proceedings of the 37th IAHR World Congress, Kuala Lumpur*.

Evaluation of the water and suspended particulate matter sources in a regulated river

L. Troudet[1], J. Le Coz[1], J.B. Faure[1], and B. Camenen[1]

[1] Irstea, UR Riverly, 5 rue de la Doua, CS 20244, 69625 Villeurbanne Cedex, France.
laura.troudet@irstea.fr, jerome.lecoz@irstea.fr, jean-baptiste.faure@irstea.fr and benoit.camenen@irstea.fr

1. Introduction

Long term flux data in rivers are required for a better understanding of particulate transfers from the continental areas to the seas in order to manage water resources, pollution, hydropower generation, etc. Estimating Suspended Particulate Matter (SPM) fluxes in rivers requires continuous time series of both discharge and SPM concentration. While discharge data are usually available for long periods at high frequency, SPM concentration data are limited to recent years through the development of turbidimeters. As turbidity stations are often scarce, usually reconstitution of series from empirical laws is often necessary. Moreover, such *in situ* data cannot reveal the origin of water and sediment as numerical tools can do. Our objective is to explore the interest of using a 1D numerical model to better grasp the spatial and temporal dynamics of SPM from a single event to a multi-annual period throughout complex river networks.

2. The Rhône River model

The Rhône River flows 810 km from its source in the Swiss Alps to the Mediterranean Sea in the South of France. The Rhône watershed is characterized by diverse hydrological regimes influenced by: (i) snow and glacier melting (Arve and Isère tributaries), (ii) oceanic rain (Saône River), (iii) Mediterranean storms (Cevenol rain (Ardèche, etc.) and Durance). Very few studies on the Rhône River have investigated its main tributaries to explore the origin of water and the source and fate of SPM over many years (Launay et al., 2019).

The Rhône River 1D model, developed at Irstea as part of the Rhône Sediment Observatory (OSR) program, was built from Lake Geneva to the Mediterranean Sea (545 km). Hydrodynamic equations are solved using the code Mage including operation rules of hydropower schemes (Dugué et al., 2015). Solute pollutants and SPM dynamics are simulated using the advection-dispersion module (Adis-TS). Such 1D numerical tool can be used to identify the sources of the water and SPM passing by at any point in the model network at any time.

3. Results

The studied period extends from January 2010 to November 2018 combining many flood events. 1-D model is suitable for calculating river dynamics, here computations takes around 12 hours on standard dekstop computers with quadcore processor for simulating 9 years. Discharge time-series have been correctly reproduced by the model along the Rhône River, especially during floods. For low flow periods, results are not as accurate due to hydropower scheme subdaily operations that are not included in the model. At Beaucaire, near to the outlet, the proportion of water coming from each tributary can be determined based on the injection of a numerical tracer in each tributary, with concentration equal to 1. A focus on the year 2013 (e.g. Figure 1) reveals the origin of water by decomposition of the discharge from each tributary all year long. The high temporal resolution of the hourly results is useful to focus on any hydrological event we choose in the study period.

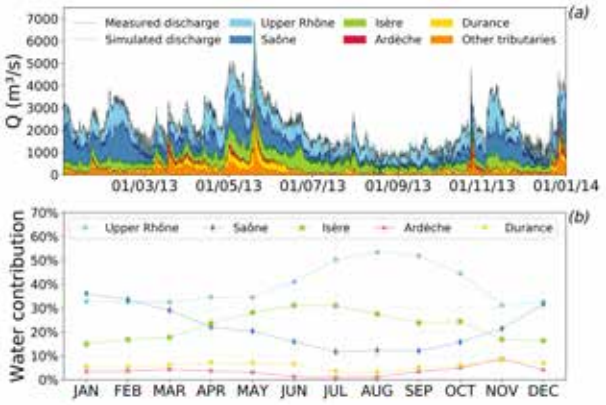

Figure 1. Decomposition of the Rhône discharge at Beaucaire in 2013 *(a)* and monthly mean contributions of major tributaries over 2010-2018 *(b)*.

The monthly mean contributions of major tributaries to the Rhône River discharge at Beaucaire are presented in Figure 1. It confirms the hydrological regime with the highest input from the Saône River in winter, and from the Arve (Upper Rhône) and Isère rivers in spring and summer. Deliveries from the Durance and Ardèche are relatively low but they correspond to short and violent events in spring and autumn. Such behaviour leads to a very different distribution of the SPM sources all year long.

4. Conclusion and perspectives

The Rhône 1D model can reproduce precisely past hydrological events during multi-annual periods at high spatial and temporal resolution, which is useful to understand the SPM dynamics, deposit and resuspension along the river. Long-term SPM concentration series for the tributaries are reconstructed in order to compare past events simulated to stratigraphic records and estimate SPM fluxes.

Acknowledgements

This work is part of the OSR project funded by the Plan Rhône and the ERDF (European Union).

References

Dugué, V. et al. (2015) Accounting for hydropower schemes' operation rules in the 1D hydrodynamic modeling of the Rhône River from lake Geneva to the Mediterranean sea. In *Proc. 36th IAHR Congress*, The Hague, The Netherlands, paper 3366.

Launay, M. et al. (2019) Numerical modelling of the suspended particulate matters dynamics in a regulated river network. *Science Total Environment*, 665:591–605.

Interaction of buoyant river plumes with vegetation and consequences for sediment transport and deposition

Hemanth Vundavilli[1], Julia C. Mullarney[1], Iain T. MacDonald[2], Karin R. Bryan[1]

[1] Coastal Marine Group, University of Waikato, Hamilton, New Zealand, vvssrhemanth@gmail.com
[2] National Institute of water and Atmospheric Research, New Zealand,

1. Introduction

River plumes are the primary mechanism delivering sediment to the coastal environment. Near the coast, river banks and deltas are often lined with aquatic vegetation, such as mangroves, which can dissipate wave and tidal energy, and trap these sediments (Mullarney et al. 2017). While much previous work has elucidated the dynamics of freshwater plumes, the interaction of these buoyant plumes with vegetation is relatively less well understood. We aim to identify the key processes that play a role in sediment deposition and erosion patterns within a mangrove-lined river delta using an idealised numerical model.

2. Methodology

Our model system is based on the Firth of Thames (FOT), New Zealand, a modern flat-fronted deltaic system, in the Hauraki Gulf, in the North Island. A ~1-km wide mangrove forest has colonised the southern end of the Firth, and the river banks. The FOT has been simplified with a grid that has a symmetric geometry with respect to the longitudinal axis with a single river input at the centre (Figure 1).

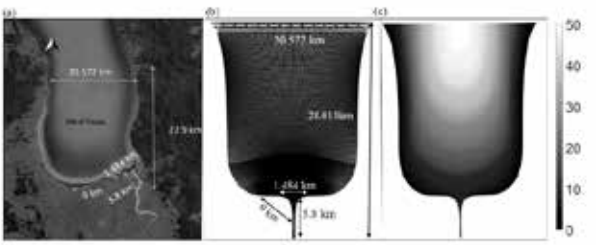

Figure 1: (a) Firth of Thames field site with key dimensions shown. Idealised symmetric model grid (b) with open boundary (dashed red line) and river boundary (solid red line) and bathymetry in m (c).

2.1 Model setup

We use the Delft3D modelling suite, which includes a hydrodynamic solver for the unsteady non-linear shallow water equations, morphology, and vegetation modules. The grid was composed of three domains with resolutions varying from 170 x 160 m in the upper grid, 15 x 6 m in the mangrove regions and 20 x 20 m in the river (Figure 1b). There were 5 sigma-layers in the vertical. The model consists of a single river input at the centre at the southern end forced with a constant freshwater discharge of 70 m^3s^{-1} and mud concentration of 0.1 kg m^{-3}, and a northern open boundary was forced with a M2 tide with an amplitude of 1.3 m. Initial salinity in the model was set at 31 ppt. To represent the different environments within the model domain a spatially varying bottom roughness was used. The model was run with a 1-m initial bed layer thickness for a simulation time of one month with a morphological factor of 12.

3. Results

Model results indicate that wind direction strongly influenced plume spread (Figure 2), and hence, sediment deposition patterns.

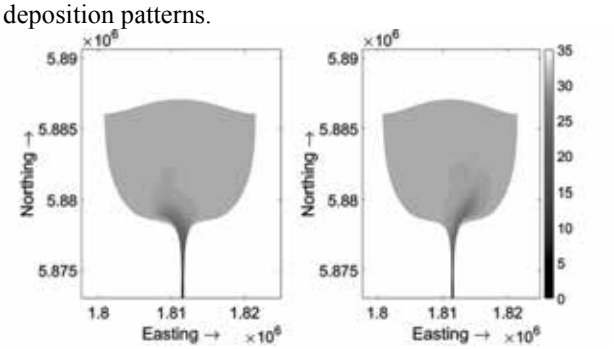

Figure 2: Model results (focused on the plume area) showing salinity (ppt) in the surface layer for a variety of wind scenarios. Wind speeds were 5 m/s from (a) 0 degrees (b) 300 degrees

Preliminary results indicate sediment deposition occurred at the mudflat, and deep inside the forest; whereas the fringe area experienced erosion (Table 1). This pattern of erosion and deposition are consistent with field observations collected in FOT (Lovett, 2017).

Observation Point	Initial bed layer	Final sediment thickness	Erosion/Deposition
Forest	1 m	1.25 m	Deposition
Fringe	1 m	0.87 m	Erosion
Mudflat	1 m	1.45 m	Deposition

Table 1: Observed erosion/deposition depths within different environments in the model.

We will present results from the across-shore momentum balance to help elucidate the observed erosion/deposition patterns.

Acknowledgements

Acknowledgment is made to the Donors of the American Chemical Society Petroleum Research Fund for support of this research.

References

Mullarney, J.C., Henderson, S.M., Norris, B.K, Bryan, K.R., Fricke, A.T., Sandwell, D.R. and Culling, D.P. (2017), A question of scale: How turbulence around aerial roots shapes the seabed morphology in mangrove forests of the Mekong Delta, *Oceanography* 30(3): 34-47.

Lovett, N.J. (2017). *Sediment transport in the Firth of Thames mangrove forest, New Zealand* (MSc thesis), the University of Waikato, Hamilton, New Zealand. Retrieved from https://hdl.handle.net/10289/11568

Source-to-sink modelling of sediment dynamics in the South Island of New Zealand

Y. Walley[1], A. Henshaw[2] and J. Brasington[3]

[1] School of Geography, Queen Mary University of London, London, United Kingdom. y.r.s.walley@qmul.ac.uk
[2] School of Geography, Queen Mary University of London, London, United Kingdom. a.henshaw@qmul.ac.uk
[3] Department of Earth and Ocean Sciences, University of Waikato, New Zealand. james.brasington@waikato.ac.nz

1. Introduction

Landscape evolution is governed by the interplay of uplift, climate, erosion and the discontinuous pattern of sediment transfer through the catchment system. This pattern is modulated by the interaction of key network characteristics such as the distribution of transport capacity and resultant zones of sediment storage. Given the long timescales involved in the episodic transfer of sediment, patterns of storage are often out of phase with the driving rates of uplift and erosion. An understanding of how sediment is modulated through network topology over associated timescales presents significant implications for the understanding of river response to disturbance events, and floodplain asset management. This research project investigates the role that drainage network topology plays in modulating the pattern of sediment transfer from source to sink, using numerical models of sediment storage and transfer and focusing on the dynamic environment of the South Island of New Zealand.

2. Context and Rationale

The processes that control the flux and storage of sediment have been widely researched at small scales, from individual grains, to the transfer of sediment pulses through a reach (e.g. James, 2010; Lisle et al., 2001), and the impact of intersecting tributaries (e.g. Knighton, 1980; Rice, 1998). There remains a lack of integration between the mechanics of individual sediment pulses and theoretical sediment transfer through catchment-scale networks. Recent research has centred around confluence environments (Benda, 2008; Benda et al., 2004) and 'geomorphic hotspots' (Czuba and Foufoula-Georgiou, 2015, 2014; Walley et al., 2018) at the catchment scale, as key nodes where individual sediment wave evolution and catchment-scale connectivity intersect.

At the catchment scale, network configuration becomes a significant control on the modulation of sediment flux in river systems, through the configuration of effective and ineffective tributaries (Rice, 1998) producing a pattern of discontinuous downstream transport. Where research has previously focussed on tributary interactions at the reach scale, there remains a lack of understanding around the role of network configuration on modulating patterns of sediment routing across entire catchments.

3. Approach

This research project identifies representative topological structures from a range of networks, which then inform topologically varied modelling of sediment connectivity. Fluvial systems are identified across the South Island of New Zealand as networks of connected links extracted from digital terrain data, and key parameters of topology calculated for each link and catchment. These parameters are used to classify catchments into topological 'types', from which one network is identified as representative of each class. The resulting catchments parameterize a river network sediment transport model (Czuba and Foufoula-Georgiou, 2015, 2014) and the CAESAR landscape evolution model (Coulthard et al., 2013). This numerical framework is used to establish the role of network topology in determining the spatial and temporal patterns of sediment transfer.

References

Benda, L., 2008. Confluence environments at the scale of river networks, in: Rice, S.P., Roy, A., Rhoads, B.L. (Eds.), River Confluences, Tributaries and the Fluvial Network. Wiley & Sons Ltd., pp. 271–300.

Benda, L., Andras, K., Miller, D.J., Bigelow, P.E., 2004. Confluence effects in rivers: Interactions of basin scale, network geometry, and disturbance regimes. Water Resour. Res. 40.

Coulthard, T.J., Neal, J.C., Bates, P.D., Ramirez, J., De Almeida, G.A.M., Hancock, G.R., 2013. Integrating the LISFLOOD-FP 2D hydrodynamic model with the CAESAR model: implications for modelling landscape evolution. Earth Surf. Process. Landforms 38, 1897–1906.

Czuba, J.A., Foufoula-Georgiou, E., 2015. Dynamic connectivity in a fluvial network for identifying hotspots of geomorphic change. Water Resour. Res. 51, 1401–1421.

Czuba, J.A., Foufoula-Georgiou, E., 2014. A network-based framework for identifying potential synchronizations and amplifications of sediment delivery in river basins. Water Resour. Res. 50, 3826–3851.

James, L.A., 2010. Secular Sediment Waves, Channel Bed Waves, and Legacy Sediment. Geogr. Compass 4, 56–598.

Knighton, A.D., 1980. Longitudinal changes in size and sorting of stream-bed material in four English rivers. Geol. Soc. Am. Bull. 91, 55–62.

Lisle, T.E., Cui, Y., Parker, G., Pizzuto, J.E., Dodd, A.M., 2001. The dominance of dispersion in the evolution of bed material waves in gravel-bed rivers. Earth Surf. Process. Landforms 26, 1409–1420.

Rice, S.P., 1998. Which tributaries disrupt downstream fining along gravel-bed rivers? Geomorphology 22, 39–56.

Walley, Y., Tunnicliffe, J., Brierley, G., 2018. The influence of network structure upon sediment routing in two disturbed catchments, East Cape, New Zealand. Geomorphology 307, 38–49.

A free water surface measurement using camera synchronization control device

H. Koseki[1], T. Yasuda[2], A. Yorozuya[3] and H. Yasuda[4]

[1] Public Works Research Institute, Ibaraki, Japan, h-koseki@pwri.go.jp
[2] Yasuda Survey Co., Ltd., Tochigi, Japan, ys-tpo@bc9.be.jp
[3] Public Works Research Institute, Ibaraki, Japan, yorozuya@pwri.go.jp
[4]Research Institute for Natural Hazards & Disaster Recovery, Niigata, Japan, hiro@gs.niigata-u.ac.jp

1. Introduction

For understanding propagation of flood waves, water gauges are installed in every 1 km or some tens of kilometers. On the other hand, water surface distribution appears on sand waves such as dune or bar. When the distribution can be measured, bed shape or water depth can be estimated using previous study (e.g. Yalin & Bishop, 1977). The photogrammetry with plural camera is one of the key technologies to create the distribution.

There two requirements for the distribution in river, one is to cover area with several tens of meter, the other is to have density with several tens of points/m^2. Some studies were successful in covering several tens of centimetre in flume (e.g. Tsubaki & Fujita, 2005), but there is no study satisfying these requirements in river, because it's difficult to synchronize time of images in the field. The present study introduced a setup of a commercial camera and camera synchronization control device (SCD) using GPS clock. Point could on the surface in wide area was created using Structure form Motion (SfM) technique. Finally, the verification of accuracy was conducted.

2. Instruments & Site

The setup consists of one camera, one SCD and one shutter release cable. The camera body is SONYa7II with SEL2870 lens. The camera is used in auto mode except manual focus adjusting with distance from the camera to the water surface. The SCD transmits a signal to the camera for taking a picture at every one minute based on GPS clock. Authors set five setups on the bridge. The point cloud is created using PhotoScan manufactured by Agisoft, Russia.

For verification of the accuracy, the elevation was measured using Total Station (TS), which is tracking the target equipped with the top of a tethered boat. In addition, Workhorse Rio Grande ADCP, manufactured by Teledyne RD Instruments in USA, is equipped with the boat to measure water depth and velocity.

The measurement site locates at a transition place from riffle to pool, therefore, we can see easily the wave and white bubbles of the surface. There are 6 reference points on the ground for geometric transformation of images.

3. Result

3.1 Coverage

The accuracy in horizontal and vertical axes was less than 10cm. One set of the images covers maximum 50m long in flow direction and 25m in cross-sectional direction.

3.1 Point measurement

For understand time variation of the water surface, point measurement was conducted using the boat tethered at one place as possible. The sampling duration is more than 5 min, therefore, there are more than 300 samples which is enough to calculate averaged value (TS-Ave.) and standard deviation σ. Water surface elevation from the point cloud is averaged value, which is called Image-Ave, using more than 50 points. The results are shown in Table 1. Range of three standard deviations is 0.02~0.035 m. At No.1 and 2, Image-Ave. are within the 95% confidence interval. At No. 3, difference is 0.03m between the Image-Ave. and the confidence interval, which is a small difference for wavelength and height.

	Total Station		Image
No.	Ave.+2 σ	Ave. -2 σ	Ave.
1	89.08	88.99	88.98
2	89.06	88.92	89.09
3	88.94	88.83	88.86

Table 1: Result of point measurement.

3.2 Line measurement

For comparison wavelength and wave height, the result of longitudinal profiles is shown in Figure 1. TS and the present method measured between 0~45 m and 25~60 m from upstream, respectively. These profiles have same phase of wavelength and wave height. Densities of these are 50 points/m by the method and 1 point/m by TS. Frude number is 0.6~1.1 calculated using ADCP results. The bed elevation is measured two times and the second one is shown as Bed 2 in Figure 1. The shapes are almost same and the difference in the elevation aren't much. Estimated water depth is 0.95m using the formula proposed by Yalin & Bishop (1977). The measured value is about 1.5m.

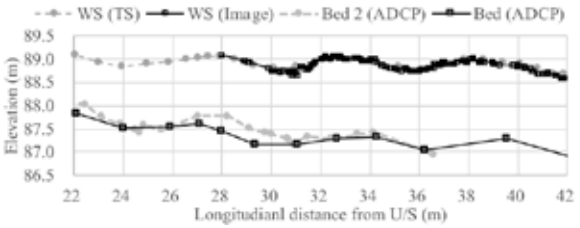

Figure 1: Comparison the longitudinal profiles.

4. Conclusions

The measurement system can get points cloud of water surface in 50m by 20m area using commercial cameras and the developed time synchronize devices. The point measurement result is within 95% confidence interval. The longitudinal profile is identical with the result of TS.

References

Tsubaki, R. and Fujita, I. (2005). Stereoscopic measurement of a fluctuating free surface with discontinuities, *Measurement Science and Technology*, 16, pages 1894-1902

Yalin, M., Bishop, B. (1977). On the physical modeling of dunes. *Proceedings of 17th Congress IAHR*, pages 25-32.

Spatial variation of surge phenomenon during very shallow water periods on intertidal mudflats

Qian Zhang[1], Zheng Gong[2], Changkuan Zhang[1], Beibei Xu[1]

[1] Jiangsu Key Laboratory of Coast Ocean Resources Development and Environment Security, Hohai University, Nanjing, China, zhangqian@hhu.edu.cn

[2] State Key of Laboratory of Hydrology-Water Resources and Hydraulic Engineering, Hohai University, Nanjing,

1. Introduction

Intertidal flats are extensive coastal areas with water depth changing periodically, leading to the frequent occurrence of the "very shallow water" (water depth on the order of 10 cm) periods. Researches have shown that this special period, which is sometimes characterized by velocity and suspended sediment concentration (SSC) surges(Wang *et al.*, 1999; Zhang *et al.*, 2016), makes remarkable contribution to sediment transport and morphodynamical processes (Nowacki&Ogston, 2013; Shi *et al.*, 2019). This study aims to explore the spatial variation of the surge phenomenon on different elevation of tidal flats and to improve the understanding of sediment transport processes during very shallow water periods.

2. Field campaigns

Three stations on the upper, middle and lower intertidal mudflats along Jiangsu coast, China, were chosen for measurements of near-bed flow and SSC (Figure 1). The Nortek Vectrino Profiler was used to measure near-bed profiles (3-6 cm above bed) of velocity with 1 mm vertical resolution at a frequency of 25 Hz. Distance from the transducer to the seabed was recorded at 1 Hz. Meanwhile, SSC at 5 layers above bed were collected by OBSs. Wave height and direction were calculated from the high-frequency velocity data, and bed shear stress was calculated with the turbulent kinetic energy method after wave-turbulence decomposition.

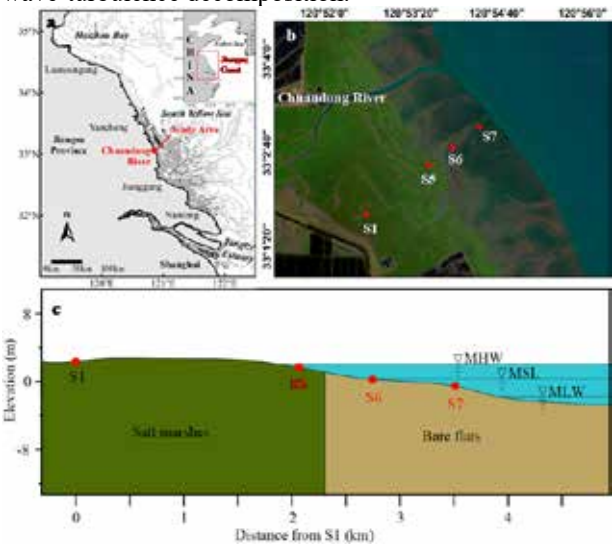

Figure 1 (a) Location of the study area; (b) Joint hydrodynamic and sediment measurements were collected at S5, S6 and S7 on intertidal mudflats in the summer of 2016. (c) Cross section of the mudflat profile, based on elevation data collected in December 2015.

3. Results

Observation reveals that the very shallow water processes varied largely at three stations. Velocity surges decayed a lot as flat elevation increased, while at the upper intertidal flat, no velocity surge was observed. However, SSC surges were detected to be strong at both stations on middle and lower intertidal flats, with advection and suspension to be the dominant factor, respectively. Furthermore, suspended sediment stratification, suspended sediment flux and bed load flux are calculated to explore the sediment transport processes during very shallow water periods. At lower intertidal flats, bed sediment can be resuspended by surge flow and well mixed into the water column during the very shallow water periods, contributing up to 25% of the onshore suspended sediment flux during flood tides, although they last only 10% of the flood duration.

Acknowledgments

The author would like to thank the colleagues and students helped in the field work. This work is supported by the National Natural Science Foundation of China (51620105005，51879095)

References

Nowacki, D.J., &Ogston, A.S., (2013). Water and sediment transport of channel-flat systems in a mesotidal mudflat: Willapa Bay, Washington. Continental Shelf Research, 60, Supplement,S111-S124. https://doi.org/10.1016/j.csr.2012.07.019

Shi, B.,Cooper, J.R.,Li, J.,Yang, Y.,Yang, S.L.,Luo, F.,Yu, Z., &Wang, Y.P., (2019). Hydrodynamics, erosion and accretion of intertidal mudflats in extremely shallow waters. Journal of Hydrology, 573,31-39. 10.1016/j.jhydrol.2019.03.065

Wang, Y.P.,Zhang, R.S., &Gao, S., (1999). Velocity variations in salt marsh creeks, Jiangsu, China. Journal of Coastal Research, 15 (2),471-477.

Zhang, Q.,Gong, Z.,Zhang, C.,Townend, I.,Jin, C., &Li, H., (2016). Velocity and sediment surge: What do we see at times of very shallow water on intertidal mudflats? Continental Shelf Research, 113,10-20. https://doi.org/10.1016/j.csr.2015.12.003

Effect of pier shape on the local scour

K.V.S. KrishnaReddy[1] and V. Chandra[2]

[1]Indian Institute of Technology Madras, Chennai, India. kvskreddy.09@gmail.com
[2]Indian Institute of Technology Madras, Chennai, India. vc@iitm.ac.in

1. Introduction

Scour is the process of river bed erosion due to the action of flowing water. Local scour occurs when the stresses induced around the local area of pier (Kothyari, 2007). Generally, bridge piers are designed as circular type cross-section, and the shape and size of the pier influence the extent of maximum local scour (Melville and Sutherland, 1988). Apart from the circular shaped pier, researchers have attempted studies with different shaped piers such as rectangular and aerofoil (Vijayasree et al., 2017). Pier shape is a significant factor and obtaining an optimum shape can reduce the scour depth. Most of the existing studies to estimate the scour depth are for uniform shaped piers (Jones et al., 1992). In practice, compound piers also exist, having an enlarged footing at the base of a uniform shaped pier. Very few investigations have incorporated the effect of compound piers on the scour formation (Kumar et al., 2012). Therefore, it becomes important to study the effect of circular footing with modified piers in scour reduction.

The present study aims to reduce the local scour around the pier by modifying its shape using two modified piers along with a circular pier, to find the optimal shape against the local scour. Further, the effect of circular footing with modified piers is studied, which is important in foundation design.

2. Experiments

Experiments are performed in a rectangular glass-walled flume filled with sand (d_{50}=0.46 mm) under clear water conditions at a flow depth (h) of 12 cm. Two modified piers are used (M2 and M3) with the cross-sectional area equivalent to that of a circular pier (M1) having diameter (D) equal to 5 cm. Where, pier M2 is combination of semi-circle and triangle in which pier is oriented to the flow direction in either way (M2a and M2b) and M3 has a groove with projection on the semi-circular face of M2.

In addition, experiments were conducted with isolated and compound piers (a circular footing of size 2D is for piers mentioned above) under steady and hydrographic flow conditions. Figure 1 shows the temporal variation (T^*) of non-dimensional scour depth (H^*), which is the ratio between the maximum scour depth observed (h_s) and the pier diameter (D). Where T^* is the ratio of time of measurement (t) to the total duration of the experiment (T~300 minutes). From the results, it can be observed that modified piers produced minimum local scour depth compared to the circular pier because of their less effective width to the approach flow and the modified pier shape weakens the down flow and horseshoe vortex. More details will be presented in the main paper.

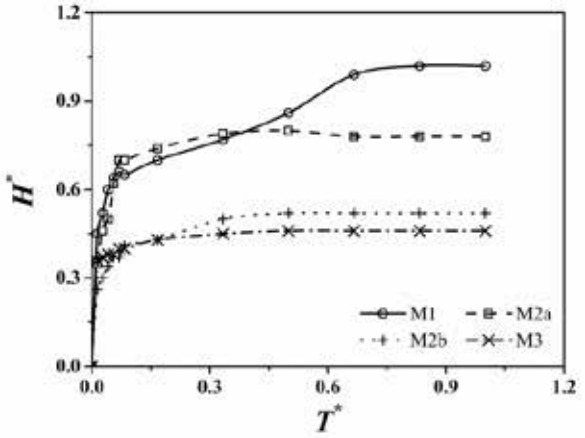

Figure 1: Temporal variation of scour depth ratio for isolated piers under steady flow conditions

3. Conclusions

Following conclusions are made from the present experimental study.

- Under steady flow conditions, the reduction in the scour depth for the modified piers M2a, M2b and M3 compared to M1 are 23.5%, 50%, and 55%, respectively.
- The scour depth further reduced by 49% with the introduction of a circular footing to M1 pier. However, it shows an insignificant effect with the modified pier shapes in scour reduction.

Acknowledgements

We express our sincere thanks to the Science and Engineering Research Board (SERB), Government of India, for funding this project work.

References

Jones, J. S., Kilgore, R. T., and Mistichelli, M. P. (1992). Effects of footing location on bridge pier scour. *J. of Hyd. Eng.*, 118(2):280-290.

Kothyari, U. C. (2007). Indian practice on estimation of scour around bridge piers-A comment. *Sadhana*, Vol. 32, No. 3:187-197.

Kumar, A., Kothyari, U. C., and Raju, K. G. R. (2012). Flow structure and scour around circular compound bridge piers–A review. *J. of Hydro-Env. Res.*, Vol. 6, No. 4:251-265.

Melville, B. W., and Sutherland, A. J. (1988). Design method for local scour at bridge piers. *J. of Hyd. Eng.*, 114(10):1210-1226.

Vijayasree, B. A., Eldho, T. I., Mazumder, B. S., and Ahmad, N. (2017). Influence of bridge pier shape on flow field and scour geometry. *Int. J. of River Basin Management*:1-21.

Modelling the influence of longshore tides on cross-shore sediment dynamics under moderate wave conditions

V.H. Hewageegana[1] A. Canestrelli[1]

[1] Department of Civil and Coastal Engineering, University of Florida, Gainesville, FL, USA

1. Introduction

The influence of tides on cross-shore sediment dynamics of a longshore-uniform beach is studied by means of a 1D numerical model (XBeach). The model is modified to include longshore tidal currents induced by water level gradients. The effect of tides on cross-shore sediment dynamics is quantified by analyzing the change in suspended sediment concentration (SSC), sediment advection velocity and sediment transport. The effect of tides is decoupled in its two main components, i.e., water level fluctuations and tidal currents. Water level fluctuations modulate wave orbital velocities and sediment advection velocity, therefore affecting both resuspension of sediments and cross-shore sediment transport. Tidal currents favor sediment resuspension due to the increase in applied shear stress on the bed. The effects of water level fluctuations and tidal currents on sediment dynamics vary in the cross-shore direction: tidal currents drive the changes in deeper water depths while water level fluctuations dominate the changes observed in shallow water. Therefore, while at shallow waters tidal range is a good indicator of the influence of longshore propagating tides on cross-shore sediment dynamics on a uniform beach, at deeper waters, tidal period and tide length also play an important role. To the authors' knowledge, at present no study has undertaken a systematic investigation of the combined effect of water level fluctuation and longshore tidal currents on cross-shore sediment dynamics for longshore uniform beaches.

2. Methodology

Separate model scenarios were generated incorporating the two main tidal effects for varying short wave and tidal conditions. Four model scenarios used were: (A) short waves propagating over a constant water level and no tidal currents (reference case); (B) short waves propagating over an oscillating water level and no tidal currents; (C) short waves propagating over a constant water level with tidal currents; (D) short waves propagating over an oscillating water level and tidal currents

3. Results

Figure 1 illustrates the tidally averaged increase in SSC for scenario D compared to the reference. At deeper water depths (-5m), the longshore tidal currents increase the SSC due the increased bed shear stress. At this depth water level fluctuation is not strong enough to change the SSC. As the water depth reduces, the effect of tidal currents on SSC wanes owing to higher frictional effects which dissipates the tidal current. At shallower depths (-2m), the change in SSC by water level fluctuation (scenario B) and scenario D overlaps each other. Figure 2 shows the change in tidally averaged suspended sediment transport rate for scenario D compared to the reference. The suspended sediment transport varies due to the change in SSC and advection velocity. Change in suspended sediment transport rate also shows a similar pattern to that of SSC.

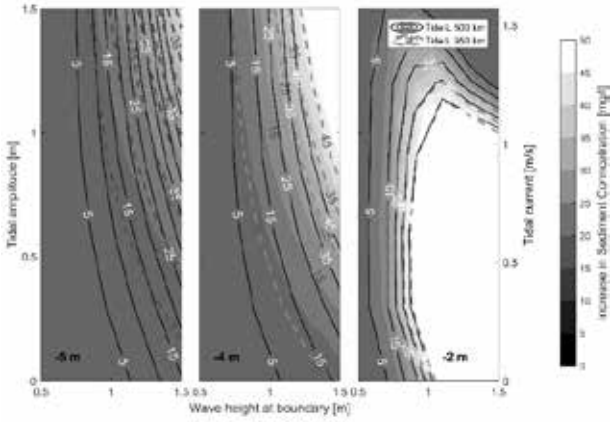

Figure 1: Increase in tidally averaged SSC due to the effect of water level oscillations and tidal currents (scenario D) compared to the reference case (Scenario A). The solid background colors shows the change in SSC due to water level fluctuations only (Scenario B).The contour lines provide the increase SSC for tides with a wave length of 500km and 950km (Scenario D).The right Y axis (Tidal current [m/s]) refer to the tidal current of tide with 500km wave length.

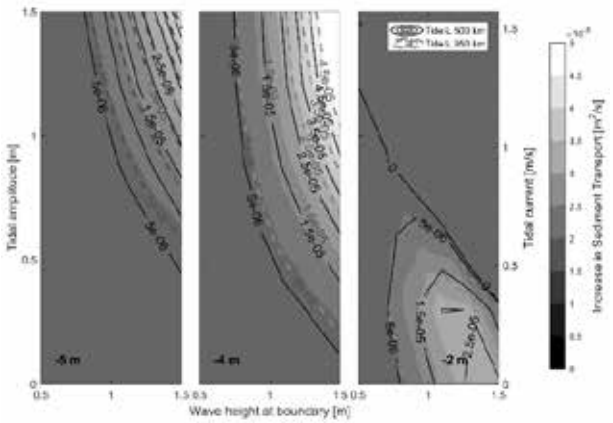

Figure 2: Increase in tidally averaged cross-shore suspended sediment transport due to the effects of tide. (Figure layout similar to Figure 1)

4. Conclusions

Tides have an important influence on cross-shore sediment dynamics. Tidal water level fluctuations are important in changing the SSC and advection velocity at shallower depths, while tidal currents can act as an additional mobiliser of sediments in deeper water depths. Tidal wave length becomes important in the process as the tidal velocities depend on the tidal wave length. At intermediate depths, both tidal currents and water level fluctuation influence changes in SSC and sediment transport.

Mechanisms underlying the formation of branching creeks on flanking tidal flats along a large channel: A morphodynamic study

Y. Zhang[1,2], Z. Zhou[1,2], A. Finotello[3], A. D'Alpaos[3], C.K. Zhang[2]

[1] State Key Laboratory of Hydrology-Water Resources and Hydraulic Engineering, Hohai University, Nanjing, China, ying.zhang95@hhu.edu.cn, zeng.zhou@hhu.edu.cn

[2] College of Harbour, Coastal and Offshore Engineering, Hohai University, Nanjing, China, zhangck@hhu.edu.cn

[3] Department of Geosciences, University of Padova, Padova, Italy, alvise.finotello@unipd.it, Andrea.dalpaos@unipd.it

1. Introduction

Tidal channels, typical features in coastal and estuarine systems, display a variety of morphological patterns. Their formation and evolution depend on the interplay between hydrodynamic processes, sediment dynamics and topography. Though widely distributed in tidal environments, branching creeks on flanking tidal flats along a large channel have received limited attention. Field observations by Mariotti and Fagherazzi (2011) in Willapa Bay show hydrodynamics on the tidal flat and the channel differ remarkably during a tidal cycle. Large velocities occur in creeks branching from the main channel when the flow concentrates in the channel and the tidal flat becomes exposed. In contrast, when the water surface level increases, water in the branching creek starts to flow along the channel and the lateral creek tends to be inactive. Such flow variation indicates that the topography near the main channel can influence hydrodynamics, sediment transport and hence the formation of branching creeks especially during the ebb tides. Previous studies show that a concave cross-section profile tends to generate larger deposition rates compared to a convex profile due to the associated larger horizontal velocity gradient (van Maren and Winterwerp, 2013). A gentle initial slope of the tidal flat tends to accelerate the formation of tidal channels in an open-coast environment (Xu et al., 2017). This study aims to unravel the mechanisms underlying the formation and evolution of branching creeks along a large channel, with a specific focus on the role of the cross-sectional profiles with different shapes and curvatures.

2. Method

A morphodynamic model (Delft3D) is used in this study. The model domain is characterized by a single main channel, with flanking tidal flats on both banks, extending toward a closed land boundary. A harmonic tide with a tidal period of 12 h and an amplitude of 1.5 m, propagates at the along-channel direction. Several types of cross-section profiles are considered by changing the shape and curvature (see Fig 1). Ellipses are adopted for creating convex-up cross-section profiles and circles for concave-up ones. Quantitative analyses on geometric parameters of generated creeks then are conducted to explore the response of tidal creeks morphology to changes in cross-section profiles.

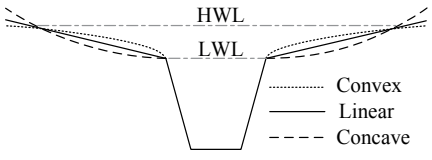

Figure 1: Schematic cross-sections used in the model.

3. Preliminary Results

Model results indicate that the model can reproduce the formation of parallel creeks along the main channel. Here we examine the effects of concave-up cross-section profiles. As the decrease in curvature of the initial profile (i.e., increase in the profile slope), more branching creeks perpendicular to the main channel form at the landside (see Zone 1). A gentler slope seems to favor the formation of creeks on the bank. Larger creeks tend to develop close to the sea boundary (in Zone 2) due to stronger tidal forcing. The number of creeks appears to be the largest when the concavity of the initial profile is intermediate (Figure 2b). It is also worth mentioning that the main channel becomes curved due to erosion and deposition near the channel banks. Though not reported here, the role of profile shapes (i.e., concave-up, convex-up and linear profiles) are also being investigated.

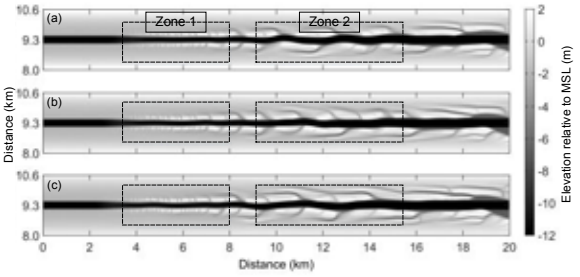

Figure 2: Simulated bathymetries after 8 years with decreasing concavity of initial cross-section profiles.

4. Conclusions

The formation of branching creeks on flanking tidal flats along a large channel depends on the feedback between flow and local topography. Numerical model results suggest that the number, morphology and long-term evolution of these creeks are affected by the cross-section profile of tidal flat adjacent to the large channel. The creeks generated at landside area are smaller and denser than the creeks at seaside area. A gentler cross section slope tends to favour the creek development.

References

Mariotti, G. and Fagherazzi, S. (2011). Asymmetric fluxes of water and sediments in a mesotidal mudflat channel. Continental Shelf Research, 31(1): 23-36.

van Maren, D.S. and Winterwerp, J.C. (2013). The role of flow asymmetry and mud properties on tidal flat sedimentation. Continental Shelf Research, 60: S71-S84.

Xu, F., Coco, G., Zhou, Z., Tao, J. and Zhang, C. (2017). A numerical study of equilibrium states in tidal network morphodynamics. Ocean Dynamics, 67(12): 1593-1607.

Numerical modeling on meander chute cutoffs using hybrid deterministic-stochastic method

Z. Li[1] and M. H. García[1]

[1] Dept. of Civil and Environmental Engineering, University of Illinois at Urbana-Champaign, Urbana, USA.
Email: zhil2@illinois.edu and mhgarcia@illinois.edu

1. Introduction

The development of a chute cutoff locally shortens and straightens a meandering river channel, excavating a large volume of floodplain sediment as the chute channel deepens and widens. The formation process of chute cutoffs contains stochastic components (Grenfell *et al*., 2014). The heterogeneity of floodplain material, the random density distribution of vegetation and the nature of turbulent flow can easily overturn the whole cutoff process.

A key challenge to numerically model chute cutoff is on how to simulate a stochastic process via a deterministic fundamental framework. Conventionally, in the field of river dynamics modeling, bank line shift is subjecting an effective mathematical framework: linearly correlating erosion rate with the a) excess velocity or 2) excess shear stress. The former family of methods, named HIPS method (Hasegawa, 1977; Ikeda *et al*., 1981), always takes the form,

$$\zeta = E(U - U_0) \tag{1}$$

and the latter family of methods, named physically-based method (Motta *et al*., 2012a), takes the form,

$$\zeta = K_d(\tau - \tau_c) = K_d'(\tau/\tau_c - 1) \tag{2}$$

where ζ is erosion rate $[L/T]$, E is the non-dimensional erosion coefficient, U is the near bank flow velocity, U_0 is the mean velocity, K_d and K_d' are the erosion coefficient in different forms, τ is the near bank shear stress, τ_c is the critical bank shear stress.

E , K_d and K_d' are cite specific and highly variable soil properties (Motta *et al*., 2012b). They are required to be specified in models using soil jet testing results or values extracted from historical records. The parameters can easily range several orders of magnitude and thereby bring uncertainties, especially in long-term simulations. It also leads to the process completely deterministic, unless one decides to randomize the parameters (Posner and Duan, 2012). In this study, a hybrid deterministic-stochastic method is applied to numerically model chute cutoffs. The model assumes Gaussian distributions of both bank shear stress and the critical bank shear stress to evaluate the bank erosion risk. The method is tested using a simplified bench scale chute cutoff, which is scaled down from a natural chute cutoff in Wabash River.

2. Results

The qualitative comparison of the sand bar development between the model and its prototype is shown in Fig 1.

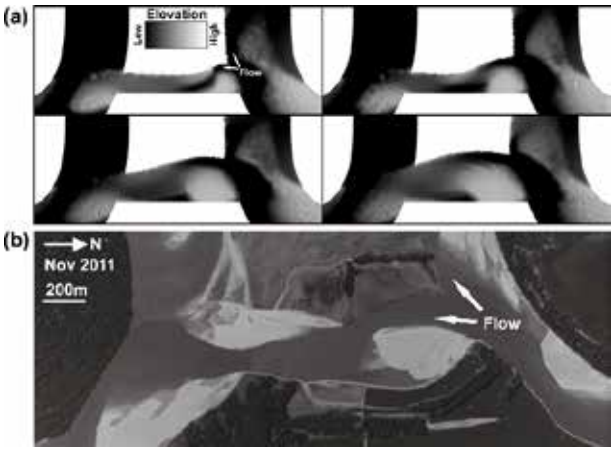

Figure 1: (a) Modeled bar development;
(b) Aerial imagery of Mackey Bend, Wabash River.

3. Conclusions

The conventional modeling method "sweeps a large amount of physics under the rug" (Parker *et al*., 2011) and it naturally rejects stochastic components to be modeled in the complex hydro- and morpho-dynamic process. The present method provides a new look that a chute cutoff can evolve to diverse shapes with stochastic components being considered.

References

Grenfell, M. C., Nicholas, A. P., & Aalto, R. (2014). Mediative adjustment of river dynamics: The role of chute channels in tropical sand-bed meandering rivers. *Sedimentary Geology*, 301, 93-106.

Hasegawa, K. (1977). Computer simulation of the gradual migration of meandering channels. *Proceedings of the Hokkaido Branch, Japan Society of Civil Engineering*, 197-202 (in Japanese).

Ikeda, S., Parker, G., & Sawai, K. (1981). Bend theory of river meanders. Part 1. Linear development. *Journal of Fluid Mechanics*, 112, 363-377.

Motta, D., Abad, J. D., Langendoen, E. J., & Garcia, M. H. (2012). A simplified 2D model for meander migration with physically-based bank evolution. *Geomorphology*, 163, 10-25.

Motta, D., Abad, J. D., Langendoen, E. J., & Garcia, M. H. (2012). The effects of floodplain soil heterogeneity on meander planform shape. *Water Resources Research*, 48(9).

Parker, G., Shimizu, Y., Wilkerson, G. V., Eke, E. C., Abad, J. D., Lauer, J. W., ... & Voller, V. R. (2011). A new framework for modeling the migration of meandering rivers. *Earth Surface Processes and Landforms*, 36(1), 70-86.

Posner, A. J., & Duan, J. G. (2012). Simulating river meandering processes using stochastic bank erosion coefficient. *Geomorphology*, 163, 26-36.

The effects of vegetation intensity on river morphodynamics

T. Kyuka[1], S. Yamaguchi[2], Y. Inoue[3,] H. Kon[4] and Y. Shimizu[5]

[1] Graduateschool of Engineering, Hokkaido University, Sapporo, Japan. t_kyuka@eng.hokudai.ac.jp
[2] The Civil Engineering Research Institute for Cold Region, Sapporo, Japan. kawamura-s@ceri.go.jp
[3] Graduateschool of Engineering, Hokkaido University, Sapporo, Japan. amfate2033@icloud.com
[4] Graduateschool of Engineering, Hokkaido University, Sapporo, Japan. hkon@eng.hokudai.ac.jp
[5] Graduateschool of Engineering, Hokkaido University, Sapporo, Japan. yasu@eng.hokudai.ac.jp

1. Introduction

Growing vegetation on floodplain has been known to affect river channel morphodynamics. For instance, vegetation reduces channel (sandbars) movability and prevents bank erosion, leading into a channel meander related to a reduction in the number of channels (Tal and Paola 2010: Jang and Shimizu 2007). On the other hand, in the steep-gradient rivers, both the plane distribution of vegetation patches and the intensities of vegetation itself on floodplain considerably effect on different channel morphodynsmics such as a long-term maintenance of island braiding under the vegetation effects (). However, the basic knowledge of vegetation effects such as plane distribution and vegetation intensities on floodplain on channel morphodynamics have been lacked yet.

The objectives of this study are to know the fundamental characteristics of vegetation intensities on channel meandering by means of flume experiments. The initial channel form was sine-generated meandering curve, and two types of vegetation (alfalfa, bentgrass) were used in the experiments. Then, flow path, bank erosion and channel deformation were compared under the different growing rate of vegetation. The experimental results are used for numerical modelling as the next step of this research.

2. Methods

Experiments were conducted in a 26.0-m-long and 3.0-m-wide rectangular flume having a bed slope of 1/161, located at the civil engineering research institute of cold region, JAPAN. The flume bed consisted of uniform grain size material (the mean grain size d_m = 0.765). As an initial channel shape, 0.20-m-wide of sine-generated curve channel with a meander angle of 28.7° and 0.02-m-hight of low flow path with a triangle-shape were prepared at the center part of the flume. At the inlet and outlet sections of the flume, plywood boards were installed to prevent bed deformation during the experiments, and the volume of the supplied sediment was determined not to arrow both bed aggradation and degradation at the just downstream part of the inlet section of the flume.

Hydraulic parameters in the experiments were as follows, water discharge of Q = 0.0010^3/s, initial non-dimensional shear stress of τ_* = 0.08 and initial normal depth of h_0 = 2.0 cm. Four experimental cases are summarized below. No vegetated case is Case 1, and different vegetation intensity cases are Case 2 to Case 4. In Case 2, as relatively weak vegetation intensity, bentgrass is used (average length of stem: 20mm, root: 7mm). While, in Case 3 and Case 4, as relatively high strong vegetation intensity, mature alfalfa (average length of stem: 30mm, root: 40mm) and immature alfalfa (average length of stem: 7mm, root: 7mm) are used, respectively.

3. Results and Conclusions

Figure 1 shows the results of channel deformation in each case. In Case 1, scroll bar formation was developed as time advances at the meandering part. In contrast, different results were confirmed in other cases. In Case 2, relatively weak vegetation intensity resulted in a widening of the channel width at the only meandering part. In Case 3, relatively strong vegetation intensity led to channel incision because of little bank erosion. Due to the flow concentration into the low flow path and little sediment supply from banks, channel bed degradation was occurred. Moreover, quite different channel deformation was confirmed in Case 4. Immature alfalfa with low vegetation intensity on floodplain promoted the formation of new channels. According to figure 1, although new flow channels did not reach Chute cutoff, vegetation accelerated flow concentration even on the floodplain, especially the places of weak vegetation intensity, leading into the development of the new flow path. In this experiment, since the vegetation density was large enough, so in actual rivers, the influence of vegetation on channel morphodynamics may be small at the places where the scroll bars are formed.

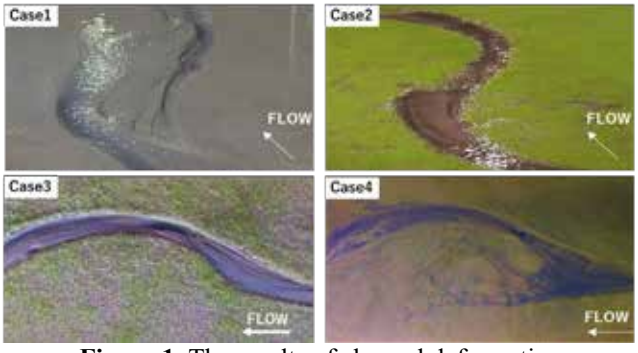

Figure 1. The results of channel deformation in Case1 to Case 4

References

Tal, M. and Paola, C. (2010): Effects of vegetation on channel morphodynamics: Results and insights from laboratory experiments. *Earth Surface Processes and Landforms*, 35: 1014-1028. doi: 10.1002/esp.1908

Jang, C. L. and Shimizu, Y. (2007): Vegetation effects on the mor-phological behavior of alluvial channels. *Journal of Hy-draulic Research*, 45: 763-773, 2007.

Van Dike, W. M., Teske, R., Van de Lageweg, W. I. and Kleinhans, M. G.: Effects of vegetation distribution on experimental river channel dynamics, *Water Resources Research*, Vol.49, pp. 7558-7584, 2013.

Index of Authors